Achim Röder

Vom Fachbereich VI
(Geographie/Geowissenschaften)
der Universität Trier
zur Erlangung des akademischen Grades
Doktor der Naturwissenschaften
(Dr. rer. nat.)
genehmigte Dissertation

A Remote Sensing Based Framework for Monitoring and Assessing Mediterranean Rangelands. Case Studies from Two Test Sites in Spain and Greece

Betreuer:
Univ.-Prof. Dr. Joachim Hill

Berichterstatter:
Univ.-Prof. Dr. Joachim Hill
appl. Prof. Dr. Willy Werner

Datum der wissenschaftlichen Aussprache: 7. 12. 2005

Trier, 2005

Acknowledgements

Just as this work has been evolving and growing, so has the number of people who have helped to make it possible in one way or the other, by sharing their ideas, energy and time at work and – most importantly – beyond. To do them all justice is an impossible task; hence, a simple ‘Thank you!’ to all friends who accompanied me in these past years.

Still, I owe particular words of gratitude

to Prof. Dr. Joachim Hill, head of the Remote Sensing Department and my first supervisor, without whose scientific guidance and experience this work would not have been possible. My knowledge of Mediterranean processes and remote sensing concepts has vastly benefited from his expertise. Most importantly, I owe him the chance to work in a European research environment, for which I am very grateful;

to Prof. Dr. Willy Werner, for accepting to act as the second supervisor for this work despite many other obligations. With his profound knowledge he complemented a remotely sensed view with a valuable ecological perspective;

to Prof. Dr. Patrick Hostert, for his friendship and encouragement. He was a part of this project from the very beginning and shared long hours in the office and in field. My deepest gratitude for his support in the final phase – his ability to create time in a tight schedule was amazing. I am indebted to him for still answering the phone, and, not the least, to Viola Neukam for letting him;

to the colleagues I had the pleasure to work with in GeoRange, who shared data and insight that are the basis of many analyses undertaken here, and who provided invaluable hours of Mediterranean hospitality: Prof. Dr. Vasilios Papanastasis, Dr. Mihailis Vrahnakis, Dimitrios Chouvardas and all the staff at the Aristotle University in Thessaloniki; Stefan Sommer and Wolfgang Mehl at the JRC/Ispra; Dr. Giuseppe Brundu at CFVA/Sardinia; Dr. Juan Puigdefabregas at EEZA/Almeria. In particular, my sincere gratefulness to Dr. Beatriz Duguy, Dr. Thomas Kemper, Dr. Gabriel del Barrio and Prof. Dr. Georgios Tsiourlis for making project work much more than a job;

to all the student staff who contributed to the project in the past years: Silke Peine, Sebastian Mader, Markus Hampen, Henning Buddenbaum, and especially to Samuel Bärisch for his support in data processing and his talent to solve problems; special thanks are due to the students who supported the project and this work with excellent diploma theses: Björn Waske and Sebastian Schiefer for advancing the initial stages with their methodological works; finally, to Tobias Kümmerle, for his dedication and efforts in the last stage of the project and – most of all – for ‘quapping’ hours;

to all colleagues at the Remote Sensing Department, from whose experience and knowledge I was privileged to benefit in the last years, and who make working in the department a pleasure; especially Dr. Thomas Udelhoven and Dr. Thomas Jarmer for help whenever needed; and not the least to Hermine Marx for sympathy, catering, and for ‘making things work’.

to Martin Schlerf for sharing highs and lows of finishing a PhD and for ‘the carrot or the stick’ this takes;

to my family, most of all to my parents, Inge and Horst Röder, and to my grandmother, Hedwig Kiefer; for their support and care throughout the years and generously accepting that visits were rare in the last months.

The last and biggest ‘thank you’ goes to the person whose energy, endurance and belief during the last year has only made this possible: my partner Anja Brassel. Thanks a million for our years together and for being there!

Achim Röder Trier, December 2005

Contents

List of Figures

List of Tables

1 Introduction and scope of the work

Natural hazards and resulting disasters, such as earthquakes, volcanic eruptions, floodings and others are threatening human welfare and the associated damages and tragedies are repeatedly raising public awareness. Thinking globally, their environmental impact and resulting consequences are at least equalled by processes that rather manifest on a longer time scale, such as the degradation and desertification of fertile lands. These may result in the accelerated reduction or even destruction of fundamental resources supporting human live, with abandoned lands being the final consequence. Such degradation processes can partially be due to climatic phenomena and gained widespread attention in the 1970s with the catastrophic drought leading to the Sahel crisis.

Ever since, there have been numerous initiatives at an international level to promote environmental protection, conservation of biodiversity, or sustainable development, such as the United Nations Conference on Environment and Development (UNCED). Among a series of resolutions and conventions originating from this event, the United Nations Convention to Combat Desertification (UNCCD) was adopted in 1994. Its mandate often appeared limited to irreversible desertification, illustrated by images of overgrazed, barren lands and approaching dunes (Helldén, 1991). Although these situations are a major concern, Annex IV of the Convention explicitly lists the European part of the Mediterranean basin as a threatened region. Beside the Convention, different international networks address these problems. For instance, the Land Use and Land Cover Change (LUCC) project is a programme element of the International Geosphere-Biosphere Programme (IGBP) and the International Human Dimensions Programme on Global Environmental Change (IHDP), and has been set up as an interdisciplinary programme aimed at improving the understanding of the land use and cover change dynamics and their relationships with global environmental change. One of its thematic foci lies in the characterisation and investigation of degradation processes, and the possible contributions of spatial data sets and the related interpretation techniques. The Land Degradation Assessment in Drylands (LADA) project initiated by the Food and Agricultural Organisation of the UN (FAO) aims to generate up-to-date information on ecological, economical, social and technical aspects of land degradation in drylands, including a combination of traditional knowledge and modern science, to guide an integrated assessment and cross-sectoral planning and management of land resources in drylands.

Addressing factors relevant in the land degradation context, climate acts as a background and multiplying factor (Mulligan et al., 2004), while often human interventions are the ultimate cause for resource degradation (Hobbs et al., 1995). Although the Mediterranean basin has been strongly utilised for long periods of time, significant land-use transformations were observed in recent times. These are often related to economic consequences of countries joining the European Union and there is ample evidence on the changes this brought about to local economy (Dubost, 1998). These include urbanisation and industrialisation, often concentrated in coastal areas, added to by the growing importance of tourism. On the other hand, rural areas often experienced a corresponding migration of young people to such centre regions, causing widespread land abandonment and aging of rural communities, while at the same time there was a growing demand for agricultural products both on national and

international markets. There is a multitude of interacting processes, as a result of which both intensification and extensification of resource utilisation are observed in close proximity. (Perez-Trejo, 1994; Van der Leuuw, 1999)

At a scientific level, the European Union responded to the challenges expressed in the UNCCD by making desertification and degradation research a priority topic in its different Framework Programmes. Given the obligation to identify areas at risk, to evaluate the impact of management decisions and to implement mitigation actions in relation to the Convention, the potential of earth observation satellites was recognised, as reflected in a history of initiatives focussing on remote sensing and modelling approaches. In the context of DeMon-I, (Integrated Approaches to Desertification Mapping and Monitoring in the Mediterranean Basin), the definition and derivation of degradation indicators from remotely sensed imagery was pursued. Its successor, DeMon-II, aimed at the conceptual extension and operational applicability of data processing and interpretation, which was demonstrated in different case studies. Besides, different projects were established with a focus on landscapes dynamics and modelling approaches in a land degradation context, such as the MEDALUS (Mediterranean Desertification and Land Use) or ModMed (Modelling Mediterranean Ecosystems Dynamics) initiatives. (Lacaze et al., 1996; Legg et al., 1998; Geeson et al.2002; Hill et al., 2003; Röder et al., 2002)

More recently, marginal lands in European Mediterranean countries have been identified as areas especially threatened by land degradation and have been given particular attention in the research project GeoRange (Geomatics in the Assessment and Sustainable Management of Mediterranean Rangelands). Its most prominent objective was to find pathways towards the establishment of a consistent approach for characterising the state of rangelands, retrospectively assessing their development, and to supply recommendations for optimised management of these lands. (Hill et al., 2001; Röder et al., 2002)

The research presented here was in parts carried out in the frame of the GeoRange project and has evolved from the experience gained therein. It analyses the use of remote sensing and geoinformation processing approaches to set up land degradation monitoring and analysis capabilities for Mediterranean rangelands that are applicable in different local contexts. Reflecting both environmental and socio-economic complexes, such a framework should allow for the monitoring of processes and trends, support the integration of multiple data sources and their interpretation, and ideally provide information relevant to decision-makers.

Due to their multi-functional character, rangelands are characterised by a complex of interacting, mutually-dependant processes. On a higher abstraction level, these can be characterised by the time scale on which they operate as ‘slow’ or ‘fast’ processes (Mulligan et al., 2004). These processes may be represented by ‘typical’ disturbance factors, such as fire and grazing.

Remote sensing enables addressing land degradation at a range of spatial and temporal scales (Hill et al., 2004) and its potential for a regular monitoring of Mediterranean regions has long been recognised. Hill et al. (1996) have formulated a number of requirements for a general-

ised monitoring framework and stressed the importance of standardised processing and interpretation approaches.

Given the complexity of processes and spatial patterns encountered in Mediterranean rangelands, the implementation of a scientifically sound interpretation framework requires an equally sound conceptual basis. This will be established by answering two sets of questions. The first relates to the identification of key processes:

- Which are the main processes operating in Mediterranean rangelands?
- How are ecological and socio-economic complexes connected?
- What are their implications for land degradation?

The second set involves the ‘translation’ of the answers to these questions into a data processing and interpretation strategy.

- Which scales are to be addressed and what type of sensor is needed?
- What data processing steps are required and what are appropriate strategies?
- Which data interpretation approaches are suitable to address the target processes identified before?
- How can remote sensing based results be enhanced by the integration with other sources of information?

These questions will be discussed in the following sections and allow to conclude on key elements of a remote sensing based rangeland monitoring framework. The further work will systematically address these by making use of two pilot areas. Referring back to the above questions, the different elements will be reviewed and as a conclusion, a scientific framework for Mediterranean rangeland monitoring and analysis based on remote sensing data and auxiliary information will be presented.

2 Land degradation in Mediterranean rangelands

Processes of desertification have appeared throughout the history of mankind and it were Greeks and Romans who used the term “agri deserti” to indicate grazed or agriculturally used lands that were deprived of their productive potential (Rubio, 1995). In historical times, the term “desertification” was introduced to soil science to describe degraded soils and plant communities (Aubreville, 1949). Until today, it has been used in varying contexts and gained worldwide attention with the United Nations Conference on Desertification (UNCOD) held 1977 in Nairobi. In 1992, the United Nations Conference on Environment and Development agreed on the ‘Convention to Combat Desertification’, which was adopted in 1994 (UNCCD, 1994). It defined desertification as “…land degradation in arid, semi-arid and dry sub-humid areas resulting from various factors, including climatic variations and human activities”. In Annex IV of the local Annexes, the specific conditions encountered in the European Mediterranean were explicitly acknowledged and unsustainable utilisation of water resources, uncontrolled wildfires and inadequate land use were identified as primary triggers of desertification (UNCCD, 1994).

Although a general consensus was reached in the Convention, Mainguet (1994) concluded that “… after the discussion […] of the existence or non-existence of desertification, I have great difficulty in accepting the use of the word ‘desertification’ at all, because it so often implies an irreversible condition. I prefer the term ‘land degradation’…”. Several authors questioned the concept of ‘desertification’ to be uniformly applied (e.g. Helldén, 1991; Stafford-Smith & Reynolds, 2002). As a consequence, it should be confined to the irreversible expansion of desert-like conditions, while ‘land degradation’ relates to processes that negatively affect the natural potential of an ecosystem. This may include its biological productivity, its landscape structure, ecosystem functioning including energy and nutrient fluxes and explicitly includes economic, social and cultural structures (Thomas & Middleton, 1994; van der Leeuw et al., 1998, 1999; Stafford-Smith & Reynolds, 2002).

The following sections aim at identifying and characterising relevant factors that determine the ecological state of Mediterranean rangelands and their temporal dynamics. This is a crucial step in the definition of a remote sensing based monitoring framework, as its different elements must be based on a thorough understanding of major processes (e.g. Hill et al., 1995c, 1996).

2.1 Rangelands

In the Mediterranean Basin, the majority of land surface can be considered as “ranges” or “rangelands”, which are defined as “...those areas of the world which by reason of physical limitations – low and erratic precipitation, rough topography, poor drainage, and/or cold temperatures – are unsuited to cultivation and which are a source of forage for free-roaming native and domestic animals, as well as a source of wood products, water and wildlife. They include grasslands, shrub-steppe, desert scrub, savannah, open woodlands, grazed forests, mountain meadows, riparian areas, wetlands and tundra. All areas of the world that are not barren deserts, farmed, or covered by bare soil, rock, ice, or concrete can be classified as

rangelands (Holechek et al., 1989)". This broad definition has a strong focus on parts of the world such as North America or Australia, where rangelands are large, homogeneous areas and water is often a limiting factor (Williams et al., 1968; Holechek et al., 1989).

In the Mediterranean Basin, the landscape structure is different from that. 'Rangelands' defined as non-arable, marginal lands are much more interwoven with cultivated areas, and there is a variety of highly heterogeneous ecosystems (Di Castri, 1981). Besides, we find completely different conditions of ownership. Following the small-structured character of the landscape, land is often also split into many small parcels.

'Rangelands' are not exclusively related to livestock use and production alone. Rather than a land use in itself, a range is a kind of land with many uses, including forage for domestic and wild animals, water supply, wood fuel supply, wildlife cover, and aesthetics. Most of the problems of rangelands result from these partly competing land uses and increase with population growth, increasing urbanisation, and interests in preservation (Heady & Child, 1994).

A major factor when comparing Mediterranean rangelands to those found in the Americas or Australia is their different history of land utilisation. While e.g. in North America the introduction of domestic grazing animals has taken place only relatively recently, Mediterranean landscapes show a history of utilisation by man that spans back over millennia (e.g. Gomez-Sal, 1998; Di Pasquale et al., 2004). Traditionally, they have often reached an equilibrium state with the demands and pressures exerted on them and traditionally represented an important resource for local populations. This equilibrium was often attained within a semi-natural environment, as man had already widely replaced Mediterranean forests with evergreen and sclerophyllous vegetation types following the Neolithic revolution (Di Pasquale et al., 2004).

2.2 Desertification and land degradation in the Mediterranean basin

As stated before, degradation processes may be the result of a combination of climatic background, ecological conditions and socio-economic determinants (e.g. Mulligan et al., 2004). A major change in one of the components may cause the system to depart from previous 'steady-state' equilibrium and start feedback loops. While natural conditions in the Mediterranean explain its general disposition to degradation, various authors stress that it is most frequently human interventions that initiate a degradation of resources (e.g. Hobbs et al., 1995; Blondel & Aronson, 1995; Gomez-Sal, 1998; Papanastasis & Kazaklis, 1998). There is a wide range of disciplines engaged in research on ecological conservation, optimisation of productivity and management/administrative interventions. It is out of the scope to provide an exhaustive overview of these different fields or completely reflect the ongoing debate related to degradation problems here. Rather, the interrelated factors and processes are sketched. Subsequently, the focus will be set on specific problems which will illustrate opportunities of a remote sensing based monitoring and assessment framework for Mediterranean rangelands under pressure (compare sections 2.3, 2.4, and 3).

In an attempt to develop a systematic approach, Perez-Trejo (1994) suggests to partition the desertification complex into three interlinked processes: physical, biologic and socio-eco-

nomic. Although he argues that degradation commonly results from multiple interacting driving forces, he differentiated the major complexes and their relations (Fig. 2.1).

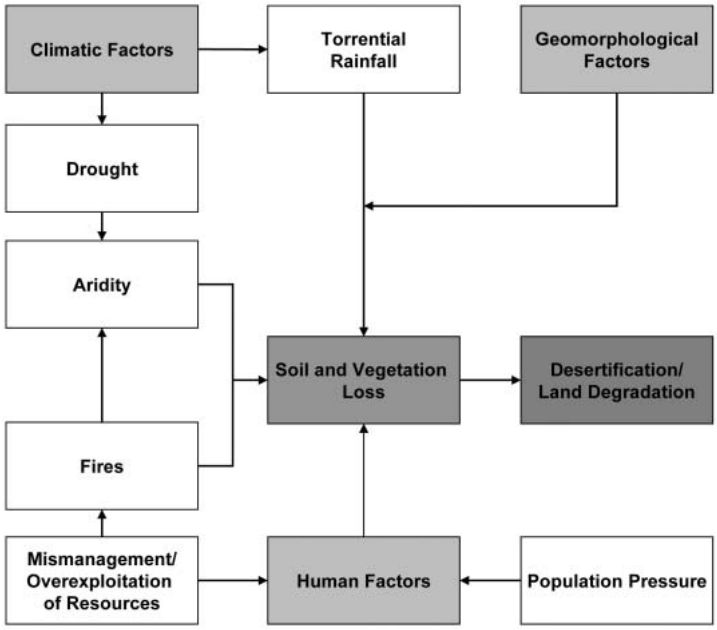

Fig. 2.1: Factors directly or indirectly affecting the desertification complex (Perez-Trejo, 1994, mod.)

Climate represents the background in front of which the other factors operate. Mediterranean climate is generally characterised by dry, warm to hot summers and mild, wet winters. Strong seasonal changes concerning the onset of rainy season may occur with corresponding implications for vegetation periods. In addition, excessive rainfall events may occur, which yield enormous amounts and intensities of precipitation. Finally, climatic conditions are locally modified according to elevation and aspect (e.g. Linés-Escardo, 1970; Rother, 1984; compare sections 4.1.1 and 4.2.1).

In the second major complex, the status of soils is depending on geological conditions, topography, vegetation cover, and the climatic regime. Accordingly, soils may show a generally higher or lower disposition to erosion, the risk of which is modified according to geomorphological properties and vegetation cover. Ultimately, precipitation amounts and intensities are the driving factors for linear and sheet erosion.

The soil-vegetation interaction is of major importance in the degradation system, and it has been extensively studied (e.g. Thornes, 1985; Francis & Thornes, 1990; Mulligan et al., 2004). Evidently, bare soil is most prone to erosion, which disrupts nutrients and organic matters in the topsoil by splash detachment and removes them. This may lead to rills and gullies or sheet erosion processes. Other processes include soil sealing through splash on bare soil, reducing infiltration and encouraging overland flow. Depending on the transport capacity this may again result in rill and gully erosion sparked by any hollow in the surface. As this processes increases gradients it can be considered a positive erosion feedback loop (e.g. Thornes, 1985). This process is theoretically limited by the amount of rainfall or exhaustion

of the surface once the bedrock surface is reached (Kirkby, 1980). In addition, bare soils that are deprived of their protective vegetation cover are frequently subject to soil surface crusting and salinisation, depending on climatic conditions (e.g. Thornes, 1990; Mainguet, 1994).

On the other hand, vegetation cover has shown to reduce these effects by stabilising the soil, slowing down overland flow, reducing splash impact, and preventing capillary rise effects in the soil (Francis & Thornes, 1990). However, it was also argued that the last effect depends on vegetation types and densities and additional weight was attributed to the protective function of the surface litter layer (Thornes, 1985). In addition, increased vegetation cover is associated with increases in evapotranspiration rates, which is an important factor for hydrological properties and local water balances (Boer, 1999). On the other hand, it was shown that on bare soils the invasion and succession of plants also leads to a positive feedback loop, as increasing cover increases shade, infiltration and ultimately soil moisture and nutrients from breakdown litter. With increasing competition among plants this process is limited by the maximum biomass to be attained under given ecological conditions (Thornes, 1985). As the rate of growth was shown to be reduced by erosion trough removal of nutrients and reduction in productivity a ‘competition between erosion and vegetation’ was stated (Thornes, 1985).

Mulligan et al. (2004) reinforce the role of climate in this context, as climate forcing determines the magnitude of erosion effects. With reference to the soil-vegetation interaction described previously, they describe a potential positive feedback loop that leads to self-sustaining, accelerated erosion that might even feed “…back to the climate with a degraded vegetation leading to increased surface albedo, reduced convection, reduced cloud formation, reduced rainfall and thus further vegetation degradation [through prolonged aridity]” (Mulligan et al., 2004). In addition, the more degraded a system is, the less it can act as a buffer for climatic extremes. These process complexes are subsumed in the conceptual model of soil-vegetation interaction depicted in Fig. 2.2. Given the driving function of the specific Mediterranean climate, it is evident that the whole system might dramatically change as a result of climate change. As the implications of different climate change scenarios on Mediterranean degradation processes are highly diverse and partially speculative, they are not further addressed here. An overview is for instance given by Jeftic et al. (1995, 1996).

Finally, water and hydrological properties form the last major complex to be considered, as the degradation of ecosystems is often accompanied by changes in groundwater level through changed infiltration rates, as well as reduced surface water quality (Perez-Trejo, 1994).

This is the natural background against which human interventions with the landscape unveil their dynamics. Although the Mediterranean basin has been strongly utilised for long periods of time, recently significant land-use transformations are obvious in many regions of the European Mediterranean. This may encompass both intensification and extensification of resource utilisation (Fig. 2.3).

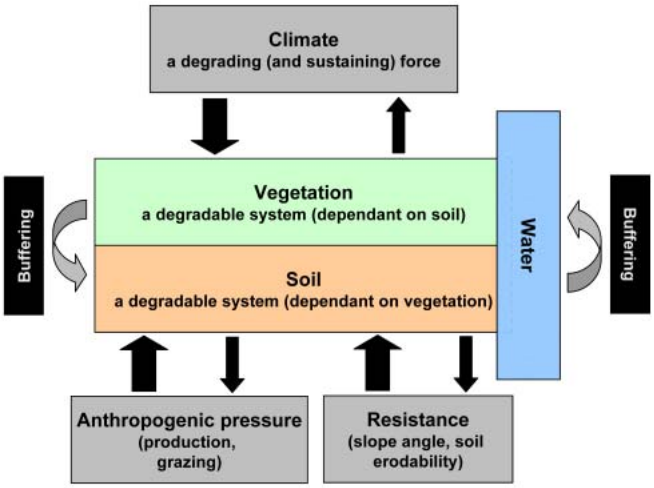

Fig. 2.2: Conceptual model of soil-vegetation interactions in the desertification system Mulligan et al., 2004)

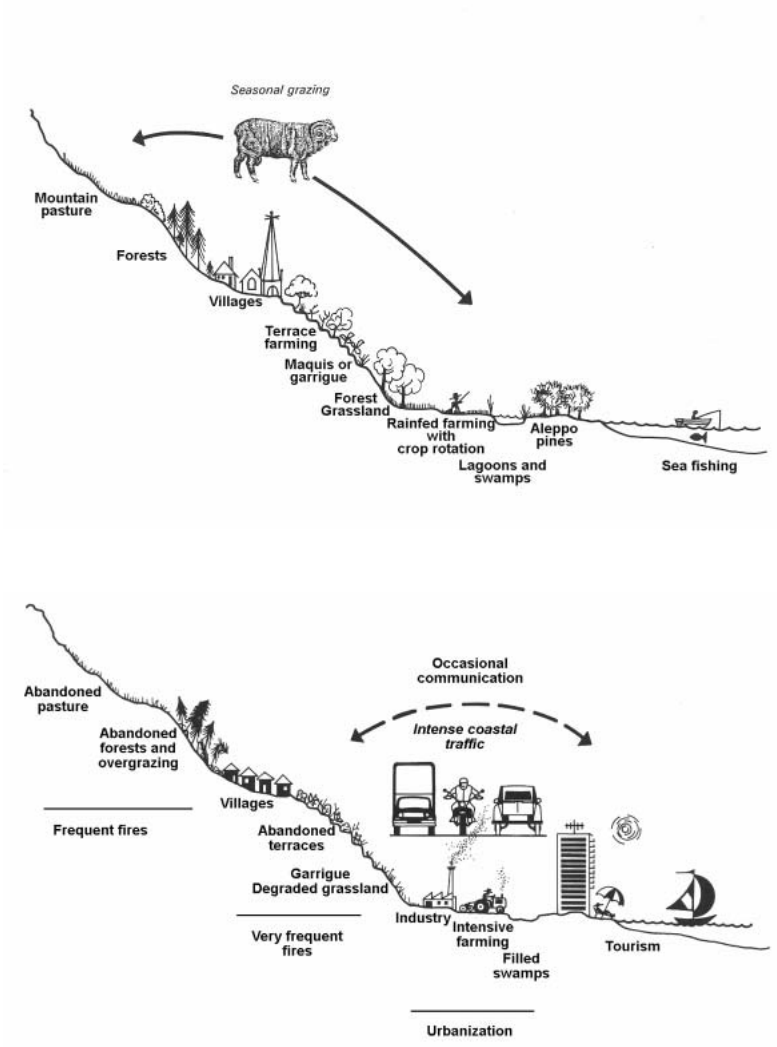

Fig. 2.3: Schematic illustration of changes in land-use patterns in the Mediterranean basin. Top: traditional land use systems in different elevation zones; bottom: recent land use system with intensification in coastal areas and abandonment and ecosystem degradation at higher altitudes (Hobbs et al., 1995).

Fig. 2.3 shows an example for changes in land-use patterns leading to landscape fragmentation and the widespread degeneration of landscape mosaics (Hobbs et al., 1995). In particular, it is evident how these transformations often occur in different directions of utilisation intensity depending on elevation zones. Etienne et al. (1998), Gomez-Sal (1998) or Papanastasis & Kazaklis (1998), among others, report on conflicts that often arise from competing demands on rangelands, for example between past and present uses following land use transitions or between ecological and economic priorities. For instance, policies to promote grazing sometimes provoked land degradation by overgrazing, fire prevention measures may be in conflict with ecosystem conservation, massive afforestation may negatively affect biodiversity, or even counteract fire prevention measures. Finally, land abandonment may result in shrub encroachment, increasing the risk of wildfires and reducing runoff and infiltration with significant consequences for groundwater tables and receiving water bodies (Etienne et al., 1998; Gomez-Sal, 1998; Papanastasis & Kazaklis, 1998; Noy-Meir, 1998).

With respect to human interventions, Perez-Trejo (1994) identifies major factors that contribute to accelerated soil erosion and resource degradation:

- Human exploitation exceeding the natural carrying capacity of the land resource
- Under-exploitation and abandonment of land due to population migration
- Increase in population and escalation of human needs
- Socio-political processes that put pressure on rural communities to orientate their production towards national and international markets
- Socio-economic processes that reduce the market value of rural products and cause the prices of rural people's needs to escalate
- Processes of national development, especially programmes for expansion of farmlands for production of cash crops, that exacerbate conflicts over land and water use and often reduce areas available to marginalized communities

Further to these, there are a number of factors that exert an indirect influence. The growing importance of tourism in the European Mediterranean has increased pressure on coastal environments, increased the demand for many rural goods while at the same time promoting rural abandonment through migration to urban/touristic centres with more attractive jobs. Further important aspects are changes in irrigation strategies or the introduction of cash-crops in large areas that may significantly affect ecological conditions by converting marginal lands into intensively utilised agricultural areas (Perez-Trejo, 1994).

Within this complex framework, two aspects emerge as important agents of land degradation: grazing and fire. While also directly related, they decisively affect vegetation cover, soil condition and are also of high relevance for questions of biodiversity. They can be considered being located at opposite ends of the temporal scale range of processes determining the shape of Mediterranean rangelands. While grazing is rather a long-term, gradual process, fire – although of relevance in the long-term as well – has spontaneous and direct consequences on the ecosystem. For this reason, the present study establishes a methodological framework to monitor the development of rangelands affected by these processes.

To base this framework on a sound understanding of relevant processes, the following sections provide a more detailed appraisal of the implications of fire (section 2.3) and grazing (section 2.4) in a Mediterranean context

2.3 Fire

Fire is an important factor in Mediterranean ecology, although its characteristics have changed considerably. Its occurrence is not exactly predictable and although it is an irregular disturbance in the short term, it may attain a regular character at longer observation scales.

2.3.1 Historical perspective

Various authors have stressed that Mediterranean rangelands in their present form are the result of thousands of years of human interventions and should hence be conceived as 'cultural landscapes' (e.g. Thirgood, 1981; Rackham & Moody, 1996). These interventions began with natural resource utilisation of the hunter-gatherer societies and reached a first culmination during Neolithic times when the landscape was converted to a mosaic of forests and agriculture. Fire was an important tool to open areas which had been forested before. The remaining woodlands were used as a source of fuel, timber and wood for buildings, weapons, and tools (Trabaud, 1981). The use of biomass has hence been termed '…the most important factor in the relationship between man and forest in the Mediterranean over the last eight millenia, from the Neolithic Age until the first half of the twentieth century' (Di Pasquale et al., 2004).

It is assumed that natural fires have influenced vegetation ever since the appearance of the first terrestrial plants and have hence become one of the most important evolutionary factors. According to Schüle (1990), evidence of fires dates back more than 1,500,000 years ago. The origin of the use of fire by man is assigned to the middle Paleolithic age, where it is assumed that fires were ignited to open the landscape to favour hunting and the spread of vegetation species used by humans and for livestock nutrition (Di Pasquale et al., 2004). Accordingly, fire was termed 'the most ancient technique for the management of vegetation' (Trabaud, 1981). Ever since, the high frequency of fires has played a major role in shaping the rangelands found today, where, together with other factors, they led to the establishment of plant succession patterns and semi-natural climax communities which are adapted to these disturbances (Trabaud, 1994).

Especially in the Northern Mediterranean, fires have been rated to be largely intentional and man-induced. Besides accidental ignition, main reasons include the creation of agricultural land, land for building, or the enhancement of grazing capacity. Concerning the latter, expected positive effects of fires are the opening of shrublands and forests, the removal of impalatable species, or the promotion of attractive fodder species, although doubts on such benefits have been expressed concerning long-term effects on pasture productivity (e.g. Holechek et al., 1989; Blondel & Aronson, 1995; Wagner, 2001). In general, an increasing tendency of fires has been reported for most European Mediterranean countries, only a part of which may be related to climate (Vázquez & Moreno, 1993; Moreno et al., 1998; Moreno, 1999).

It is accepted that in adapted communities, fire initiates an autosuccession process which ultimately leads to the same or similar plant communities as before, although relative abun-

dances of specific plants may vary. Accordingly, modifications of this process may only be expected if the frequency of fires exceeds or falls below the period required by plants for regeneration or maturation (e.g. Trabaud, 1994). Summarising, fire is a major force initiating succession cycles of vegetation in the Mediterranean basin. The long history and frequency of fires have resulted in fire-adapted (and –sustained) plant communities that differ from the potential natural vegetation, and are now conceived as 'steady-state' or 'pseudo-climax' communities (Blondel & Aronson, 1995).

2.3.2 Fire risk

In the Mediterranean basin, the hottest and driest seasons coincide, which is one of the main reasons for the generally high fire risk in summer. In addition, there is a high variability in precipitation and in exceptionally dry years the problem is further aggravated (Schultz, 2000). Different authors have linked the most devastating fire events in past years to prolonged, exceptionally dry periods in Spain and elsewhere in the Mediterranean (e.g. Millán et al., 1998; Moreno et al., 1998). Wood and leaves of the sclerophyllous species are characterised by high concentrations of etheric oils and resin which increases flammability and leads to highly explosive fire behaviour, especially in old communities with a high amount of dry biomass (Schultz, 2000). In recent years, it is agreed that in many areas the accumulation of dry and dead biomass is closely related to the common trend of abandonment of Mediterranean marginal lands (e.g. Naveh, 1994; Vallejo et al., 2004). This represents an important change in concepts, since, as a reaction to the appearance of degradation processes imposed by grazing, many countries have taken decisive measures to exclude livestock from many areas (e.g. Thirgood, 1981). Together with strong migration movements away from rural areas, this has led to what is now called 'under-utilisation' or, more specifically, 'undergrazing', leading to the noted accumulation of flammable biomass (Seligman & Perevolotsky, 1994).

Both the risk of fire ignition and patterns of fire propagation are essentially determined by composition and structure of plant communities. Different methodologies exist to classify these into fuel types (e.g. Rothermel, 1972; Anderson, 1982; Finney & Ryan, 1995; Van Wagtendonk, 1996). Common to all these approaches is the assignment of dense shrublands with high amounts of flammable dry or dead biomass to the high risk fuel types. This is aggravated by the fact that dead fuels respond quickly to changing meteorological conditions, increasing fire risk even at short drought periods (e.g. Viegas, 1998). Another important factor is the spatial configuration of the landscape, i.e. the pattern of fuels characterised by size, shape and their mutual arrangement. In this respect, it has been emphasised that the presence of a heterogeneous mosaic of different fuel types considerable reduces the connectivity of the landscape with respect to fire propagation (White & Pickett, 1985; Forman, 1995, 1996). This is strongly opposed to the homogeneous landscapes dominated by fire-prone fuel types, which frequently evolve after land abandonment. These are abundant in many Mediterranean regions, and have been reported to favour rapid fire expansion (e.g. Christensen, 1985; Wiens, 1995). There may, however, appear conditions where the landscape patchiness does not affect fire behaviour, especially in the case of crown fire at extremely dry conditions when vegetation moisture falls below certain thresholds (e.g. Turner, 1994).

Depending on the local dynamics of land use transformations, fire became a major concern for forest managers in Mediterranean countries in the second half of the last century (Moreno et al, 1998; Naveh, 1994; Pausas & Vallejo, 1999). Before the increasing frequency of wildfires, reforestation was conceived for watershed protection, dune fixation, and wood production, in addition to its role in promoting rural employment. More recently, strategies for fire prevention have been developed, including reforestation, reduction of competition for plants on recovering areas, mechanical clearing of flammable biomass, the creation of firebreaks and water tanks, or prescribed burning of high risk areas (Riggan et al., 1994; Naveh, 1994; Vallejo et al., 2004).

2.3.3 Plant resilience and post-fire dynamics

When assessing the effect of fire on plants and plant communities, two aspects need to be distinguished. One is the specific adaptation of plants to fires, such as the bark of *Quercus suber*, which efficiently protects these trees from fires of low to moderate intensity (Trabaud, 1994). On the other hand, in fire-affected ecosystems a wide variety of regeneration traits may be observed, which allows plants to recover after fires, which hence determines their resilience to fire (Keeley, 1986). By definition, resilience refers to 'the pace, manner, and degree of recovery of ecosystems following natural or human disturbance (Westman, 1978)'. With reference to plant adaptation to fires, traditionally four general types of 'pyrophytes' have been identified: 1) pyrophytes with passive resistance (constitution, high water content in tissues, e.g. *Quercus suber*); 2) vegetatively regenerating pyrophytes with the capability to sprout after destruction of the above-ground organs by epidermic shoots or below-ground resprouts (e.g. *Quercus coccifera*); 3) pyrophytes with an indirect resistance that creates an unfavourable environment for plants around them; 4) social pyrophytes that regenerate by seeds (e.g. *Pinus ssp.*) (Kuhnholtz-Lordat, 1958, after Trabaud, 1994). Keeley (1986) extended and differentiated this concept to the community level. As a first important group of plants, directly after fires 'there is a flush of deciduous suffrutescent and herbaceous plants arising from soil-stored seed or dormant bulbs or other underground parts' (Keeley, 1986). With the process of shrub cover gradually closing, this temporary component often returns to its pre-fire, dormant status. On a longer term, plant regeneration and development is either based on obligate resprouting, obligate seeding or facultative resprouters as an intermediate form (Keeley, 1986). Resprouting species rely on below- or above-ground vegetative parts, and frequently begin producing seed crops at an early resprouting age, which are adapted for long-distance dispersal via birds or wind (e.g. Whelan, 1995). These seeds are often sensitive to heat, such that, depending on the intensity and heat of fires, they may be destroyed (Mooney & Hobbs, 1986). On the other hand, in the case of long-term absence of fire, resprouting plants may gain dominance as they are able to rejuvenate from their base and are long-lived. Seeder plants rely on the production of seed banks which are stored either on the plant or in the ground (Quinn, 1994). Commonly, these species rarely have well-developed dispersal properties, while their seeds are very long-lived, and require a germination cue from fire, which may be triggered by heat or charred wood in the case of fire-annuals (Keeley, 1986). This reproduction trait makes plants extremely vulnerable in the time following germination but prior to seedling establishment. Comparing resilience to fire of plants surviving by resprouting or seed reproduction, a number of important differences can be noted, which

strongly relate to the frequency of fire cycles (Keeley, 1986). Resprouting plants quickly recover following fires, but they require long fire-free periods to develop seeds and expand their stands. Seeder species require longer time to recover, and, even more importantly, they require fire-free periods to reach sexual maturity and develop seed banks for post-fire reproduction. Once this level is reached, they may survive long fire-free periods depending on the viability of their seeds, but despite this their stands do not easily expand on account of their lack of dispersal properties. Owing to the variety of fire-adaptations, 'the resilience of plant communities to perturbations […can be considered] a function of the composite resiliences of the assemblage of different species populations in the community (Keeley, 1986)'. Beside the evolutionary effect of fires, other disturbances have operated simultaneously, such as grazing or cutting, which have contributed to shape today's Mediterranean landscapes (Trabaud, 1981).

On a general level, some aspects play a determining role on post-fire succession, such as the plant age (availability of viable buds or seeds), the season of burning (i.e. whether the plant is in its active or in its dormant state, determining the amount of mobilised resources destroyed by fire), and especially the post-disturbance environment (Mooney & Hobbs, 1986). Environmental conditions may differ significantly compared to pre-fire conditions. Although, in case they are not washed off, there may be an initial surplus in nutrients and minerals, a net loss has been reported on longer terms. Moreno (1999) found that at certain fire recurrence intervals to which ecosystems have adapted, initial losses in minerals and nutrients are balanced as plant cover develops, while a net loss is evident if these intervals increase. Top soil layers may be sterilised as a result of the impact of high fire temperatures on the microfauna, and both decreases in cation exchange and soil-water holding capacity have been reported (Christensen, 1994). Besides, soil surfaces may become less permeable by water, adding to the increased surface runoff due to the lack of protective vegetation. Finally, the removal of the vegetation layers leads to a modification of the local radiation budget (Mooney & Hobbs, 1986). In addition, herbivores prefer regenerating to mature plants, such that the presence of seedlings in relations to herbivores determines whether this disturbance initiates a major change in plant communities in comparison to the pre-fire state (Quinn, 1986).

Concluding, the maintenance of plant communities adapted to fire in a patchwork landscape relies on the existence of a disturbance regime that is 'unpredictable in time and space in the short term, but predictable in the long term (Blondel & Aronson, 1995)'. The identification of fire recurrence cycles and plant dynamics on a landscape scale are important factors that need to be considered in a remote sensing based monitoring framework.

2.3.4 Fire as an agent of degradation

Fire is an important ecological factor and most of today's 'pseudo-climax' plant communities in fire-prone Mediterranean areas are adapted to this disturbance. Trabaud (1981) concluded that '…there is no clear evidence of fire as an agent of desertification. Without the action of man, fire is only an agent of disturbance interrupting the long term succession.' Especially the *Pinus ssp*. widely abundant in many fire-affected ecosystems are well-adapted to fire, provided fire recurrence cycles are not too frequent to impede reproduction through seed production (e.g. Agee, 1998). This being undisputed, Moreno (1999) argued that fire is still an im-

portant factor in the context of resource degradation, since due to the interventions of man in the last decades, fire cycles depart from the pattern to which ecosystems had adapted. A further increase in fire frequency as a result of climate change scenarios has been discussed, which may be triggered by generally increased temperatures and decreased rainfall amounts (Moreno & Oechl, 1994).

Summarising, depending on its recurrence, fire contributes to the deterioration of natural resources through a number of possible implications:

- Threat to human welfare through fires and associated costs for fire-fighting
- Economic loss of timber and biomass used as burning fuel, fodder,…
- Long-term loss in net primary productivity
- Loss of recreational areas
- Destruction of animals and their habitats
- Threat to fire-adapted species on account of increased fire recurrence rates
- Soil sealing
- Deprivation of the soil from the protective vegetation cover, increased susceptibility to erosion from wind and water or disturbance through animal tramping
- Reduction in soil fertility through long-term loss in nutrients and minerals, sterilisation of top soil layers, changed hydrological properties, destruction of soil fauna and flora…

(e.g. Specht, 1981; Brown, 1990; Christensen, 1994; Naveh, 1994; Vallejo & Alloza, 1998; Moreno, 1999; Vallejo et al., 2004)

2.4 Grazing

Despite the long history of grazing, its character has repeatedly changed through the times. Different grazing schemes effectuate different impacts, hence an understanding of grazing-related processes and their consequences for land degradation are vital in the formalisation of monitoring and interpretation approaches.

2.4.1 Historical perspective

Beside cutting and fire, grazing is the major factor responsible for the shape of Mediterranean landscapes. Especially in the last 10,000 years, grazing has probably been the main factor contributing to the degradation and the loss of many forest features of the Mediterranean (e.g. Thirgood, 1981; Di Pasquale et al., 2004). According to Le Houérou (1981), the breeding of sheep and goats began in the eastern Mediterranean between 12,000 and 8,000 B.P., that of cattle somewhat later (8,500 to 7,000 B.P.). About 6,000 years ago, during the Neolithic period, peoples were already acquainted with cereal agriculture and extensive grazing by small ruminants, but still depended mainly on hunting. About 2,000 B.C. the climate became more arid and game became less plentiful. At that time, sheep and goats became established as the main grazing livestock which is proved by findings in kitchen middens, and evidence of

transhumance exists for many regions of today's Mediterranean Europe dating back to these times. Ever since, periods of intense degradation changed with periods of stability and regeneration. Often, these were coupled with demographic developments as a result of political situations, economic prosperity, wars, famines etc, which frequently even resulted in cultures shifting from nomadic to sedentary systems and back. (Le Houérou, 1981)

During the 19th and at the beginning of the 20th century, vegetation was severely damaged as a result of rapidly growing human populations, mechanisation of farming, extension of fires, use of herbicides and overgrazing (Blondel & Aronson, 1995). More specifically, this effectuated the replacement of forests by shrublands, the spread of evergreen plants at the expense of deciduous trees and changes in plant and animal communities (Blondel & Aronson, 1995). Together with agro-pastoral activities, a closely interwoven semi-natural landscape developed, representing a man-maintained equilibrium (Naveh, 1988).

In the developed countries of the Northern Mediterranean, the following period was determined by two major factors. A rapid growth of income per inhabitant and a slight rate of demographic growth led to the shrinking of animal numbers and land abandonment in many poorer regions (Le Houérou, 1981). In addition, livestock animals were held responsible for damages to Mediterranean ecosystems resulting from intensified grazing, such that decisive measures against sheep and mostly goats were effectuated (Papanastasis, 1998). This led to the exclusion of livestock animals from many regions, especially forests.

In the last decades, the political and socio-economic framework has largely changed as a result of the accession of Mediterranean countries to the European Communities (e.g. 1981 in Greece). Most of these countries have been net receivers of funds ever since and have consequently benefited from numerous funding schemes. Especially in least favourite areas, instruments such as the European Regional Development Fund (ERDF), the European Social Fund (ESF) or the European Agricultural Guidance and Guarantee Fund (EAGGF) have strongly affected and altered rural infrastructure and economies. Most importantly, the Common Agricultural and Rural Policy (CAP) has made livestock grazing profitable again, leading to re-increasing animal numbers in wide parts through per-capita subsidies (Dubost, 1998). Despite rising animal numbers, this partial reactivation of rural economies did not coincide with returning to traditional practices everywhere. Rather, sedentary systems were frequently installed (Legg, 1998). Today, high to very high stocking rates are frequently observed, where large flocks are sustained by the provision of additional feedstuffs, provision of water at the shelters and by returning animals to the sheds in the evenings or even during the day at the hottest midday hours (Oba et al., 2000; Yiakoulaki, 2002). In addition, the network of roads and tracks has increased in many Northern Mediterranean countries sparked by European supporting funds, enhancing the accessibility of formerly remote areas. In many regions, shepherds take benefit of this to transport their flocks to different pastoral areas.

2.4.2 Grazing impact

When livestock arrived in the Mediterranean, they did not enter a grazing-free environment, but replaced the existing wild herbivores to a large extent. For this reason, plant communities had already developed a large range of defensive mechanisms against grazing (Noy-Meir, 1998). According to Quinn (1986), one can distinguish two general traits: tolerance and de-

fence. The latter includes spininess (*Sarcopoterium spinosum*), chemical repulsion (for instance through ethereal oils, aromatic plants), prostrate form (*Polygonum idaeum*), high regeneration capacity (*Acer creticum*), isolated distribution in cliffs or growth in protected niches less accessible to animals (e.g. herbs under phrygana or in rocky outcrops) (Margaris, 1981; Quinn, 1986; Papanstasis, 1998; Noy-Meir, 1998). Grazing affects plants and plant communities in various ways. Most obviously, plant function is immediately disrupted by grazing in response to the reduction in photosynthetic leaf area (Briske & Noy-Meir, 1998). On the other hand, there are environmental modifications for surviving plants, which include reduced competition, increased photosynthetic irradiance, or the opening of gaps (Briske & Noy-Meir, 1998). Changes imposed by grazing relate to morphological and functional types of plants and to species composition. In grasslands, these frequently encompass shifts from perennial to annual species, from plants with large seeds to those with many small seeds, from space-monopolizers to colonizers, and palatable to less palatable species with chemical or physical defences. In general, with increased grazing intensity three selection factors become important: the ability to avoid being grazed, the ability to regrow after defoliation and the ability to colonise open space. Strong grazing frequently results in plant communities dominated by species adapted to at least one of these (Noy-Meir, 1998). In grazing areas dominated by evergreen woody species, a wide range of plant compositions constituting the ‘matorrals’ may be noted. These are frequently considered degradation stages of the ‘natural’ vegetation present before human intervention. Extensive treatise of such development traits in different ecosystems and under varying utilisation schemes are found for instance in Le Houéourou (1981), Aronson & Blondel (1995), Tsiourlis et al., (1998), Quézel (2004) or Di Pasquale et al. (2004). Common to all of these is the decrease in biomass of both woody and herbaceous components proportional to grazing intensity. This is often reflected by decreasing rates of primary productivity and hence one important element in the context of land degradation in Mediterranean rangelands (Holechek et al., 1989; Papanastasis, 1998). The effect of strong grazing on plant specimen is illustrated in Fig. 2.5. In addition, plant communities may experience an increase in the relative abundance of grazing-resistant or –tolerable species (Le Houérou, 1981). Given the long history of grazing in the Lagadas area, shrublands and grasslands are believed to represent the local manifestations of grazing-determined plant communities (compare sections 4.2.5 and 4.2.6).

The majority of woody species are grazed by livestock in varying degrees. Given the availability of both woody and herbaceous vegetation, sheep act as feeders and prefer the latter. On the other hand, goats act as browsers and are particularly suited to forage on woody plants. Beside their ability to thrive on woody plants alone, the agility of goats (Fig. 2.4), their extreme resistance to thirst and their ‘intelligence’ in seeking food makes them perfectly adapted even to degraded environments (Le Houérou, 1981; Legg et al., 1998; Nastis, 1998).

Fig. 2.4: Goat grazing on steep and rocky slope (left) and in *Quercus* tree (right)

Among species completely ignored by livestock animals are most gymnosperms (especially *Abies, Cedrus, Cupressus, Pinus, Taxus*), many Apiaceae and Asteraceae, almost all Liliaceae, many Fabaceae (e.g. *Genista, Ononis*), many Brassicaceae and the Euphorbiacea (Le Houérou, 1981). Generally, "[…] a plant species is the more eaten, the more growing organs it has: young shoots, buds, seedlings, and sometimes flowers". Especially goats prefer young shoots and seedlings, which may prevent regeneration of disturbed vegetation (e.g. Quinn, 1986; Briske & Noy-Meir, 1998).

The impact of grazing is not limited to modifications of the plant composition. Overgrazing triggers the reduction of vegetation cover, thus increasing the risk of soil erosion (e.g. Thornes, 1990; Pickup & Chewings, 1994). This is often aggravated by the creation of trails through repeated passage of animals, which may act as starting features for linear erosion. The compaction of soil through trampling may in turn decrease infiltration rates (e.g. Perez-Trejo, 1994; Rhoades et al., 1964; Thornes, 1985; White, 1987). The loss of stratum causes different negative effects, such as reduced water availability for plants, reduced fertility and a change in soil texture (Le Houérou, 1981; Thrash, 1997). The above described effects are amplified by topography gradients. Positively, the nutrition content of the soil may be affected by dung of domestic animals (Thrash & Derry 1999).

Especially strong effects occur if grazing and fire coincide, for instance where shepherds apply prescribed burning to improve pastoral quality. Although an increase in short-term pastoral value may be attained as grasses and herbs are abundant in the first year after fires, an effective regeneration of vegetation is usually prevented by browsing of young seedlings (Le Houérou, 1981). If fires are frequent, pyrophilous plant species are favoured and will successfully compete for resources. This in turn must be seen as a form of land degradation, as pyrophilous vegetation is potentially less productive than non-pyrophilous vegetation (Fox & Fox, 1986; compare section 2.3).

2.4.3 Grazing management in rangelands

As outlined before (section 2.4.1), livestock grazing was blamed for a lot of negative effects on ecosystems some decades ago, and restrictive policies were introduced in many areas. It is agreed that grazing at intensities exceeding the local carrying capacity may cause sever damage to natural resources, with all consequences identified in section 2.4.2. On the other hand, with the introduction of the term 'cultural landscapes' (e.g. Thirgood, 1981), it was recog-

nised that the appearance of today's rangelands in the Mediterranean is owed to their utilisation history. Zervas (1998) states that gradual degradation of mountainous and hilly grassland and shrubland areas has taken place not only due to overgrazing and livestock concentration, but also because of undergrazing of certain areas. The extensification or total abandonment of less accessible rangelands leads to an increase in combustible biomass, a higher temperature within stands in the summer and increased fire risk (Briske & Noy-Meir, 1998). This is added to by considerations of the aesthetical value of rangelands in there present form, which is threatened by the encroachment of shrubs where no utilisation is present (Briske & Noy-Meir, 1989).

Complemented by evidence supplied by different authors, the attitude towards livestock animals has changed in the last years, and it was acknowledged that – properly managed – grazing animals may represent an important element in the maintenance of rangelands (Seligman & Perevolotsky, 1992; Papanastasis, 1998). It is obvious that stocking rates should not exceed the carrying capacity to avoid the negative implications described before (section 2.4.2). On the other hand, undergrazing may lead to equally negative effects regarding the encroachment of shrubs with an associated risk of fires, modifications of hydrological systems or the disappearance of grazing-adapted species (e.g. Noy-Meir, 1998). If the focus is moved from cover as such to biodiversity, numerous studies show that appropriate levels of grazing help to maintain the highest diversity. Noy-Meir (1998) reports on different investigations in Spain, all yielding highest biodiversity at moderate grazing rates. Tsiouvaras et al. (1998) showed the same tendency in a fencing experiment in Northern Greece. Quinn (1986) investigated the result of grazing in different environments and at systems traditionally grazed or ungrazed. For two replicates in a traditionally grazed Mediterranean area in Southern France, he analysed plots of two different grazing intensities and a control plot where grazing was excluded. The result were consistently higher diversity values with increasing grazing intensities, while the ungrazed test plots showed a significance decrease in diversity. These results are also in accordance with Milchunas et al. (1988), who developed a model predicting species richness in grazed sub-humid grasslands.

Noy-Meir (1998) argues that conservation of the full biodiversity of Mediterranean flora (and fauna) has a considerable economic value beyond its scientific, aesthtetic and ethical value. This is mostly due to the richness in species bears high genetic potential for breeding and to the touristic potential resulting from populations of geophytes and annuals in winter and spring. As plant communities are now considered to be dependent on appropriate utilisation, "[…] continuation of livestock grazing and production is not only compatible with conservation, but is actually a necessary component of a conservation strategy" (Noy-Meir, 1998). This was recently confirmed by Rowntree et al. (2004) who assessed the result of varying grazing intensities on soil erosion and concluded that grazing intensities need not necessarily translate directly into soil erosion rates. Seligman & Perevolotsky (1992) state that "[…] whilst a herder will regard rangeland as forage for his livestock – and an oak grazed down to a dense dwarf shrub is simply a well exploited forage plant – a forester or environmentalist will regard the domestic ruminant as a pest that threatens the forests or restricts the proper development of woody vegetation" (Fig. 2.5, further illustrations in sections 4.2.6 and 10.3).

Fig. 2.5: Effects of grazing at different intensities on *Quercus coccifera* shrubs: *Quercus* shrub grazed down to ground level (left); umbrella shape after parts of the shrub have grown outside of reach of animals (right)

It must be concluded that the assessment of land degradation and the impact of grazing must be based on a proper definition of the range management goals (Narjisse, 1998). Corresponding to the multi-functional character of Mediterranean rangelands, these might be dominated by enhancing productivity and pastoral value, conserving biodiversity, watershed protection, erosion prevention, recreative purposes etc. Noy-Meir (1989) concludes that an optimum management strategy for Mediterranean rangelands should provide for the diversification of grazing intensity over the landscape. Accordingly, each edaphic-climatic region should have zones of different grazing pressures, ranging from heavy pressure to complete protection in areas less accessible for grazing. This changed attitude is also reflected in European Union policies along with the call for sustainability. Manifested in the Common Agricultural Policy (CAP) directives, grazing is now facilitated in less favoured areas. Subsidiary payments in order to support these areas are being distributed based on per livestock unit (Dubost, 1998). The latest reform of the CAP further emphasised the importance of rural development (CAP 2003).

In order to proceed to concrete management scenarios and recommendations, a large number of studies and assessment models exist (e.g. Westoby et al., 1989; Walker, 1993). For instance, the ‘state-and-transition’ model proposed by Westoby et al. (1989) allows to define specific desired ecological states and plant communities, while the management actions needed to be applied to move from one community to another represent the transitions or thresholds. This approach may be further extended by introducing the term ‘rangeland health’, and assign thresholds indicating when an ecosystem is at the risk of irreversibly shifting to an unhealthy state.

In the previous section the diverse interactions between livestock animals with rangeland environments were outlined and discussed. The monitoring framework to be developed needs to adequately consider these, and allow for the characterisation of long-term trends in a spatially differentiated manner, as in heterogeneous areas no uniform impact of grazing can be expected.

3 Remote sensing based monitoring of rangelands – conceptual considerations

Remote sensing data are of considerable value in the context of monitoring environmental processes. With the history of operational earth observation sensors spanning back over three decades they allow to retrospectively analyse the state and development of ecosystems on different scales and with different spatial coverage (Kramer, 2002). Remote sensing data adhere to the principles of repetitiveness, objectivity and consistency, which are prerequisites in the frame of monitoring and surveillance (e.g. Graetz, 1996; Schott, 1997; Hill et al., 2004). In order to unfold their full potential, standardised approaches and interpretation schemes are required. Based on these, the integration and harmonisation of approaches in the frame of 'ecosystem observatories' based on earth observation satellite data and additional information has been suggested, with the goal of serving requirements of policy-making, planning and land management (e.g. Dubost, 1998; van der Leeuw, 2000; Hill et al., 1995c, 1996). Local scale observatories could be an important element complementing small scale observation and early warning systems, which are currently being implemented in different thematic contexts, such as the UNCCD regional Annexes (UNCCD, 1994). These could be used, for example, in the analysis of hot spot areas that are identified through small-scale approaches. This study aims at identifying key requirements of a remote sensing and geoinformation based framework for monitoring and assessing the state of rangelands.

3.1 Sensor systems and the question of scale

Environmentally relevant processes operate at largely different spatial and temporal scales, and the area to which they extend may considerably differ depending on the landscape structure (Turner et al., 2001). For instance, a vegetated patch may appear homogeneous at a coarser scale, while with increasing scale resolution a more and more differentiated matrix of plant composition emerges (Wiens, 1995). The question of perspective and scale needs to be considered in the design of any observation scheme, as different requirements necessitate different investigation scales (Turner et al., 2001). This is particularly true for disturbance processes whose return interval, size and spatial variation have direct implications for the selection of spatial and temporal scales as well as areal extension (White & Pickett, 1985). Hence, there may be a considerable difference in scales relevant to land managers landscape ecologists, botanists, etc. (Turner et al., 2001).

Addressing the selection of adequate remote sensing sensor systems for questions of rangeland monitoring, these concepts translate directly into specific characteristics of sensor systems and platforms, such as geometric resolution, spatial coverage, repetition rate and history of data acquisition. These need to be selected depending on target processes and areas, and on the type of information product desired, which is in turn dependent on potential end users. In addition, these systems are equipped with a largely varying number of spectral bands determining their information content (e.g. Hill et al., 2004). Fig. 3.1 illustrates this for a selection of sensors.

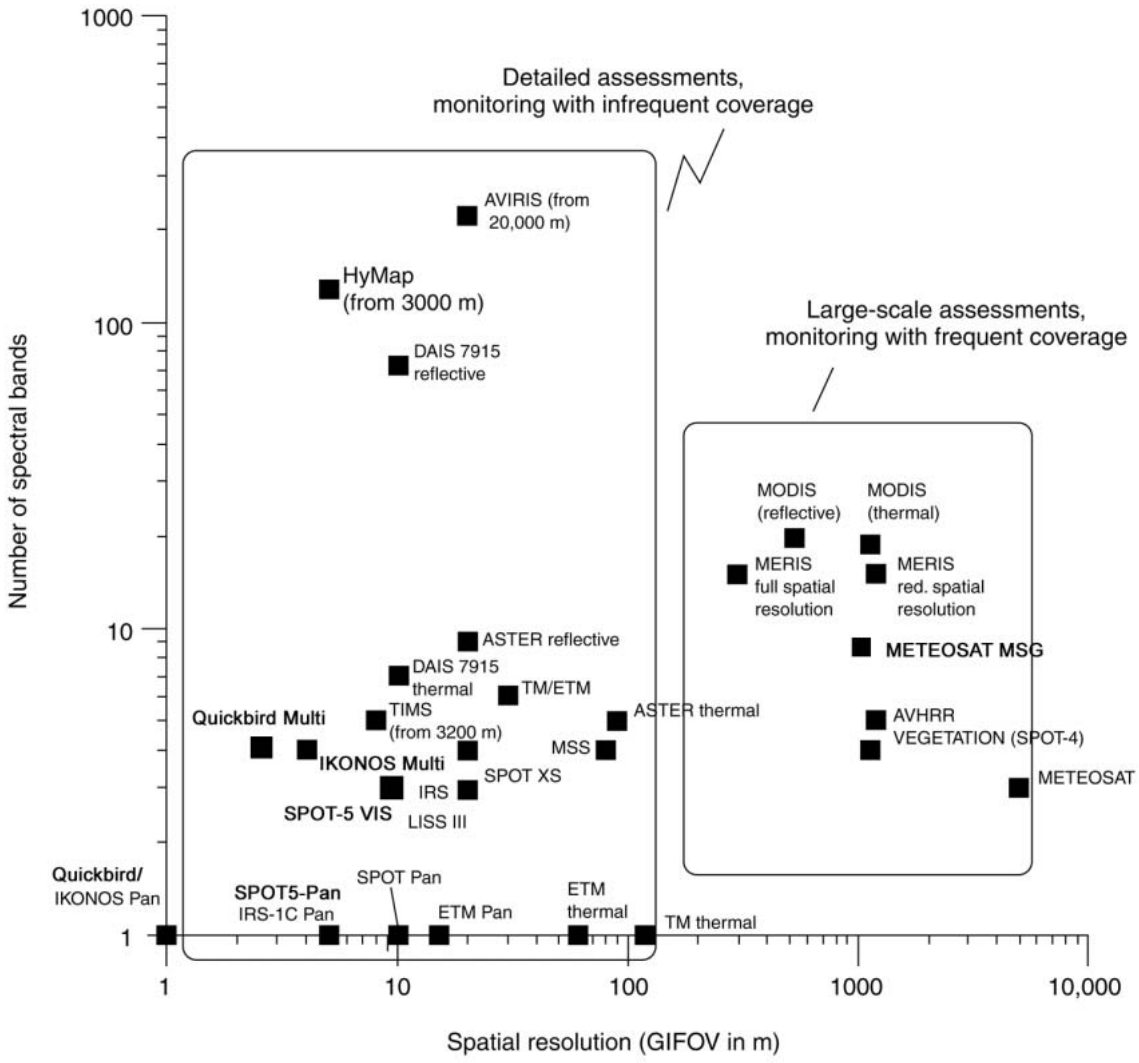

Fig. 3.1: Spatial and temporal coverage of selected sensor systems (Hill et al., 2004, mod.)

A lot of these sensors do not fulfil the criteria of routine availability or the time span covered is not sufficient. For instance, hyperspectral sensors (e.g. HyMap, AVIRIS, DAIS) are experimental airborne sensors. Equipped with excellent spectral capabilities and a high geometric resolution (depending on flight elevation), they are only available on demand and cover relatively small areas. Data from very high resolution (VHR) satellite sensors, such as QuickBird or IKONOS, may be generally acquired upon request at regular intervals, but these have only been available since 1999 and 2001, respectively. Furthermore, as of the time or writing, these data are very costly. It becomes clear that while certain systems offer very high temporal repetition rates and cover large areas, such as quasi-geostationary meteorological satellite systems (e.g. METEOSAT) or the NOAA-AVHRR and SPOT-Vegetation systems, this is achieved at the expense of a lower of spectral resolution. On the other hand, systems which provide adequate spatial and spectral resolution show lower repetition rates (e.g. Landsat, Spot), which makes possible influences by cloud cover a more severe issue to be considered. Although there have been considerable innovations in sensor design with increased spectral (e.g. MODIS, ASTER on the Terra platform; Hyperion on EO-1, MERIS on the

Envisat platform) or geometric resolution (e.g. IKONOS, QuickBird), these data can at present only complement more extensive data bases.

Strategies aiming at supporting policy-makers at trans-national levels often require data covering large areas while accepting a higher degree of spatial generalisation as provided for instance by NOAA-AVHRR or MODIS data. On the other hand, characterising spatio-temporal developments of natural resources relevant to land managers and local planning authorities suggests employing regional to local scale data (Tueller, 1995). Appraising these facts, the Landsat sensor system appears most suited as it provides an appropriate compromise between spatial detail, spatial coverage and spectral resolution. The Multi-Spectral Scanner (MSS) was launched on ERTS-1/Landsat-1 as early as 1972 and it was followed by two successor systems. In 1982, the Landsat-4 platform was launched carrying both the MSS and Thematic Mapper (TM) sensors. With the launch of Landsat-5 in 1984, this new system fully replaced the MSS, although the latter was still part of the payload and continued to acquire information. In 1999, Landsat-7 was placed in orbit carrying the Enhanced Thematic Mapper sensor (ETM+). Starting with the launch of Landsat-4, the platform operates in a polar orbit at 705 km of altitude, and covers an area of 185*185 km with 7 spectral bands and a geometric resolution of 30*30 m for the bands in the reflective wavelength domain (thermal infrared: 120 m) at a repetition rate of 16 days[1]. Landsat data have been successfully employed in the frame of different multi-temporal studies (compare sections 3.4.2 and 3.4.3), the performance of the Landsat sensor systems have been widely documented (e.g. Royer et al., 1987; Markham & Barker, 1987; Mika, 1997; Goward et al., 2001; Masek et al., 2001). At present, the future of the Landsat sensor family remains unclear. Alternative systems with similar capabilities and temporal coverage are ASTER (Terra platform) or ALI (EO-1 platform).

3.2 Standardisation requirements

Satellite imagery exhibits a number of unique properties, which result from the technical process of recording images of a part of the Earth's surface in combination with characteristics of the sensor and the satellite platform. This denies a direct comparison of images from different dates, although this is a mandatory component of a surveillance system. The following section provides a brief reference to the most important image properties while adopted processing strategies and corrections are described in chapters 5 and 6.

3.2.1 Geometry

The interplay between satellite platform, sensor and the Earth surface results in geometric distortions that prevent a direct integration with other spatial data bases.

As a result of the opto-mechanical image acquisition of the Landsat sensors and the rotation of the Earth, different sources of error emerge, which are accounted for by the system correction applied to Landsat-MSS and -TM data prior to delivery (Richards & Jia, 1999; USGS, 1984; http://ltpwww.gsfc.nasa.gov). In addition to these systematic or system-inherent errors, images acquired with opto-mechanical scanners show a typical cartographic representation of

[1] Landsat-7 ETM+ additionally provides one panchromatic channel at 15m resolution, and a thermal infrared band with 60m resolution.

the Earth's surface, with a parallel projection in along-track and a central projection in across-track viewing direction. It is the latter that significantly influences cartographic comparability, with the magnitude of distortion depending on the distance of the pixel from the satellite nadir and the elevation of the surface element. Consequently, especially in terrain with a strong relief gradient, it is crucial to adequately account for this terrain-induced distortion to ensure the consistency of satellite images with each other, as well as with other sources of spatial information (Welch et al., 1985; Itten et al., 1992; Pala & Pons, 1995).

Finally, combining the resulting data set with additional information layers and producing maps requires transferring this planar space-oblique mercator projection into a pre-defined reference cartographic projection system (Lillesand & Kiefer, 2000). The type of reference system depends largely on the geometric resolution of data employed, the scale to be addressed by the analysis, and the spatial extension of target areas. For local to regional scale applications (1:250,000 or larger) and target areas in mid-latitudes, the UTM system is widely used. In addition, there is a range of locally adapted spheroids and datums, such that the UTM system can be well adapted to different areas. In areas at very high latitudes, other ortho-projected references systems with more narrow zones may be more convenient. For instance, in Argentina a modified version of the German Gauss-Krueger system is widely used (e.g. Bonham-Carter, 1994).

3.2.2 Radiometry

Early multi-temporal image analyses have often been confined to a comparison of classification results from different periods (e.g. Price 1987a). For these cases, radiometric processing may be neglectable or simple correction approaches may be sufficient (Song et al., 2001). However, with the development of quantitative analysis techniques, changes becoming apparent from multi-temporal analyses should only result from intrinsic surface properties, while stable areas show near-to-identical spectral signatures (e.g., Hall et al., 1991; Vogelmann et al., 2001). The signal at the sensor is a result of solar irradiance received at the ground, which interacts with surface elements, and a part of which is reflected back towards the sensor. However, the direct interpretation of multi-temporal data sets based on spectral properties of these surface elements is impeded by radiometric properties of satellite images, which can be summarised under two major components.

- Sensor calibration: Incoming radiance is converted to a digital signal, which can be described by a calibration function. The further radiometric processing of satellite images requires physically meaningful values; hence it is necessary to calibrate the digital numbers in satellite images to radiance values. Since the sensitivity of detectors is known to decay with sensor age, the same incoming radiance signal will not result in the same radiance value for different dates, and the corresponding error can be expected to propagate through the subsequent processing and interpretation chain (e.g. Teillet et al., 1997; Thome et al., 1997a). Calibration procedures are further complicated when different sensor systems need to be integrated within one multi-temporal data base. This poses a severe problem in establishing a multi-temporal data base for surveillance purposes.

- Atmosphere- and topography-induced distortions: The signal recorded at the sensor is a result of solar radiance propagating through the Earth's atmosphere, interacting with the surface, and being partially reflected back through the atmosphere towards the sensor. Besides surface properties, which are the target information required, there are a number of factors affecting this signal. These comprise
    - the distance between Earth and Sun,
    - geometric viewing constellation between sun, sensor and earth surface, including the slope and orientation of the surface,
    - the constitution of the atmosphere, as characterised by gaseous and aeorosol components and their concentration. (e.g. Tanré et al., 1990; Schott, 1997).

In order to meet the criteria for a general monitoring framework formulated before, it is mandatory to remove these influences of topography, illumination, shadows, viewing directions and atmospheric properties to attain physical quantities (i.e. surface reflectance) that can then be considered to be primary indicators for further interpretation, (e.g. Schott, 1997; Du et al., 2002). As a consequence, in terms of radiometric standardisation, a monitoring framework needs to incorporate three general components:

- a sensor component
- an atmosphere component
- a topography component

3.3 Indicators

Different authors have described criteria to assist in an objective identification of land degradation or conditions that favour it. Physical factors include for instance:

- Reduced vegetation cover (frequently accompanied by increasing dominance of annual over perennial plants) and increased soil exposure
- Increased rate of movement of soil particles and corresponding change in the soil-bedrock relation
- Increased soil compaction
- Reduced rate of litter accumulation
- Ingress of light-demanding invasive plants
- Change in the phenology of the vegetation
- Increased frequency of fires
- Increase in the woody (resprouting) element of vegetation

(Groves, 1998; Perez-Trejo, 1994)

With the growing importance of aspects of environmental quality or sustainability in planning and policy-making, there is a growing need for the definition of generally accepted indicators

and benchmarks. The European Environmental Agency (EEA) has defined the 'Driving Forces–Pressures-States-Impacts and Responses' model (DPSIR) to offer a basis for analysing the inter-related factors that impact on the environment (http://org.eea.eu.int/documents/brochure/brochure_reason.html). Despite this and other initiatives (e.g. OECD, 2001; Klug et al., 2003), indicators remain widely scattered. Remote sensing and other spatial data have been identified as one major source of information for indicator development (e.g. Kosmas et al., 1999; UNEP, 2003) The proposed indicators often make use of spectral properties (e.g. Huete et al., 1985; Baret & Guyot, 1991), object shapes or object patterns (e.g. Blaschke & Hay, 2001) or landscape metrics (e.g. Frohn, 1997; McGarigal, 2002). A number of research projects have been specifically targeted towards formulating remote sensing and GIS based indicators in different fields, such as SPIN (Spatial Indicators for European Nature Conservation, http://www.spin-project.org) or EON2000+ (Earth Observation for Natura 2000, http://www.eon2000+.org). Very recently, the Desertlinks initiative (Combatting Desertification in Mediterranean Europe, Linking Science with Local Stakeholders, http://www.kcl.ac.uk/desertlinks) has developed a 'Desertification Indicator System for Mediterranean Europe' (DISforME), which includes physical and ecological, economic, social and institutional indicators.

It has to be noted that no indicator of degradation directly inferable from earth observation data exists. Rather, suitable indirect indicators need to be defined, which can be related to processes of erosion, degradation, increase of flammable biomass etc. (Verstraete, 1994b). In fact, soil and vegetation properties are tangible items which can be assessed using remote sensing approaches (e.g. Lacaze et al., 1996). Secondly, land degradation essentially operates in the time dimension. Correspondingly, indicators need to be derived for a sequence of time steps as proposed within this surveillance framework (Graetz, 1996). This in turn makes it mandatory that the chosen indicator can be calculated in a standardised and straightforward manner once it is established.

Among different potential indicators, UNEP (2003) as well as the DISforME framework suggest 'vegetation cover' as an indicator of ecological condition. Vegetation cover can be defined as "…the percentage of soil, which is covered by green vegetation as seen in a vertical view from top, corresponding to the single layered projection of green foliage cover. [It is also] known under the term projected foliage cover (PFC), [and is…] closely related to leaf area index (LAI)" (DISforME).

Proportional vegetation cover is closely related to above-ground biomass (e.g. Tsiourlis, 1998; Chiarucci et al., 1999; Röder et al., 2003) and as such an indicator for the productivity of an ecosystem. Many authors demonstrated that in a wide range of environments, both run-off and sediment loss decrease exponentially as the percentage of vegetation cover increases (e.g. Francis & Thornes, 1990). For instance, DISforME identifies a value of 30 to 40 % vegetative cover the critical threshold below which accelerated erosion dominates in a sloping landscape, varying with types of vegetation, rain intensity and land attributes (Francis & Thornes, 1990). On the other hand, an increase in biomass above a certain threshold may result in the accumulation of flammable material accompanied by a higher fire risk (Seligman & Perelovotsky, 1992). Within the DPSIR system, vegetation cover is a 'state' indicator and is

closely linked to indicators such as ‘Soil organic matter content’, ‘Soil depth’, ‘Erosion risk’, ‘Soil erosion’, ‘Erosion protection’, ‘Ecosystem resilience’, ‘Land use type’ or ‘Fire risk’. There are different opportunities to inferring information on vegetation cover from remote sensing data, which are given further attention in section 3.4.1.

3.4 Remote sensing of rangelands

Different studies illustrate perspectives of remote sensing applications in Mediterranean-type rangelands. Given the scope of this work, fields of major importance, which are highly inter-related, include:

- Characterisation of vegetation properties in rangelands
- Remote sensing based approaches in burned area mapping and fire management
- Rangeland monitoring approaches
- Approaches specifically targeted at grazing impact assessment

The following section will particularly focus on methods of direct relevance in the context of this study and, where available, refer to their application in a Mediterranean context.

Remote sensing of rangelands has a long tradition in non-European rangelands with their specific properties (e.g. Foran, 1987; Pickup, 1996; Pickup et al., 1988). Reflecting the long tradition of this field in the USA, Tueller (1991, 1995, 2001) has highlighted the potential of remote sensing in mapping and managing large rangeland areas in a series of papers. These describe a range of potential mapping approaches and emphasises the suitability of Spectral Mixture Analysis in a rangeland context. In particular, the question of mapping scales corresponding sensors, including aerial photography and video camera acquisitions, airborne hyperspectral data, medium-resolution imagery (i.e. Landsat-MSS, -TM), coarse-resolution scale remote sensing devices (NOAA) and radar systems is addressed. For mapping scales of 1:50,000 and regular observations, Landsat data represent the best compromise between spectral and spatial detail, data availability and acquisition costs.

3.4.1 Derivation of vegetation-related information

Using remote sensing data, ‘vegetation’ can be characterised at different scales and using a range of methodological approaches, depending on the target information required.

Numerous studies address the issue of sparse vegetation mapping. Traditionally, the derivation of vegetation-related information has been based on the calculation of simple spectral indices such has the Vegetation Index (VI) or Normalised Difference Vegetation Index (NDVI). While their application is simple and efficient, such indices suffer from a number of drawbacks, such as the influence of soil background especially for bright soils and sparse vegetation canopies, or saturation effects for very dense vegetation layers (e.g. Huete et al., 1985; Baret & Guyot, 1991; Verstraete, 1994b). Some authors suggested introducing a soil line as a reference, resulting in the Soil Adjusted Vegetation Index (SAVI), or the Perpendicular Soil Adjusted Vegetation Index (PSAVI). These helped to resolve some of these ambiguities, but for variable soils and lithological backgrounds the concept of a universal soil

line can not be maintained (e.g. Huete, 1988; Baret et al., 1991; Verstraete, 1994a; Rondeaux, 1995; Gilabert et al., 2002). Other approaches include the Global Environmental Monitoring Index (GEMI; Pinty & Verstraete, 1991), or transformations of the data feature space, such as the Tasseled Cap transformation (Kauth & Thomas, 1976). Another problem common to these indices is the comparability of index values derived from remote sensing systems with different spectral characteristics. Nonetheless, vegetation indices are still widely used in manifold applications and are still being further developed (e.g. Turner et al., 1999; Gilabert et al., 2002).

All of the above mentioned indices remain confined to the pixel as the reference spatial entity, which poses different problems when highly heterogeneous Mediterranean environments are regarded. In these cases, the average size of homogeneous surface features frequently lies below the pixel size, such that the recorded values have to be considered mixtures of different materials (e.g. Fisher, 1997; Cracknell, 1998). Consequently, the pixel signal can be assumed to be a combination of the reflectance of a limited number of surface features. Provided the availability of information on these reference materials, the signal can be decomposed into proportions of these materials, which is known as 'Spectral Mixture Analysis' (SMA) (e.g. Smith et al., 1985, 1990a, b; Adams et al., 1986, 1993). Elmore et al. (2000) have demonstrated the superiority of vegetation cover derived using SMA over NDVI for sparsely vegetated areas, and various authors have successfully applied the methodology to infer information on vegetation or soil cover in a quantitative way in different environmental settings (e.g. Roberts et al., 1993; Smith et al., 1994; Lacaze, 1996; Garcìa-Haro et al., 1996; Shoshany & Svoray, 2002; Hostert et al., 2003a). Ustin (1996), Roberts et al. (1993, 1998), Okin et al. (1998, 2001) and McGwire et al. (2000) have demonstrated the potential of the method when applied to hyperspectral data, but these studies are largely concentrated on Mediterranean ecosystems of California. An extension of the approach is represented by multi-date unmixing approaches (e.g. Shoshany & Svoray, 2002; Rogan et al., 2002; Kuemmerle et al., 2006) or the establishment of multiple endmember setups (MESMA; Okin et al., 1998; Roberts et al., 1998; Garcìa-Haro et al. 2005). Beside vegetation, soil-related parameters have been successfully derived from remote sensing data using a variety of approaches. For instance, Hill et al. (1995a) used SMA to relate soils and bedrock fractional cover to degradation status for a test site in Southern France. Hill & Schütt (2000) used an empirical function derived from soil samples and hyperspectral measurements to infer a linear relation between reflectance and soil organic matter, which was upscaled to Landsat-TM imagery using a forward-backward spectral unmixing approach to restore soil-related information.

The selection of appropriate approaches needs to take into account the spectral separability of surface materials given the spectral dimensionality of the sensor employed. Where soils are spectrally similar to the prevailing bedrock, no distinction with high confidence is possible. On the other hand, vegetation has a unique spectral signature compared to other materials and has hence been selected as the target indicator in this study (compare chapter 7).

In many cases, it is aimed at relating information on vegetation cover to other structural parameters, such as LAI, above ground biomass etc. (Lacaze, 1996; 2005). Calvaõ & Palmeirim (2004) investigated the spectral behaviour of *Cistus* shrubs, and related NDVI as well as

spectral reflectance in single bands to biomass estimates. Although a satisfactory relation between NDVI and biomass was attained, they observe deviating patterns in the empirical function due to very bright background materials, making this study in fact a strong case for basing analyses of sparsely vegetation areas on SMA. In another study, Fang et al. (2005) investigated different approaches to characterise semi-arid rangelands based on NDVI, EVI, surface broadband albedo, LAI and FPAR, and their comparability when derived from Landsat ETM+ and MODIS data. Results were shown to be consistent between both sensors for the indices, while MODIS data overestimated LAI and FPAR. However, their approach of deriving 'biophysical' indicators is dependent on an exhaustive reference data base of ground LAI and spectral measurements. It requires well characterised plots which are homogeneous and cover a wide range of values, and is hence confined to specific experimental conditions. Other authors have successfully related information from multi-temporal series of satellite images to ecological process models to infer structural and chemical indicators of vegetation (Tabarand, 2000; Nouvellon et al., 2001)

Further to these approaches of deriving specific, quantitative indicators, traditional and enhanced classification methods are still widely used to differentiate vegetation communities (Friedl & Brodley, 1997; May et al., 1997). Sometimes these are combined with sophisticated stratification approaches or make use of decision trees, rule-bases and object-related information (San Miguel-Ayanz & Biging, 1996; Shandley et al., 1996). By combining multiple dates and sensors, improvements to single-date classifications could be attained in may cases (Vinas & Baulies, 1995; Grignetti et al., 1997). A second major group of approaches to vegetation mapping makes use of hypertemporal data sets and phenological information contained therein. Frequently, such approaches are based on small-scale sensors, such as NOAA-AVHRR, MODIS etc. (Justice et al., 1985; DeFries et al., 1995; Ehrlich & Lambin, 1996; Moody & Johnson, 2001). An overview of existing methods and studies is provided for instance by Shoshany (2000).

3.4.2 Evaluation of processes in fire-affected rangelands

The crucial step in designing an interpretation framework is to include the temporal component. Frequently, these are based on different diachronic comparison techniques of a limited number of images (Lu et al., 2004b), sometimes under consideration of multiple sensor systems to address various spatial scales. Different facets of relevance to the factors fire and grazing impact need to be discussed in this context.

Fire monitoring has long been recognised as a major remote sensing application. In principal, two effects of fires need to be recognised that manifest differently in remote sensing data. The first is the deposition of charcoal and ashes, which persists for limited times only; the second is the alteration of the vegetation structure (fire scar), which may be discernible for long times after the fire (Chuvieco & Congalton, 1988). Remote sensing based approaches frequently concentrate on spectral manifestations of the second effect.

When addressing the variety of concepts and approaches, the question of scale on which fire is addressed determines the choice of sensor system. Furthermore, methods used are conditioned by the respective aspect of fire-related investigations, such as

- estimation of fire risk and fuel characterisation
- mapping of burned areas
- monitoring of fire-affected areas, with an emphasis on the assessment of post-fire behaviour

Although not directly addressed in this study, the estimation of **fire risk and determination of fuel loads and types** is an important contribution of remote sensing data to fire prevention. Detailed information can be found in Chuvieco et al. (2002a), Agouado et al. (2003), Chuvieco et al. (2003) and Kötz et al. (2004), fire simulation models making use of this input are described for instance in Finney & Ryan (1995) or Duguy et al. (2005).

Fire perimeter mapping has often been addressed at small scales using hypertemporal datasets, such as NOAA-AVHRR, MODIS, METEOSAT etc. As for the amount of data to be processed, major attention is devoted to the definition of automatic and semi-automatic fire perimeter extraction techniques (e.g. Fernández et al., 1997; Barbosa et al., 1999; Pereira, 1999). These approaches are especially useful when information on fires and affected areas is to be supplied for large administrational units. For instance, the European Commission regularly reports on forest fires in Europe based on a standardised analysis of IRS-WiFS data (Barbosa et al., 2002; EC, 2001, 2002, 2003, 2004).

On larger scales, mapping of burned areas is addressed using different concepts.

Various authors use spectral indices to detect fire affected areas (e.g. Chuvieco & Congalton, 1988; Chuvieco et al., 2002b). In most cases, indices are used as a method to support feature extraction by image enhancement through thresholding. Such approaches may encompass unitemporal thresholding or classification techniques and bitemporal change detection methodologies comparing pre- and post-fire images (e.g. Koutsias et al., 1998, 2000; Kushla & Ripple, 1998). For instance, Salvador et al. (2000) used a long series of Landsat-MSS (1975-1993) data in a diachronic study to map fire-affected areas in northern Spain by calculating the NDVI difference between consecutive dates.

Other transformation approaches include the application of principal component analysis to a single image or a stack of pre- and post-fire images (Siljeström & Moreno, 1995; García-Haro, 2001), or the utilisation of tasseled cap transformations and subsequent differencing (Patterson & Yool, 1998; Rogan & Yool, 2001).

Due to its potential in the spectral discrimination of sparse vegetation canopies from background materials, SMA has been employed in different studies on burned area mapping. Shimabukuro et al. (1998) have used the fractional estimate of the shade component to map deforestation in the Amazon Region. SMA may even be used to discriminate ash, charcoal etc. and hence conclude on fire severity, but this approach appears more appropriate for data recorded with hyperspectral sensors due to their higher spectral dimensionality (Caetano et al., 1994; Cochrane & Souza, 1998; Riaño et al., 2002).

Coppin et al. (2004) and Lu et al. (2004) provide extensive review articles on change detection techniques. Corresponding to the studies presented in the previous section, most articles cited make use of bi-annual image acquisition dates, while the respective time slices often

relate to irregular intervals depending on knowledge of processes or events to be assessed. This is a convenient means of addressing a known disturbance at specified dates and enables incorporating seasonal information in vegetation-related analyses. However, these techniques do not allow to adequately incorporate 'slow' processes, i.e. gradual vegetation changes over long periods after fires or in response to grazing; nor do they represent a suitable framework for a regular observation of short-term, unpredictable events (Mulligan et al., 2004).

With their concentration on diachronic analysis, the above studies on the identification of fire scars are a specific case of **multi-temporal analyses**. Beyond these, remote sensing data offer considerable potential in the analysis of post-fire effects and dynamics on the long-term. Many studies address this issue using a limited number of images and covering only little time spans. Ricotta et al. (1998) have used a set of three images acquired before and after a fire event to monitor effects of fire and post-fire dynamics on the landscape structure using fractal indices. Marchetti et al. (1995) used a series of 3 Landsat-TM data sets along with exhaustive auxiliary data sets to analyse the evolvement of five major Mediterranean vegetation types following a major fire event, where they used a qualitative classification approach based on an index calculated from near and short-wave infrared bands. A further review of remote sensing methods in a fire context is provided in Chuvieco (1999).

While these studies remained confined to relatively short periods, Diaz-Delgado et al. (2003) presented a study incorporating 8 Landsat-TM images which covered a 3-year period after a large fire north of Barcelona. This was complemented by a series of Landsat-MSS pre-fire data sets covering a similar time span and extensive ground-based mapping of fire severity. The data sets were acquired at irregular intervals, starting with the first post-fire image at 13 days after the fire. Using the NDVI, they analysed the difference between the closest pre- and post-fire images to infer information on fire severity (termed 'damage'), while the difference between the last image in the post-fire series to the pre-fire situation was interpreted as 'unrecovered NDVI'. In addition, they found significant positive correlations between their 'damage' parameter and fire severity classes mapped on the ground.

Twele (2004) presented an extensive comparative study on fire mapping approaches and post-fire regeneration for a fire event in the *Massif de L'Étoile*, Southern France, which was based on a multi-temporal Landsat-TM/ETM+ data set. He compared a variety of methods for burned area mapping and post-fire monitoring and concluded that SMA most accurately revealed the spatial variability as mapped in the field. Similar to Diaz-Delgado et al. (2003), he analysed post-fire recovery over 5 years, and derived integrated profiles for stands dominated by *Pinus halepensis* and *Quercus coccifera*. These temporal cover profiles were shown to differ in their immediate response after the fire, but converge towards the end of the observation period.

Although these studies incorporate a larger number of satellite images, they are tailored towards a specific fire event and are not suitable for a regular, long-term monitoring concept due to their irregular acquisition dates.

The most extensive remote sensing based study on local-scale post-fire dynamics in the European Mediterranean was presented by Viedma et al. (1997). They used a set of 9 Landsat-TM

images covering the period from 1984 to 1994 to evaluate ecosystem recovery after fires. Following radiometric normalisation and derivation of NDVI estimates, they assessed post-fire dynamics in different vegetation types known from auxiliary data. Consistent with the theory of auto-succession (Trabaud, 1994), different regrowth patterns were observed which could be mathematically described using an exponential function. This approach remains limited due to the radiometric normalisation and its utilisation of the NDVI. Nonetheless, it does contain elements suitable for a monitoring concept with its approach in selecting satellite images at regular dates to characterise long-term processes at suitable periods of time.

3.4.3 Evaluation of processes in grazing-affected rangelands

Aspects of temporal coverage attain even higher weight when grazing is the target factor. Mulligan et al. (2004) state that it is a 'slow' process, hence consideration of the factor 'time' is mandatory for the investigation of grazing-related degradation. Secondly, the influence of grazing needs to be assessed using an indirect indicator that is tangible with remote sensing instruments, such as vegetation cover (Graetz et al., 1996; Hill et al., 2004, compare section 3.4.1). Given the reported influence of livestock foraging on vegetation cover (e.g. Le Houérou, 1981) grazing impact may be assessed by integrating information on vegetation cover development with auxiliary information (e.g. Legg et al., 1998; Hostert, 2001). As a consequence, two different approaches appear suited to assess the impact of grazing:

- the assessment of temporal trends that are triggered by grazing
- the identification of spatial trends in rangelands that result from locally differentiated impact of grazing

To the present date, only Hill et al. (1998) and Hostert et al. (2003b) have attempted a per-pixel, long-term analysis of **temporal trends in vegetation cover** using dense time series, and aimed at interpreting this in the context of the local grazing regime. Especially Hostert et al. (2003b) focused on integrating quantitative assessments based on one image per year over a period of 20 years with available auxiliary data to investigate the impact of livestock grazing.

In the context of research on land use/land cover change, such a characterisation of gradual processes has so far not gained major attention. Coppin et al. (2004) and Lu et al. (2004) provide extensive overviews on the techniques employed at present. These include for instance change vector analysis (Johnson & Kasischke, 1998), multitemporal PCA (García-Haro et al., 2001) or image differencing (Rogan & Yool, 2001). Frequently, variations are accounted for by using combinations of images to characterise one time slice. According to their findings, these methods remain confined to the comparison of a discrete and often limited number of such slices. For instance, Petit & Lambin (2001) have aimed at quantifying processes of land-cover change in Zambia by supervised classification of three SPOT images from 1986, 1992 and 1997. They suggested a combination of image differencing between two-date combinations with comparison of change in land use classes to characterise land use change. This was achieved at the level of land use classes in total and on the pixel level and the interpretation was related to census data on a non-spatial level. This approach is well-suited to characterise major changes in land use classes and provide a 'from-to' change matrix or transition trajecto-

ries. On the other hand, it is deemed incapable of quantifying change of a specific indicator (e.g. vegetation cover) within a land use class. Especially the characterisation of gradual, long-term trends is not possible using only two time steps.

Such local scale applications are often accompanied by approaches based on small-scale land use change analyses that focus on seasonal dynamics (e.g. Lambin, 1996; Lambin & Ehrlich, 1997). In a recent study Geerken & Ilaiwi (2004) analysed desertification processes in Syria by integrating local knowledge with multi-temporal data sets from Landsat-MSS/-TM and NOAA-AVHRR. Based on visual interpretation, they inferred patterns of aeolian transport of sediments, while NDVI differencing between two images was used to identify dynamics of rain-fed cultivated fields. In addition, temporal trends in biomass were assessed by comparing NDVI cycles to precipitation patterns, which allowed to distinguish human-induced changes from those triggered by precipitation. The different information was integrated with local knowledge and socio-economic information to characterise human-induced degradation through cultivation practices and grazing, and suggest options for rehabilitation.

With respect to grazing, a second major group of studies is less concerned with the temporal dimension, but sets a focus on the identification of **spatial trends** of grazing impact based on remotely sensed imagery. Pickup & Chewings (1988) showed systematic changes in green vegetation or soil cover with increasing distance from water sources which they related to animal distribution patterns. As these trends are often not discernible visually, or can be masked by strong vegetation response to rainfall variations, they suggest employing statistical techniques to describe trends (Pickup & Chewings, 1994; Pickup et al., 1998). Investigating cattle grazing in Australian rangelands, these statistics were related to the distance from waterholes and decreasing pressure with increasing distance could be proven. Harris et al. (2003) employed airborne hyperspectral imagery from the AVIRIS sensor to detect grazing gradients based on sub-pixel green vegetation cover derived from SMA. These studies are based on the concept of piospheres[1] as a manifestation of the impact of a spot disturbance on a landscape at an environmental resource patch (e.g. Lange, 1969; Forman & Gordon, 1981). In arid to semi-arid environments, where water is the limiting factor, animal's activities are often most pronounced around watering points, while with increasing distance from these points their impact on the environment attenuates. The piosphere is hence a zone of decreasing grazing pressure radiating outwards from watering holes, its extent being limited by the maximum distance where no impact can be observed (e.g. Lange 1969; Andrew & Lange, 1986; Thrash & Derry, 1999). Foraging behaviour or trampling being the most common disturbances, a variety of parameters have been observed to be directly related to the distance from the disturbance point. These include biomass, plant density, species composition, green vegetation cover, the ratio of annuals to perennials or nutrition quality (e.g. Andrew & Lange, 1986; Pickup et al., 1998; James et al., 1999), but also soil compaction, runoff, infiltration rate, erosion rate, livestock trails or dung accumulation (e.g. Andrew & Lange, 1988; Thrash & Derry, 1999). As water is not the limiting factor in the rangelands addressed in this study, an adaptation of the

[1] The expression is derived from 'pios' which means 'to drink' in the Greek language.

concept to accommodate a specific Mediterranean perspective is required to support its applicability (compare section 10.2.1).

3.5 Elements of a remote sensing based rangeland monitoring and assessment framework

Notwithstanding the presence of a vast number of case studies it was stated that a commonly applicable framework of 'linking people to pixels' yet remains to be defined (e.g. Fox et al., 2002; Rindfuss et al., 2004). Hill et al. (1995a, c; 1996) have sketched the scenario of an observatory for the Mediterranean, but despite previous efforts (e.g. Hostert, 2001) a systematic approach to the implementation of such a concept has not yet been attempted. A remote sensing based monitoring and assessment framework for Mediterranean rangelands should allow for monitoring of processes and trends, support their interpretation and ideally provide information relevant to decision-makers. From the previous sections, some basic requirements and elements can be identified. These will be addressed in the further sections of this work as indicated in the following.

Referring to the processes to be accounted for (sections 2.3 and 2.4) and the sensor system characteristics (section 3.1) Landsat images from different sensors were selected for procurement of the time series. They provide for consistent retrospective data sets at appropriate spatial coverage, spatial/spectral resolution and repetition rate. The processes to be evaluated are 'slow' processes (Stafford-Smith & Reynolds, 2002; Mulligan et al., 2004) with regards to long-term grazing impact and post-fire recovery; on the other hand they also show unpredictable, short-term characteristics as concerns fire events. In addition, effects may only manifest on time scales at the order of decades. Hence, long-term data sets with a sufficient density are needed. The data acquisition strategy needs to account for external factors such as data costs, processing efforts, data availability etc.; consequently, one image per year was acquired. The data sets employed are presented in Appendix A.

The interpretation of satellite image time series requires that differences in the spectral content of the images relate only to change in surface properties, to enable the application of quantitative interpretation approaches. This necessitates a **standardisation** of the satellite image data base, i.e. a full geometric and radiometric correction of all images (Hill et al., 1996). The different **processing** steps need to incorporate the sources of distortions raised in section 3.2 and will be discussed in chapter 5 and 6.

The ecological state of rangelands needs to be characterised at different times to allow for their temporal assessment. As many relevant processes can only be measured using indirect **indicators**, their selection is a crucial issue. While the concentration on soil or bedrock information depends on the spectral contrast defined by environmental conditions and the spectral dimensionality offered by the sensor, proportional vegetation cover is a suitable indicator. It may be interpreted both with respect to fire/post-fire recovery as well as in relation to grazing. Given the opportunities and limitations discussed before, SMA will be used to derive this information from all data sets incorporated in the data base (chapter 7).

Following the data processing and derivation of indicators, the further steps need to focus on the processes that affect Mediterranean rangelands.

Concerning fire, the first objective is to identify, **map** and label **burned areas**. In principle, this can be achieved be partitioning the multi-temporal data set in a large number of bi-temporal data sets for classical differencing. Subsequently, the long-term data set needs to support the statistical characterisation of **post-fire dynamics**, which will be based on **linear trend analysis** (chapter 9). Ideally, this quantitative information should be complemented by an identification of vegetation communities. A classification is complicated if only one image per year is available. Hence, the applicability of an alternative approach to **map** major **structural vegetation types** under the given data configuration, will be assessed in section 9.5.

In addition to a remote sensing based trend analysis, it is essential to identify relevant **drivers** based on **data integration and analysis** of auxiliary information and datasets. Depending on data availability, these may include climate data, information on geology, pre-fire vegetation, soils, or socio-economic information (e.g. Wilkinson, 1996; Burrough & McDonnell, 1998). Especially digital elevation models are of importance in this context, as they are routinely available (for instance DEMs derived from the Shuttle Radar Topography Mission) and allow a range of topography-related GIS operations (section 9.4).

In rangelands particularly affected by grazing, the multi-temporal analysis needs to focus on long-term change imposed by grazing. **Spatio-temporal trends and patterns** will be identified using linear trend analysis similar to the post-fire assessment, although in this case singular disturbances are expected to be less important (section 10.1).

Identifying the presence of a causal connection between observed trends and the socio-economic regime requires **data integration** with specific reference to grazing properties. Hence, socio-economic data, such as stocking rates and their development, livestock behaviour, infrastructure etc. play an essential role. In addition, topography partially determines grazing behaviour and is hence assessed based on digital elevation data (section 10.1.2 to 10.1.6).

Making use of the piosphere concept (section 3.4.3) it will be investigated whether the available data enable to model spatial disturbance patterns resulting from grazing and infer **spatial trends** in rangelands complementing temporal trends (section 10.2).

The test sites of **Ayora** (section 4.1) and **Lagadas** (section 4.2) will be used to represent the two aspects ‘fire’ and ‘grazing’ and their associated processes. Beside the interpretation of causes and consequences of observed environmental processes, opportunities and limitations associated with the different steps will be critically discussed the respective contexts.

These results will support the definition of a **formalised interpretation framework**, the identification of shortcomings and the formulation of recommendations for a refinement and potential extension (chapter 11).

4 Pilot areas

4.1 The Ayora study area

The Ayora study area belongs to the province of Valencia and is located about 60 km south-west of the city of Valencia and 80 km west of the *Cabo de la Nao*. The area covered in this study is defined by a frame corresponding to 39° 20’ 15.13’’N / 1° 10’ 33 ‘’W (ULX/ULY) and 38° 49’’ 53.19’’N / 0° 32’ 3.53’’W (ULX/ULY). Within this, a total area of 1902 km^2 is covered by this study.

From a bio-geographical point of view, the area belongs to the *Valenciano-Tarraconens*e sector of the *Valenciano-Catalano-Provenzial* phytogeographical province (Vázquez & Moreno, 1993). Fig. 4.1 indicates the location of the test area on the Iberian Peninsula, Fig. 4.2 provides an overview of the topography of the area.

Fig. 4.1: Location of the Ayora test area on the Iberian Peninsula (data: ESRI Maps & Data)

As many other rural Mediterranean areas, the Ayora region has undergone major socio-economic changes which have also affected the appearance of the land. The whole area comprises 60 municipalities with 17,600 inhabitants, with an average population density of less than 14/km^2. Most of the population is concentrated in the 3 urban areas of Ayora, Enguera and Mogente. Since 1900 the region experienced a decrease in population by 15 % and by 8 % since 1980 (Vallejo et al., 2001). In parallel, an overall increase in population is noted for the latter period for the province of Valencia, illustrating the widespread urbanisation process, since these figures are triggered by the population increase of urban Valencia as one of the most dynamic cities in Spain (source: Eurostat, http://epp.eurostat.cec.eu.in). In parallel to the decreasing rural population, abandonment of traditional agricultural practices and areas occurred, especially in the mountainous areas. Today, cultivated land is mostly located in the large valleys around the actual test area where agricultural mechanisation is feasible.

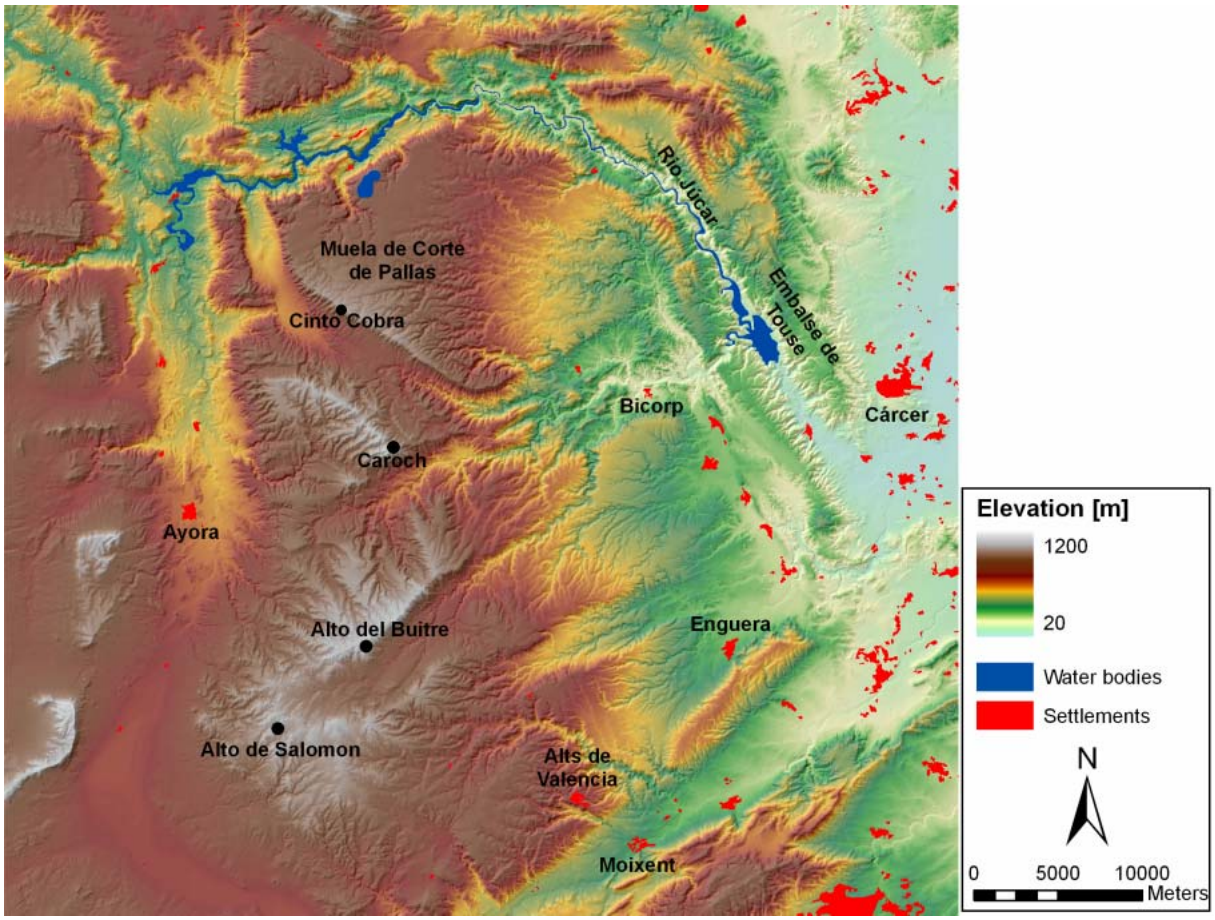

Fig. 4.2: Topography of the Ayora test area (DEM: CNIG, vector data: Fundacion CEAM)

With its mountainous character the test area is a clearly delineated landscape unit. To the West, it is bordered by the agricultural valley of *Ayora*, while to the North the marked canyon sculptured by the *Rio Júcar* is a natural boundary (Fig. 4.2 and Fig. 4.3).

Fig. 4.3: Canyon of the *Rio Júcar*

The southern border is given by the valley of the *Rio Cañoles*, and towards the East there is a transition to the agricultural plains of the Levant, which are heavily used for orange plantations. While this transition is more gradual in the Southwest, there is a clearer limitation in the Northwest given by the *Rio Jùcar* and the *Embalse de Tous*. Within this landscape unit, elevations rise to more than 1000 m asl, with the maximum elevation reached at the *Caroch* with 1126 m asl. Generally, the area appears as a compact mountainous block, structured by a few major valleys. In the North it does show a more undulating character, with a large elevated plain of the *Muela de Corte Pallas* (Fig. 4.4 and Fig. 4.5) and the highest elevation of 1018 m asl at the *Cinto Cabra*.

Fig. 4.4: *Muela de Corte de Pallas* (eastern part, view southwest)

Fig. 4.5: Rugged topography of the southern test area

From this plain, small rivers drain towards the *Rio Júcar*. Separated by a large tectonic fault running from north-west to south-east, the southern zone is characterised by a more rugged

surface, with a number of valleys and intermediate hills and peaks, such as the *Alto del Buitre* (1095 m asl) or the *Alto de Salomón* (1063 m asl).

4.1.1 Climate

The Mediterranean area is governed by a typical seasonal climatological framework. In summer, it is influenced by the system of subtropical anticyclones from which the dry trade winds originate. In winter, the planetary circulation system moves towards the equator, and the Mediterranean basin is also affected by the cyclones of the middle latitudes and the dominating system of the west wind drift. In autumn and spring the Iberian Peninsula is directly affected by westerly winds, while in winter this belt moves even further South (Linés Escardó, 1970). During the winter season, cold periods may even lead to frost and snow especially at higher altitudes. The season of favourable water supply does not coincide with the season of high temperature, which results in a serious climate-driven limitation for plant growth especially when winters are cool or cold (Schultz, 2000).

Despite generally dry conditions, exceptional rainfall events do occur at times. In summer these often result from convection cells that foraminate the atmospheric inversion associated with trade wind zones, while in winter they are triggered by frontal rains or cyclones. With extremely high intensities these events are often catastrophic and result in high rates of surface flow and considerable erosive processes, while only small shares are actually received by the soil and made available to plants (Fisher & Bowen-Jones, 1969).

In the Ayora area, this general framework is somewhat modified. Precipitation is higher in autumn and spring than in winter (compare Fig. 4.6), and its genesis differs from the pattern observed for the western part of the Mediterranean Peninsula. Generally, precipitation in the Ayora region is mostly attributed to disturbances developing or regenerating in the Mediterranean and the Northeast of the peninsula, which may originate from decaying jet stream or through the advection of unstable polar air into the Mediterranean in autumn and winter (Linés Escardó, 1970). On the other hand, cyclones travelling with the westerly jet stream branch usually weaken above the land mass and have hence only little effect on eastern Spain. Consequently, the presence of meridional circulation types increases the probability of precipitation in eastern Spain, while strongly latitudinal circulation rather favours precipitation on the western side of the Iberian peninsula due to cyclones travelling with the jet stream (Linés Escardó, 1970). Especially in September, October and, occasionally, November cyclone cells which develop in the Gulf of Léon and the Strait of Gibraltar are important. In addition, low pressure cells at the Balearic Islands often lead to extended and intensive rainfall events (Costa, 1987). If cool air masses are present, this situation may result in rainfall sums of 200 to 350 mm within 24 hours (Linés Escardó, 1970). In winter, precipitation may result from advection of polar air exceeding the Pyrenees Range and Cantabrian slopes. However, in winter anticyclonic conditions are frequent, causing a decrease in precipitation compared to the autumn situation. In spring, low pressure cells at Gibraltar and the Balearic Islands again augment precipitation which nonetheless ranges below autumn amounts (Costa, 1987). In summer, the Azores high pressure system belonging to the subtropical anticyclonic pressure belt blocks currents from the Atlantic and leads to dry conditions. In their combination, the described meteorological patterns also result in relatively high rainfall variability in eastern

Spain compared to the western Iberian Peninsula, and often cause a gradient of decreasing precipitation from East to West (Linés Escardó, 1970).

Based on the system developed by Walther (1955), Fig. 4.6 shows climate charts of stations from these two zones accompanied by a chart representing the city of Valencia which is based on a longer data record. Unfortunately, no records were available for stations on the higher elevations of the central test area.

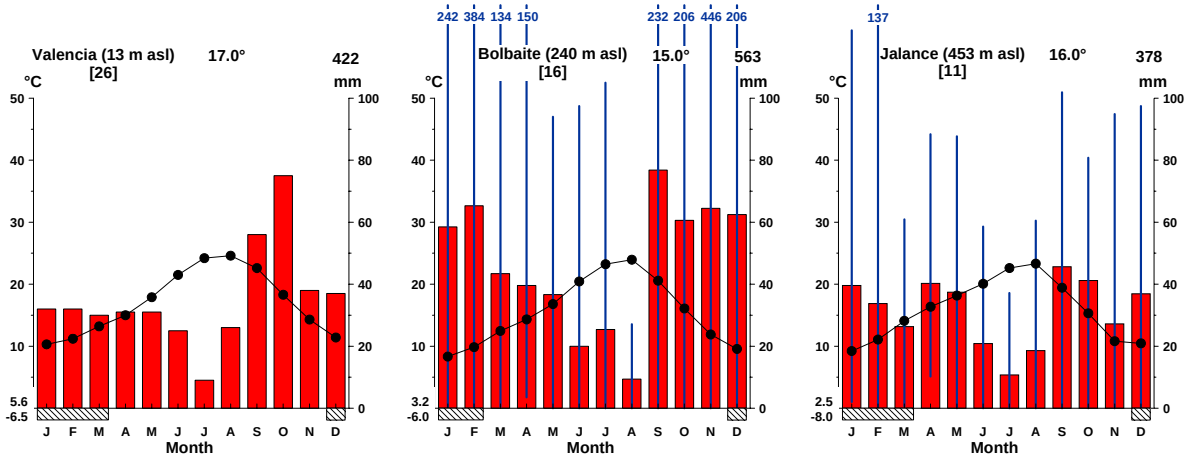

Fig. 4.6: Climate charts for the Ayora test site and the city of Valencia after the chart system developed by Walther (1955). Where full records were available, blue lines show the minimum and maximum precipitation amounts recorded during the observation period; values exceeding 130 mm were clipped and are indicated by labels with the actual precipitation values (data from Müller, 1996 and Fundacion CEAM)

Data for the stations of Bolbaite and Jalance have been recorded by the Spanish National Meteorological Service and made available through Fundacion CEAM, while data for Valencia are taken from Müller (1996). Bolbaite represents the agricultural region to the East of the core mountain area, while Jalance is located in the Ayora Valley.

The city of Valencia shows a typical distribution of temperature and precipitation, with four arid months in summer and a temperature maximum in late autumn. Although based on slightly different periods of record, the stations of Bolbaite and Jalance reflect the East-West gradient with a difference in average precipitation over 16 and 11 years of 185 mm. The distribution is largely corresponding between the two stations, with major amounts of precipitation occurring in early autumn and a secondary maximum in spring, while winter precipitation is somewhat lower and summers are mostly dry. Mean yearly temperatures only differ by 1° C, but minimum temperature indicators are lower in the western site and four instead of three frost months are observed. Most importantly, both stations display the high variability in precipitation which is typical for the area. Since the stations employed are located in lower zones, temperature profiles may differ in the higher altitudes of the core area, and frost periods may be even more prolonged. An altitudinal gradient could not be quantified as both stations are located in lower zones and no stations are present in the higher altitudes; hence, a spatial interpolation was not possible.

4.1.2 Geology

The test site is situated in the transition zone between the massive of the north-eastern *Cordillera Ibérica*, the *Cordillera Bética* ranging from the *Andalusian Mountains* to the *Balearic Islands* and the coastal plains of the *Levant* (Sole Sabaris, 1978a; Gutiérrez Elorza, 1994). The Ayora test area is associated to the *Iberian Cordillera* which has been formed during the alpidic orogenetic phase in the Tertiary. The north-eastern outliers of the *Betic Mountain* range are directly adjacent in the South, and the border is represented by the valley of the *Rio Cañoles*.

The *Iberian Cordillera* is characterised by Mesozoic sediments dating to Triassic to Cretaceous periods. They have been mostly deposited under submarine conditions corresponding to the different transgression phases from which only the Meseta was excluded (Sole Sabaris, 1978b). They form a disconcordant layer upon the older, folded palaeozoic sediments. At the end of the Cretaceous, the sea had retreated and subairial erosion became the dominating factor. Opposed to typical facies of the alpidic orogenese, the *Iberian Cordillera* shows no significant metamorphism (Gutiérrez Elorza, 1994a). On the other hand, karstic phenomena are common following dissolution processes in the carbonatic rocks deposited in Jurassic and Cretaceous ages (Gutiérrez Elorza & Peña Monné, 1994).

In the geological map (Fig. 4.7) the topography structure depicted in Fig. 4.2 and the central mountainous block can well be perceived against the surrounding areas.

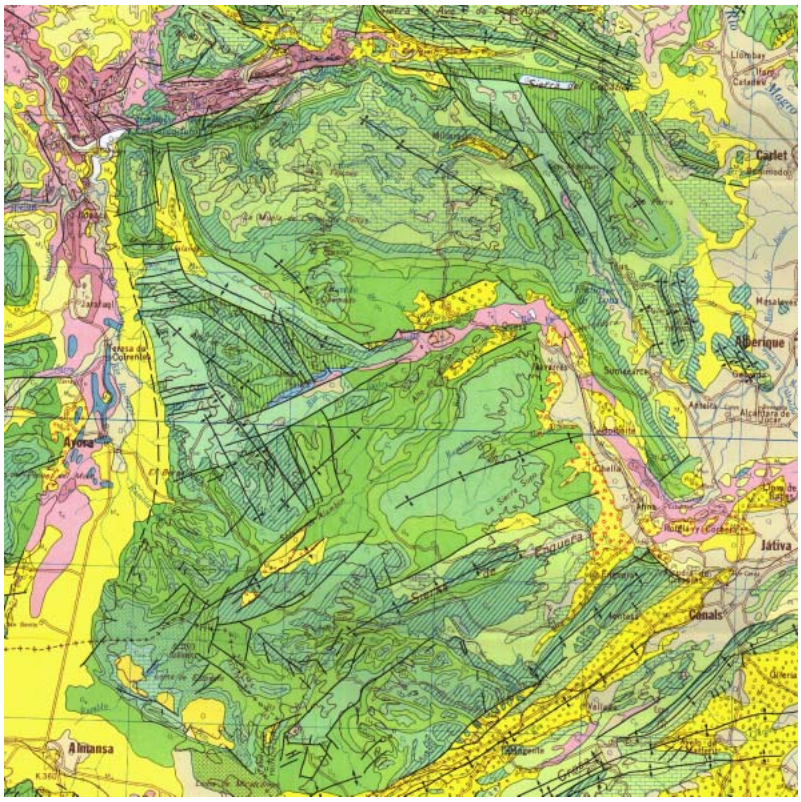

Fig. 4.7: Geological map 1:200,000 (IGME, 1987; Sheet 63)

Except for local deviations associated with tectonic faults, the mountain block of the Ayora test area is dominated by three types of calcareous bedrock, limestones, dolomites and marls,

with local contributions of sandstones and clays. All of these have been deposited during the upper and lower Cretaceous period. Along the carved wall of the canyon in the North towards the *Muela de Corte de Pallas*, a sequence of sediments from lower Cretaceous to upper Cretaceous can be found. The *Muela de Corte de Pallas* is a gently undulating plain, its northern and eastern part being dominated by different limestones from the upper Cretaceous, while in the West a combination of limestones and marls are present.

Towards the South, this zone is bordered by a belt of limestones which does also show an E-W differentiation. Its eastern part, until the disturbance at *Bicorp*, is made up of limestones and marls from the lower Cretaceous, while the western part is more heterogeneous and consists of sediments of the upper Cretaceous, mostly limestones and marls.

The major northern and southern complexes of the test area are separated by an E-W running fault. South of this line, the pattern of the lower Cretaceous present in the North appears again with limestones and marls, as well as sandstones, clays and marls. In the central part, a large unit characterised by limestones and marls of the upper Cretaceous is present. The western and southern parts of the southern complex show a higher degree of heterogeneity, which is also reflected in the more rugged impression visible in Fig. 4.2. Corresponding to the strong relief gradient and structured by numerous fault troughs, sediments from upper and lower Cretaceous times are present, with limestones, marls and dolomites being abundant.

This mountain block is clearly delinated in the West by the valley of Ayora with Quarternary and Neogeneous sediments along its eastern side, while the slightly more elevated areas in the West do also show Triassic sediments. The southern perimeter of the test area is also characterised by sediments of these two periods, complemented by marls of the Negoenous in the former riverbed of the *Rio Cañoles.* In the North and Northeast, the canyon of the *Rio Júcar* has dug deep in the Cretaceous series. East of the main mountain block, a broad valley runs in parallel to the *Rio Júcar*. It connects to the agricultural plain in the South and to the bed of the *Rio Escapona* in the North, this being a tributary to the *Rio Júcar* in the *Embalse de Tous*. Further west from *Bicorp* it continues as a series of marked faults and disturbances reaching almost to the cañyon of the *Rio Júcar* with its SW-NW leg and the *Ayora* valley with its ENE-WSW leg. There are some other lower troughs within the mountainous block, where Neogenous deposits are found, which are usually employed for agricultural land use.

Concluding, despite minor variations resulting from specific sedimentation characteristics, lithological properties are very homogenous in the test area.

4.1.3 Soils

Only little information on soils or soil types was available for the Ayora area. Generally available information, such as the European Soil Database, proved being too generalised and inaccurate to infer information on a suitable scale. Here, the whole area is associated to the class ‘chromic cambisols’ exclusively. Most common soils in the area are superficial soils developed over limestone (*Chromic Luvisol, rendzic Leptosol*), deep soils developed over marls (*Calcaric Regosol*) and *Calcaric Phaeozem* (Vallejo et al., 2004). Soils on marls without protective vegetation are characterised by deep erosion and gravel accumulation. The loss of organic matter and fine particles lead in turn to downhill accumulation

In addition, a number of general indications on expected soil development can be drawn based on knowledge of bedrock and climate conditions. According to Schachtschabel et al. (1989), mild, wet winters in combination with dry hot summers frequently result in the development of reddish *chromic cambisols* with low contents of organic matter and low acidity. These are especially frequent under sclerophyllous vegetation and over calcareous bedrock. Where secondary accumulation of carbon occurs, these soils appear as *calcic cambisols*, while a reduction of clay in upper soil horizons and an accumulation in lower horizons result in *chromic Luvisols*. On limestone, rubification often causes deep red soils (*Terrae rossae*) that are typical for the Mediterranean. *Rendzic Leptosols* are typical in areas where soil development is limited or which have been subject to erosion (Schachtschabel et al., 1989). According to Gutiérrez Elorza (1994) R*endzinas* are by far the most common soils on calcareous bedrock within the *Cordillera Ibérica*. In the Ayora test area, this general pattern is expected to adequately describe relevant processes and deviations are only encountered in accumulation areas, where alluvial soils are present. Additionally, in locations where low relief energy or topographic depressions coincide with dry conditions, soil water rising due to capillary processes may lead to a salinisation of the top soil, which is however frequently reversible and has not been reported for the Ayora area.

Given the relative homogeneity of bedrock described in section 4.1.2, it can be assumed that there is no large variance in soil types. In addition, their development is expected to be differentiated according to topography. For instance, Boer et al. (1996) found soil depth to be strongly influenced by a combination of spatial variation in topography-driven processes related to sediment transport and insolation budgets. These are essential for soil development since they trigger evapotranspiration rates and related soil moisture conditions and hence play an important role in determining weathering rates, soil structure and soil erodibility. As a consequence, moderate slopes and accumulation zones are associated with deepest soils. On the other hand, steeper slope can be expected to be connected with less developed rendzinas or even lithosols. The influence of slope is accordingly modified by the availability of moisture, which is both affected by the factors discussed before, as well as by soil texture and the structure of underlying bedrock.

In limited locations, karst processes lead to quick draining of water, resulting in poor soils even if other boundary conditions are generally favourable.

In the absence of spatially differentiated information on distribution of soil types in the test site, the strong influence of topography and the relative homogeneity of bedrock suggest to attribute specific reference to the factors ‘aspect’ and ‘slope’ in the interpretation process due to their importance for soil-related processes and characteristics.

4.1.4 Hydrology

In accordance with the climate regime, the hydrological network shows a high variability of water availability. Rivers draining to the Mediterranean Sea are usually perennial and transport less than half the amount of water than rivers connected to the Atlantic Ocean (Sole Sabaris, 1978c; Schultz, 2000). In many cases, catchments are relatively small and rivers are short, draining directly to the receiving water course or the sea. The erosive effect of rainfall is largely determined by relief energy, soil depth and presence of protective vegetation cover

(e.g. Francis & Thornes, 1990). An exception of the impact of torrential rainfall is presented by areas subject to karst processes where water is drained quickly and may appear in different locations in the form of karst wells (Gutiérrez Elorza, 1994).

In the Ayora test site, numerous small watersheds correspond to the rugged topography especially in the centre of the area (compare Fig. 4.2). Most of the associated rivers are perennial (Sole Sabaris, 1978c). Following the Spanish terminology, they are accordingly termed '*Rambla'* on topographic maps (Fig. 4.8 left).

Fig. 4.8: Small 'Rambla' in the *Muela de Corte de Pallas*

Fig. 4.9: *Embalse de Cofrentes*

The most important exception is the *Rio Júcar* which permanently holds water and represents the major water receiving course to which the small rivers drain after relatively short courses. Being allochthonous in nature, it rises on the *Sierra de Cuenca* and is one of the few rivers with a significant length that drain to the Mediterranean Sea.

Within the Ayora area, there is a series of dams in the north-west of the test site (*Teresa de Cofrentes, Embalse de Embarcadero, Corte de Pallas, Preba del Naranjero*, Fig. 4.9) as well as in the East (*Embalse de Tous*), such that the annual water regime of this river is not representative. Only in the South and Southeast of the test sites there is an exception to this pattern. Here, rivers discharge to the *Rio Cañoles*, which however connects to the *Rio Jucár* east of the actual test area.

4.1.5 Vegetation

The European Mediterranean zone is frequently delineated by the distribution of characteristic plants and vegetation types, such as sclerophyllous forest and shrub formations, or the occurrence of the olive tree (*Olea europaea*) (Schultz, 2000). A further zonation is present along an altitudinal gradient which is especially dependant on local climatic conditions. Along these gradients, significant changes in dominant species are observed, such as 'replacement' of sclerophyllous by deciduous trees or the occurrence of low alpine shrubs at high elevations. Quézel (1981) has accordingly defined 5 altitudinal zones of Mediterranean vegetation: thermo-, eu-, supra-, montane- and oro-Mediterranean, the upper and lower limit of which depend on local conditions. He argues that the current vegetation is 'a direct consequence of climatic modifications since the last glacial withdrawal' and '…the explosion of Neolithic civilisations of herders and farmers, which had a profound influence on the natural ecological equilibrium brought about by gradual climatic warming over more than 10 millennia (Quézel, 2004)'. Disregarding azonal vegetation, he proposed the general scheme depicted in Fig. 4.10.

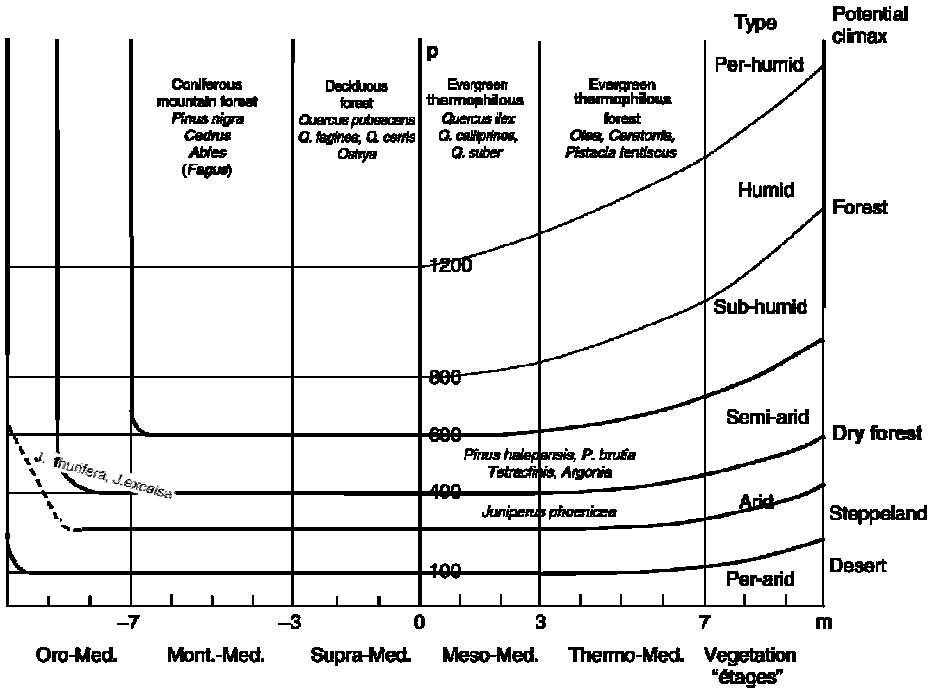

Fig. 4.10: Major structural vegetation types according to climatic types and vegetation layers (p: mean annual rainfall; m: mean temperature of the coolest month) (Quézel, 2004)

Between the appearance of man in the Mediterranean (estimated at 1 Mio years ago) and today, Le Houérou (1981) distinguishes six major phases of human interventions with the natu-

ral landscape. Especially since the Neolithic revolution these have led to significant modifications of vegetation composition through setting of fire, grazing, agriculture, but also as a result of industrial needs, urbanisation etc. As a consequence, plant communities corresponding to the natural potential vegetation are only found in isolated locations, while in most locations vegetation is in a semi-natural state and develops towards a secondary climax (Trabaud, 1994)

The potential natural vegetation in the Ayora region has been described by Rivas-Martinez (1987) and is shown in Fig. 4.11.

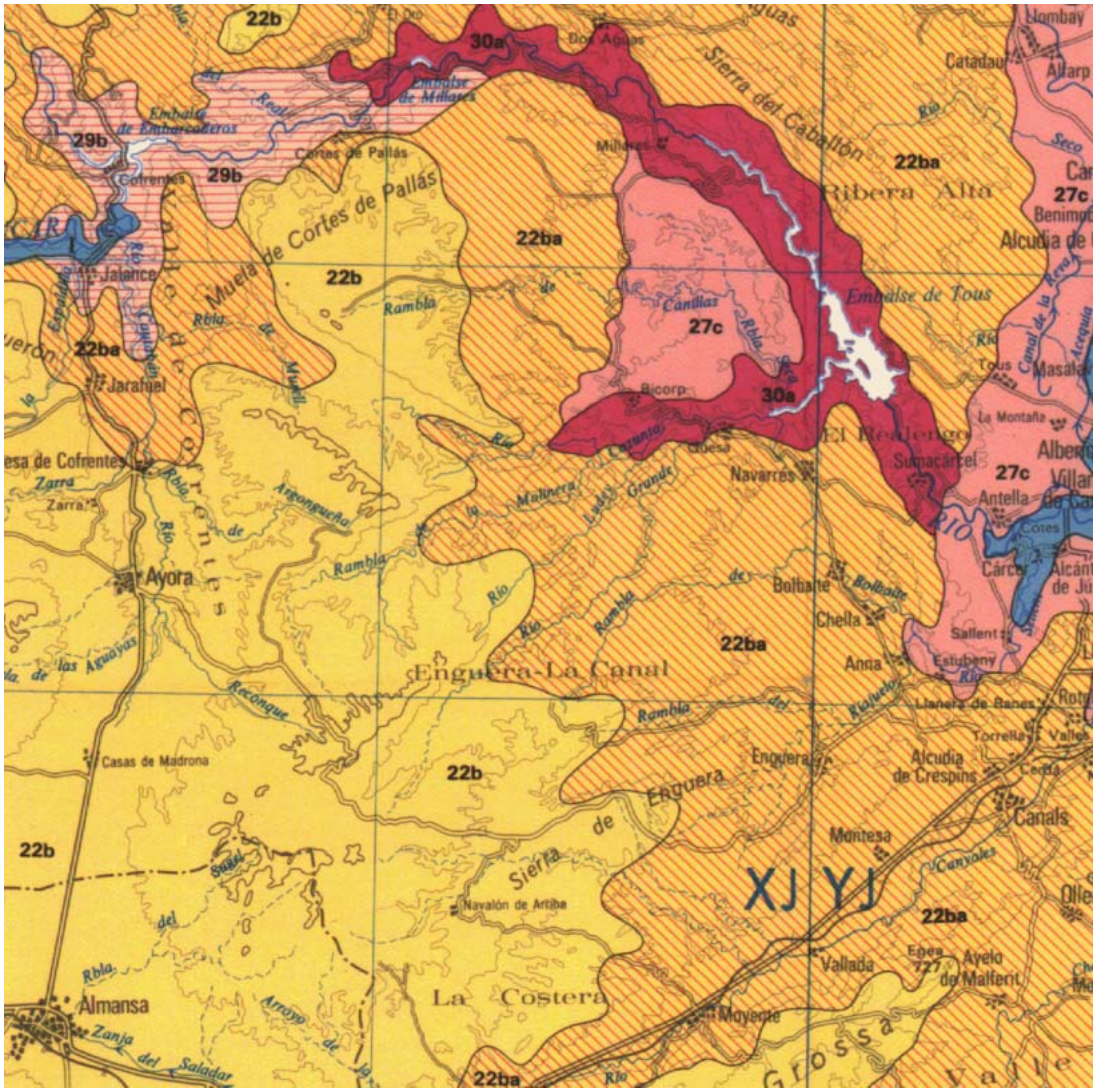

Fig. 4.11: Potential natural vegetation of the Ayora test site (Rivas-Martinez, 1987)

Each of these zones relates to specific dominant species (Table 4.1). The *Bupleuro rigidi–Querceto rotundifoliae sigmetum* (‘H 22b’) is partially complemented by *Pistacia lentiscus* (‘H22ba’). The term ‘mattoral’ has been introduced to characterise woody shrub formations (Ruiz de la Torre, 1971, after Tomaselli, 1981). These formations are often separated from forests by the height of individuals; in addition, their physiognomy does often not show a differentiation into trunks and stems because they are ramified from the base (Tomaselli, 1981). They can be further characterised according to their height or cover. Transitions to grasslands

and forests are gradual and arborescent individuals may be present in matorrals (e.g. Quézel, 2004).

Table 4.1: Potential natural vegetation: dominant plant species in different development stages of the associations found in the Ayora area

	Bupleuro rigidi-Querceto rotundifoliae sigmetum (H22b)	**Rhamno lycioidis-Querceto cocciferae sigmetum (H29)**	**Querco cocciferae-Pistacieto lentisci sigmetum (I30a)**	**Rubio longifoliae-Querceto rotundifoliae sigmetum (I27c)**
Forest	*Quercus rotundifolia* *Bupleurum rigidum* *Teucrium pinnatifidum* *Thalictrum tubersoum*			*Quercus rotundifolia* *Rubia longifolia* *Quercus coccifera* *Smilax aspera*
Dense matorral	*Quercus coccifera* *Rhamnus lycioides* *Jasminum fruticans* *Retama sphaerocarpa*	*Quercus coccifera* *Rhamnus lycioides* *Pinus halepensis* *Juniperus phoenicea*	*Pistacia lentiscus* *Quercus coccifera* *Chamaerops humilis* *Olea sylvestris*	*Cytisus patens* *Hedera helix* *Retama sphaerocarpa* *Genista valentina*
Degraded matorral	*Genista scorpius* *Teucrium capitatum* *Lavandula latifolia* *Helianthemum rubellum*	*Sideritis cavanillsii* *Linum suffruticosum* *Rosmarinus officinalis* *Helianthemum mariflorum*	*Erica multiflora* *Rosmarinus officinalis* *Anthyllis cytisoides* *Cistus clusii*	*Ulex parviflorus* *Erica multiflora* *Thymus piperella* *Helianthememum lavandulifolium*
Grassland	*Stipa tenacissima* *Brachypodium ramosum* *Brachypodium distachyon*	*Stipa tenacissima* *Lydeum spartum* *Brachypodium ramosum*	*Brachypodium ramosum* *Ononis minutissima* *Phlomis lychnitis*	*Brachypodium ramosum* *Sedum sediforme* *Brachypodium distachyon*

The vegetation climax states given in Table 4.1 are hardly encountered in the Ayora area. Plant communities found today are strongly influenced by management actions such as reforestations, fuel breaks or clearings, as well as the pressure and disturbance regime, i.e. land use or land use change, grazing and fire. Given a total of 124,929.06 ha of burned land in the area for the period between 1978 and 2000 (compare section 9.1), fire has strongly altered the composition of the vegetated surface. Even previous to 1979, the area was dominated by *Pinus halepensis* and *Pinus pinaster* with contributions of *Quercus ilex*, indicating fire events prior to the period investigated in this study. Today, the physiognomic appearance of vegetation and composition of plant communities appears to be related to the fire history of the respective area. In general terms, the current vegetation of the Ayora site corresponds to a mosaic of matorrals or shrublands with different development stages and species compositions, covering the range from sparse shrublands with high presence of grasses (mainly Mediterranean gorselands with *Brachypodium ssp.*) to very young regenerated pine forests with a dense understory. The following description of the current vegetation cover and species composition is based on field prospection carried out in 2001 and 2002 (Vallejo et al., 2002, 2004).

The large wildfire event in 1979 has affected major parts of the test site, but there were numerous fires occurring thereafter, such that on a basic level the test area may be differentiated into three zones of similar fire history (during the period observed): areas not affected by fires, areas affected only by the fire in 1979 and areas affected by more than one fire with a more recent fire event in the 1990s.

Where no fires occurred during the last 30 years, tall matorrals and forests are found which are dominated by *Pinus pinaster* individuals. The understorey consists of shrub species such as *Rosmarinus officinalis, Juniperus oxycedrus, Erynacea anthyllis* and *Bupleurum fruticescens*. Additionally, grasses are abundant, of which *Brachypodium retusum* is most frequent. In addition, other tree species, such as *Juniperus phoenicea* and *Quercus ilex* are found in isolated places. The understorey of theses areas is partially affected by grazing, since livestock frequently passes through them (Fig. 4.12).

Fig. 4.12: Central area unaffected by fires during the observation period with matorral/forest dominated by *Pinus ssp.*

Areas affected by fires during the last 30 years are characterised by shrublands of different height and density, depending on the time elapsed after the last fire. Where fires did not occur for a longer time period, thick matorrals with 1 to 1.5 m height are generally found. Individuals of *Quercus ilex* (height 1.5-2 m) may be present as well as *Pinus halepensis* and *Pinus pinaster*, but in some locations the latter may also result from reforestation schemes. In addition, *Ulex parviflorus* is widely abundant, often with high amounts of dead and hence highly flammable biomass.

Where fire events were more recent, low (< 50 cm) and sparse shrublands prevail, with few grasses and tree species. Depending on the substrate, *Quercus coccifera* (on limestone) or *Erica multiflora* (on marl) are the most dominant species.

Based on the topography-stratified sampling of 113 plots using a transect method, typical categories of plant communities could be inferred in fire-affected areas. The percentages given in brackets relate to the relative frequency of the respective species at the sampled plots.

- Open shrublands. Here, shrub species do not present a ground cover higher than 20 % and the most abundant shrub species is *Ulex parviflorus* (19.7 %), although *Quercus coccifera* and *Quercus ilex* may be punctually common. The highest cover portions are attained by *Brachypodium retusum* (48.5 %), which exceeds the numbers in any other of the identified species The average aboveground biomass (photosynthetically active and non-photosynthetically active) is 1,263.6 g/m^2, mostly contributed to by *Ulex parviflorus* and *Quercus coccifera* (41.2 % and 14.5 % of it, respectively).
- Kermes oak shrublands. This unit corresponds to *Quercus coccifera* shrublands (38.8 %) with a herbaceous layer mainly composed by *Brachypodium retusum* (42.5 %). Other resprouter species, such as *Pistacia lentiscus* and *Juniperus oxycedrus*, are common. Seeder species (*Ulex parviflorus* and *Rosmarinus officinalis*) show lower abundances compared to other described communities. These shrublands are usually found on limestone and non-agricultural soils. Two species show different behaviour in relation to fire recurrence: *Cistus albidus* presents clearly higher covers in plots which burned twice than in those burned once, whereas *Rosmarinus officinalis* shows the opposite pattern. The average aboveground biomass reaches 1,816.6 g/m^2 and *Quercus coccifera* accounts for 54 % of it.
- Gorselands. These shrublands are characterised by the dominance of *Ulex parviflorus* (30.1 %), a much lower presence of other seeder shrub species (*Rosmarinus officinalis*, 13.1 %) and the absence of resprouter shrub species (*Quercus coccifera* or *Juniperus oxycedrus*). The herbaceous layer consists both of *Brachypodium retusum* (29.2 %) and *Brachypodium phoenicoides* (14.1 %), the latter showing the highest cover among all vegetation types. This shrubland category mainly occurs over North-facing slopes and set-aside agricultural areas, over soils developed on marls and in elevated areas. The average total biomass is 1,579.4 g/m^2, of which 63.5 % is accounted for by *Ulex parviflorus*.
- Shrublands with Pine. These dense shrublands are dominated by *Rosmarinus officinalis* (33.6 %) and, in a lesser extent, *Ulex parviflorus* (16.8 %). A notable tree layer composed of *Pinus halepensis* (25.2 %) is present, although the vegetation structure is typically shrubby with individuals of *Pinus halepensis* surpassing the height of the shrubs. The herbaceous layer is of less importance (*Brachypodium retusum*: 18.2 %). This community is only found on areas burned once and lowlands that have never been cropped. It reaches the highest average total biomass (4,431.9 g/m^2) of which *Pinus halepensis* contributes 66.9 %.
- Mixed rosemary shrublands. This is the vegetation type most widely represented in the Ayora site under a range of different environmental conditions. The average cover percentage for *Rosmarinus officinalis*, *Ulex parviflorus* and *Quercus coccifera* are 29.1 %, 22.4 % and 17.8 %, respectively. The herbaceous layer is also well developed and mainly represented by *Brachypodium retusum* (29.6 %, lower than in other shrubland types). The average total biomass is 1,798.2 g/m^2. *Rosmarinus officinalis*, *Ulex parviflorus*, *Juniperus oxycedrus* and *Quercus coccifera* account for most of it (26.5 %, 17.9 %, 15 % and 14.6 %, respectively). Extreme peaks may result where *Pinus halepensis* punctually occurs.

- Rosemary shrublands. This type of shrublands is common in forest areas burned once, above 800 m, on soils developed over limestones (or limestones mixed with marls), and preferably over South-facing smooth slopes. *Rosmarinus officinalis* (29.1 %) and *Ulex parviflorus* (22.4 %) are the dominant species. The cover of *Brachypodium retusum* is lower than for other types (11 %), whereas other grasses (*Helictotrichon filifolium* and *Stipa offneri*) show higher relative abundances compared to other plots *(*with 9 and 3 %, respectively). The average total biomass is 1,748.7 g/m^2.

(Vallejo et al., 2002, 2004)

Fig. 4.13 to Fig. 4.18 provide examples of different plant communities found in the test area.

Fig. 4.13: Sparse, open shrubland dominated by *Brachypodium ssp.*

Fig. 4.14: Mixed shrubland with *Quercus coccifera, Rosmarinus officinalis* and *Ulex parviflorus*

Fig. 4.15: Shrubland dominated by *Quercus coccifera*

Fig. 4.16: Dense mixed shrubland with *Pinus* individuals

Fig. 4.17: Transition shrubland – matorral with individuals of *Pinus halepensis* and *Pinus pinaster*

Fig. 4.18: Mixed matorral with *Pinus halepensis* and *Quercus ilex*

Comparing the actual distribution and composition of plant communities with the potential natural vegetation sketched in Table 4.1, the influence of recurring wildfires on the appearance of the Ayora test site is evident. Today, its vegetation cover shows a pattern that is determined by a combination of local environmental boundary conditions and fire recurrence cycles. Beside purely floristic questions, two major factors need to be considered in the following: the soil-protective function of vegetation and its importance in the context of landscape-resilience to fire (compare sections 2.2 and 2.3). Protection of the soil from erosion processes is strongly depending on vegetation cover and the risk of erosion is highest where bare soils are present. Where vegetation cover is present, soil loss rates may vary depending on species composition, the type of rainfall event and the saturation of the soil (e.g. Francis & Thornes, 1990; Sala & Calvo, 1990). On the other hand, the direction and effectiveness of fire propagation depend on the amount of biomass as well as on fuel types. These are defined according to the composition of plant communities as well as different structural and chemical parameters, such as dry biomass, moisture content, content of ethereal and resin oils etc. (e.g. Rothermel, 1972; Anderson, 1982; Viegas, 1998).

4.2 The Lagadas study area

The Lagadas test area is defined to match the border of the County of Lagadas, which belongs to the Region of Central Macedonia. Situated north of the Chalkidiki peninsula and east/northeast of the city of Thessaloniki, the surrounding frame is located at 22° 56’ 53.89’’ E / 41° 00’ 01.41’’ N (ULX/ULY) and 23° 45’ 59.17’’ E/ 40° 28’ 39.37’’ N (LRX/LRY). The County covers approximately 2060 km^{2}and extends about 60 km N-S and about 70 km E-W. Within the administrative structure of Greece, it belongs to the prefecture of Thessaloniki and the district of Central Macedonia, and harbours some 70,000 residential inhabitants (County of Lagadas, www.nath.gr/lagadas).

The location of the test area in northern Greece is shown in Fig. 4.19, Fig. 4.20 gives a detailed view of the topography of the area and delineates the County border.

Fig. 4.19: Location of the Lagadas test area in northern Greece (base data: ESRI Maps & Data)

Lagadas County is bordered by the *Aegean Sea*, the *Gulf of Orfanos* in the East and the *Gulf of Thessaloniki* in the West. Its border follows in wide parts the perimeter of the watershed of *Mygdonia Valley* (Fig. 4.20). The landscape is clearly structured into different elevation zones and transitions between these. While natural vegetation partially corresponds to these zones, there is a mosaic of land uses of various types and intensities according to which different pressure systems operate. There are some major zones of intensive agriculture, but it is especially the mosaic of rangelands used for grazing, with embedded smaller agricultural plots, which requires major attention.

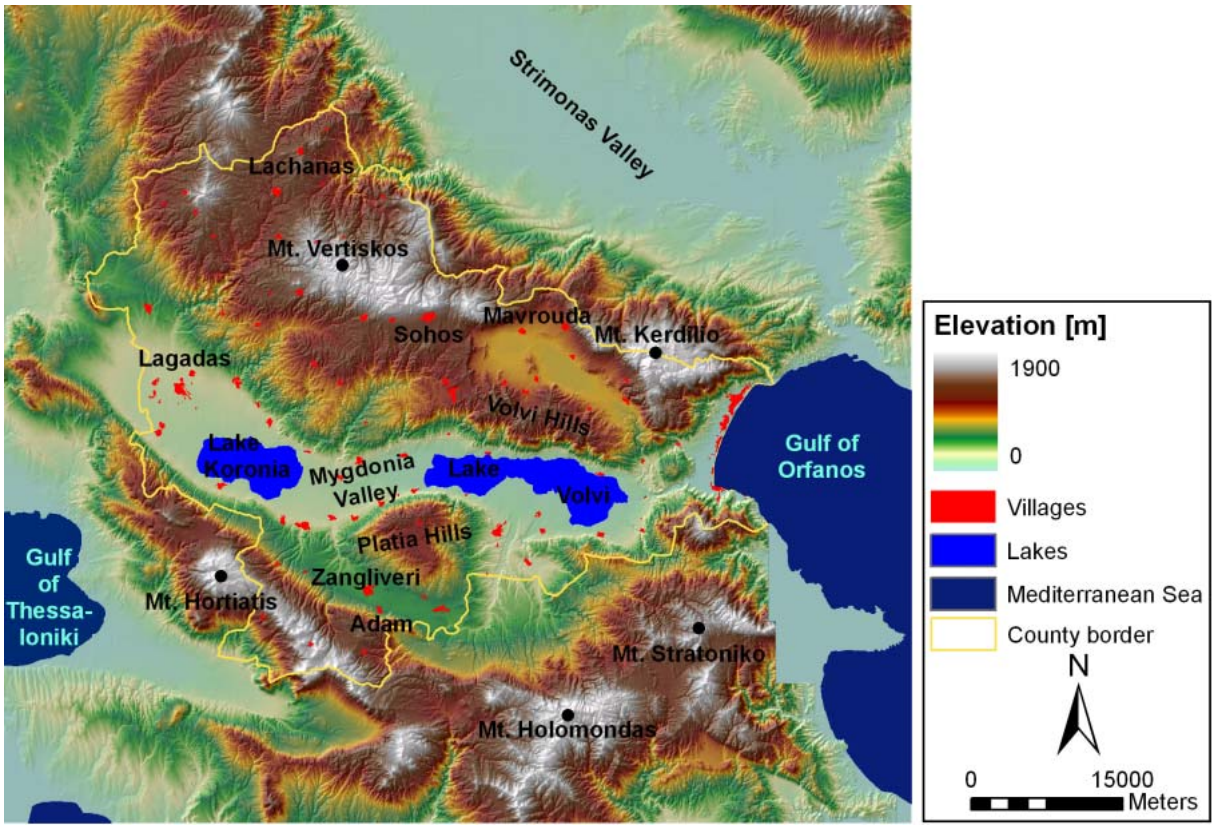

Fig. 4.20: Topography of the Lagadas test area (hillshaded DEM; source: Geoapikonisi Ltd.)

The two lakes in the main valley are major landmarks of the area and of considerable importance for the local economy. *Lake Koronia* is used as the main source of irrigation, while *Lake Volvi* presents important fishing grounds. The plain of *Mygdonia Valley* is predominantly used for settlement and intensive agricultural use sustained by high degrees of irrigation. North of the valley, elevations rise from 70 m asl at the level of *Lake Koronia* (*Lake Volvi*: 36 m) to 1103 m asl at *Mt. Vertiskos* and 1095 m asl at *Mt. Kerdilio*. In this northern section, the large depression at *Mavrouda* is notable, which is the second major agricultural zone in Lagadas County. South of the valley of *Mygdonia*, elevation rises steeply towards *Mt. Hortiatis* (1201 m asl) and *Mt. Holomondas* (1163 m asl). There is a gently undulating trench rising from the western edge of *Lake Koronia* in ESE direction which is the main agricultural zone here. This belt is separated from the main trough by the compact *Platia Hills*.

While the highest areas are mostly covered by thermophilous forests and the two major plains are used for intensive agriculture, it is especially the undulating areas in between that can be characterised as rangelands and that are at the scope of this study.

4.2.1 Climate

In principal, the climate of the region corresponds to the seasonal climatic framework typical for the Mediterranean as described in section 4.1.1. From May through to October, the 'Meltemi' winds with a strongly northern component dominate over Greece and the Aegean Sea. The weather is dry and skies are very clear, effectuating high amounts of solar irradiance and high temperatures, most of all at higher distances from the Sea. Major precipitation at these times is coupled to convective events when air masses foraminate the inversion, espe-

cially in the case of thunderstorms (e.g. Lienau, 1989). In winter, cyclones travelling east bring extensive amounts of rainfall, but the exact position of these cyclones is highly dependent on the type of westerly circulation, high- or low-index. A special situation may arise when North-South gradients evolve and cause northerly winds which may result in extensive rain- and snowfall during the winter months (Lienau, 1989; Furlan, 1977).

In general, the western coast of Greece receives higher precipitation and temperature differences between summer and winter are less pronounced. In comparison, the County of Lagadas is characterised by a transition towards a continental climate component, with higher temperature gradients and lower precipitation rates. Macedonia in general and Lagadas County in particular show a sub-mediterranean precipitation regime and maximum rates are encountered in spring and autumn.

A further modification of the local wind, precipitation and irradiance patterns is exerted by local relief conditions, resulting in mountain-valley or land-sea breezes. Given the structure of Lagadas County (Fig. 4.20), luv- and lee-effects determine local precipitation rates depending on the respective wind direction. Although this is highly variable, a general influence of elevation can be noted. With increasing elevation, precipitation rates increase while temperatures decrease (compare Fig. 4.21), which is especially important with regard to vegetation periods, the occurrence of frost etc (e.g. Huttary, 1950).

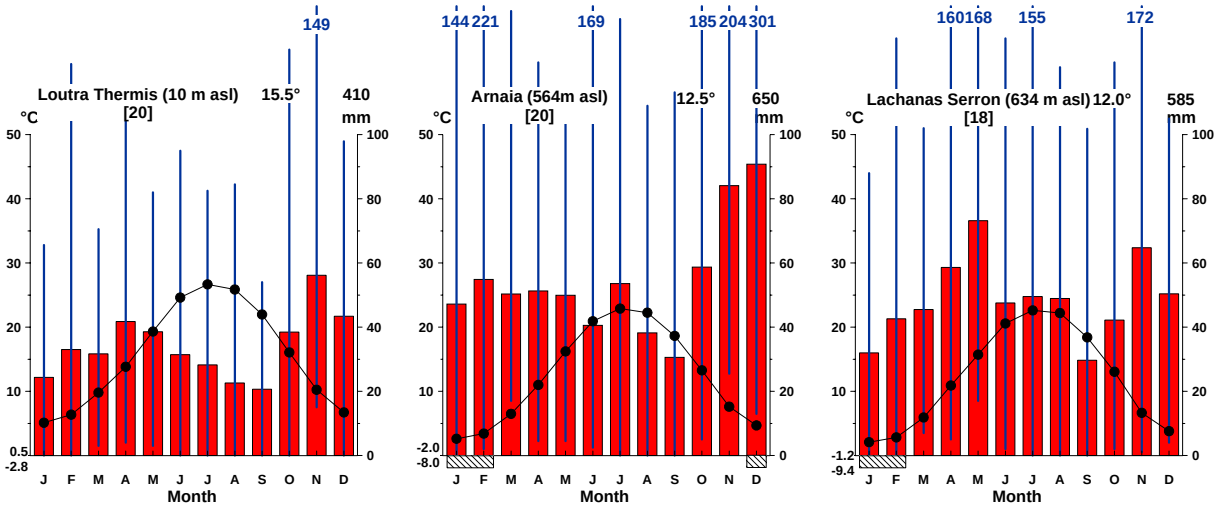

Fig. 4.21: Climate charts for the Lagadas test site after the climate chart system developed by Walther (1955). Blue lines show the minimum and maximum precipitation amounts recorded during the observation period; values exceeding 140 mm were clipped and are indicated by labels with the actual precipitation values (data by NAGREF)

All data have been recorded by the Greek National Meteorological Service and made available through NAGREF. *Loutra Thermis* is located just outside the County perimeter, southeast of *Thessaloniki*. *Arnaia* lies on the mountainous ridge separating the valley of Mygdonia from the *Gulf of Orfanos*, and *Lachanas Serron* is the northernmost village in the County (compare Fig. 4.20).

First of all, the influence of elevation on temperature and precipitation is evident, with the earlier decreasing and the latter increasing from the low-elevation to the two high-elevation stations. This is underlined when the maximum precipitation records are viewed. In addition, the shift of the precipitation peaks to spring and autumn is evident for *Loutra Thermis* and *Lachanas Serron*. Comparing the two high-elevation stations, the differences in precipitation magnitude are apparent. The station of *Lachanas Serron* shows a stronger seasonal component, while *Arnaia* shows a more balanced record for the first months of the year, with peaks occurring in November and December. Two reasons must be noted here: the close proximity of the Sea triggering a stronger maritime component and local circulation systems. Secondly, the West-East orientation of the *Mygdonia* depression, which facilitates the passage of cyclones travelling with a westerly current that cause advective rains at the eastern mountain ridge.

According to Konstantinidis & Tsiourlis (2003), the study area can be classified as semi-arid to sub-humid and be sub-divided into three zones. A thermo-mediterranean semi-arid climate type that can be found in the zones of low altitude (up to 200-300 m asl) with an annual precipitation of around 450 mm. The second zone can be described as meso-mediterranean sub-humid, covering the altitudinal range from 200-300 m asl up to an altitude of 600-800 m asl. Here, winters are considerably cooler, however frost is rare. The amount of precipitation is higher, summing up to approximately 550-800 mm per annum. The third zone is the sub-mountainous region above 600 m asl in north-oriented slopes and above 1000 m asl in the south-oriented ones, where the climate is continental with several days of snow and an average precipitation of 800 mm (Konstantinidis & Tsiourlis 2003; Le Houérou 1981).

4.2.2 Geology

Greece is generally assigned to two major geological formations. The Hellenides-Orogene, which is primarily made up of sediments and magmatites and aligns in direction of NNW-SSE. The second major formation consists of crystalline and metamorphic masses, which govern most of northern and northeastern Greece, the Rhopode-Kyklade Massif and the Serbo-Macedonian Massif. In general, the area of Lagadas County belongs to the Serbo-Macedonian Massif which follows the general NNW-SSE tendency (Jacobshagen, 1985; Meyer & Kockel, 1985).

The eastern boundary of the Massif is delineated by a series of faults which mark the transition to the wide *Strimonas Valley*. To the West, multiple foldings separate it from a marginal trough evolved as a subduction zone on the continental slope between the Serbo-Macedonian Massif on the Eurasian continent and the ancient Axios Ocean (Pippan, 1976; Psilovikos, 1993). The Massif is further structured by a series of intersecting grabens and troughs, such as for instance the valley of *Mygdonia*, which were filled with thick sedimentary deposits, mainly of contintental sources with marine and brackish intrusions.

Fig. 4.20 highlights the pronounced topographic structure of the test site. This results from neotectonic activities, which have ‘recently’ activated exogenic processes and initiated substantial tectonic activity, testified in the County by earthquakes and the presence of mineral springs (Psilovikos & Sotiriadis, 1983; Psilovikos, 1993; Goldsworthy et al., 2002).

A detailed study on the neotectonic graben complex of the Promygdonia Basin (corresponding to Mygdonia watershed) can be found in Psilovikos & Sotiriadis (1983). They distinguish three major lithological zones.

- The eastern part, which includes *Mt. Kerdilio*, along the borderline with the *Strimonas Basin*, made up of gneiss, biotite-hornblende gneiss, amphibolite and marble horizons. They belong to the Kerdillion formation as the lower and oldest rock group of the Serbo-Macedonian Massif and date to the Paleozoicum – Pre-Paleozoicum.
- The central part, including the mountains of *Vertiskos* and *Holomondas*, which consists of three sub-units:
    - Vertiskos formation with mica-gneiss, mica-schist, biotite gneiss, amphibolite, augen gneiss, schistose granite sills, pegmatoids and metasediments (paleozoic to prepaleozoic)
    - Amphibiolites, pegmatitic gabbros, uralitic leucogabbros on the eastern side of Volvi hills and serpentinized peridotite dunite on the western side of the graben at *Mavrouda* (paleozoic to prepaleozoic)
    - Local granitic intrusions of different character (mesozoic).
- The western-southwestern part along the mountains *Hortiatis-Holomondas*, consisting of phyllites, quartzites, sandstones, flysh type sediments with limestone olistholiths as well as bedded limestones, marbles, dolomite and shale marls. With lower abundance, ryolite, acid tuff and quartzite form the known volcano-sedimentary series (scythian-permian-jurassic).

These types of bedrock form the basement of the *Promygdonia Basin* and are the source for neogeneous and quartenary sediments deposited in the grabens, of which *Mygdonia Valley* is the most prominent. Psilovikos & Sotiriadis (1983) identify three topographically closed areas: the *Vromolimnes* between *Mt. Kerdilio, Mt. Vertiskos* and *Volvi Hills* at the northeastern part of the basin; the *Marathoussa*, between *Mt. Stratoniko, Mt. Holomondas* and the *Platea Hills* at the southeastern part of the basin; and the *Zangliveri*, between *Mt. Hortiatis* and the *Platea Hills* and the southern part of the basin (Psilovikos & Sotiriadis, 1983).

In a simplified representation, Fig. 4.22 indicates the major types of bedrock that are encountered in the test area as a result of the processes and properties described in the previous section.

Metarmophic rocks – represented by different gneiss varieties – are dominating along with pyroclastic intrusions. The main valley of *Mygdonia* and other tectonic depressions are characterised by alluvial sediments. To the contrary, limestones, tertiary deposits and basic rocks only appear in isolated and highly confined locations (Savvaidis et al., 2000).

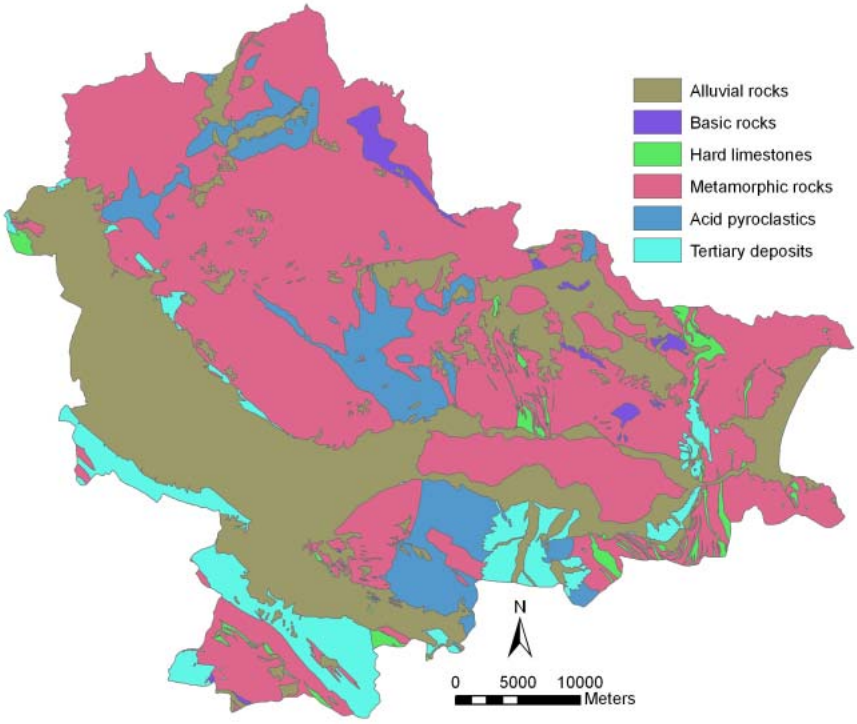

Fig. 4.22: Major types of bedrock and sediments in Lagadas County (source: IGME geological map 1:50,000)

4.2.3 Soils

Under Mediterranean climate conditions, soil formation processes are very slow (compare section 4.1.3). Due to the slow weathering rate of the given bedrock most soils are generally shallow and in a rather low development stage. This is especially pronounced where slopes are steeper and ablation of particles occurs (e.g. Schultz, 2000; Boer et al., 1999).

In the Lagadas area, soils emanating from the metamorphic minerals are generally neutral to moderately acidic and poor in nutrients. They include a low level of bases and organic matter, and a high content of silicate and iron. Soils evolving from granodiorites, that are rich in silicates, are acidic. Clay mineral formation takes place due to processes of chemical weathering and soils can therefore be rich in clay (Konstantinidis & Tsiourlis, 2003). Important soil types for the Lagadas area are:

- Leptosol and Regosols: Shallow Leptosols evolve on hard silicate basic rock. These raw soils dominate especially in the hilly and mountainous areas and comprise a major fraction of sand and loam, frequently associated with a layer of duff (Lienau, 1989). Regosols are poorly developed, shallow soils that are not limited in depth by the bedrock. Both Leptosols and Regosols are poor in nutrients. They have a low capacity to store water and are not attractive for agricultural usage (Schultz, 2000).
- Cambisols: The mesotrophic or oligotrophic Cambisols are possible relicts from other periods, as they have properties which must have developed under different climatic conditions. The advanced stage of development of these soils is manifested in a high fraction of clay minerals and a loss of carbonates in the upper layer (Schultz, 2000).

They show a slightly developed profile with an A-, B- and C-horizon, but without sharp boarders between the layers.

- Alluvial soils: Quarternary alluvial soils constitute a major class in the area. They are predominantly found in the Mygdonia Basin as well as in the other depressions and grabens. These dark soils often hold a fluctuating ground water level and are highly fertile (Papanastasis, 2003b). As a result of the specific tectonic properties of the Lagadas area (compare sections 4.2.2 and 4.2.4) they are frequently characterised by the presence of sediments deposited in the former lakes under a wide range of sedimentary regimes, i.e. marine, lagoonal, estuarine, brackish, lacustrine, fluviolacustrine, deltaic, fluvial and alluvial (Psilovikos & Sotiriadis, 1983). Depending on the properties of the former lakes and the type of sediments deposited, soils that have evolved under submarine conditions may be very fertile, with high water capacities and pore volumes (Schachtschabel, 1989).

Fig. 4.23 gives a generalised overview on major patterns of soils in the test area.

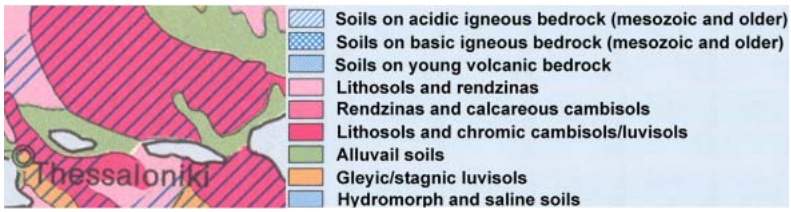

Fig. 4.23: Major soil types in Greece (subset taken from Lienau, 1989, after Kayser & Thompson, 1950)

Soil depth is primarily connected to topographic aspects and land use (Lienau, 1989; Boer et al., 1999; compare also section 4.1.3). In the mountainous rangeland areas that are mainly utilised for grazing, dominantly shallow soils and occasionally even bare bedrock occurs. This, together with the slow soil formation processes, makes the area highly vulnerable to soil erosion. On the other hand deep, fertile and well-developed soils prevail in depressions as well as in arboreous regions. (Konstantinidis & Tsiourlis, 2003; Papanastasis, 2003b).

4.2.4 Hydrology

Specific Mediterranean properties result from the uneven distribution of precipitation and the torrential nature of many rainfall events. Their general implications for soil erosion have been previously discussed (section 4.1.4). Lagadas County is associated with the wider Mygdonia watershed and is divided into 14 sub-watersheds. A dense network of rivers, ditches and ravines covers the region. Surface runoff collects in the drainage system and can scale up to torrents in the rainy season, contributing substantially to erosion in the area. On the other hand these rivers easily run dry in the hot summer period (Papanastasis, 2003a).

Referring back to the geological setting of the area (section 4.2.2), especially the graben structures are of interest in the context of hydrological properties. The presence of these grabens and the connected intramountainous plains led to the establishment of a number of lakes. The *Vromolimnes grabens* were uplifted in the lower Quarternary, cut off from the sea and filled

with fresh water which drained towards *Lake Volvi*. In 1950 both lakes were artificially drained. This plain, north of Lake Volvi, is well visible in Fig. 4.20 at the village of *Mavrouda*. It is now used for intensive agriculture due to the presence of fertile sediments and alluvial soils (Psilovikos & Sotiriadis, 1983). In the South, the small grabens of *Doubia* and *Adam* were tectonically separated from the *Marathoussa* and *Zangliveri* grabens during the Quartenary and another small lake formed at *Adam*, which was also artificially drained (Psilovikos & Sotiriadis, 1983).

The most important changes, however, have taken place in the main valley of *Mygdonia*. Here, the large *Mygdonia Lake*, covering 500 km^2, was cut off from the *Strimonas Basin* at the beginning of the Quarternary and filled up with water. The present *Lakes Volvi* and *Koronia* are the only remnants of this large ancient lake and of considerable importance for the local economy. *Lake Koronia* is used as the main source of irrigation, while *Lake Volvi*, with a total surface area of 68 km^2 the second largest freshwater lake in Greece, presents important fishing grounds. This hydrological system has experienced severe ecological threats due to strong utilisation. In 1975, the lakes have been listed under the RAMSAR list of wetlands of international importance, but in the last years especially *Lake Koronia* has experienced a reduction in water level of 90 % (Karavokyris et al., 1998).

The tectonic activity described here and in section 4.2.2 is reflected in the landscape structure. Although elevation from the main valley to the peaks rises gradually, a sequence of deep valleys and channels cuts through the generally undulating areas and connects high elevation zones and intermittent depressions to the bottom of the valley. Frequently, these channels and gullies show a high altitude gradient. Depending on the availability of water, which is highly variable (compare sections 4.1.1 and 4.2.1), they may carry considerable sediment loads (Psilovikos & Soitaridis, 1983). The magnitude of these processes is closely linked to recent tectonic movements, as a result of which erosion processes were widely activated. As the present-day lakes are very important, the drainage network providing them with water provides an important element in the interacting ecological and socio-economic factors of Lagadas County.

4.2.5 Vegetation

In a biogeographical sense, Greece lies at the intersection of Europe, Asia and Africa, where the European character and the Mediterranean and Balkan European sub-division are of greatest influence for most taxa. Especially the eastern Mediterranean is of interest, as it is situated at the biogeographic crossroad between the continents (Di Castri, 1991).

Historically, the Mediterranean has experienced major invasions of plant and animal species. Invasions are promoted due to the climatic framework, disturbance such as fire events or grazing, and interactions by man. With respect to the long history of utilisation of the Mediterranean, the present pattern of plant communities considerably differs from the potential natural vegetation (e.g. Le Houérou, 1981; Trabaud, 1994; Quézel, 2004; compare also chapter 2). Groves (1991) concludes, that a large proportion of the plant species in the Mediterranean Basin stems from northern Europe or from other regions of Mediterranean climate (e.g. *Eucalyptus, Casuarina, Pinus*).

In general, high diversity at all ecological levels may be found in Greece (i.e. genetic, population, species, habitats, communities, ecosystems). Throughout its complex geological and ecological history, tectonic, eustatic, climatic and biotic interactions have created highly changing environmental conditions. Especially water and temperature stress during the summer months, year-to-year fluctuations of the distribution of rainfall, and topographic diversity exert major effects on plant populations (Raven, 1973; Legakis, 1998).

The Southeast of Europe is located at the interface of the Euro-Siberian, the Mid-European and the Irano-Caspian floristic zones, whereas the higher peaks of the mountains are covered by flora of sub-alpine type. Northern Greece has a close climatic, physiognomic and phytosociological relation with the continent and is considered an area of transition from the thermo-mediterranean to the meso-mediterranean zone (Braun-Blanquet, 1952). Corresponding to the climatic conditions and the altitudinal gradients (section 4.2.1) three vegetal domains can be distinguished. The thermo-mediterranean zone is referred to as *Quercion ilicis* and the potential vegetation is forest of evergreen, sclerophyllous species also known as high, dense maquis (Konstantinidis & Tsiourlis, 2003). In higher altitudes, plants adapt to cooler conditions in winter by shedding of leaves; hence thermophilous deciduous forests prevail in this zone. Within this *Quercion confertae* association, oaks (*Quercus frainetto, Quercus pubescens)* as well as chestnuts (*Castania sativa*) are characteristic. Above elevations of 600-1000 m asl a zone of sub-mediterranean, continental vegetation follows. Here the climate is more cold and humid and several species of beech form typical Mediterranean mountainous forests (*Fagion moesiacae* association*),* with *Fagus moesiaca* being the one most abundant. Furthermore, *Fagus orientalis* and *Fagus sylvatica* thrive in this region (Dafis, 1975; Le Houérou, 1981; Konstantinidis & Tsiourlis, 2003).

Although thermo-mediterranean evergreen forests and meso-mediterranean broadleaved woods are the potential natural vegetation for the major part of northern Greece, sclerophyllous shrublands dominate due to the human interaction through cutting and grazing activities (Lienau, 1989; compare also chapter 2). This vegetation formation can also be described as sclerophyllous pseudo-maquis, the dominating vegetation formation of the *Sklerea* biome (King et al., 1997). Today, it is typical for the eastern Mediterranean, especially where semi-arid and sub-humid climate types dominate (Le Houérou, 1981). In many locations, these vegetation communities are interpreted as degraded forests and dominate at altitudes below 600 m asl.

In the context of the GeoRange project, Konstantinidis & Tsiourlis (2003) procured a spatial data base of habitats of Lagadas County at scale 1:20,000 shown in Fig. 4.28. It is based on the Natura 2000 habitat key (Dafis et al., 1999). Natura 2000 is the EU network of conservation areas designated by the Member States under the habitat directive (EEC/92/43 Directive) in 1992. The following compact description is largely based on their findings.

Shrublands of varying density are dominating in Lagadas County, where they account for around 46 % of the land cover. According to their density, these typical rangeland communities can be subdivided into three distinctive units: dense (shrub/tree-fraction of 70-100 %), medium dense (shrub/tree-fraction of 40-70 %) and sparse (shrub/tree-fraction of 10-40 %), the latter forming a transition to grasslands.

With its resistance to grazing due to its spiny small leaves, its resilience to fires and its competitiveness due to fast resprouting and coppicing abilities, the kermes oak (*Quercus coccifera)* is by far the dominant species. Also *Quercus ilex* is present in high percentages. They are accompanied by characteristic Mediterranean evergreen species such as *Pistacia lentiscu*s, *Phillyrea media, Olea europaea* var. *sylvestris, Erica arborea,* constituting the association *Oleo-Lentiscetum*. In the higher altitudes of this zone (300-500 m asl) deciduous Mediterranean shrubs like *Spartium junceum* and *Crataegus monogyna* are also encountered (Konstantinidis & Tsiourlis, 2003). Herbaceous species, especially aromatic *Labiatae* and *Fabaceae,* are numerous in this area, represented for instance by *Anemona hortensis, Medicago ssp., Trifolium ssp., Allium ssp. Melica ciliate,* among others (Konstantinidis & Tsiourlis, 2003). In the grasslands the main species are for example *Hieracium ssp., Bromus ssp., Holcus lanatus, Poa bulbosa, Dactylus glomerata, Rumex acetosella, Daucus carota, Thymus vulgaris* and *Melica ciliate* (Konstantinidis & Tsiourlis, 2003). Frequently, grass communities consist of a high number of annual species together with some perennial grasses (Lienau, 1989). As these grasslands are a result of intense grazing activities, thorny shrubs are favoured. Species like *Quercus coccifera, Crataegus monogyna, Juniperus oxycedrus* and *Prunus spinosa* belong to this group.

Fig. 4.24 to Fig. 4.28 depict typical manifestations of the rangeland area of Lagadas, more images illustrating the occurrence of different types of rangelands can be found in Fig. 10.8.

Fig. 4.24: Transition between grasslands and sparse/medium dense shrublands

Fig. 4.25: Sparse degraded shrublands

Fig. 4.26: Dense shrublands

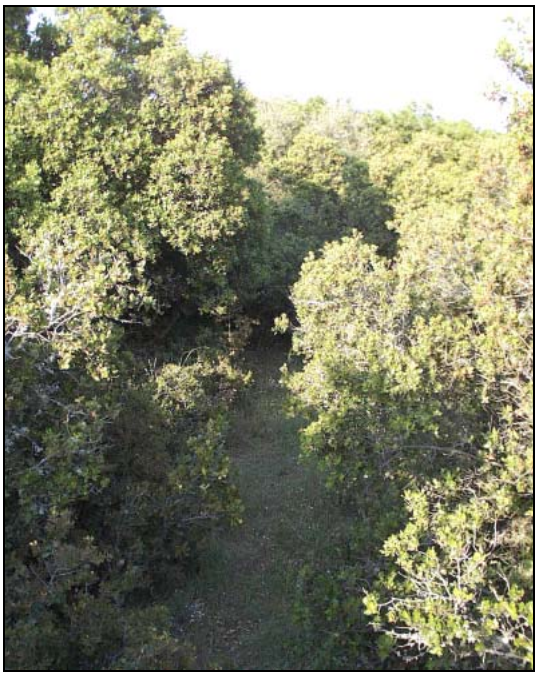

Fig. 4.27: Dense shrublands with trees of *Quercus coccifera*

The thermophilous oak forests (*Quercion frainetto*) occur in the meso-mediterranean zone covering elevations from 300-400 m asl to 600-800 m asl. A major part of these forests has been degraded to shrubland communities through grazing and intense forestry activities. However, especially at higher altitudes spacious oak forests can be found which are mainly composed of *Quercus frainetto, Quercus pubescens* and *Fraxinus ornus*. In the dense shrub layer *Quercus coccifera, Juniperus oxycedrus, Rosa canina, Coryllus avellana* and *Carpinus orientalis* thrive. The herbaceous layer presents species such as *Viola reichenbachiana, Pteridium aquilinium Brachypodium sylvaticum, Trifolium ssp., Veronica chamaedrys* and *Lapsana communis*. Common grasses are *Poa nemoralis, Carex caryphyllea* and *Dactylus glomerata*. Where conditions are more humid and irradiation rates are higher, these forests are often associated with *Castania sativa* (Chestnut) and *Quercus dalechampii; e*specially on clay-sandy soils this is frequently observed (Konstantinidis & Tsiourlis, 2003). The warmer conditions also allow thermo-mediterranean species to advance to these habitats (e.g *Quercus ilex, Pistacia lentiscus*). Additionally, a transition zone to the domain of beech and mixed beech woods (*Fagion Moesiacae)* can be found, with species such as *Fagus moesiaca, Fagus orientalis, Abies borisii regis*, and *Pinus nigra (*Spanos et al., 2001*).*

The zone of deciduous, sub-mountainous beech forests (*Fagion moesiacae*) is predominantly found in elevations above 600-800 m asl. Characterised by trees species of *Fagus moesica* and *Fagus orientalis,* further species include *Castania sativa* and some oak species (e.g. *Quercus dalechampii*), *Fraxinus ornus* and *Sorbus torminalis* (Konstantinidis & Tsiourlis, 2003). In addition, the shrub layer is predominantly composed of *Ilex aquifolium, Acer platanoides, Rubus ideus* and *Taxus baccata*. Characteristic is also the abundance of grasses and forbs, especially in gaps and forest clearances. The term ‘forbs’ accounts for all the herbaceous species except grasses and include both annuals and perennials (Papanastasis, 2003a). Typical species are for instance *Poa nemoralis, Dactylus glomerata, Luzula forsteri, Pteridium aquilinum, Melica uniflora* and *Viola hirta*. On acidic locations *Luzula-Fageteum* beech

forests prevail. Here the dominating tree species is *Fagus sylvatica* and the forests are characterised by the presence of *Luzulo luzuloides.* Typical is also the occurrence of acidophilous species such as *Vaccinium myrtillus* and *Mycelis muralis* (Konstantinidis & Tsiourlis, 2003).

Furthermore, a number of small habitats are found which are confined to highly specific environments, such as the dune-, halophytic- and rocky coast-habitats, accounting for 0.1 % of the County surface, or the plane woods, *Salix* and *Populus* galleries and reed beds found along rivers and the lakes, representing another 0.7 % of the total area (Konstantinidis & Tsiourlis, 2003).

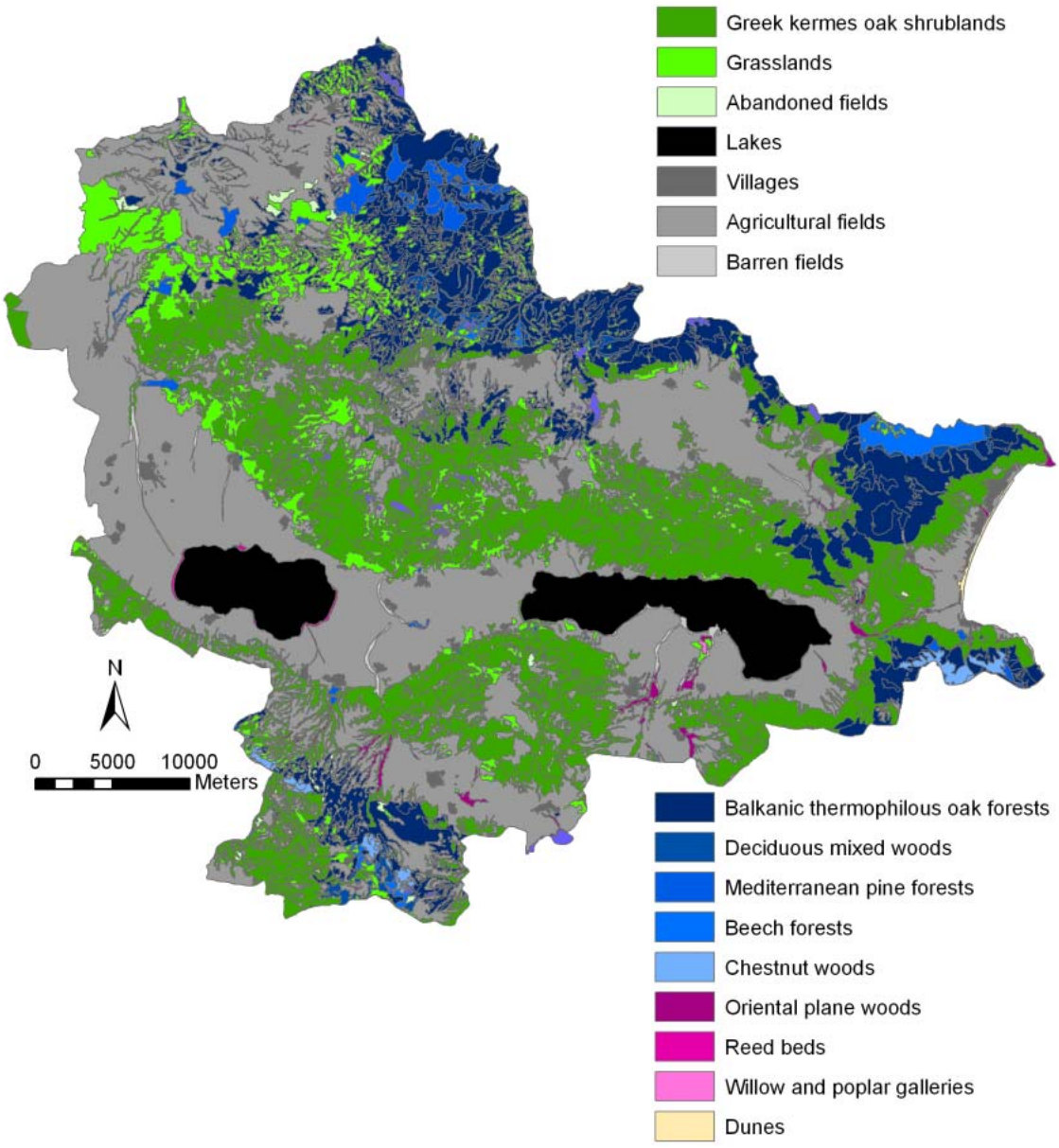

Fig. 4.28: Major vegetation formations in the Lagadas area. Vectors were derived from aerial photography and field surveys; they are based on the Natura 2000 habitat key (Konstantinidis & Tsiourlis, 2003)

Fig. 4.28 shows a simplified and aggregated representation of this spatial database. From a floristic point of view, highest diversity in the County can be found in the niche habitats and at higher altitude zones. On the other hand, agricultural areas and rangelands account for the majority of the surface of Lagadas County. These rangelands represent a valuable landscape element with respect to the local economy, but also due to their ecological and aesthetical value (e.g. Papoulia et al., 2003; compare also section 2.1 and 2.4). They will hence be at the focus of the further analysis (chapter 10).

4.2.6 The grazing system

Although livestock grazing is an important factor in the County of Lagadas, the proximity of the industrial and economical centre of the city of Thessaloniki as well as the tourist centres of the Chalkidiki peninsula provide for additional sources of income beside rural activities. This contributes to the specific properties of the area compared to other grazing regions in Greece, which are still more oriented towards traditional pastoral systems.

In the region of Thessaloniki and Macedonia, large rangeland areas favour extensive or semi-intensive pasture farming. Around 30 % of the total number of sheep in Greece and approximately 32 % of Greece's goats can be found in this area (Hadjigeorgiou et al., 1998). In Lagadas County, rangelands amount to 98,761 ha, differentiated into evergreen shrublands (73 %), grasslands (16 %), deciduous shrublands (7 %), partially forested areas or open woodlands (3 %) and abandoned fields (1 %) (Papanastasis, 2003a). In this environment, livestock breeding of almost exclusively sheep and goats has been the most important factor for centuries. It is mainly carried out for meat production of dominantly lambs and kids, and secondly for milking and manufacturing of dairy products (Hadjigeorgiou et al., 1998). Historically, the husbandry system can be characterised as a shepherded, extensive grazing system, a land use form which is especially adapted to less favoured areas (Hadjigerogiou et al., 1998). The system is mainly based on rangeland utilisation where shepherds guide their animal flocks through the grass- and shrublands. In the winter period, animals are occasionally held in paddocks and during late summer and early autumn the herds find additional nourishment in the form of cereal stubble on agricultural land after harvesting (Yiakoulaki et al., 2002). As with most regions of the European Mediterranean, grazing activities have been of dominant influence on the landscape configuration found in the Lagadas region today. Especially by the end of the 19th and the beginning of the 20th century, when the number of inhabitants and domestic animals largely increased, the forests of the Lagadas area underwent severe degradation and were to a large extent transformed into *Quercus coccifera* shrubland. In addition, forests were also transformed into agricultural land in the 1920's and 1930's, resulting in severe land degradation and erosion (Papanastasis, 2003b). From the 1950's and 1960's on, this process was partially reverted and the general reduction in the number of animals described before was also effective in Lagadas. This in turn resulted in areas of undergrazing or complete elimination of grazing (Papanastasis, 1998). Forests spread again, also due to intensive reforestation and urbanization in the 1960's and 1970's. The latter moreover lead to a further decrease in domestic animals and to an abandonment of agricultural land.

Following further reductions in animal numbers, it was only with Greece joining the European Union in 1981 that animal numbers rose again. However, despite of constantly high

numbers of animals, the grazing system of the Lagadas area has undergone severe changes in the past decades. If formerly shepherds were travelling long distances with their flocks and staying out in the rangelands over night in a kind of transhumance system, they nowadays only carry out daytrips (Yiakoulaki et al., 2002). This dramatically limits the area that is actually being grazed, leading to over-grazing for regions where livestock is concentrated and often animals are held in sheds for considerable time. In the last years an increasing but still extensive use of feedstuffs makes the production system semi-intensive. Feedstuffs given to the animals include for instance corn, wheat, barley, rye, oat and alfalfa hay and are used to increase milk production and prolificacy (Yiakoulaki et al., 2002).

On the other hand, undergrazing of less accessible locations occurs, especially the traditional summer pastures in mountain regions received a great reduction in grazing pressure (Zervas, 1998). As a result, further forest dispersion occurred, in particular at higher elevations and shrublands have become thicker and thicker through the years due to the lack of grazing influence (Papanastasis, 2003b). As a consequence, rangelands develop towards their natural climax state or, where areas are severely degraded, towards a pseudo-shrub vegetation climax state. Today, the rangelands are communally grazed with stable grounds. Especially the trend towards milk production, that has been observed over the last years, lead to a more sedentary grazing system in the Lagadas area (Tsiourlis, 2003).

It is notable, that the grazing system applied in most of the Lagadas region is considerably different to the grazing activities that are carried out in other parts of northern Greece (e.g. the Chalkidiki peninsula). There, the shift in grazing systems is not as advanced and more traditional ways of rangeland utilization are implemented (Tsiourlis, 2003). For the study area, seasonal trends became obvious in the last years due to the fact that the actual grazing activity is carried out only during a few hours every day. In winter the animals graze mainly during the day. In the hot summer, grazing is carried out chiefly in the morning and in the evening while animals remain ruminating in the shade during the afternoon. The composition of flocks is usually mixed and includes both sheep and goats (MODMED, 1998; Fig. 4.29).

This seasonality is superimposed by modifications of the grazing scheme according to the respective elevation. Domestic animals graze during the entire period of the year at the low zone (< 200 m), 9-10 months at moderate altitudes (200-600 m) and 6-7 at higher elevations (600-1000 m) (Papanastasis, 2003b). Animal statistics according to the National Statistical Survey of Greece (NSSG) are given in Table A.1 (Appendix). The figures reflect the general trends described before. Fig. 10.2 depicts the history of stocking rates in the different communities, and it is evident that developments differ depending on the elevation and location in relation to other landuses. Nonetheless, total animal numbers and stocking rates are rather high in some communities.

Fig. 4.29: Mixed flock of sheep and goats on grassland patch

Due to rural abandonment and urbanisation, shepherding is mainly carried out by men of the older generation. According to Hadjigeorgiou et al. (1998) more than 82 % of the shepherds are older than 45 years. Animal husbandry is labour-intensive and not as profitable as the cultivation of crops like tobacco or cotton. Thus efficiency of animal farms can often only be maintained if family work prevents the farmer from paying wages to farm hands (Hadjigeorgiou et al., 1998). In addition, European Union policy plays an important role for animal breeding in the region. Considering the expansion of the European Community, it is unsure whether subsidiaries will be available to livestock farmers to a comparable extent as they are nowadays. In addition, an increasing demand for dairy products and to some extent for goat meat can be observed over the last years, making animal husbandry slightly more attractive to producers (Hadjigeorgiou et al., 1998). Farmers have chiefly reacted to changes in the socio-economic framework and the principles of subsidiary payments by intensifying grazing systems while the total number of animal farms has declined. The net income of farmers primarily depends on the number of animals, and hence flock size is expected to further increase in the future. At the same time a further shift from transhumance towards more sedentary, lowland grazing systems and paddock breeding is the most likely scenario (Boyazoglou & Flamant, 1990; Hadjigeorgiou et al., 1998).

5 Geometric data processing

Systematic and non-systematic geometric distortions result from the design and operation of satellite platform and sensor system in combination with characteristics of the Earth surface. As stated in sections 3.2.1 and 3.5, these need to be accounted for when to enable a multi-temporal analysis and integration of different sources of date.

The Landsat sensors are 'whiskbroom scanners', employing an oscillating mirror to reflect incoming radiance to the detector system. It consists of 16 detectors for each of the bands in the reflective wavelength domain for the Thematic Mapper (MSS: 6). The resulting image covers a swath width of 185 km. The most important geometric errors resulting from the given constellation are:

- Earth rotation skew
- Panoramic distortion depending on the distance of a pixel from nadir
- Distortions resulting from the planar representation of the curved surface
- Scan time skew distortion resulting from the onward movement of the platform
- Pixel size distortions resulting from a varying oscillation speed of the mirror
- Variations in platform speed, elevation and orientation
- Geometric inaccuracies resulting from different locations of the detector planes

(USGS, 1984; Richards & Jia, 1999)

The system correction applied to Landsat-MSS and -TM data prior to delivery accounts for these errors, where systematic components can be treated in a standardised manner, while non-systematic components are accounted for using specific tracking devices hosted on the satellite platform (USGS, 1984).

In addition to these distortions common to all Landsat-based sensors, MSS data exhibit an oversampling in across-track direction, where the ground sampling distance is 57 m, while the instantaneous field of view (IFOV) is 79 m, leading to a 22 m overlap between adjacent pixels (aspect-ratio-distortion). Images displayed with pixel sizes of 79*79 m^2 appear stretched in x-direction and incorporate a low-pass effect. Consequently, a spatial deconvolution is applied to MSS data prior to further correction to account for this effect (USGS, 1979; Richards & Jia, 1999). MSS data included in this work were pre-processed accordingly.

System-corrected data sets are available in a planar space-oblique mercator projection, and need to be transferred into a reference cartographic projection system (Lillesand & Kiefer, 2000). The relation between 'distorted' image and 'reference' system is established by identifying corresponding points in the distorted satellite image and in reference data sets, such as aerial orthophotos, ortho-referenced satellite images or topographic maps. Recently, it has also been proposed to employ illuminated digital elevation models (Hill & Mehl, 2003). These 'ground control points' (GCPs) are employed to calculate a transfer function between distorted image and reference system. Depending on the type of data to be processed and the

distortions to be corrected, transfer functions may range from linear functions to polynomials of higher orders. Considering the quality of Landsat data and the system correction already applied, transfer to a reference map projection involves only translation, rotation and change of scale, such that a first-order polynomial (affine projection) is sufficient (Bähr, 1985; Richards & Jia, 1999).

The transfer function between image coordinates (x', y') and reference coordinates (x,y) can thus be expressed as

$$x = a_0 + a_1 x' + a_2 y' \text{ and } y = b_0 + b_1 x' + b_2 y' \tag{5.1}$$

where the constants a_0, a_1, a_2, b_0, b_1 and b_2 can be retrieved based on a minimum of three GCP pairs. If more GCPs are available, the potential error can be minimised by minimising the following equation

$$\sum_{i=1}^{n}\left[x_i - \left(a_0 + a_1 x_i' + a_2 y_i'\right)\right] \text{ and } \sum_{i=1}^{n}\left[y_i - \left(b_0 + b_1 x_i' + b_2 y_i'\right)\right] \tag{5.2}$$

with n = number of GCPs

The accuracy attained by this function can be assessed using the root mean squared error (RMSE), defined as

$$RMSE_x = \sqrt{\frac{\sum_{i=1}^{n}\left(x_i - x_i'\right)^2}{n}} \text{ and } RMSE_y = \sqrt{\frac{\sum_{i=1}^{n}\left(y_i - y_i'\right)^2}{n}} \tag{5.3}$$

for x- and y-directions, and

$$RMSE_{xy} = \sqrt{\left(RMSE_x^2 + RMSE_y^2\right)} \tag{5.4}$$

for the total RMSE.

However, it has to be noted that these error estimates only correspond to the GCP pairs.

Once the transfer function has been established, the indirect method is commonly employed in order to avoid the occurrence of data gaps. This departs from the destination grid and assigns the respective location in the (distorted) source grid. Different resampling algorithms are available to calculate the digital numbers in the corrected image from the pixel values neighbouring the target position in the distorted image. Here, 'cubic convolution' resampling was chosen, which does modify the original pixel values, but results in a smoother output (Richards & Jia, 1999).

The Universal Transverse Mercator (UTM) system was chosen as a reference, which is one of the most widely used coordinate systems for local to regional scale applications, resulting in accurate planar representations for map scales of 1:250,000 or larger. It is a cylindrical conformal projection system, subdividing the globe into 60 zones of 6° longitude each, which are characterised by their centre longitudinal meridians (Hake, 1982). In order to minimise distortions across the zone, a scale factor equal to 0.9996 is applied at the central meridian. A

number of reference spheroid and datum definitions exist, which aim at best representing the Earth's surface for a given area. These are expressed through their inverse flattening distance and the length of their major and minor axes (spheroid), and by their position compared to the WGS84 reference position (datum) using seven parameters (x-y-z translations, ω-θ-κ rotations, and scale variation) (Malling, 1992).

5.1 Topography-induced distortions

Images acquired with opto-mechanical scanners show a typical cartographic representation of the Earth's surface, with a parallel projection in along-track, and a central projection in across-track viewing direction. It is the latter which distorts the image, with the magnitude of distortion increasing with distance from the satellite nadir and the elevation of the surface element. Evidently, this source of error is essentially non-systematic, and can not be accounted for by transfer polynomials. However, if the elevation is known, sensor elevation and distance from nadir can be employed to calculate the magnitude of the resulting radial pixel-shift. Especially in terrain with a strong relief gradient it is crucial to adequately account for this terrain-induced distortion, which may lead to shifts of several pixels, thus greatly hampering the interpretation of multiple data sources. The shift can be calculated according to

$$\Delta X = \frac{H_p \cdot x}{H_S} \text{ or } \Delta X = H_p \cdot \tan(\Theta) \qquad \text{[m]} \qquad (5.5)$$

with ΔX = offset of a pixel x
H_p = elevation of the given location x
H_S = altitude of the satellite platform
$\tan(\Theta)$ = angle between nadir and the line connecting platform and pixel

(Itten et al., 1992; Pala & Pons, 1995).

5.2 Ayora

For the Ayora test site, the most common UTM adaptation for the Iberian Peninsula was chosen (Table 5.1).

Table 5.1: Cartographic reference projection for the Ayora test site

Projection system	UTM, Zone 30
Longitude of central meridian	0:00:00.000000° E
Latitude of central meridian	0:00:00.000000° N
False easting	500,000 meters
False northing	0 meters
Scale factor at meridian	0.9996
Spheroid	International 1909
Semi-major axis	6378388.0
Semi-minor axis	6356911.94613
Datum	European 1950 (Portugal, Spain)
dx dy dz dω, dθ, dκ, ds	-84, -107, -120, 0, 0, 0, 0

As a geometric reference for collecting GCPs, official topographic maps (1:25,000) procured by the Centro Nacional de Informaciónes Geográfica (CNIG) were available for the test site. For the Landsat-TM images, GCPs were collected iteratively, which was complicated by a lack of adequate image features. Easily decipherable features, such as major roads, road crossings etc. are missing in the core area, where different types of rangelands and forests prevail. These are only accessible by tracks and small roads, which are difficult to locate in satellite imagery with the given resolution. Nevertheless, a number of major firebreaks and other landmarks could be identified in both satellite imagery and maps, such that a satisfactory distribution of GCPs was attained.

During the time of geometric data processing, a new software tool became available which facilitates GCP collection through an automatic process[1] based on local correlations (Hill & Mehl, 2003). Using one uncorrected and one corrected master image, their relative orientation has to be approximated using 3 GCPs. Employing this preliminary orientation, the algorithm calculates window-based correlations between the images, thus identifying candidate GCPs where highest correlations appear. Compared to a visual collection of GCPs, this approach overcomes limitations of human perception, which is strongly biased by known surface features, and also identifies corresponding locations based on pattern properties. This way, a large number of candidate GCPs can be retrieved, which then undergo a visual inspection and plausibility check prior to processing.

The corrected TM image for 1984 was degraded to 90 m and then resampled to 79 m resolution using bilinear interpolation to match the geometric resolution of MSS and the low-pass effect associated with the MSS sampling characteristics (compare section 5). The correlation

[1] The software tool 'findgcp' was developed by Wolfgang Mehl at the Joint Research Centre of the European Commission, and was kindly made available for this study.

analysis algorithm described above was then employed to identify a large number of GCPs for the subsequent resampling process.

The geometric correction directly incorporated a digital elevation model based on 10 m contours from 1:10,000 topographic maps, with an estimated vertical accuracy of 3 m and an original horizontal resolution of 25 m. This had been resampled to match the resolutions of TM and MSS using a bilinear interpolation. Table B1 (Appendix) gives the number of GCPs included in the calculation of the transfer function and the corresponding RMSE estimates.

All single and total RMSE values indicate an estimation of the transfer function with subpixel accuracy, which is important for the subsequent pixel-based trend analysis. Further to that, a visual inspection by overlays confirmed the high quality of the correction with good coincidence between satellite images of different dates as well as between satellite images and the 1:25,000 topographic map.

5.3 Lagadas

In addition to the general UTM zones, a specific Greek UTM adaptation exists. Since most local data are stored in this projection format, it was chosen as the reference projection for this study, and specifications are given in Table 5.2.

Table 5.2: Cartographic reference projection for the Lagadas test site

Projection system	Transverse Mercator
Longitude of central meridian	24:00:00.000000° E
Latitude of central meridian	0:00:00.000000° N
False easting	500,000 meters
False northing	0 meters
Scale factor at meridian	0.9996
Spheroid	GRS 1980
Semi-major axis	6378137.0
Semi-minor axis	6356752.31414
Datum	EGSA87
dx dy dz dω, dθ, dκ, ds	-199.799; 74.281; 246.454; -8.678e-08; 2.424e-09; 3.248e-08; -1.7e-08

In Greece, the availability of geographic data has traditionally been limited due to military restrictions. Large scale topographic data are hence not available for many regions. For this reason, a 1:50,000 topographic map formed the geometric basis to collect GCPs for the Lagadas test site. The Landsat-TM image acquired June, 5th, 2000 was employed as the reference, for which GCPs were iteratively collected. Digital elevation data with 30 m resolution were acquired, which were procured from photogrammetric analysis of aerial photography. Following the correction of the master image, the GCP retrieval algorithm described before was used to derive GCP pairs for the remaining TM images.

Employing the identified GCPs and the DEM, the satellite images were geometrically referenced following the principle described in section 5.1, and the number of GCPs and RMS estimates are given in Table B.2 (Appendix).

Sub-pixel accuracy could be attained for all corrected images. As far as the limited quality of the topographic map permitted, the visual comparison of satellite images and the reference confirmed the generally high accuracy. Comparison between images showed a very high coincidence even in the terrain with a strong relief gradient. As a result the time series of satellite imagery can be considered highly consistent within itself, but care has to be taken when overlaying this information with auxiliary spatial information.

For a small area at the core of the Lagadas test site, a Quickbird image was acquired in 2003 (geometric resolution at nadir: panchromatic band: 0.61*0.61 m^2, multispectral bands: 2.44*2.44 m^2). Given the specific properties of the Quickbird image acquisition strategy, the image consists of four overlapping tiles, two recorded on July, 3rd, and August, 3rd, 2003, respectively. Different off-nadir looking angles correspond to the different acquisition dates (Table 5.2). The single tiles were delivered as standard image type, i.e. a photogrammetric correction accounting for sensor orientation and camera properties had already been applied, resulting in geometric resolution of 0.6*0.6 m^2 (panchromatic) and 2.4*2.4 m^2 (multispectral). A rough correction for topography-induced distortions using a digital elevation model with 250 m resolution had also been performed. Using the GPS data recorded during image acquisition, the resulting image was projected to a standard UTM reference grid with WGS84 ellipsoid and datum. In addition, an auxiliary data set of Rational Polynomial Coefficients (RPC) was delivered. These describe the mathematical relationship between object space and image space by polynomial functions with 59 coefficients and 10 parameters. Mosaicking of the separate tiles revealed limitations of this standard image rectification: strong differences in viewing angles along with the rather coarse approximation of the relief led to shifts of ~120 m for corresponding features in the overlapping areas, and an estimated accuracy of 23 m (given by Digitalglobe©).

This rather low accuracy called for a refined processing of the single data sets. The information in the auxiliary files was used to re-establish the image characteristics prior to the standard processing and combine it with a sensor and camera model (Leica Geosystems, 2003b). In order to enhance the results, the auxiliary GPS information was complemented by selected field-based GPS positions of well-distributed landmarks identified in the Quickbird image tiles[1]. Using this information and elevation data from the DEM, the Quickbird data were ortho-rectified, and shifts between corresponding surface features were eliminated. Finally, the resulting image was reprojected to the Greek UTM system. (Table 5.3). This processing routine had to be run separately for all image tiles and the panchromatic and multi-spectral bands. Fig. 5.1 illustrates the accuracy of different processing steps when separate tiles are mosaicked.

[1] GPS measurements were kindly carried out by Dr. Georgios Tsiourlis from the National Agricultural Research Foundation – Forest Research Institute (NAGREF-FRI) of Greece, using a Garmin 3+ GPS. 23 positions were measured, with an estimated average accuracy of 3.9 m.

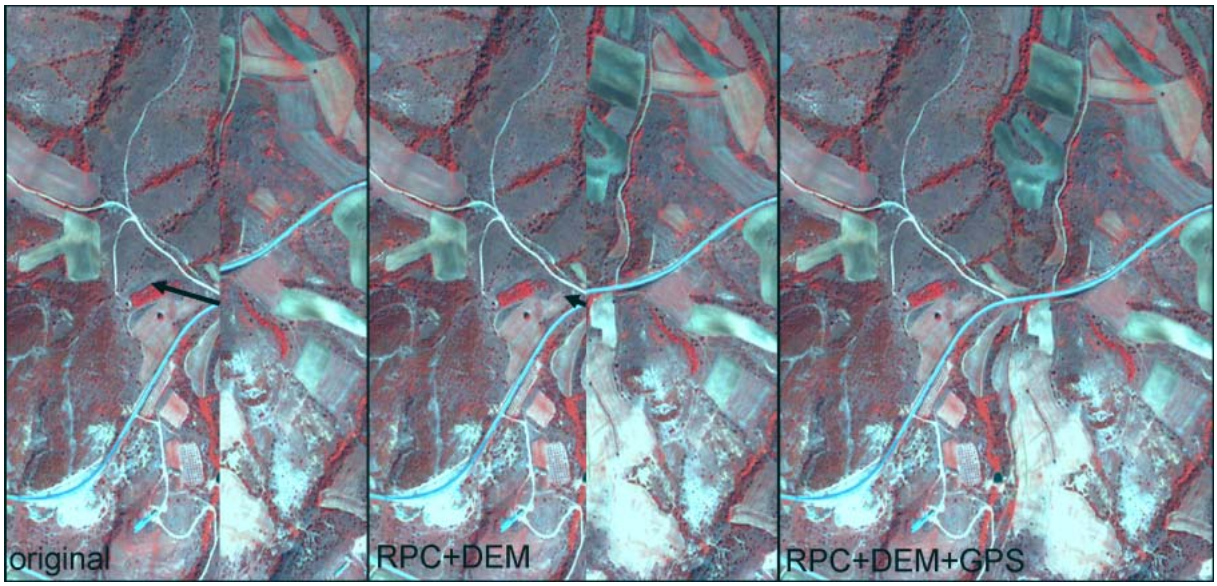

Fig. 5.1: Accuracy of different geometric processing steps shown for mosaicked Quickbird tiles. Left: original tiles; centre: correction using rational polynomial coefficients supplied by Digitalglobe and DEM; right: same as centre, but including GPS-measured ground control points

An overlay with Landsat-TM imagery and the topographic map revealed the achieved accuracy for the full processing (RPC+DEM+GPS), and error estimates are given in (Table 5.3).

Table 5.3: Accuracy attained for processing of the single Quickbird tiles using RPCs and additional reference points

Tile	RMSE (m)
July, 3rd, 2003 (1)	0.7
July, 3rd, 2003 (2)	0.5
August, 3rd, 2003 (1)	1.1
August, 3rd, 2003 (2)	0.9

For comprehensive information about principles of photogrammetric data processing and specific issues related to ortho-rectification of very high resolution satellite imagery refer to Kraus (1996, 1997), Toutin (2002), Toutin et al. (2002), Cheng et al., (2003a, b), Leica Geosystems (2003a, b) or Toutin (2004).

6 Radiometric processing

Early multi-temporal image analyses have often been confined to a comparison of classification results from different dates or periods (e.g. Price, 1987a). With the development of advanced analysis techniques, it has frequently been stated that changes becoming apparent from multi-temporal analyses should only result from intrinsic surface properties, which determine the radiance signal reflected back towards the sensor after irradiation has interacted with the surface (compare sections 3.2.2 and 3.5). While there may be limited cases where radiometric correction is negligible, or simple correction approaches are sufficient (Dinguirard & Slater, 1999; Song et al., 2001), many approaches addressing changing land cover properties will strongly benefit from a full radiometric correction of satellite imagery (e.g. Hall et al., 1991).

Consequently, influences of topography, illumination, viewing geometry and atmospheric properties need to be removed to attain physical quantities that can be used as primary indicators for further interpretation, such as surface reflectance (e.g. Schott, 1997; Du et al., 2002). Orientation of surface elements towards the sun and the sensor as well as neighbouring areas significantly modify the signal recorded at the sensor through variation in illumination properties and shadowing. While a number of simple correction approaches exists (e.g. Holben & Justice, 1981; Conese et al., 1988), an exact correction of these effects requires the integration of digital elevation information (e.g. Itten et al., 1992; Conese et al.; 1993; Hill et al., 1995b).

If a radiometric correction is to be based upon modelling of the radiative transfer through the atmosphere, knowledge of the detector sensitivity is fundamental. Calibration factors characterise the transfer function from digital numbers into physical radiance values, upon which radiative transfer models are commonly based.

6.1 Sensor calibration

Most of the methodologies developed for radiometric correction of satellite imagery start from the physical quantity of spectral at-satellite radiance (L). Given this, knowledge of the sensor calibration is mandatory for subsequent quantitative interpretation approaches. Calibration of remote sensing devices adapted to the time of image acquisition becomes necessary since there are significant changes in the sensitivity of the detectors with time. Conventionally, sensor calibration is expressed as:

$$L_\lambda = a \cdot DN + b \tag{6.1}$$

with L_λ = spectral at-satellite radiance [$mWcm^{-2}\ sr^{-1}\mu m^{-1}$]
a = sensor gain
b = sensor offset
DN = digital number

Alternatively, some authors describe the sensor transfer function according to:

$$L_\lambda = L_{\min\lambda} + \left(\frac{L_{\max\lambda} - L_{\min\lambda}}{DN_{\max}} \right) \cdot DN \tag{6.2}$$

with $L_{\min\lambda}$ = spectral at-satellite radiance for DN=0 [mWcm^{-2} sr^{-1}µm^{-1}]
$L_{\max\lambda}$ = spectral at-satellite radiance for DN=DNmax [mWcm^{-2} sr^{-1}µm^{-1}]
$DN_{\max}$ = maximum DN

or express it as 'Counts per unit radiance' [DNmW^{-1}cm^{-2}sr^{-1}µm^{-1}]. In this case, the 'offset' term can not be retrieved and is often neglected due to its relatively low influence on the signal. Frequently, pre-flight offset values are used instead (Elachi, 1987).

There is a variety of possible causes for the degradation of detector sensitivity, such as the stress of platform and sensor during launch or shifts in sensitivity due to differences in ambient and vacuum pressure conditions. Once in orbit, other potential influences are high-energy irradiance, cyclic thermal inputs from passing in and out of the Earth's shadow, and a general decrease in sensor sensitivity as well as the performance of the calibrator lamps with increasing sensor age. While these effects can be monitored by the internal calibration devices hosted on most sensor systems, these do not characterise degradation of the foreoptics, which may for example be caused by condensation of outgased material onto the cold mirror after launch. Hence, using only internal calibration factors for sensor calibration seems questionable (Holm, 1987; Hill, 1990; Brockmann, 1992). Different research groups have tried to complement internal calibration factors by running vicarious calibration experiments both ground-based and using calibrated spaceborne sensors. These experiments are most commonly carried out in large and homogeneous environments with high reflectance surfaces, such as the White Sands Desert (New Mexico, USA), Lunar Playa (Nevada, USA), or the area of La Crau (Southern France). More recently, Saharan and Arabian desert sites have been introduced for the purpose of vicarious calibration campaigns. Besides, there have also been efforts to establish utilisation of the moon as a stable reference (Gu et al., 1992; Santer et al., 1992; Kieffer & Wildey, 1996; Cosnefroy et al., 1996, 1997; Thome et al., 1997a, b; Rondeaux et al., 1998; Teillet et al., 2001b). Teillet et al. (1997) have provided a framework to characterize land surface used for calibration experiments. A review of approaches to and status of sensor calibration in general can be found in Teillet et al. (1997) and Dinguirard et al. (1999).

The good radiometric performance and sensor calibration of the Landsat-5 Thematic Mapper have been extensively studied and described (e.g. Holm, 1987; Price, 1987a, b; Chavez, 1989; Slater et al., 1986, 1987; Biggar et al., 1994; Vogelmann et al., 2001; Black et al., 2003). It has been stressed that the on-board calibration is especially suited to monitor within-scene variation of the sensor's sensitivity and that it does provide a precise view of the sensor's behaviour on the order of hours to months. For longer periods it needs to be complemented by vicarious calibration exercises (Thome et al., 1997a). In order to describe the temporal development of the detectors, Teillet & Fedosojevs (1995) have proposed a time-dependant calibration function, where sensor gains are expressed as a function of days since launch of Landsat-5 making use of the calibration factors attained from the White Sands measurement

campaigns. While this approach does not approximate non-linear changes in sensitivity, which are indicated by the White Sands measurements, it compensates for irregularities in the acquisition date of these measurements and does provide a tool to infer best-possible estimations of the sensitivity for any image acquisition date.

In this study, Landsat-5 TM calibration has been calculated using a time-dependant function (Fig. 6.1), which is based on the White Sands measured factors as published by Thome et al. (1997a, b). For more recent acquisition dates, estimates provided by Teillet et al. (2001a) following a cross-calibration experiment during the tandem phase of Landsat-5 and -7 were employed. Since notation of these factors does not identify offset parameters, these were set to post-launch values given by Markham & Barker (1986).

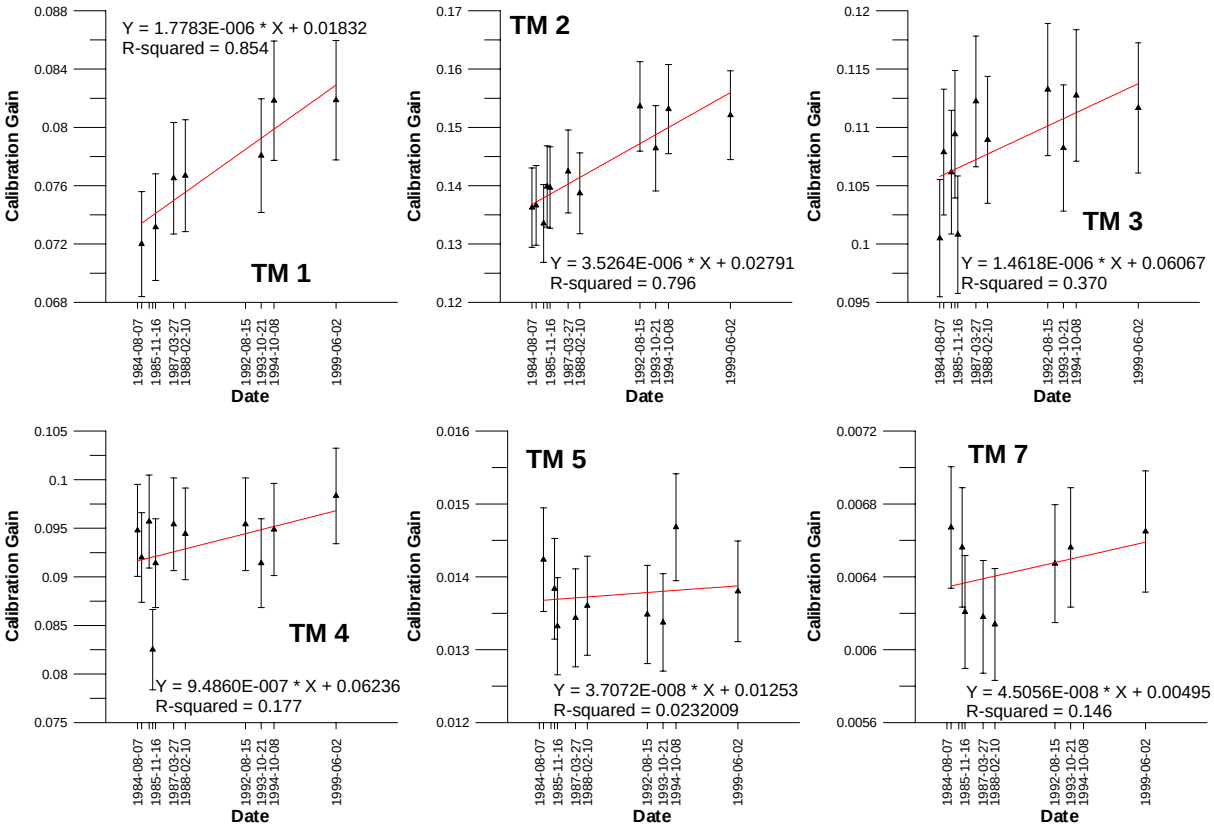

Fig. 6.1: Visual representation of the time-dependant calibration function and the ground based measurements employed; error bars delineate ± 5 % accuracy margins for measurements as given by the authors (Thome et al., 1997b; Teillet et al., 2001)

It is obvious that measurements for all bands show a tendency of degrading sensor sensitivity, although values are clearly fluctuating. Since it can not be inferred which results might be more significant than others, it has been decided to base the calibration function on this linear regression function, and correspondingly the time-dependant function has been calculated.

With the successful launch of Landsat-7, one focus of calibration related research is now set upon validating and complementing the inflight-calibration provided with the data (e.g. Markham et al., 1996; Teillet et al., 2001a; Thome et al., 2001; Black et al., 2003; Chander & Markham, 2003; Markham et al., 2003). In addition, USGS regularly releases updated cali-

bration factors extracted from the internal calibration data stream (http://landsat7.usgs.gov/cpf/). These factors were employed to correct the Landsat-7 images in this study.

In contrast to the exhaustive documentation available for Landsat-5 TM and Landsat-7 ETM+, only little corresponding information exists for the Landsat-MSS sensors, which had been started with the ERTS-1 mission in 1972. According to Price (1987 a, b), during the early period of operational Earth observation engineering challenges were given highest priority and efforts were rather dedicated to construction and maintenance of reliable and long-lasting devices. In addition, image interpretation was largely confined to different classification methodologies for which quantitative physical values were not required. The prerequisite to convert digital numbers to meaningful parameters was only promoted later by the development of quantitative interpretation techniques. For this reason, sensor calibration information for the MSS sensors remains limited to information provided from pre-launch and post-launch calibration (Markham & Barker, 1986, 1987), and does not allow to characterise sensor degradation effects (Price, 1987a). Royer et al. (1988) have analysed radiometric properties of the MSS sensors on board of Landsat systems 1 to 5 based on pseudo-invariant targets and could show significant variations in detector sensitivity both for individual sensors and between sensors. Following Markham & Barker (1987), Pickup et al. (1994) have tried to overcome sensor calibration limitations by performing an empirical line normalisation. They used dark and bright targets to standardise a number of MSS images, and calibrate these to a common standard. This approach is suitable for standardisation of MSS images from different dates, but it does not resolve general ambiguities in the available calibration constants, which may propagate through subsequent radiometric processing steps. Since for the Ayora test site incorporation of images from the MSS sensor systems was mandatory, an approach to radiometric intercalibration was developed, which has been described by Röder et al. (2001, 2005). A simplified version of has already been successfully applied by Hostert et al. (2003a).

On the one hand, a direct intercalibration between Landsat-TM and -MSS is denied by the different spectral setup of these sensors. On the other hand, the Landsat-4 and -5 systems host both the TM and MSS sensors and calibration factors for Landsat-TM are extensively documented (e.g. Thome et al., 1997a, b). As a consequence, synoptic datasets can be acquired, where identical ground segments are recorded under identical atmospheric conditions with different sensor systems. Differences in the recorded signals can then exclusively be attributed to sensor properties, while neither variations in surface properties nor different atmospheric conditions need to be considered. Therefore, Landsat-TM can be used as a calibrated reference to derive calibration factors for Landsat-MSS, provided the differences in spectral and geometric setup of the sensors can be overcome. A detailed description of this approach is provided in section 6.3.4.

6.2 Correction of atmospheric and topographic distortions

The effects of the atmosphere on the signal recorded by earth observation satellites have been extensively investigated (e.g. Tanré et al., 1979, 1981; Diner & Martonchik, 1984a, b; Tanré et al., 1987). It has been concluded that influences of topography, illumination, shadows,

viewing directions and atmospheric properties should be removed to attain physical quantities that can be used as primary indicators for further interpretation, such as surface reflectance (e.g. Schott, 1997; Du et al., 2002). Besides a number of simplified approaches, such as scene averaging, flat-field or empirical line correction (e.g. Roberts et al., 1986; Richards & Jia, 1999), numerous approaches based on full modelling of atmospheric processes have been proposed (e.g. Teillet, 1986; Kaufman & Sendra, 1988; Tanré et al., 1990; Itten et al., 1992; Vermote et al., 1997; Hill et al., 1995b). For most of these, it is desirable to dispose of detailed atmospheric measurements at the time of image acquisition to parameterize the atmosphere model; however, such information is often not available. Different simplified approaches have been suggested to solve this shortcoming, including radiometric normalisation based on known or pseudo-invariant targets (e.g. Schott et al., 1988; Moran et al., 2001) or simple histogram-based haze removal (Richards & Jia, 1999). An alternative approach to derive the driving atmospheric parameters for aerosol scattering directly from the image itself has been proposed by Teillet & Fedosejevs (1995). They suggest using dark targets of known reflectance in an iterative approach to characterise the aerosol optical thickness, which can then be used to parameterise radiative transfer models.

6.2.1 Radiative transfer modelling

The complex interrelation between passage of radiance through the atmosphere, surface properties and the signal recorded by a sensor can be expressed as a set of equations.

Following calibration of digital numbers to 'at-satellite radiance' L, the 'equivalent at-satellite reflectance' ρ* can be calculated according to

$$\rho^* = \frac{\pi \cdot L}{E_0 \cdot \mu_0 \cdot d} \tag{6.3}$$

with ρ^* = spectral at-sensor-reflectance

L = spectral at-satellite radiance [$mWcm^{-2}\ sr^{-1}\mu m^{-1}$]

E_0 = solar irradiance at the top of the atmosphere [$mWcm^{-2}\mu m^{-1}$]

μ_0 = cosine of the solar zenith angle

d = daily variation in sun-earth distance obtained from $d = 1/au^2$; au denotes the average distance from sun to earth in astronomical units

The value of ρ* in reflective wavelength domain is directly related to the surface reflectance factor ρ_t of a given target, but is modified by atmospheric gas absorption and scattering by aerosols and molecules (Tanré et al., 1990).

Given this, atmospheric attenuation and modification of solar radiance propagating through the atmosphere towards the ground and back towards the sensor after interacting with the ground need to be described in order to convert ρ* into the target reflectance at the ground, ρ_t. A number of different radiance fluxes can be differentiated, which contribute to the signal recorded at the sensor (Fig. 6.2).

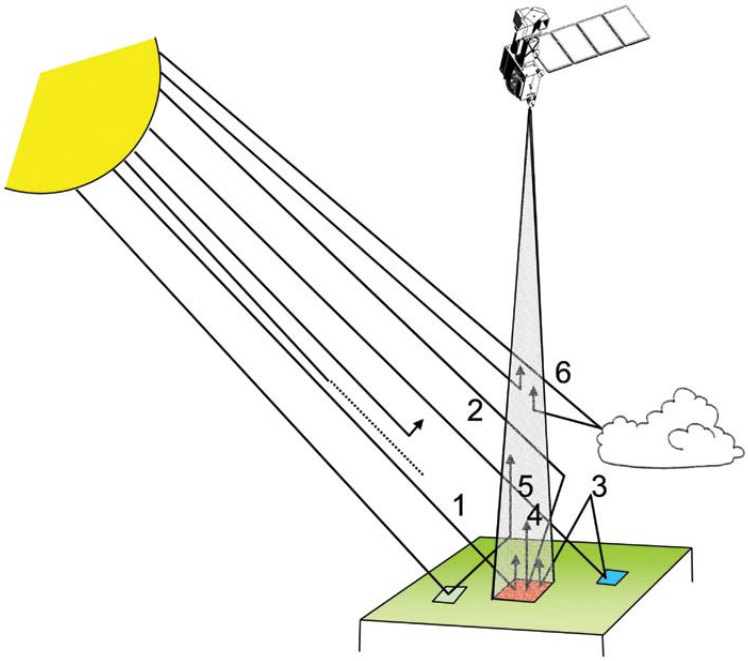

Fig. 6.2: Radiance fluxes and relevant processes between sun, sensor and surface (after Tanré, 1985; descriptions in the text)

According to this characterisation, three downwelling fluxes may be identified:

1) irradiance resulting from downwelling, direct transmission through the atmosphere ($t_{dir\downarrow}$) in dependency of the cosine of the solar zenith angle (μ_s)

2) irradiance determined by diffuse transmission ($t_{diff\downarrow}$) in dependency of μ_s

3) diffuse irradiance after multiple scattering determined by background reflectance ($<\rho>$) and spherical albedo (s)

Three radiance fluxes are received at the sensor:

4) target reflectance (ρ_t), modified by upwelling, direct transmission of the atmosphere ($t_{dir\uparrow}$) in dependency of the observation zenith angle (μ_b)

5) background reflectance ($<\rho>$), modified by diffuse transmission of the atmosphere ($t_{diff\uparrow}$) in dependency of the observation zenith angle (μ_b)

6) atmospheric path radiance (ρ_{at})

All of these terms are subject to the influence of gaseous constituents of the atmosphere, which are accounted for through the gaseous transmission factor (t_{gas}). The most important absorbing constituents are oxygen (O_2), ozone (O_3), water vapour (H_2O), carbon dioxide (CO_2), methane (CH_4) and nitrogen oxide (N_2O). O_2, CO_2, CH_4 and N_2O can be considered globally invariant, while O_3 and H_2O show a variable spatio-temporal distribution. O_3 varies depending on season and latitude, while H_2O is highly variable and hence is a complicated factor to be considered in radiative transfer models. This is especially important given that the short- and mid-wave infrared bands of the Landsat sensors are affected by atmospheric water vapour.

For a Lambertian surface, the relevant interactions in the surface-atmosphere system can be summarised according to:

$$\rho^{*} = t_{gas}\downarrow\uparrow \cdot \left\{ \rho_{at} + \frac{T\downarrow \left[t_{dir}\uparrow \cdot \rho_{t} + t_{diff}\uparrow \cdot \langle \rho \rangle \right]}{1 - \langle \rho \rangle \cdot s} \right\} \tag{6.4}$$

with T = total downward transmission

Solving for ρ_t yields

$$\rho_{t} = \frac{\rho^{*}}{t_{gas}\downarrow\uparrow} \cdot \frac{\cdot \left(1 - \langle \rho \rangle \cdot s\right) - \rho_{at} \cdot \left(1 - \langle \rho \rangle \cdot s\right) - T\downarrow \cdot t_{diff}\uparrow \cdot \langle \rho \rangle}{T\downarrow \cdot t_{dir}\uparrow} \tag{6.5}$$

Provided that the gaseous composition of the atmosphere is known and given the information on exoatmospheric irradiance, all unknown factors can be solved by introducing the optical thickness τ as the quantity driving the radiative transfer. This represents the total extinction of a vertical light beam passing through an air volume and is mostly determined by density and size distribution of molecular and aerosol particles in the atmosphere and on their scattering and absorption properties. Hence, transmission terms can be calculated based on τ.

In this context, it is important to adequately consider the variable scattering behaviour of atmospheric constituents for different viewing angles. While the molecular (Rayleigh) phase function is uniformly varying with viewing/backscattering angle, the aerosol (Mie) phase function depends on the type of aerosol, which can be described by three constants approximated by a two-term Henyey-Greenstein function (Henyey & Greenstein, 1941). Details on molecular and aerosol phase functions and their approximation can be found in Aranuvachapun (1983, 1985), Henyey & Greenstein (1941) and Irvine (1965).

Consequently, atmospheric path radiance, spherical albedo and background reflectance can be calculated incorporating the optical thickness and pre-defined atmospheres (e.g. Kneizys et al., 1980, 1988; Berk et al., 1999), such that the radiative transfer equation is fully dependant on the optical thickness τ.

The optical thickness τ is composed of two components. The first is represented by the Rayleigh optical thickness τ_r, given by

$$\tau_{r} = 0.0088 \cdot \lambda^{(-4.15+0.2\lambda)} \tag{6.6}$$

with τ_r = Rayleigh optical thickness
λ = Wavelength [micron]

which is invariant and solely depending on the wavelength.

The second component is the aerosol optical thickness τ_a, which varies in space and time and is hence the determining factor for the accuracy of radiative transfer models. The aerosol optical thickness τ_a can be expressed using the Ångstrom relation given by

$$\tau_a = \beta \cdot \lambda^{-\alpha} \tag{6.7}$$

with τ_a = Aerosol optical thickness
β = atmospheric aerosol concentration
α = aerosol size distribution

(Ångstrom, 1964)

In principle, precise estimation of the aerosol optical thickness requires sounding, either based on ground measurements or from a balloon, parallel to the image acquisition. Since this is rarely possible, approaches for image-based estimation of τ_a have been proposed (e.g. Ahern et al., 1977; Royer et al., 1988; Teillet & Fedosojevs, 1995), which have suitably been termed 'dark-target approach'. It makes use of reference targets of known reflectance and corresponding surface targets retrieved from the images. Then, the radiative transfer model is parameterised and τ_a set to an initial value corresponding to an aerosol-free atmosphere. This is iteratively increased until the best match is attained between reference reflectance spectrum and the corrected image-based spectrum. Most frequently, dark objects such as seas, lakes or forests are utilised for this approach. This matching is performed on a band-wise basis, such that the correlation coefficient of the logarithmic regression between the estimated aerosol optical thickness and the corresponding central wavelength can be employed as a quality measure of the estimation.

Implementation of the radiative transfer in this work is based on the work of Tanré et al. (1979, 1981, 1985, 1987) and the 5S code (Tanré et al., 1990). The adaptations applied have been described in more detail in Hill & Sturm (1991), Hill (1993), Hill et al. (1995b), Hostert (2001) and Hill & Mehl (2003). In general, these comprise a number of assumptions, which are made to ensure acceptable processing times.

- The atmosphere is considered to be horizontally homogeneous, and absorbing atmospheric gases (H_2O, O_3, CO_2, O_2) are assumed to accumulate at the top of the atmosphere and at the top of the layer between the earth surface and the sensor altitude.
- Lambertian scattering behaviour is assumed and bi-directional reflectance functions are not considered.
- The target surface is assumed to be illuminated by the sun with extraterrestrial irradiance E_0, and a uniform hemispherical sky. In contrast to (<ρ>) and (s), direct illumination from neighbouring terrain is not considered.
- Nadir viewing is assumed for each pixel, since the Landsat systems show a small side-looking angle.
- The surface reflectance is not assumed to be uniform to account for the influence of background radiation from the target environment scattered into the sensor's field of view. A simple correction formalism is adopted to eliminate the major part of this environmental contamination, provided that the aerosol optical thickness is known.

In the present implementation, five different scattering phase functions representing typical aerosol types are available. Transmission values for different atmospheric compositions were

derived using the Modtran 4 code (Berk et al., 1999). Hadjimitsis et al. (2004) emphasised the importance of parameterising radiative transfer models with specific, adapted gaseous transmission characteristics rather than applying a single standard set of parameters for different scenes with variable conditions, which may result in poorer results than those derived from simple empirical models. For different contents of atmospheric water vapour, transmission coefficients are given for H_2O, CO_2, O_3, trace gases, N_2, HNO_3, CO, CH_4, N_2O, NH_3, NO, NO_2 and SO_2 and at a resolution of 5 nm. While O_2, CO_2, CH_4 and N_2O can be considered globally invariant, O_3, H_2O are highly variable. With respect to Landsat-MSS and -TM bands, H_2O is the most relevant parameter, with its concentration significantly affecting bands 4, 5 and 7 (Vermote et al., 1997). This is underlined by Fig. 6.3, which shows the spectral setup of Landsat-TM in relation to atmospheric water vapour transmission.

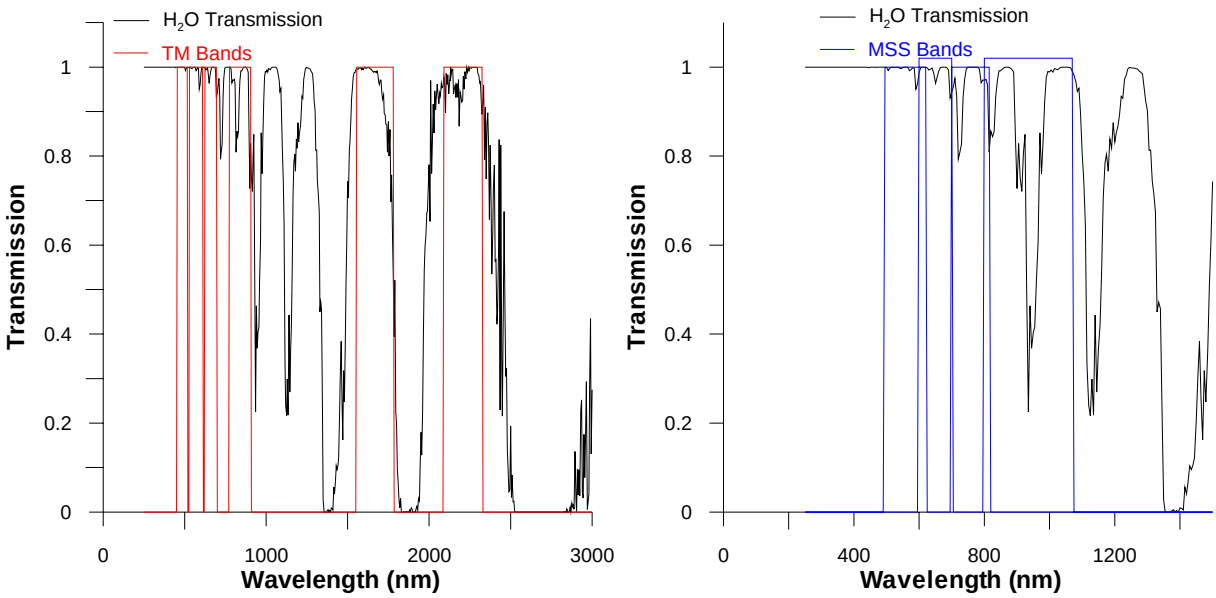

Fig. 6.3: Spectral setup of Landsat-TM and -MSS in relation to atmospheric H_2O transmission; transmission calculated from the Modtran-4 code for a mid-latitude summer atmosphere and a water vapour concentration of 2.92 g/cm^2

To estimate aerosol concentration from the images using the dark target approach, a library of water reflectance signatures from inland lakes was available based on Dekker et al. (1992) and Dekker & Donze (1994). These were complemented by a clear sea water spectrum extracted from a Landsat-TM image of Sardinia, acquired in August, 1985, which was atmospherically corrected with high confidence and supposed to represent open sea conditions.

6.2.2 Integrated topography correction

Further to these considerations and adaptations, a number of authors have demonstrated the strong influence of relief on local illumination and reflectance properties (e.g. Justice et al., 1981; Woodham & Gray, 1987; Itten et al., 1992; Conese et al., 1993). Since the above considerations of the radiative transfer are only valid for horizontal surfaces, a number of approaches have been proposed to minimise topographic effects, such as index calculations based on the variation of the reflectance signal (Holben & Justice, 1981), or image transfor-

mations (Conese et al., 1988). However, an exact quantification is only possible using digital elevation data, allowing to characterise the sun-surface-sensor constellation for each pixel. A simple approach has been proposed based on a cosine correction (e.g. Civco, 1989; Colby, 1991), but since this only incorporates the direct irradiance flux it often results in over-correction (e.g. Itten et al., 1992). The anisotropy index presented by Hay & McKay (1985) and Hay et al. (1986) differentiates direct and diffuse irradiance terms and thus enables a more precise topographic correction. The approach adopted in this work follows ideas presented by Conese et al. (1993) and makes use of the anisotropy index, which is supported by the fact that direct and diffuse radiance fluxes are treated separately in the 5S model.

The direct irradiance flux can be corrected by dividing incoming radiance by the cosine of the angle between the surface normal and the incoming radiance. On the other hand, the diffuse radiance term consists of isotropic and anisotropic components. The anisotropic component has its maximum in the circumsolar and circumzenithal region (Iqbal, 1983) and is cosine-corrected analogous to the direct irradiance term. The isotropic component is corrected irrespective of the position of the sun, by considering the visible sky portion (H), derived from digital elevation data, and the anisotropy index (k), which is defined as the ratio between direct irradiance at the ground and exoatmospheric irradiance. The corrected radiance reaching a pixel is then calculated as

$$E_{cor} = \left(E_0^{'} \cdot t_{dir} \downarrow \cdot \frac{\mu_s}{\gamma} \right) + \left(k \cdot E_0^{'} \cdot t_{diff} \downarrow \cdot \frac{\mu_s}{\gamma} \right) + \left[(1-k) \cdot E_0^{'} \cdot t_{diff} \downarrow \cdot 0.5 \cdot (1+\theta_n) \cdot H \right] \quad (6.8)$$

with E_{corr} = topography-corrected irradiance received at the ground
E_0 = exoatmospheric irradiance corrected for gaseous absorption
γ = cosine of the angle between surface normal and sun zenith
k = anisotropy index
θ_n = cosine of the slope
H = visible fraction of the sky

(Hill et al., 1995b)

In the technical implementation of this correction approach within the modified 5S code, the negligible circumzenithal portion of the anisotropic irradiance is not considered. Hence, in the case of slopes oriented away from the sun, direct and anisotropic diffuse irradiance terms are disregarded, and only isotropic diffuse irradiance is considered. For large slope angles surface reflectance properties may significantly depart from Lambertian behaviour, resulting in an overcorrection of these areas. The consideration of bi-directional reflectance functions would be desirable in this context, and the introduction of a correction factor accounting for this effect has been suggested (e.g. Gu & Gillespie, 1998; Herold et al., 2000; Riaño et al., 2003). However, these often require information of surface types, which can in turn often not be derived with satisfying accuracy prior to radiometric correction. Here, a threshold angle is introduced, and locations with higher slopes are corrected using this angle.

More details on the approach and its technical implementation can be found in Hill et al. (1995b), Hostert (2001) and Hill & Mehl (2003), alternative approaches to topographic nor-

malisation may for example be found in Colby (1991), Itten et al. (1992) or Gu & Gillespie (1998).

6.3 Ayora

As described in Appendix A.1.1, a series of 9 Landsat-MSS and 14 Landsat-TM/ETM+ images were available for the Ayora test site. Since Landsat-MSS data require specific processing, procurement of these data will be treated in section 6.3.4 and following.

Following the approach described in section 6.2.1, the estimation of driving parameters for the radiative transfer calculations based on water targets was pursued. The Ayora test site includes the *Rio Júcar*, which is dammed in some places such that water bodies extending to a few pure pixels can be found in the imagery. In addition, an artificial lake was established at *La Cortada* is included for the first time in the 1985-image. The original full TM scenes extend to the Mediterranean Sea in the East, such that also sea water signatures were considered. Consequently, different water signatures based on an average of several pixels were extracted for each scene. These uncorrected water signatures were employed together with a set of reference reflectance signatures for different water types to estimate the wavelength-dependant aerosol optical thickness. However, no meaningful results could be attained, since the estimates either showed unrealistic Ångstrom-relations or low correlation coefficients for the regression between optical depth and wavelength as described in section 6.2.1. Obviously, this must be attributed to a lack of suitable reference water reflectance spectra.

As a consequence, an alternative iterative approach was followed, making use of expert knowledge gained in past experiments, which intended to enable radiometric correction of the full time series of data while safeguarding its radiometric consistency. In a first step, a comparison of the atmospheric state of the different scenes was performed based on the water signatures extracted before (Fig. 6.4).

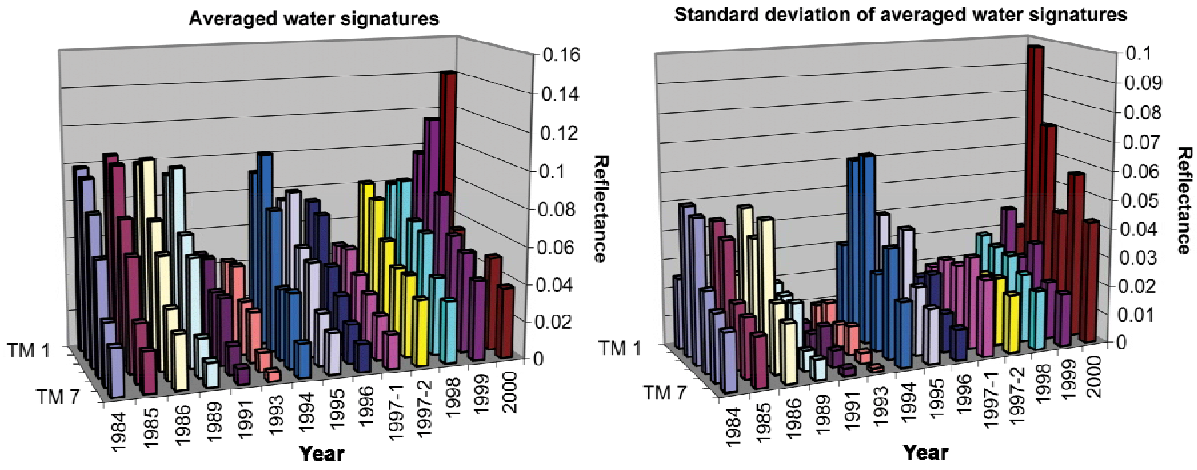

Fig. 6.4: Averaged reflectance spectra and corresponding standard deviations for water targets in different scenes

These signatures were firstly converted to at-satellite radiance. Then the radiative transfer model was parameterised based on clear sky aerosol scattering, an Ångstrom-relation with β=0.1 and α=1, and transmission characteristics of a typical mid-latitude summer situation. Although the resulting water reflectance signatures do not represent real conditions of the respective scene and date, they visualise differences in atmospheric conditions at the different dates. Fig. 6.4 depicts both the average reflectance spectrum for a given year, and the standard deviation for the 6 signatures assessed.

The scenes clearly differ both with respect to the average reflectance level for all targets, as well as concerning the variability between the 6 water signatures analysed for each image, as depicted by the standard deviation. This effect is especially obvious when comparing years 1991 or 1993, with low reflectances and standard deviations, and years 1999 or 2000 with significantly higher estimates especially for reflectances.

Two major factors affect these results both within scenes and between scenes: atmospheric conditions and water properties. Relating to the first, the general type and magnitude of atmospheric disturbance affect the level of reflectance. In addition, the heterogeneity of atmospheric conditions over the scene triggers the variation between the signatures for a single date. The latter effect may be accentuated by the open sea area which is not considered in the actual processing of the data, since the final frame remains limited to the area covered by the digital elevation model. With respect to water properties, several factors can be noted. Climatic conditions encountered in the different years may result in low water levels and hence a reduction of the extension of water bodies and the availability of 'pure' pixels. Besides, more shallow water bodies exhibit higher spectral contributions of bottom of rivers and lakes to the recorded signal. Furthermore, the level of reflectance and the signature are affected by water turbidity and the concentration of different water constituents, such as chlorophyll or sediment particles of different size. Finally, water may reflect higher due to the so-called 'white-cap' effect, caused by waves and the resulting spray on the water surface (e.g. Sathyendranath et al.; 1989; Dekker & Peters, 1993; Dekker & Donze, 1994). During selection of the open-sea targets, potentially affected areas had been excluded through a through visual inspection.

Following these analyses, the 1993 scene was chosen as the reference, corrected first and utilised as a master image for the subsequent correction of the remaining images. This was supported by its position in the middle of the TM time series, clear atmospheric conditions following the above analysis, and the fact that a number of ground truth datasets had been procured in 1993.

6.3.1 Sensitivity analyses

Pior to the actual radiometric correction process, a sensitivity analysis was carried out to assess the influence of the driving parameters. It was based on 19 targets representing different surface types or homogeneous mixtures thereof averaged from a number of pixels in the 1993 image. The image was radiometrically corrected following the approach described in sections 6.1 and 6.2. The model was iteratively run with systematically varying gaseous transmission coefficients, aerosol scattering models and Ångstrom-relations. It is evident that a variation of the aerosol optical depth mainly affects TM bands 1-3, while there is no influence on the near-

and shortwave-infrared bands. This general behaviour is modified depending on the parameters for α and β, and is solely depending on the factor β at 1 µm. The effect of varying water vapour is concentrated on bands 4, 5 and 7, which are affected by major water absorption bands (compare Fig. 6.3). The shortwave bands are influenced by absorption processes of other elements (e.g. O_3), but since the concentration of these elements is almost constant, so are absorption/transmission parameters for bands 1 to 3.

Fig. 6.5 shows column-wise the resulting spectra for an area dominated by limestone (col. 1), an area covered by forest (col. 2), and a water sample extracted from the *Rio Júcar* in the North of the test site (col. 3).

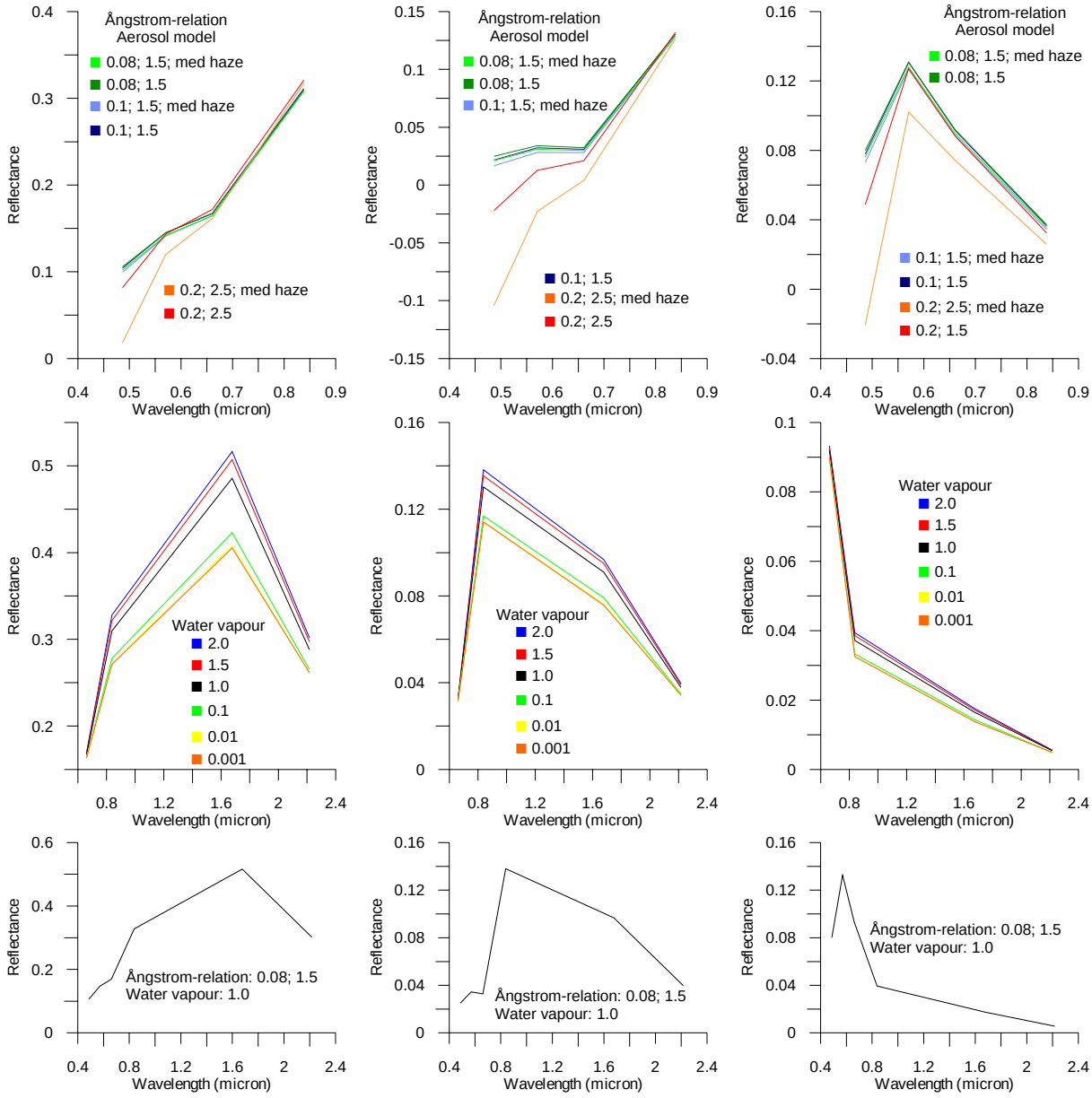

Fig. 6.5: Sensitivity of the radiative transfer model to variations of Ångstrom-relation, aerosol phase function and water vapour transmission (columns: different targets, rows: driving parameters; discussion in the text)

The first row of graphs shows the wavelength domain between 0.4 and 0.9 μm, indicating the effect of varying Ångstrom-relations and aerosol phase functions for a fixed gaseous transmission corresponding to 2.92 g condensed water vapour per cm^2, as a standard for mid-latitude summer conditions. The term 'med haze' indicates aerosol scattering behaviour corresponding to medium haze conditions while the other models were parameterised using a phase function representing continental clear sky conditions. Apparently, assuming hazy conditions in the radiometric correction yields lower reflectance values for identical Ångstrom-relations, and the effect is more prominent for shorter wavelength positions. Especially, a change in the β factor of the Ångstrom-relation significantly influences the radiometric correction. Since it acts as a multiplicative factor, an increasing concentration of atmospheric scatterers also results in lower reflectance estimates. Besides, it is underlined that this domain is essentially related to the shorter wavelengths, and reflectance values converge for TM band 4 in the near infrared.

The second row of graphs shows the effect of varying atmospheric water vapour contents and hence of gaseous transmission. Employing the Modtran 4 code, water vapour concentrations were varied as a fraction of the Mid-Latitude standard value of 2.92 g/cm^2, and consequently been named '2.0' for double concentration, '0,1' for the 10^{th} fraction etc.

The third row shows the reflectance spectrum attained after parameterising the radiative transfer model with β=0.08, α=1.5, clear sky conditions, and the standard gaseous transmission values as given before.

6.3.2 Radiometric correction of the TM time series

Auxiliary data required for the radiometric and topography correction, such as sun position, flight elevation of the sensor, time of image acquisition etc. were extracted from the header files supplied with the satellite imagery.

The radiometric correction of the reference image from 1993 was carried out first[1], followed by the subsequent parameterisation of the remaining images. In the case of Ayora, the selection of invariant homogeneous surface types (e.g. Schott et al., 1988) was complicated by the high frequency of fire events and their large extension. As a result of this highly dynamic landscape, the number of invariant targets covering the full time series is limited. Following iterative adaptations, the radiative transfer models were parameterised according to the calibration factors and parameters given in Tables B3, B4 and B.5 (Appendix), respectively.

A visual inspection of the results underlines the effects of the radiometric processing and the effect of correcting for topography-induced illumination variations (Fig. 6.6). It is composed of three parts representing different processing stages. Part (a) shows the uncorrected image using the same lookup-table that is deployed for the radiometrically corrected image, which is shown in part (b). As a result of the strong scattering due to aerosols, the uncorrected image

[1] AtcPro 3.0 was designed by Prof. Joachim Hill, University of Trier, under the Delphi programming environment, and implements the processing scheme described in section 6.2. Horiz is a C code developed by Wolfgang Mehl, Joint Research Centre of the European Commission. It calculates the information layers necessary to directly incorporate the radiometric correction in the radiative transfer model, such as the cosine between surface normal and sun illumination, local horizon, visible fraction of the sky, slope or shaded positions (compare section 6.2.2). Details can be found in Hill & Mehl (2003).

shows a strong bias towards the blue wavelength region, which is removed after radiometric correction. Part (c) shows the result of radiometrically correcting the image without considering topography-induced illumination variations. The effect of the topography correction leads to a reduction of relief impression, and its success was additionally assessed using surface spectra from different aspects, as given in Fig. 6.7.

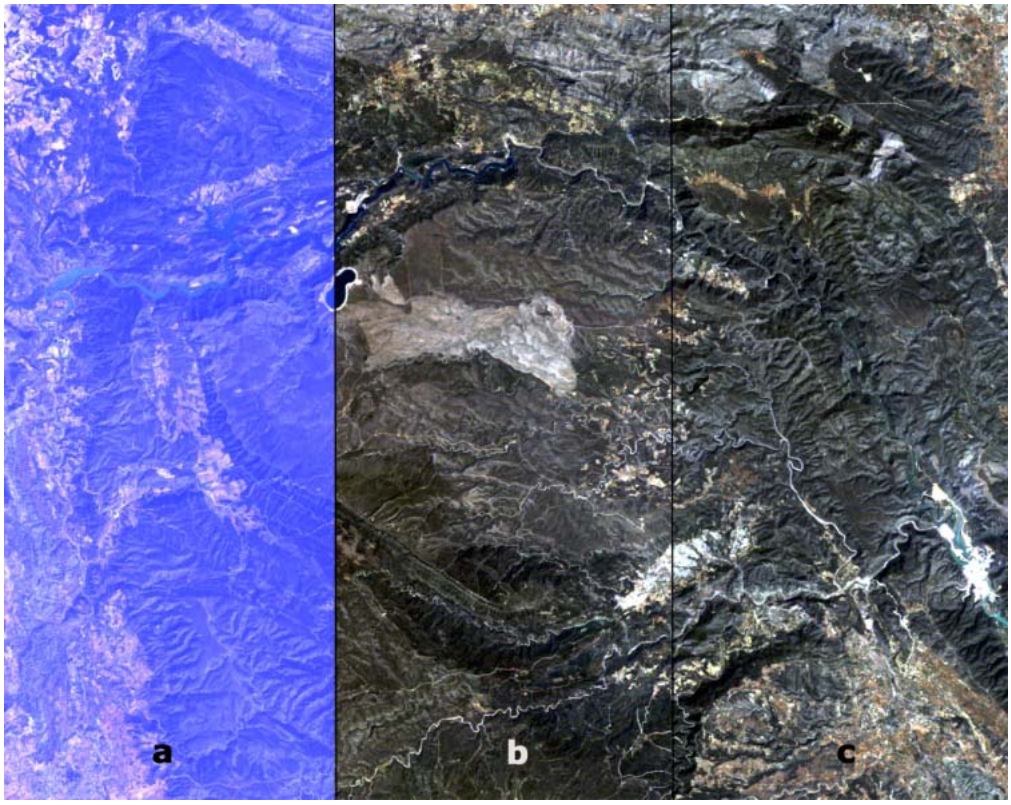

Fig. 6.6: Uncorrected vs. corrected image subset in true colours (RGB = TM 3-2-1) and using identical stretch. a: raw image; b: full radiometric and topography correction including topography; c: radiometric correction without consideration of topography

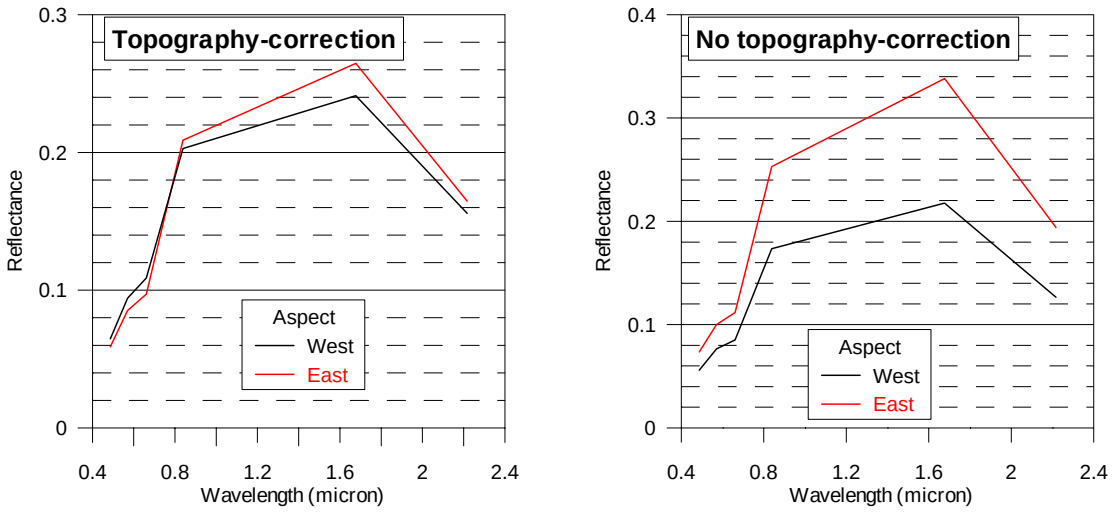

Fig. 6.7: Spectra taken from east- and west-facing slopes after radiometric correction with and without topography correction

Reflectance signatures derived for similar surfaces but different aspects are significantly differing when specific illumination conditions are not accounted for. East-facing slopes show higher reflectance values due to higher insulation in the morning hours, while spectra for East and West-exposition clearly converge as a result of including topography in the radiometric correction process

6.3.3 Validation of the radiometric correction of the TM time series

Different radiometry validation steps were carried out for the 1993 scene, since deficiencies in the radiometric quality of the master image will propagate through all other data sets as a consequence of the adopted processing strategy.

Firstly, a pixel purity index (PPI) was calculated to identify spectrally 'pure' pixels. A random vector is calculated in the multi-spectral feature space, here corresponding to the 6 TM bands. All pixels are projected on to this vector according to their spectral reflectance, and a pre-defined percentage of pixels at the outermost positions along this vector are marked as 'extreme' pixels (e.g. Boardman et al., 1995). This procedure was run for 500 iterations, and only pixels which did not differ more than 5 DNs from the minimum and maximum of the respective vector were identified as candidate pure pixels in each iteration. Finally, a mask of pure pixels was produced showing the number of identification instances for each pixel. The term 'pure' has to be utilised with care in this context, since although the procedure does identify 'extreme' pixels, only some of these do also represent 'pure' surface materials. Also, 'corrupted' pixels may by located using this approach. Disregarding these, spectral reflectance values were extracted for the remaining pixels, and the NDVI was calculated. Only pixels showing either very high or very low NDVI values were considered for the further validation, while intermediate values as potential mixtures of different surface types were excluded. Pixels indicating non-vegetated surfaces were labelled with their most probable bedrock/soil type using the available vector-based information on lithology. This data base of 'pure' reference surfaces was then compared with a library of hyperspectral reflectance spectra which had been collected during various spectral measurement campaigns and for different typical Mediterranean environments (Preissler, 1996; Hostert & Preissler, 1997; Retzlaff et al., 1998; Röder & Hostert, 1998; Röder, 2002). After spectral resampling to match the TM bands, this information was utilised to compare image-derived spectra with reference spectra. Variations in the reflectance level resulting from albedo effects were accounted for through scale factors (Fig. 6.8). Rather than averaged spectra, single spectra were plotted displaying the typical variety of reflectance shapes observed. It also has to be noted, that the locations chosen may actually belong to different geological classes due to scale-dependant generalisation in map digitising. The hyperspectral measurements utilised for this analysis are found in Fig. B.1 (Appendix).

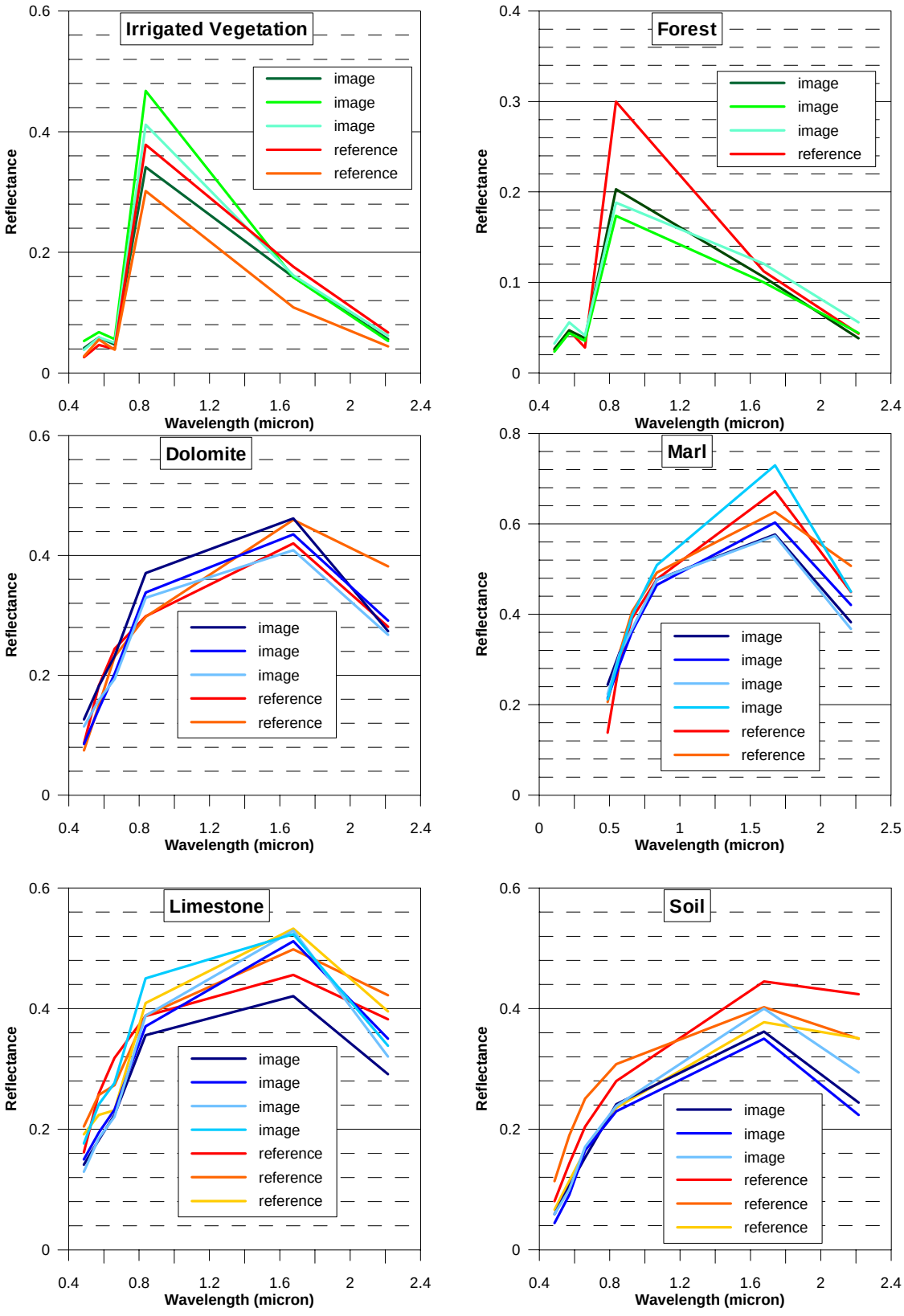

Fig. 6.8: Comparison between image-based and reference reflectance spectra for typical surface types

Since no reflectance measurements of irrigated vegetation have been available, integrated measurements of dense shrubs of *Euphorbia characias* were employed, which also show high contents of leaf water. The spectrum utilised to assess ‘forest’ spectra is a laboratory meas-

urement of a stack of pine needles (*Pinus halepensis*), which explains the obvious deviations comparing measured and image-derived spectra. Generally, in the case of vegetation the scale difference between hyperspectral measurements and reflectances integrated by a pixel is most important to consider. The latter exhibit influences of background reflectance, non-green vegetation elements and a contribution of shading. Especially if stacks of leaves or needles need to be employed, pixel-based spectra of vegetation should be considered as a qualitative indication for correctly pre-processed images.

Assessing different bedrock and soil types, it has again to be noted that given the TM pixel size of 30*30 m^2, even 'pure' spectra are commonly composed of more than one surface material, although one may be dominant (Cracknell, 1998). This is aggravated by the heterogeneity of Mediterranean landscapes. For instance, this effect is obvious in the 'Limestone' sample. Here, reference reflectance measurements of typical limestone rocks with a partial cover of lichens exhibit the typical bend in the reflectance curve at TM band 3, resembling a weak vegetation absorption feature at 0.66 µm. The spectra extracted from the radiometrically corrected image using the PPI show a similar feature, but this is much less pronounced due to the fact that even in areas dominated by bedrock, soil patches and even sparse vegetation elements contribute to the reflectance signal. This effect does also hold true for the other samples, explaining deviations between image-derived and measured spectra.

For some limestone samples, differences in the shape or gradient of the reflectance curves beyond albedo effects may occur in the SWIR. The main reason for this are differences in the carbonate content of different types of limestone, resulting in a stronger absorption feature at 2.34 µm for rocks with higher carbonate concentrations. As TM band 7 ranges from 2.097 µm to 2.349 µm a stronger absorption in this spectral domain will result in lower integrated reflectance spectra and trigger the stronger decrease between bands 5 and 7. For soils, clay minerals show an absorption feature at 2.2 µm, which can lead to a similar effect provided a certain moisture content. Notwithstanding the constraints arising from a comparison of integrated reflectance values on pixel level with punctual reflectance measurements, the analysis demonstrates the quality of the radiometric correction of the 1993 image.

Following the processing of the master image, the full TM time series was corrected. The radiative transfer model was parameterised for the individual scenes to support the closest match between the pseudo-invariant target sets. Target areas were defined to represent homogeneous surface types or stable mixtures of different surface materials, and areas ranged between 1.35 and 7.2 ha (15 to 80 pixels). An adequate size of these target areas is important to account for possible deviations in geometric accuracy through averaging of a larger number of pixels. When validating the consistency of the time series, it was unavoidable that some targets were subject to 'disturbances' at certain dates, which may affect the assessment. These encompass for instance climatological conditions resulting in dryer soils, lower water levels, less photosynthetic activity etc.; furthermore, target areas may be obscured by clouds, areas dominated by lithological background may be influenced by low but photosynthetically vigorous amounts of vegetation etc. Where such obvious cases were detected, they were eliminated from this validation step. Average reflectance, standard deviation, minimum and maximum values were calculated for the remaining signatures (Fig. 6.9). In addition, individual

reflectance curves are included in Fig. 6.9 as dotted lines to illustrate the range of different spectra.

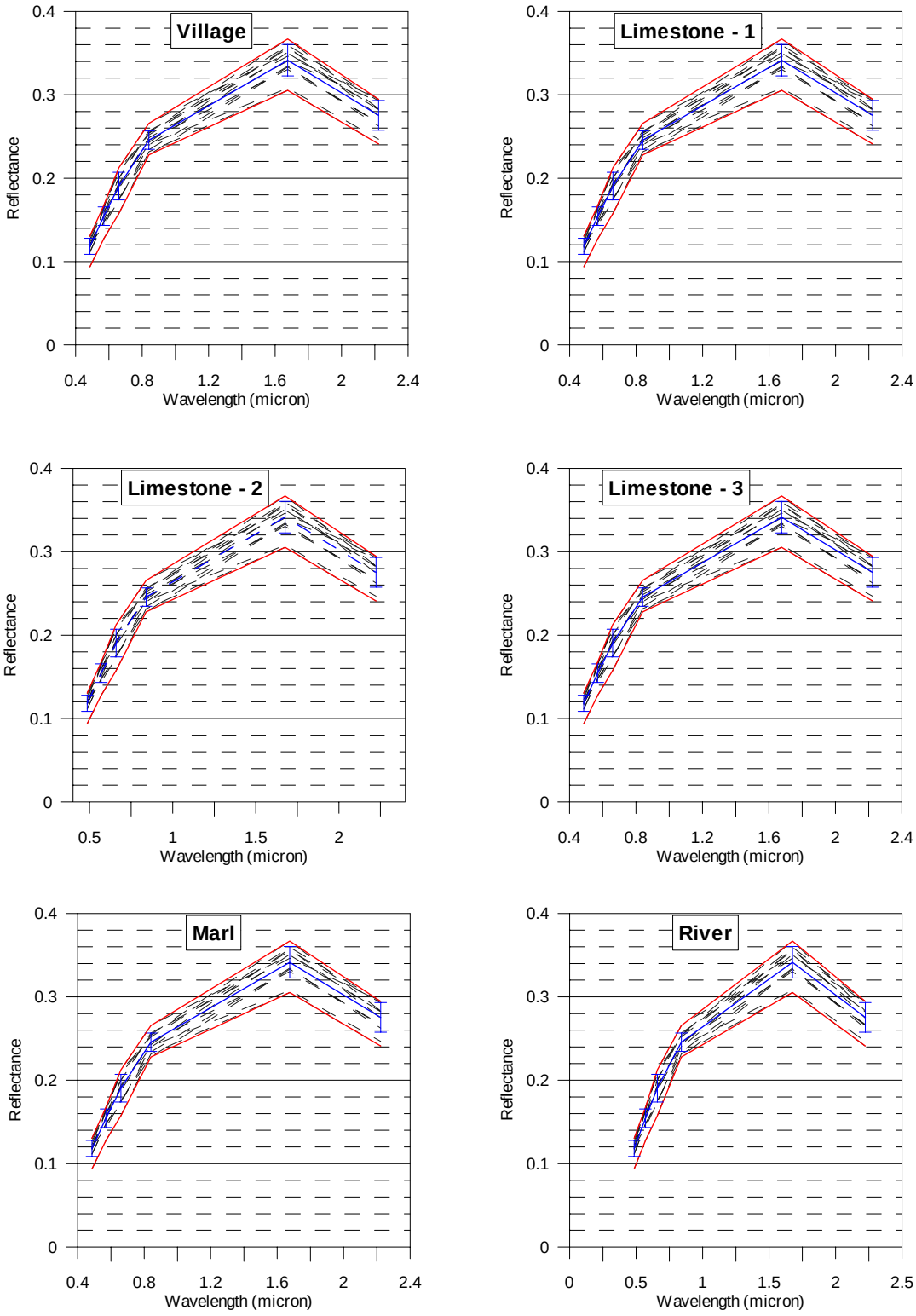

Fig. 6.9: Reflectance values for invariant targets after radiometric correction of the TM time series. Blue lines show average reflectance and standard deviations, red lines indicate overall minimum and maximum value for each feature, dotted black lines show the single spectra (features include 15 to 80 pixels, scenes where the respective area was obscured by clouds were excluded)

It is evident that especially the spectra dominated by bedrock material show a high resemblance for the different dates, while targets comprising certain amounts of vegetation show a higher fluctuation. In general, the correspondence of the spectra after radiometric correction underlines that the prerequisite of high radiometric consistency between the data sets is met, thus supporting the further quantitative assessment of the Ayora data set.

6.3.4 TM – MSS intercalibration scheme

For various reasons no reliable information on the development of the sensitivity of the MSS sensors exists (section 6.1), although this information is crucial in the process of radiative transfer modelling. This problem is further aggravated by the fact that the period from 1972 to 1984 is covered by 5 different MSS sensors, which share major technical specifications, nonetheless calibration factors differ between them. Notwithstanding these constraints, the objectives pursued at the Ayora test site made the integration of Landsat-MSS data an essential prerequisite, such that alternative solutions to radiometrically correcting the MSS data sets were needed. As a consequence, a methodology for radiometric intercalibration to derive updated MSS calibration constants was developed (Röder et al., 2001; Hostert et al. 2003a; Röder et al., 2005). For the Ayora test site the synoptic data set acquired June, 1st, 1984 was employed to derive the calibration constants according to the methodology depicted in Fig. 6.10.

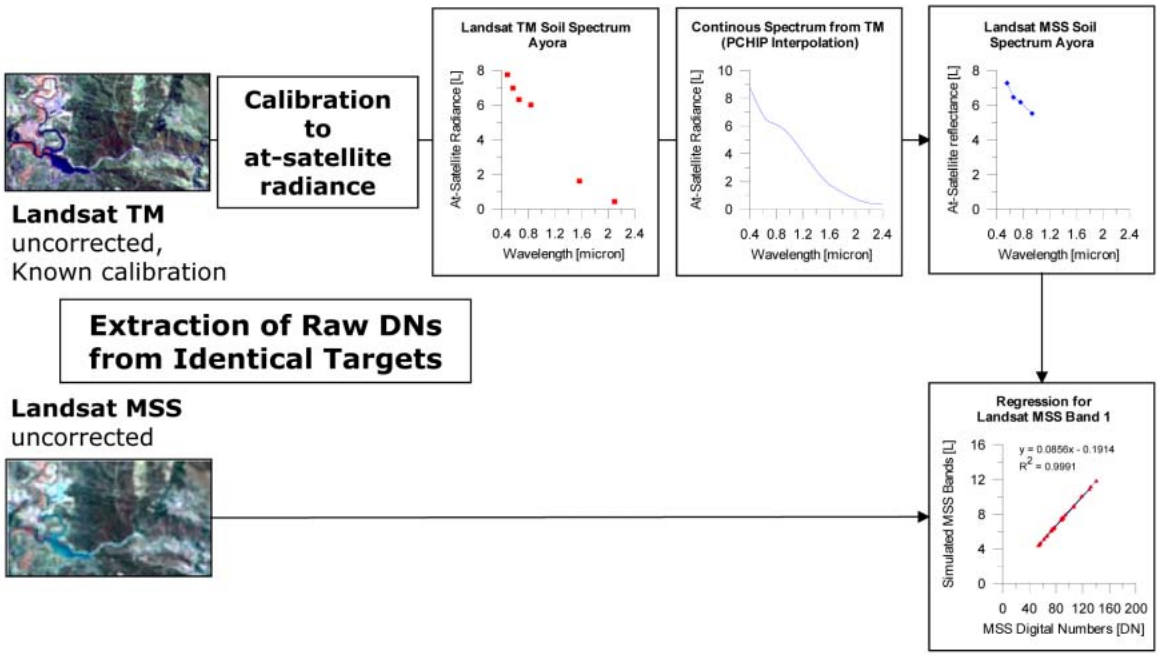

Fig. 6.10: Principle of radiometric intercalibration between Landsat-MSS and -TM (further explanations in the text)

Employing known calibration factors, Landsat-TM data are converted to at-satellite radiance values [$mWcm^{-2}\mu m^{-1}sr^{-1}$], representing the energy received at the sensor after propagation of solar radiance through the atmosphere, interaction and reflectance at the Earth's surface and propagation back through the atmosphere towards the sensor. Using the centre wavelengths of the different TM bands, an interpolation algorithm is employed to calculate continuous radi-

ance spectra between 0.4 and 2.4 µm. From this continuum, those values are extracted and averaged that range between the lower and upper bandpasses of the MSS bands, resulting in a simulated MSS radiance signal [$mWcm^{-2}\mu m^{-1}sr^{-1}$]. Then, corresponding digital numbers can be extracted from the MSS image to attain data pairs. These values correspond to the channel-wise calibration function of a sensor, which is given by Eq. (6.1). In order to support a unique solution to this equation, the described procedure is run for a variety of surface elements with different brightness levels. The resulting number of value pairs is then used in a channel-wise regression analysis to yield gain and offset values for the MSS channels. Using these gain and offset parameters, MSS digital numbers are converted into at-satellite radiance allowing a subsequent radiometric correction. Given the spectral setup of Landsat-TM vs. -MSS it is obvious that especially the simulation of MSS band 4 radiances needs to be executed carefully, since unlike MSS bands 1-3 the interpolation of continuous radiance spectra is not anchored on both sides by closely neighbouring TM bands, because MSS band 4 is shifted towards longer wavelengths compared to TM band 4, and TM band 5 is located in the SWIR.

Extensive sensitivity analyses were carried out to test different geometric input sensor resolutions and interpolation algorithms. Details on these are provided in Röder et al. (2005). As a result, the intercalibration was carried out using the calibration data set of 38 test areas with a minimum size of 316 m^2, and using the piecewise cubic hermite spline algorithm along with the original TM resolution of 30*30 m^2. Table 6.1 shows the derived set of calibration factors and the correlation coefficients of the regression analysis. In addition, post-launch values are given for comparison purposes.

Table 6.1: Calibration factors derived for the Ayora test site

	Ayora dataset			**Post-launch**	
	gain	offset	r^2	gain	offset
MSS 1	0.0856	-0.1914	0.9991	0.1035	0.3
MSS 2	0.0733	-0.1454	0.9990	0.0687	0.3
MSS 3	0.0655	-0.557	0.9757	0.0559	0.4
MSS 4	0.0602	-0.1772	0.9925	0.0469	0.3

Derived and pre-flight estimates vary on the magnitude of 6 to 24 %, underlining the necessity to employ adapted coefficients.

6.3.5 Radiometric correction of the MSS master scene and validation

Since for the 1984 TM scene, the parameterisation of the radiative transfer model had already been inferred, the corresponding MSS data set could directly be corrected once the required auxiliary layers for the topography correction were calculated for the native spatial resolution of 79*79 m[21].

Various reasons compromise a validation of radiometrically corrected Landsat-MSS data. First of all, there is a considerable time lag between the date of spectral reference measure-

[1] Spatial resampling of the digital elevation model available in 30*30 m grid has been carried out using bilinear interpolation.

ments compared to the image acquisition dates. More importantly, though, is the geometric resolution of Landsat-MSS, which makes it highly improbable to identify spectrally 'pure' pixels that could be compared to hyperspectral measurements from the field. As a result of this unbridgeable scale gap, an indirect validation approach was chosen. It makes use of the slightly shifted mean band positions of Landsat-TM and -MSS, such that an integrated 10-channel reflectance spectrum can be produced. A successful application of the methodology should yield continuous reflectance spectra from radiometrically corrected TM and MSS imagery. This investigation was carried out firstly for the calibration set of targets, resulting in highly consistent shapes, which had to be expected since these data had served to build the intercalibration regression. The second step consisted in producing the same spectra for a validation target set comprising 37 targets. In addition, the radiometric rectification was also carried out using the same atmospheric parameters, but the post-launch sensor calibration values. Consistent reflectance spectra were observed for almost all targets of the validation data set using the calibration parameters derived from the intercalibration process, while the post-launch calibration values led to significant inconsistencies, which is shown exemplarily in Fig. 6.11. Reflectances are given in DNs with a scaling factor of 340 applied.

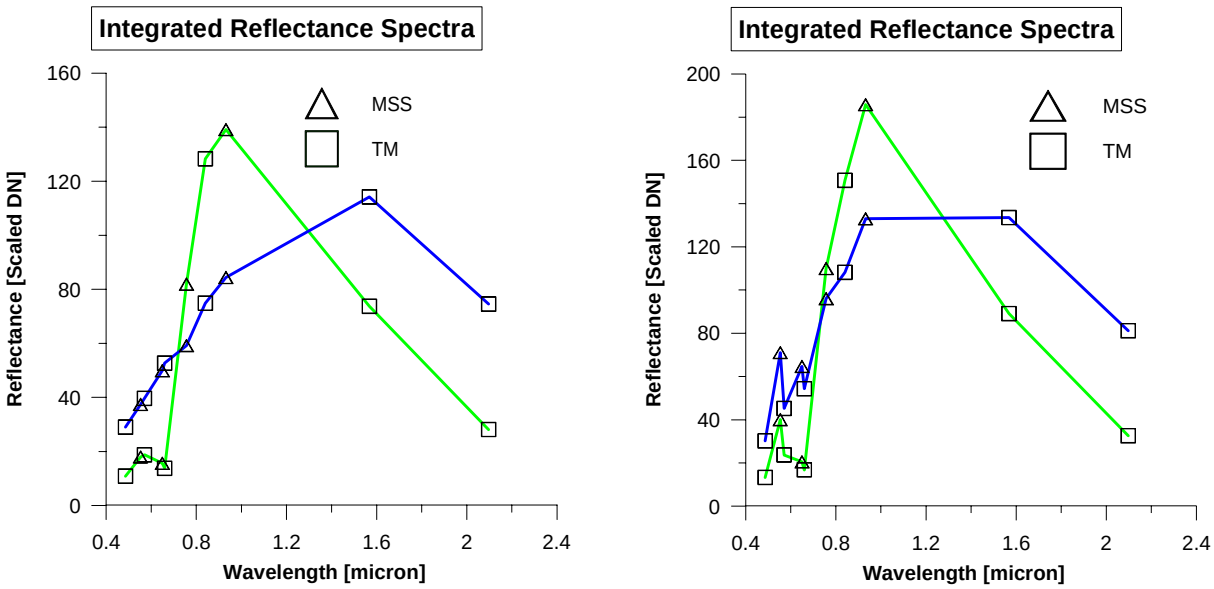

Fig. 6.11: Integrated reflectance spectra from radiometrically corrected synoptic Landsat-TM and -MSS data set (left: radiometric correction using intercalibration factors; right: radiometric correction using post-launch factors)

Fig. 6.11 clearly underlines the necessity to base the radiometric correction of Landsat-MSS data on calibration factors adapted to the sensor sensitivity at the time of image acquisition, rather than employing pre-flight or post-launch values.

Six targets exhibited minor fluctuations, which are mostly confined to the visible portion of the wavelength spectrum and which are most pronounced for non-continuous reflectance spectra, such as for vegetation. Possible reasons for this effect may be inhomogeneities within the target areas in conjunction with a suspected difference in sensitivity of the two sensors for some surface types. Especially vegetation features appear to be resolved slightly differently,

which may result from the configuration of the MSS channels. These cover significantly broader wavelength increments and are hence not able to resolve the characteristic absorption features of photosynthetically active vegetation in the visible part of the spectrum due to chlorophyll and carotin absorption. Nonetheless, the variations observed still range well within the aspired overall accuracy of the full radiometric processing chain of ±2.5 % reflectance (Fig. 6.12).

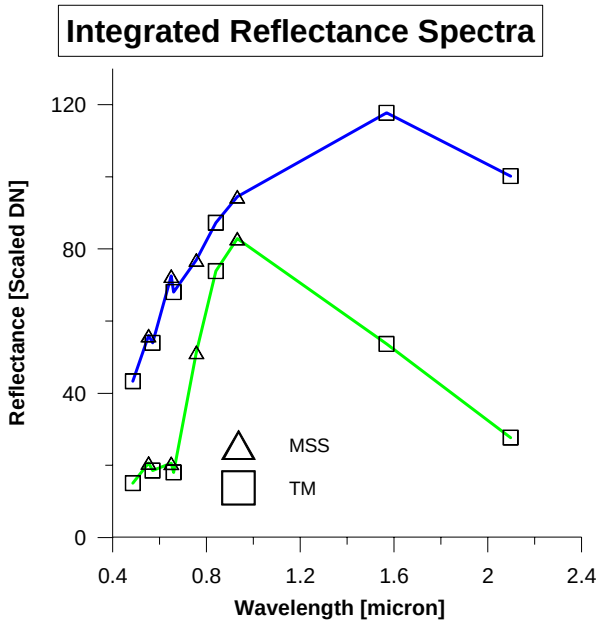

Fig. 6.12: Integrated reflectance spectra from radiometrically corrected synoptic Landsat-TM and -MSS data sets showing minor fluctuations

These results support the design of the developed intercalibration approach, and suggest that synoptic datasets of Landsat-TM and -MSS can be used to derive the essential sensor calibration parameters to perform a full radiometric correction of Landsat-MSS data.

6.3.6 Radiometric correction of the MSS time series and validation

It follows from the intercalibration methodology that the derived factors are only valid for the scene that has been employed for their derivation. Therefore, correction of the older Landsat-MSS data sets required an additional normalisation step, in which these images were adapted to the corrected master image using an empirical line approach and a number of pseudo-invariant targets that were iteratively defined between image pairs. Empirical line correction is a straightforward adaptation of uncorrected slave to a corrected master image. However, pursuing this approach would exclude the correction of topography-induced illumination variations, which were identified to be important factors affecting the radiometric properties of satellite images. Hence, this option has been disregarded in favour of a more complex constellation of calculating the linear relation between radiometrically uncorrected master and slave images. The result of this procedure is an uncorrected slave image with atmospheric distortions resembling the master image. As this adaptation only incorporates linear atmospheric effects, similar atmospheric conditions between slave and master image will result in a more accurate normalisation. Then, full radiative transfer modelling is possible,

employing the atmospheric parameters and calibration factors of the master image, as well as the corresponding auxiliary layers on illumination variation due to topography. Again, it has to be noted that results will be more accurate if sun positions are similar for both scenes. In case of vastly differing conditions, only that share of topography-induced effects will be adequately corrected that can be modelled using a linear function. Since the scenes considered in this study are all dating from the summer season, this aspect can be considered less problematic as in the case of images acquired at significantly lower sun elevations, when a difference of some days may result in largely differing illumination conditions.

The processing sequence of applying a linear normalisation model followed by a non-linear radiative transfer model leads to a mis-matching of reflectance values between pseudo-invariant targets to match with high coincidence if variations between slave and master scene depart from linearity. In order to account for this effect, the pseudo-invariant areas were analysed again after the radiometric correction, and a further optimisation was carried out based a second linear regression between corrected slave and corrected master image. This processing workflow for radiometric correction of the MSS images provided the best compromise between limiting data modification while adhering to the standards required for further quantitative data analysis. Consequently, processing parameters correspond to the ones given in Table B.5 (Appendix) for the TM image from June, 1st, 1984. The number of targets included in the normalisation as well as the empirical relations applied are given in Table B.6 (Appendix).

Validation was carried out utilising the same approach adopted for the TM series. However, the poorer radiometric resolution of the Landsat-MSS sensor further complicated the identification of pseudo-invariant areas which could be considered spectrally ‘pure’ and denied transferring the targets employed for the TM data set. In addition, the large wildfire in 1979 affected more than 1/3 of the core test area. Consequently, validation targets were defined to reflect unchanged conditions through relatively large areas characterised by a stable mixture of a limited number of different surface materials. A total of 21 targets were selected with sizes range 23 and 530 ha (35 to 849 pixels) and most elements ranging around 200 ha (320 pixels). As can be inferred from the results depicted in Fig. 6.13, the reflectance estimates showed reasonable shapes and a high degree of consistency.

Obviously, the radiometric correction approach adopted for the Landsat-MSS based time series yields radiometrically consistent results and thus enables the further quantitative analysis of the full time series.

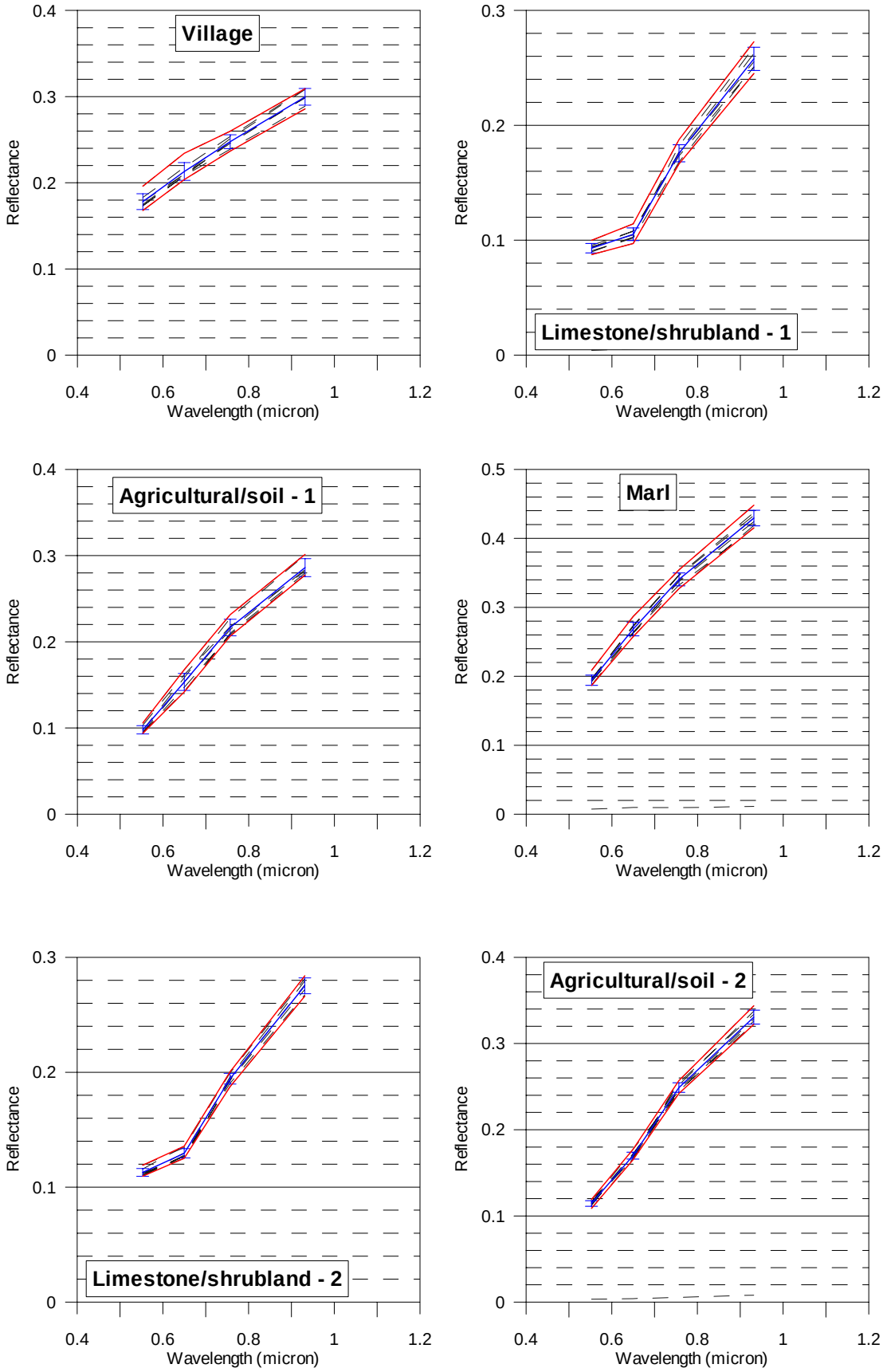

Fig. 6.13: Reflectance values for invariant targets after radiometric correction of the MSS time series (compare Fig. 6.9)

6.4 Lagadas

Radiometric correction of the Lagadas time series was carried out following the principles described for the Ayora test site in section 6.3.

In a first step, water signatures were extracted from Lakes Volvi and Koronia, and from the open sea surrounding the Chalkidiki peninsula south of the test area. It was assessed if these could be employed to infer the driving parameters for the radiometric correction following the dark target approach. Similarly to the Spanish site, image-derived and reference water signatures proved to be incompatible, leading to unrealistic estimations for the Ångstrom-relation. Thus, the strategy successfully developed for the Ayora test site was adopted. The water signatures extracted before were calibrated to at-satellite radiance values and radiometrically corrected using clear sky aerosol scattering, an Ångstrom-relation with β=0.1 and α=1, and mid-latitude summer transmission characteristics. Fig. 6.14 shows average reflectance spectra for the different years and the corresponding standard deviation.

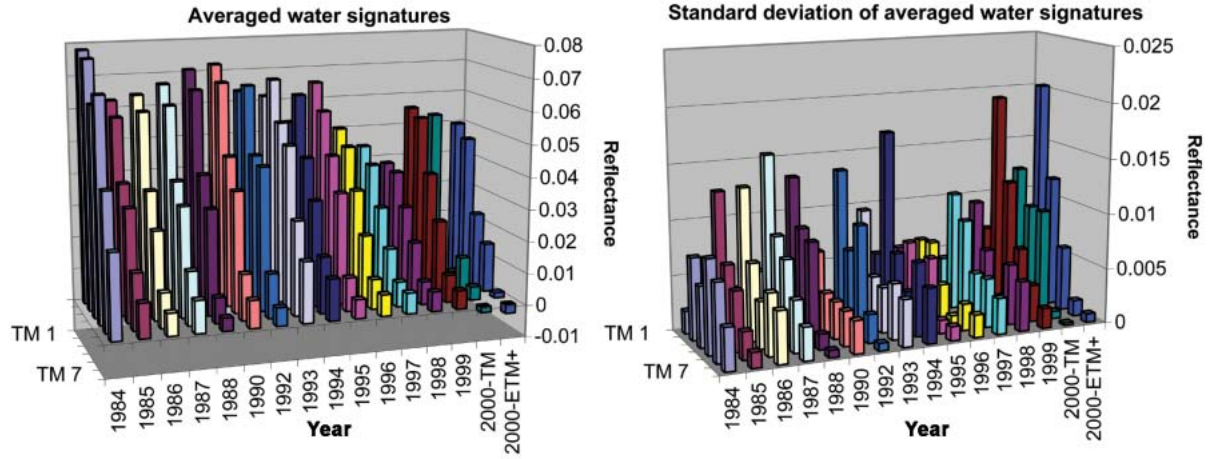

Fig. 6.14: Averaged reflectance spectra and corresponding standard deviations of water bodies and open water for different scenes

Based on this evaluation, the image acquired in 1996 was selected as a master image, since the averaged water signature shows both, an intermediate brightness level, as well as a low standard deviation, the latter indicating homogeneous conditions over the full area. In contrast to this, images from the years 1992 to 1995, which are better placed within the time series, show rather high standard deviations, suggesting that atmospheric conditions are more variable across these images.

6.4.1 Radiometric correction of the TM time series

A total of 26 calibration/validation targets was defined, which could be identified in the images of the time series. Similarly to the Ayora region, these can only partially be considered invariant over time, which is owed to the high heterogeneity of Mediterranean landscapes. Subsequently, the different radiative transfer models were defined using the parameters given in Table B.7 (Appendix) and the sensor calibration function described before.

6.4.2 Validation of the radiometric correction of the TM time series

Validation of the master image was conducted using pixel purity index to identify 'pure' pixels, which were assessed in relation to a spectral library (Fig. 6.15).

In the reference hyperspectral signatures (shown in Fig. B.2, Appendix), typical effects of atmospheric water vapour appearing in field measurements were eliminated, resulting in gaps in hyperspectral curves, which do not affect spectral resampling to Landsat-TM bands.

The spectra utilised to assess 'vegetation' are field measurements of different tree and shrub species which are typical for the Lagadas rangelands, such as *Quercus coccifera*, *Calicotome villosa* or *Sarcopoterium spinosum*, while image-spectra showing irrigated vegetation were approximated using hyperspectral measurements of plants with a high leaf water concentration, such as *Urginea maritima* or *Euphorbia characias*.

Assessing the different bedrock and soil spectra, it has again to be noted that comparability is constrained by scale differences between field measurements of 'pure' materials and satellite-based measurements potentially integrating various surface types or, for example, identical bedrock types at different weathering stages. In some cases differences in the reflectance spectra occur in band 5 and band 7 only. This is evident in the 'Bedrock 3 – Limestone' graph, where reflectance decreases much stronger from band 5 to band 7 for the image spectra. The main reason for this is a difference in the carbonate content of different types of limestone, resulting in a stronger absorption feature for rocks with higher carbonate concentrations as outlined in the corresponding section for the Ayora site (section 6.3.3).

Beside the limitations arising from comparing measurements of different spectral and spatial scales there is a good coincidence between reference and image spectra. It does prove the validity of the radiometric correction of the 1996 master image, which was then utilised in the subsequent iterative correction of the remaining images.

Following the processing of the master image, the full TM time series was corrected. Radiative transfer models were parameterised to yield the closest match for the pseudo-invariant target sets defined before. Target areas were defined to represent homogeneous surface types or stable mixtures of different surface materials, and areas ranged between 5.49 ha and 45 ha (61 to 500 pixels), while four very large areas were defined to integrate stable rangeland areas and water bodies exceeding an area of 200 ha or 500 ha (2533 or 6470 pixels), respectively. Average reflectance signatures were extracted for all sites and average reflectance, standard deviation, minimum and maximum values were calculated over the full time span. Together with dotted lines to represent individual reflectance curves, the result is shown in Fig. 6.16.

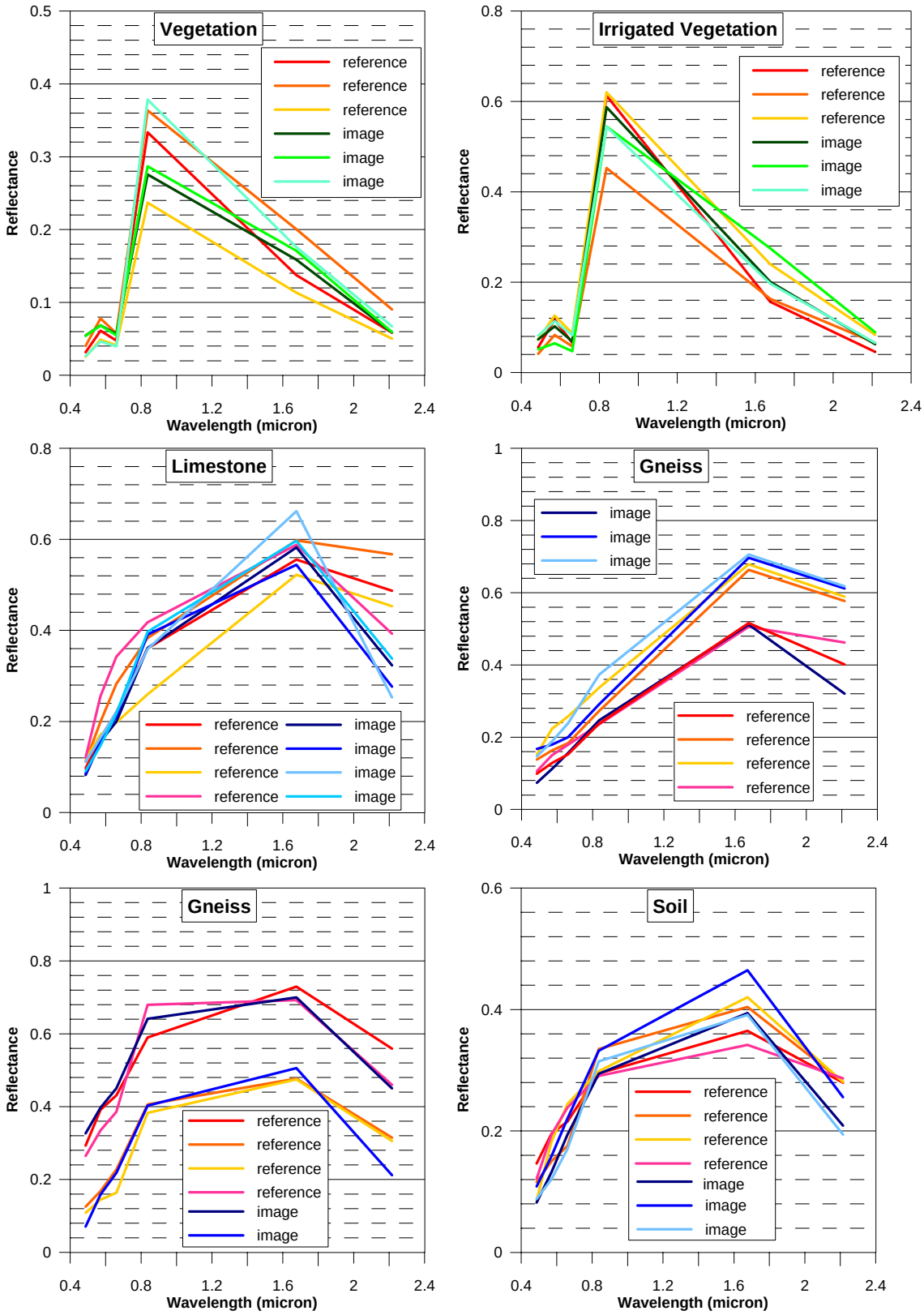

Fig. 6.15: Comparison between image-derived and reference reflectance spectra for typical surface types

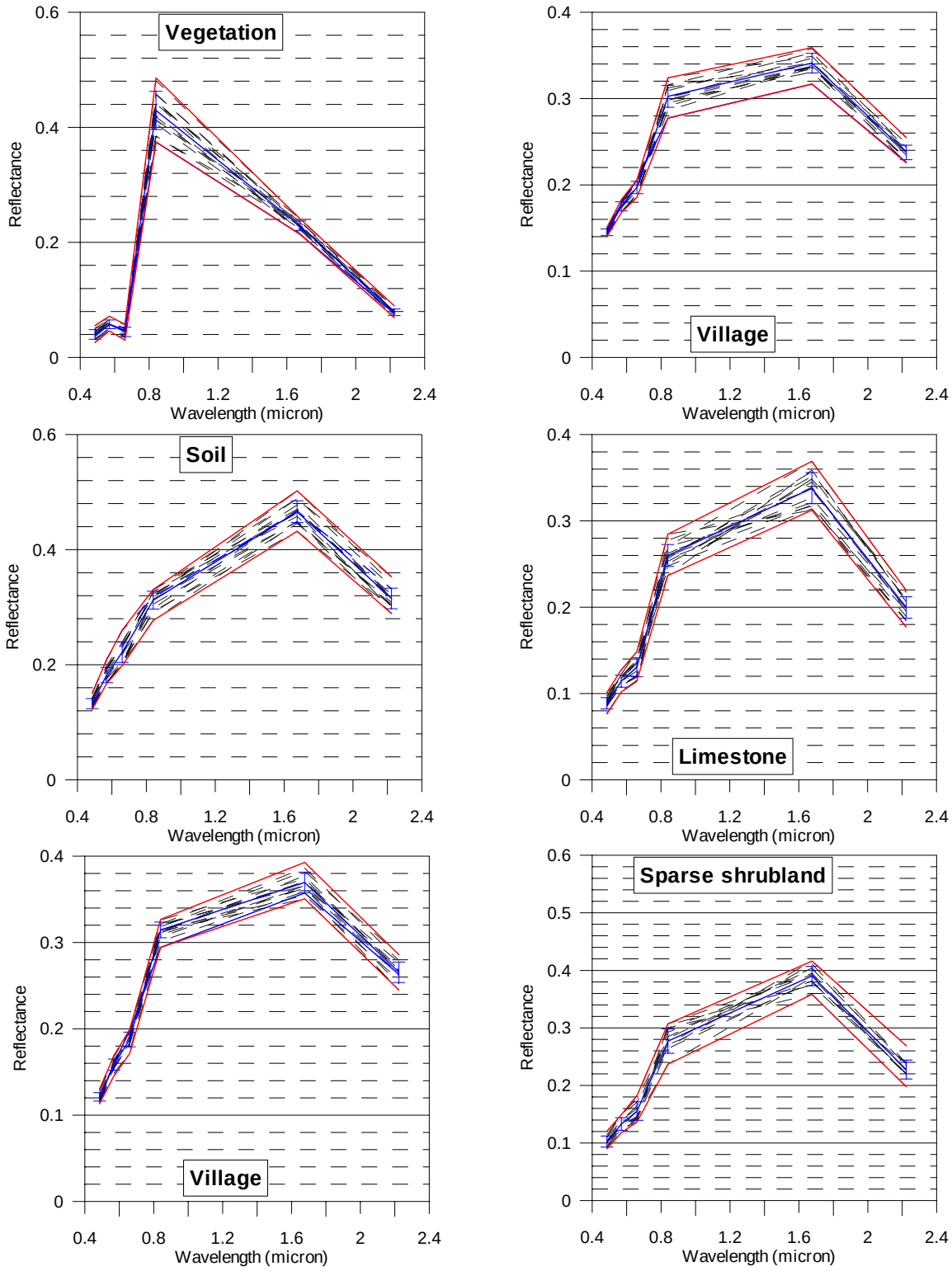

Fig. 6.16: Reflectance values for invariant targets after radiometric correction of the TM time series (compare Fig. 6.9)

The represented targets show minor fluctuations, which may result from differences in climatological conditions or photosynthetic activity (compare section 6.3.3), but also from violations of the criterion of invariance between different years.

The target representing a dense and relatively stable stand of sclerophyllous oak forests shows spectra slightly differing as a function of vitality and phenology. Nonetheless, the shapes of the spectra correspond very well. Two targets represent the town of Lagadas and the village of Sochos. Villages mostly meet the requirements of being invariant if the settlement structure undergoes no significant modifications. The integrated signal may only be disturbed by the phenology of vegetation that is always present in settlements, especially through small garden cultivations. Also, like bedrock, sealed surfaces will show different behaviour depending on wetness, and finally a certain degree of weathering may occur over the years. In the present case, both village targets are highly consistent over time. In addition, two targets are shown which are characterised by dominating limestone rocks ('Limestone') or very sparse shrubland cover. Small villages do often show a spectral behaviour that is very similar to the dominating bedrock formation, which can be clearly seen in Fig. 6.16. The limestone- and shrubland-targets show a somewhat higher variability compared to the villages, but still standard deviation ranges well within a margin of ±2 % reflectance. Even minimum and maximum values are close to the averaged spectrum. In the case of the shrubland target, a slightly higher variation can be noted in the visible bands, resulting from the influence of vegetation.

Summarising, validation based on pseudo-invariant targets confirms the radiometric consistency of the data set following correction for atmospheric disturbance and effects of topography.

6.5 Summary of the radiometric correction chain

Despite the availability of simplified correction approaches, it has repeatedly been stressed that a radiometric correction meeting high quantitative standards should be based on full radiative transfer modelling. Ideally, such a transfer model comprises three components accounting for sensor sensitivity, atmospheric conditions and variations of illumination as a function the sun-surface-sensor constellation. The approach presented here integrates these three components. It makes use of continuous experiments to update the internal sensor calibration, a set of pre-defined atmospheric characteristics defined by aerosol models, aerosol optical depth and gaseous transmission coefficients, and by a model to calculate the required auxiliary information on the influence of the relief based on digital elevation models and the sun position. In the current approach, all of these components are treated within one integrated processing scheme, and allow for a precise radiometric correction of multi-spectral and multi-temporal sets of satellite images from different sensor systems.

While, depending on the quality of the digital elevation model, information on topography-dependant illumination can be calculated with a high degree of accuracy, the other two components are associated with a certain error potential. Both internal or updated sensor calibration are subject to different sources of error, which were discussed in detail in section 6.1. Fig. 6.1 visualised the variations associated with the calibration measurement experiments. However, the adopted approach to calculate time-dependant functions partially balances these variations.

Characterisation of atmospheric conditions at the time of image acquisition is highly desirable and may be available from ground observations or from sounding balloons, but these remain

mostly constrained to experimental setups. Alternatively, methods to directly estimate the driving parameters from the image data have been presented, but the lack of suitable reference water spectral libraries is often an obstacle to benefiting from these. Trying to overcome these limitations and make processing of larger volumes more straightforward, this study presented an operational approach where a suite of images is radiometrically corrected based on one or more master images, following initial analyses of the respective general conditions, and utilising sets of pseudo-invariant targets. Finally, an essential step determining the quality of the radiometric correction is already inherent in the geometric rectification, which has to lead to an accurate overlay of digital elevation model and satellite image. If this prerequisite is violated, artefacts will hamper the quality of radiometrically corrected images especially in mountainous areas.

The implementation of this approach strongly depends on an accurate correction of the designated master image(s). This requires the availability of an appropriate spectral library that can be employed to calibrate the model and validate its results.

Depending on the thematic context addressed, it may prove necessary to integrate further sensor systems. In the present study, monitoring of the fire events in the Ayora region made the backward extension of the time series a mandatory task. This required incorporating Landsat-MSS data into the multi-temporal data base, which is complicated by the lack of suitable information on sensor calibration. An approach to radiometric intercalibration of sensor systems with different spectral setups was hence developed, tested and applied. It makes use of twin data sets acquired with different sensors under identical conditions, which limits the applicability of the resulting calibration factors to the matching data set. Employing linear relationships between a master scene and the other scenes enables to correct images from different dates and sensors provided they have the same spectral characteristics. However, this involves applying linear functions between uncorrected images, followed by the application of the radiative transfer model derived for the master image. It is evident that this application of linear relations to account for the essentially non-linear processes of atmospheric scattering and extinction has to be exerted with great care. Where atmospheric conditions largely differ between the master and slave image, this may cause inaccuracies for some cases. In the present study, a second normalisation step was applied to further reduce this effect. Nonetheless, it was shown that the topography correction is absolutely mandatory for any quantitative analysis, which denies directly applying a linear normalisation between uncorrected slave and corrected master image. Given this lack of suitable alternatives, it is concluded that limitations of applying this approach to correct Landsat-MSS data have to be accepted for the sake of large multi-temporal data bases.

For both data series, validation of the quantitative consistency was carried out using pseudo-invariant areas, the availability of which may greatly vary between different areas depending on the landscape heterogeneity. In the present case, this validation confirmed the accuracy attained for both the Ayora and the Lagadas site, supporting the subsequent quantitative interpretation as presented in the following chapters.

7 Spectral Mixture Analysis

Depending on the type of indicator and the surface features being investigated, an appropriate analysis scheme is essentially determined by the spectral and geometric properties of the data. The instantaneous field of view (IFOV) of the TM sensor integrates the spectral response of a surface area covering 30*30 m^2 (MSS: 79*79 m^2). Especially in heterogeneous landscapes with patches of surface features, the pixel size often exceeds the size of single surface elements, resulting in pixels composed of features with different spectral characteristics. According to Fisher et al. (1997), four different types of mixed pixels can be distinguished: sub-pixels containing features smaller than the actual pixel size, boundary pixels including border lines between different land cover types, intergrade pixels comprising fuzzy transitions between classes, and linear sub-pixels containing narrow line features. When assessing such mixed pixel signals, it is important to be aware of the type of mixing depending on the type of interaction of the downwelling radiance with the surface, i.e. linear mixing when irradiating energy interacts only one time with the surface, or non-linear mixing, which may occur when interacting surface types are viewed (e.g. sparse vegetation cover which does not fully cover the underlying soil) or when, for example, dense vegetation canopies lead to processes of multiple scattering (Guyot, 1990; Ray & Murray, 1996).

A number of data transformations and spectral indices exist, which aim at inferring information about vegetation cover. Many of these are affected by drawbacks, which were discussed in section 3.4.1. Different authors have assessed the potential of deriving vegetation properties based on physically-based reflectance models (e.g. Goel, 1989; Jacquemoud and Baret, 1992; Verstraete, 1994a; Jacquemoud, 1995; Atzberger, 2000). These models have originally been developed for uniform agricultural areas or homogeneous forests, and transferring them to heterogeneous, sparsely vegetated plant communities has not yet become operational using satellite images of moderate spectral and spatial resolution.

An alternative approach to derive quantitative proportional information is 'Spectral Mixture Analysis' (SMA), which dates back to early work of Horwitz et al. (1971), Detchmendy & Pace (1972) and Horwitz et al. (1975). Parallel to advances in sensor systems, the method was developed and enhanced by Smith et al. (1990, 1994), Adams et al. (1986, 1989) and Settle & Drake (1993). It has been successfully tested and applied in numerous studies covering mostly natural (e.g. Roberts et al., 1993; Foody & Cox, 1994; Garcia-Haro et al., 1996; Ustin et al., 1996; Tompkins et al., 1997; Okin et al. 1998; Garcia-Haro et al., 2001; Roberts et al., 1998; Okin et al. 2001; Shoshany & Svoray, 2002; Hostert et al., 2003b) but also urban environments (e.g. Small, 2003, 2005; Wu, 2004). Especially for areas with sparse vegetation, the superiority of SMA to traditional indices has been discussed and proven (e.g. Hill et al., 1995a; Elmore et al., 2000). Using tripod-based near-orthogonal observations of vegetation cover in Southern France, Twele (2004) attained excellent correlations with image-based cover estimates.

While most frequently linear spectral mixture is employed to characterize the relative abundance of surface materials, it is evident that in some cases the assumption of linear mixing is not valid and a number of approaches have addressed non-linear spectral unmixing (e.g. Rob-

erts et al., 1991; Sabol et al., 1992; Borel & Gerstl, 1994; Ray & Murray, 1994; Foody et al., 1997). While it seems desirable to account for non-linear mixture effects, the required a-priori knowledge of surface patterns strongly constrains this concept for studies with an experimental setup.

7.1 The spectral unmixing approach

Spectral mixture analysis (SMA) is based on the assumption that the majority of spectral variation encountered in multispectral imagery can be ascribed to a mixture of a limited number of surface materials, which can be characterised by reflectance spectra (Smith et al., 1990). Most frequently, these mixtures occur at the sub-pixel level, resulting in mixed-pixel spectra. SMA attempts to model the multispectral reflectance recorded in a pixel as a mixture of representative 'prototype' spectra, which are termed 'spectral endmembers' (EM). The approach computationally decomposes multispectral measurements into a finite number of pure spectral components by describing the recorded signal as a result of linear spectral mixing (e.g. Adams et al., 1986; Smith et al., 1990) and yields the relative abundance of the different endmembers in a pixel.

Linear unmixing does hence represent a transformation of pixels from the n-dimensional feature space to the mixing space defined by the endmembers. In mathematical terms, linear spectral mixture analysis can be expressed as:

$$\mathrm{A} \bullet \mathrm{X} = R \tag{7.1}$$

with A = n-m dimensional matrix, with n=number of spectral bands of the image, and m=number of spectral endmembers
X = Abundance vector of the respective EMs
R = reflectance vector (corresponding to the pixel value)

The actual unmixing is then executed by inverting equation (7.1):

$$\mathrm{X} = R \bullet \mathrm{A}^{-1} + \mathrm{E} \tag{7.2}$$

with E = overall residual error

A unique solution to this system is possible if the number of spectral endmembers equals the number of spectral bands. If the problem is underdetermined, i.e. the number of unknown fraction components (i.e. abundances) exceeds the number of spectral bands by one, a solution can still be obtained by assuming that the set of endmembers is exhaustive. In this constrained approach, the sum of the computed endmember proportional weights (fractions) is forced to be equal to 1. Frequently, the number of bands does exceed the number of endmember spectra such that the linear mixing model is over determined. In this case, a solution can be obtained making use of the pseudo-inverse:

$$\mathrm{X} = \left(\mathrm{A}^{\mathrm{T}} \bullet \mathrm{A}\right)^{-1} \bullet \mathrm{A}^{\mathrm{T}} \bullet R + \mathrm{E} \tag{7.3}$$

with A^{T} = transposed matrix of spectral endmembers (A)

Equation (7.2) minimises the mean-squared error in fitting the abundance estimates to the data, and renders the computation of abundance estimates equivalent to a rotational transform of the image.

An alternative expression is given by

$$R_i = \sum_{j=1}^{n} F_j \bullet RE_{ij} + \varepsilon_i \text{ and } \sum_{j=1}^{n} F_j = 1 \quad (7.4)$$

with R_i = reflectance of the mixed spectrum in band i
RE_{ij} = reflectance of the endmember spectrum j in band i
F_j = fraction of endmember j
n = number of spectral endmembers
ε_i = residual error in band i

This equation is solved through a least squares regression, while constraining the sum of fractions to one. A unique solution is possible as long as the number of spectral components (endmembers) does not exceed the number of bands plus one. However, it has been emphasised that the intrinsic dimensionality of the data is lower than the number of bands due to autocorrelation between bands (e.g. Settle & Drake, 1993; Small, 2004). For instance, Small (2004) gives a maximum of 4 EM for Landsat ETM+ data; however, this number has also been shown to depend on the spectral contrast of the selected endmembers in relation to the sensor sensitivity and the spectral variance within the image (Drake & Settle, 1989). Different approaches exist to assess the spectral dimensionality, such as the Principal Components Analysis (PCI) or the Minimum Noise Fraction (MNF) transformation (e.g. Green et al., 1988; Gillespie et al. 1990).

Composition of the endmember sets is the crucial step in spectral unmixing. Different approaches to identification of suitable reference endmembers exist. These may be derived from the image itself and different methods have been proposed to optimise this extraction (Boardman et al., 1995; Garcìa-Haro et al., 1999). Notwithstanding the high operationality of this approach, its validity for sensors with medium to low spatial resolution has been questioned, since most frequently no spectrally ‘pure’ pixels can be expected (Bateson & Curtis, 1996). Alternatively, the utilisation of spectral databases has been suggested, which incorporate hyperspectral reflectance measurements of different surface materials (e.g. Hill et al., 1995a, 1996; Preissler et al., 1998). Employing such data bases, measurements can be resampled to match the spectral resolution of the respective sensor.

Some authors have additionally suggested to include an artificial shade endmember, which is supposed to account for albedo differences between different pixels, and which models shading effects. While Adams et al. (1986) suggest using a zero reflectance spectrum, Roberts et al. (1993) have introduced a canopy-reflectance spectrum derived from residual analysis. While macro-effects resulting from topography were eliminated by the radiometric correction, micro-shading determined by the surface roughness is still present in the data, and plays a substantial role especially in vegetation canopies. Once a suitable endmember model is determined and the abundance estimates for the different components is calculated, a normalisa-

tion of the results with respect to the shade component can be performed by proportionally assigning it to the other fractions. The required normalisation is calculated according to eq. (7.5):

$$f = \frac{1}{(1 - F_{Shade})} \text{ and } \sum_{j=1}^{(n-1)} F_j \bullet f = 1 \tag{7.5}$$

with f = shade normalisation factor
F_{Shade} = fraction estimate for the shade endmember
F_j = fraction estimate for endmember j

Different statistical analysis approaches exist to assess the performance of unmixing models and support their optimisation.

Firstly, fractions resulting from the unmixing process should range from 0 to 1. Different error terms can be calculated such as the average root-mean-squared (RMSE) error, which is derived according to

$$RMSE = \frac{\sum_{k=1}^{m} \left[\sqrt{\left(\sum_{j=1}^{n} \left(R_{jk} - R_{jk}' \right)^2 \right) / n} \right]}{m} \tag{7.6}$$

with R_{jk} = modelled reflectance in band j and pixel k
R_{jk}' = measured reflectance in band j and pixel k
n = number of spectral bands
m = number of pixels

The RMSE provides a measure of the spectral variability explained by the model, and its calculation per pixel yields an RMSE image that allows a visual assessment which surface materials may not have been correctly presented in the model.

Finally, the spectral band residuals can be calculated by transforming equation (7.4):

$$\varepsilon_i = R_i - \sum_{j=1}^{n} F_j \bullet RE_{ij} \tag{7.7}$$

The spectral band residuals provide additional indicators of modelling errors. Positive residuals occur when the measured spectrum has higher a reflectance than the modelled spectrum at a specific wavelength. This points at the presence of absorption features which were lacking in the measured reflectance signature. Negative band residuals indicate the presence of absorption features in the measured spectrum that are less pronounced or not even present in the modelled spectrum.

Aiming at an enhancement of the methodology, it has been suggested to improve quantification of the fraction of specific ‘foreground’ targets by optimising modelling of the ‘background’ (e.g. Smith et al., 1990a; Hill et al., 1996). This can for instance be achieved by accounting for different geologic and soil background surface types, if derivation of the fraction

of green vegetation is desired. This concept has, for example, been implemented by different authors through the concept of Multiple Endmember Spectral Mixture Analysis (MESMA). It assumes that the number of different endmember spectra may be high throughout the full image, although a single pixel can be explained by a limited number of these. Correspondingly, the method is based on analysing a large number of possible endmembers, which may be organised in spectral libraries, and determine for each pixel the model of optimal fit (e.g. Okin et al., 1998; Roberts et al., 1998). This can lead to an improved model performance and a more accurate estimation of abundances, especially when surface classes do not occur throughout the whole image (e.g. geological strata) and a high variability of materials exists in the image (Garcìa-Haro et al. 2005). While theoretically the method is only limited by the computational cost, the estimated fractions may still be inaccurate, even if all occurring materials are provided in the form of possible endmembers. Especially when endmembers are themselves of mixed nature, such as for instance dry vegetation (Ustin et al., 1993), or in the case of errors in calibration, radiometric rectification, or the presence of system noise, erroneous abundances may result. Most importantly, not every mathematically valid model can be explained physically and correctly reflects 'real-world' situations. Hence, approaches based on MESMA have to be exerted with great care, and only if knowledge of local conditions enables to stratify and constrain the model to sensible endmember combinations.

Consequently, spectral mixture analysis of the two time series of Landsat-TM/ETM+ and MSS data was executed employing highly constrained or completely fixed endmember models and reference spectra were drawn from representative spectral libraries.

7.2 Ayora

A database of hyperspectral reflectance measurements has been available for the Ayora test site. The spectra were measured using an ASD Fieldspec Pro II spectroradiometer, which measures reflectance in 2151 bands at a spectral resolution of 1nm. A spectralon panel was used as spectral reference. Measurements were acquired in the frame of different field campaigns in Mediterranean areas (Preissler, 1996; Hostert & Preissler, 1997; Retzlaff et al., 1998; Röder & Hostert, 1998; Röder, 2002). Especially the spectra provided by Retzlaff et al. (1998) were useful in this context, since these had been acquired at a test site directly adjacent to the Ayora area, with a similar environmental setting. Spectra were measured on site for different vegetation types and plant species, integrating green components as well as stems and branches. Dense vegetation samples were selected for this exercise to reduce the background contribution to a minimum. These were complemented by laboratory measurements of fresh leave and needle stacks. Bedrock and soil samples were measured in field as well as under laboratory conditions, measuring both natural and freshly cut rock surfaces, as well as soil samples in their original and in sieved and homogenized state.

Spectral mixture analysis of the Ayora data set comprised definition of an endmember model for the most recent scene and validation of the results using field data. Subsequently, the mixture model was applied to the full time series.

7.2.1 Endmember selection

Endmember models are supposed to characterise the spectral variance encountered in an image. The Landsat-TM image acquired on June, 21st, 2000 was utilised as a reference and its spectral variance was assessed. This can be done by visualising the n-dimensional feature-space in a sequence of 2-dimensional plots for different two-band combinations. Possible endmember spectra can be included to detect which endmembers best cover the spectral variance (Fig. 7.1).

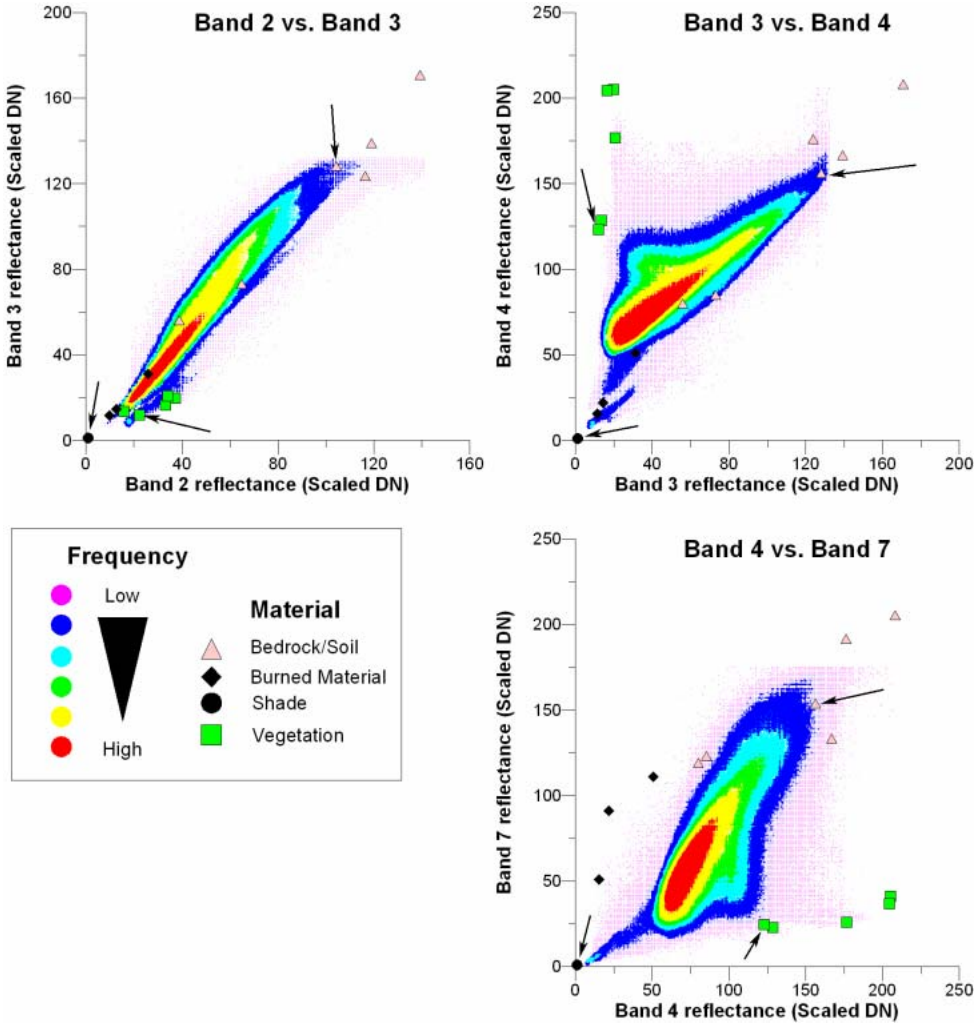

Fig. 7.1: Feature space images showing different band combinations and including candidate EMs and actually employed EMs (marked with arrows)

It is evident that the spectral variance covered by two-band combinations is vastly differing for different combinations. For instance, the band 2/band 3 feature space shows a high colinearity. To the contrast, especially combinations of bands from the visible and the near-infrared wavelength region show a peculiar shape. It is essentially composed of a straight line, which forms the basis for a perpendicular plane converging into a single point. In similar form, this has for example been described by Kauth & Thomas (1976) in their tasselled cap concept. The 1:1 base line is related to soil and bedrock background, while the orthogonal peak of the shape is governed by photosynthetically active vegetation, resulting from its spectral behav-

iour between TM bands 3 and 4. In theory, if only a single soil type was present, pure soil pixels would orientate along this base line depending on their spectral brightness. Correspondingly, pixels whose reflectance is composed by a mixture of these basic surface types are located in the plane between these 'extremes'.

For the Ayora test site, it was mandatory to include Landsat-MSS data in the analysis, since only these cover the time of the most devastating fire in the region in 1979. This further aggravates the constraints arising from the spectral dimensionality of the data. With two bands in the near infrared wavelength domain, and the two bands in the visible being highly intercorrelated, a maximum of three endmembers could be chosen (Fig. 7.2). For a better consistency between the MSS- and the TM-based data sets, this model was applied to both, although it had to be expected that the residuals and error estimates might be higher than what could be expected for the TM data. Nonetheless, it was assumed that for the reasons given above derivation of the green vegetation fraction should still be possible with a high degree of accuracy. The following fixed endmember model was set up for the Ayora test area.

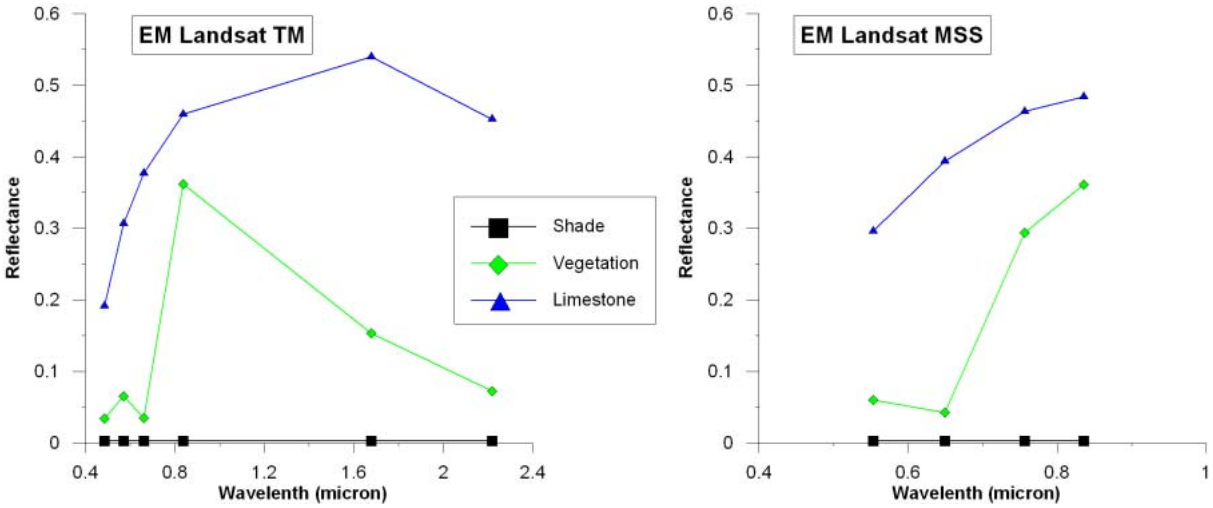

Fig. 7.2: Endmember model deployed for the Ayora test site (left: TM; right: MSS)

An artificial shade endmember was included as a zero reflectance spectrum. In addition, green vegetation was represented by a spectrum derived from a stack of needles from *Pinus pinaster* and a limestone spectrum was included to account for the bedrock. These two components represent the most frequent vegetation and bedrock types.

7.2.2 Spectral Mixture Analysis of the reference image

In a first step, the spectral mixture model was applied to the reference image acquired in 2000. The result is shown in Fig. 7.3 in an RGB representation.

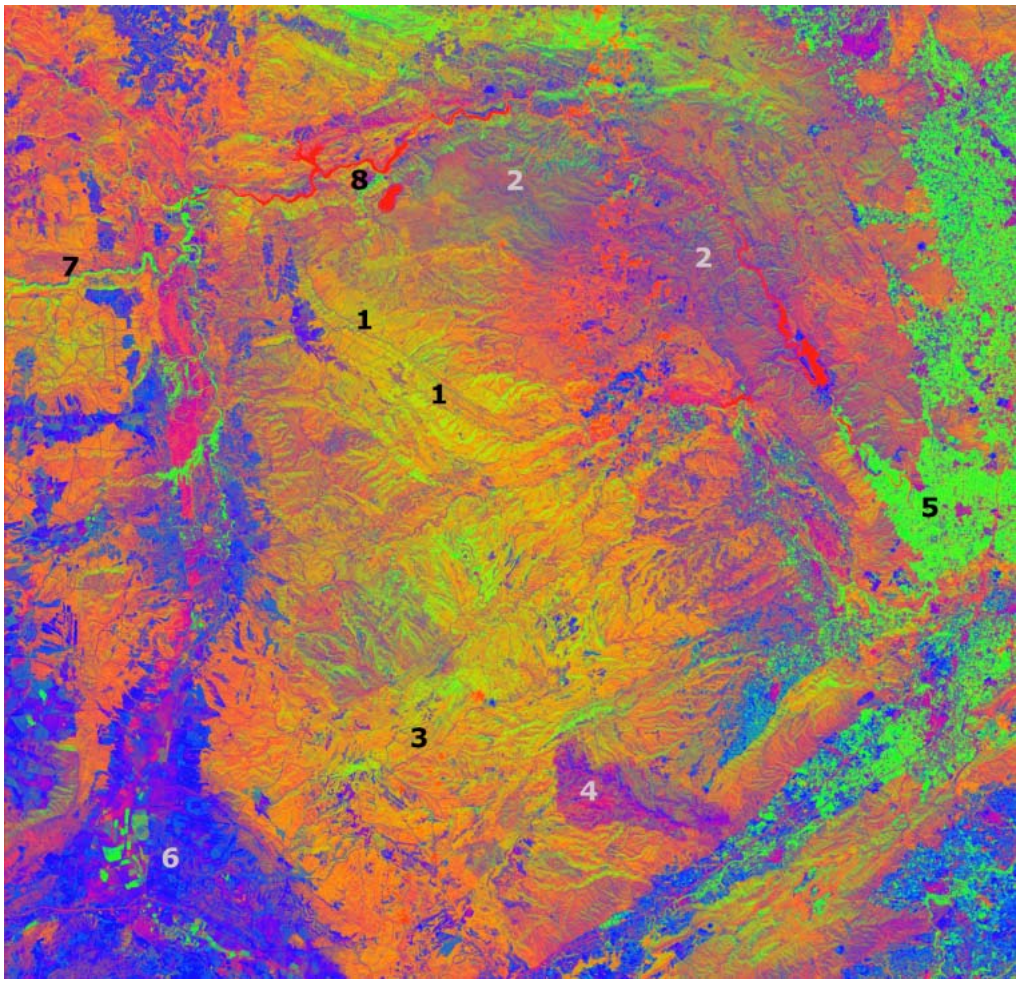

Fig. 7.3: Colour representation of fractions resulting from spectral mixture analysis for the 2000 TM image (R = Shade, G = Vegetation, B = Bedrock)

Most parts of the test site are characterised by shades of chartreuse to orange, indicating high fractions of vegetation and shade where vegetation is prominent (1). In areas with very sparse vegetation, blue, purple and violet colours dominate (2), triggered by high bedrock fractions, which may be accompanied by high shade fractions due to brightness effects. In the same way, roads or fire breaks appear as blue to purple lineaments (3). Also, areas recently affected by fire display shades of purple, and can be visually detected by their shape (4). Burned material and ashes are abundant after fires and contribute to the reflectance signal in the respective locations. However, since the spectral reflectance of burned bark or ash resembles a shade spectrum and due to the limitations explained before, these were not been included in the endmember model. Hence, where high shade fractions are observed these may also relate burned materials.

Fig. 7.1 includes the regions surrounding the test site. Here, agricultural areas show a highly specific behaviour. For instance, the orange cultivations east of the test area produce a large vegetation fraction, which corresponds to the bright green colours (5). This is mainly due to the fact that the endmember model has been parameterised to reflect the vegetation in the test area itself, whose reflectance is not as pronounced as that of irrigated vegetation. On the contrary, the Ayora valley bordering the test site in the West is dominated by bare soils and rocks, resulting in a dominance of the bedrock endmember. Especially in the South, the pattern of field plots is apparent, with harvested plots contrasting sharply with crops (6). Similarly, dense vegetation accompanying narrow rivers triggers a strong response of the vegetation endmember (7). Broader river sections as well as the artificial lake in the North are easily discernible with a strong shade endmember signal (8).

The resulting fraction distributions are partially skewed, and 99.9 % of all values lie between 0 and 1. Values exceeding 1 or negative values are scattered, and only occur outside the test area where the environmental setting does not correspond to the one reflected by the endmember model. This occurred for example in areas covered by irrigated vegetation, where vegetation fractions above one were compensated for by the algorithm trough negative shade fractions. Similarly, areas dominated by very bright marls show bedrock fractions above 1 and these were compensated for by very low to slightly negative shade and vegetation fractions. Fig. 7.4 shows the histograms for vegetation, bedrock, shade and the RMSE.

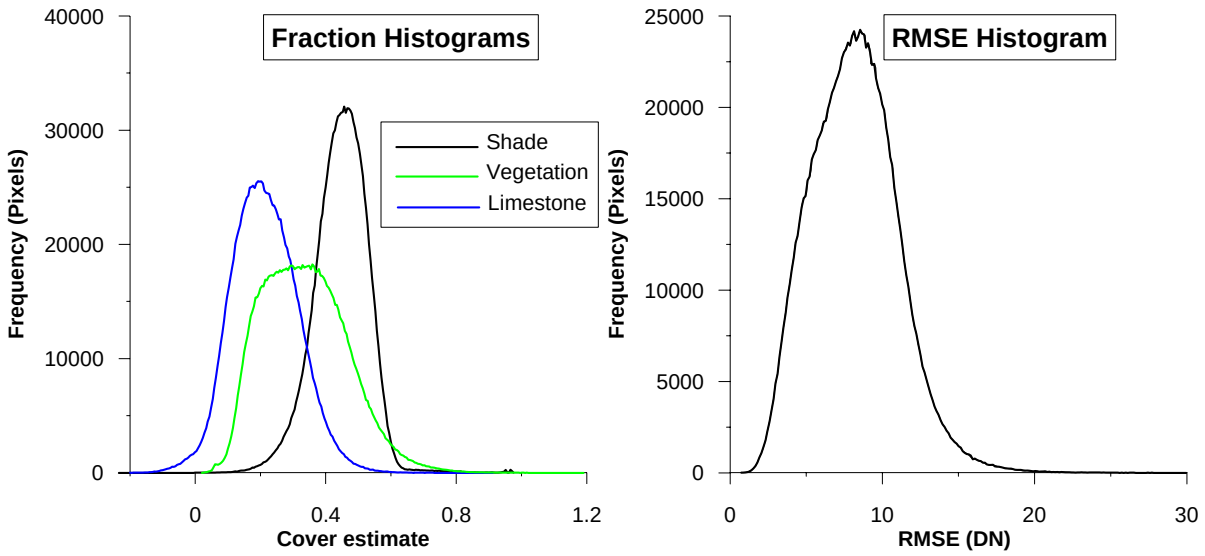

Fig. 7.4: Histograms of the fractions resulting from spectral mixture analysis of the 2000 reference image and the RMSE

The histogram of the RMSE has its maximum at 7.5 DN scaled reflectance, corresponding to 2.2 % reflectance that is not explained by the endmember model. The spatial distribution of the RMSE is shown in Fig. 7.5.

Spatial patterns are still visible in the image, indicating that the 3 endmember model does not equally represent the full area. Especially prominent are regions where bare rocks or soils are

present which differ strongly from the limestone spectrum employed, such as for instance agricultural fields or in formerly burned areas.

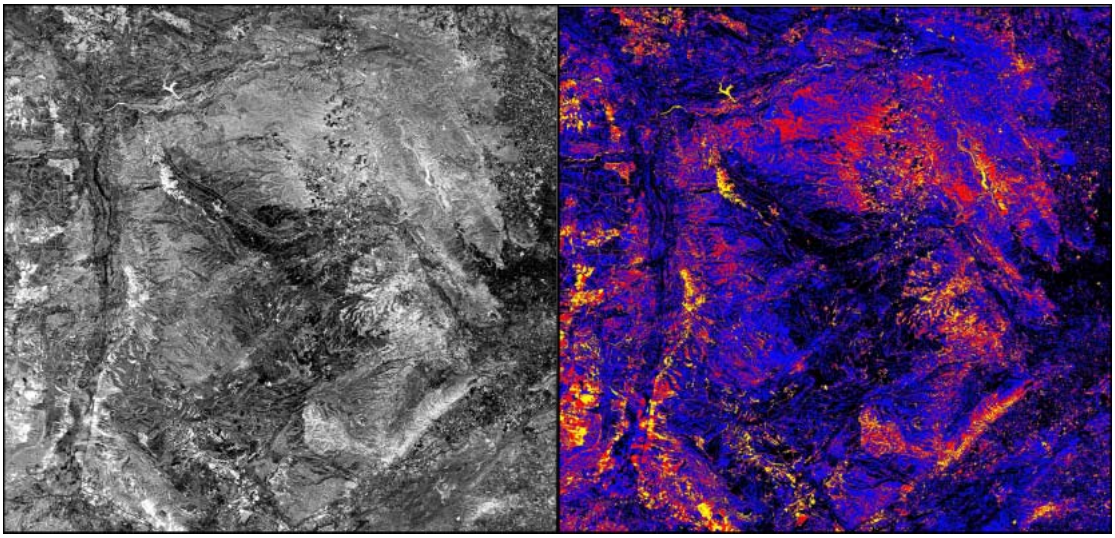

Fig. 7.5: RMSE resulting from spectral mixture analysis of the 2000 image (Left: grey scale; right: black = 0-2 %, blue = 2-3 %, red = 3-4 %, yellow > 4 %)

Nonetheless, the RMSE is considered satisfactory low given the above mentioned limitations. Hence, normalisation of the vegetation and bedrock fractions with respect to shade was executed according to eq. (7.5) This leads to stretching the current value range, thus also pronouncing positive and negative exceptions of the desired range between 0 and 1. In order to suppress undesired noise while at the same time keeping information on where this actually occurred, fractions after normalisation were saturated at -0.2 and 1.2 for negative and positive exceptions, respectively. The result of this operation are true surface abundances for vegetation and background, as depicted in Fig. 7.6.

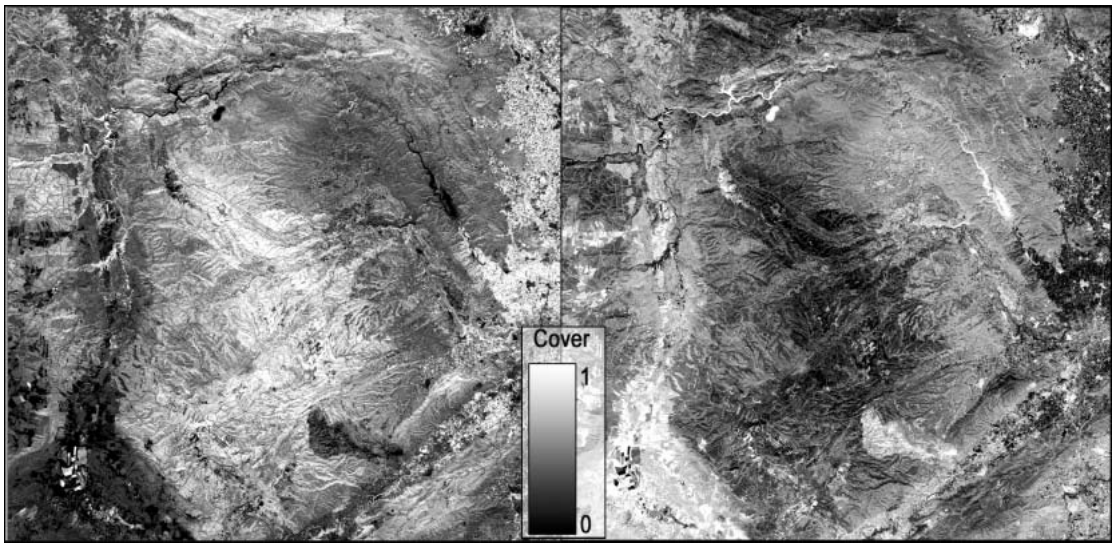

Fig. 7.6: Abundance estimates for green vegetation and lithological background for 2000 derived after SMA and shade normalisation

Validation of the vegetation abundance estimates was based on botanical field surveys undertaken in 2002 and 2003 that were conducted to assess the species composition of fire-affected areas in relation to terrain position. The different plots were located using non-differential GPS and four x-shaped 20 m transects with 40 cm sampling distance were defined for each. At each position, a stick was employed to record contact with each plant for four storeys or, in case of total absence of plants, plant litter, bare soil, rocks etc was surveyed. Since these data could not have been used for a validation of satellite imagery, a number of interpretation steps proved necessary. Herbaceous species assumed to be already dry as well as dead plant material were eliminated from the further analysis. Assuming a vertical projection, it was assessed for each point whether a plant part was touching the stick and if so it was assigned a cover value of 1. In this way, the 200 points associated to one plot were averaged to yield estimated ground cover. These 93 plots were intersected with the satellite-derived green vegetation cover estimates by extracting the corresponding information for a 30 m buffer around the respective plot position. This was necessary to account for possible errors in matching the satellite data with field plots that may result from limitations in precision of the non-differential GPS measurements and the built-in reprojection algorithms used to transfer geographical into UTM coordinates. On the other hand, potential pixel to sub-pixel shifts resulting from geometric ortho-correction of the satellite data may add to the geometric ambiguity. Then, averaged pixel values for the buffers were assessed in relation to the field-based data (Fig. 7.7).

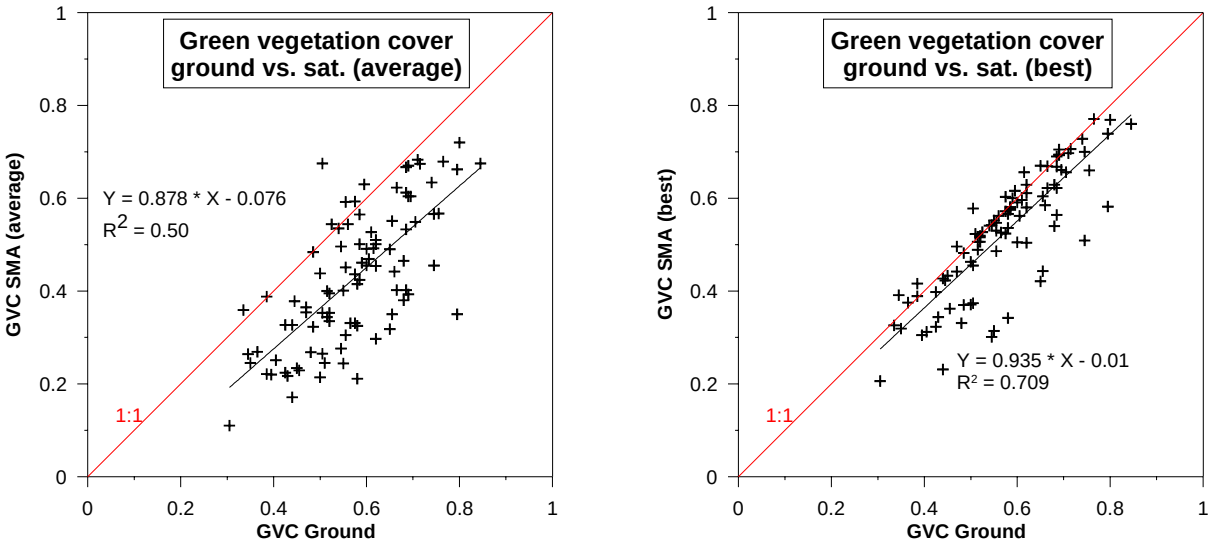

Fig. 7.7: Ground-based vs. satellite-derived green vegetation cover, left: buffer averaged from 30 m buffer, right: best fit pixel from within this pixel, indicating the best possible accuracy for the given data

A gain of the regression function close to 1, but a negative offset of 7.5 % is discernible. Results deviate significantly from the 1:1 line and an r^2 of 0.5 illustrates the strong scattering of data pairs. It can be assumed that a number of reasons inherent in mapping of the field data and linking them to satellite-based information are responsible for this result. In a second step, it was also assessed which could be expected to be the best relation for the given data, presuming that in the heterogeneous landscape field plots should be related to exactly one pixel

in a buffer area representing the geometric deviation margin. Correspondingly, the right section of Fig. 7.7 represents a 'best-pixel' plot, where for each buffer the pixel closest to the field estimate was selected.

A far better match between the two sources results, with the gain of the function being close to 1, an offset of 0.01 and a more satisfactory r^2 of 0.709. This underlines the assumed influence of the high spatial heterogeneity in vegetation cover, with averaging of strongly varying cover estimates leading to the strong discrepancies observed in Fig. 7.7 (left). To the contrary, if the best fitting value of an area corresponding to the potential geometric error is employed, the two data sources clearly align much better. Evidently, two groups of value pairs seem to be inherent in the data. One is oriented close to the 1:1 line, a second group of values is oriented along a straight line with a strong bias towards the field-based estimates.

Summarising, Fig. 7.7 illustrates the difficulty in upscaling plot-related measurements to information derived from moderate-resolution satellite sensors. This is aggravated by the mapping scheme applied in the field, which was originally focused on botanical assessments rather than satellite data verification. A number of points have to be discussed in this respect, which can be summarised into four major components:

- The interpretation approach applied to integrate the highly specific field survey into green cover per plot was based on a binary information, expressing plant contact with the reference stick at any storey with either '1' for present or '0' for absent. Then, a vertical projection integrated these four layers, and if one layer was set to '1', the whole position was counted as '1' meaning 'ground fully covered'. Obviously, this is an unacceptable simplification in the case of very sparse vegetation cover, and violates the basic concept of leaf area index. One leaf or needle touching the reference stick would indicate the same ground cover as a dense shrub or tree, leading to an over-estimation of ground- in relation to satellite-derived data. Also, stems and barks were not eliminated from the integration exercise, which leads to an over-estimation of ground-based information. This manifests in the figures in values orienting in parallel to the 1:1 line, but with a considerable offset indicating higher values mapped in field. Exclusion of these 7 values would change the regression functions to $y = 0.9696x - 0.1134$ ($r^2 = 0.6067$) and $y = 1.0106x - 0.0386$ ($r^2 = 0.8509$) for averaged and best pixel estimates, respectively.
- There is a high degree of heterogeneity apparent in many locations. Where adjacent pixels show strongly differing cover estimates, it is clear that a pixel-based assessment is highly error-prone in case of geometric inaccuracies even at a sub-pixel level. On the other hand, averaging of various pixels might also result in erroneous values.
- Depending on the IFOV of the sensor, integration of patches of dense vegetation with sparsely vegetated patches may occur. This 'bordering effect' is likely to introduce a low pass effect and deprive the satellite image analysis of some of its fidelity. Similarly, for plots which are heterogeneous, (e.g. bare soil/bedrock surfaces covered with isolated shrubs), the exact orientation of transects will strongly influence the results. The field plots had been selected to represent different relief positions. This aggravates

this problem in the case of very narrow relief features, which frequently display highly different plant communities in relation to neighbouring areas.

- There is a time lag of 2 respectively 3 years between the satellite image and field data acquisition. Firstly, surface properties may have changed between the dates. Secondly, due to meteorological conditions, it is not clear whether herbaceous vegetation has been mapped at the same phenological state in both years and the satellite image. Unfortunately, this could not be verified using the existing meteorological data which were only available until 2000.

These aspects need to be considered when trying to upscale field-related information to sensor level. Although some problems can not be resolved, it is concluded that if field campaigns are specifically targeted towards integration of plot-related measurements with satellite data, a more generalised approach to infer vegetation ground cover shall help to solve some ambiguities. Also, it seems desirable to stratify field plots to reflect areas which are homogeneous across various adjacent pixels, minimising the noise introduced by possible geometric deviations. Finally, exact co-registration of field plots and satellite data is of paramount importance. The locating of field plots should be carried out with the highest possible accuracy by using differential GPS and reprojecting coordinates using dedicated transfer functions instead of the simpler algorithms integrated in most GPS devices.

Notwithstanding, the spatial variation encountered in the field is clearly reproduced by the SMA-based estimates. In addition, the spectral mixture approach is known to be very robust when green vegetation is assessed. Hence, it can be assumed that applying the model to the full time series will yield stable results that can be interpreted with high confidence.

7.2.3 Spectral Mixture Analysis of the full time series

TM and MSS endmember models were then applied to the time series. Table 7.1 indicates the RMS error margins attained for the test site.

Table 7.1: RMSE attained from spectral mixture analysis of Landsat-TM/ETM+ and -MSS satellite imagery

Image	RMSE	Sensor
am19750629	6.203278	MSS
am19780710	6.401691	MSS
am19790512	6.226875	MSS
am19800602	6.267132	MSS
am19810606	6.670964	MSS
am19820610	6.411795	MSS
am19840601	6.387342	MSS
am19850722	6.454070	MSS
at19840601	7.355686	TM
at19850722	7.595912	TM
at19860623	9.410546	TM

Image	RMSE	Sensor
at19890717	8.203013	TM
at19910402	6.110445	TM
at19930407	7.605806	TM
at19940528	7.795246	TM
at19950531	8.801256	TM
at19960704	9.258522	TM
at19970402	8.824040	TM
at19970621	8.352394	TM
at19980507	9.253910	TM
at19990627	8.981456	TM
at20000621	8.234521	ETM+

In a final step, it was assessed whether the significantly lower spectral dimensionality of Landsat-MSS in relation to TM does also affect the final vegetation estimates employing the synoptic data set from 1984. A total of 59 homogeneous target areas were defined, which cover the full range of estimated green vegetation fractions, with sizes between 10 and 140 ha. For these, average cover estimates were extracted from both data sets and analysed using regression analysis (Fig. 7.8).

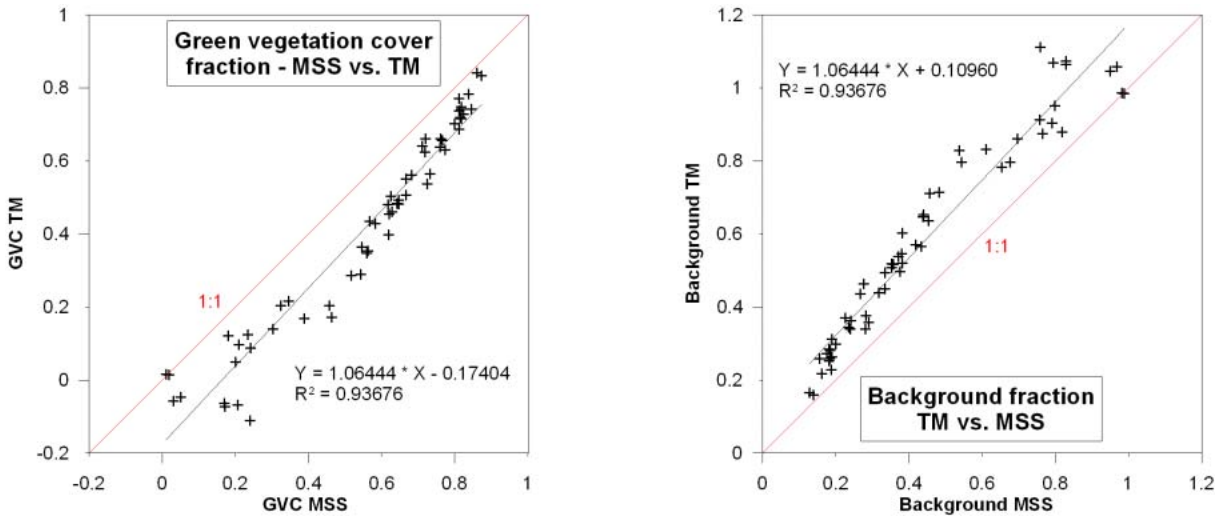

Fig. 7.8: Green vegetation cover derived from spectral mixture analysis of Landsat-TM and MSS using the synoptic data set and congruent endmember models for the respective spectral resolution

Although a general coincidence exists, data pairs appear scattered in regions with low vegetation cover. The MSS sensor produces lower estimates, but with increasing cover levels the value pairs converge towards the 1:1 line. In the range between 0.2 and 0.5 (GVC MSS) residuals do not show normal distribution, but are biased to TM between 0.2 and 0.3 (GVC MSS) and biased to MSS between 0.4 and 0.5 (GVC MSS). In the four band feature space of Landsat-MSS, spectral separability of different materials is obviously attenuated in comparison to the 6 band feature space of Landsat-TM. The value distribution in the two sensor scatter plots is depending on specific local conditions, and patterns differing from the one visible here have been derived for other environments (e.g. Hostert et al., 2003a). When areas are almost fully covered by vegetation, the signal is mostly determined by one surface type, which explains the better coincidence of value pairs with the 1:1 line at higher vegetation levels apparent in Fig. 7.8. Since the regression function shows a high correlation with r^2 of 0.9368, it was decided to apply the derived coefficient to the MSS data to ensure that the satellite data time series is quantitatively consistent.

As a result of these processing steps, vegetation cover maps were prepared for all dates, an example of which is shown in Maps D.1, D.2, D.3 and D.4 (Appendix) for different dates.

7.3 Lagadas

Candidate spectral endmembers were supplied from the different spectral libraries described before. These were complemented with specific measurements conducted on site during a field campaign in May 2002 and in the laboratory using representative samples collected in the area (Röder, 2002). For rock samples, both weathered and freshly cut surfaces were measured, while soils were recorded in their natural and in sieved state. All measurements were carried out using an ASD II Fieldspec Pro spectroradiometer and a Spectralon reference panel. Different endmembers were evaluated with regard to their position in the feature space (compare section 7.2.1) and the endmember model presented in Fig. 7.9 was deployed.

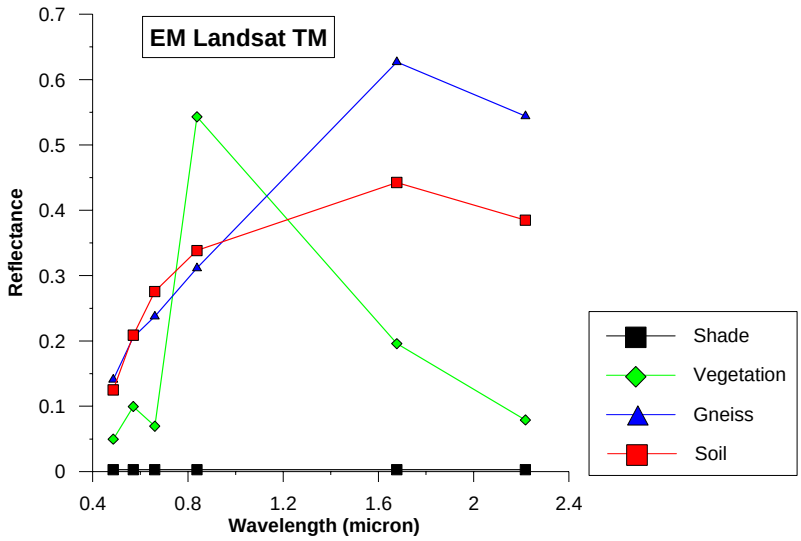

Fig. 7.9: Endmember model deployed for the Lagadas test site

No Landsat-MSS data were used such that benefit could be taken from the higher spectral dimensionality of the data set. For this reason, a multiple endmember model composed of four endmembers was employed: an integral measurement of a *Quercus coccifera* shrub, a laboratory sample of a weathered gneiss sample, and a Cambisol. The shade and vegetation components were forced to be included in any model, while the two endmembers for the background were alternatively used depending on which model yielded the lowest root mean squared error. With regard to the subsequent shade normalisation, the latter was based on an either/or-decision, safeguarding that the same number of endmembers was present in any pixel.

7.3.1 Spectral mixture analysis of the 2000 reference image

The described endmember model was firstly applied to the image acquired on June, 5th, 2000. The result for the full area is shown in Fig. 7.10, the perimeter of the administrative border of Lagadas County is depicted in yellow.

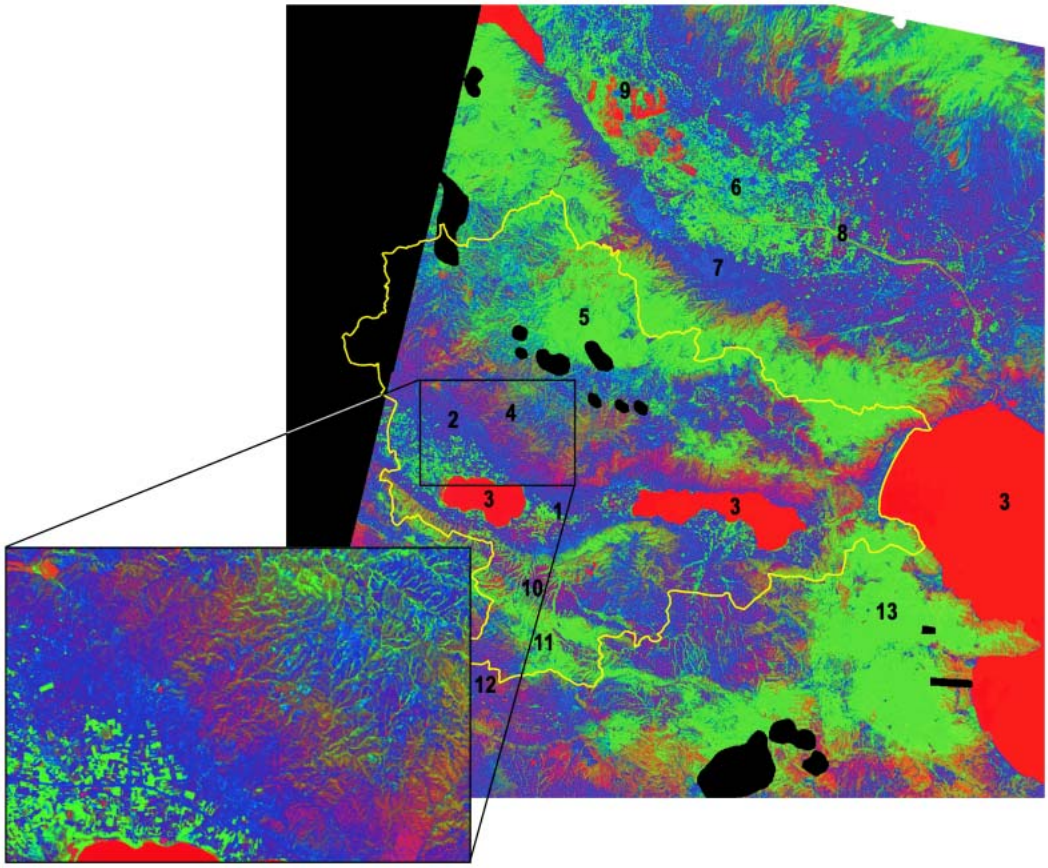

Fig. 7.10: Colour representation of the fractions resulting from spectral mixture analysis for the 2000 TM image (R = Shade, G = Vegetation, B = Bedrock; Lagadas County border in yellow). Numbers relate to major landscape units that can be visually differentiated (further discussion in the text)

Although the model has to be considered simplified considering the large area (approx. 7,200 km^2), the landscape structure is well represented by the resulting fraction image. Mygdonia valley at the centre of the image is characterised by agricultural patchwork patterns, resulting from a mixture of fields and bare soil after harvesting (1). Surrounding these fields are extended areas where bedrock or soils are abundant, which appear in shades of blue in the same way as villages, which can therefore not be distinguished in this representation (2). Lakes Volvi and Koronia show high fractions of shade, corresponding to the deep red colour which is also visible for the visible parts of the Mediterranean sea (3). Moving north, elevation rises in a sequence of slopes with intervening planes, which are frequently used for agriculture, towards the highest elevations of the Mount Vertiskos area, which are dominated by dense deciduous oak forests. The intermediate areas are characterised by the rangelands mainly investigated here, where the typical mixture of green vegetation and bedrock with varying amounts of shade leads to different shades from green to blue (4). Green and orange tones indicate higher amounts of vegetation in steep and narrow valleys, as visible in the zoomed view. Rangeland vegetation is composed of shrubs, herbs and grassland; hence, grass that is already dry might partially contribute to the background signal due to the high spectral similarity between dry vegetation and soils. The oak forests are in their verdant phase in June, which triggers the strong vegetation signal (5). Elevation declines again towards the plain of Strimonas, which is used for intensive irrigated cultivation (6) embedded in a matrix domi-

nated by background materials (7). Again, the typical patchwork of fields and bare soil is clearly visible, as well as the villages embedded in these fields which can be identified by their shape. This plain is transgressed by the Strimonas river which drains towards the Mediterranean Sea. It is visible as a narrow red line accompanied by a green band, corresponding to the irrigated vegetation along the river, from which a network of irrigation channels departs (8). The peculiar red to orange colours within this area result from rice fields where high water levels lead to an increased shade signal (9).

South from Mygdonia valley, the landscape structure is similar, albeit with smaller patches. Rangeland areas of different steepness interact with embedded planes, which are frequently used for agriculture. Here, steep valleys transgressing different plane levels in North-South direction with high amounts of vegetation are prominent (10). The highest areas of Mount Hortiskos area are dominated by sclerophyllous oak forests (11). Descending slopes towards the Chalkidiki peninsula have experienced strong degradation effects. Vegetation cover was reduced by wildfires and heavy grazing in many locations, resulting in dominating blue to red colour tones (12) due to the high contribution of background and shade. In the Southeast, the elevated areas surrounding Mount Stratoniko are covered by deciduous oak forests corresponding to a high vegetation signal and bright green colours (13). For illustration purposes, Fig. 7.11 displays the RGB representation of the spectral mixture analysis results draped over the DEM available for the area. The grey patches correspond to clouds.

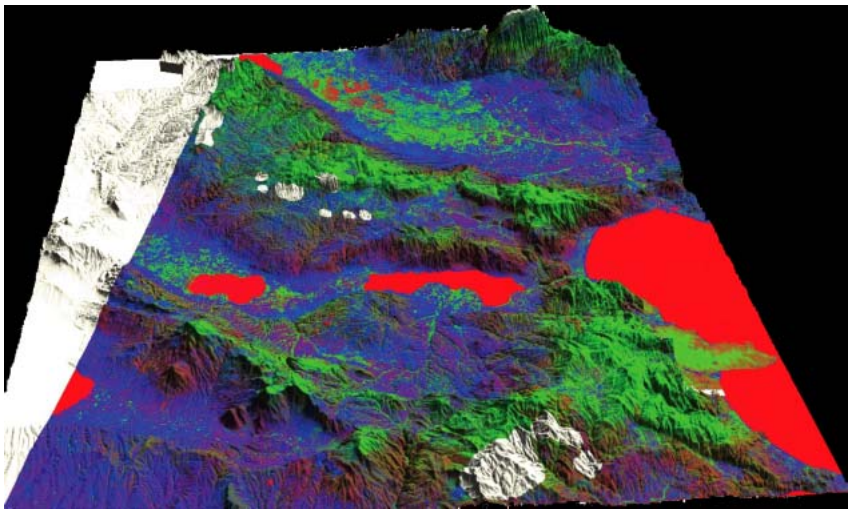

Fig. 7.11: Result of the spectral mixture analysis for the 2000 TM image (R = Shade, G = Vegetation, B = Bedrock) displayed over a DEM (compare Fig. 7.10)

The fractions resulting from the SMA are mostly between 0 and 1 (Fig. 7.12).

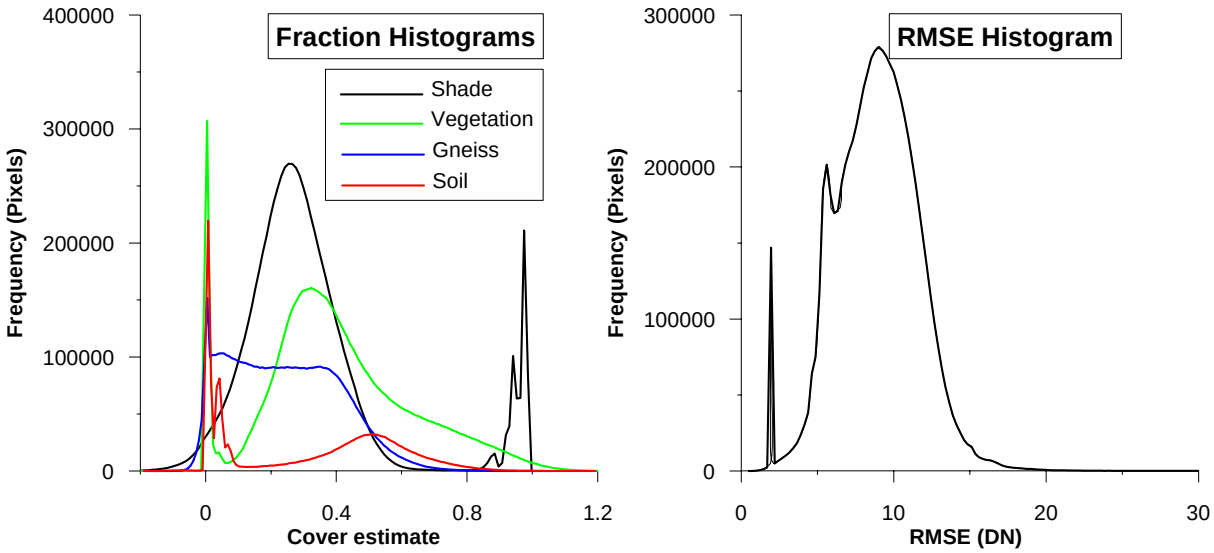

Fig. 7.12: Histograms of the fractions resulting from spectral mixture analysis of the 2000 reference image and corresponding RMSE

Opposed to a normal distribution, a peak occurring close to 0 for the surface material endmembers is contrasted by a peak around 1 for the shade endmember. Two reasons are responsible for this effect. Firstly, the full image contains a significant portion of water bodies, for which the model has not been parameterised. For these features, their low reflectance results in high shade estimates, which are balanced by correspondingly low, and sometimes slightly negative, estimates for the other endmembers. Secondly, in areas where dense deciduous oak forests or irrigated vegetation determine the signal, vegetation fraction estimates above 1 are possible. This is due to the fact that the endmember model was set up to best reflect the grasslands and woodlands where *Quercus coccifera* is the dominating species, and where lower vegetation signals are expected for dense canopies. For this reason, positive exceptions for such areas are compensated for by negative shade proportions. The RMSE displays a similar distribution, with a peak around 1 DN corresponding to the water bodies, and its average around 9 DN corresponding to 2.6 % reflectance.

This results from applying a constrained endmember model to a large, heterogeneous area. While this approach can not be expected to explain all the spectral variance, it ensures a temporally and spatially consistent result and the operational applicability of the model for the full time series. Table 7.2 shows that the average RMSE is lower for most scenes.

The grey scale representation shows that spatial patterns are not very pronounced, suggesting a general agreement of the endmember model with real world conditions. The colour coded representation depicts areas with relatively high RMSE above 3 % reflectance (Fig. 7.13). High RMSE values correspond to the area surrounding villages and fields inside Mygdonia valley. The ground surface is to a large degree covered by fine textured soils and dust. Like agricultural soils these are not represented in the endmember model. Higher RMSE values also appear in the areas of dense deciduous vegetation. In addition, sealed surfaces are usually associated to high RMSE values. To the contrary, the rangeland areas show RMS errors corresponding to a maximum of 2 % reflectance, such that the model can be considered satisfactory for the intended analysis of processes driving the development of rangelands.

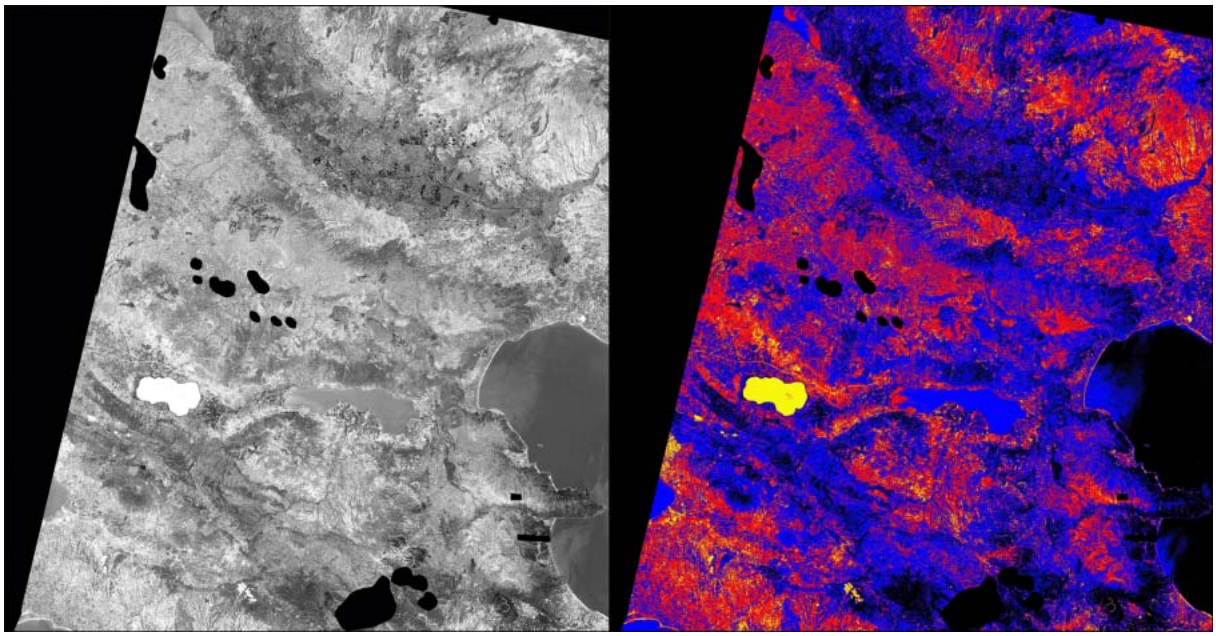

Fig. 7.13: RMSE resulting from spectral mixture analysis of the 2000 image (Left: grey scale; right: black = 0-2 %, blue = 2-3 %, red = 3-4 %, yellow > 4 %)

Subsequently, shade normalisation was carried out following the principle described before, and the gneiss and soil spectral classes where integrated into a single lithological background class (Fig. 7.14).

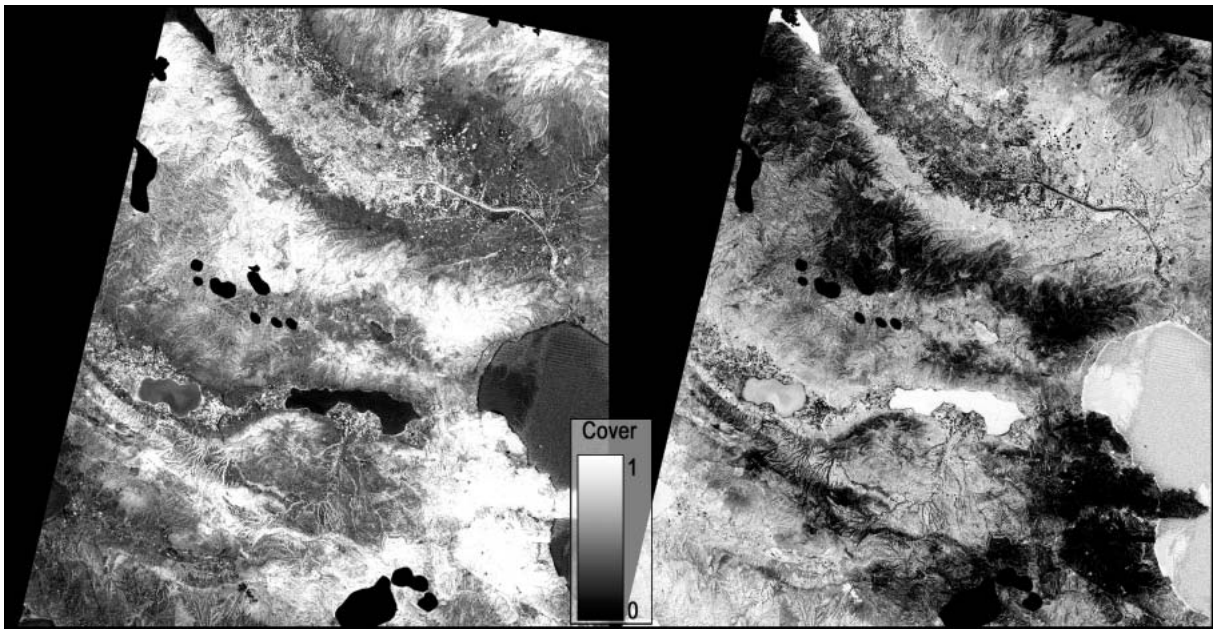

Fig. 7.14: Abundance estimates for proportional green vegetation and lithological background for 2000 derived from SMA after shade normalisation

Validation of the vegetation abundance estimates was based on a limited number of field plots assessed in May and June 2002. These plots were designed to represent four distinctly different types of grassland/shrubland areas: grasslands with a very low presence of shrubs, and sparse, medium dense, and dense shrublands. For the latter, only two plots were selected,

three were chosen to represent the other types, resulting in a total of 11 plots. For each of these plots, two diagonal transects with a length of 35 m and intersecting at the centre coordinate were defined. Along each transect, 8 sampling locations of 1 m diameter were visually assessed. For each of these locations, the cover of trees, shrubs, forbs and grass was recorded separately, and integrated into a single cover estimate for the different categories. These 11 plots were intersected with the satellite-derived green cover estimates by extracting the corresponding information for a 30 m buffer around the coordinates (compare section 7.2.2). Averaged pixel values for the buffers were then assessed in relation to the field-based data (Fig. 7.15).

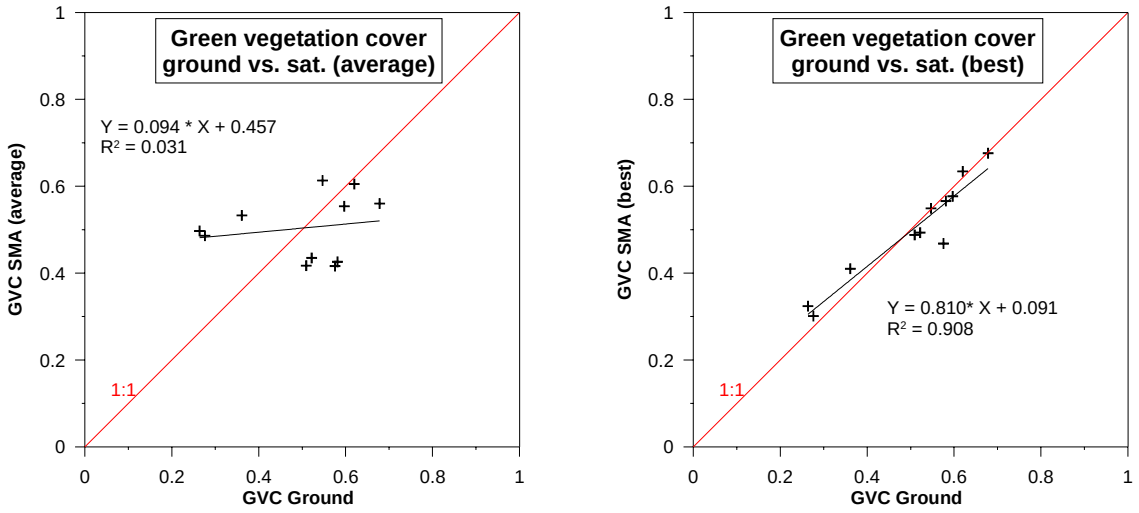

Fig. 7.15: Ground-based vs. satellite-derived green vegetation cover for June, 2000; left: buffer averaged, right: best fit pixel (compare Fig. 7.7)

Results are in accordance with the observations made in the context of the Ayora study (section 7.2.2). However, the number of available plots is significantly lower, which manifests in a strong scattering of value pairs when assessing the averaged satellite-based estimates. In this case, no trend at all can be inferred from the data. Notwithstanding this, the best-pixel estimation yields agreeing value pairs, which arrange close to the 1:1 line, and a regression with r^2 of 0.975, a gain of 0.81 and an offset of 0.091.

The limited availability of field plots poses the biggest problem in validating the TM-based vegetation cover estimates for Lagadas. In addition, trying to delineate homogenous shrubland types and characterising these on an area corresponding to one single pixel of a satellite image appears highly questionable. To illustrate this, Fig. 7.16 displays a small subset of the Lagadas rangeland area as imaged from Quickbird in July/August 2003 (panchromatic channel, 0.6 m resolution), overlaid with a Landsat-grid. It is evident how ambiguous any delineation of shrubland communities is.

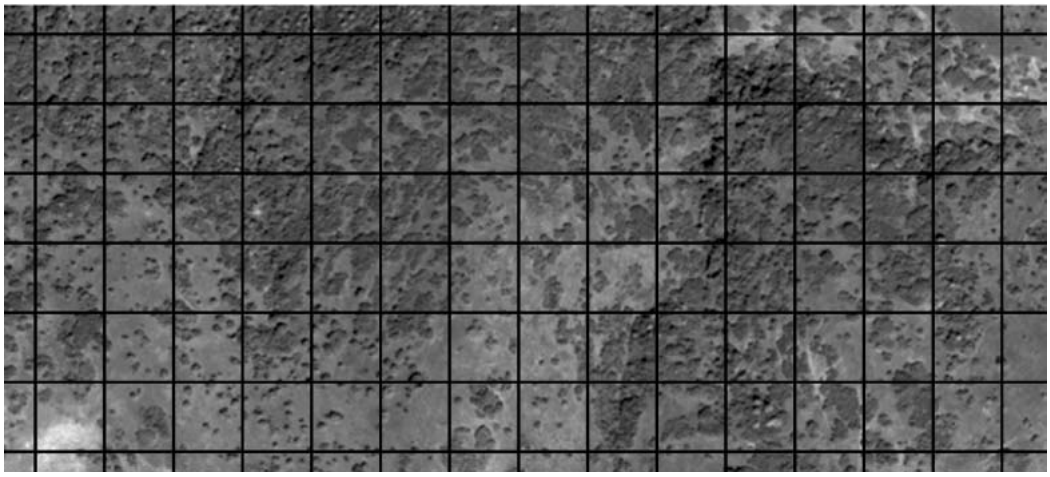

Fig. 7.16: Illustration of heterogeneous shrub distribution in Lagadas rangelands by a sample from a Quickbird image acquired July/August, 2003 overlaid with grid corresponding to Landsat-TM spatial resolution

Beside these problems, all points raised in section 7.2.2 also apply in the present case, but are aggravated by the small number of samples. Especially the time lag between satellite image acquisition and field data reception has to be noted, since in highly dynamic rangeland areas the meteorological framework strongly influences phenological cycles in different years.

Aiming at an additional validation, the second TM image available for 2000 was used to complement this analysis. This image was acquired on August, 16th, when herbaceous species were expected to consist of non-photosynthetic active vegetation only and only shrub and tree species as well as evergreen forbs contribute to green vegetation. Structural information on the same plots was available from a different field campaign. Tree and shrub cover were estimated by plot-integrated estimates of projected cover. After spectrally unmixing and processing with the same endmember model, the same validation steps were carried out using the field estimates of woody vegetation cover (Fig. 7.17).

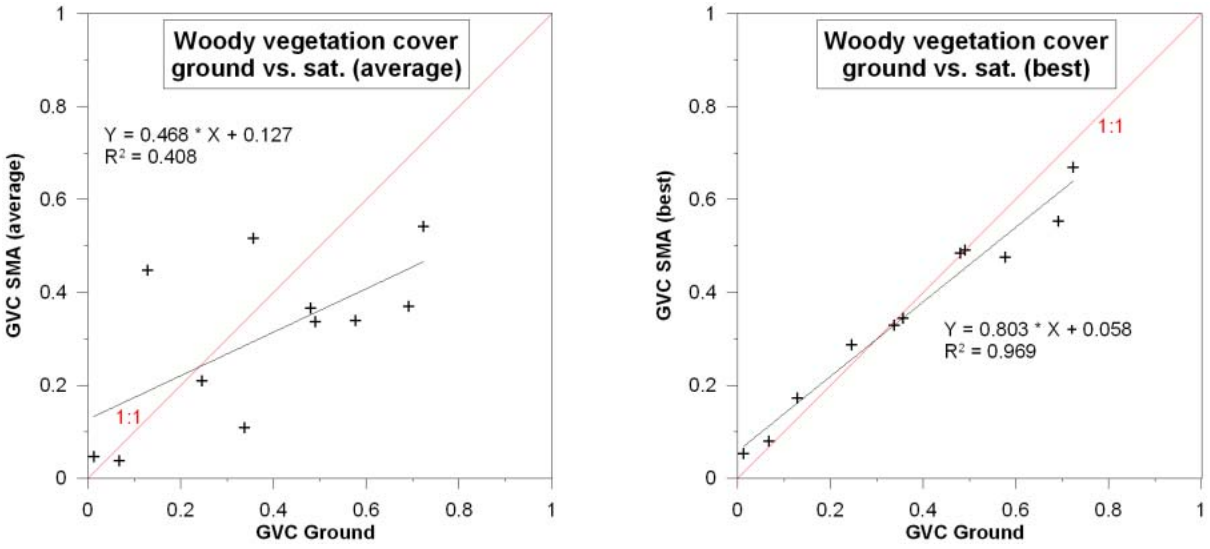

Fig. 7.17: Ground-based vs. satellite-derived green vegetation cover for August, 2000; left: buffer averaged, right: best fit pixel (compare Fig. 7.7)

Obviously, the pattern corresponds to the one found for the earlier image. The average plot again points at the problem of spatial heterogeneity of the landscape. Yet, the best-pixel estimate is again highly consistent between image- and field-derived values.

Considering the plot-based validation of the unmixing results together with the statistical estimates and documented robustness of the method, the unmixing model defined for Lagadas was accepted for further analysis of the time series.

7.3.2 Spectral mixture analysis of the full time series

Following the initial analysis and validation, the TM/ETM+ endmember model was applied to the time series (Table 7.2). Examples of the green vegetation cover maps for selected dates are presented in Maps E.1, E.2 and E.3 (Appendix).

Table 7.2: RMSE attained from spectral mixture analysis of Landsat-TM / ETM+ satellite imagery

Image	RMSE	Sensor
lt19840703	8.346945	TM
lt19850519	6.751818	TM
lt19860623	7.581724	TM
lt19870610	6.883214	TM
lt19880714	9.426712	TM
lt19900704	8.749487	TM
lt19920623	7.791471	TM
lt19930712	8.471217	TM

Image	RMSE	Sensor
lt19940528	7.939477	TM
lt19950702	9.303941	TM
lt19960704	7.703033	TM
lt19970621	6.843122	TM
lt19980710	7.966624	TM
lt19990611	7.655773	TM
Lt20000605	9.136886	ETM+
lt20000816	8.390090	TM

7.4 Discussion of the adopted spectral mixture analysis scheme

Spectral Mixture Analysis has been shown to be a highly suited approach when assessing vegetation cover in sparsely vegetated regions, and it has been successfully applied in different studies in semi-arid conditions. Although this has been confirmed in the context of this study, the different steps involved require a critical review of the uncertainties entailed.

First of all, the spectral dimensionality of the input dataset largely influences the possible representation of the spectral variance within an image. In cases where Landsat-MSS data need to be incorporated, this obviously leads to a reduction in the number of endmembers that can be represented in the model. Even in the case of Landsat-TM with its higher spectral dimensionality, high redundancy between bands has to be noted. For instance, separating dry vegetation from soils with only one image is hardly feasible. In addition, in many cases soils do not sufficiently differ from underlying bedrock and can hence not be discriminated. Given this, it is often considered advisable to utilise highly constrained endmember models. Although this is done at the expense of a higher overall RMSE, it does ensure a higher spatial consistency of resulting fractions compared to more flexible models. The selection of endmembers is obviously the crucial step in SMA. Here, the availability of spectral libraries containing a large number of reference measurements for different surface materials greatly

enhances the approach, since at the geometric resolution of Landsat-TM or -MSS most pixels must be expected to be a mixture of different materials.

When executing the SMA, assuming linear mixture for all surface types must be rated critical. Especially in the case of vegetation canopies of different densities, this simplification appears problematic. However, without a-priori knowledge of local conditions the establishment of non-linear mixture models is a complex task and contradicts the prerequisite to base spectral image interpretation on operational procedures for analysis of extensive time series. Similarly, the shade normalisation employed represents a simplification, since it assumes that the artificial shade component is equally distributed among the different surface materials. Hence, the approach suggested here must be considered a compromise between meeting conditions of quantitative validity and operational applicability.

Another important aspect is the selection of appropriate spectral references for vegetation. Typically, plant communities are variable through space and time. Hence, if endmembers are selected to represent typical conditions, they may not be equally appropriate in all locations or for all dates of a time series. For instance, an endmember representing sclerophyllous, woody vegetation may yield higher abundance estimates if the actual vegetation is dominated by herbaceous species at the time of photosynthetic activity. This has to be kept in mind in the context of temporal interpretation of green vegetation cover when plant succession processes occur. In the case of woody vegetation, a higher estimation of the shade fraction can be expected compared to herbaceous vegetation, which adds to the ambiguities of shade normalisation. Notwithstanding, specific treatise of these processes, for instance through stratified application of different vegetation references, would require a-priori knowledge that is mostly not available while at the same time introducing spatial discontinuities that greatly hamper the interpretability of results.

One of the problems common to most studies making use of SMA for vegetation analysis is the satisfactory validation of results. While solutions have been successfully demonstrated in the context of homogeneous areas and under controlled sampling designs specifically aimed at SMA validation (e.g. Elmore et al., 2000; Twele et al., 2004), this study has illustrated the problems arising when dealing with highly heterogeneous, patchy, and fragmented landscapes. This is aggravated even more if test areas are not repeatedly mapped through field visits, or where data not specifically collected for the purpose need to be used. While one problem is related to the considerable lag in spatial scales between satellite data and field estimates, another problem simply arises from different demands on the data. Remote sensing data are integrating surface elements, necessitating corresponding field information. In this case details on vegetation species appear negligible in relation to cover estimates for the largest possible unit. On the other hand, ecologists or botanists often place a higher emphasis on very specific, often plant-sociological analyses which are difficult to synchronise with satellite-based cover estimates (Brogaard & Ólafsdóttir, 1997; Congalton & Green, 1999). This has been illustrated by the Ayora study, where an excellent data base of field information was available, but where the focus resulted in a sampling strategy which almost denied matching these data with satellite imagery.

Secondly, defining areas to be considered of homogeneous composition in field relating to homogeneous areas in satellite imagery is almost impossible given the spatial configuration of many Mediterranean rangelands. This has been illustrated for the Lagadas area using the Quickbird panchromatic image with a resolution of 0.6 m in the panchromatic band. Finally, the composition of plant communities largely influences the comparability of field- and satellite-derived data. Species with strong phenological dynamics exhibit strongly varying photosynthetic activity in different seasons depending on the respective meteorological conditions. Hence, if field information has not been collected in parallel to the image acquisition, this may introduce considerable ambiguities in validation exercises.

Consequently, if it is not feasible to conduct validation campaigns specifically for the interpretation of satellite imagery, it is often mandatory to integrate field data in a flexible way, depending on the respective specifications. One possibility to get an impression of the theoretical correlation is the best-pixel approach employed here, since otherwise geometric inaccuracies together with the high spatial variability of landscapes often deny to match the two data levels on per-pixel basis, while buffer averaging introduces a low-pass effect that has been shown to reduce the comparability of the cover estimates. One solution to this problem would be the stratification of field campaigns based on preliminary analysis of satellite images, for example using a simple vegetation index, and then defining target field plots in homogeneous patches. In addition, validation based on field work can at least be complemented by statistical accuracy estimates, such as assessing fraction and RMSE histograms or their spatial distribution using local knowledge.

Concluding, SMA can be considered a robust approach especially when green vegetation is analysed since its specific spectral properties can be distinguished from other surface materials with high confidence. Beside quantitative estimates of target materials for which the model is optimised, SMA has proven to adequately reproduce landscape structures with respect to the limited number of reference materials included. Nonetheless, the model performance might be enhanced if suitable ground reference data were available, which might particularly reduce the resulting error estimates.

As a result of these processing steps, spatially explicit vegetation cover maps can be provided for all dates as a first important information product. They provide an objective and synoptic view over large areas both for present and past times, as shown exemplarily in Appendix D and Appendix E.

8 Time series interpretation

In this study, multi-temporal data sets with one image for every year where acquisitions with a satisfactory quality had been available were employed. Vegetation is the target variable of this approach, which required that the images cover comparable phenological dates in the respective years. Image acquisition dates have been selected to ensure comparability, but it has to be noted that deviations due to phenological dynamics do occur.

From multi-temporal image data with a sufficient temporal coverage spatial patterns of temporal trends may be derived using time series analysis techniques. According to Schlittgen & Streitberg (1999), the analysis of trends involves consideration of two deterministic and two stochastic components:

Deterministic

- Transient component (trend)
- Cyclic component

Stochastic

- 'Memory' effects
- Red and white noise

The additive stochastic components represent 'disturbances' when assessing long-term trends in vegetation development. While 'white noise' relates to random disturbances, which might for example result from data processing, 'red noise' encompasses all kinds of autocorrelated disturbance effects. The 'memory' effect relates to environmental conditions or events which are not independent, but influenced or determined by prior states. The deterministic component can be differentiated into the transient component, representing the actual long-term development and the cyclic component. The latter includes seasonal effects, which may, for instance, be interpreted as phenological cycles when appearing in vegetation-related time series.

In the case of hypertemporal data sets, such as small-scale data from the NOAA-AVHRR sensor family, a number of interpretation approaches exist, which are suited to address and partially separate the different components. These encompass Fourier analysis (e.g. Andres et al., 1994), change-vector analysis (e.g. Lambin & Strahler, 1994a, b), principal component analysis (Townshend, 1987; Eastman & Fulk, 1993; Lambin & Strahler, 1994a; Anyamba & Eastman, 1996; Turcotte et al., 1993; Benedetti et al., 1994) or wavelet transform (Brunsell & Gillies, 2003), among others. Typically, amplitude and phase values derived from Fast Fourier Transforms provide a measure of important land use characteristics; amplitude values for twelve or six months appear closely related to the vegetation response to annual rainfall and temperature patterns, while the phase of the annual growth cycle provides information to differentiate various responses due to phenological dynamics. The wavelet transform is an efficient tool to overcome some restrictions resulting from the exclusive use of the power spectrum (i.e. loss of time information). Wavelet analysis of surface phenologies can provide in-

formation on events affecting vegetation, such as fire, drought, land use conversion or climate fluctuations (Brunsell & Gillies, 2003).

Although it is obvious that interpreting time series in this manner may provide interesting information, these approaches remain limited to data sets with equidistant value pairs. Besides, given the population of time series with one image per year, such methods are not suitable, and the detection of the underlying temporal patterns would require a temporal resolution at the order of days to months. Rather, characterisation of trends in rangelands that might indicate degradation of resources has to be based on assessing the first, transient component. This may, however, be difficult to be separated from the other components; especially the cyclic and the white noise component have to be considered sources of ambiguity.

8.1 Multitemporal statistics

Utilising the available Landsat-MSS/TM/ETM+ data set, quantitative characterisation of the development of a target variable (i.e. green vegetation cover) is undertaken by means of linear trend analysis. The regression is calculated to minimise the sum of least squares between given and estimated values for each fix point, and yields a function of the type

$$y_t = g \cdot t + o \tag{8.8}$$

with y_t = vegetation cover at date t
t = date of image acquisition (e.g. in days since launch of sensor)
g = regression coefficient (gain)
o = regressions constant (offset)

The offset of the resulting function characterises the level of vegetation cover estimated for the date of sensor launch. Alternatively, it can be related to the starting date of the observation period if t_0 is set to the date of the first image acquisition. The gain describes the direction and magnitude of the development over the monitoring period. It is possible to calculate this regression function on a per-pixel basis, such that the temporal development can be illustrated in a spatially differentiated way.

Different methods exist to assess the statistical robustness of the approach and mathematically describe the trends. The strength of the correlation between time and vegetation cover can be described using the correlation coefficient (r), from which the coefficient of determination' or 'explained variance' can be calculated by raising r to the second power. In addition, different parameters characterising the variation of a data set may be assessed, such as the standard deviation (sd) or the coefficient of variation (v), which relates sd to the mean value of the data. In the present context, these parameters are sometimes of limited use, especially if there is a low value range of target variables, and the gain of the regression function is low. For instance, in the case of stable vegetation, a low gain, indicating that there is no trend, will be accompanied by a low correlation coefficient. In this case, the factor 'vegetation cover' is not dependant on the factor 'time'. The term 'trend' always describes a change of a certain parameter with time, but areas where no change has happened are equally important. This may even be an indication of ecologically valuable areas in case of stable, high abundances of

vegetation cover. Hence, multi-temporal statistical analyses should be extended beyond exclusively focusing on the characterisation of trends.

Further to the parameters detailed before, a two-sided t-test can be used to evaluate the statistical significance of the regression coefficient derived from the trend analysis (Bahrenberg et al., 1990). This is a valid approach if the number of samples is large enough to be considered representative. Although in some cases a minimum number of 30 samples have been suggested, the lower total number available in these time series can still be rated satisfactory given that each year within the observation period is represented by one image. While in cases of very low sample numbers, no significant trends may be expected, a very high number of samples will increase the probability of significance regardless of real conditions. Corresponding to the previous sections, a low variance of vegetation cover will result in insignificant trends for these areas, which correspondingly need to be analysed in a different manner.

As a result of these considerations, the 'root mean squared error' (RMSE) is suggested as a complementary parameter, which is calculated according to

$$RMSE = \sqrt{\frac{\sum_{x=1}^{n}\left(y_x - \hat{y}_x\right)^2}{n}} \tag{8.9}$$

with y_x = observed value (i.e. vegetation cover) at sample x (i.e. date *t*)

$\hat{y}_x$ = value estimated at sample *x* using the linear regression function

n = number of samples

This formulation exclusively depends on the deviation between observed and estimated values, and is hence independent of the direction and magnitude of the regression coefficient. The RMSE can also be normalized to account for the absolute level of values observed.

8.2 Temporal profiles

The conceptual framework for monitoring and assessing typical rangeland processes to be developed here is based on densely populated multi-temporal data sets. This requires interpreting information on temporal behaviour for a given location in a given thematic context. Hence, beside the technical implementation of the pixel-wise trend analysis, one important component of this framework is the appraisal of the temporal profiles that can be expected.

The temporal behaviour is commonly determined by interacting environmental and anthropogenic factors; however, noise due to errors present in multi-temporal data sets may lead to profiles which are not interpretable. This may be caused both by data-inherent errors, but also be introduced at the different stages of data pre-processing. As a result of variations in the accuracy of the geometric rectification, matching pixels may not always represent exactly the same location in field. The radiometric correction process may not be equally successful for all and/or throughout all images, such that observed changes between images may partially relate to processing artefacts. Finally, the adopted approach of spectral mixture analysis in-

volves a number of simplifications that might result in varying accuracy of vegetation characterisation in different local contexts, especially where surface properties strongly differ from the model applied. In addition, variations of target parameters are frequently present in multi-temporal data, but if these do not result from error sources described before they will not be referred to as 'noise' but are assumed to comprise information that needs to be adequately interpreted. Hence, it is necessary to define how a given temporal behaviour, which is characterised by the different statistical parameters described in section 8.3, is interpreted and rated.

This means that criteria have to be defined which help to 'translate' statistical parameters derived from the pixel-wise trend analysis into a spatial representation indicating environmental processes. To illustrate this, a set of typical temporal profiles extracted from the Lagadas multi temporal data set is shown in Fig. 8.1. Included are the statistical significance (α) estimated from a t-test, the corresponding RMSE normalised by the data mean ($RMSE_{norm}$) and the coefficient of determination (r^2). The gain is given in its original form, i.e. related to days. For a thematic interpretation it may be converted to rate of change estimates related to one year or the total observation period (compare chapter 9 and 10).

Plots a and b show typical profiles representing obvious negative and positive trends. While $RMSE_{norm}$ shows low to moderate values, the trends are clearly supported by statistical parameters and may characterise areas, where the presence or termination of strong grazing leads to a decrease or an increase of vegetation cover, respectively. On the contrary, plots c and d visualise stable behaviour with time, where residuals are equally distributed around the regression line, gains are close to zero, and $RMSE_{norm}$ values are low. These profiles are statistically not significant. Nonetheless, they clearly represent stable environmental conditions, which manifest on a high level in the case of the sclerophyllous oak forest (plot c). Plot e demonstrates how a slightly negative trend is 'disturbed' by a single event in the year 1996. A drastic reduction in vegetation cover is followed by a rapid increase, which may be the result of a fire event, followed by rapid growth of early succession species. In rangeland areas, this is frequently observed as a result of intentional burning of unpalatable shrubs. Although a significant trend could be derived from this series and the normalised RMSE is still on a moderate level, it results in a rather low r^2. It is obvious that this type of trend needs to be specifically analysed. Plot f shows a strong decrease between 1987 and 1990, followed by a period of stability. While α and r^2 are similar to plot e, the $RMSE_{norm}$ is rather high. In addition, residuals are not equally distributed around the regression line, indicating a violation of the conditions for a valid regression analysis. In fact, this profile suggests separating the series in two periods, where the first period may relate to heavy grazing and a corresponding decrease in vegetation cover, which then remains stable on a very low level for the second period. This is potentially a result of continued grazing prohibiting vegetation recovery. Similarly, plot g might also indicate a slightly negative trend until 1995, followed by an equally moderate increase thereafter. Variance in this case is much lower, resulting in lower estimates of α and r^2, while $RMSE_{norm}$ is still on a relatively high level, such that this profile is more difficult to interpret. Finally, plot h is an example of a profile that does not seem to represent an interpretable behaviour. A significant positive trend is derived, which is, however, not supported

by $RMSE_{norm}$ or r^2. The profile was derived from the agricultural areas of the Mygdonia valley, explaining the obvious fluctuation of vegetation cover.

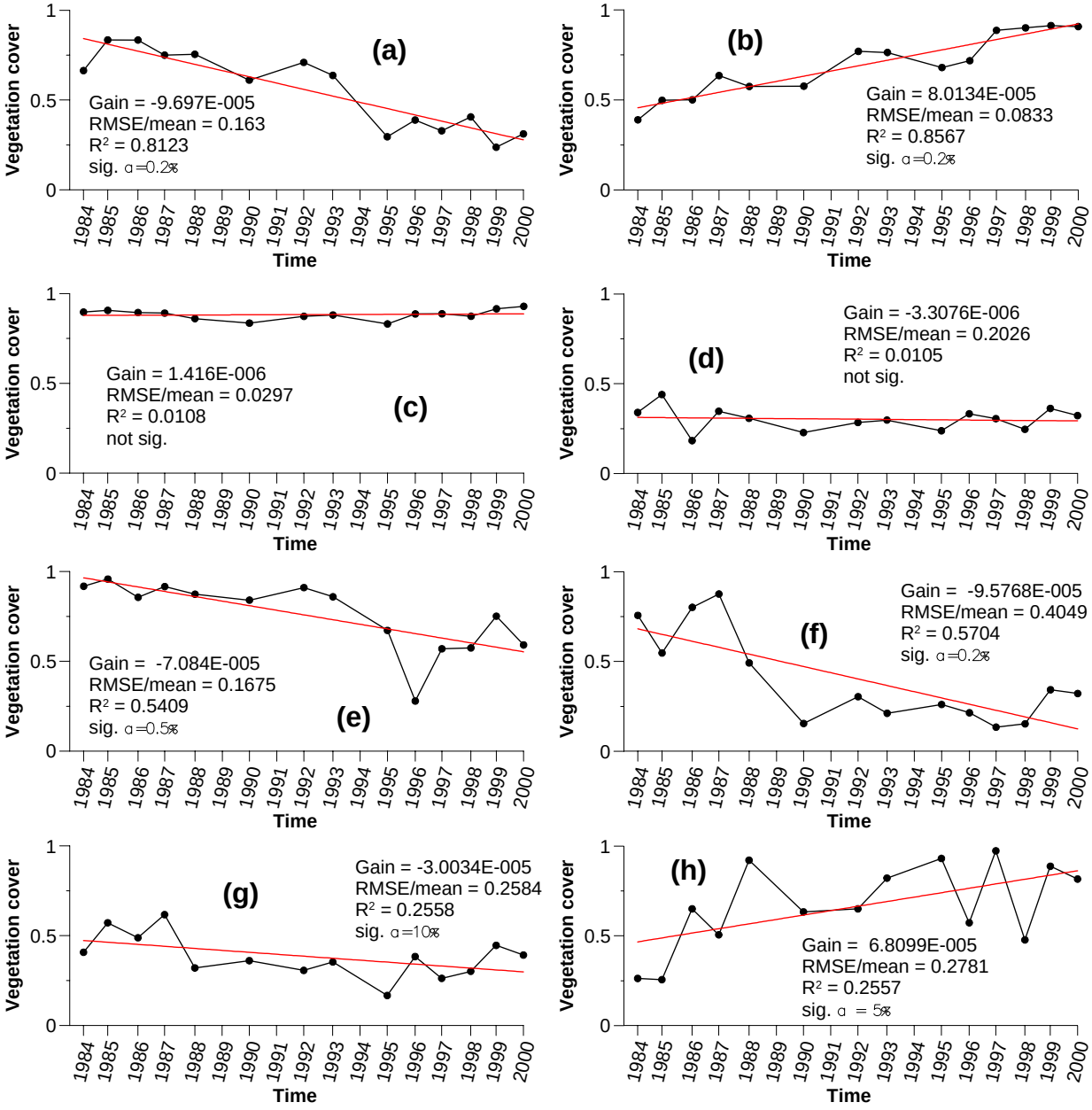

Fig. 8.1: Sample temporal profiles of green vegetation cover in the Lagadas area, illustrating negative (a, e, f, g), positive (b, h) and indifferent (c, d) temporal development as a result of different factors and how these 'translate' into statistical parameters; more specific explanations in the text

Although agricultural areas will not be considered in the further analysis, it underlines that exclusively assessing trends based on statistical significance or correlation parameters might lead to a considerable misconception. In the case of real 'trends', where a change in vegetation cover is apparent with time, it is especially 'disturbed' or 'multiple' trends that require careful assessments. In addition, it has been shown that in the case of natural, undisturbed development, stable areas fail to be identified using statistical trend descriptors, where con-

sideration of the RMSE or $RMSE_{norm}$ may be used to additionally characterise these areas. As a means of tackling 'disturbed trends', evaluation of vegetation cover changes between consecutive dates is suited to identify disturbance dates.

Finally, although care has been taken to select scenes acquired at comparable dates and hence comparable vegetation phenology, temporal profiles do exhibit a fluctuating pattern as a result of the respective climatic conditions in single years. This effect is most prominent for areas where plant communities dominated by herbaceous species react sensitive to climatic boundary conditions, while for instance dense sclerophyllous forests are less sensitive to phenologic variations. Although such patterns affect the temporal profiles, it has been shown that they can be used to actually identify different types of vegetation communities (e.g. Hostert, 2001; Hostert et al., 2004).

Different types of information may hence be extracted from time series of satellite data if the necessary knowledge of individual boundary conditions and local environmental settings exists.

8.3 Implementation of the regression analysis

The temporal analysis using the full data set has been implemented based on the principles of regression analysis and calculated on a per-pixel basis[1]. A number of different statistical and auxiliary parameters are computed to describe the profiles:

- Regression gain (g)
- Regression offset (o)
- Regression sigma (σ)
- T-test (t)
- Correlation coefficient (r)
- Root Mean Squared Error (RMSE)
- Relative Error ($RMSE_{norm}$)
- Maximum Residual
- Time of Maximum Residual
- Standard deviation
- Mean
- Coefficient of Variation (v)
- Number of valid cases

In addition to these parameters, a binary mask is produced for each year as auxiliary information. It marks locations where the difference to the preceding year exceeds a threshold that

[1] The software package 'timestats' employed here was developed by Dr. Thomas Udelhoven at the Remote Sensing Department, University of Trier, under the IDL programming environment.

may be defined prior to the analysis. This is especially important in cases where various disturbances, such as fire, clearcutting etc., occur, since the maximum residual criterion only identifies the largest deviation. Prior to the execution of the multi-temporal, statistical analysis cloud masks have been prepared for all images where clouds are present and the flagged locations are excluded from the further calculations.

Residual analysis can be employed to assess whether linear regression analysis is valid to describe the temporal behaviour and to identify locations where the presence of two distinctly different trends in one profile violates the foundation for a single linear analysis. Such cases may indicate a change in boundary conditions or pressure factors. The separation of the profile into two trend functions would be adequate, but this is statistically problematic due to the associated reduction in the number of samples and not feasible when working with image data and consequently thousands of individual profiles. These possible cases are partly accounted for using the threshold masks, since pixels which exhibit one or more exceptions from threshold can be separately analysed, as will be presented in the following sections.

It is essential to adequately ‚translate' these parameters into spatially explicit and consistent information on the temporal behaviour of vegetation, that may then be linked to auxiliary information to identify the drivers behind trends. The underlying rules and thresholds to support this translation have to be defined in the respective thematic context of the investigated sites and will consequently be treated in sections 9.2 to 9.4 for Ayora and section 10.1 for Lagadas.

9 The Ayora case study

The Ayora region is a typical example of a semi-arid to sub-humid Mediterranean region that is strongly affected by recurrent wildfires. The region has undergone dramatic land use changes in the past decades, with widespread land abandonment and a strong reduction in grazing activities. These must be considered when assessing the fire regime. Local management authorities have implemented various measures to prevent fires and mitigate their negative effects, but a systematic assessment of fire events for longer periods and large areas, which might assist in refining management interventions, has not been available so far.

As a consequence of this, a monitoring framework for rangelands being subject to large fire events should comprise the following elements:

- Exact mapping of fire dates and perimeters
- Characterisation of post-fire dynamics on a quantitative level
- Characterisation of the state of landscape units in relation to their potential vegetation cover
- Identification of driving factors for post-fire dynamics
- Characterisation of post-fire vegetation succession at the level of plant communities

9.1 Fire events and perimeters

In areas affected by wildfire events, accurate mapping of fire perimeters is an important task to identify areas of recurrent fires or to assess the benefit of management interventions. In the Ayora area, fire perimeters were available for a limited number of years and sites, which have been mapped using orthophotos and local knowledge of foresters and fire workers. This is a valuable source of information, but it may be biased by different factors. For instance, visual mapping often tends to strongly generalize. Also, a field-based perspective is not equally consistent and objective for all areas. These aspects make remote sensing based approaches a suitable alternative, since it is impartial and supports the repeated assessment of the same areas.

In chapter 8, Fig. 8.1e depicts a typical temporal profile of fire affected areas. In the case of the Ayora test site, locations may even be affected by more than one fire. Other disturbances of vegetation communities, such as grazing, clearcutting, or building of new plantations, are not present except for spatially constrained vegetation removal associated with fire prevention measures, and minor extensions of existing agricultural plots. For these reasons, a multi-temporal interpretation scheme needs to focus on characterising specific disturbance events (i.e. fire) and subsequent vegetation regeneration rather than identifying long-term trends. In this context, mapping of fire perimeters using a threshold analysis is a key step to identify the year and exact perimeter of such events. In a second step, this information can be used to stratify the trend analysis for a given region. Setting the year of a fire event as a starting date for the given area, the linear trend represents the quantitative recovery of vegetation following this fire, provided no second fire event occurs. Succession after fires involves an evolution of

plant communities and the earliest phase is dominated by grasses and other herbaceous species, which are responsible for a fast increase in green vegetation cover. This is followed by a less rapid increase in cover as the abundance of woody species increases. Depending on climatic conditions and phenological stages at the time of image acquisition, the transition from herbaceous to woody vegetation might theoretically event result in a decrease of vegetation cover (compare chapter 7).

The trend analysis is carried out on a per-pixel-basis. For this reason, it was necessary to resample the TM images to match the geometric resolution of MSS data, which was achieved by spatially averaging abundances derived from SMA.

The fire perimeter maps that had been available from the Spanish Forestry Service supported the definition of a suitable threshold for the minimum difference in vegetation cover between subsequent years for fire event identification. In principle, the threshold can be applied in two different ways; either based on a relative or an absolute difference. Employing the relative difference, fluctuations at low vegetation cover levels, which might result from phenological variations, are erroneously characterised as fires. This introduces considerable fluctuations in the data. To the contrary, employing an absolute threshold effectively suppresses these fluctuations at the expense of omitting fire events in areas with very low cover levels. In the present case, fires are most frequent in areas with moderate to dense cover. After iterative testing using the available ground truth data an absolute threshold of 30 % cover change was chosen, which correctly represented the available perimeters. Integrating this threshold into the trend analysis leads to a set of fire perimeters for the period 1975-2000. These have been labelled according to the acquisition year of the image succeeding the fire. This data set can be utilised to produce fire perimeter maps for use in GIS. This is an important information product to assess the impact of past management actions. It shows a higher degree of detail compared to conventional fire mapping based on a combination of aerial photographs and field information. Typical differences between the fire perimeters derived using the present approach and traditional methods are visualised in Fig. 9.1 based on the fire perimeter identified for 1994.

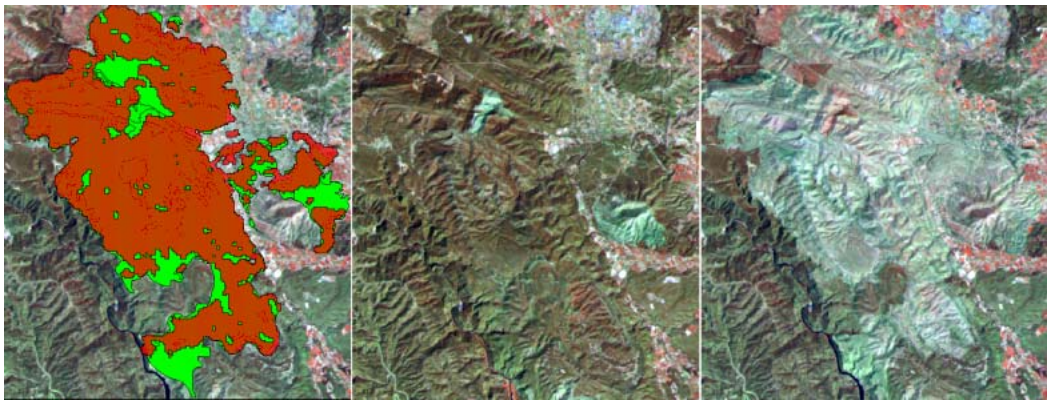

Fig. 9.1: Fire perimeters provided by Spanish Forestry Service (green) and derived in this study (red) compared to corresponding satellite images in 1993 and 1994.

In general, the two perimeters coincide very well. Notwithstanding, the satellite-based approach obviously neglects some areas which have been mapped using conventional methods.

The first patch is composed of two sub-patches. The first of these has obviously not been affected by the fire, probably as a result of the fire break that is visible just north of this area. The second sub-patch is an area without vegetation as a result of a smaller fire preceding the image acquisition, which has accordingly been mapped and attributed to the year 1993. The other disparities result from the methodological difference between applying a threshold focusing on areas with a significant reduction in vegetation cover, in contrast to the higher degree of generalisation associated with conventional, interactive mapping approaches. Depending on the problem addressed, or the severity of fires, the threshold of 30 % cover difference may be modified accordingly.

The method is an efficient means of precisely identifying fire perimeters over long time periods. For reasons of data availability, only one image per year is used; hence, it is not possible to yield the exact dates for the fire events.
As a second information product, the recurrence of fires at a given area can be assessed, which can assist in assigning different fire risk categories (Fig. 9.2).

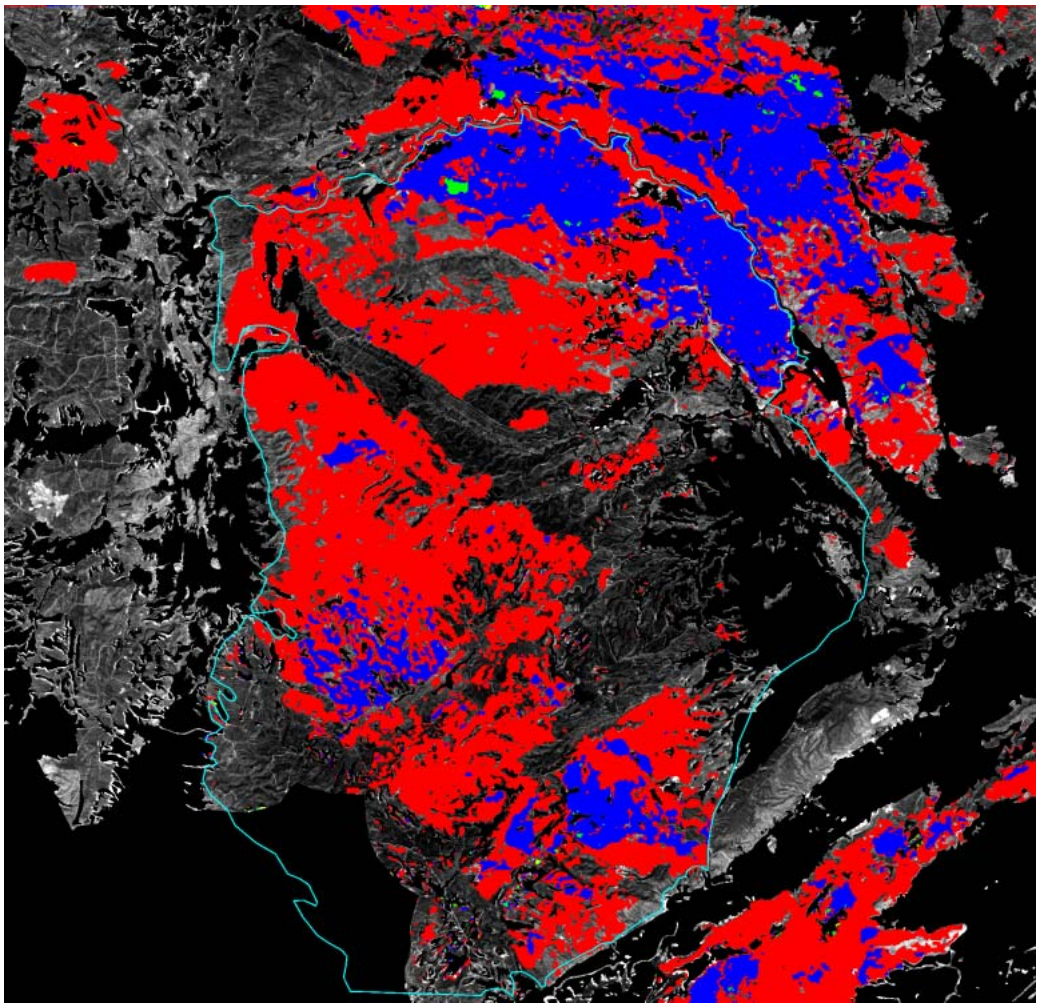

Fig. 9.2: Number of fire incidents (1975-2000) derived from pixel-based integration of fire perimeter data. Red: 1 fire, blue: 2 fires, green: 3 fires (core area depicted in cyan)

Most of the central test area not used for agricultural purposes has been burned once or twice, while fires are less frequent in the region west of the Ayora valley. The core area to be analysed in more detail in the following sections is depicted in cyan.

The spatial extension of fire affected regions clearly shows the severity of the fire problem in the Ayora area. Table 9.1 lists the total surface affected in the different years.

Table 9.1: Fire affected areas per year according to multi-temporal threshold analysis ([1] ach fire per pixel counted; [2] only one fire per pixel counted in case of recurrent fires, [3] agricultural areas excluded)

Year	Burned area (ha, Full)	Burned area (ha, Core)
1978	348.26	88.62
1979	11267.52	615.85
1980	32665.90	31584.65
1981	517.38	0
1982	1351.78	274.70
1984	3582.33	16.22
1985	6074.37	2658.66
1986	19362.02	16062.06
1989	84.25	84.25
1991	1342.43	1263.80
1993	7952.92	4807.90
1994	8306.76	396.93
1995	29079.3154	12541.48
1996	102.98	21.21
1997	322.03	322.03
1998	207.19	46.18
1999	308.31	236.53
2000	2043.31	2043.30
Total[1]	124929.06	73064.46
Total[2]	97801.46	59159.28

	Full area (ha)[3]	Core area (ha)[3]
	190211.14	107289.59
Burned area (%)[1]	65.67	68.1
Burned area (%)[2]	51.41	55.14

The fire in 1979 (according to the described approach labelled ‘1980’) was the largest fire during the period observed. Although ambitious management plans have been launched in its wake, a number of large fires have followed since, most prominently in 1986 and 1995. The latter corresponds to one of the most devastating fire events in the history of Spain, the general pattern emerging from the area statistics reflects the fire history for the whole of Spain given by Moreno et al. (1998). The severity of the problem is also reflected by the percentage of burned area, amounting to more than 50 % for both the full and the core area that have been burned at least once.

9.2 Vegetation dynamics in unburned areas

In the following sections, the assessment of vegetation dynamics in unburned areas and areas affected by fires is exemplarily presented for the major fire incidents in the core area. As outlined in Fig. 9.2, this is situated east of the Ayora valley and bordered in the North and East by the *Rio Júcar*. This area was defined to represent a consistent landscape unit and excludes the large agricultural areas of the Ayora valley and the orange plantations west of the mountain range towards the plain of Valencia. In addition, the *Rio Júcar* is a natural border in the North, although the region north of the river shows landscape features similar to the area in the South and the interpretation scheme could theoretically be extended to the northern territories.

Maps D.5 and D.6 (Appendix) show the spatial pattern corresponding to the areas that have not been subject to any fire between 1975 and 2000, complemented by t-tested significance. The gain parameter from linear regression analysis represents the rate of change per day. This could be used to calculate the rate of change for the period observed which characterises the overall rate of vegetation cover increase. These areas have been extracted by masking all fire areas as well as agricultural areas. It has to be comprehended that the agricultural mask is based on information dating back to 1989, such that newer agricultural plots are not represented. Positive change, negative change and stability of vegetation cover are often spatially continuous, while especially at the western rim of the core area they also appear in scattered form. The significance map shows that both positive as well as negative change are associated with significance levels of α=10 % or higher. On the other hand, relatively stable areas with only little or no change are characterised as insignificant. These compact maps provide an indication of the associated rates of change and their statistical significance.

Furthermore, a synoptic analysis of different parameters resulting from the trend analysis is expected to support a better spatial differentiation of zones with similar temporal behaviour or environmental dynamics. In accordance with chapter 8, consideration of the RMSE may increase the information content in areas with stable conditions. A composite was produced that integrates the gain rate, the RMSE and the average vegetation cover for the full observation period between 1975 and 2000 (Fig. 9.3). Numbers indicate positions of temporal profiles shown in Fig. 9.4.

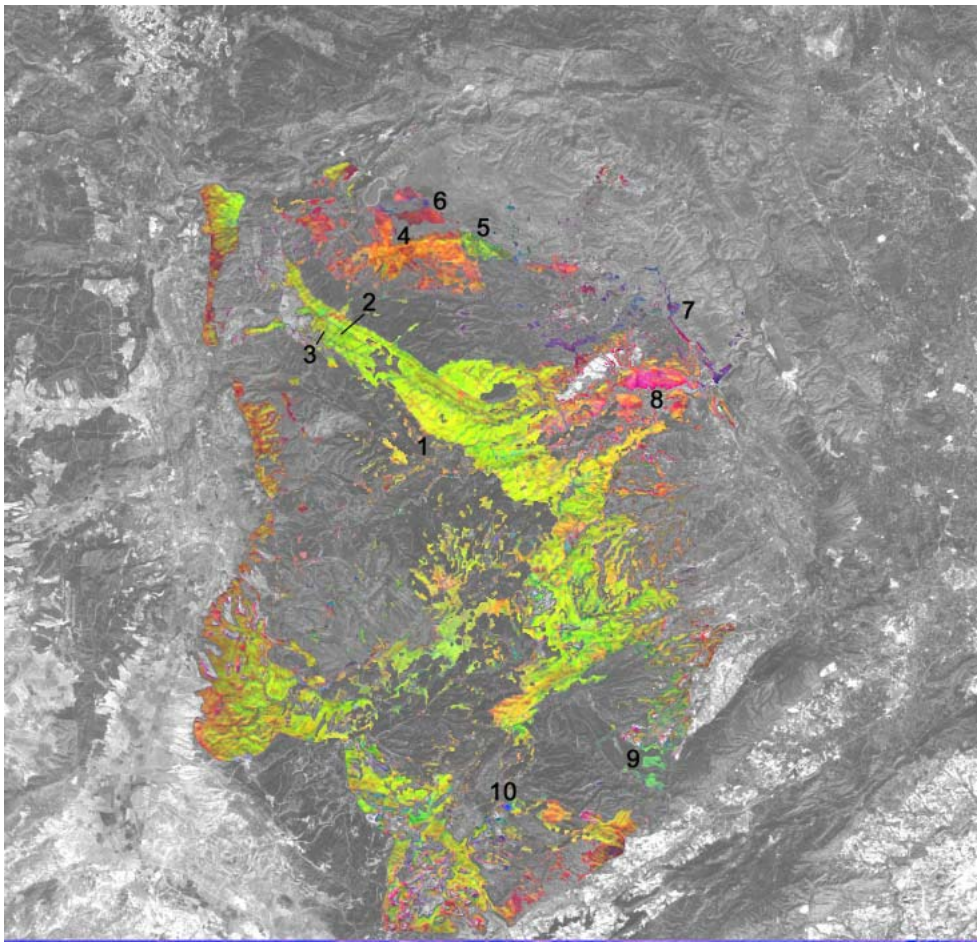

Fig. 9.3: Multi-temporal analysis of areas not affected by fires during the observation period. R = trend gain, G = average cover of the time series, B = RMSE of the linear trend function; agricultural areas are excluded; the numbers correspond to the profiles shown in Fig. 9.4

Typical temporal profiles were extracted to characterise these major groups (Fig. 9.4), which are specified according to the numbers in Fig. 9.3. Profiles 1-1 and 1-2 give two examples of development resulting in yellow tones, which are caused by an increase in vegetation cover on a high cover level, and with a relatively low RMSE. Both profiles show a higher degree of fluctuation during a first phase, which is succeeded by a smoother second one. Typically, this indicates a change in plant composition with a transition from grasses and herbs to shrub and tree species. Profiles 2-1 and 2-2 belong to the same area, but no clear increase in cover is present. Thus, the contribution of the red colour is reduced compared to example 1, such that the high level of vegetation cover leads to green colour tones. Between these two typical manifestations, transitions in colours and corresponding profiles exist, representing the undisturbed, nowadays forested areas. The photos displayed in Fig. 4.12 and Fig. 4.18 have been taken in these areas. Profile 3 illustrates the linear pattern visible within this compact forested area. It shows a decrease in vegetation cover followed by stability on a lower cover level. Together with its shape, this indicates the creation of fire breaks between 1982 and 1984, where the associated removal of vegetation has not exceeded the threshold level, which was confirmed by available maps. The photo shown in Fig. 9.5 was taken from within a large fire break and more such bare strips can be seen in the background.

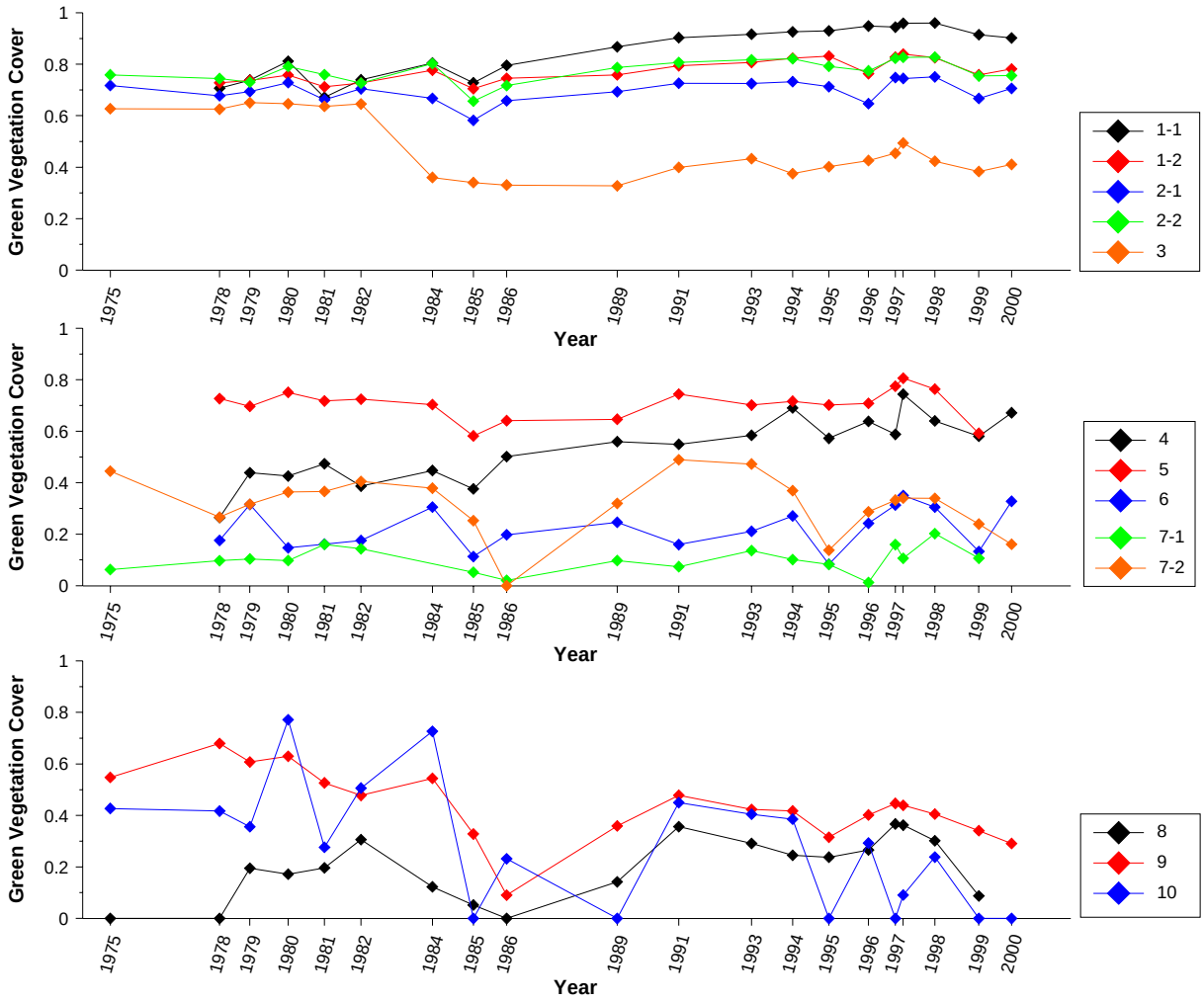

Fig. 9.4: Temporal profiles of the development of green vegetation cover in areas not affected by fires during the observation period. The numbering of the profiles corresponds to Fig. 9.3 and the profiles illustrate typical pattern groups inferred visually from multi-temporal statistics (Fig. 9.3)

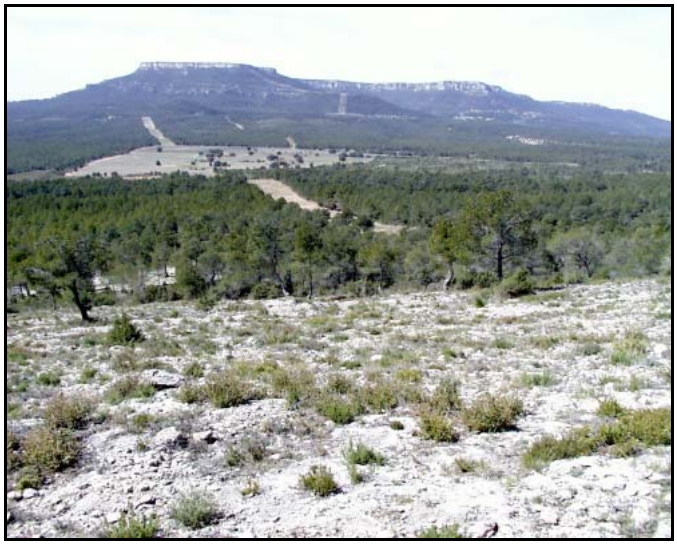

Fig. 9.5: Network of fire breaks in the Ayora test area

Profile 4 represents the area dominated by shades of red to orange and brown. The reason is an increase in vegetation cover resulting from reforestation measures that have been initiated in this area in the mid 1980s. Directly adjacent, dark shades of green can be noted, which are similar to plots 1 and 2. As illustrated by profile 5, they correspond to undisturbed vegetation which is stable on a relatively high level. In the patch characterised by profile 6, a strong pink component is present in generally dark red colours. Vegetation in this area is dominated by sparse grasses and low shrubs, which manifests in the profile in a fluctuation with a correspondingly high RMSE, and a very weak positive tendency.

Profiles 7-1 and 7-2 represent the linear feature in the East of the core area, where pink to dark purple tones prevail. Profile 7-1 appears similar to profile 6, with cover estimates fluctuating on a relatively low level. This area corresponds to a narrow valley and varying amounts of available water are expected to cause the apparent fluctuation. Profile 7-2 also relates to this linear patch, but was extracted from the zone with dark purple to blue colours. As can be seen, a slight overall negative trend can be inferred, decreasing the intensity of the red colour component in the hue composition. Similar to 7-1, a high fluctuation is apparent, although on a higher overall level. Both profiles show a drastic reduction in vegetation cover especially for 1986 and 1995. An analysis of the fire masks for the corresponding years confirmed that the fire perimeters for both years are directly adjacent. This suggests that the location has actually been affected by these fires, without having been identified due to the threshold. This exemplifies one limitation of the approach, where locations may be neglected if they are close to, but below the threshold. Although this could be solved by lowering the critical value, it would on the other hand introduce considerably more noise in the fire masks, hence the fixed-threshold approach is maintained.

Profile 8 corresponds to a compact area with a bright pink colour. Here, the absence of vegetation in 1986 follows a general trend of the preceding years. Hence, a fire-effect is not obvious. It can rather be suspected that this patch is dominated by plant communities with a strong response to varying water availability, supposedly a combination of grasses and other low herbaceous species. This is supported by the high fluctuation in cover estimates, which occurs on a moderate overall cover level.

Profile 9 represents patches with a cyan colour tone. The profile shows an effect similar to profile 7-2 and assessing the fire masks confirmed that this patch is directly adjacent to the 1986 fire area. In contrast to 7-2, the overall trend is negative, which results in the red colour component being set to almost zero. The high fluctuation after the fire points at the presence of grasses and herbaceous species strongly affected by the amount of available water.

Finally, the small patch illustrated by profile 10 shows an almost pure dark blue colour. This is explained by the strongly negative trend and an extreme fluctuation of cover estimates. It is situated in close proximity to agricultural lands, and must be expected to represent a location not included in the agriculture mask.

Concluding, the synoptic interpretation of parameters resulting from the multi-temporal statistical analysis differentiates spatial patterns even in generally ‘undisturbed’ areas. Comparing Fig. 9.3 with Map D.5 and D.6 (Appendix), this would remain undisclosed when solely

considering rates of vegetation increase or statistical significance. Especially assessing the fluctuation of temporal profiles using the RMSE must be noted in this context. Fig. 9.3 shows a spatial distribution of areas with a stable or slowly recovering vegetation cover on high general levels, which are 'surrounded' by areas characterised by temporal profiles with more fluctuations. Their properties were analysed using representative pixels, and unique groups of temporal behaviours can be noted. Particularly, the temporal profiles can in some cases be related to major groups of plant communities, since herbaceous species are distinctly different from areas dominated by shrubs and trees.

9.3 Vegetation dynamics in fire-affected areas

Corresponding to the previous representation, the following sections address fire-affected areas which are exemplarily presented for the major fire incidents in the core area. Maps D.7 to D.14 (Appendix) show rates of change and t-tested significance for the fires in 1980, 1986, 1993 and 1995. Overall rates of change were calculated from the gain parameter. Nonetheless, the resulting absolute figures differ depending on the time that has elapsed since the last fire. For reasons of comparability, it was opted to transform the gain to an average yearly rate of change. This maintains comparable dimensions for all fire events from different years, but it needs to be interpreted considering the respective overall period referred to.

The analysis of post-fire dynamics was carried out for the largest fire events in the core area, which occurred in 1980, 1986, 1993 and 1995. It was conducted using a temporal stratification approach, where the respective fire year was set as the starting date for the linear regression. The resulting maps, indicating yearly gains of green vegetation cover and t-tested significance are shown in Map D.7 to D.14 (Appendix). All maps show increasing vegetation cover following the fire events, although the calculated gain rates do vary. In some locations, however, the post-fire behaviour is characterised by stable or even negative gains. This mostly results from subsequent fire events which disturb the regeneration. This is especially obvious for 1980, with 4 subsequent fire events affecting different parts of the area. The gain rates were converted to yearly rates, hence it is important to comprehend the overall time elapsed after the respective fire event when assessing the overall vegetation recovery. For the 1980-fire this results in notable overall increases on the quantitative vegetation cover level, which is confirmed by the accompanying maps of trend significance. Significance levels of α=2 % are attained for the regions burned only once, while areas affected by a second fire can be clearly identified since they show no statistical significance. For the 1986-fire, this is similar, although the area in the North, which was only burned once, does show varying α-levels, and even an area without a significant trend can be noted. The respective maps for 1993 and 1995 are less homogeneous, and although both regions have not been subject to subsequent fires significance of the trends seems to be weak. In these cases, the low number of samples in the regression analysis is a critical issue and significance levels may not be interpretable.

As a further means of characterisation, integrated temporal profiles were prepared (Fig. 9.7). These represent the development of green cover estimates averaged from areas with a similar fire history, which have been attained by segmenting fire zones using all fire perimeters. This was done considering fires before and after the regarded event. Although the study aims at

assessing post-fire dynamics, the resulting profiles show the full period to provide a better impression of the specific characteristics of the respective patch. For instance, the 1980 fire has been separated into a southern and a northern fire zone. Then, the southern zone has been further distinguished into the large patch that has only been burned once, the area that has been burned again in 1993, and the smaller patch further south, which has also been burned once. Similarly, the northern fire zone has been separated into the area only burned in 1980, and the zone where a second fire in 1995 occurred. Fig. 9.6 shows the resulting patches using the numbering and colour coding of the temporal profiles in Fig. 9.7.

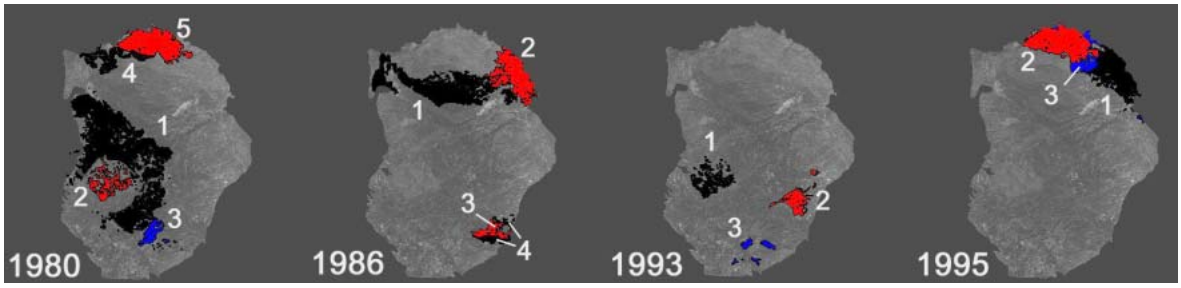

Fig. 9.6: Patches of identical fire history used to create integrated temporal profiles

First of all, it is obvious that almost each continuous fire zone is at least partially affected by more than one fire. In the graphical representation, this results in corresponding patches for different years, such as for instance patches 1980-2 and 1993-1 or 1986-2 and 1995-1. While most of these segments result from intersecting fires, the patch represented by profile 1993-1 is completely located within the perimeter of the large 1980-fire (southern zone).

Where patches are directly adjacent and rather compact, the profiles are frequently close to being identical before the second fire takes place. Especially for the 1986-fire area this is striking, but relates also to the 1995-fire area, where initial differences in profiles result from earlier fires. For the 1980 fire, this behaviour is also apparent in the southern fire zone, where the large, compact patch (profiles 1980-1 and -2) is highly consistent prior to the second fire in 1993. The smaller patch 3 behaves similar to 1980-1 but on a lower cover level. Also, the northern 1980-fire zone shows a deviating behaviour, with a stronger increase in cover beginning in 1986. After occurrence of the 1995-fire, which affected patch 1980-5, the temporal profiles converge again. In contrast, the 1993-fire patches, which are smaller and more scattered, appear less consistent over time. While prior to the fire in 1993 this is an expression of the different fire history, the curves are parallel following the 1993 fire event. Generally, both of the more recent fires in 1993 and 1995 seem to be characterised by two opposing trends after the fires. In both cases, a quick recovery is followed by a decrease in cover, which also explains the spatial representations and lacking statistical significance visualised in the maps shown in Appendix D.

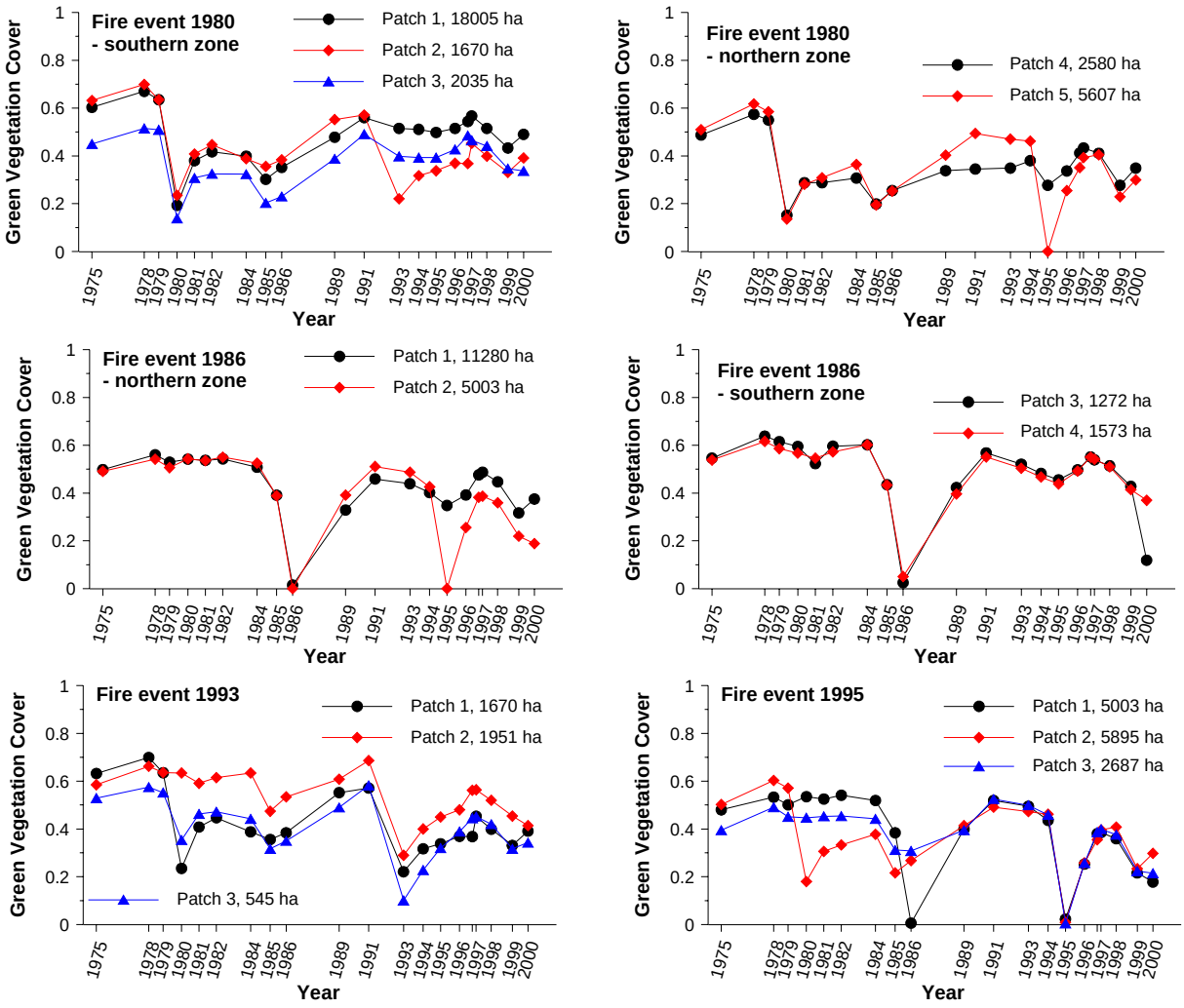

Fig. 9.7: Integrated temporal profiles characterising major fire events, differentiated according to year of fire and to coherent patches depicted in Fig. 9.6

Concerning the magnitude of vegetation loss from fires two effects are generally important: On the one hand, the fires in 1986 and 1995 resulted in a complete destruction of vegetation, i.e. zero cover estimates in the respective years. On the other hand, the 1980- and 1993-fire events are both characterised by bottom levels of vegetation cover of more than 10 %. Although this appears to give an indication of the fire strength, it is more probable that in these cases there is a lag between the actual fire date and the time of image acquisition. In the case of the 1980-fire, it is known that the actual event took place in 1979, such that the relatively high level of vegetation cover must be attributed to a partial regeneration that has already taken place, and a similar effect is suspected for the 1993-fire area.

Focusing on post-fire dynamics, different phases of the temporal profiles of green vegetation cover relate to different stages of plant succession, and frequently follow the exponential shape described by Viedma et al. (1997). Succession following fires commonly starts with grasses and other herbaceous species, which are adapted to fire disturbance as sprouters or seeders (‘pyrophytes’), and often recover quickly as a result of the ‘mineral flush’ after fires (e.g. Christensen, 1994). They commonly develop through shrub-dominated communities with single, isolated trees at a later stage, to eventually become dense matorrals or forests,

given undisturbed conditions for sufficiently long periods. The effective manifestation of such a post-fire succession is determined by a combination of local physical conditions, the climatological framework and the presence or absence of further disturbance factors during the recovery phase (e.g. Quinn, 1986; Whelan, 1995). Generally, it is accepted that following fires an autosuccession takes place, where pre-fire species are present immediately after the fire, even if the relative abundance or frequency of individuals changes later. Accordingly, no secondary succession occurs, and modifications of this process may only be expected if the frequency of fires exceeds or falls below the period required by plants for regeneration or maturation (e.g. Trabaud, 1994).

According to field observations (Vallejo et al., 2002, 2004), different types of shrublands with and without trees can be found, but apart from the areas unaffected by fires (compare section 9.2), forests have not re-evolved in notable extensions during the period considered. Six typical communities were identified, which were described in more detail in section 4.1.5:

- Open shrublands: low shrub cover; dominance of *Brachypodium retusum* and *Ulex parviflorus*
- Kermes oak shrublands: dominance of *Quercus coccifera* shrublands with a herbaceous layer mainly composed by *Brachypodium retusum*; usually on limestone and non-agricultural soils
- Gorselands: strongly dominated by *Ulex parviflorus*; mainly on North-facing slopes and abandoned agricultural areas.
- Shrublands with Pines: dense shrublands dominated by *Rosmarinus officinalis* and *Ulex parviflorus*, with high numbers of *Pinus halepensis*; in areas burned once and lowlands that have never been cropped.
- Mixed rosemary shrublands: almost equally composed of *Rosmarinus officinalis*, *Ulex parviflorus* and *Quercus coccifera*, most abundant shrubland type in the test area
- Rosemary shrublands: dominance of *Rosmarinus officinalis* and *Ulex parviflorus;* in previously forested areas burned once, above 800 m, on limestone, and preferably on South-facing smooth slopes.

Assessing the temporal development in the Ayora region (Fig. 9.7), two major patterns may be separated. All profiles related to the 1980-fire show a relatively fast increase at the first date succeeding the fire, following which the further increase clearly slows down. Also, the pre-fire level is not reached in any of the plots before a second fire, although no disturbance by fire occurred during a period of 13 and 15 years. Although this is partially attributed to the fact that the lowest cover estimates for 1980 are already recorded in an early state of recovery, this behaviour is striking when compared to the 1986-fire. Here, vegetation recovers to almost the pre-fire level within 5 years. Following this fast recovery, a fluctuating pattern can be noted where no second fire occurs (1986-1, 1986-3), which appears in similar form in profiles 1980-1, -2 and -4. Similar effects appear for the 1993- and 1995-fire events, but in both cases the time following these events is too short to allow for in-depth interpretation.

The fast recovery following directly after fires is connected to the rapid colonisation with grasses and herbaceous species. Depending on local conditions, especially *Brachypodium retusum*, *Ulex parviflorus* and *Rosmarinus officinalis* can be expected. Then, the extension of resprouters such as *Quercus coccifera*, or in rarer cases *Pistacia lentiscus* and *Juniperus oxycedrus* leads to a partial closure of the canopy and a consequent reduction of the lower canopy. As outlined before, this transition to different shrubland types depending on local conditions, is much slower, and does not necessarily manifest in a further increase in vegetation cover. Although at subsequent stages, tree species (*Pinus halepensis*, *Pinus pinaster*, in rarer cases *Quercus ilex*) are appearing, conversion of these shrublands of different composition and density to forests was not observed in the test area during the period viewed. In the case of pine regeneration, the frequency of fire recurrence is of great importance. If undisturbed periods are not long enough to allow pines to reach sexual maturity and produce viable seed banks, they are not able to locally recover through an autosuccession process; rather, their re-evolvement depends on seed migration (e.g. Vallejo & Alloza, 1998). Contrarily, *Quercus ssp*. are able to quickly resprout after fires. Consequently, some authors have termed *Quercus coccifera*-dominated shrublands a 'disclimax' or 'alternative steady state' (e.g. Blondel & Aronson, 1995). Often, the development of these shrublands is associated with the accumulation of large amounts of flammable biomass, which greatly enhances the risk of new fires and consequently diminishes the probability of succession towards forests (e.g. Naveh, 1994; Moreno et al., 1998; Vallejo & Alloza, 1998). The profiles shown in Fig. 9.7 illustrate the strong initial recovery effect resulting from the availability of high amounts of mineral nutrients after fires, if these are not washed off by rain events, as well the stable cover behaviour thereafter. Although this recovery pattern is positive in terms of protecting soils from erosion, a long-term reduction in productivity has been reported from different investigations. For instance, Specht (1981) analysed different sclerophyllous woodlands, where, in the first years after fires, highest increases in phytomass were recorded. This was, however, followed by an overall decrease in net primary productivity of these areas.

Besides, the availability of water plays a key role in the actual post-fire dynamics. Both initial recovery rates as well as fluctuations apparent in all profiles during longer undisturbed periods are strongly influenced by this factor. In section 9.4.1 ('climate'), it is further investigated whether this suspected influence is supported by available precipitation rates.

Beside the analysis of post-fire dynamics through recovery rates of green vegetation cover, or its characterisation using integrated profiles, it is often important for land managing authorities to assess the present state of an ecosystem in relation to a reference state on a spatially differentiated basis, for instance to assess the recovery state of vegetation at a given date. This information is difficult to infer from the maps based on the gain of the post-fire trend analysis. One way of providing this type of information is by relating vegetation cover at a given date and location to the theoretical maximum for this location, or to the theoretical maximum for a larger area. Making use of the available data, this has been implemented by integrating the series of vegetation cover estimates for the period observed and yield two indices providing the required information. Firstly, vegetation cover at each time step available was related to the maximum for the same area, i.e. pixel, for the full period covered, which was assumed to represent the theoretical maximum for that area. Secondly, a ratio was calculated between the

vegetation cover given at a certain date and location, related to the overall maximum for all dates and for the full area under investigation. This value was derived from unburned locations under exclusion of agricultural areas. Examples for both approaches are given in Fig. 9.8.

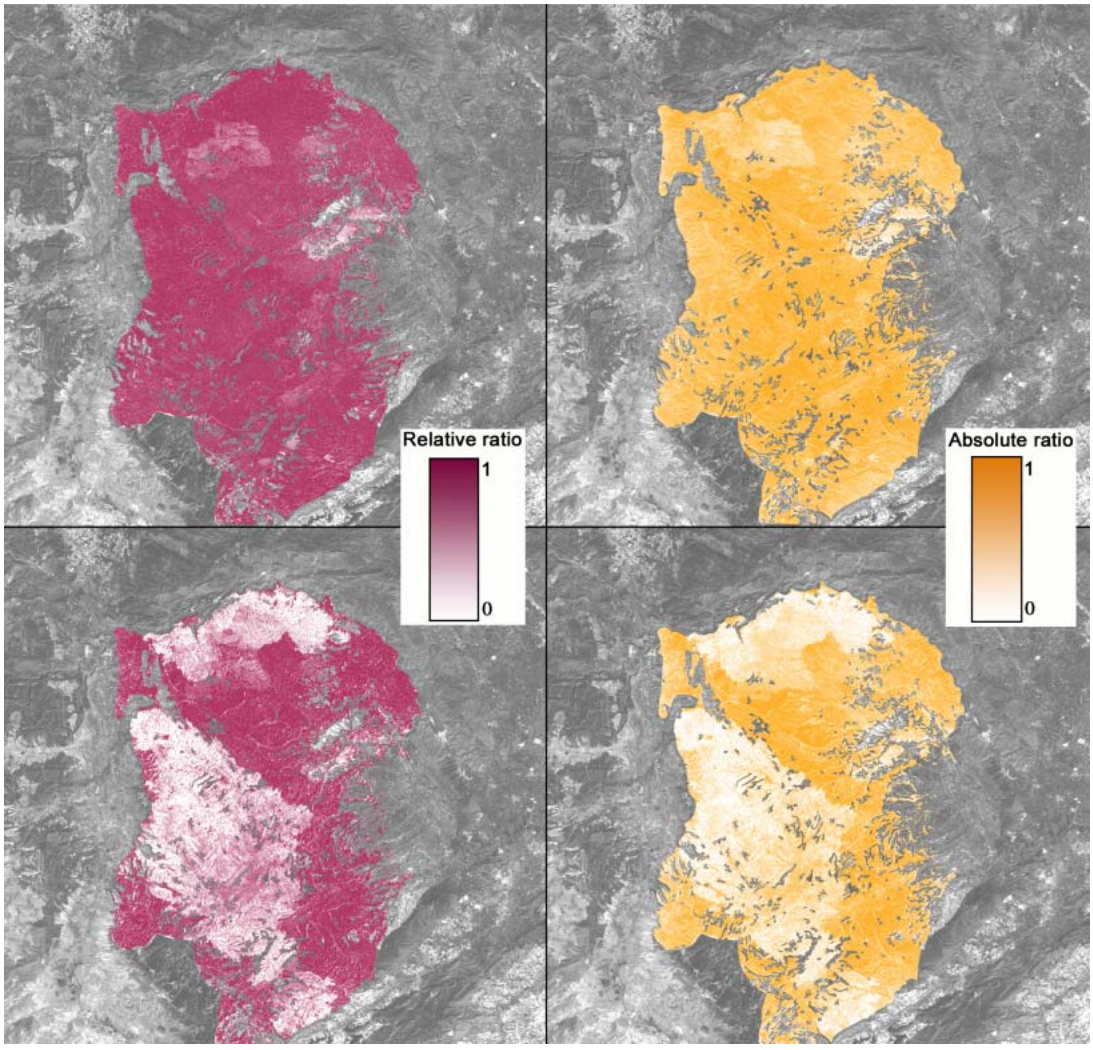

Fig. 9.8: Spatial representation of vegetation cover in relation to different maxima (top: 1979; bottom: 1980). The local maximum (left) was approximated by the maximum vegetation cover at the given pixel, the global (potential) maximum (right) was given by the maximum vegetation cover value for the full area (the analysis was confined to the core area and excluding agriculture)

A clear spatial differentiation results for the exemplary images of 1979 and 1980. Comparing both, the local relation shows a stronger gradient, since each pixel is related to the maximum at the same location. The global ratio appears slightly attenuated, since all pixel values are compared to the same, highest pixel value throughout the time series. It is important to note that this approach may involve uncertainties where plant communities with strong fluctuations in vitality are dominating. It may result in over-estimations for years where herbaceous species were recorded in stages of high photosynthetic activity as compared to years where these plants are already in their senescent stage. However, the effect is rated less critical the

higher the abundance of woody species is, although these may show variations on a lower level, too. However, given the typical plant communities and succession patterns of the Ayora test area, this effect would only affect isolated pixels and dates and is hence not expected to compromise the overall spatial representation. Although both indicators are calculated from simple ratios, they were found helpful in visualising the temporal development while at the same time incorporating specific local conditions. For instance, foresters were frequently interested in knowing the date when vegetation cover has returned to a certain fraction of the potential maximum that can be expected, which is supported by this type of representation.

9.4 Driving factors and regeneration patterns

The integrated temporal profiles discussed before assist in identifying general trends of vegetation recovery for larger areas. A first and objective criterion for their spatial definition is to employ fire perimeters, and further separate these according to corresponding overall fire history (compare section 9.4.1). As this implies averaging cover estimates across zones with varying physical conditions, it might result in a loss of information. This suggests to further analyse the spatial variation of post-fire dynamics and to assess whether driving factors for these processes can be identified. The following, exemplary investigations are confined to the 1980- and 1986-fires, for which a sufficient time between the major fire and the last image in the time series is given.

In the frame of specific case studies, the question of driving factors is often solved using complex ecological models. These often remain concentrated on specific local conditions and are frequently highly demanding in terms of spatially explicit input data. For these reasons, such investigations are out of scope in the context of outlining a general assessment and monitoring framework of rangeland degradation processes. Nonetheless, one component of a general framework should be a generalised approach to understanding apparent patterns and trends based on available auxiliary information. Most importantly, information on topography may be derived from digital elevation models, since these are an essential part of the presented strategy from the very beginning of dataset procurement.

In the context of the Ayora case study, different parameters were derived from the DEM. In addition, available data on bedrock and lithology were utilised as well as precipitation records. Employing selected fire patches from the 1980- and 1986-fires, it was investigated, which of these factors exert a discernible influence on the changes in vegetation cover following the respective fire events. The results are depicted in a series of integrated temporal profiles of vegetation cover stratified for categories of different factors. Underpopulated categories were not considered, since they are easily biased towards isolated exceptional values.

This is complemented by a spatial, synoptic interpretation of parameters from the regression analysis, corresponding to the respective analysis of unburned areas. It aims at distinguishing spatial patterns that can provide additional information on spatial regeneration patterns.

9.4.1 Physiographic stratification

Aspect

In Mediterranean regions, the most important influence of local aspect relates to the solar irradiance. Together with the slope of the respective surface element, it determines local short wave radiation budgets, which control the evapotranspiration of vegetation or the ground water balance trough transpiration. In conditions where the availability of water is limited, locations receiving high amounts of irradiance are less favourable since more available water is lost through transpiration effects (e.g. Kirkby et al., 1990; Boer, 1999). This negative effect is not compensated for by the correspondingly higher amounts of photosynthetically active radiance (PHAR). Furthermore, soil-related processes are also influenced by this factor complex. In addition, in case of advective precipitation regimes, meteorological conditions and the influence of luv- and lee-effects are partially determined by the aspect. In the present case, aspect was stratified according to 8 classes. Fig. 9.9 shows the corresponding integrated temporal profiles, Table 9.2 indicates the respective area in the different classes.

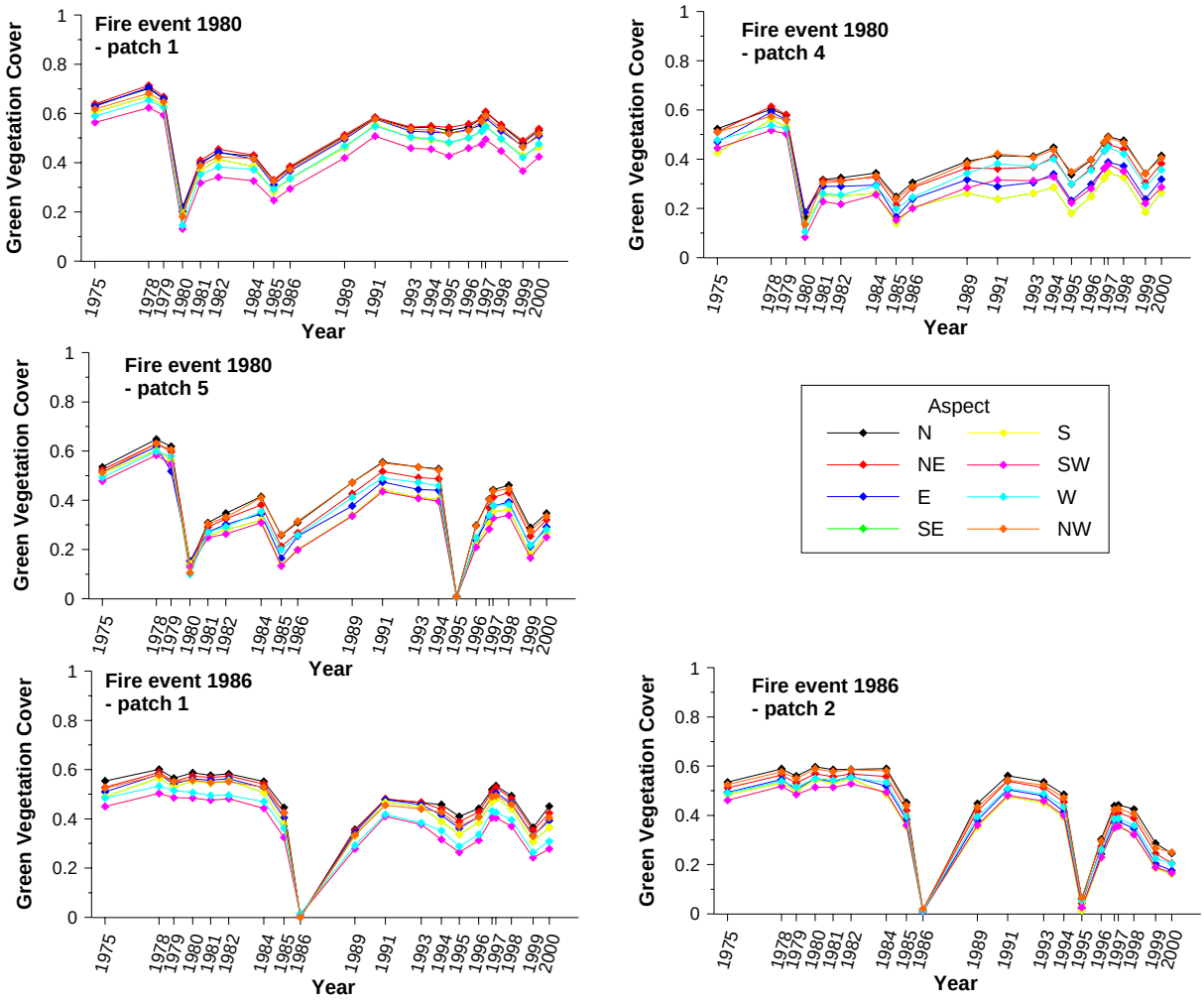

Fig. 9.9: Vegetation dynamics stratified by aspect, differentiated according to year of fire and to coherent patches depicted in Fig. 9.6

Table 9.2: Area integrated in major aspect zones (%)

Fire patch	N	NE	E	SE	S	SW	W	NW
1980-1	16.07	14.39	10.60	12.51	11.37	9.40	11.28	14.37
1980-4	18.14	16.37	13.05	10.16	8.39	7.83	9.45	16.60
1980-5	17.23	20.05	15.24	12.36	12.54	5.67	5.14	11.77
1986-1	15.71	19.57	17.44	14.60	11.11	6.57	6.15	8.85
1986-2	11.96	17.47	17.41	12.86	11.37	12.57	8.73	7.63

Apparently, all patches show a very consistent behaviour. Areas which receive the highest amounts of solar irradiation, with aspect S, SW and W, show the lowest vegetation cover estimates. Contrarily, locations oriented N, NE and NW show the highest values. This illustrates very well the described influence of aspect for the Ayora area, and must hence be considered a major factor determining post-fire vegetation succession.

Elevation

In mountainous areas of the Mediterranean basin, elevation significantly affects the composition of plant communities, especially through its effect on the length of the vegetation period and the commencement of the dry summer period. In the core area, elevation ranges from 47 m to 1124 m and it was classified to five classes with intervals of 250 m each. The few classes ensure that these are representative due to the respective number of samples. Fig. 9.10 exemplarily shows the results for two fire dates and five different patches, the numbering of which corresponds to the numbers shown in Fig. 9.6. Table 9.3 shows the respective integrated areas.

Table 9.3: Area integrated in elevation zones (%)

Fire patch	1 (<250 m)	2 (250-500 m)	3 (501-750 m)	4 (751-1000 m)	5 (>1000 m)
1980-1	0.0	0.0	80.8	13.2	6.0
1980-4	0.0	15.6	31.8	52.7	0.0
1980-5	0.0	14.2	71.1	14.7	0.0
1986-1	10.7	23.3	37.3	28.7	0.0
1986-2	14.6	78.3	7.0	0.0	0.0

Patches 1980-1 and 1986-2 show highly congruent temporal profiles for all elevation zones present. For patches 1980-4 and 1980-5, the highest elevation zone shows the lowest cover estimates throughout the time series, while in patch 1986-1 the highest zone is associated with the highest cover estimates. The different patches do not suggest a dependency of vegetation cover on elevation categories, which is coherent for the different locations. It can be assumed that the elevation gradient in the respective plots is not large enough to clearly differentiate vegetation dynamics, for instance through varying local precipitation regimes or significant differences in temperatures and vegetation phenology. It can, however, be suspected that in cases where a clear differentiation between the single profiles is apparent, this might be due to an indirect influence of another factor. Table 9.4 describes the relative distribution of aspect classes in the different elevation classes to assess a potential indirect influence.

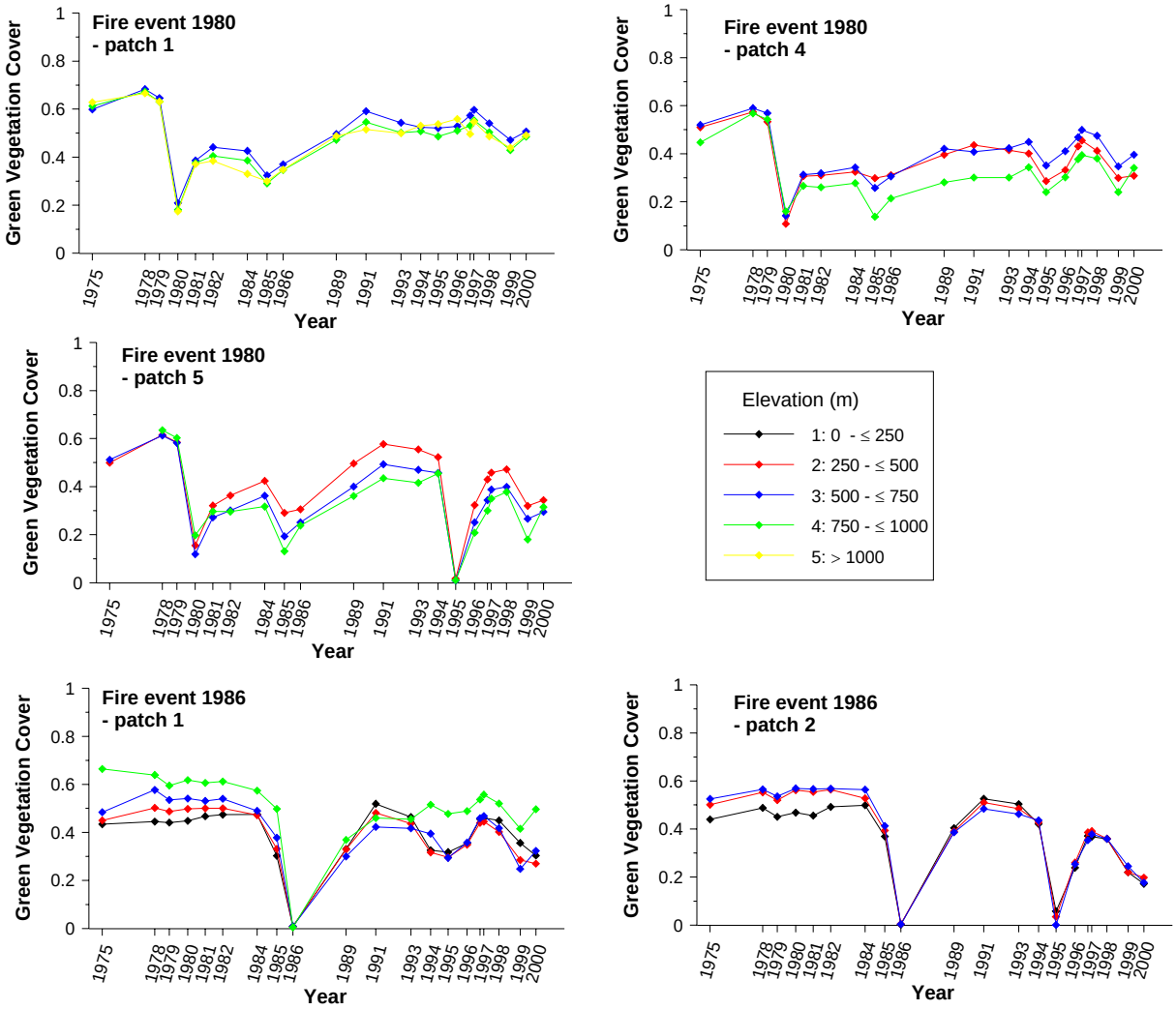

Fig. 9.10: Vegetation dynamics stratified by elevation, differentiated according to year of fire and to coherent patches depicted in Fig. 9.6

Table 9.4: Percentage of aspect-classes in different elevation zones for heterogeneous patches

	1980-4			1980-5			1986-1			
Elev. / Aspect	251-500	501-750	751-1000	251-500	501-750	751-1000	0-250	251-500	501-750	751-1000
flat	0.0	0.0	0.4	0.0	0.0	0.4	0.2	0.0	0.0	0.0
North	21.0	22.8	15.7	27.9	17.6	10.2	12.6	11.4	13.4	23.4
Northeast	12.8	14.7	18.1	24.6	18.6	19.7	20.3	18.4	18.9	21.3
Northwest	19.6	18.6	14.5	16.5	11.9	8.6	3.4	8.1	9.4	10.8
East	7.4	8.6	14.5	15.7	11.3	28.2	24.0	17.2	16.6	16.3
Southeast	10.5	7.2	12.1	5.6	11.9	15.9	23.9	14.6	13.2	13.1
South	13.5	6.6	8.1	1.5	16.6	6.4	10.0	11.1	13.4	8.4
Southwest	7.1	9.1	7.8	1.6	6.8	5.5	2.6	11.4	7.3	2.9
West	8.1	12.3	8.8	6.6	5.2	5.1	3.0	7.8	7.8	3.8

Patches 1980-4 and -5 both occupy the northern part of the plateau of *Muela de Corte Pallas*, as well as the steep, North-facing slopes towards the *Rio Júcar*, where elevations drop down

from about 800 m at the edge to about 250 m at the river bed. In both cases, the cross-tabulation confirms that higher values in the temporal profile occur in elevation classes with a higher relative abundance of favourable orientations (i.e. N, NE, E, NW), which explains the variation observed within and between the respective patches. While the two classes of lower elevations are mostly positioned on the slope, the 'high altitude' class does also incorporate a certain area of the plateau, which is rather inclined towards S/SE. This is also reflected in the cross-tabulated aspect areas. In addition, water redistribution as a function of topography may additionally affect the different vegetation succession patterns and higher inflow rates may be expected for the steeper slopes towards the *Rio Júcar*.

The cross-tabulation reveals the same indirect effect in an opposite way for patch 1986-1 which is located on the southern fringe of the plateau and extends east of the *Rio Júcar*. Here, it is the highest elevation class that shows the highest cover estimates. This class is associated with a significantly higher percentage of North-oriented pixels compared to the other zones.

Slope

Slope is directly related to precipitation runoff and the erosive potential and also affects vegetation through its influence on soil development and the related water retention capacity. In addition, together with aspect, slope is an important factor determining the amount of solar irradiance at a given location. It is calculated in degrees using the digital elevation model; hence, the micro-relief is not resolved due to limitations in the spatial resolution. The resulting slope factors were classified in 6 major slope classes according to AG Bodenkunde (1982), which may also be related to erosion potential. The resulting profiles are shown in Fig. 9.11, while Table 9.5 indicates the area summarised in these zones.

Table 9.5: Area integrated in slope zones (%)

Fire patch	1 (0-2 °)	2 (2-5 °)	3 (5-10 °)	4 (10-15 °)	5 (15-20 °)	6 (>20 °)
1980-1	6.2	17.5	35.7	25.5	15.1	6.2
1980-4	14.9	21.0	29.3	20.5	14.3	14.9
1980-5	17.7	18.2	29.0	21.4	13.7	17.7
1986-1	13.0	29.2	33.1	16.1	8.6	13.0
1986-2	14.6	78.3	7.0	0.0	0.0	14.6

Only patches 1980-4 and -5 do show a differentiation of temporal profiles by slope classes, while for the remaining patches vegetation cover is largely similar. In both cases, the steepest slope classes correspond with the highest vegetation cover throughout the period observed. To the contrary, no clear pattern is apparent for the minor slope classes.

Again, this indicates that the apparent differentiation according to slope classes for patches 1980-4 and -5 is an indirect effect, and corresponding to the previous section the possible influence of aspect was assessed by cross-tabulation (Table 9.6).

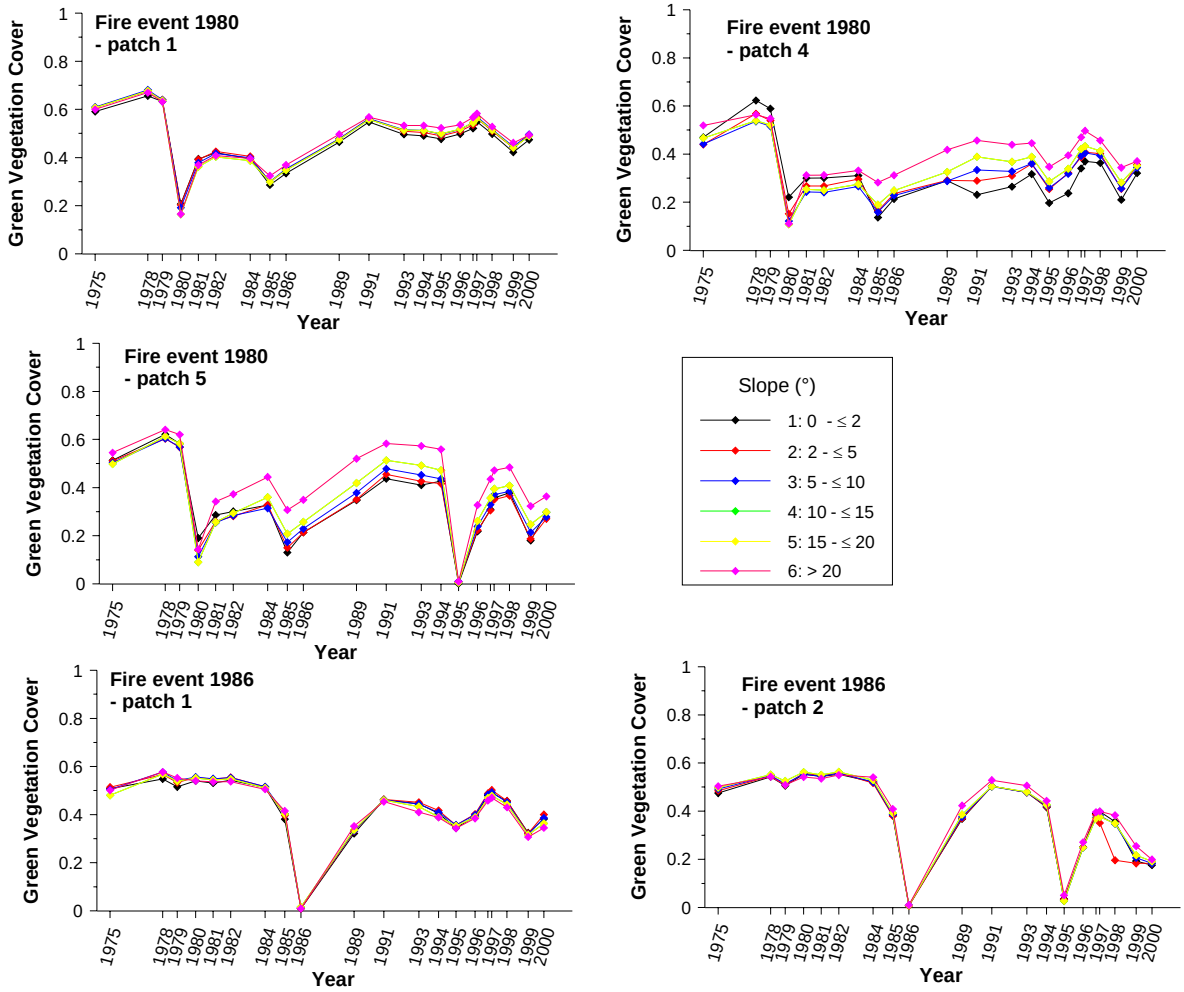

Fig. 9.11: Vegetation dynamics stratified by slope, differentiated according to year of fire and to coherent patches depicted in Fig. 9.6

Table 9.6: Percentage of aspect-classes in different slope zones for patches 1980-4 and -5

	1980-4						1980-5					
Aspect \ Slope	0-2°	2-5°	5 - 10°	10 - 15°	15 - 20°	>20°	0-2°	2-5°	5 - 10°	10 - 15°	15 - 20°	>20°
Flat	1.2	0.0	0.0	0.0	0.0	0.0	0.5	0.0	0.0	0.0	0.0	0.0
North	15.2	17.8	18.3	17.1	19.0	22.7	5.4	12.7	15.8	20.4	25.5	30.6
Northeast	19.9	21.9	13.6	18.6	15.2	12.0	18.2	15.9	20.8	23.3	20.9	17.9
Northwest	11.6	13.0	13.0	15.8	21.5	22.7	4.1	5.3	8.1	14.3	18.4	25.9
East	21.5	15.5	10.2	8.9	6.3	6.3	27.6	17.0	12.1	12.5	11.8	6.6
Southeast	16.3	9.7	13.0	9.7	9.0	5.3	17.6	18.6	13.2	8.0	6.7	3.9
South	3.7	9.9	13.8	7.8	8.7	8.3	12.6	17.8	18.5	11.2	8.7	4.5
Southwest	5.2	5.6	8.1	11.2	7.6	10.1	9.4	8.9	6.7	5.1	1.7	2.2
West	5.5	6.8	9.9	10.8	12.8	12.6	4.5	3.7	4.8	5.3	6.2	8.4

For both patches, the steeper slopes show a higher relative abundance of North- than South-oriented pixels. This explains the marked difference in vegetation cover profiles, where slope classes larger than 20° and between 15° and 20° exhibit the highest values throughout the

period observed. In the lower slope classes, there is also a notable percentage of northern aspects, but this is balanced by the East/Southeast-oriented areas. Especially for patch 1980-5, the zones with low slopes of up to 10° show a high percentage of areas with aspect East/Southeast/South corresponding to the overall inclination of this plateau.

Relief categories

Further to the analysis of single terrain variables, it was analysed whether an influence of major landscape mesoforms on vegetation dynamics can be identified.

Given climatic conditions in the test area, water availability was assumed to be of major importance. First, water redistribution is strongly governed by topography, which is especially important given the rugged terrain of the Ayora area and the limited availability of water. Del Barrio et al. (1996) have developed a methodology to derive relief categories from digital elevation models where processes of water redistribution are explicitly considered.

This methodology was refined and adapted to conditions of the Ayora test site. Different topographic variables were computed from the 30 m DEM: slope, profile and plan curvature, catchment size, wetness index, sediment transport index, distance to the nearest stream, and insolation factor. An unsupervised classification of the resulting matrix yielded 23 preliminary classes, which were aggregated to 10 superclasses using sequential agglomerative hierarchical non-overlapping (SAHN) cluster analysis (Sneath & Sokal, 1973). They were then related to landscape mesoforms or relief categories and the resulting data set was made available for this study (Del Barrio et al., 2001).

Classes 9 and 10, gullies and streams, were found to be directly adjacent and were merged to a single class in this analysis. Results obtained for this class have to be treated carefully, since the target features are essentially linear in nature and did not exceed 30 m in width. This means that when intersecting this class with the 79 m multi temporal data set, pixels will be associated that are not exclusively related to gullies and streams, but are also determined by the signal from surrounding surface elements. The resulting profiles are shown in Fig. 9.12 while Table 9.7 indicates the respective area.

Table 9.7: Area integrated in major relief zones (%)

Fire patch	Alluvial fans	Flood areas	Areas near channels	Foot-slopes	Terrace fronts /steep valley sides	Mid-slope sections	Steep upper-slopes	Plateaus / mountain tops	Gullies / streams
1980-1	1.35	0.00	0.00	3.70	8.96	49.70	15.20	8.78	12.32
1980-4	2.11	0.00	0.00	14.08	29.70	7.18	4.18	23.65	19.10
1980-5	6.56	0.00	0.00	19.51	17.15	26.11	2.40	16.35	11.92
1986-1	21.65	1.35	4.60	10.27	11.30	29.09	3.35	7.18	11.23
1986-2	31.83	0.00	2.23	24.97	29.12	0.00	0.00	0.97	10.88

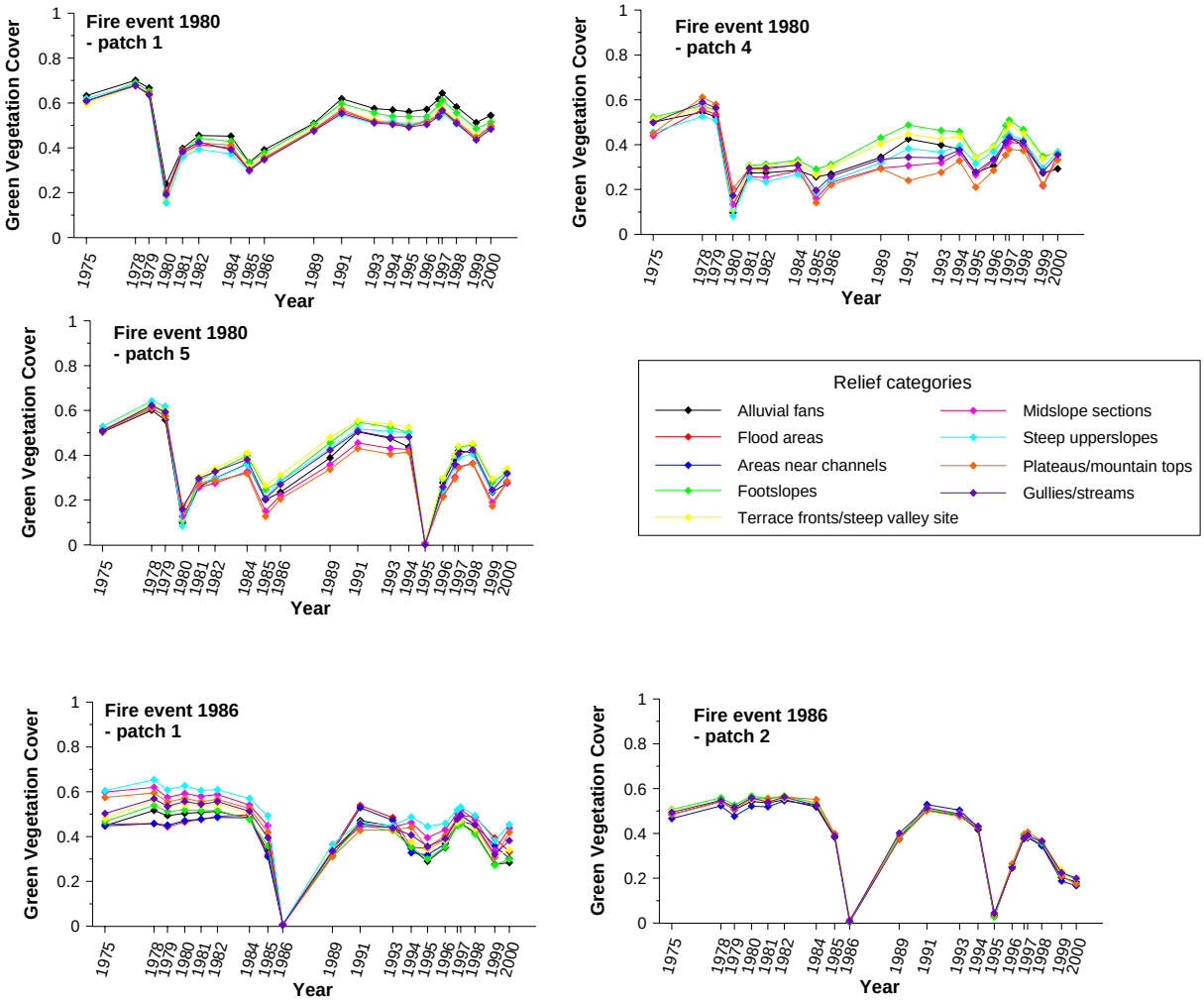

Fig. 9.12: Vegetation dynamics stratified by relief categories, differentiated according to year of fire and to coherent patches depicted in Fig. 9.6

Results for different relief types do not show a consistent pattern for the patches investigated. Profile 1980-1 displays a parallel arrangement of the profiles throughout the full period with only minor differences in the cover level. The highest values are found for ‘alluvial fans’ and ‘footslopes’, indicating a higher availability of water. In plot 1980-4, a more heterogeneous course of the single profiles is visible. It is the ‘footslopes’ class that shows the highest cover values throughout the observation period. Alluvial fans take an average rank, but the very small abundance of this class in the 1980-4 fire patch denies further interpretation. Also, the ‘terrace fronts/steep valley sides’ class exhibits high estimates, while lowest values are found for the ‘plateaus/mountain tops’ and ‘midslope’ classes. The described pattern is repeated in profile 1980-5.

Beside the effects of water redistribution incorporated in the relief classes, this behaviour is attributed to the aspect-factor (compare paragraphs ‘elevation’, ‘slope’, ‘relief categories’ this section), which is assessed using cross-tabulation in Table 9.2, Table 9.9 and Table 9.10.

Table 9.8: Percentage of aspect-classes in different regionalisation zones for patch 1980-4

Aspect \ Topo class	Alluvial fans	Foot-slopes	Terrace fronts /steep valley sides	Mid-slope sections	Steep upper-slopes	Plateaus/ mountain tops	Gullies /streams
Flat	0.00	0.00	0.00	0.00	0.00	0.39	0.76
North	22.22	26.97	20.51	16.79	28.78	14.79	14.92
Northeast	17.46	15.35	12.72	17.97	9.35	19.58	14.20
Northwest	17.46	19.96	21.95	12.74	21.58	11.80	19.91
East	7.94	4.61	7.08	11.90	2.88	20.62	14.10
Southeast	4.76	7.24	5.64	11.81	6.47	15.56	12.53
South	11.11	8.77	7.90	11.39	5.04	5.58	7.95
Southwest	7.94	8.55	9.44	7.85	17.99	6.23	6.24
West	11.11	8.55	14.77	9.54	7.91	5.45	9.39

Table 9.9: Percentage of aspect-classes in different regionalisation zones for patch 1980-5

Aspect \ Topo class	Allu-vial fans	Flood areas	Areas near channels	Foot-slopes	Terrace fronts/ steep valley sides	Mid-slope sections	Steep upper-slopes	Plateaus/ mountain tops	Gullies/ streams
flat	0.00	0.00	0.00	0.00	0.00	0.00	0.00	0.40	0.09
North	18.24	0.00	0.00	23.76	25.94	14.10	32.42	8.41	15.37
Northeast	22.35	75.00	0.00	23.76	16.83	18.99	18.68	18.95	18.34
Northwest	16.47	0.00	0.00	13.07	9.33	12.21	6.59	23.00	17.50
East	11.76	0.00	0.00	6.03	6.54	16.47	2.75	16.97	11.73
Southeast	14.71	0.00	0.00	7.99	8.16	19.04	4.95	13.56	13.95
South	5.49	25.00	0.00	2.84	3.23	8.72	3.85	8.88	4.96
Southwest	4.31	0.00	0.00	5.48	8.30	4.46	7.14	4.20	5.00
West	6.67	0.00	100.00	17.06	21.68	6.01	23.63	5.63	13.07

The cross-tabulation (Table 9.8, Table 9.9) supports the hypothesis of a strong influence of the aspect-factor for plots 1980-4 and -5. Given the fire perimeters, steeper slopes and terrace fronts are all oriented North, hence leading to lower evapotranspiration rates. This adds to the generally better water supply in the 'footslopes' and 'alluvial fans' zones and triggers the high cover estimates found for these classes. To the contrary, the 'plateaus/mountain tops' and 'midslope' zones correspond to the undulating, higher areas of the *Muela de Corte Pallas*, where a higher percentage of East/Southeast/South-oriented areas has to be noted. It is characterised by less favourable conditions and vegetation cover dominated by sparse and rather low shrubs.

This behaviour is contrasted for the 1986-fire zone, which is heterogeneous within itself. In plot 1986-1 the profiles of 'steep upperslopes', 'midslope sections' and 'plateaus/mountain tops' show the highest cover values, while 'gullies/streams', 'flood areas', 'footslopes' and 'alluvial fans' range below. Even if gullies/streams and flood areas are disregarded following their small relative size this behaviour is striking. Table 9.10 shows the results for cross-tabulation of the 1986-1 fire patch, stratified for terrain zones, with aspect.

Table 9.10: Percentage of aspect-classes in different regionalisation zones for patch 1986-1

Aspect \ Topo class	Alluvial fans	Flood areas	Areas near channels	Footslopes	Terrace fronts/ steep valley sides	Midslope sections	Steep upperslopes	Plateaus/ mountain tops	Gullies/ streams
Flat	0.00	1.20	0.00	0.00	0.00	0.00	0.00	0.08	0.05
North	13.58	11.95	9.29	11.27	13.14	19.68	18.45	17.82	16.85
Northeast	21.83	17.53	18.70	15.71	16.63	21.54	15.98	21.53	17.40
Northwest	18.16	29.48	28.35	16.03	12.85	16.39	14.83	19.48	18.39
East	16.09	23.51	27.99	11.91	11.78	13.51	12.03	13.96	15.16
Southeast	10.06	12.35	9.05	14.10	17.94	9.68	12.85	7.41	9.05
South	7.37	0.80	2.05	12.66	8.63	4.25	3.95	6.62	6.37
Southwest	5.79	0.40	1.57	9.72	8.34	4.55	7.91	4.50	8.47
West	7.11	2.79	3.02	8.60	10.71	10.40	14.00	8.60	8.26

The ‘plateaus/mountain tops’ and ‘midslope’ zones show high percentages of North-oriented areas, which corresponds to their relatively high vegetation cover estimates. However, the ‘steep upperslopes’ section, that shows the highest cover estimates, does not show a corresponding pattern. In addition, the adjacent patch 1986-2 does not show any clear differentiation according to relief classes. This indicates that other boundary conditions influence vegetation dynamics in this area, which exceed the terrain characteristics represented in the relief categories.

Lithology

The lithological background is a major factor determining vegetation structure and dynamics through its influence on soil development. In addition, geology, relief and hydrological conditions are closely related. The lithological background strongly affects water availability, which is not only important in the context of plant water availability, but also since it triggers pedological processes and properties. This includes the concentration of clay minerals as well as the acidity milieu, which in turn strongly determines the development of plant communities (Schachtschabel et al., 1989).

The digital lithological map available from the Forestry Service of the regional administration of Valenciana was employed to differentiate major lithological classes. These are described according to the bedrock types ordered by their relative significance, and summarised according to the major substrate. Following section 4.1.2, calcareous sediments are largely dominating the core area, which are differentiated into dolomites and limestones. Only minor contributions of sandstones or marls are present. Frequently, these major formations appear in combinations. Other substrates or sediment types remain confined to geological faults as well as channels and valleys. In the available data set, these frequently encompass the class ‘conglomerates’, whose lithologic composition varies depending on the components and binding material, and which is hence difficult to interpret.

Employing these aggregated classes, the stratified analysis yielded results shown in Fig. 9.13, complemented by the area of the respective class in Table 9.11.

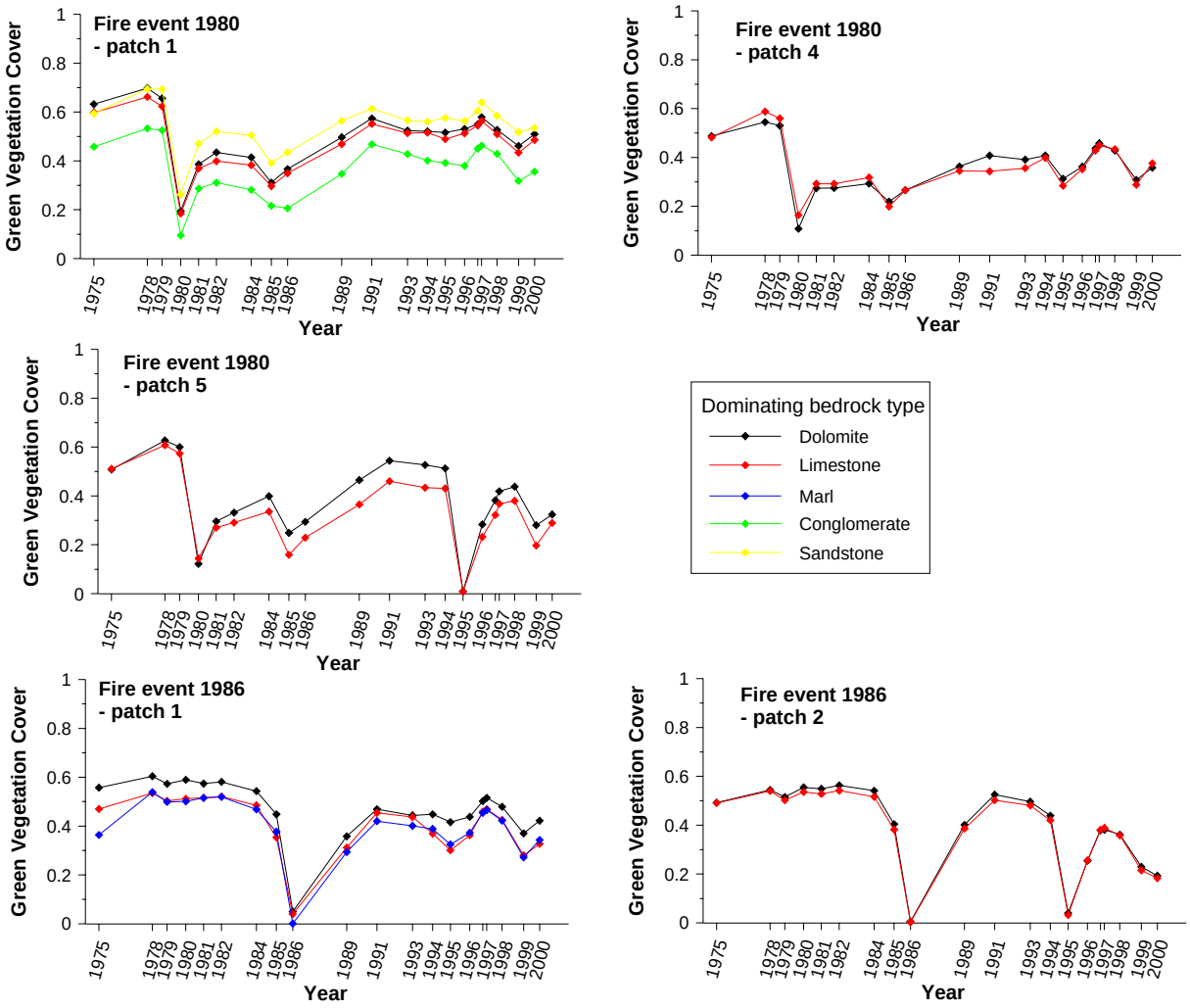

Fig. 9.13: Vegetation dynamics stratified by lithological categories, differentiated according to year of fire and to coherent patches depicted in Fig. 9.6

Table 9.11: Area integrated in major relief zones (%)

Fire patch	Dolomite	Limestone	Marl	Sandstone	Conglomerate
1980-1	51.9	44.3	0.0	1.3	2.5
1980-4	41.2	58.8	0.0	0.0	0.0
1980-5	44.2	55.8	0.0	0.0	0.0
1986-1	44.4	53.5	2.2	0.0	0.0
1986-2	40.7	59.3	0.0	0.0	0.0

Table 9.11 indicates that the distribution of classes does only allow a serious interpretation of the ‘dolomite’ and ‘limestone’ substrates. Profiles 1980-5 and 1986-1 show higher vegetation cover estimates for the dolomite- compared to the limestone-dominated formations. This is especially interesting in the case of patch 1980-5, where both substrates display almost identical vegetation cover before the fire, while after both the 1980- and 1995-fire a regular offset is maintained with the ‘dolomite’ class ranging above the ‘limestone’ class.

For this reason, it was analysed for patches 1980-5 and 1986-1 whether, corresponding to the above sections, a notable influence of the factor aspect may be observed. Table 9.12 gives the

cross-tabulated aspect percentages for ‘dolomites’, ‘limestones’ and ‘marls’ zones, the other zones were disregarded due to their little relative size.

Table 9.12: Percentage of aspect-classes in different bedrock zones for patches 1980-5 and 1986-1

	1980-5		1986-1		
Lithol. cl. / Aspect	Dolomite	Limestone	Dolomite	Limestone	Marl
flat	0.0	0.1	0.0	0.0	0.0
North	22.7	13.9	17.6	14.9	12.0
Northeast	22.1	17.8	18.6	20.6	18.0
Northwest	16.4	8.6	9.9	8.3	12.0
East	13.3	15.4	16.4	18.7	12.0
Southeast	9.5	13.3	13.4	16.0	13.6
South	7.2	17.6	10.9	10.1	16.4
Southwest	3.3	8.0	6.5	6.0	6.0
West	5.5	5.3	6.6	5.3	9.9

For patch 1980-5 it is indeed confirmed that the effect visible in the profiles might relate to the influence of the factor ‘aspect’. This is, however, not maintained for the 1986-1 fire zone, where no clear differentiation according to aspect classes can be noted for the different lithological zones. It indicates that in this case further variables affect the temporal behaviour. It may be reasoned that the dolomite formations are generally more compact and water drains less easily, leading to a higher supply of water compared to limestone formations. As this is only visible for two of the assessed fire patches, it must be assumed that pedological and lithological properties are not adequately resolved by the existing generalised data and intricate mixtures of materials are not accounted for.

Climate

Climatological conditions play an outstanding role for the development of vegetation and the differentiation of plant communities through combined effects of temperature and precipitation. The climatological regime is differentiated by local topography, which modifies solar irradiation and hence temperature as a function of elevation, slope and aspect. Precipitation is affected by relief through luv- and lee-effects in the case of advective precipitation, and is also differentiated according to elevation. In addition, intensive rainfall events occur as a result of convective processes (compare section 4.1.1). Especially during the dry summer months these have a high erosive potential and hence influence on vegetation.

Precipitation must be seen as a factor governing the dynamics of vegetation in general. As such, it both determines the magnitude and manifestation of immediate post-fire dynamics, but also the more gradual, long-term plant development. It is responsible for the fluctuating patterns in the temporal vegetation cover profiles, although these vary in magnitude depending on the plant communities viewed.

As stated before (section 4.1.1), meteorological stations are unevenly distributed around the test area. They surround the core mountainous area and frequently records of different stations

have not been collected at corresponding dates and times or information for long periods is missing. It has been shown by Waske (2003) that the available data are not sufficient for a spatial interpolation that adequately incorporates relief influences. For this reason, the amount of rainfall is considered here in a global way for the whole region.

Making use of two meteorological stations located close to the village of Ayora, precipitation in the different years was characterised in relation to the respective image acquisition date. The amount of available water was calculated by summarising rainfall in the given year between January and the image acquisition date and dividing this by the long-term average for the same period. This way the amount of water available during the vegetation period before acquisition of the respective image was evaluated. Fig. 9.14 illustrates the amount of available water in different years in relation to three characteristic temporal profiles.

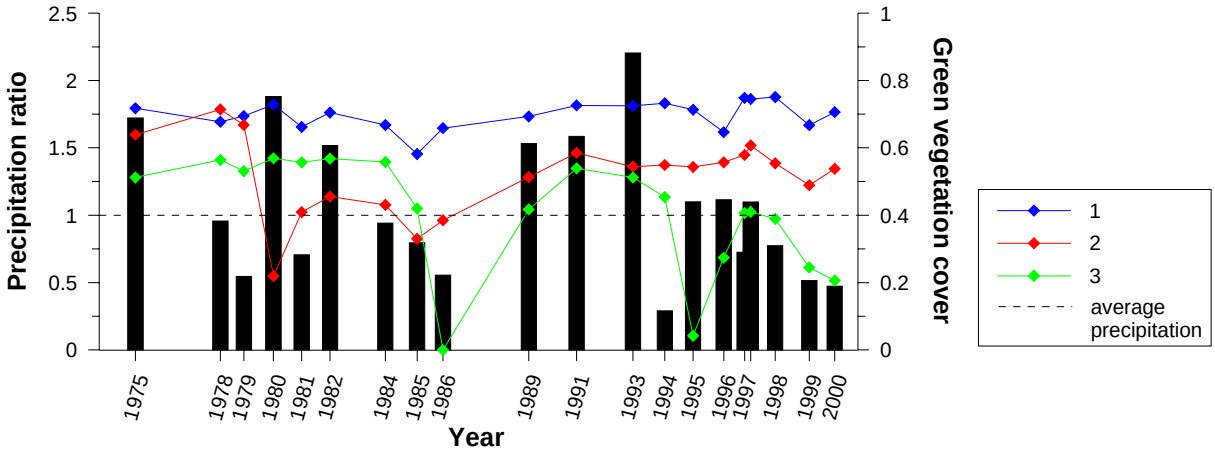

Fig. 9.14: Relative precipitation in relation to different profiles of vegetation cover. The precipitation index was calculated by summarising rainfall in the given year between January and the image acquisition date and dividing this by the long-term average for the same period. The temporal profiles relate to: unburned (profile 1), burned in 1980 (profile 2), and burned in 1980 and 1995 (profile 3)

In general, most vegetation pulses can be directly related to periods of high water availability. Periods with decreasing vegetation cover often coincide with lower amounts of available water, although this response frequently shows a temporal lag of one vegetation cycle.

This may be attributed to the vegetation's physiological adaptation to the highly variable Mediterranean regime. Another noteworthy determinant is the date of image acquisition relative to the onset and duration of the dry period following constraints of image availability.

The profile representing the 1980-fire underlines the effects of a favourable supply of water, pronounced by a long period between the actual fire event (which was known to have happened in 1979) and the acquisitions of the image (1980). As a result, derived vegetation cover estimates are already at a level of almost 50 % at the bottom point of the curve to which the fire event is assigned. It is interesting to note that the major fire years 1980, 1986 and 1995 are all characterised by decreasing cover estimates in the year preceding the fire. These are associated with precipitation below average, suggesting that the data analysis actually reflects typical situations of increased fire danger following exceptionally dry periods. With

reference to the general situation in Spain, different authors have confirmed this pattern of extreme climatological conditions preceding major fire events (e.g. Moreno et al., 1998; Millán et al., 1998). On a shorter time scale, this effect is accompanied and aggravated by a quick response of dead fuels to changing meteorological conditions. This means that where high amounts of dead, flammable biomass are present, even short periods of drought lead to an exponential increase in the risk of fire (Viegas, 1998).

Summarising, it has to be comprehended that the precipitation figures are solely based on two neighbouring stations in the Ayora valley. Neither modification of rainfall through relief nor the effect of elevation, temperature and aspect on actually available amounts of water are adjusted for. Although this representation of precipitation conditions does involve certain generalisations and could not fully explain all fluctuation patterns, direct effects of precipitation variation on vegetation cover development or the risk of fires are evident, which illustrates the impact of climatic properties on both fire risk and post-fire plant succession.

It can be concluded from the factor-related analysis of integrated profiles that the availability of water is the most important driving parameter for plant regeneration following fires. From the range of topography-related parameters, aspect is exerting the most discernible influence on vegetation dynamics through the differentiation of insolation. Additional explanations of apparent spatial regrowth patterns may be derived from secondary parameters based on terrain analysis which incorporate information on water redistribution. On the other hand, it was shown that apparent correlations between vegetation cover and the factors ‘elevation’ and ‘slope’ are strongly triggered by aspect. These dynamics are generally influenced and modified by the precipitation regime

More influencing factors may be present, which are not tangible using the existing data. Especially the influence of bedrock and soils may play an important role, but this could not be verified on account of the high level of generalisation associated with the lithology dataset, and the lack of suitable local scale information on soils. Attempts to employ the European Soil Database (European Union Publication Office, 2004; http://eusoils.jrc.it) failed to solve this shortcoming, since the scale of 1:1,000,000 results in the class ‘chromic cambisols’ for the whole area. Given the relative homogeneity of the geological situation, it can however be assumed that there is no large bedrock-related variance in soil types. With respect to soil development over carbonatic rocks, rendzinas are expected under less favourable conditions, while chromic cambisols or luvisols result from chemical soil development (Schachtschabel et al., 1989) (compare section 4.1.3). This pattern is only expected to be modified in accumulation areas where alluvial soils are present. Concerning soil depth, Boer et al. (1996) found this parameter to be strongly influenced by a combination of spatial variation in topography-driven processes of sediment transport and the insolation budget. Related evapotranspiration rates and soil moisture conditions control weathering rates, soil structure and soil erodibility. Hence, deepest soils are expected in locations with low slope angles and in accumulation zones, while in areas with higher slope angles less developed rendzinas or even lithosols may occur. The influence of slope is modified by the general amount of available water, as well as by soil texture and the structure of underlying bedrock. Where this is affected by karst and water is drained quickly, poor soils may result despite otherwise

favourable conditions. According to the expected domination of topography over bedrock type for the spatial differentiation of soils, the factors ‘aspect’, ‘slope’ and ‘relief categories’ do partially incorporate the expected spatial variation due to soils in the area.

9.4.2 Analysis of multi-temporal statistics

The factor-related analysis described in section 9.4.1 is complemented by a synoptic analysis of different parameters from the regression analysis. Similar to the section 9.2, spatial patterns are visually identified that can provide additional information on spatial regeneration patterns. These are characterised using temporal profiles for representative positions.

1980-fire

Corresponding to section 9.2, Fig. 9.15 shows a combined representation of gain, average cover and RMSE estimates for the stratified trend analysis of the 1980-fire, complemented by exemplary temporal profiles in Fig. 9.16.

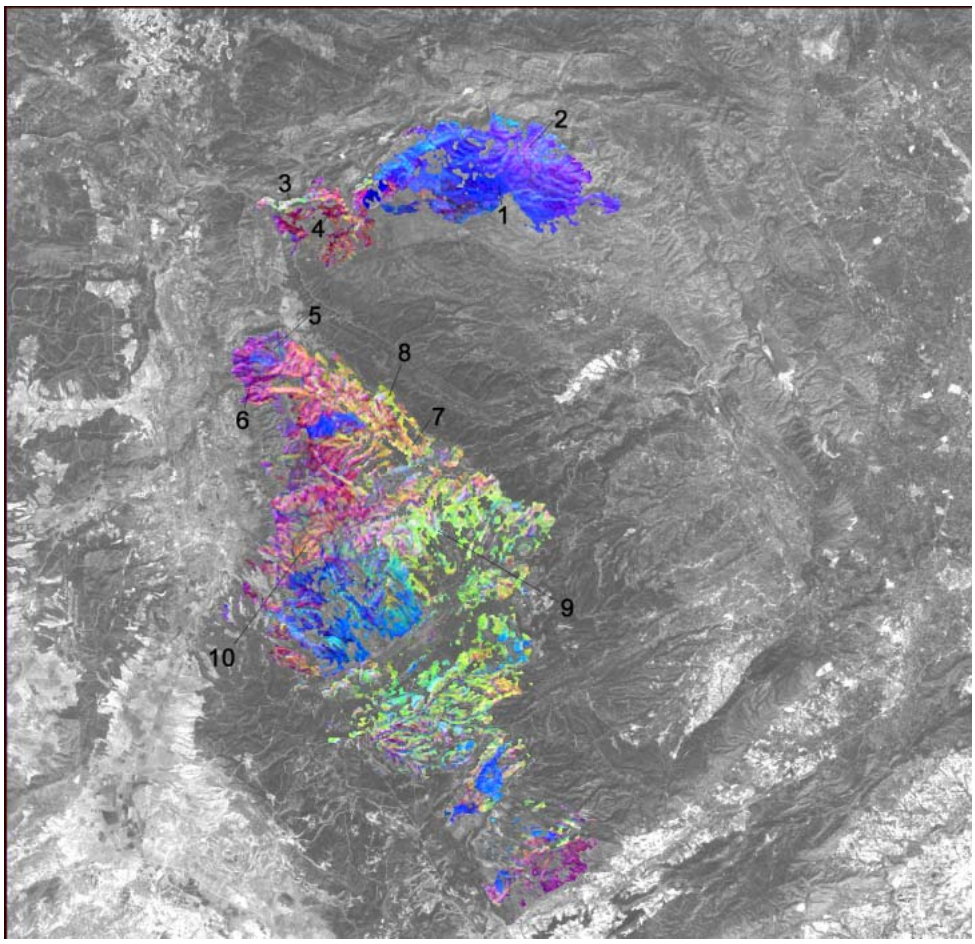

Fig. 9.15: Multi-temporal analysis of areas burned in 1980. R = trend gain, G = average cover of the time series, B = RMSE of the linear trend function; agricultural areas are excluded; the numbers correspond to the profiles shown in Fig. 9.16

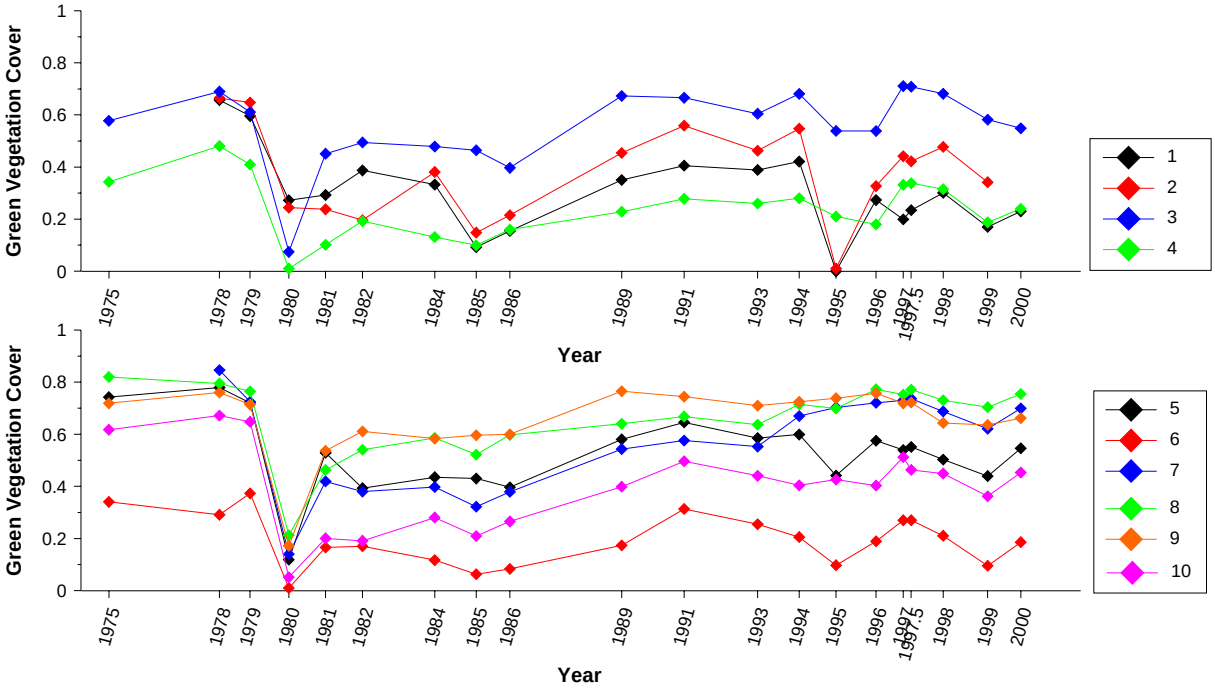

Fig. 9.16: Temporal profiles of the development of green vegetation cover for representative areas burned in 1980. The numbering of the profiles corresponds to Fig. 9.15 to and the profiles illustrate typical pattern groups inferred visually from multi-temporal statistics (Fig. 9.15)

For the northern fire zone, the areas burned once and twice are easily separated, as the second fire in 1995 leads to a higher RMSE, resulting in dark purple to blue colours depending on the overall development. Profiles 1 and 2 represent this characteristic. Both show relatively high cover estimates in 1980, which has already been explained by the acquisition date in relation to the date of the fire. It is striking that following the fire, both profiles behave rather stable with a high fluctuation at the same time, indicating recovery rates are rather slow. After the 1995-fire, which reduced vegetation cover to zero, recovery rates are again different between the two profiles, and especially for profile 1 the curve remains on a very low level. During field observations, this region was characterised by sparse and low shrubs (Fig. 4.4). As stated in section 2.3, it must be expected that the recurrence of two fires within relatively short time had a negative long-term effect on soil fertility; in addition, seeder species may not have managed to reach sexual maturity between these two fire events. As a consequence, colonisation of the area with pine tree species could be considered improbable and would rely on immigration of seeds from surrounding areas.

Profile 4 represents an area burned only once, where recovery is very slow and remains on a very low level, while profile 3 displays a high recovery dynamic. A strong increase after the fire, related to the colonisation with herbaceous species and augmented by the availability of higher amounts of minerals after the fire, is followed by a slight decrease corresponding to the extension of a shrub canopy and a slight long-term increase thereafter, which also exhibits high fluctuations. All three parameters do hence contribute to the differentiation of relevant processes, resulting in the bright colours. An analysis of the digital elevation model showed that profiles 1 and 4 correspond to mostly South-facing slopes, while profiles 2 and 3 are generally oriented towards North (compare Table 9.13). This corresponds to conclusions from

section 9.4.1 (‘aspect’) and emphasises the importance of aspect as a factor strongly affecting vegetation dynamics. According to Vallejo et al. (2003), areas burned twice are characterised by different shrubland types and an absence of a notable tree layer. In areas facing north, these are expected to be dominated by *Ulex parviflorus* and a grass layer of *Brachypodium retusum*. On areas burned only once, shrublands dominated by *Quercus coccifera* or *Rosmarinus officinalis* form the general matrix within which *Quercus ilex* individuals occur, which are complemented in different patches by *Pinus halepensis* and *Pinus pinaster*.

Similar to this, the southern fire zone exhibits a high degree of structural differentiation compared to the gain-maps in Appendix D. Again, areas burned twice can be identified by their shades of blue. The processes depicted by their corresponding colour combinations in the northern zone are also present here, although in more different shades. Profiles 5 to 10 show the temporal development from different regions which were only burned once. Similar to the northern zone, there is a considerable variability in the post-fire dynamics of these different regions. Profile 6 represents the dark pink areas, which are characterised by a weak gain and a moderate RMSE at a very low cover levels. Again, this corresponds to an area characterised by very sparse vegetation, which is strongly dominated by a sparse cover of low shrubs. In comparison, the other profiles show generally higher recovery rates, and already the 1980-cover estimates are about 15 % higher than profile 6. A quick recovery followed by a generally moderate increase can be observed, corresponding to the succession phases described above. Different variances in the profiles suggest that the floristic composition varies in these different regions.

Profiles 5 and 8 slightly differ from the general behaviour. Profile 5 represents the northern part of the southern fire zone with rather low rates of cover increase following the initial recovery ‘flush’; this results in a total increase of about 40 % for a period of 20 years only. To the contrary, profile 8 stands for a steady increase in vegetation cover, resulting in estimates of almost 75 % in 2000. This profile generally resembles the post-fire trajectory that has been described by some authors to approximate major recovery phases, with a strong initial recovery being followed by a progressively attenuated increase towards a saturation point (e.g. Trabaud, 1994). The southern 1980-fire zone can be generally ascribed to the one-fire or two-fires vegetation compositions. Since only 13 years elapsed between both fires, the probability of pine maturation between the fires is even lower, such that the area burned twice is not expected to show any notable tree layer apart from reforestation plots. Contrarily, the remaining area can be expected to follow the main shrubland composition described briefly in section 9.3 and in more detail in section 4.1.5.

Possible ‘upper’ and ‘lower’ limits of the range of present plant communities are exemplarily depicted in Fig. 9.17 and Fig. 9.18.

Fig. 9.17: Dense shrubland with trees in the 1980-fire area

Fig. 9.18: Sparse, open shrubland in the 1980-fire area

A wide range of manifestations of the typical plant communities described before exists, which – depending on fire regime/recurrence and local conditions – follow the general scheme described before. In addition to Fig. 9.17 and Fig. 9.18, additional representative images are found in section 4.1.

Table 9.13: Elevation and Aspect for the profiles shown in Fig. 9.16

	1	2	3	4	5	6	7	8	9	10
Elevation [m]	721.00	499	414	786	729	811	828	905	803	803
Aspect	SE	NE	N	S	W	S	NE	NE	W	S

Supported by Table 9.1, it is concluded that aspect is the decisive factor and exerts a significant influence on vegetation recovery in the different zones. This is further underlined by the fact that for the three South-facing slopes considered green vegetation cover estimates actually reach zero, while for the remaining positions there has already been a notable recovery at the time of image acquisition. This observation coincides well with the analysis conducted in section 9.4.1. In addition, all profiles show secondary pulse of vegetation recovery in 1989 and 1991, which correspond to the higher amounts of rainfall received in these years (compare section 9.4.1 – climate).

1986-fire

A corresponding representation is given for the parts of the core area that were affected by the 1986-fire, and the same graphical representations are provided in Fig. 9.19 and Fig. 9.20.

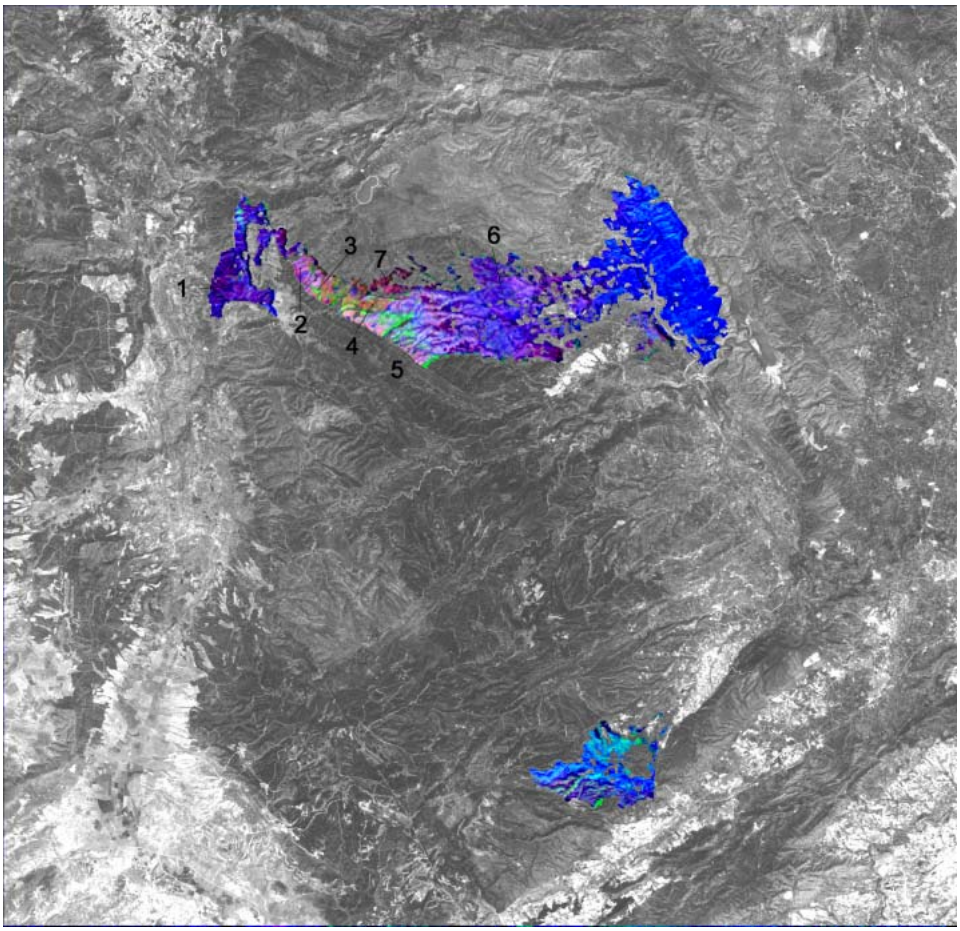

Fig. 9.19: Multi-temporal analysis of areas burned in 1986. R = trend gain, G = average cover of the time series, B = RMSE of the linear trend function; agricultural areas are excluded; the numbers correspond to the profiles shown in Fig. 9.20

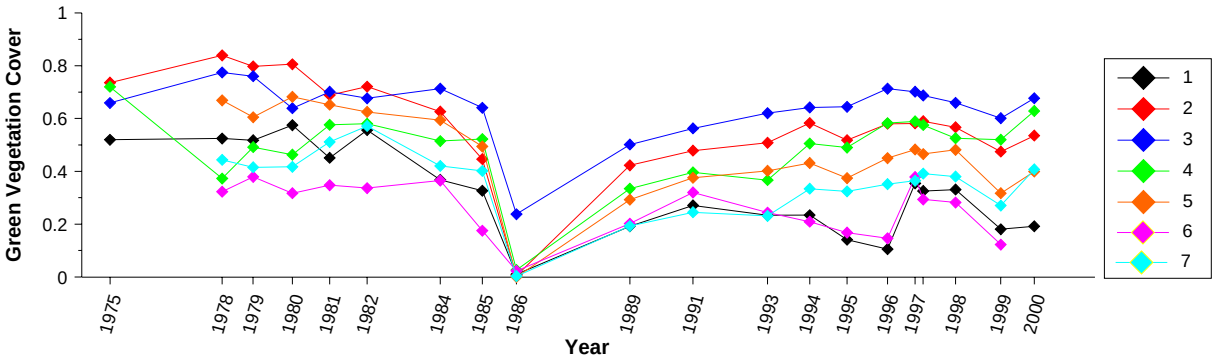

Fig. 9.20 Temporal profiles of the development of green vegetation cover for representative areas burned in 1986. The numbering of the profiles corresponds to Fig. 9.19 and the profiles illustrate typical pattern groups inferred visually from multi-temporal statistics (Fig. 9.19)

Similar to the 1980-fire, areas burned twice appear in deep blue and the extraction of profiles was confined to the large fire zone in the North affected by one fire only. From a visual inspection, a regular pattern may be deduced, with two corresponding zones in the West and East with dark purple to blue colours. Towards the centre of this patch, brighter pink tones can be noted, with an intermediate zone with colours varying from dark orange/brown to green shades. The extracted profiles follow this East-West transition. In addition, profile 7 represents the smaller patch, characterised by dark pink to red colours, which is appended in the North of the middle section. Profiles 1 and 6 exhibit a similar post-fire behaviour, with recovery on a low cover level and pronounced fluctuations, indicating unfavourable conditions. According to the systematics described before, open shrublands prevail in these areas, where interspersed herbaceous species are more prone to phenological variations and hence produce a relatively high fluctuation. The photos displayed in Fig. 9.21 and Fig. 9.22 were both taken in the eastern part of the one-fire zone, represented by profile 6.

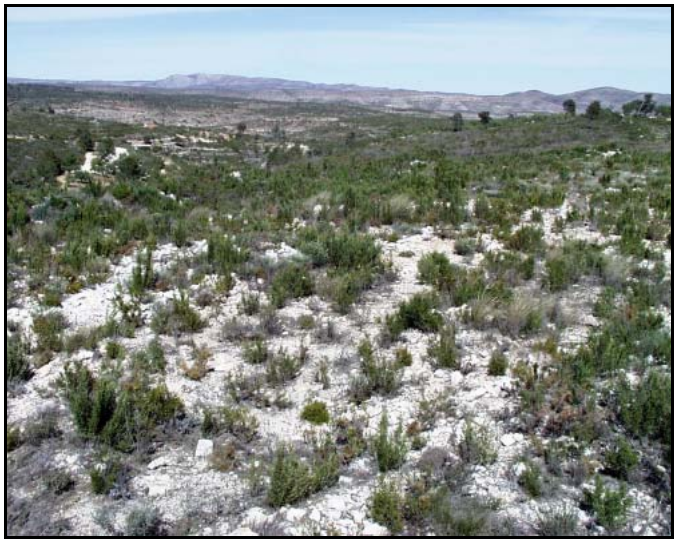

Fig. 9.21: Sparse, open shrubland in the East of the 1986-fire area burned once

Fig. 9.22: Sparse, open shrubland in the eastern part of the 1986-fire area burned once

Proceeding west, profiles 2, 3 and 4 show much higher recovery rates with differing variation. Especially profile 3 represents favourable conditions, since at the date of image acquisition vegetation cover already exceeded 20 % and a rapid increase to maximum cover levels follows. Profile 5 marks the transition zone to less favourable conditions. After a quick recovery directly after the fire no significant further increase can be observed. Assessing the reason for this spatial variation, a distinct zonation according to relief can be noted, where profiles 1 and 6 correspond to lower altitudes, while areas of higher increase rates are associated with higher altitudes. In addition, an influence of aspect is likely. Table 9.14 lists these two parameters for the profiles.

Table 9.14: Elevation and aspect for the profiles shown in Fig. 9.20

	1	2	3	4	5	6	7
Elevation [m]	673	880	941	922	786	549	874
Aspect	W	SE	NW	N	SE	W	N

For the profiles along the W-E transition, a combined influence of elevation and aspect explains most of the cover estimates, while profile 7 appears opposed. Here, albeit being exposed North and at a high elevation, low cover estimates appear. It must hence be expected that further factors are responsible for this differentiation.

As indicated before, the level of detail of the lithological map was not sufficient to analyse these questions. For the investigated fire patch, the geological map 1:200,000 (IGME) indicates different ‘limestone’ facies of the Cretaceous, two of which show contributions of marls. In addition, the map identifies an area dominated by a combination of calcareous sandstones, clays and marls. Although this may indeed represent conditions differing from the other zones, no clear coincidence is apparent between the gradient in Fig. 9.19 and transitions between geological classes. Nonetheless, small-structured patterns of bedrock variation at scales not resolved by this map might be responsible for some of the effects that are not explained by the factors employed here.

In general, except for locations represented by profiles 1 and 6, shrublands of varying density and composition can be expected in the other zones according to the respective local combination of determining factors. Although a forest-like community has not evolved, individuals of *Pinus halepensis*, *Pinus pinaster* and *Quercus ilex* represent the most frequent tree species.

9.5 Characterisation of plant communities

It was demonstrated how the recovery of vegetation cover can be characterised on a quantitative level. This is especially important with regard to the soil-protective function of vegetation. In addition, the characterisation of the development of plant communities has been identified as a desired information product for land managers and ecologists. Such a characterisation would complement the picture of vegetation succession and help to assess fire resilience. Although plant species may - to a certain degree – be be differentiated using airborne hyperspectral remote sensing data (e.g. Roberts et al., 1991, 1998; Lewis et al., 2000; Okin et al., 2001; Schmidt et al., 2004), this is not possible using data with the spectral and geometric resolution of Landsat-TM or even -MSS. Alternatively, a series of such data sets for one phenological vegetation period may be employed to infer such information based on knowledge of phenological cycles (e.g. Cihlar, 2000; Alvarez et al., 2003; Camacho-de-Coca, 2004; Lobo et al., 2004); similarly, hypertemporal data with a coarser spatial resolution may be utilised (e.g. Justice et al., 1985; Tucker et al., 1985; Lu et al., 2001; Moody & Johnson, 2001). In the present case, these options were not supported by the setup of the multi-temporal data base. Hence, a feasibility study investigated whether it is possible to identify a limited number of major structural vegetation classes based on the available data and by making use of existing auxiliary information.

This approach is based on a more intensive exploitation of all information layers provided by the SMA (compare section 7.2). Especially the shade component contains valuable information that has so far not been directly incorporated into the analysis process. Adams et al. (1995) have classified multispectral images of the Brazilian Amazon using endmember fractions. Lu et al. (2004a) have compared different classification methods to infer information on land use in the Amazonian basin. They concluded that using fraction estimates from SMA, especially the shade component enhances classification results as it contains valuable information related to vegetation structure. Shimabukuro et al. (1998) have presented an approach using shade fractions derived from SMA to infer structural vegetation types and information on deforestation in the Amazon region. Sabol et al. (2002) investigated how the evolution of pacific forests following clearcuts and replantations reflects in fractional proportions of different endmembers. Further, Small (2005) and Rashed (2005) have discussed the value of the synthetic shade endmember in the context of urban remote sensing applications. The method proposed here is based on the hypothesis that different vegetation units may yield the same vegetation cover estimates, but that their respective shade abundance varies as a function of structure and species composition. For instance, a dense forest is expected to produce a much higher shade fraction, as a result of its complex structure with large LAI values and high proportions of non-photosynthetic vegetation. In comparison, dense grass- or shrublands with similar or even higher cover estimates are expected to yield lower shade fractions. Similarly, the fraction of identifiable background signal may be used for an additional differentiation of

units. Based on these assumptions, a rule-base for classification into four categories using all bands provided by the SMA was defined. The target classes were: sparse shrubland, dense shrubland, sparse forest (sparse matorral) and dense forest (dense matorral).

As a reference, the vegetation/fire perimeter map prepared on the basis of the conditions encountered in 1989 was employed. As described in Appendix A.1, this map differentiates a higher number of plant communities and growth characteristics than what could be expected to be derived from the tested approach, such as different types of forests and shrublands as well as different levels of crown cover. Unfortunately, some areas are also mapped as 'burned areas', and the respective fire year is given instead of information on vegetation in 1989. For these reasons, vegetation units were aggregated to finally represent four major classes, which can be considered to be the main post-fire vegetation succession stages: sparse shrubland, dense shrubland, sparse forest, and dense forest. Referring to the major communities identified before, the 'sparse shrubland' class refers to the herbaceous-dominated communities following fires, as well as to sparse, open shrublands described before (for instance Fig. 9.18, Fig. 9.21, Fig. 9.22). The 'sparse forest' class relates to the transition stage between shrublands and forests, where a high number of tree individuals is present in a matrix of dense shrublands, but no closed crown canopy is yet established (compare Fig. 4.16 and Fig. 4.17).

From this reference map, agricultural areas were excluded as well as areas for which no information was available, i.e. the areas mapped as 'burned areas'.

Assessing the histograms of the fractions derived from SMA, it is possible that the position of their maximum and the shape and type of distribution vary between different years within certain ranges. This results for example from general variations in the brightness level of different images as a result of the moisture content of the soil. It also depends on the photosynthetic activity of vegetation which is affected by many factors. As a consequence, it was not feasible to apply fixed classification thresholds, since the classes were assigned based on very narrow histogram intervals, such that the classification was highly sensitive to these variations. Hence, image statistics were calculated for all SMA results prior to normalisation, and the thresholds were expressed as functions of the respective mean and standard deviation, which significantly increased the robustness of the approach. In order to avoid ambiguous class assignments, information on water bodies and settlements was introduced in the respective data matrices derived from vector data sets, which hence consisted of 5 layers: water (binary), settlement (binary), vegetation, background, and shade. The, hierarchical classification tree shown in Fig. 9.23 was developed and applied: to the results of the linear spectral mixture analysis for 1989. This procedure yielded a map of the four target vegetation units, which was compared with the reclassified reference map (Fig. 9.24).

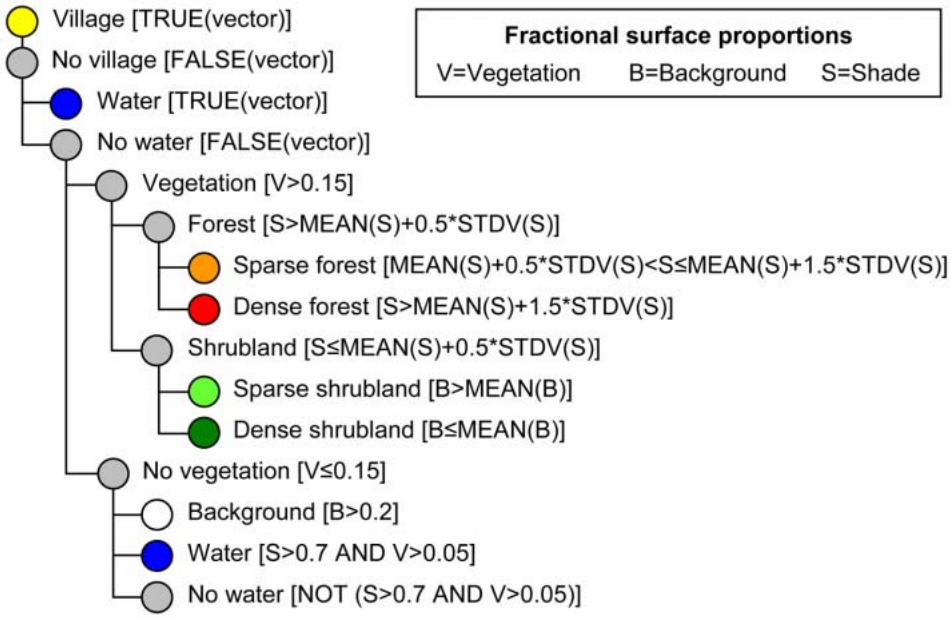

Fig. 9.23: Classification rule-base for major vegetation units. Coloured circles indicate derived target classes, grey circles relate to superclasses required in the decision tree structure; classification rules are given in brackets

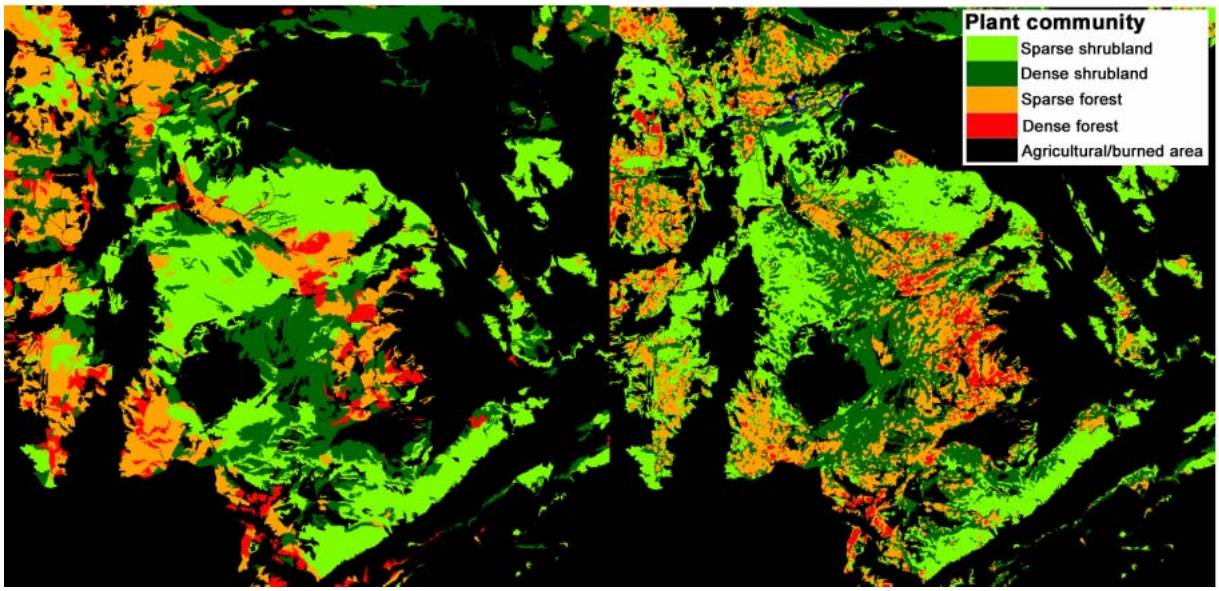

Fig. 9.24: Major vegetation units derived from the reclassification of the vegetation reference map (left) and the rule-based classification of SMA results from 1989 (right) using the rule-base presented in Fig. 9.23

Apparently, major units of the reference map are well reproduced in the classified image. Where deviations appear, it needs to be considered that the reference map was based on visual mapping, which is commonly associated with stronger generalisation compared to the classified image that is based on pixels as the smallest entity.

In a further step, the rule-base was applied to an image from 1979. The resulting vegetation formation map was visually evaluated[1] and was used in the context of fire simulation experiments for the 1979-fire (Duguy et al., 2005). Such generic applicability supports transferring the rule base to other data sets and the classification scheme was applied to the full suite of images. For the example of the 1979-fire, the majority of forests and dense shrublands present in the area prior to the fire event is destroyed, and sparse shrublands are dominating after the fire (Fig. 9.25).

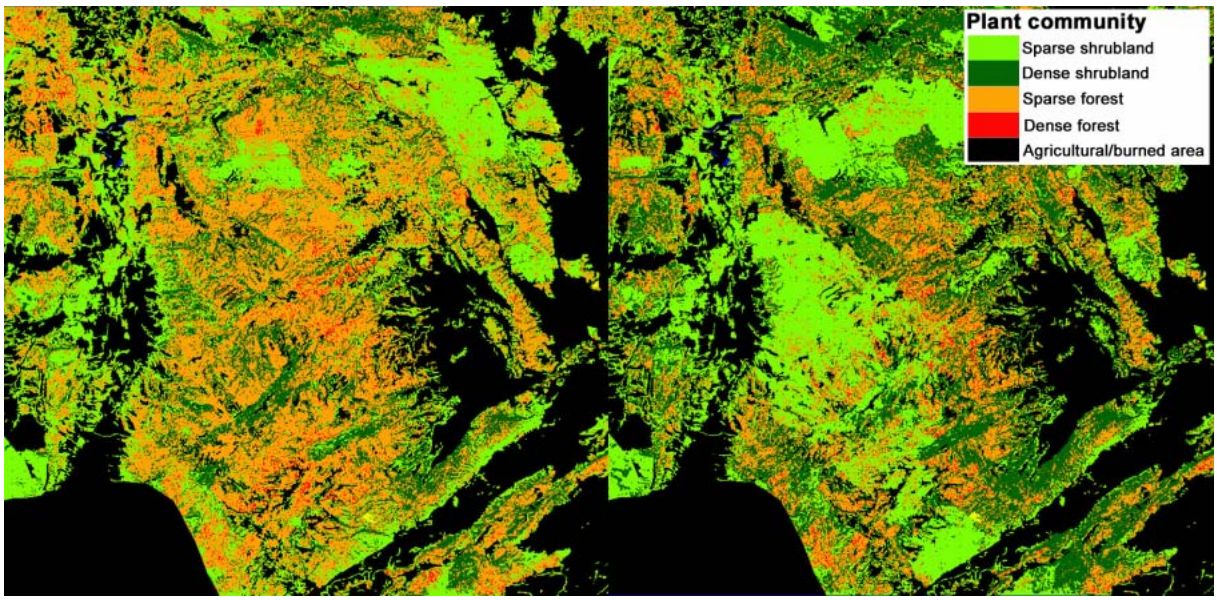

Fig. 9.25: Rule-base classification of major plant communities before and after the fire in 1979 (left: 1979, right: 1980) using the rule base depicted in Fig. 9.23

Employing this dynamic classification rule-base, plant community classes were derived for the whole time series.

In some locations, the reported variations in histograms for consecutive years were found to exceed the general behaviour and could not be balanced by the dynamic assignment of classification thresholds. In such cases, class assignments may show positive followed by negative development, indicating ‘succession’ followed by ‘regression’ of plant communities, such as for instance from ‘sparse forest’ to ‘dense shrubland’. This may also occur where plant communities are in a transitional state between two major classes, and phenological variations cause these their assignment to different classes in different years.

Summarising, the results demonstrate the potential of SMA-based analysis to derive information on structural vegetation formations and post-fire dynamics beyond green vegetation cover for larger areas. It complements multi-temporal approaches for single phenological cycles and satisfactorily reproduces major succession stages of vegetation. In order to support an analysis on the pixel-level, additional validation data are needed to further develop this classification

[1] A visual assessment of the results for 1979 was carried out by Dr. Ramon Vallejo, Dr. Beatriz Duguy and Dr. José Antonio Alloza from the Fundación CEAM (Valencia, Spain) using knowledge of specific plots and topographic maps.

scheme. For instance, the availability of new orthophotos or imagery from very high resolution sensors, such as Quickbird or Ikonos, would provide a means to independently validate the results and refine the classification. Future work has to concentrate on stabilising the approach and on minimising the effects of variations in the histograms of the different abundance channels. Fuzzy thresholds might support the analysis especially where pixels are located at the transition zone between two classes, which is so far the major obstacle in considering this approach operational.

9.6 Summary and discussion: fire dynamics in the Ayora rangelands

An interpretation scheme for large areas affected by recurrent fires was developed. Owing to the specific properties of time series dominated by disturbance events, the habitual concept of linear regression analysis to describe the temporal behaviour of a target indicator was modified and extended. It accommodates both requirements of land managers and ecologists, and provides, beside exact fire perimeters, information on vegetation succession on a quantitative level following a stratified and multi-temporal analysis. Exploiting results from the different analysis steps, a suite of additional information products with high practical relevance can be derived.

Based on the quantitative indicator of green vegetation cover, which was also used to produce vegetation cover maps for each year, the first important step was to identify the years of major fire events, exactly locate the corresponding perimeters and characterise these both in the form of fire maps and area statistics. Making use of the fire perimeters in a spatio-temporal stratification, post fire recovery was calculated on the level of green vegetation cover and it was shown how the validity of the derived trends can be supported by their statistical significance. For all fire patches, vegetation was shown to quickly recover directly after the fire event which is strongly owed to the higher availability of minerals after fires, provided these have not been washed off (e.g. Christensen, 1994).

If no second fire occurs, the initial evolvement of mostly herbaceous species is followed by a gradual development and closure of a shrub layer as a result of resprouting or seedling establishment (e.g. Keeley, 1986). With the colonisation of tree individuals, a possible development to adolescent and later mature pine forest stands begins. This development largely depends on local conditions and no succession to a forest was observed in the burned areas during the observation period. In general, it has been stated that pine trees require an average of 15 years to reach sexual maturity (Trabaud, 1994; Vallejo et al., 2004), from which on they can be considered resilient to fires. In this case, the autosuccession following fires is expected to ultimately result in similar plant communities as present before. In the test area, locations not subject to any fire during the observation period are expected to represent typical fire-adapted climax states, with *Pinus pinaster*, *Pinus halepensis* being dominant tree species above a shrub and herbaceous layer (compare section 4.1.5). Given a higher frequency of fires, the concept of autosuccession is expected to result in ‘steady-state’ shrublands characterised according to the dominance of *Quercus coccifera*, *Rosmarinus officinalis* or *Ulex parviflorus*, while the development of pine trees is suppressed.

Alternatively to the approach adopted here, a post-fire date could be utilised as the starting point for the temporal stratification. This would reduce the influence of herbaceous species on the calculated recovery rates, but on the other hand decision upon such a starting date would be ambiguous, as succession occurs in a sequence of transitions.

In the case of Ayora, fire is the outstanding factor controlling environmental processes and conditions, as emphasised by the statistics of areas affected by wildfires given in Table 9.1. The analysis of Moreno et al. (1998) confirms that the Ayora region is among the Spanish regions most affected by wildfires in the past years. In the past decades, the region has been subject to socio-economic processes that are typical for many regions of the European Mediterranean. The number of local residents in the rural area of the Ayora test area has declined, while the city of Valencia has experienced a steady increase in population. The corresponding changes in local economical structures have led to widespread land abandonment and significant changes in land utilisation schemes. In the Ayora region, grazing activities have been strongly reduced and the subsequent encroachment of shrubs and accumulation of flammable biomass has been reported as one factor contributing to the recurrence of fires (e.g. Vallejo & Alloza, 1998; Moreno et al., 1998). With an increasing thickness of the existing shrub layer, this effect is further aggravated by the limited accessibility of such areas. Assessing the size of fire perimeters provided in Table 9.1, a recurrent pattern of fire perimeter extensions rising from low area figures towards large fire events may be inferred. This effect may be related to an increase in flammable biomass after fires if the area as a whole is viewed. Once recovering shrublands have attained a certain density and amount of biomass, they represent enormous fuel loads during the dry season. They are potential ignition points or areas through which fire fronts may easily propagate before previously unaffected areas are reached, especially where land abandonment contributes to this accumulation of flammable biomass (e.g. Riggan et al., 1994; Naveh, 1994; Finney & Ryan, 1995). As one consequence, almost the full area has been burned at least once during the period regarded. In most cases large fire events are preceded by generally drier years, accompanied by a slight decrease in green vegetation cover, as stated for instance by Millán et al. (1998) and Moreno et al. (1998). Again, such fire-prone conditions following extended dry periods pose even higher risks in areas dominated by shrublands with high portions of dry matter (e.g. Viegas, 1998). This effect is especially apparent for the three largest fires in 1980, 1986 and 1995 (compare Table 9.1, Fig. 9.7 and Fig. 9.14). Accordingly, the analysis of implications from likely climate change scenarios pinpoints at a further aggravation of fire events in the future (Rambal & Hoff, 1998).

Following the large fire event in 1979 (labelled ‘1980’), a number of management interventions and mitigation schemes were introduced. These include afforestations (*Pinus halepensis*, less frequently *Pinus pinaster* and *Quercus ilex*) as well as fuel load reduction in limited areas. More importantly, considerable efforts have been attributed to the creation of an extensive network of fire breaks, which is largely kept free of vegetation to limit the spread of fires and to provide access for fire workers (Fig. 9.5). In addition, water tanks were installed. In recovering areas, a number of measures have been applied, such as the removal of regrowing vegetation following a striping pattern, aiming at reducing competition and thus promoting faster recovery (Vallejo et al., 2004). As a result of both field inspections and the remote sensing based analysis, these efforts have generally been rated not successful. Considering the

budget spent on human work resources alone of 1,700,000 €, it must be stated that although a higher protection from fires could be realised within the area burned in 1980, wide areas were burned in the remainder of the test area. In addition, a high mortality of seedlings was noted. It was concluded that efforts should concentrate on changing fuel models by reducing the amount of dry biomass both through mechanical removal as well as controlled grazing, or by introducing woody resprouters and tree species considering local conditions. Generally, promoting a higher fragmentation of the landscape was considered an important option to counteract fire propagation. The creation of complexly shaped woody patches was proposed to increase forest expansion, which should be complemented by ensuring connectivity through the establishment of corridors between different patch types (Forman, 1995, 1996; Vallejo et al., 2004; Del Barrio et al., 2004). Beside these efforts to re-establish mature vegetation, immediate measures may prove necessary where an immediate risk of erosion might result from the strong rainfall events following fires. In these cases, emergency seeding has been proposed as one possible solution (Vallejo & Alloza, 1998).

In a further interpretation step, it was analysed whether a stratification of fire patches according to factors that potentially influence vegetation characteristics enables to draw more specific conclusions on post-fire dynamics or their environmental drivers. This was based on the digital elevation model as one component of the monitoring framework that is routinely available. Additional analysis investigated the benefit to be gained from auxiliary information, the availability of which may vary from case to case. Results were not fully consistent, with patches showing no differentiation at all, while many others exhibited different regeneration patterns corresponding to different stratification zones.

Although minor disturbances may decisively influence the average of cover estimates, most areas clearly recover concerning green vegetation cover, if very slowly in some instances. It is generally accepted that a climax plant community typical for fire-affected areas could be expected given enough time and a disturbance frequency that does not exceed the one to which the recovery traits of the respective plants are adapted. Its potential floristic composition is reflected in the area not affected by fires during the period covered by this study. There, mature *Pinus pinaster* and *Pinus halepensis* individuals are dominating, and the understorey is composed of shrub species such as *Rosmarinus officinalis*, *Juniperus oxycedrus*, *Erynacea anthyllis* and *Bupleurum fruticescens*, and a grass layer dominated by *Brachypodium retusum*. In addition other tree species, like *Juniperus phoenicea* and *Quercus ilex* are locally interspersed.

It was shown that the factor ‘aspect’ most decisively determines vegetation properties, which results from its strong influence on insolation and evapotranspiration rates and hence the availability of water. In addition, terrain features which control redistribution of available water were identified as a second major component. Given the importance of the water as the major limiting factor for vegetation development, amount and temporal distribution of rainfall mostly affects vegetation development and succession. Precipitation is responsible for most of the yearly variability of vegetation development in sub-humid to semi-arid ecosystems. This emphasises the importance of precipitation and water availability as a major factor governing the behaviour of vegetation in the semi-arid conditions of the Ayora region. Furthermore,

although the area is relatively homogeneous as to underlying bedrock, it is plausible that local variations in pedogenetic processes are another determinant of vegetation characteristics, which could only partially be verified for topography-related properties using the available information.

The presented approach is considered an efficient component of a monitoring strategy for fire affected rangelands, since the most important types of spatial and non-spatial information can be derived exclusively based on remote sensing data and digital elevation models. A number of factors need to be discussed in this context.

Population of the multi-temporal data set

The way in which time series are aiming at approximating 'real world' processes needs to be accounted for when interpreting the results. In the present example, it was opted to address each year of the total period, provided suitable data are available. Consequently, a fire may have occurred – in the extreme cases – one day prior to the image acquisition date or one day after the time of acquisition of the preceding image, or at any date in between. Although unlikely, more than one fire may have occurred during this interval, which will be summarised as one fire by the given approach. Where a certain lag between the date of fire and the date of image acquisition is the case, regeneration has already taken place. This can, for instance, be noted for the 1980 fire event, which is known to have happened already in 1979. For this reason, the vegetation cover estimates for 1980 are already on the order of more than 10 %. It follows that the starting point for the subsequent trend is relatively high, such that the derived gain parameter will be lower than for dates where vegetation is still recorded following fires at very low levels. This effect could be counteracted by the introduction of more images, but this is not feasible for various reasons, such as data costs, processing efforts or availability of images at suitable dates.

Assessment of green vegetation cover

The multi-temporal analysis of vegetation dynamics is based on green vegetation cover derived from spectral mixture analysis (compare chapter 7). The spectral resolution of the Landsat-TM and especially the Landsat-MSS sensor denies to differentiate plant species from spectral properties. The endmember model employed was set up to represent typical overall physical conditions and variability of the whole test area, while accounting for limitations of the spectral dimensionality of Landsat-MSS. Concerning the assessment of vegetation, this means that the endmember adapted to represent the typical mixture of shrublands with pine trees is also applied in cases where different types of vegetation are present in reality, such as in areas dominated by herbaceous species. In addition, vegetation often includes varying amounts of dry components depending on its phenological stage. Both of these factors have to be considered when assessing the results, and have been discussed in the context of the different phases of post-fire dynamics shown in the integrated vegetation cover profiles over time. A stratification of endmember sets according to local conditions might appear desirable, but in the case of vegetation this is not feasible due to a number of reasons. First of all, the stratification according to plant communities would require prior knowledge on the spatial distribution of different species. Secondly, plant communities are not static, such that a continual

adaptation of stratified endmember models would be necessary. Finally, the application of a large number of individual endmember models, where both target and background components vary, has been found to create offsets at the boundary between models that do not reflect real conditions, these often being characterised by transitional states between communities. As a consequence, a unified model was applied to the full investigation area. The higher data consistency is expected to balance the potential inaccuracy where specific plant communities are not exactly represented.

Rate of change

The calculated recovery rates are based on the gain factor of the linear trend analysis. This is originally calculated as a function of days since the first date of image acquisition by a given sensor, but should be converted into a more easily comprehensible figure. In this study the average rate of change per year (%) was calculated, which enables to compare the figures for different fire events. It is important to note the total time during which vegetation has developed at this rate, which will of course result in different total cover depending on the length of time. This could alternatively be visualised by relating the calculated gain to the total time elapsed between the date of fire and the last day assessed.

The adopted temporal stratification equally considers different stages of post-fire succession when calculating the linear gain rates. It encompasses both the strong initial recovery of herbaceous species, and then the more gradual further increase associated with the transition to shrublands of varying species composition and density. Alternatively, the second year after the fire could be chosen as the starting date, assuming that the resulting gain would in this case exclude the initial recovery phase. This is, however, critical, as there is no clear breakpoint between the different transitional phases. Furthermore, plants associated with initial vegetation recovery already offer important protection from soil erosion processes, although the degree of protection increases with further plant succession (e.g. Francis & Thornes, 1990).

Integrated temporal profiles

Beside the spatial representation of average recovery rates and trend significance, integrated profiles are a means of visualising an overall trend of a given area which is homogeneous with respect to the stratification parameter. In a first step, this has been done for the major fire events in the core study area, which were again stratified according to their overall fire history. In this way, the effect of smaller ‘disturbances’, such as minor agricultural activities, clearcuts or newly created fire breaks, is minimised by averaging large areas. On the other hand, this does also involve a certain attenuation of fidelity in the data. Consequently, this type of integration provides an overall view on the temporal development of larger areas, which may be complemented by a more spatially differentiated assessment of the development in relation to different influencing factors. In this study, this has been pursued by stratifying the larger patches with homogeneous overall fire history into smaller units according to classes of the factor evaluated. This can help to clarify the influence of different factors, but increases the risk of introducing noise through small deviating units, since the strata averaged in this interpretation step are much smaller than the ones involved in the first step.

Referring to the requirements postulated at the beginning, points 1 to 4 were shown to be tangible items using the proposed analysis strategy for remote sensing data covering local to regional scales. In addition, an approach was suggested to derive further information on post-fire succession of major classes of plant communities. Although the results attained in this study have demonstrated the potential of the method, further refinements are needed before it can be operationally applied. Especially, specific calibration and validation data sets or maps are needed covering different points in time. Fig. 9.26 provides a schematic representation of the different components of the proposed monitoring and interpretation framework for fire-prone areas of the Mediterranean.

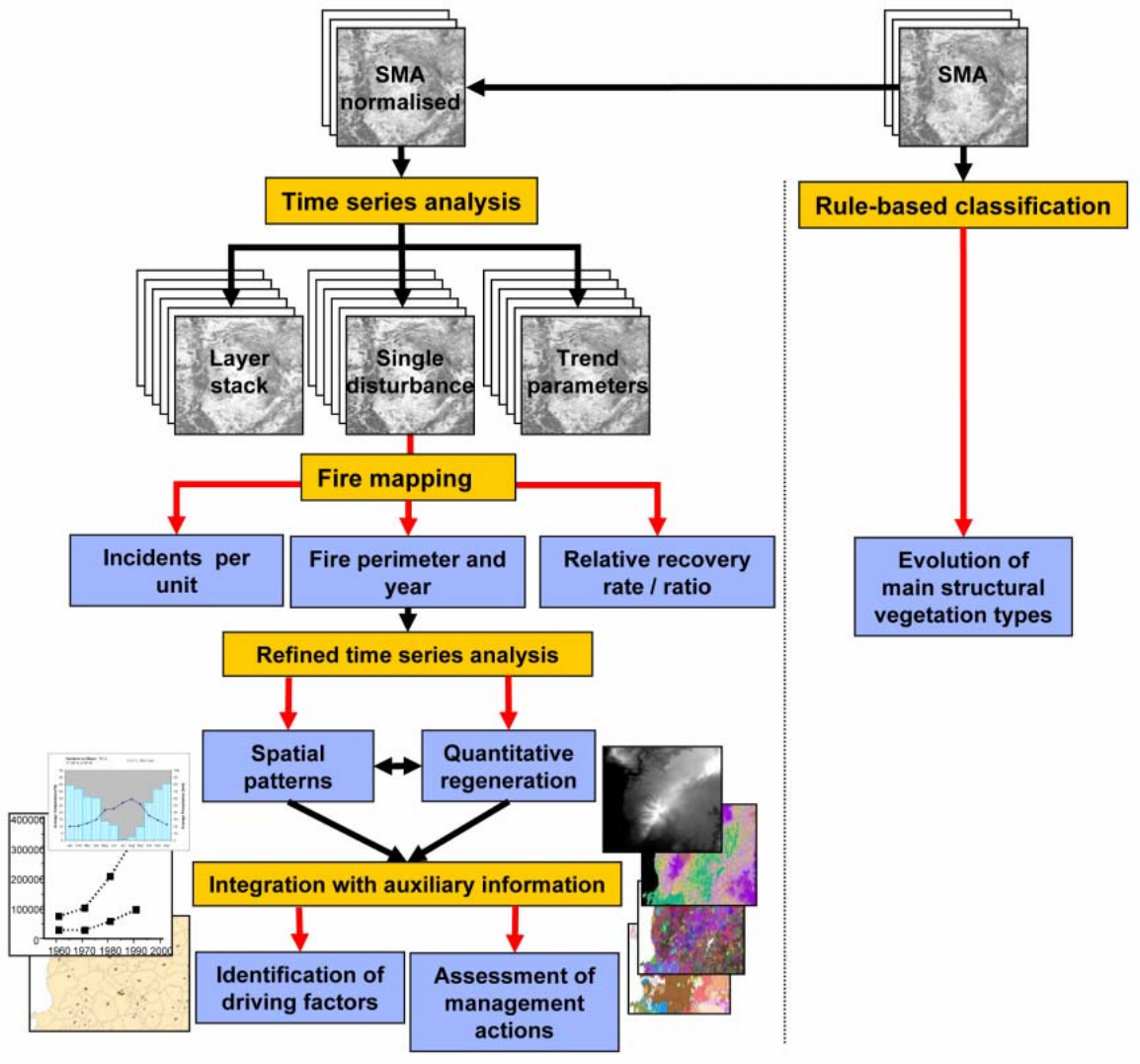

Fig. 9.26: Interpretation scheme for fire perimeter mapping and monitoring of post-fire regeneration (red arrows indicate the preparation of information products)

10 The Lagadas case study

The Lagadas test area is typical for the highly interwoven mosaic of land uses and land cover types found in many European Mediterranean regions. North and south of the main trough with Lakes Volvi and Koronia, the landscape is clearly structured into different elevation zones and transitions between these (compare section 4.2). While natural vegetation partially corresponds to these zones, there is a mosaic of land uses of various types and intensities according to which different pressure systems operate. There are some major zones of intensive agriculture, but it is especially the mosaic of rangelands used for grazing, with embedded smaller agricultural plots, which requires major attention.

For such areas, a long-term monitoring framework needs to enable the identification and assessment of the complex interactions between environmental conditions, land use types and socio-economic pressures. In the case of Lagadas, especially grazing-related processes are at the focus of this study (compare sections 2.4 and 4.2.6). Hence, important factors to be considered are:

- Characterisation of long-term trends of vegetation cover in rangelands
- Identification of relations between grazing system, grazing impact and the physical and socio-economic framework
- Consequences of grazing-induced landscape modifications

It can be assumed that gradual processes dominate in the Lagadas area. Although the setting of fire to improve pasture quality and remove unpalatable species is a common shepherding practice, this remains confined to limited areas. Larger 'singular disturbances' only occur in the deciduous forests in the high-elevation zones, where both cutting for wood production and – in rarer cases – fires may occur. As the work is centred on rangelands, trends and processes in these forest areas are only briefly touched here.

10.1 Long-term trends

In the proposed observation framework, the understanding of local processes is approached in a first step by assessing the temporal behaviour of target indicators, in this case green vegetation cover derived from SMA (compare section 7.3). The focus here was laid on overall development rather than the identification of short-term disturbances. Hence, the linear trend analysis was calculated for the period from 1984 to 2000 according to the principles set out in chapter 8. The resulting overall rates of change of vegetation cover based on the trend function, as well as its t-tested significance, are shown for the full area in Maps E.4 and E.5 (Appendix).

10.1.1 Spatial patterns of multi-temporal statistics

In the North of the target area, the belt of deciduous, thermophilous oak forests dominated by *Quercus ssp*. and, to a lesser extent, *Fagus ssp*. extends from Northwest to Southeast. These forests extend to both sides of the northern County border (compare section 4.2.5). In Map E.4 (Appendix) this unit is represented as a matrix of locations showing no change,

within which adjacent compact patches of positive and negative development are present. While these forests can mostly be considered stable over time, clearcuts have been applied in some parts for timber production. Also, isolated fires have occurred. These events lead to sharp breaks in the temporal profiles and, depending on the respective dates (i.e. position in the temporal profiles), may cause a positive or negative gain exceeding the neutral interval. They are mostly responsible for the pattern related to this ecological unit. The strongest decrease in vegetation cover can be found close to the Mediterranean Sea, in this case caused by a fire event in 1992 following which a *Quercus coccifera*-dominated shrubland has been established (Konstantinidis & Tsiourlis, 2003). The small patch with the strongest negative development in the North of this area was burned in 1995. In all cases, vegetation cover did not attain its previous level, leading to the overall negative tendency. The significance estimates (Map E.5/Appendix) show corresponding levels of α=10 % or higher for the disturbed locations, resulting from the overall dynamics during the observation period (compare chapter 8). In comparison, the surrounding, undisturbed areas show stable cover estimates with no obvious trend in most parts. There exist, however, also locations where the trend results from undisturbed gradual development and is supported by t-tested significance, but these are very rare.

Moving South to the lower elevation zones, agricultural areas are abundant. These are embedded in the rangelands at the scope of this work, which become dominant towards Mygdonia Valley. There is a general partition in an eastern part, corresponding to the area north of Lake Volvi, and the area directly adjacent in the West. In the East, a compact agricultural plain is nested between the deciduous forest zone and the Mt. Volvis mountain range (Mt. Volvis: 654 m asl) from which elevation drops down steeply towards Lake Volvi. The main mountain block is the only larger rangeland area characterised by a clear increase in green vegetation cover and corresponding significance levels. The slopes towards the lake show more patches with negative than positive trends, but are mostly associated with neutral behaviour. West of this area, the transition from the forest zone to the bottom of the valley is more gradual and undulating in general. Here, agricultural areas appear more scattered and arrange especially along flat areas. There is only one area where negative trends are visible for a compact patch, while for the remainder a mixture of positive and negative trends can be inferred. The value of the gains is only moderate, and overall neutral areas prevail.

The plain of Mygdonia Valley is predominantly used for settlement and intensive agricultural use sustained by high degrees of irrigation. East of this belt, a mountainous ridge separates this trough from the coast. It is also dominated by dense shrublands and forests of *Quercus coccifer*a, but thermophilous species appear as well in the highest areas (Konstantinidis & Tsiourlis, 2003). Here, the same processes described for the high elevation forest zone operate and negative trends are visible.

South of the valley of Mygdonia, elevation rises steeply towards the Mt. Hortiskos range (1201 m asl) and Mt. Holomondas (1163 m asl) in the East. There is a gently undulating trench rising from the western edge of Lake Koronia in ESE direction which is the main agricultural zone here. In the Lake Volvi area, there is a compact mountain block between this trench and the lake. The topographic structure south of the main valley is reflected in the rates

of change, as both larger patches showing positive trends are related to higher elevations. In addition, locations showing negative development and supporting significance levels appear in lower areas which appear unsuited for agricultural use due to relief gradients. Beside these compact patches, the remaining areas show a mixture of moderate increase and decrease within a matrix of neutral pixels, which is similar to the pattern observed north of the main valley. Correspondingly, highest significance levels are attained where strong gains occur, while in the more disperse areas trends are insignificant or characterised by lower levels.

Appraising the possible development scenarios, it is clear that the estimation of significance levels may not be appropriate in all cases. Following the suggestions formulated in chapter 8 and the examples given for the Ayora test area, the RMSE was evaluated as a further means of assessing temporal profiles (Map 7/Appendix). The most pronounced patterns and patches do reflect those described before. Especially the disturbed forest patches show high RMSE values. However, in this representation the stable behaviour of undisturbed forests is clearly represented by lowest RMSEs. In addition, locations where a positive trend is not an indirect result of a disturbance event do also show low RMSE values and can thus be separated form disturbed patches. It is also striking that most of the grazed rangelands where significance levels of α=10 % or higher were not attained do nonetheless show medium RMSE values. This indicates that in some cases trends are weak but still a consistent temporal profile is present. Again, the two grazed regions north of the Mygdonia Valley are easily separated, but for the western area most locations with insignificant trends do show only moderate RMSE values.

South of Mygdonia Valley, the situation is somewhat different. Especially south of Lake Koronia, compact areas with both significant trends and low RMSE values appear in the mountain range of Mt. Hortiatis. This indicates a positive or negative development of green vegetation cover not resulting from isolated disturbance events and calls for further interpretation. In the rangeland area between the agricultural trench and Mygdonia Valley, for which the gain map shows a generally positive trend, patches with high RMSE estimates appear. Where these are also characterised as insignificant, the cause may be a high amount of grasses which trigger higher fluctuations in the data. Finally, the rangelands south of the eastern part of Lake Volvi show mostly moderate RMSE estimates, corresponding to no significance estimates better than α=10 % and neutral or slightly negative gains. However, two patches stand out with high RMSE estimates in areas with significant negative trends pointing at a disturbance event during the observation period.

Concluding, the analysis of gain, t-tested significance and RMSE as statistical parameters relevant for the temporal development of green vegetation cover in the test area reveals major patterns of stability, recovery or degradation. It is evident that given the spatial scale of Maps E.4, E.5 and E.6 (Appendix), it is especially compact patches that appear highlighted, while for large parts of the grazed rangelands no overall consistent tendency can be inferred.

10.1.2 Driving factors of spatial trends: grazing pressure

As in the whole of Greece, livestock grazing has a very long tradition in the County of Lagadas (e.g. Hadjigeorgiou et al, 1998; compare sections 2.4.1 and 4.2.6). According to Papanastasis (1998), the grazing system has undergone major changes in the past years, which

are reflected in the figures on animal numbers given in Fig. 10.1. During the 1960s grazing animals were increasingly held responsible for land degradation and restrictive policies were introduced. Together with an accelerated urbanisation this led to decreasing animal numbers and a spread in forests. With Greece joining the European Union in 1981, the introduction of the Common Agricultural Policy and the associated subsidy system made grazing profitable again and caused a general increase in animal numbers (Dubost, 1998). Nonetheless, this general trend greatly varies for the different communities. For instance, the communities of Volvi, Sohos, Peristera, Nea Appolonia and Kryoneri show steady increases since 1981 and total figures of more than 10,000 animals in 2002, while the number for other communities continually decreased and now range close to zero (e.g. Vertiskos, Petrokerasa). At the same time, the grazing system in the Lagadas area greatly changed in past decades, with transhumance being replaced by a sedentary system characterised by a concentration of grazing locations, pronounced daily grazing cycles centred around paddocks and the provision of feedstuffs to increase milk production and prolificacy (e.g. Zervas, 1998; Yiakoulaki et al., 2002; Yiakoulaki & Papanastasis, 2003; Yiakoulaki et al., 2003).

Animal numbers were made available for decades between 1961 and 2002 and on community level from the National Statistical Service of Greece and the Direction of Agriculture (NSSG, 2002). Unfortunately, 1981 was missing and hence had to be calculated from the 1971 and 1991 figures through averaging. This census includes information on cattle, sheep and goats, but does not discriminate between animals kept in sheds or as roaming livestock. As cattle is usually kept in sheds and only grazed on the farms it has not been considered in the further analyses. The development of goat and sheep numbers is shown in Fig. 10.1, the figures are given in Table A.1 (Appendix).

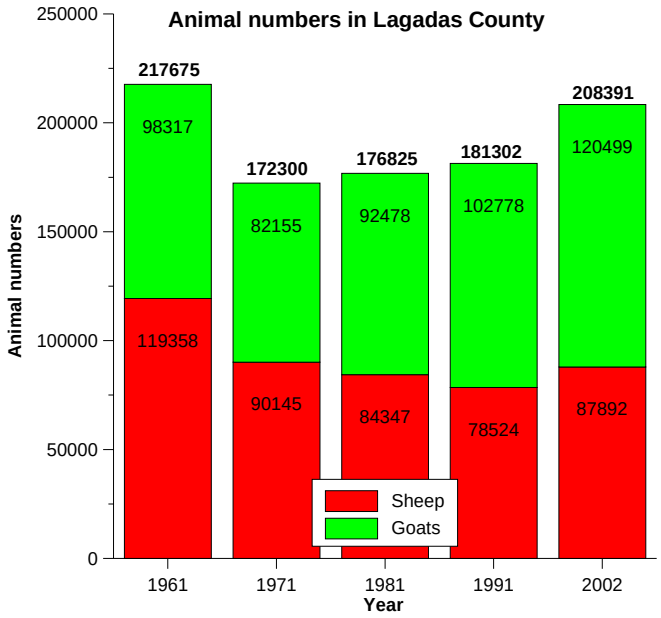

Fig. 10.1: Development of sheep and goats figures in Lagadas County between 1961 and 2002 (NSSG, 2002)

In total, animal numbers have not dramatically changed during the period covered by the data. This being undisputed, there has indeed been a significant reduction in animals between 1961 and 1971, following which numbers have steadily risen to almost attain their 1961-level in 2002. It is also interesting to note that there has been a change in the relative weight of sheep and goats, with about 15 % more goats in 2002 compared to a dominance of sheep in 1961 and 1971.

As the grazed rangelands in the test area are made up of grasslands or shrublands with varying composition of grasses and shrubs, they provide the diet for both browsing and feeding livestock. Hence flocks are usually composed of sheep and goats; for this reason total animal numbers will be employed in the following sections.

Similarly to Hostert et al. (2003b) it was analysed whether a relation between the development of green vegetation cover, as derived from SMA, and the development of stocking rates can be found. A mask of landuse types was derived using unsupervised classification and iterative thematic clustering of two Landsat-TM/ETM+ images from 2000 where the habitat GIS served as a reference. Using this information, areas not suitable for grazing, i.e. settlements, dense forests and agricultural areas were excluded from the community-related vector information. The latter may appear arguable as Yiakoulaki et al. (2003) report that sometimes animals are also led to harvested fields to feed on stubbles. This does not follow a regular grazing scheme and occurs outside the period covered by satellite imagery in late summer. Hence, the effect is similar to the provision of additional feedstuffs and can not be quantified. Using only the grazed community area made sure that averaged vegetation cover on community level was deduced in a correct manner and allowed to calculate adjusted stocking rates. On the county level, this stratification reduces the total area of 206,027 ha to 78,300 ha of grazed lands.

Fig. 10.2 shows the development of stocking rates for the time span covered by the following section. For visualisation purposes, the full communities are employed here rather than the stratified perimeters. Evidently, there is no uniform tendency in stocking rate development. More importantly, most communities show moderate to low stocking rates given the carrying capacities indicated for example by Tsiouvaras et al. (1998) for this area. As a conclusion from a fencing experiment, they suggested a stocking density of 1.1 sheep/ha for moderate grazing, while grazing pressure is considered heavy starting from 3 sheep/ha. Following Chouvardas & Papanastasis (2004), stocking rates for goats and sheep in total were classified as shown in Fig. 10.2. With ascending rates, these classes are rated as follows: lightly grazed, properly grazed, heavily grazed and very heavily grazed. The communities adjacent to the Mediterranean Sea show low stocking rates throughout the time considered. In addition, there are a number of other communities where stocking rates have decreased to a lightly grazed state, especially in the north-western and northern parts at higher elevations. On the other hand, the reduction in stocking rates in some communities has created one consistent belt that is rated as ‘properly grazed’ according to Chouvardas & Papanastasis (2004). Apart from these zones, there is a clear dominance of communities where livestock grazing is expected to exceed the natural carrying capacity and was rated ‘heavily grazed’ or even ‘very heavily grazed’. As a consequence, it can be expected that a long-term analysis of green vegetation

cover development should indicate a corresponding decrease of vegetation cover and level of degradation.

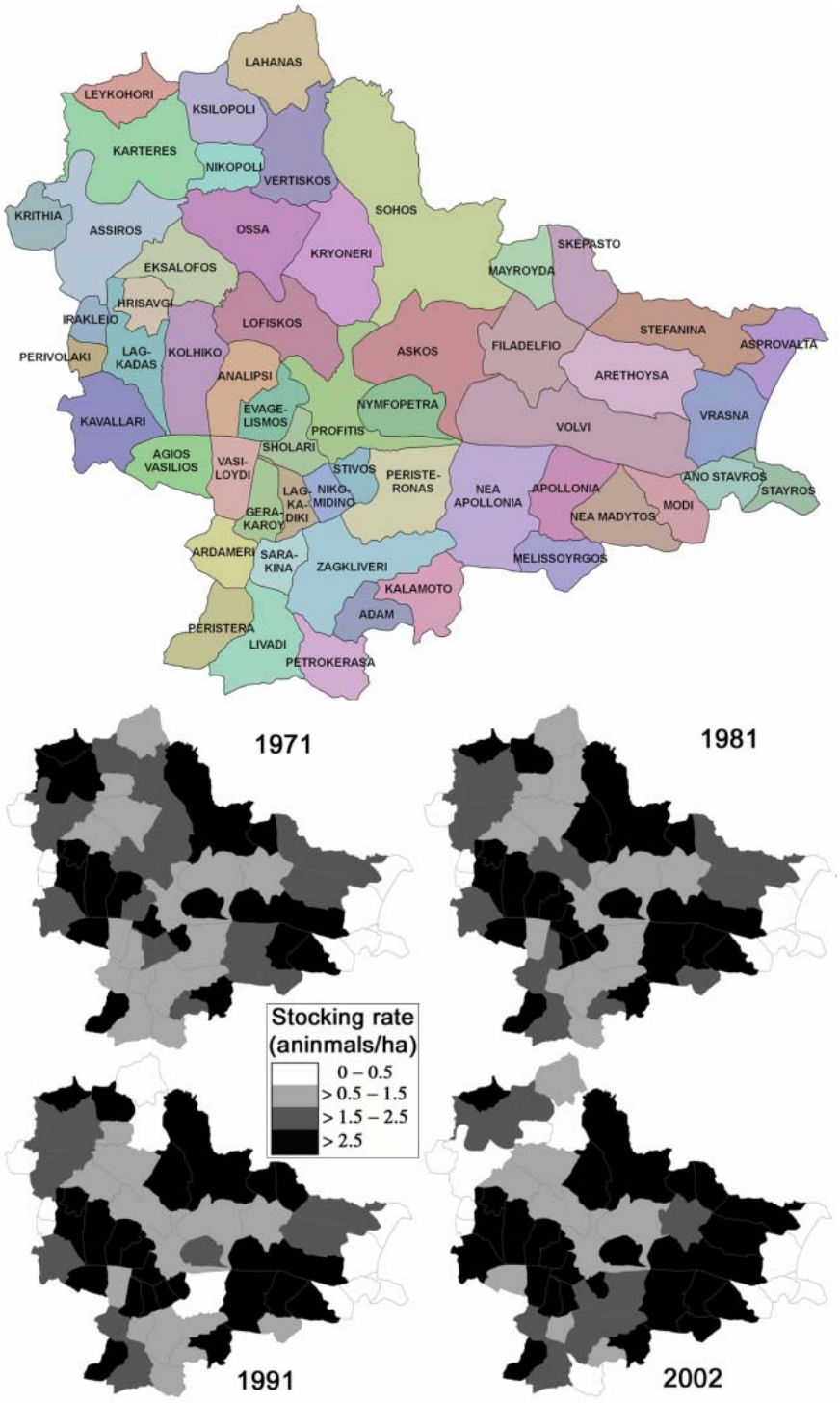

Fig. 10.2: Development of effective stocking rates in Lagadas County between 1981 and 2002. Effective stocking rates were calculated by excluding agricultural and urban areas

Using the stratified community perimeters, average green vegetation cover was related to stocking rates at the different observation dates to investigate if a direct dependency can be

proven. In order to suppress phenological variations at the different dates, the trend function calculated for each pixel (compare section 10.1.1) was used to calculate green vegetation cover for 1981, 1991 and 2002. This implied extrapolating beyond the observation period, but as this accounted only for 3 and 2 years, respectively, it could be assumed to be supported by the given multi-temporal data set. As a result, temporal trajectories relating vegetation cover to stocking rate at a given time were computed for each community. According to Ghossub (2003) community borders are respected by the shepherds, which is a prerequisite for this type of spatio-temporal analysis. The resulting 47 temporal trajectory plots are individually shown in Figs. C.1 and C.2 (Appendix), and Fig. 10.3 shows selected examples representative for the categories described below.

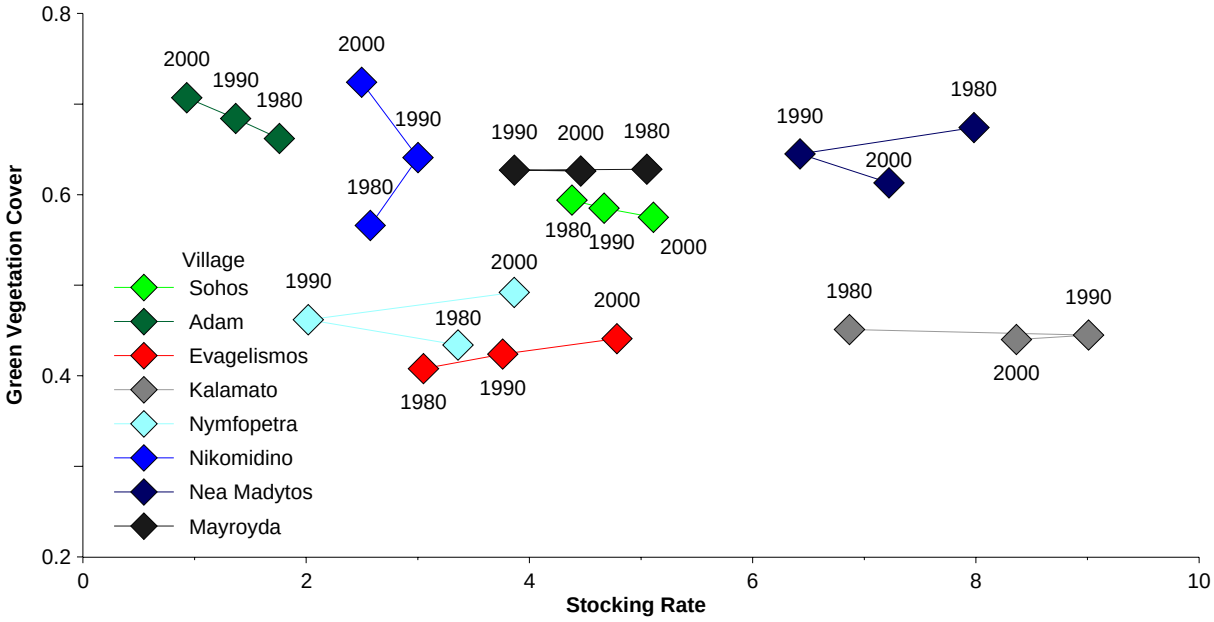

Fig. 10.3: Temporal trajectories of the relation between vegetation cover and stocking rate at three decades. Vegetation cover estimates were derived using the linear trend function for each pixel, animal numbers for each community are provided in Table A.1 (Appendix)

The range of stocking rates strongly varies between different communities. Where high stocking rates occur in communities with only little grazed area (Lagkadas, Scholari), it must be assumed that animals are mostly kept at the houses and in sheds.

Assessing the different plots, major groups of trajectories can be differentiated. Group A represents communities with a continuous negative relation between stocking rate and vegetation cover. Here, increasing stocking rates imply decreasing average cover and vice versa. This behaviour can be found for the villages of Sohos and Adam (Fig. 10.3). In the community of Sohos more than 12,600 sheep and goats were recorded. Although the community area is large, high stocking rates are noted here as a considerable part of the community area is not suitable for grazing, such as the agricultural areas and the thermophilous forests in the North. The increase in stocking rates during the two decades assessed is accompanied by a moderate decrease in vegetation cover. The village of Adam shows the same relation, but here a decrease in stocking rates and a corresponding increase in vegetation cover are present. In this

case, stocking rates developed from the ‘heavy grazing’ to the ‘proper grazing’ classes, which might explain the stronger gradient in vegetation cover compared to Sohos, where stocking rates indicate heavy grazing for the full period.

Group B also relates to a continuous development, but with an adverse relation. In this case, increasing stocking rates coincide with increasing vegetation cover, while the complementary effect is not observed. In Fig. 10.3, the community of Evagelsimos shows a strong increase in stocking rates which fall in the ‘heavy grazing’ category throughout the observation time. Notwithstanding, an increase in vegetation cover can be noted. It must be assumed that concentration processes and/or a diet strongly based on feedstuffs are responsible for this pattern. Especially the good road infrastructure in the valley of Mygdonia makes the provision of nutrition very convenient. In addition, agricultural fields occupy a significant portion of the area, such that grazing of animals on harvested fields may also play a role. All in all, groups A and B account for 21 out of the considered 45 cases.

A third major group of trajectories (group C) is characterised by a significant change in the direction of the relation between stocking rate and vegetation cover, indicating a transition from type A to type B or vice versa. Different factors may contribute to this behaviour, which mostly relate to the degree of ‘artificiality’ of the local grazing system compared to traditional roaming, or the general level of stocking rates. In the first case, increasing stocking rates are (over-)compensated for by the provision of additional feedstuffs and/or the local concentration of animals (Nymfopetra). This is especially important where villages are located in the valley of Mygdonia or at major transport routes and the good accessibility and infrastructure supports the concentration and intensification of grazing systems. The second major factor is the general level of stocking rates. Where these are very high, even a change in the direction does not necessarily translate in a corresponding regeneration of vegetation. This is further emphasised where agriculture is the dominant land use and only little generic grazing areas exist. In these cases, rangelands can not be set aside for regeneration purposes and overgrazing of the remaining areas results (Nea Madytos). On the other hand, vegetation cover may increase independently of minor changes in stocking rates if these are generally at a level that is sustained by the local environment (Nikomidino).

In the last group (D), vegetation cover remains stable regardless of changes in stocking rates (Mayroyda). Where this effect occurs at high stocking rate levels, it must be assumed that the modern feeding and animal keeping practices complementing the traditional pastoral system have led to the creation of an equilibrium that sustains high stocking rates within a given range (Kalamato).

In Lagadas County, livestock grazing has been an important component of the rural economy for long periods. In such areas, the analysis of green vegetation cover development in relation to stocking rates based on temporal trajectories would be expected to yield a negative relation where stocking rates are moderate to high. Stable vegetation cover would relate to stocking rates at a proper grazing level (i.e 0.5 to 1.5 animals per ha according to Chouvardas & Papanastasis, 2004), where the rotating system allows rangelands to recover. Positive relations would be expected where stocking rates lay below local carrying capacities leading to increasing vegetation cover and a corresponding encroachment of shrubs and trees. The trajec-

tories shown in Fig. C.1 and Fig. C.2 (Appendix) and in Fig. 10.3 support this theoretical function only in a limited number of cases. Besides, there is a variety of examples where the spatio-temporal pattern illustrated by the trajectories exhibits a clearly deviating pattern. There are a number of possible reasons subsumed as 'human factors' and related to the recent socio-economic framework. These encompass the enhanced accessibility of many locations, the local concentration of flocks in sheds and the provision of additional feedstuffs. As such, the changed political framework after Greece's accession to the European Communities in 1981 has a great indirect influence. In addition, the proximity of the city of Thessaloniki as an industrial capital of Greece and the Chalkidiki peninsula as a tourist attraction have changed the income structure and are partly responsible for changes in the rural economy and income sources. Comparing these results to the ones presented by Hostert et al. (2003b) for central Crete, it is striking that the increase in animal numbers is far lower in magnitude for the Lagadas region, which might also relate to good alternative sources of income.

The Lagadas area is characterised by specific properties terms of topography, spatial configuration of land uses and pastoral system. The fact that in contrast to the transhumance system the animals are nowadays usually grazed during the day and return to the same shed in the evening suggests that the impact of grazing can only to a certain extent be unveiled at the community aggregation level. The results from the temporal trajectory analysis underline this and suggest that degradation effects induced by livestock grazing manifest on finer scales and are also driven by a combination of socio-economic factors (e.g. Oba et al., 2000).

Consequently, the following sections address the identification of patterns of stability, regeneration and degradation and possible driving factors (sections 10.1.3, 10.1.4 and 10.1.5).

10.1.3 Degradation index

As a consequence of the limitations described before (i.e. section 10.1.1), it was tried to integrate information provided from the linear trend analysis to enhance the interpretability based on an ecologically relevant parameter. Similar to the approach adopted by Hostert et al. (2003b), a degradation index was formulated. It combines information on the direction and magnitude of the trend with the average level of vegetation cover during the observation period. The major advantage of deriving this index from information layers resulting from the trend analysis is the incorporation of the time dimension.

As selection of single dates for the vegetation cover parameter may introduce a bias, the long-term average vegetation cover per pixel was chosen. Given the possibility of strong trends, considerable ranges may punctually occur; hence, average cover values were assigned to three classes: low (0-35 %), medium (35-70 %) and high (>70 %) average cover. Similarly, overall gain rates were classified as follows: strong decrease (<-15 %), decrease (-15 - -5 %), increase (5-15 %) and strong increase (>15 %). The range between -5 % and 5 % was set to neutral to accommodate for possible errors in the processing and interpretation chain. In addition, it can be assumed that changes below this upper and lower limits are negligible considering the observation time span of 16 years.

Map E.7 (Appenix) shows the resulting spatial representation of the pixel-based degradation status modelled this way. Although the patterns shown in the vegetation cover change map

(Map E.4/Appendix) are reflected, a better differentiation is observed. Areas with strong trends appear pronounced, but especially in regions with moderate trends the introduction of the level of vegetation cover on which these manifest enhances the spatial explicitness of the resulting map. Most importantly, in the area north of Lake Koronia, spatial patterns emerge that are not visible in the gain map.

In a first step, areal statistics were calculated for the different degradation classes. Using the spatial information on habitats, areas not used for grazing, such as thermophilous forests, agricultural or urban areas were excluded. For the remaining areas, the area per class was calculated, and the results are shown in Table 10.1 and Fig. 10.4.

Table 10.1: Areal statistics for different degradation classes (numbers indicate counts) ([1] percentage for each class; [2] percentage aggregated for trend classes)

Trend	Vegetation cover level	Degradation index	Area (ha)	Percent[1]	Percent[2]
Strong negative < -15 %	Low	11	609.030	0.56	5.86
	Medium	12	5263.74	4.85	
	High	13	487.35	0.45	
Negative < -5 - -15 %	Low	21	1450.08	1.34	17.948
	Medium	22	16444.71	15.16	
	High	23	1560.51	1.44	
Neutral -5 - 5 %	Low	31	2211.21	2.04	42.42
	Medium	32	34739.19	32.03	
	High	33	9048.15	8.34	
Positive > 5 - 15 %	Low	41	958.32	0.88	27.42
	Medium	42	19597.41	18.07	
	High	43	9182.70	8.47	
Strong positive > 15 %	Low	51	212.22	0.19	6.36
	Medium	52	4795.29	4.42	
	High	53	1888.29	1.74	
Total			108442.20	100	100

According to this representation, only less than half of the area shows a neutral behaviour given the uncertainty threshold of ±5 %. Both negatively and positively developing areas yield higher percentages for the moderate compared to the strong gain classes. In addition, within these aggregated classes, development on mean levels is dominating compared to low and high vegetation cover levels. This may, to a certain degree, also result from averaging over long periods. Notwithstanding, differentiation of trends according to the level of vegetation cover yields important additional information, as the ecological value of vegetation cover development must be rated differently depending on its overall cover level.

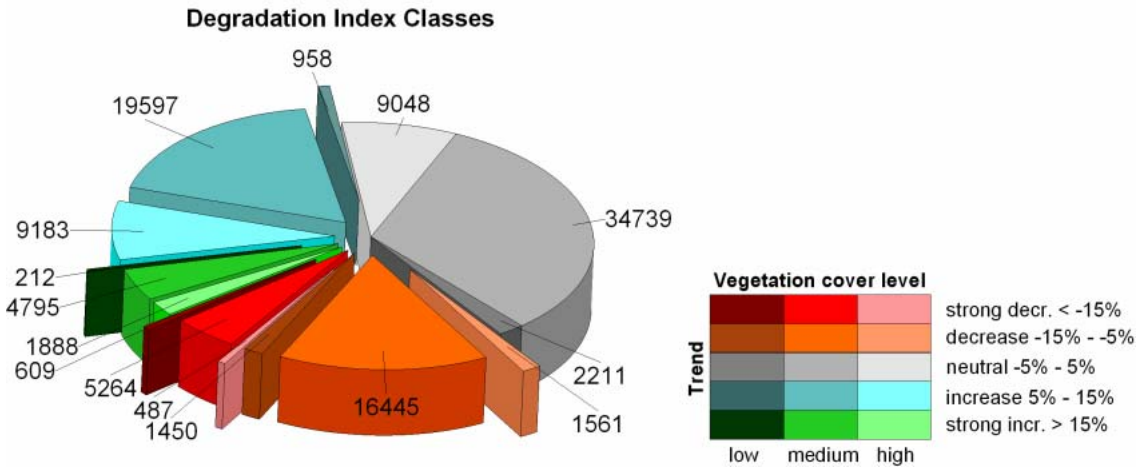

Fig. 10.4: Distribution of area assigned to degradation classes (with corresponding area in ha)

Concluding, the applied degradation index integrates two parameters that are important for a characterisation of the development of vegetation cover with regards to an ecological assessment. As it incorporates the temporal dimension of degradation it is a dynamic index and can hence only be derived from adequate multi-temporal data sets. This makes it an ideal element for monitoring concepts based on time series analysis. With respect to the Lagadas area, its spatial representation enhances results that rely on the gain of the trend function by highlighting the subtle patterns of positive and negative developments in the major grazing areas. Since these are difficult to discern given the overview map scale of 1:400,000, section 10.1.4 is focused on major rangeland areas.

10.1.4 Trends in target rangelands areas

Based on the degradation index, a limited number of sub-areas are visually analysed at larger scales in this section. Fig. 10.5 shows the perimeters of the selected areas.

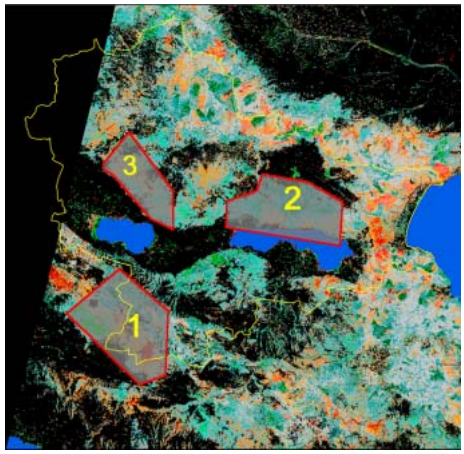

Fig. 10.5: Sub-areas used for the large-scale analysis of grazing related trends in the following sections

The **first focus area** is characterised by relatively compact patches with positive and negative trends on different average cover levels. In between these, pixels characterised as ‘neutral’ are

visible, but these are not abundant (Fig. 10.6). Comparing the spatial pattern of degradation index values with the subset of the DEM, patches with positive trends are mostly associated with the highest elevations, which appear in the subset as exposed landscape features, with elevations around 1200 m asl. To the contrary, patches with negative gains range at lower and less steep elevations. A sequence of temporal profiles representative for different patches and temporal scenarios is provided in plots 1-1 to 1-14 shown in Fig. 10.7.

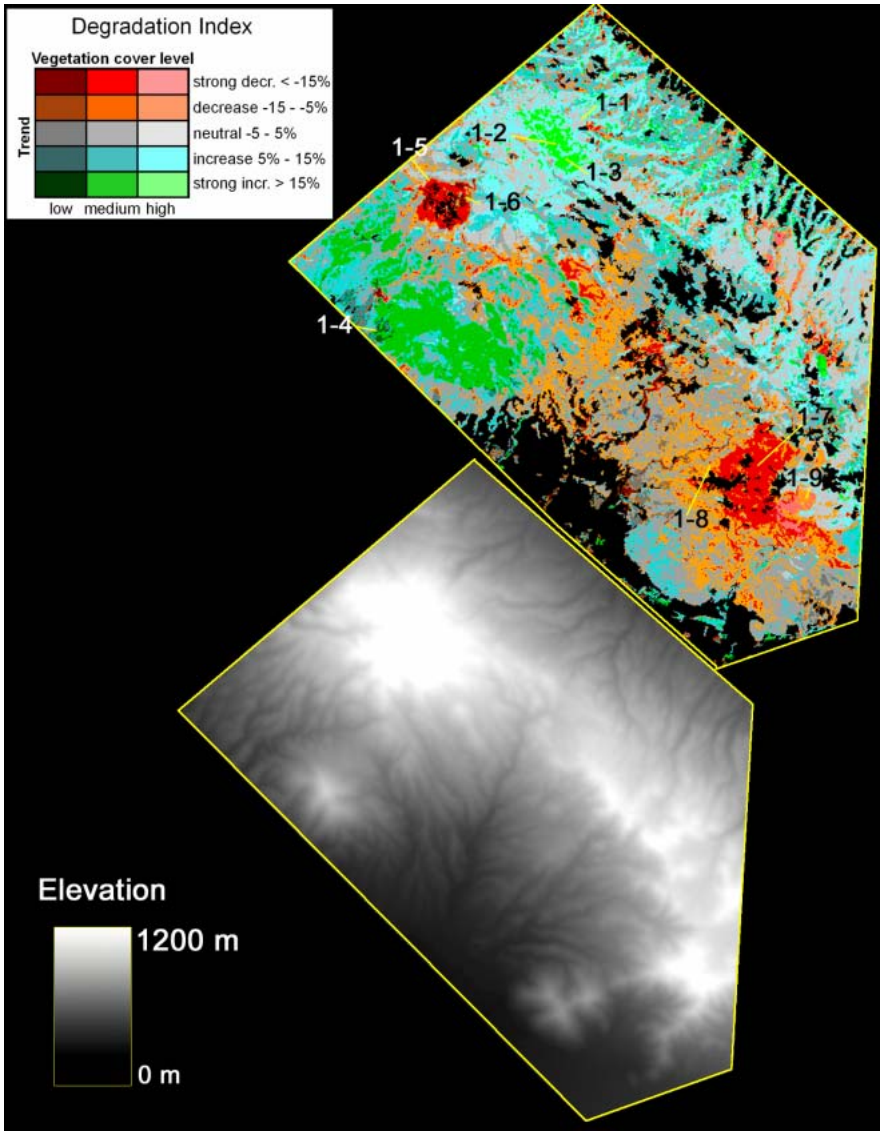

Fig. 10.6: Degradation index: focus area 1 (numbers correspond to temporal profiles shown in Fig. 10.7) and corresponding DEM-subset

Profile 1-1 represents a 'neutral' behaviour on high cover levels while profiles 1-2 and 1-3 both indicate strong overall increases in cover, although their respective shapes testify of a largely different history for this plot. While profile 1-3 relates to a continuous following a strong initial increase in green vegetation cover, profile 1-2 exhibits a major disturbance observed in 1986, potentially a fire. Nonetheless, vegetation is shown to recover quickly, such that the whole area can be considered an example for conditions not affected by permanent pressure factors. Given these conditions, dense *Quercus coccifera* shrublands may be ex-

pected at the given area. Similarly, profile 1-4 characterises the second major patch showing strongly positive trends. In this cases, the profiles depart from a rather low cover level, suggesting that the development of vegetation cover might be caused by changing pressure systems, such as for instance a reduction in grazing activities in that area. On the northern slopes of this area, a reticulate pattern of positive trends is observed. Such patterns will be exemplarily treated in the third focus area.

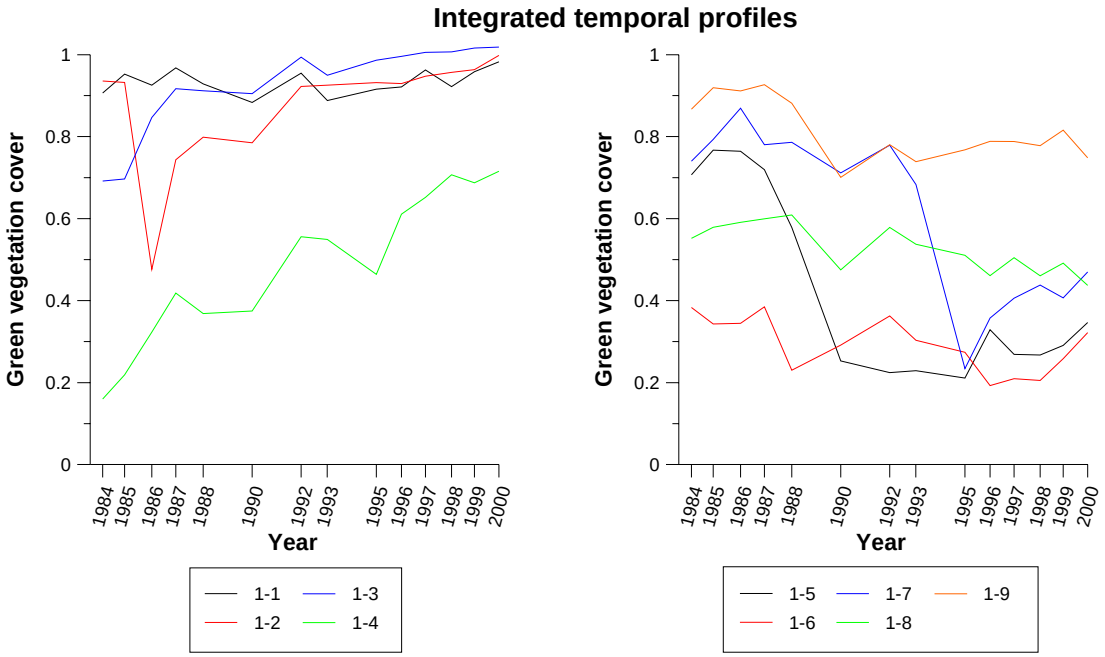

Fig. 10.7: Examples of integrated temporal profiles of green vegetation cover for representative locations with degradation index values; left: neutral-positive index; right: negative index (numbering corresponds to Fig. 10.6)

There are also areas where degradation index values indicate a negative trend, represented by profiles 1-5 to 1-9. It is evident that the smaller area in the Northwest has a different history compared to the second, larger patch in the Southeast. Profile 1-5 shows a strong but gradual reduction in vegetation cover between 1987, following which the values stabilise on a rather low level. On the other hand, profiles 1-6 is representative of moderate, gradual decrease in vegetation cover. Profiles 1-7 to 1-9 represent the largest area with negative to strongly negative trends. These mostly manifest on medium levels of vegetation cover. While it is known from field observations that this area has been heavily grazed for long periods, profile 1-7 characterises an especially serious case. Here, a fire event in 1995 has led to a decrease in vegetation cover of 45 %, aggravating the effects resulting from grazing activities. In this case, it is not known whether the fire was ignited naturally, by accident, or as an intentional measure to improve pastoral conditions. The photos shown Fig. 10.8 illustrate the degree of degradation in this area resulting from combined effects of the fire and the heavy resource utilisation that has prevented regeneration. Similar effects were for instance reported by Quinn (1986), who found that grazing after fires significantly reduced survivorship of different plants in various Mediterranean-type ecosystems.

Fig. 10.8: View over grazed and burned area corresponding to profile 1-7

The **second focus area** is located north of Lake Volvi and is clearly structured into three main zones by the degradation index (Fig. 10.9).

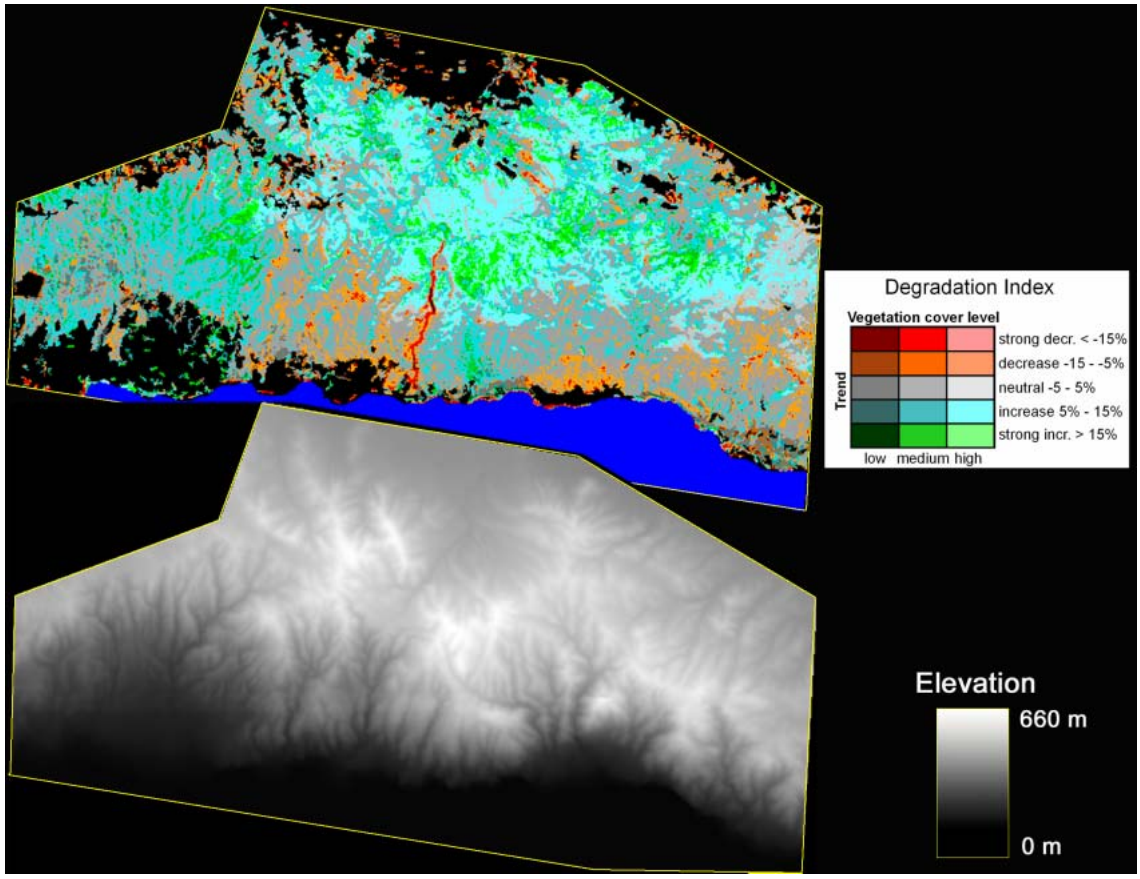

Fig. 10.9: Degradation index: focus area 2 and corresponding DEM-subset (interpretation in the text)

Zone 1 is a belt adjacent to the lake. It represents the transition zone between the valley and the higher areas and is mostly ascribed to the neutral class. In between, areas with positive and negative development are found, the previous relating to narrow valleys and gorges, the

latter to ridges in between these valleys. However, the linear feature characterised by strongly negative development results from the recent creation of a road. North of this belt, positive to strongly positive trends are abundant in the higher elevation zone and negative trends only appear in isolated patches. In addition, a third sub-area further west can be noted, which does not show this twofold zonation. It is the narrow belt between the more extended alluvial plain in the South and the agricultural zone in the North. Within this, two further subdivisions may be delineated, with the eastern patch being almost exclusively attributed to moderately and strongly positive trends. On the other hand, the westernmost patch of this focus area shows a more heterogeneous pattern, although positive trends are dominating here as well and negative trends are confined to small, isolated patches.

The **third focus area** is mostly situated north of Lake Koronia. It comprises the lower and mid-elevation ranges of the major grazing area in the County of Lagadas, which are dominated by grasslands and heterogeneous *Quercus coccifera* shrublands (Fig. 10.10). It represents the landscape that is typical for the region and that was shown in Fig. 4.24 and Fig. 4.26.

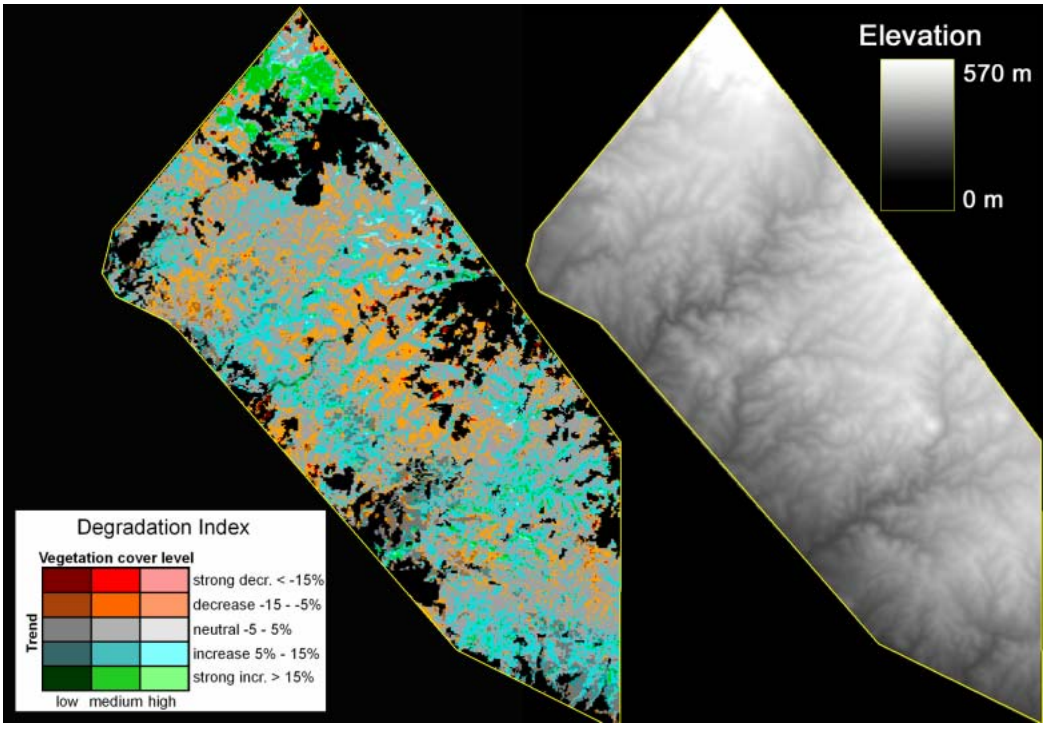

Fig. 10.10: Degradation index: focus area 3 and corresponding DEM-subset (interpretation in the text)

In the northernmost corner of this focus area strongly positive trends appear in a homogeneous patch corresponding to recent afforestation measures. Apart from this, the degradation index image (Fig. 10.10) shows a matrix of pixels with neutral status mostly on a medium cover level. Embedded, the reticulate pattern of moderate to strongly positive trends described before is most evident in the whole investigation area. A synoptic assessment with the DEM suggests that these strands correspond to narrow valleys and gorges. On the other hand, areas with negative trends show a more patchy structure and are often located on plainer areas in

between the reticulates. Both positive and negative developments are mostly on a moderate level although strongly positive trends do appear as well. Notwithstanding, the pronounced appearance of this pattern is striking and calls for its further interpretation to conclude underlying driving factors.

Similar to the temporal trajectory analysis (section 10.1.2) the numerical distribution of degradation index values shown in Table 10.1 does not support the hypothesis of a general degradation of grazed areas with respect to green vegetation cover. Rather, neutral areas are abundant, which are contrasted by positive and negative trends. These mostly manifest on moderate levels, which is an indication of general tendencies that may still be reversed. This information is complemented by spatially explicit information depicted in Fig. 10.6, Fig. 10.9 and Fig. 10.10. Grazing is assumed to be the major pressure factor in the focus areas. Its impact is disparate, leading to a differentiated pattern of stability, degradation and regeneration. A visual comparison of structures in the degradation index image with the DEM suggests a relation to relief properties. In **focus area 1** elevation seems to be the dominant factor, while in **focus area 3** patterns are rather associated with terrain features, such as narrow valleys and steep slopes, or intermediate ridges and planes. **Focus area 2** shows an intermediate behaviour since both ‘elevation’ as well as ‘relief position’ may be deduced as potential driving factors.

10.1.5 Driving factors of spatial trends: topography

In sections 10.1.3 and especially 10.1.4 it was suggested that topography and the associated accessibility of locations have a significant influence on the apparent trends in green vegetation cover. This factor complex is added to by the influence of socio-economic conditions on shepherding practices, which have in the past years changed the system from transhumance to a much more sedentary structure. In this section, it is assessed whether a correlation between topography and spatial trends can be confirmed using the available spatial information.

Based on the DEM, the influence of elevation and the terrain was investigated for the full area as well as for the three sub areas represented in section 10.1.4. In addition, a data set characterising major relief mesoforms was available. This had been computed using DEM-derived spatial information on different relevant parameters and following the procedure described in section 9.4.1.

Elevation

In a first step, elevation was stratified into classes of 250 m intervals and agricultural areas were excluded. The resulting zones were intersected with the datasets containing the total gain for the full observation period (i.e. scaled between 0 and 1), as well as with the degradation index image. For the gain related analysis, the mean gain was calculated, while for the degradation index image histograms were derived to assess the relative distribution of the classes. All of these analyses were carried out both for the full grazed observation area as well as for the three focus areas presented in section 10.1.4.

Table C.1 and C.2 (Appendix) give the numeric values for the increase in vegetation cover over the full observation period (total gain) and degradation index. Fig. 10.11 and Fig. 10.12

show the average total gain and the distribution of the degradation index classes for the different elevation zones, respectively.

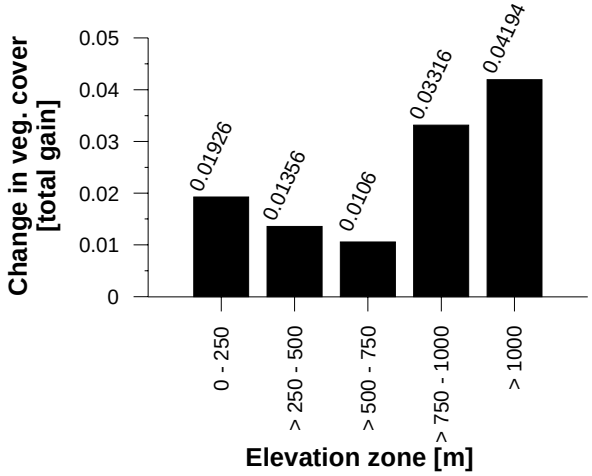

Fig. 10.11: Average total gain derived from linear trend analysis for five elevation zones and the full observation area

Obviously, there is no consistent pattern across the different zones and only the two high-elevation zones show distinctly higher averaged gain rates. However, the relevance of the information given for the highest area is somewhat limited by the smaller number of pixels included. Although the transition between the third and fourth class may relate to a difference in grazing intensities, the low value of the trends has to be noted. From Table C.1 (Appendix) it is obvious that the zones encompass a large range of positive and negative trends, such that the average can only provide a very general impression when a large area is analysed. Notwithstanding, the table also shows that this range diminishes with increasing elevation. While higher minimum numbers appear reasonable given the hypothesised relation between elevation and grazing, the lower maximum values are the result of the generally higher proportion of stable areas.

On a more differentiated level, Fig. 10.12 shows how the degradation index classes distribute within the elevation zones, while additional information is found in Table C.2 (Appendix). As this representation implies a further differentiation into different classes, the highest elevation zone is not shown here. It supports conclusions from the previous analysis, as the most evident change in class distribution is visible between elevation zones 3 (500 - ≤ 750 m) and 4 (750 ≤ 1000 m). There is a general dominance of moderate cover levels for these trends in almost all classes and at all elevations.

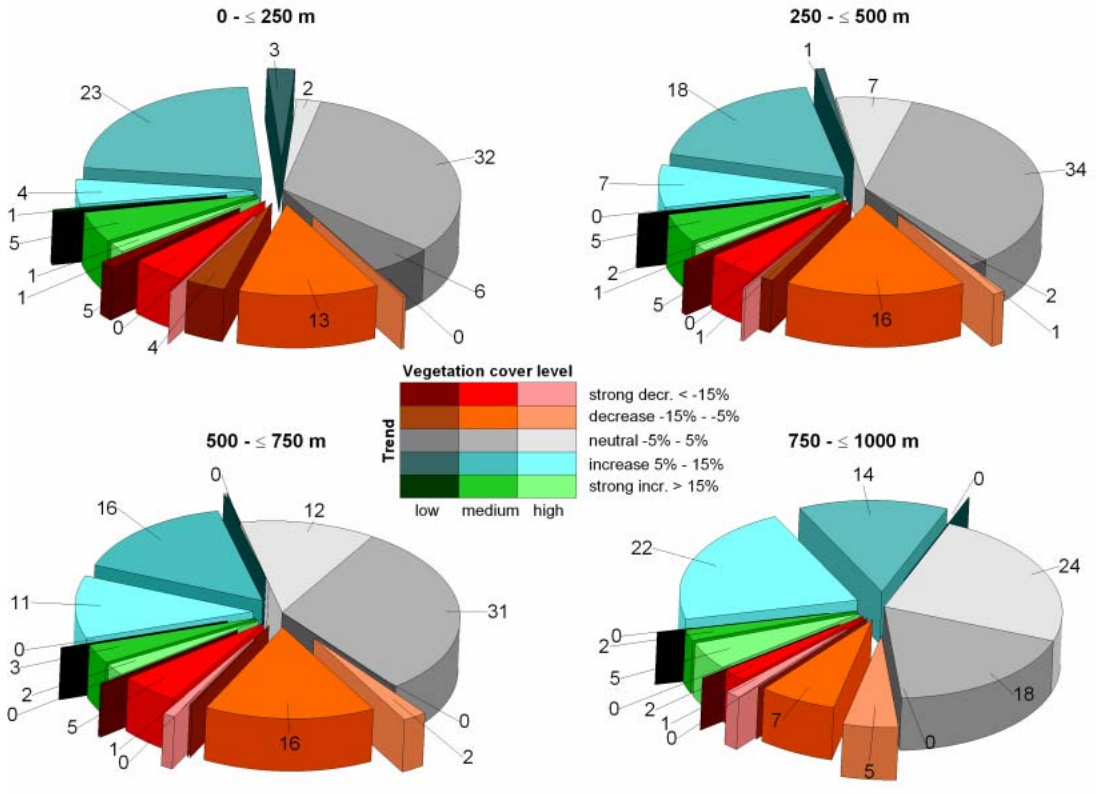

Fig. 10.12: Distribution of degradation index classes in major elevation zones and respective percentages, shown for the full observation area

Changes occurring between single classes are mostly balanced when values are considered for accumulated trend classes without considering the level cover of vegetation cover. To further illustrate this general behaviour, Fig. 10.13 shows trajectories for degradation index classes at two aggregation levels, the first relating to trend classes integrating the three vegetation cover levels, the second integrating all positive and negative trend classes ('total incr.'/'total decr.').

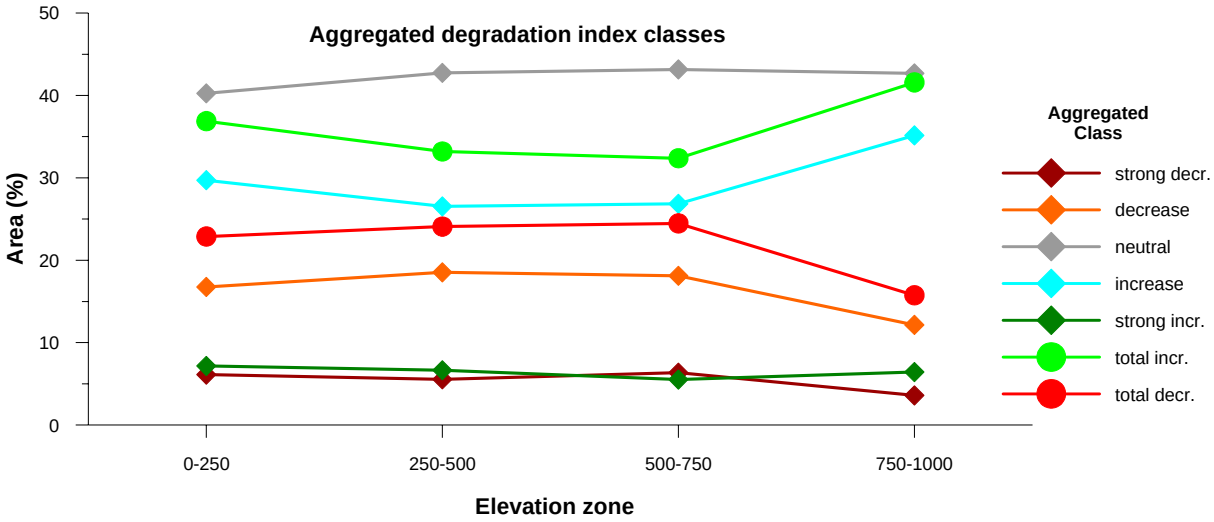

Fig. 10.13: Elevation trajectories showing relative abundance of degradation index aggregated to major classes and stratified for major elevation zones, shown for the full observation area

Fig. 10.13 further underlines that the proportions of the different classes are rather indifferent with increasing elevation from zone 1 to 3, while the strong gradient between zones 3 and 4 is highlighted. It must be concluded that despite the influence of elevation on the trend in vegetation cover, it is not the sole explaining factor if the full area is investigated.

This analysis was repeated for the three focus areas depicted in Fig. 10.5. The gain rate for the full observation period (1984-2000) averaged for the elevation zones is shown in Fig. 10.14 for all focus areas.

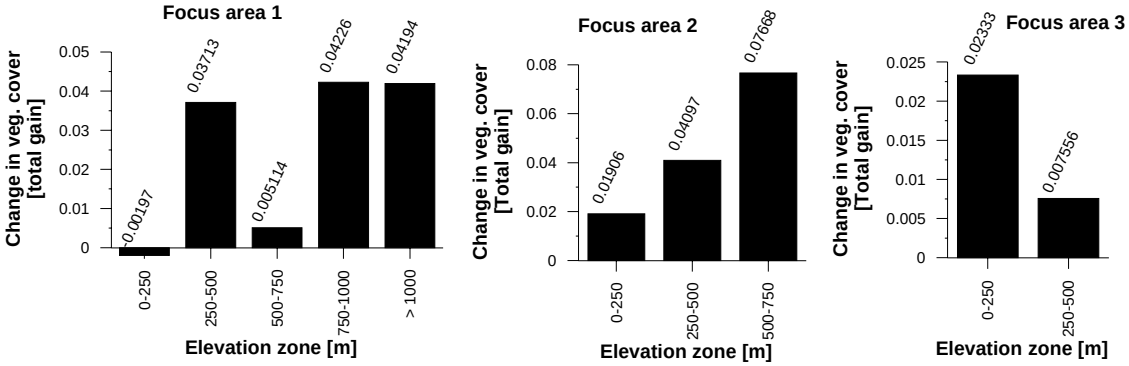

Fig. 10.14: Average total gain derived from linear trend analysis for the elevation zones in the focus areas (Fig. 10.6, Fig. 10.9, Fig. 10.10)

In addition, the distribution of the degradation index in the different elevation zones was assessed as shown in Fig. 10.15 for the aggregated classes. All tabular data can be found Tables C.3 to C.8 (Appendix).

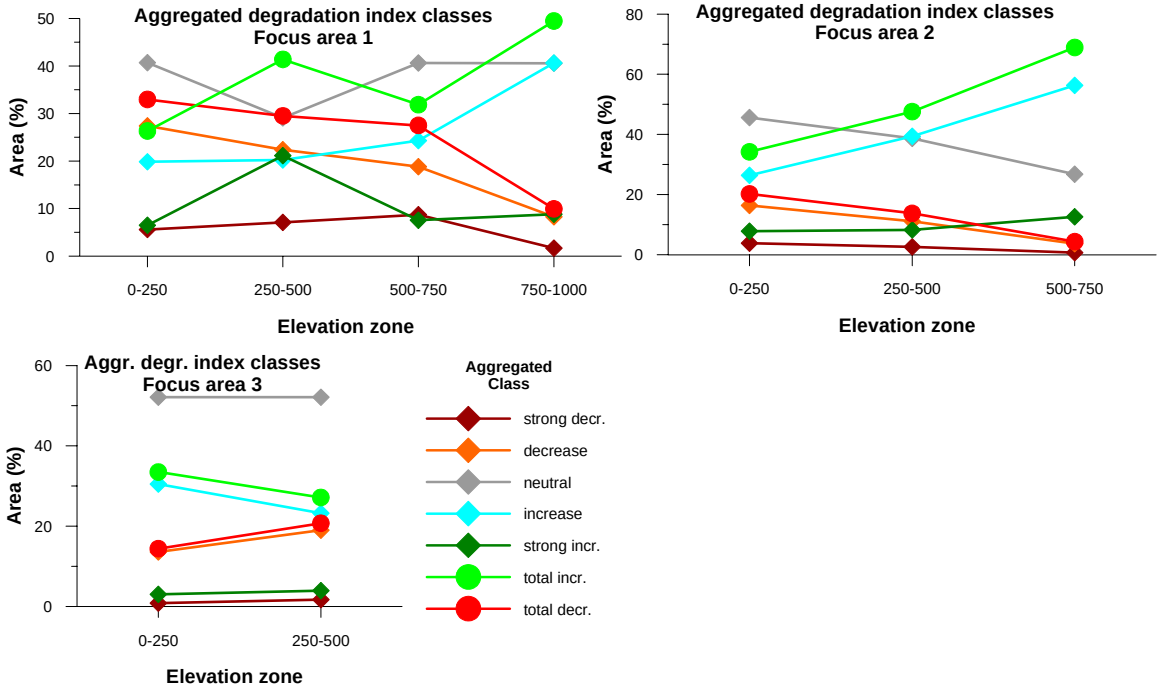

Fig. 10.15: Elevation trajectories showing relative abundance of degradation index aggregated to major classes and stratified for major elevation zones in the focus areas (Fig. 10.6, Fig. 10.9, Fig. 10.10)

The results complement the visible interpretation of the degradation index distribution in relation to the DEM (section 10.1.4) and show different patterns for the three sub-zones. While class assignments appear variable especially for the positive classes in **focus area 1**, the 'decrease' class shows a consistent reduction in relative size with increasing elevation. The 'strong decrease' class does not follow this behaviour, but remains on a generally low and undifferentiated level. Only the highest elevation zone shows a distinct distribution of pixels among the classes that corresponds to the anticipated decreasing impact of grazing with altitude, indicating a lower relative area affected by degradation. **Focus area 2** shows a consistent trend with more areas with positive vegetation cover development found at higher elevations. **Focus area 3** shows the opposite behaviour, but here the deep valleys cut into the surface form part of the lower elevation class, while the higher areas include a relatively low number of pixels in total.

Concluding, elevation appears to be one factor that contributes to the differentiation of the observation area with respect to the trends in vegetation cover. Apparently, this influence is neither uniform nor oriented in the same direction everywhere, as increasing elevation may be related to increasing or decreasing gain rates in different areas. This suggests that other important factors are present and underlines the spatial heterogeneity of process patterns even within the perimeter of Lagadas County.

Terrain attributes

Based on the DEM, a dataset characterising major landscape mesoforms was computed following the principle described in section 9.4.1 which distinguishes 10 classes. Four categories have been attributed to different sections within the systems of channels or deep valleys that are characteristic for many areas within the investigated area. To achieve larger integration zones, these were merged into a single category 'channels', and areas not used for grazing purposes, such as dense thermophilous forests, settlements and agricultural areas were excluded. The 7 zones of terrain attributes were converted to vector data and in a first step the average total gain was calculated (Fig. 10.16, Table C.9/Appendix). In contrast to the analyses related to elevation (Fig. 10.11, Fig. 10.14) classes with clearly negative gain rates occur. A separation into negative and clearly positive classes can be perceived, with the 'Hilltops' class in between. With reference to the hypothesised influence factors outlined in section 10.1.2 and 10.1.3, the relief categories are here employed as a proxy for the 'accessibility' of locations for shepherds and their flocks. From this point of view, the chart suggests a direct relation between temporal trends and accessibility of specific locations. At an average level, areas that are potentially easy to reach show a negative or no trend at all, such as the 'Low elevation divides', 'Gentle areas' and 'Convex upperslopes' classes. In contrast, areas which are presumed to require higher efforts to be reached show positive average trends. Concerning the 'Steep mid and low slopes' and 'Channels' classes this behaviour might be more determined by the relief gradient. In the case of the 'High elevation ridges and divides' it must rather be attributed to the fact that these locations are more remote from settlements due to their elevation. The 'Hilltops' category represents a very small total area and is associated with pixels in the DEM that represent the peaks of mountainous areas. For this reason it will not be further investigated in the further sections.

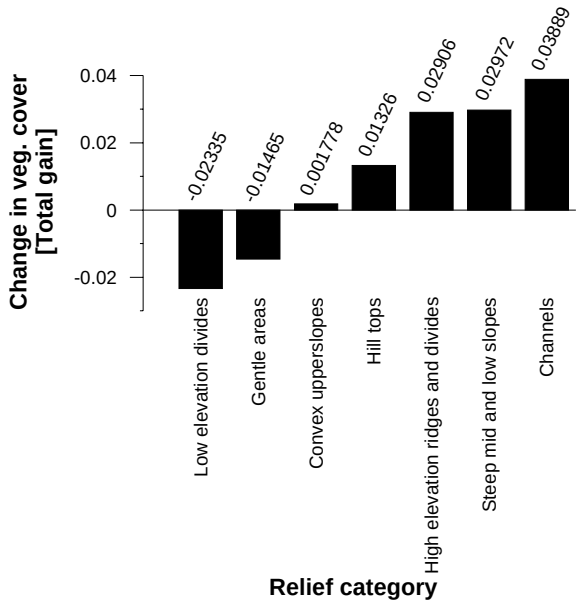

Fig. 10.16: Average total gain derived from linear trend analysis for seven relief categories for the full observation area

Analogous to the 'elevation' paragraph, the distribution of degradation index classes in the relief categories was analysed. Fig. 10.17 shows the aggregated trajectories, tabular data and differentiated charts are depicted in Table C.10/Appendix).

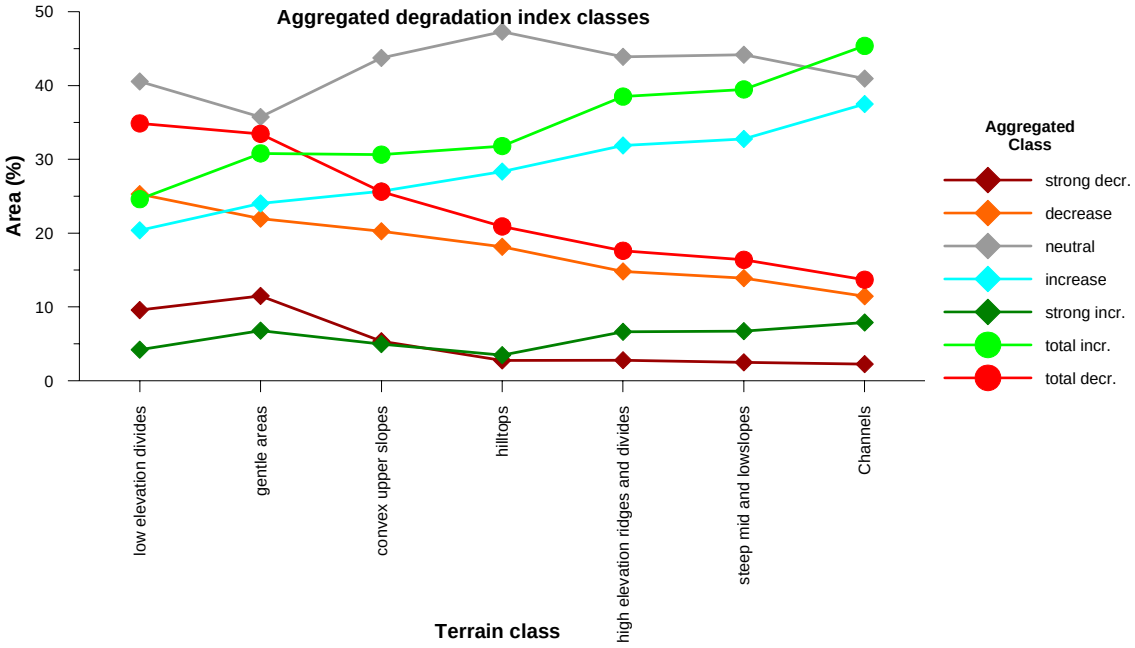

Fig. 10.17: Relief category trajectories showing relative abundance of degradation index aggregated to major classes and stratified relief categories, shown for the full observation area

The results depicted in Fig. 10.16 are supported by the trajectories of aggregated degradation index classes across the same relief categories (Fig. 10.17). The overall development is strongly driven by moderate change, although when the total gain is viewed the 'strong

increase/decrease' classes may more than proportionally affect the averaged result. The tendency illustrated in Fig. 10.16 is repeated in this representation for the different relief categories. Besides, the opposite evolvement of positive and negative index classes with an assumed aggravation of accessibility is noteworthy. In accordance with the analyses related to the total gain, this effect culminates in the 'channels' class.

Subsequently, the same analysis was carried out for focus areas 2 and 3. Focus area 1 is only located to a small part in the Mygdonia valley watershed, for which the relief category data set was available. It was hence not examined here. In both cases, the hilltops class was not considered, as it only holds very small shares of the respective area.

In both areas, sites with reduced accessibility show the highest positive change rates. In **focus area 2**, the 'high elevations ridges and divides' and the 'convex upperslopes' class do also show clearly positive values. In accordance with previous sections and the landscape structure depicted in Fig. 10.9 this might indicate a stronger influence of the 'elevation' factor here, which is supported by Fig. 10.18 and Fig. 10.14. On the other hand, in **focus area 3** the 'accessibility' factor explains to a large degree the reticulate pattern visible in Fig. 10.10. The hypothesis proposed before is underlined here, and it is interesting to note that this region is among the most heavily grazed in the County. It can hence be considered to be a good example of the selective grazing prevailing in Lagadas County.

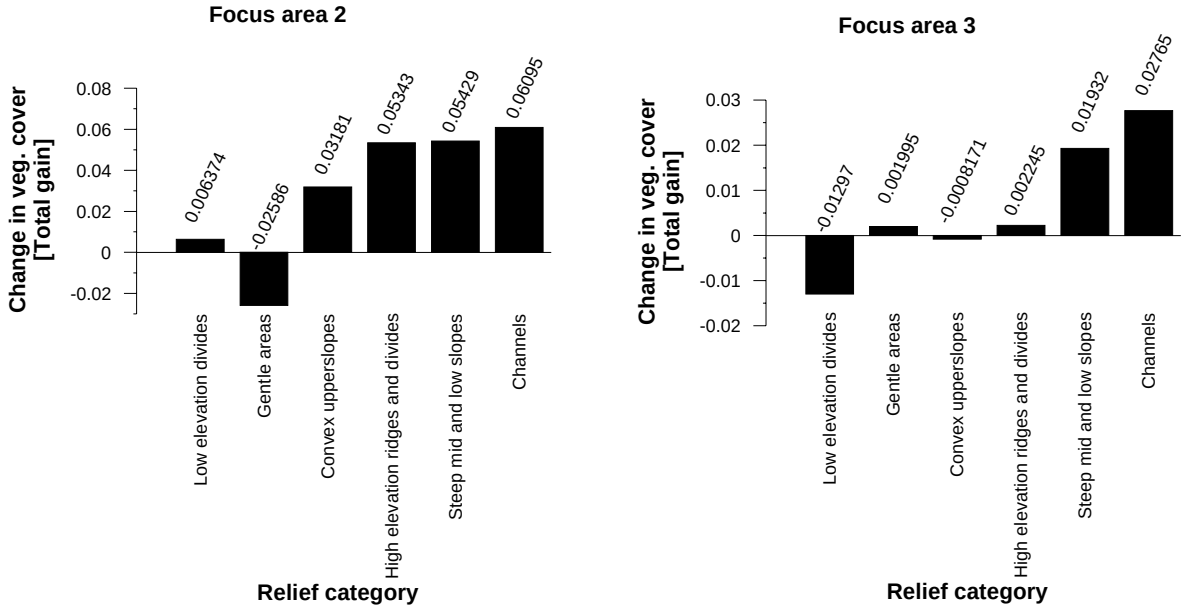

Fig. 10.18: Average total gain from linear trend analysis for the relief categories in the focus areas covered by the relief data set

The tabular data for the previous analyses related to the focus areas are provided in Tables C.11-14 (Appendix).

Section 10.1.5 underlines the influence of topography on vegetation cover development, which is considered to result from its determinant effect on livestock and shepherd behaviour. Depending on the respective location, 'easiness of access' or 'elevation' were identified as

most important factors, although the latter is often interpreted as an indirect effect of accessibility. Especially **focus area 3** appears to perfectly illustrate the effects of 'selective grazing' driven by shepherds behaviour as determined by physical factors. Beside pastoral quality, convenience of access is a major factor for shepherds who do not roam with their flock over days but follow this as a daytime profession. It is hence safe to assume that the open plains and ridges between the deep valleys are most attractive, while steep slopes or the bottoms of narrow valleys are not favoured. As a consequence, the named categories are grazed at increased or decreased intensities, while the other categories experience 'intermediate' pressure and are consequently characterised by neutral behaviour or total gains close to zero (Fig. 10.18).

10.1.6 Discussion of the multi-temporal interpretation approach

With regard to the data processing and interpretation scheme, some aspects beyond those discussed in the data processing chapters (chapters 5, 6, 7) require specific attention as they affect the derived results:

- Concerning the implications arising from the population of the satellite image time series and the derivation of green vegetation cover using SMA, it is referred to the discussion section of the Ayora case study (section 9.6), as the principal points raised there apply here as well. For the trend analysis, images were chosen to represent green vegetation cover as a whole, while the cost surface analysis was based on a late image acquisition date aiming at woody vegetation cover as the target indicator.
- As the analyses concentrated on vegetation cover as the target indicator, the exclusion of agricultural areas was an important step. Effective stocking rates for the communities were calculated on grazed areas, excluding agricultural and settlement areas. As the land cover information was based on the habitat GIS and the multi-temporal land cover classification of the 2000 Landsat-5 TM and -7 ETM+ data, their application to older dates contains some uncertainty. If changes in agricultural areas took place they were mostly effectuating an increase in area. This would cause an overestimation of stocking rates for older dates.
- In the Lagadas area, a semi-intensified, sedentary grazing system is present. Both grazing on stubbles after fields are harvested as well as the provision of additional feedstuffs to the animals are factors that can not be quantified here. They were discussed in the context of interpreting results, and although they do not affect the calculated trends they are considered an important reason for the observed patterns in relation to the high stocking rates.
- The trajectory analysis was based on decadal census data from 1961 to 2000, with 1981 missing. The values were interpolated from the 1971 and 1991 values in order to guarantee a sufficient time span covered. Beside this, these data were compiled from interviews with punctual surveys. Depending on the price and subsidy policy at the respective dates, it can not be ruled out that exaggerated or understated figures may have been provided, which would affect the derived variables. In order to reduce the influence of phenological variations, the vegetation cover estimates for the fix points were derived using the trend function. The accuracy of this approach depends on the RMSE

of the trend function, but it is believed that major deviations only appear for isolated pixels and are negligible given the averaging on community level.

- The formulation of the degradation index involves the average vegetation cover of the full period viewed. Although this is the only feasible option of characterising the general level on which trends manifest, it does involve some uncertainty. The same average value may result from a very similar range of cover estimates for the different years or from a large range of estimates. However, for 'true' trends this effect is considered by the gain of the trend function and errors are only expected for situations where cover estimates are fluctuating, such as for agricultural areas that are not excluded by the mask.
- The investigation of temporal trends in relation to topography attributes involves intersecting the two information layers. While it is straightforward for the elevation zones, the terrain feature classes include both compact areas as well as highly linear features. Where the latter do not exceed a single pixel, such as for narrow channels, the accuracy of the analysis depends on the precision of the geometric co-location of both data sets. As the same DEM was used to derive the terrain features and to support the different satellite image processing steps this is considered only a minor source of error that additionally depends on the number of pixels averaged for the different feature classes.

10.2 Spatial trends of grazing impact on rangelands

In the previous sections, temporal trends in rangelands were identified based on the development of green vegetation cover and different measures to characterise these processes were discussed. Grazing as a major factor of the rural economy is considered to strongly affect the state of rangelands. It was shown that a direct relation between stocking rates and vegetation cover is not generally present (section 10.1.2). As spatio-temporal trends manifest in highly differentiated patterns, it was concluded that investigating grazing related processes necessitates consideration of processes and driving factors on scales larger than the community scale. An opportunity is offered by approaches to piospheric analysis presented in section 3.4.3.

10.2.1 The Mediterranean perspective: modelling livestock distribution in Lagadas

Piospheric analyses have been reported from Sub-Sahara Africa in the context of wildlife management, from Australian cattle grazed rangelands (e.g. Andrews & Lange, 1988; Pickup & Chewings, 1994; Pickup et al., 1998; Thrash & Derry, 1999; Heshmatti et al., 2002) or from the Steppes of Inner Mongolia (Fernandez-Gimenez & Allen-Diaz, 2001). Also, the impacts of African large herbivores, prairie dog, kangaroos and termites have been studied based on the piosphere concept (e.g. Coppock et al., 1983; Lange & Graham, 1983; Andrew, 1988; Thrash, 1997). Remote sensing based implementations were presented in section 3.4.3.

In the described studies, watering holes are commonly the major point of livestock concentration and animals roam freely around these within the extent of the piosphere. Grazing-induced effects are usually assessed making use of circular buffers around these points, which is a

convenient approach in large, homogeneous areas. In the Lagadas area, however, three factors deny a direct application of the present concept of piosphere analysis:

- The landscape structure is very heterogeneous and areas unsuitable for grazing are intermixed with grazing areas of highly variable pastoral value.
- Water is not the sole limiting factor, as numerous watering points exist within reach of the flocks and these are being led back to their sheds each night.
- The different landscape structure results in grazing impacts on much finer scales compared to large contiguous grazing areas. Most importantly, grazing in Lagadas County follows a sedentary system. Yiakoulaki & Papanastasis (2003) report that shepherds lead their flocks away from the sheds during the day and return in late afternoon or in the evening. Depending on the season, animals may even return to their sheds during the hot hours at midday.

Hence, the spatial distribution of livestock is determined by a combination of environmental conditions and shepherd's decisions. If these specific properties can be spatially parameterised, grazing impact can be assessed using piospheric analysis adapted to specific local conditions.

This study investigates the potential and limitations of assessing the impact of grazing based on a prediction of the spatial distribution of grazing livestock as an extension of traditional analysis of circular buffers. This is demonstrated for the communities of Kryoneri, Ossa, Eksalofos, Kolhiko and Analipsi. Based on livestock concentration points, around which grazing activities evolve, four major factors were identified in collaboration with rangeland and grazing experts from the University of Thessaloniki[1] and Greek national authorities[2, 3] as affecting the selection of grazed areas:

- Distance
- Topography
- Attractiveness (nutrition value)
- Accessibility (openness)

As a consequence of the facts discussed above, circular buffers are expected to describe the distribution of grazing animals only to a certain degree. In fact, this would imply random distribution following animal's choice of location exclusively. By considering additional factors it is expected to more accurately predict the spatial behaviour of flocks based on shepherd decisions and the preferences of the animals (e.g. Legg et al., 1998). The translation of these factors into a spatial context was necessary to define an optimised zonal stratification for a piospheric analysis. The concept of cost distance modelling was employed to pursue this goal (Eastman, 1989; Douglas, 1994; Tomlin, 2000).

---

[1] Aristotle University of Thessaloniki, Faculty of Forestry and Natural Environment, Laboratory of Range Ecology (AUTh-LARE)

[2] National Agricultural Research Foundation, Forest Research Institute, Laboratory of Ecology (NAGREF-FRI)

[3] Region of Central Macedonia, Directorate of Forests

10.2.2 Livestock concentration points

The identification of the points from which animal flocks depart or where they gather is a crucial component of this approach, as the buffers or interpretation zones are calculated around these. In the Lagadas site, there are principally three categories of such points: sheds, gathering points, and watering points (Ghossub, 2003). The first two categories may be conveniently identified using aerial photographs or appropriate satellite imagery. Watering points may related to ponds, lakes, and watering devices. Especially for the first two categories it is difficult to decide whether these are used by livestock. Hence, 90 'points of livestock concentration' were mapped from Quickbird VHR data by locating sheds and gathering points Fig. 10.19 shows two examples for sheds identified from the satellite image and the corresponding shed.

Fig. 10.19: Subsets of the Quickbird image (left) with corresponding sheds (right)

Precise location of these sheds is of utmost importance, since they provide the starting and end points of daily pastoral activities and the place where additional feeding of animals takes place. As there are numerous options to provide water for the animals, this was not considered to be a limiting factor. Furthermore, Le Houérou (1998) reports that sheep and goats may sustain for long periods and walk long distances without water depending on the breed. Hence, watering points were disregarded in the further analysis which rather focused on sheds as the primary PLC.

10.2.3 Cost surface calculation

The concept of cost surface modelling is used in contexts as diverse as archaeological landscape reconstruction (e.g. Lock & Stancic, 1995), civil engineering (e.g. Feldman et al., 1995; Cowen et al., 2000; Yu et al., 2003), social sciences (e.g. Rees, 2004; Bertam, 2005) or in

landscape ecology to assess the connectivity of habitats for migration of animal species (e.g. Ray et al., 2003; Adriaensen et al., 2003; Sutcliffe et al., 2003; Osborn & Parker, 2003). In this study, the concept is adapted to the assumption that the spatial distribution of livestock animals and hence grazing activity can be modelled in dependence of the factors identified in section 10.2.1. Subsequently, the derived distribution patterns may be employed to assess the impact of grazing on vegetation cover.

The approach is based on regular grids, each layer accounting for a specific factor. For each of the factors, a functional hypothesis is formulated to characterise how this specific factor affects decisions taken by shepherds and/or grazing preferences by goats and sheep. Then, this relation is translated into a spatial information layer based on the available geodata information (compare Appendix A.2).

Each cell value in a grid represents the effort required to travel through this cell according to the respective factor, i.e. the 'cost'. The resulting layer is termed 'friction surface'. The different friction surfaces required to incorporate all driving factors need to be scaled to comparable ranges for the later integration with other surfaces. It is important that frictions of different layers exclusively relate to the considered factor and are as independent from each other as possible. High values correspond to high costs, suggesting that in the present case shepherds will avoid passing through this cell. Accordingly, each pixel in the spatial representation of the target indicator, i.e. green vegetation cover derived from SMA, is stratified according to its minimal cost required to reach the nearest PLC. This 'cost distance' is calculated to represent the accumulated costs for the shortest path to the closest PLC for each cell. Movements can be carried out in 8 directions, where the friction values are weighted 1.41 times for diagonal movements. The calculation of this accumulated cost distance surface from the friction surface(s) is commonly implemented using a 'pushbroom algorithm', that accumulates costs away from starting features throughout the image "[…] much like a pushbroom would be used to systematically clean a room. Effects then ripple through the image, much like water being pushed over a wet floor (Eastman, 1989)". Details on cost surface calculation and the related algorithms are given in Eastman (1989), Douglas (1994) and Tomlin (2000).

Using the spatial representation of accumulated costs, equal cost intervals may be derived by categorisation. Categories can then be vectorised to yield the adapted buffers for the subsequent analysis.

Cost factors – distance

From the identified factors (compare section 10.2.1), distance is the most straightforward one. It can be calculated using the PLC as starting features and using circular buffers around these points. It resembles the buffers traditionally used for piospheric analyses, but here these are an input layer to a more complex cost surface preparation. More specifically, it is important to note that the 'distance' factor does not simply represent the distance away from PLC. In fact, the Euclidian distance is intrinsically considered in the process of cost accumulation. Rather, 'distance' is introduced here as an additional scaling factor. It accounts for the fact that for the shepherd, the same accumulated cost to move through a grid cell involves different efforts depending on the distance to the home shed. For example, crossing an area with a high cost is

less probable if the flock has already roamed a longer distance and is already far away from the shed, compared to the same cost in the direct vicinity of the shed. This is accounted for by the distance factor. It was computed in the form of circular buffers around the PLC and using an average maximum travel distance away from the shed of 2000 m (Yiakoulaki et al., 2002). Hence, a scaling factor was applied to the grid resulting from the buffer analysis that rescales the distance values between 0 and 100 for a 2000 m distance (10.1).

$$F(dist) = 1 + \frac{99 \cdot dist}{2000} \qquad (10.1)$$

with $F(dist)$ = friction for distance factor
$dist$ = distance from nearest PLC[m]

Larger distances were not excluded, but these were assigned values exceeding 100, although in general frictions are scaled between 1 and 100. This expresses the assumption that shepherds may indeed move beyond this distance but only in exceptional cases, for instance where reaching the 2000 m distance was not costly, or the area beyond is particularly attractive. The resulting friction surface is depicted in Fig. 10.20.

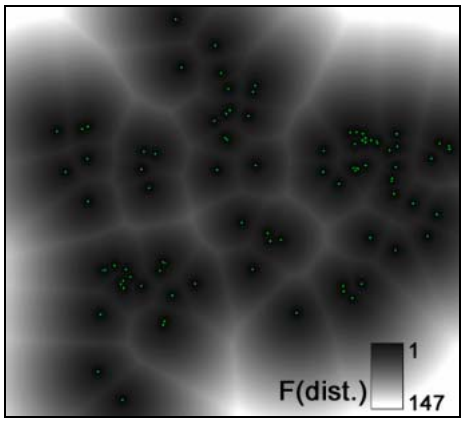

Fig. 10.20: Distance friction surface based on points of livestock concentration (PLC are indicated as green dots)

Cost factors – topography

The rangelands of Lagadas County are clearly structured according to elevation zones. In addition, there is a reticulate pattern of valleys and channels and steep slopes. The relevance of these different topography units was already demonstrated in section 10.1.5. Although goats and sheep may move on steep slopes at ease, shepherds tend to avoid such areas. Two options were evaluated to incorporate this factor.

The first is based on calculation of slope values in percent, which could be directly incorporated. In this calculation, a 90° slope corresponds to 100 %,

In a second attempt, a more differentiated approach was pursued making use of the terrain mesoform data set which was also used in section 10.1.5. By assigning the different classes

friction values between 1 and 100 it was hypothesised that, although slope contributes considerably to the definition of these classes, it is not the only factor that determines the topography-related cost to move through a cell. For instance, the bottom of a narrow valley or channel may be almost flat, resulting in low friction values if topography is only approximated by the slope. On the other hand, these areas are narrow, frequently difficult to follow, and must hence be considered less favourable than for example elevated plains or ridges. Following these considerations, friction values were assigned to different topography classes according to Table 10.2. In the terrain features data set, different categories of channels were identified according to position and transport capacity. As these represent a contiguous network they were summarised to a general 'channels' category.

Table 10.2: Friction estimates assigned to topography classes

Topography class	Friction value
Gentle areas	10
Low elevation divides	20
High elevation ridges and divides	20
Hill tops	30
Convex upperslopes	30
Channels	50
Steep mid & low slopes	70

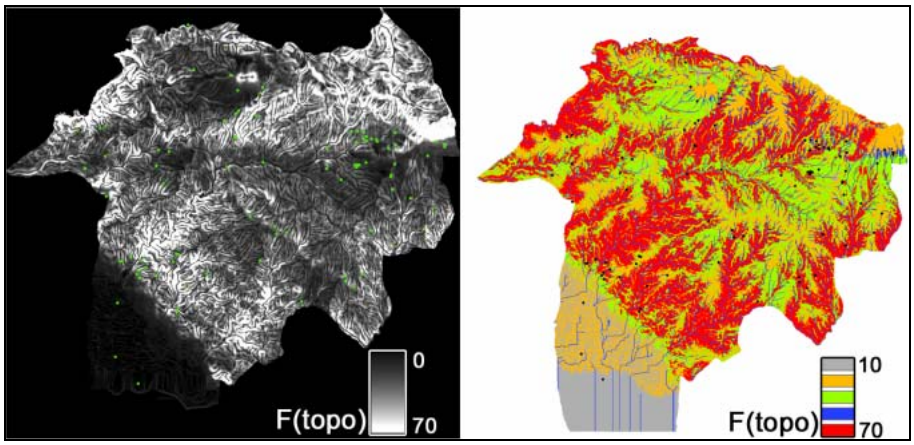

Fig. 10.21: Topography friction surface (a: based on slope; b: based on topography classes; PLC indicated as green/black dots)

Fig. 10.21 reflects the difference between both approaches, with image b being characterised by categories rather than continuous values. On the other hand, specific conditions, such as channels and narrow valleys, are clearly different when compared to the result when slope is used exclusively. In the sensitivity analyses illustrated in section 10.2.5, both approaches will be evaluated. The bottom of Mygdonia valley included in this test area is also discernible in both graphs (as well as in the following friction surfaces). Especially in Fig. 10.21 b these flat areas are exposed by generally low friction values, while the channels feeding into Lake

Koronia receive high frictions. The majority of this area is used for agricultural purposes and will be excluded from the subsequent piospheric analysis.

Cost factors – attractiveness

Several aspects need to be appraised when trying to characterise the attractiveness of an area related to nutrition value. Most obviously, patches with high amounts of green vegetation are more favourable than others, such that biomass can be assumed to be a good indicator for locations favourable for grazing. It was shown that a direct relation can be established between green vegetation cover and total above ground biomass (section 3.4.1). Thus, green vegetation cover estimated from the late spring scene available for 2000 (acquired June, 6th), including photosynthetically active herbaceous vegetation, was employed as a surrogate for total biomass. The original fractions derived from SMA were scaled between 1 and 100 according to (10.2):

$$F(attract) = 1 + 99 \cdot e^{-(10 \cdot GVC)} \qquad (10.2)$$

with $F(attract)$ = Friction for attractiveness factor

GVC = Green vegetation cover fraction (derived from SMA)

The exponential function applied mainly reflects the low grazing value of sparse patches. It also results in a strong decrease of friction values with increasing cover, resulting in favourable estimations already beginning with vegetation cover estimates of 30 %. Above 50 % cover friction values are almost at the base level.

An alternative approach to characterising the pastoral value was pursued by using the information supplied in the habitat GIS. Here, vector information on major plant communities as well as densities are provided based on the interpretation of aerial photographs and field campaigns following the Natura 2000 mapping key (Konstantinidis & Tsiourlis, 2003). This information could be transferred into friction values following some general considerations. For instance, grasslands were traditionally assigned highest nutrition values as they harbour many palatable and nutritious species and at the same time yield high values of herbage (Papachristou & Platis 1998). Only recently research findings have approved the higher value of rangeland that comprises a certain amount of shrubs, thereby increasing the amount of available edges between shrub and grassland (Papachristou & Platis 1998). Woody plants can only be grazed until they reach a certain height, while in the case of forests the understorey might be suitable. Given a variety of plants to feed on, sheep act as feeders while goats prefer browsing of woody plants (e.g. Arnold, 1987). Konstantinidis & Tsiourlis (2003) report that even open forests may be grazed in the Lagadas area, although this is not frequently observed. In front of this background, the general nutrition value of an area may be characterised considering its dominant plant community. Consequently, the information supplied in the habitat GIS was rasterised and reclassified (compare Table C.15/Appendix).

This approach is further refined by employing the information on green vegetation cover as a proxy for biomass and combining the two information sources to yield a more differentiated spatial representation of the attractiveness. To do so, the habitat information was transferred

to a raster grid and each category was assigned a code. The information on green vegetation cover was classified into three classes, low, medium, high. Both data sets were combined and each pixel was assigned a unique identifier of plant community-related nutrition value and biomass. These codes were related to friction values in the next step (Table C.16/Appendix).

Sparse shrublands with their valuable mixture of shrubs and herbaceous vegetation were given lowest friction values, differentiated according to the respective level of present biomass. Similar friction ranges were assigned to grasslands, while values are high for medium dense and dense shrublands and especially for forest classes. Within these, only open forests were considered suitable for grazing, albeit with higher frictions compared to shrublands. All areas where grazing is highly improbable were assigned the maximum friction value of 100. A special situation is encountered on abandoned fields. After these areas cease to be utilised, they are usually subject to an encroachment of shrubs to finally become dense shrublands. For this reason, abandoned fields at cover class 2 were assigned lowest friction values, as these are expected to resemble sparse shrublands (Fig. 10.22). The missing areas relate to clouds in the satellite image.

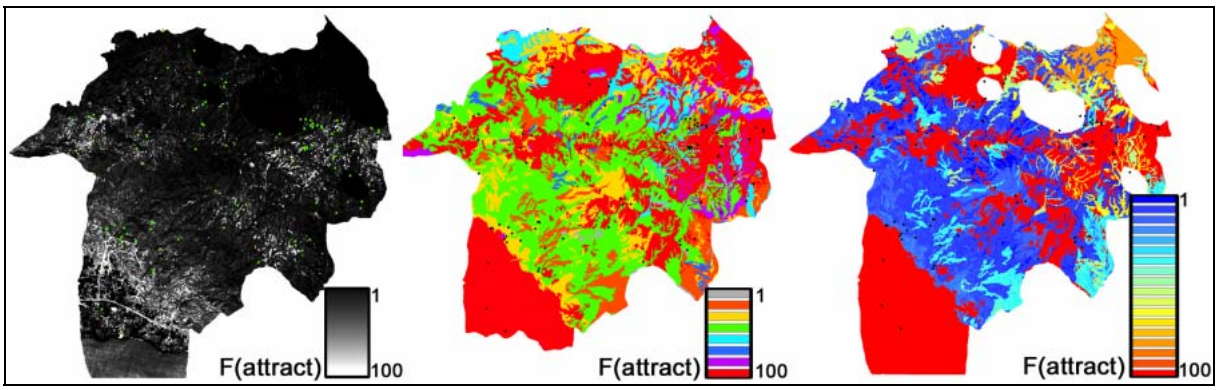

Fig. 10.22: Attractiveness friction surface. a: based on biomass derived from satellite imagery; b: based on habitat GIS classes; c: based on a combination of a and b (PLC depicted as green/black dots)

Cost factors – accessibility

Different boundary conditions might affect the accessibility of patches, such as the network of roads and tracks. In the present case, accessibility is used in the sense of 'openness' and relates to the structural land surface type. This information was derived from the vector information on Natura 2000 habitat types. In contrast to 'attractiveness', this factor relates exclusively to the density of the land cover in the case of vegetation, as animals are deterred by dense vegetation (Legg et al., 1998). Land cover classes such as villages or agricultural areas are assigned high friction values. Although these will be excluded from the buffer analysis, this is important to make sure that these areas are considered as barriers in the integrated cost surface. As such, accumulated cost tracks will favour surrounding these patches over crossing them, which reflects real conditions more realistically. Table C.17 (Appendix) depicts the classification applied, Fig. 10.23 shows the resulting friction surface. Where applicable,

Natura 2000 codes and descriptions are provided as given by Dafis et al. (1999) and Konstantinidis & Tsiourlis (2003).

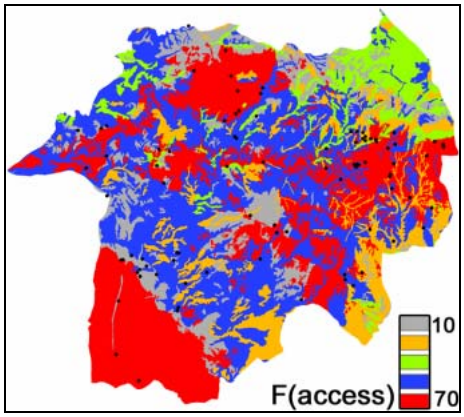

Fig. 10.23: Accessibility friction surface based on information from the habitat GIS

Integration of friction surfaces

Once the individual friction surfaces are defined, these need to be integrated. As all individual data layers were scaled to the same ranges, this is a straightforward procedure and can be accomplished by a pixel-wise calculation of the average value. This procedure implicitly assumes all factors to be of equal influence. Although objective, this approach might fail to reflect that there may indeed be factors that are more relevant to the shepherd's decisions than others. To infer the relative weights would require detailed knowledge on the tracks of flocks from which the relative weights could then be deduced on a statistical basis. In the absence of such information, an approximation can be based on questionnaires of grazing experts. Accordingly, the weights inferred by Kuemmerle (2003) at a scale from 1 to 10 were employed as shown in table Table 10.3, Fig. 10.24 shows the resulting integrated friction surfaces.

Table 10.3: Absolute and relative average expert-based weighting of the individual friction surfaces.

Factor	Absolute weight	Relative weight
Distance	9.6	0.3
Topography	8	0.25
Attractiveness	6.8	0.22
Accessibility	7.2	0.23

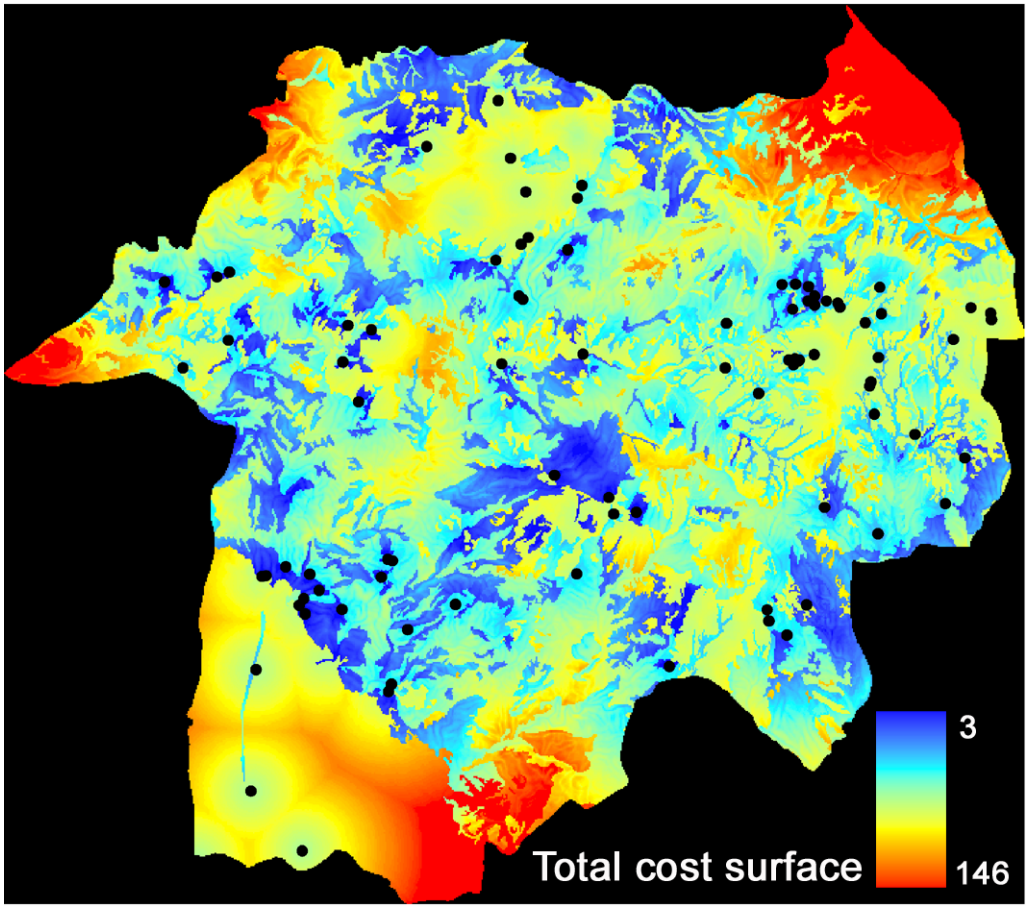

Fig. 10.24: Integrated friction surface based on ‘distance’, ‘topography’, ‘attractiveness’ and ‘accessibility’ (expert weighted, PLC indicated as black dots)

In order to estimate the sensitivity of the model to different types of input layers, a variety of integrated friction surfaces was calculated. All possible combinations to characterise attractiveness and topography were pursued. Both equal weighted and expert weighted friction surfaces were calculated, yielding a total of 12 data layers.

10.2.4 Accumulated cost distances and buffer calculation

Based on the integrated friction surfaces, accumulated costs were computed, which represent the total cost to reach the nearest PLC at the lowest cost. This was performed following the procedure described in section 10.2.3 (Fig. 10.25).

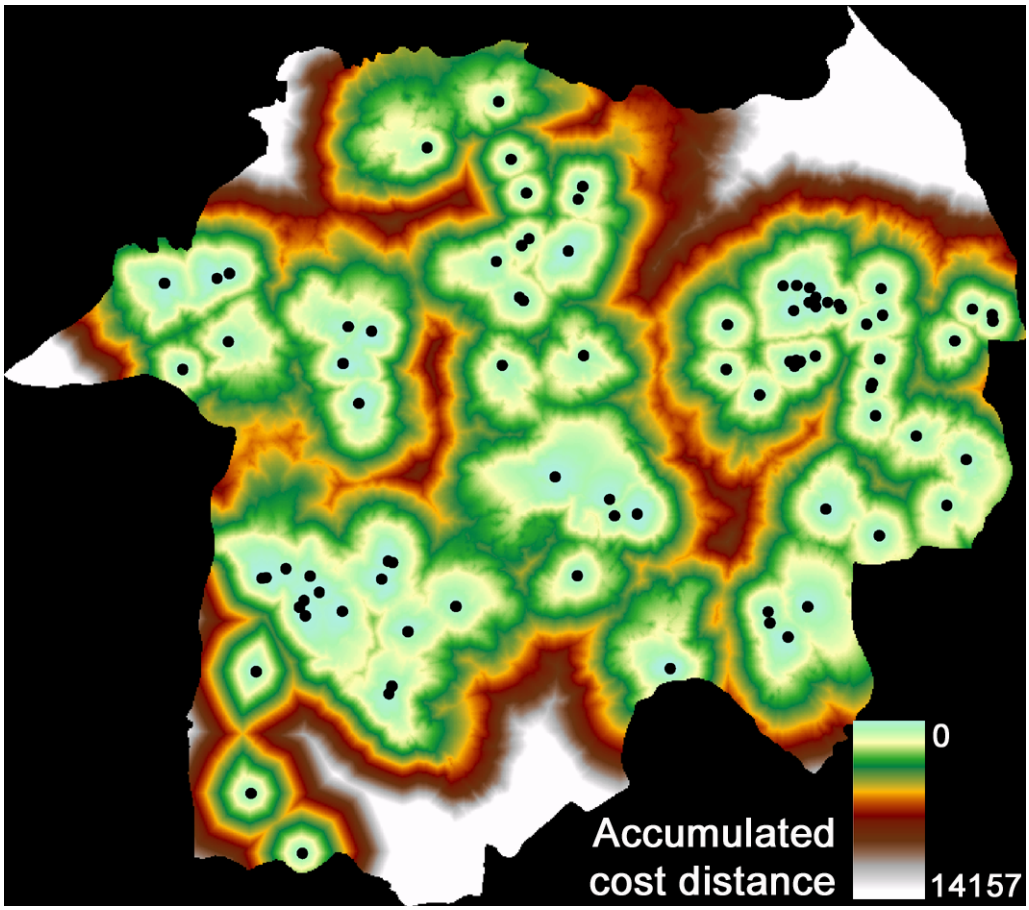

Fig. 10.25: Accumulated cost distance surface based on integrated friction surface (Fig. 10.24) and calculated using a pushbroom algorithm starting from points of livestock concentration (PLC depicted as black dots)

This data set can be considered being the spatial representation of the movement of shepherds and their flocks according to the theoretical considerations outlined in the previous sections. It forms the basis for the categorisation into zones of grazing impact (compare section 10.2.1). In doing so, the selection of the interval is the crucial issue. The resulting zones need to include a sufficient number of samples, while being narrow enough to enable the differentiation of specific conditions and detection of subtle changes. In the present study, the threshold was set to 100 following iterative testing, such that a single buffer zone represents a total cost of 100 to travel through. This cost could either result from a single cell with a total friction of 100, from 100 cells with a friction of 1, or any other possible combination. The result of this operation are adapted buffer zones around the PLC, which slightly differ in shape for the different combinations of friction surfaces. Fig. 10.26 shows a small subset of these buffers for the example shown in Fig. 10.25 in comparison to circular buffers with a radius of 100 m. It may be inferred from the orthophotos how buffers orient along the ridge in the first case, while they extend towards the open shrublands and away from agricultural area in the second. As the case of Lagadas is based on numerous PLC, multiple buffer zones are allowed. The buffers are allowed to intersect and all statistics are calculated per zone as a whole. In order to reduce the influence of very small buffer zones (or polygons) at larger cost distances, the categorised images were majority filtered using a 5*5 kernel prior to conversion from raster to vector data.

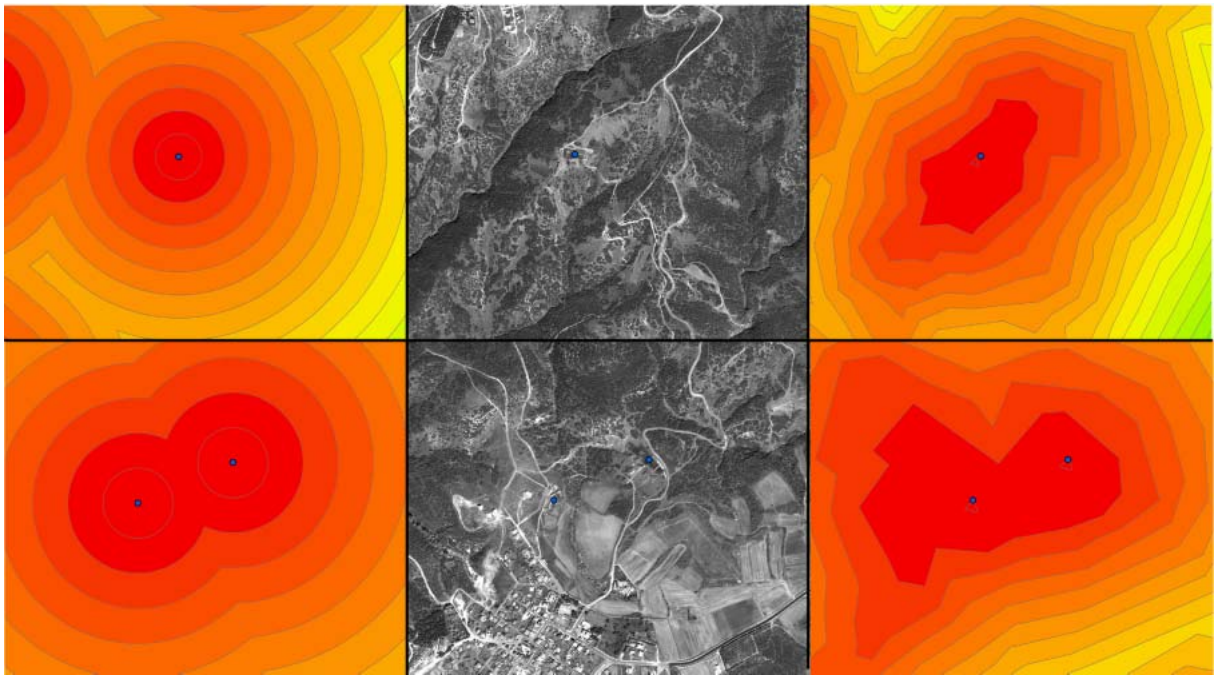

Fig. 10.26: Subset illustrating buffer zones around two PLC. Left: circular buffer zones, right: adapted buffer zones derived using the cost surface approach, centre: corresponding Quickbird subset (PLC in blue, buffers coded from red to green with increasing cost distance)

10.2.5 Results

The buffer zones derived from integrating the parameterised information on animal distribution drivers were intersected with the SMA-derived information on green vegetation cover from the Landsat-5 TM image acquired August, 18th, 2000. Given this late acquisition date, it was assumed that herbaceous vegetation was already senescent and only woody vegetation components were observed as photosynthetically active. Agricultural areas were masked using the multi-temporal land cover classification derived from a multi-temporal Landsat-TM/ETM+ data set available for 2000. Average cover, standard deviation and the number of pixels contained within the zone were extracted for each buffer zone.

Sensitivity to cost surface parameterisation

In a first step, the influence of different parameterisation approaches for the friction surfaces was assessed by deriving gradients of woody vegetation cover depending on the cost distance to the nearest PLC. While the factors ‘distance’ and ‘accessibility’ were kept constant, ‘attractiveness’ and ‘topography’ were varied employing the options described before.

The resulting curves for average woody cover and the corresponding standard deviation are depicted in Fig. 10.27, while Table 10.4 indicates the respective input data.

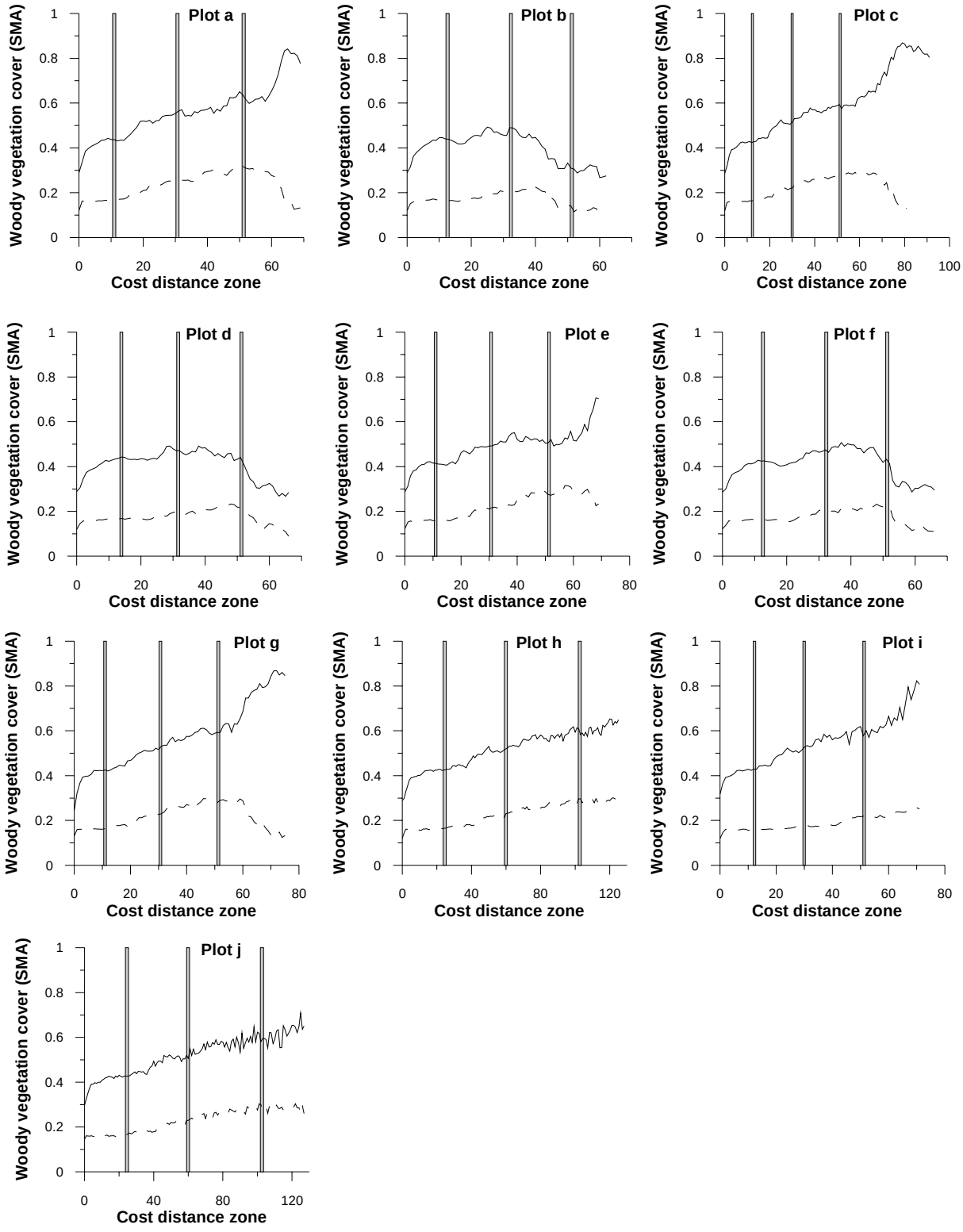

Fig. 10.27: Gradients of woody vegetation cover with increasing cost distance away from PLC (solid line: woody vegetation cover; dashed line: standard deviation). The three bars indicate the minimum, average and maximum costs that may accumulate for a Euclidean distance of 2000 m depending on the respective accumulated costs

Table 10.4: Friction surfaces used to calculate accumulated cost distances

Gradient ID	Attractiveness	Topography	Weighting	Buffer size	Filter
a	Biomass	Slope	Expert	100	
b	Biomass	Regionalisation	Expert	100	
c	Habitat	Slope	Expert	100	
d	Habitat	Regionalisation	Expert	100	
e	Habitat/biomass	Slope	Expert	100	
f	Habitat/biomass	Regionalisation	Expert	100	
g	Habitat	Slope	Equal	100	
h	Habitat	Slope	Expert	50	
i	Habitat	Slope	Expert	100	Majority 5*5
j	Habitat	Slope	Expert	50	Majority 5*5

The concept of cost distance modelling implies that the cost units to which the x-axis is scaled can be directly compared neither to Euclidian distance nor among each other. Depending on the value range of the input friction layers, accumulated costs greatly vary for different data sets. Secondly, no direct relation exists that allows converting cost to Euclidean distance, as on the same Euclidean distance accumulated costs are different depending on the respective total friction values. An indication can be given by calculating the range of accumulated costs that are attained for a given set of input parameters at a certain distance. In Fig. 10.27, the bars indicate the minimum, average and maximum costs that may accumulate for a Euclidean distance of 2000 m. It is important to note that these breakpoints were calculated based on friction values without considering their abundance. For instance, in the case of the 'topography' factor, friction values between 1 and 70 occur, but the peak of the histogram for this factor is reached at 13. It follows that the bars shown here are a theoretical indication of the range of costs, while values may vary depending in the concrete case.

Two general categories of gradients can be distinguished. The first shows increasing woody vegetation cover with increasing cost distance zones for the whole range covered by the plot (a, c, e, g, h, i, j). In the plots of the second category, a corresponding behaviour is observed until a breakpoint is reached, following which cover decreases with further increasing costs (b, d, f). The reason can be deduced from Table 10.4 and Fig. 10.21. The key separator between both categories is the parameterisation of the 'topography' factor. The steadily increasing curve is associated with the 'slope-based' friction surface, while the other gradients correspond to the 'regionalisation-based' alternative. Fig. 10.21 shows that the latter is missing part of the test area in the Northeast, as this data set is confined to the watershed of the Mygdonia valley. The missing area belongs to the open *Quercus* forests that are suitable for grazing according to Konstantinidis & Tsiourlis (2003). This area represents the highest vegetation fractions in the five communities analysed here. In this respect it is important to note that given a dense crown cover of trees the signal recorded by the satellite does not provide information on the grazed ground layer. It is, however, not very likely that animals are actually led there for grazing due to the 2000 m maximum distance criterion. In addition, when the distribution of cost unit zones is regarded it is striking that the high-cost zones responsible for the strong increase of vegetation cover in this division of the curve are exclu-

sively related to this open forest patch in the Northeast. This explains the visible deviation between both curves in the high-cost interval. Beside this effect, the consistency of gradients can be noted, especially in the low- to mid-cost unit zones that are grazed with high confidence. As an addition to the bars shown in Fig. 10.27, Table 10.5 gives the cost unit zone corresponding to 2000 m Euclidian distance if the friction value of maximum abundance in the histogram is used in the calculation.

Table 10.5: Cost unit zones for most frequent friction values (further information in the text)

Plot ID	Cost unit zone
A	25
B	34
C	29
D	39
E	26
F	35
G	29
H	59
I	29
J	59

In most cases, these values are rather close to the average bars in Fig. 10.27. Most importantly, they underline that in plots b, d and f the probability of the cost unit zones characterised by decreasing cover being visited by flocks is rather low.

The standard deviations corresponding to the cost distance zones (shown as dashed lines) generally increase with increasing cover values, indicating that as zones depart from the source points the heterogeneity within these zones increases. As this increase manifests on low to moderate levels, the classes can be considered representative. All standard deviation curves show a strong decrease in the high cost distance zones, but this is a pseudo-effect as it relates to areas to which grazing may usually no extend, meaning the theoretical considerations on which the cost surface model is developed would not be valid there. Most importantly, the units of highest cost distances only include a low number of pixels.

Concerning the processing scheme from formulation of hypotheses to creation of the analysis buffers, two conclusions can be drawn:

- Graphs c, h, i and j illustrate the effect of buffer threshold and majority filtering. Firstly, setting the threshold to 50 obviously introduces noise in the resulting gradients compared to a wider buffer interval of 100 cost units, although the general trend is maintained. This is a result of the lower number of pixels included in the cost zones in the first case, leading to a higher influence of exceptional values. On the other hand, majority filtering does not seem to improve the smoothness of the gradients. To the contrary, the gradient intervals in the mid- to high-cost unit zones even appear noisier, while no significant difference between standard and filtered gradient is observed for the low-cost unit zones. It must be suspected that for the rather narrow buffers in the

mid- to high-cost unit zones, application of a majority filter increases ambiguity where different classes are adjacent.

- Comparing graphs c and g, it can be seen that, although it is advisable to rely on local expert knowledge, the influence of differentiated weighting of the input friction images compared to equal weighting appears almost negligible.

The results from this sensitivity analysis underline the robustness of the proposed creation of an accumulated cost distance surface to model grazing preferences of livestock animals. The creation of the single friction surfaces results in slight variations of the resulting adapted buffers and hence the derived gradients, but their results remain generally constant.

Woody vegetation gradient: adapted vs. perpendicular buffers

The analysis of a spatial trend in woody vegetation cover is based on the accumulated cost distance surface corresponding to plot c in Fig. 10.27. In the chosen scenario, the calculation of attractiveness solely based on information supplied in the habitat GIS. This option implied complete independence from remote sensing data and hence the SMA model that was also applied to infer the target vegetation cover information. On the other hand, it was opted to parameterise the 'topography' factor using the slope, although the approach of using the regionalisation data set was considered more accurate. Notwithstanding, the concept of applying this analysis to a fixed perimeter corresponding to administrative units and all potentially grazed areas necessitated inclusion of the open forest area in the Northeast. As this could not be achieved using the regionalisation data set, this option was disregarded here. The buffer size was set to 100 cost units and as this was shown to effectively suppress fluctuations in the data no additional filtering was applied.

Fig. 10.28 contrasts the gradient in woody vegetation cover as a function of increasing cost distance with the gradient as a function of Euclidian distance, i.e. of circular buffers. As already shown in Fig. 10.27, the grey bars indicate the cost distance zone that is reached after 2000 m for different scenarios of friction assignment, i.e. minimum, average and maximum friction values. In addition, the position for the respective most frequent friction values for the input data is shown in Table 10.5.

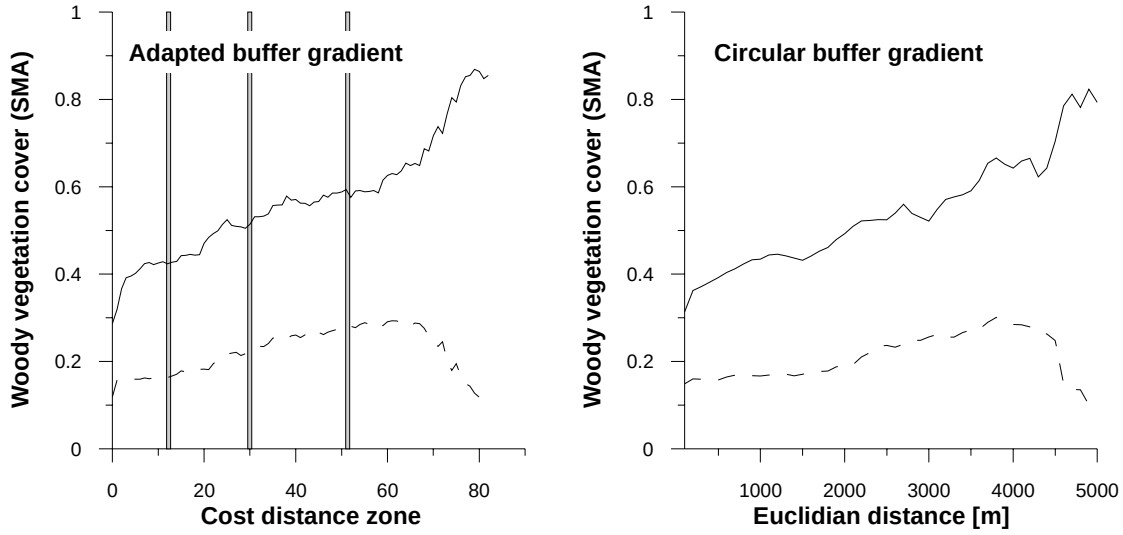

Fig. 10.28: Gradients of woody vegetation cover (solid line) and standard deviation (dashed line) derived from piospheric analysis (left: adapted buffers; right: circular buffers). The bars (left) indicate the minimum, average and maximum costs that may accumulate for a Euclidean distance of 2000 m

Both gradients are comparable in proofing a steady increase in woody vegetation cover with increasing distance from the source PLC. Also, the standard deviation curves show a similar shape corresponding to the pattern described in the context of the sensitivity analysis. This is unsurprising as the distance from shed was identified as a key driver. In the present example, it is the sole factor when regarding the Euclidian distance, while playing a vital role in the calculation of the accumulated cost surface. There, it is inserted as the factor with the highest relative weight. In addition, it is implicitly included in the calculation when accumulated costs are calculated with increasing distance from the PLC. The gradient derived using perpendicular zones is smoother, which is apparently owed to the buffers size. Further to a slightly rougher shape, that might relate to the buffer intervals, the gradient derived using the cost surface approach appears more differentiated. Even if only the minimum accumulated cost to reach 2000 m is viewed, it better resolves strong impact of grazing close to the shed. Observing the adapted buffer gradient, three to four more subsets of the curve can be distinguished. The first follows a marked breakpoint concluding the sacrifice zone. It is characterised by a very slight increase and extends beyond the minimum accumulated cost threshold corresponding to 2000 m. Subsequently, the gradient rises steeply before attenuating again, although the separation of these two components is not overly evident and they could also be interpreted as one unit. It is only slightly beyond the maximum accumulated cost threshold corresponding to 2000 m that the gradient shows its most pronounced and strong increase. This last section should be interpreted with care as it corresponds to the rather limited area of the open forest in the Northeast of the test area, whose effective relevance for grazing is unclear. Yet, even if the assessment is constrained to the potential 2000 m threshold delineated by the left bar and compared to the 2000 m perpendicular buffer gradient, the higher range of woody cover estimates underlines that the cost surface based representation reproduces the spatial pattern in a more differentiated manner.

10.2.6 Discussion of the cost surface approach

There is a direct influence of grazing animals on vegetation cover in general and their foraging behaviour may significantly affect plant community composition. In particular goats act as browsers provided the existence of a shrub layer (Arnold, 1987). In contrast to sheep, they are able to thrive on woody fodder exclusively (Le Houérou, 1981). Adding to this, effects of grazing are most obvious in the direct vicinity of sheds as these locations are under almost constant pressure. As a consequence, the greatest effect can be expected in this immediate neighbouring zone around the sheds. This has been termed 'sacrifice zone' (Thrash & Derry, 1999) and it is clearly visible in the steep initial increase in the gradient in Fig. 10.28 (until cost distance zone 10). Grazing animals prefer young shoots and smaller plants over older plants, as they are more palatable and easy to browse (Legg et al., 1998; Papanastasis 2003). Augmented by trampling effects, this is a major obstacle for the development of shrub communities in strongly grazed areas and further emphasises the direct relation between woody vegetation cover and grazing activities. The almost indifferent segment of the spectrum corresponds to the major grazing zone which is most frequently visited and which is directly adjacent to the 'sacrifice zone' (cost distance zone 10-22). Depending on the interfaces of shrubs with grassland and their accessibility, compact shrub canopies are frequently grazed from the outside, which may contribute to a further fragmentation of the landscape. In cases where shrubs manage to develop above a certain height, this may result in peculiar umbrella-like structures for single shrub specimen (Fig. 2.5).

This major grazing zone is still located relatively close to the sheds, enabling the shepherds to return their flocks to the sheds during the day, which is now a frequent habit especially during the hot midday periods in summer (e.g. Legg et al., 1998; Yiakoulaki, 2002).

Areas requiring larger efforts to travel to or which are rather distant are visited less frequently as a result of the changed practices, resulting in a significant decrease in grazing pressure. In addition, the potential grazing area is getting larger with increasing (cost) distance. The effect of low (or under-) grazing was shown in the topography-related analyses of spatio-temporal trends for the narrow channels where green vegetation cover increased over the last years. In addition, where grazing pressure is low or where the shrub cover exceeds the critical height of approx. 1.5 m, the further development of the *Quercus coccifera* shrublands is possible (Papanastasis, 2003). This is represented by the following interval which is characterised by a more or less strong increase in woody vegetation cover that is believed to be directly related to decreasing grazing pressure (22-60). In these locations, grazing does not suppress the development of a dense shrub layer. Rather, an encroachment and densification of shrubs may be expected.

Especially at high altitudes, this absence of grazing may result in the development of dense *Quercus coccifera* shrublands or even the evolvement of open forests. This may for instance be the case in the previously discussed open forest zone in the Northeast of the pilot area (beyond zone 60).

The human dimension strongly influences the effects of grazing in particular and the landscape configuration in general. First of all, shepherds are frequently interfering with the landscape. In order to promote palatable grass and herb species, shepherds are hampering the

development of a closed shrub layer by removing young specimen, thinning out shrub patches and also by setting fire (Le Houérou, 1981).

The dependency of woody vegetation cover on the pattern and intensity of livestock grazing, which is represented by the model, is but one element in the complex interaction process. The landscape configuration that determines the model parameterisation is not only the result of human utilisation, but has been a major factor determining utilisation in turn. All elements and factors influencing the distribution of grazing animals have always been a major criterion for the establishment of new sheds. In recent times, the accessibility with roads and tracks has gained additional importance in this context. No information on the development of sheds over the past years was available such that this can not be quantified. Nonetheless, it is safe to assume that the grazing regime did not only determine the present characteristics of the rangelands, but that vice versa the distribution of sheds today is – among others – to a certain degree owed to the specific matrix of shrublands, grasslands and other land cover types in the test area. In addition, a concentration of PLC close to villages or well-developed roads is observed, as these locations are most convenient when animals are only grazed for some hours a day, especially when additional forage needs to be supplied. Although agricultural areas and villages were not considered in the model-based characterisation of vegetation cover, this may also contribute to the observed gradient, as due to long human interferences these areas are expected to be more open compared to more remote locations.

Modelling the interaction between physical and socio-economic factors to predict the spatial distribution of livestock animals based on cost surfaces involves different processing steps (compare sections 10.2.3 and 10.2.4) that decisively affect the results. It is especially the formulation of the functional hypotheses on account of which the spatial information layers are created (i.e. friction surfaces) that determines the further analysis. This crucial step requires precise knowledge of the processes to be considered and relies on the availability of geospatial information suitable to represent this. The next stage involves converting the given data sets into friction values. This process requires careful execution, as the transfer functions applied to scale frictions to comparable ranges may impose an implicit weighting of different factors. Such effects may even counteract the subsequent weighting of the friction surfaces to create the integrated cost surface. The described steps are considered the most crucial in the proposed cost surface modelling approach, as the further calculation of accumulated cost distances and the selection of filtering and buffer size options are straightforward procedures. Although the sensitivity analysis has shown the procedure to operate in a robust way, a number of factors imply potential uncertainties or might be tackled using modified or alternative approaches:

- ‘Topography’: In the present study it was based on the slope due to the spatial coverage, but it is expected that the approach using relief mesoform classes described before does more accurately represent the influence of topography.
- ‘Attractiveness’/‘accessibility’: Instead of available GIS data, remote sensing based information might be used in a complementary manner. This was disregarded here due to the presence of clouds in the early image acquisition. On the other hand, using remote sensing based information exclusively is rated critical. Even if the employed

images are acquired at different dates, a certain bias may be introduced in the interpretation chain due to the autocorrelation between the data sets. Yet it must be stated that the current approach relies on the accuracy of the GIS information. Although the aerial photographs date back to 1984, extensive field work was carried out by researchers from NAGREF to update this information where required, hence the information was considered appropriate. In addition, the habitat GIS information also includes information on vegetation structures, such as different plant communities and density classes which is especially beneficial in characterising the relative pastoral value.

- 'Distance': This factor strongly relies on precise location of the PLC as well as on knowledge of the general grazing behaviour, i.e. the maximum distance animals can be expected to travel. The maximum distance exerts a strong influence on the model, as further distances are assigned exceptional costs, thus reducing the probability of remote areas being grazed according to the model.
- Using satellite images of very high spatial resolution enables to accurately map the sheds in the area. In addition, a large number of little lakes and ponds is present in the area. As these are abundant and the availability of water is not considered an essential factor determining grazing activities these were not included in the PLC data base. As the spatial distribution of sheds and gathering points is highly variable, with isolated locations occurring as well as clumped configurations, buffers were allowed to intersect and the statistics were calculated for zones belonging to the same class in total. This implies that no analysis on single PLC level can be run as in this case large cost distance zones for a specific shed might coincide with low cost distance zones for a different shed and hence corrupt the results.
- The creation of adapted buffer zones from the accumulated cost distance surface was carried out using a fixed buffer interval. As the accumulated cost distances are not increasing linearly but exponentially it is debatable whether buffers should reflect this behaviour by consecutively enlarging their intervals with increasing size. As the present study aimed at assessing the feasibility of the approach, fixed buffers were used as they facilitate controlling and understanding the results.

The focus of this analysis was set on proportional cover of woody vegetation as derived from SMA, which serves as an indicator of grazing pressure (compare section 3.3). For this reason, an image acquisition date in late summer was chosen (August, 16th, 2000), when herbaceous vegetation was expected to be already senescent. In general, this date must be chosen with care, as exceptional climatic conditions might prolong the period of photosynthetic activity of these plants and as such lead to an overestimation of woody plant cover. However, no such conditions were reported for the observation period. Also, gradients might be masked if there is a high spatial variability in rainfall and water availability, triggering different responses and states of vegetation in the area, but this could not be verified using the existing data.

Options supporting a validation of the model and the resulting gradients are highly limited. From the number of field surveys carried out in the Lagadas area (Appendix A.2), a small sample was conducted in the neighbourhood of three sheds in the vicinity of Kolchiko,

Lofiskos and Kryoneri. In this context, vegetation plots were established along line transects. The composition and coverage of vegetal layers was investigated by the scientific staff of the AUTh team at distances of 50, 100, 200, 400 and 800 meters away from the sheds. For the woody fraction, the findings are congruent to the results found in this study. An increase of phanerophytic vegetation with distance away from the sheds is the case. In addition, a strong connection of the coverage fraction of woody vegetation and mean plant height was examined (Ghossub, 2003). Yet it is not possible to validate the cost surface model itself beyond assessing the plausibility of resulting gradients. This confirms that the approach essentially requires expert knowledge of scientists who are familiar with local conditions and customs, as only this ensures that the vital factors are identified and appropriately reproduced in the model.

Summarising, the interpreting of the gradient in woody vegetation cover in relation to both physical and socio-economic factors highlights the complexity of Mediterranean rangelands and the high degree of mutual determination of natural properties and the dominating socio-economic framework.

10.2.7 Perspectives

The application of cost surface modelling to the analysis of spatial trends in rangelands as a result of grazing pressure offers considerable potential. First of all, an improvement of the model itself could be achieved if a data base with animal tracks was established. Animal tracking has become technically feasible with improvements in GPS technology. Approaches both include the attachment of automatic GPS devices to animals to monitor their tracks, which was for instance described by Ungar et al. (2005) for free-ranging cattle in the USA and Israel. Ganskopp et al., (2000) compared least-cost paths modelled using a cost surface approach to livestock trails of free-ranging cattle in rugged terrain, which were collected using GPS devices. In the context of wildlife management and conservation, GPS-based systems were developed for distribution with indigenous people to record animal sightings using simple graphical menus (e.g. Janvier & Mayaux, 2005). Whichever approach is preferred, it obviously relies on the cooperation of local shepherds. This taken for granted, it would represent a significant improvement, since the resulting tracks could help to better understand the ‘spatial decisions’ of shepherds and their flocks. Besides serving as a source of validation, this could be quantified by using multivariate statistical techniques to infer the relative importance of the identified determinants, which could subsequently be used to refine the model.

Another potential extension of the model would be the consideration of additional factors, such as the network of roads and tracks. Also, animal census data on the level of sheds might be incorporated to assign different ‘pressure weights’ to the different sheds. However, it needs to be refrained from an over-parameterisation of the model, as the inclusion of too many driving factors and regulation options may introduce pseudo-effects and reduce the interpretability of the results (Mulligan & Wainwright, 2004).

The approach bears considerable potential in the context of rangeland management. As it reproduces the combination of factors that determine the grazing pressure exerted on a certain location, it may be used to simulate the effects of management interventions. These may comprise exclusion of animals by fencing, the establishment of new sheds, the conversion of

land cover (e.g. shrublands into grasslands, opening of dense shrub areas etc.), or the creation of new agricultural areas. Once a cost surface model is established, it can be used to calculate the least costly track between a source and a target point. In the given example, the PLC may be used to determine the most plausible track along which flocks are being led and to calculate corridors where grazing pressure is expected to be greatest (Fig. 10.29).

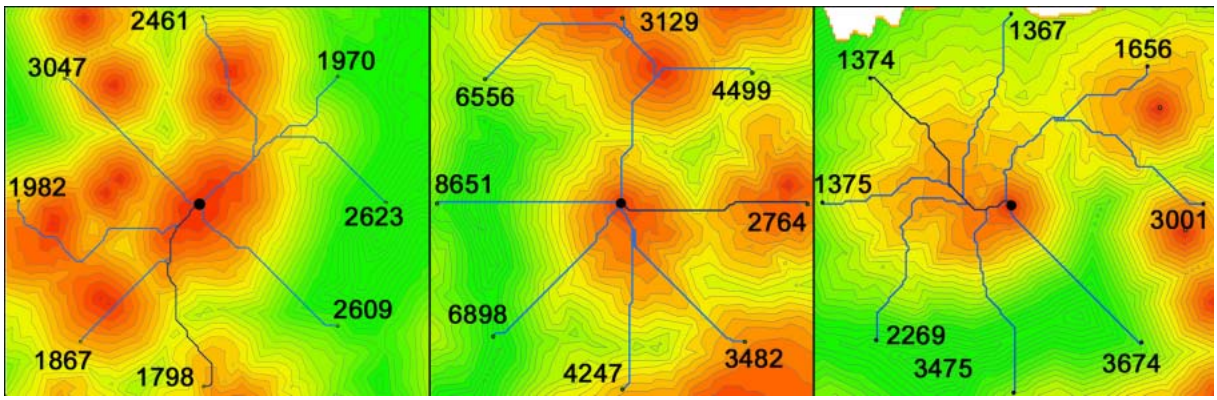

Fig. 10.29: Least cost tracks from source PLC to target positions. The targets were defined according to directional segments in clockwise order at 2000 m Euclidian distance from the respective shed (accumulated costs are coded from red to green in increasing order)

To illustrate the results of track calculation based on an accumulated cost surface, eight potential targets were defined according to directional segments, starting clockwise from North. They were fixed at 2000 m Euclidian distance from the shed and the most probable path to each was calculated. The costs accumulated along the respective tracks are shown beside the target points and the track calculated as 'cheapest' option is depicted in dark blue. For illustration reasons the cost surface is based on the parameter combination described before (e.g. section 10.2.5), although calculated for single PLC here.

Consequently, any potential intervention may be accounted for by correspondingly modifying the friction surface(s), computing total cost and accumulated cost surfaces and re-calculating least cost paths around the sheds in the area considered. The most favoured tracks may be identified by assessing a multitude of target points distributed around the investigated source point. Setting the path analysis to identify the least costly path, further spatial representations may be derived to identify grazing pressure zones, such as corridors, buffers etc.

If this model is implemented in a user-friendly environment, it may prove of significant assistance to local authorities and land managers. In the context of Mediterranean rangelands, it may serve the assessment of the potential impact of planned interventions in the landscape, or tailoring these interventions to achieve the desired steering effect in the case of livestock grazing.

10.3 Summary and discussion: trends in the Lagadas rangelands

In the previous sections it was demonstrated how time series of satellite imagery and derived information products can be integrated with auxiliary geospatial and non-spatial information to assess the temporal development of green vegetation cover in Mediterranean rangelands. Given that – beside conversion of rangelands into agricultural lands – grazing is the major factor shaping this area, no special consideration was given to singular disturbance events. In the Lagadas area, fires are mainly the result of shepherd's interventions with the landscape to improve the pastoral value and are hence confined to small patches. Notwithstanding, the interpretation scheme presented for the Ayora test site (compare Fig. 9.26) could also be applied here in a modified form.

Green vegetation cover derived from SMA was employed to assess the state of rangelands at different times and vegetation cover maps for different dates were prepared. These indicated that, beside smaller clearcuts and fires in forests at higher elevations, no major singular disturbances are to be expected.

With reference to the initial requirements, trend analysis was used to characterise long-term trends and their significance. In the absence of such information, it was hypothesised that high stocking rates might have led to widespread land degradation (e.g. Chouvardas & Papanastasis, 2004). The trend functions derived from the analysis did not give evidence of an overall negative trend. Rather, stable areas where shown to be intermixed with locations showing positive and negative trends. In addition, trends were usually moderate which also affected their statistical significance. The ecological implications of changes in green vegetation cover must be rated differently depending their level (e.g. Tsiourlis et al., 1998), as this partially determines whether trends are reversible. This information can be used as an important element when rangeland management is based on state-and-transition models, which explicitly rely on temporal development and general level of vegetation cover as input information (e.g. Westoby et al., 1989; Society for Range Management, 1995). For this reason, a degradation index was calculated similar to the one presented by Hostert et al. (2003b), which was found to more clearly represent spatial structures in the results of the trend analysis. Based on these information layers, statistics could be calculated for the different classes, showing that half of the grazed area shows a stable behaviour, while the remaining area shows increasing or decreasing vegetation cover.

Assuming grazing to be of major importance in explaining these patterns, major emphasis was given to identifying the relation between the grazing system and its impact under consideration of the physical and socio-economic boundary conditions. Firstly, the relation between the development of stocking rates and vegetation cover was investigated using temporal trajectories. Although, according to Tsiouvaras et al. (1998) and Chouvardas & Papanstasis (2004), stocking rates are often above sustainable degrees, only a limited number of villages showed the expected correlation. In these cases, increasing stocking rates triggered a decrease in green vegetation cover, while decreasing rates corresponded to increasing cover estimates. Different groups of trajectory patterns were identified, and it was concluded that additional factors affect the impact of grazing, such as the provision of additional feedstuffs.

It was also concluded that effects of grazing need to be investigated at a resolution finer than community level. From the spatial distribution of degradation index values it was stated that the grazing system must be considered highly selective in terms of areas visited (compare section 4.2.6 and section 10.1.5). Hence, it appears that the accessibility largely determines if and how strongly locations are subject to grazing. In this sense, the properties of relief features have a high relevance. Steep slopes and narrow valleys are much more difficult to reach than undulating plains. Beside its relevance for the factor 'accessibility', elevation plays an additional role in the context of availability of fodder, which is different in different climatic zones as partially determined by elevation (Yiakoulaki et al., 2002). In areas where grazing pressure is low, or has been reduced due to changed shepherding preferences, a positive feedback loop is often observed. Once the resulting encroachment of shrubs exceeds a certain threshold, shrublands become thicker and less permeable for grazing animals. This further reduces the attractiveness of such locations and contributes to the establishment of dense shrub layers. These effects were investigated for three sub areas representative of the different trend patterns. Making use of available information on relief mesoforms and elevation, it was shown that these were related to trend and degradation patterns and that the impact of grazing is strongest where areas show a high pastoral value and are easily reached. On the other hand, inaccessible regions, such as the narrow valleys and channels abundant in the area, are rather characterised by clearly positive trends.

Additional factors influencing the accessibility of areas are the proximity of sheds and roads. The network of roads and tracks has strongly increased in the past years, partially as a result of funding through the EU contributions granted under different funding schemes, such as the European Regional Development Fund (ERDF), the European Social Fund (ESF) or the European Agricultural Guidance and Guarantee Fund (EAGGF). With most parts of Greece being eligible to the highest funding levels, these grants have significantly affected rural infrastructure in past years.

Livestock grazing in the Mediterranean dates back to 12,000 to 8,000 B.P. and has led to a general regression of vegetation that mostly relates to the conversion of forests to shrublands (e.g. Blondel & Aronson, 1995; Mazolleni et al., 2004). While the traditional grazing system characterised by transhumance was considered at equilibrium with the given rangeland resources (e.g. Blondel & Aronson, 1995; Gomez-Sal, 1998), the change to a sedentary and more intensive system modified the landscape (compare section 4.2.6 grazing and section 10.1.2). This development is strongly affected by the subsidy policy of the European Union and a generally changing socio-economic framework (e.g. Le Houérou, 1981; Blondel & Aronson, 1995; Dubost, 1998). In the Lagadas area, the proximity of the industrial and economical centre of the city of Thessaloniki as well as the tourist centres of the Chalkidiki peninsula provide for additional sources of income beside rural activities. This contributes to the specific properties of the area compared to other grazing regions in Greece, which are still more oriented towards traditional pastoral systems.

Referring back to the points raised in the introduction to chapter 10, several aspects emerge. In principal, two processes seem to operate simultaneously, causing adverse effects.

Overgrazing

In areas easily accessible, especially where the interface of grasslands and shrublands provides for good fodder quality for sheep and goats, **overgrazing** is frequent. This severely damages vegetation through direct effects on shrub specimen (Fig. 10.30), changes plant composition to a dominance of grazing-resistant species (e.g. Fensham et al., 1999; Alados et al., 2004) and accelerates erosion through a reduction in ground cover and trampling effects which are especially grave in uphill positions (e.g. Thornes, 1990; Trimble, 1990). Sparse shrublands are most threatened by these effects, as they offer the highest pastoral value (Papachristou & Platis, 1998). Investigating biodiversity based on the bird fauna, Papoulia et al. (2003) found that in the Lagadas area sparse shrublands show the highest number and density of species. Both measures decline for grasslands as well as for dense shrublands, and only the thermophilous oak forests show a comparable density of birds.

Fig. 10.30: Effects of strong grazing on *Quercus coccifera* shrubs: 'sculpture grazing'

Undergrazing

On the other hand, inaccessible areas might even be considered **undergrazed** when compared to historic equilibrium states. Especially the increase in shrub vegetation in the valleys and channels as well as in upland areas is a critical aspect with respect to the hydrological properties in the watershed. During the last years a reduction in water levels of the two freshwater lakes, both of which are protected under the RAMSAR convention, has been observed. Especially for Lake Koronia this attained high magnitudes and the regression of the shoreline can be easily comprehended from the satellite images. For the period from 1972 to 1998 the water table was reported to have declined by almost 90 % (Karavokyris et al., 1998). Although this is largely owed to an increased uptake of groundwater for irrigation of arable lands in the valley zone, the reduction of water infiltration and discharge rates of the narrow valleys sig-

nificantly contributes to this problem. Papanastasis (2003) reports that irrigated fields are mainly used to produce intensively irrigated crops (e.g. maize, alfalfa), which are provided to grazing animals as feedstuffs.

Management implications

It has been stressed that, properly managed with varying stocking rates and seasonal cycles, grazing may be an important tool for conserving rangeland biodiversity and health. Floral biodiversity was shown to be higher in areas grazed according to local carrying capacities compared to areas where grazing was completely excluded. In addition, livestock grazing has been reported to reduce the risk of wildfires resulting from woody biomass accumulation (section 2.4.3). As a consequence, various measures were suggested in the County of Lagadas to improve the ecological health of rangelands and establish a sustainable local economy. Basically, these include

- incentives and regulations to provide for an extensivation and even distribution of grazing according to local carrying capacity
- the conversion of irrigated agriculture in the Mygdonia valley to less intensive uses
- the establishment of additional sources of income through tourism and recreation
- the establishment of environmental protection areas

(Papanastasis, 2003a).

The concepts and results presented in section 10.1 confirm the complexity of processes presented in section 2.2. They offer a framework for regular monitoring and interpretation in a local context. In particular, the characterisation of trends over longer periods could be shown to refine some of the initial assumptions on grazing-related degradation.

Beside this, a second major complex of the proposed interpretation framework explored the mutual determination of the landscape configuration and the existing grazing scheme. Beside characterising overall spatial trends in rangelands for single dates, it aimed at identifying pathways of making geoinformation processing techniques more useful to land management authorities. The proposed methodology is based on representing major driving factors of the distribution of livestock animals in a landscape in a spatial form. Using functional hypotheses to convert these into friction raster data sets, an artificial cost surface could be derived, which represents the landscape's suitability for grazing according to the present grazing regime. The methodology was shown to perform in a robust manner and yielded a clear spatial trend of woody vegetation cover in relation to (cost) distance from the points of livestock concentration (PLC). The approach is considered appropriate to provide land managers with a tool to evaluate implications that regulations on grazing areas or modifications of the range compositions are likely to have on the distribution of grazing animals. With its present parameterisation, it confirmed that the sedentary grazing system present in the Lagadas area is vastly different from the traditional habits. As shepherding is now mostly conceived as a daytime profession, the impact of grazing is largely driven by the distance shepherds are willing to move away from their sheds in relation to the accessibility of the respective location. Given the importance of additional feeding at the sheds, the nutritional quality only modifies the

spatial distribution pattern, which is in accordance with the previous conclusions on the effects of stocking rates and vegetation cover. Given the long tradition of livestock grazing in the Mediterranean basin, it is clear that the present landscape configuration and the gradient derived from the cost surface analysis are not exclusively the result of the current grazing regime and the sheds that were used as the source points for the analysis. Rather, the mosaic of shrublands and grasslands resulting from decades of pastoral activities have – together with the road and track network – also contributed to the selection of sites for the creation of sheds. The conclusions from this study thus underline the high degree of mutual interactions and feedbacks between Mediterranean rangelands and their utilisation over centuries. Technical aspects and limitations of this exploratory study were discussed in the respective context in section 10.2.6

Summarising, the proposed interpretation framework for grazed Mediterranean rangelands was shown to address the most important requirements formulated before. Grazing-related rangeland processes can be effectively monitored at local scales using a specific degradation index (section 10.1.3) and related to physical and socio-economic boundary conditions as shown in section 10.1.2, 10.1.4 and 10.1.5. A second component enables to predict grazing animal behaviour and assist in managing rangelands. Fig. 10.31 illustrates the major steps involved.

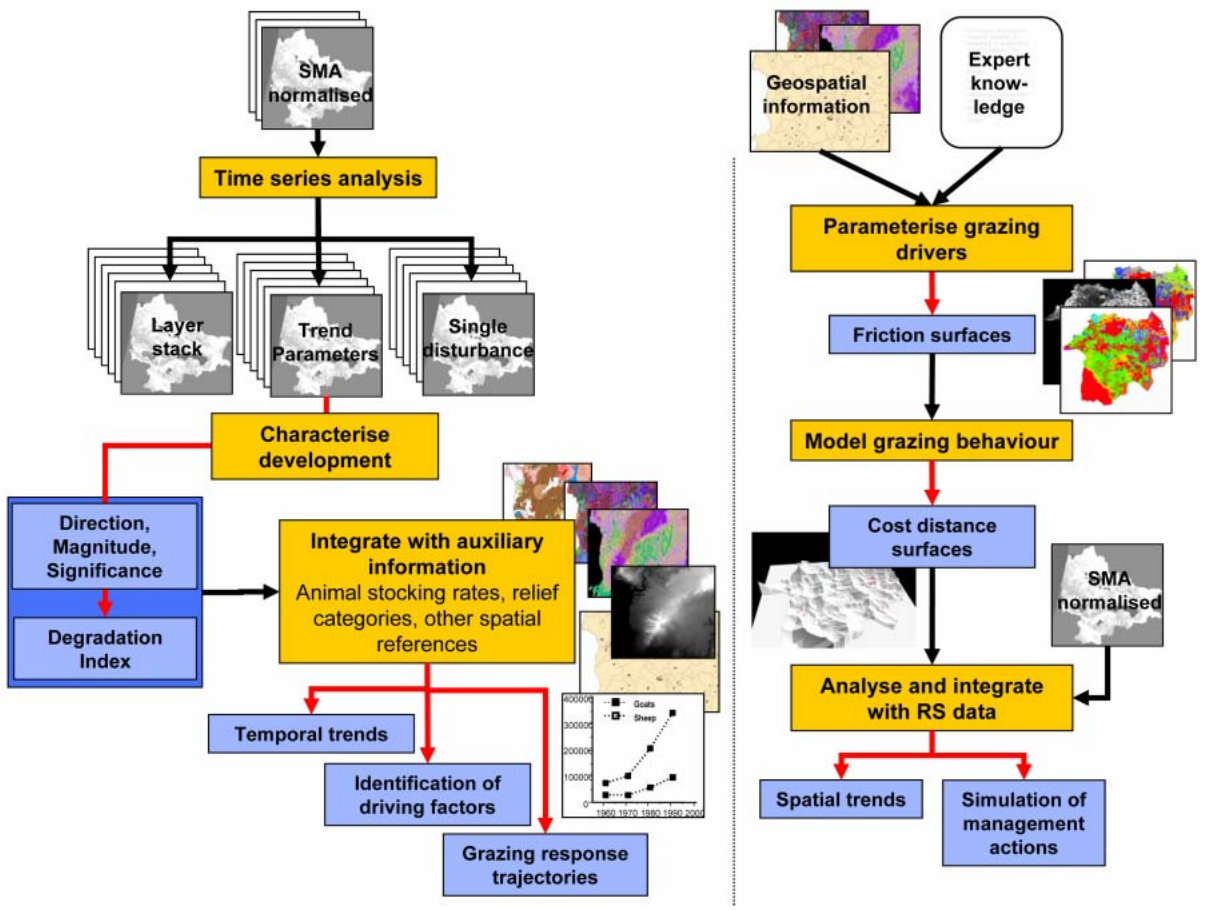

Fig. 10.31: Interpretation scheme for identification of spatio-temporal and spatial trends in grazed rangelands (red arrows indicate the preparation of value-added information products)

11 Summary and discussion

Results and methodological issues have already been discussed in the specific context of the sites in sections 9 and 10. This section intends to conclude on general aspects of a transferable monitoring and assessment framework in relation to the questions raised in the introduction. This will be complemented by the identification of conceptual extensions and modifications of this framework.

Mediterranean rangelands are marginal lands which are interwoven with cultivated and urbanised areas. The small-structured character of the landscape is reflected by a variety of ecosystems. Although these have been utilised for long periods of time, major land use transitions in the past decades have caused conflicts, as a result of which these lands are frequently threatened by land degradation processes.

Two important driving factors of rangeland ecosystems leading to degradation processes have been addressed in this research: fire and grazing. Due to their presence in the Mediterranean basin for millennia, a state of equilibrium was often attained between pressure factors due to traditional land use practices and the environment. In recent decades, major changes in national and local economies as well as sociological frameworks have increased the pressure on rangelands and disrupted these from established steady-states. As degradation is a gradual rather than a spontaneous process, its assessment needs to incorporate the temporal dimension, to which remote sensing approaches can substantially contribute. On a general level, singular disturbance events may be distinguished from ‘slow’ processes, although the first may also follow a pattern in the long run.

From the evaluation of these effects in section 2 it can be concluded that the effect of grazing on plant communities or soil erosion rates is best described as a gradual, long-term process. As many plant communities are adapted to it, grazing may contribute to the heterogeneity and biodiversity of rangelands. On the other hand, it may also lead to a severe disturbance of plants through defoliation, the destruction of the soil-protective vegetation cover or the compaction of soils through trampling, with manifold consequences for infiltration and runoff. The socio-economic framework decisively affects the impact of grazing through grazing patterns and intensities. Fire as disturbance is not *per se* negative. Frequently, ecosystems may rely on it as a regeneration factor, depending on fire-recurrence cycles in relation to the time required by plant communities to reach sexual maturity. Increased fire frequencies lead to a departure from these patterns, resulting in plant communities often dominated by shrubs that are in turn more prone to fires. Beside their impact on plant communities, fires may also trigger soil impoverishment and erosion through changes in structural soil properties or the destruction of the protective vegetation layer.

This research intended to establish a consistent monitoring and interpretation framework for rangelands affected by these factors, which should be transferable to other local contexts. To enable this, the factor ‘grazing’ represented regions where pressure is gradually exerted and requires a long-term assessment. On the other hand, ‘fire’ requires consideration of both, non-

predictable short-term disturbances that pose specific mapping requirements and long-term effects associated with post-fire recovery.

Data input

The issues outlined above have direct implications on the initial question of scale and sensor requirements. Depending on the dimension of fires and the required minimum mapping unit, small-scale approaches are convenient, but these are not appropriate for a differentiated assessment of post-fire dynamics driven by diverse local factors. The impact of grazing manifests in relation to the landscape structure, which necessitates plot- or at least local-scale observations given Mediterranean conditions. As the assessment should be based on a consistent data set incorporating a maximum observation period, Landsat data are particularly suited as a base data set and both time series were composed of Landsat TM and MSS data.

The composition of the satellite image data set depends on the objectives pursued (e.g. Pax-Lenney & Woodcock, 1997) and requires consideration of various aspects. Firstly, comparable stages of vegetation phenology should be analysed. Secondly, information on vegetation types could be derived from seasonal patterns reflected in a series of two or more images per time slice considered. Thirdly, fire mapping is frequently undertaken using images that are recorded directly before and after the fire.

Meeting all of these requirements would imply setting up an extensive data set. This is denied by the objective of transferability in the case of fire-related analyses, as the relevant processes are spontaneous. One image per year is required to exactly obtain the respective year of fire occurrence, although the monitoring of grazing-related processes could also be based on multi-temporal composites at larger intervals, i.e. two or three years. Concluding, the strategy followed to procure the satellite image data base will always be decided upon the trade-off between conceptual requirements and data acquisition and processing costs.

Data standardisation

The second, crucial factor in the framework relates to data standardisation. The analysis of multi-temporal data sets and their integration with other spatial information layers requires that identical positions are compared and spectral differences exclusively result from different surface properties. The geometric rectification of satellite data to a reference projection system using digital elevation data is a straightforward task. Using semi-automatic approaches to ground control points retrieval enhances the operability and results in high between-scene accuracies. On the other hand, the rectification of a master image may be complicated in areas where clearly identifiable landmarks are rare, or when geometric references (i.e. maps) are not available at sufficient scale or quality. As an alternative to traditional identification of ground control points, the utilisation of illuminated digital elevation data was recently suggested, allowing to significantly increase their number and hence contribute to a higher overall precision (Hill&Mehl, 2003).

The accuracy of the radiometric correction largely determines the possible accuracy of further results and is a prerequisite for quantitative interpretation approaches such as SMA. It must be based on an accurate sensor calibration and may necessitate the application of sensor cross-

calibration approaches for older systems. Sensor calibration is an extensive field of research and numerous approaches and calibration constants are available depending on the data processing status. During system correction at European pre-processing facilities for Landsat data, images acquired with MSS and TM sensors are calibrated with constant parameter sets. Rather than using these for DN to radiance conversion, the time-dependent calibration function used here is considered to best represent the decay of sensor sensitivity and ensure the quantitative consistency of the data. With the introduction of new sensor systems, an increase in calibration accuracy is expected from enhanced internal calibration capabilities of the sensors. Numerous approaches to radiative transfer modelling exist. The degree of sophistication needed may vary depending on the application and simple empirical line and topographic normalisation corrections may accelerate data processing. The objective of quantifying vegetation cover with maximum accuracy in areas with strong relief influence denied using these methods. This is confirmed by the accuracy attained from directly incorporating topography-related illumination effects in the radiative transfer model.

Indicator extraction

The analysis of temporal dynamics of rangelands must be based on feasible target indicators, which are commonly based on the spectral information content and related to the vegetation or soil complex. The latter depends on the respective spectral contrasts between soil and bedrock, determined not only by soil development processes but also by the spectral resolution of the sensor employed. On the other hand, the vegetation signal may be identified with high confidence. Being closely connected with different driving factors it is a suitable indicator and can be derived using SMA with higher precision compared to traditional vegetation indices. These models might be extended by including endmembers for ashes, charred bark or dry vegetation (Asner & Heidebrecht, 2002; Román-Cuesta et al., 2005), or by including variable endmember sets. Given the low spectral contrast between dry vegetation and soils in many environments their separation is rated critical. Especially in the case of Landsat-MSS data an extension of the number of endmembers is generally not supported by the spectral dimensionality of the data. The interpretation of results from multiple endmember sets may be rather complex depending on the degree of flexibility assigned to the model. Applying such sets to a large number of scenes may seriously compromise the consistency of the multi-temporal data and was hence disregarded in favour of a constrained model set up to yield ‘stable’ results.

In total, the data processing chain proposed and employed in this study enables a quantitative interpretation of the data and may be deployed in a standardised way. Notwithstanding, the single steps require a profound conceptual knowledge and are frequently associated with considerable efforts.

Interpretation of results

Once multi-temporal data bases are established, analysis and interpretation approaches are required to specifically consider target processes and local conditions. In this study, best use of the data sets is made by characterising trends in vegetation cover based on a linear trend analysis. While the present data sets did not allow inferring cyclic or non-linear trend compo-

nents, it was possible to identify linear long-term trends and further analyse these based on different statistical parameters.

With reference to specific objectives of the **Ayora** test site, the scheme was extended to provide accurate fire perimeter maps assigned to the year of occurrence based on sequential diachronic analyses. Subsequently, the trend analysis was repeated following a temporal stratification to quantify post-fire recovery rates for areas affected from different fires. The RMSE of the trend function could be related to plant communities. Different value-added analysis products could be procured using the remote sensing data set, such as a characterisation of fire recurrence and cycles on a per-pixel basis. In addition, pixel-based indices were calculated that indicate the level of vegetation cover for each date in relation to local and global potential maximum values derived from the time series. Although this is a simplified conceptual approach, it was shown to be of high practical value for land managers.

While the remote sensing based analysis efficiently incorporates the temporal dimension of changes in rangelands, their interpretation in relation to driving factors can only be achieved by their integration with auxiliary spatial and thematic information. This can not be completely formalised as the availability of such data is highly variable in different regions affected by land degradation processes. In the frame of the two case studies presented in this work, it was demonstrated how specific data may be used to further interpret remote sensing based results.

In the fire context, physical boundary conditions are important driving factors. It was concluded from stratification operations that topography, and particularly aspect, is the key driver for vegetation recovery. The most favourable conditions are found where lower solar irradiation rates effectuate better water supply for plants. Such analyses would greatly benefit from the availability of a gridded climate data set complementing irradiation rates with information on locally available amounts of water. Although records from a number of meteorological stations were available, their spatial distribution did not allow for an interpolation. Despite this, the long-term records enabled to relate pulses in the temporal vegetation cover profiles to years with favourable water supplies. Especially shortly after fires, when herbaceous vegetation is dominating, an immediate response to climatic forcing could be observed, while for communities dominated by trees a response was delayed and only occurred in cases of prolonged drought. Such drought periods also preceded the major fire events in the area. The remote sensing analysis suggests that management actions deployed in the area following the large fire in 1979 were not successful. Almost the full area was burned during the observation period, many locations even twice. This recurrence rate seriously threatens the regeneration of pines and favours the creation of dense shrublands. These represent high fuel loads and are easily propagated by fires; hence management intervention should focus on creating a landscape configuration that mitigates fire propagation and on deploying locally adapted replantation of tree species.

Employing one image per year allows to relate fire events and perimeters to a specific fire season; however, this event may have taken place at any date covered by the diachronic set considered. This affects the resulting recovery characteristics, as the starting date for the post-fire trend analysis may depart from a higher cover level in the case of a large lag between the

fire and the respective post-fire image. Alternatively, data may be specifically acquired to address a particular fire event at local scale. This requires prior knowledge of the fire date and approximate location, which could be based on a precursory analysis of hypertemporal imagery or making use of specific value added products (e.g. MODIS fire product). In this research, this uncertainty was accepted as the focus was set on a transferable concept that should based on time series at regular intervals.

Assessing the impact of grazing in the **Lagadas** rangelands, the trend analysis and the derived degradation index revealed a small-structured pattern of stability, negative and positive development in close proximity. In the integrated analysis, both physical and socio-economic factors were considered. In areas dominated by grazing, information on stocking rates at different dates and for spatially discrete units is important. Temporal trajectories derived by relating community-based, decadal stocking rates to green vegetation cover showed distinct patterns. Only some villages exhibited a negative correlation between stocking rate and vegetation cover, while in many other cases deviating relations occur. Concluding, the remote sensing based analysis does not support the hypothesis of an overall degradation of resources as a result of increased animal numbers. It does, however, reflect the transformation of traditional to more intensified grazing schemes. Concentration processes lead to a highly selective grazing of favourable areas and degradation effects are clearly visible. Frequently, the importance of free grazing appears to recede, where stocking rates are independent of pastoral resources and animals are mostly kept in sheds. On the contrary, less favourable areas experience an increase in vegetation cover, with subsequent feedback loops on local ecosystem dynamics.

Making use of information on topography, it was shown that trends in vegetation cover appear related to the accessibility of locations. While negative trends are more abundant in plain areas, positive trends are observed in steep valleys and channels, with ecological implications on the local drainage system. As these findings were expected to translate into spatial trends, the feasibility of modelling livestock behaviour in rangelands was assessed. Based on knowledge of shepherd's behaviour and animal preferences, information on animal sheds, topography and a habitat map were employed to approximate the distribution of animals. A spatial trend of increasing woody vegetation cover with increasing distance away from livestock concentration points was observed which is in accordance with previous conclusions. As the concept is based on expert knowledge of the grazing regime, it may be refined using new information or geospatial data sets or if major boundary conditions are changed. It is hence considered a useful element of an interpretation strategy in grazing-affected rangelands.

Drawing from the different results of the geomatics analyses, the critical management issue in Lagadas is not necessarily to reduce the utilisation of rangeland resources by grazing animals. As a proper level of grazing is expected to entail ecological benefits, it was proposed to promote a more balanced spatial distribution of grazing with stocking rates being adapted to sustainable local carrying capacities. The provision of incentives should hence appraise the landscape preservative function of extensive grazing, while the implementation of a 'per-head' quota that has long been pursued appears to be counterproductive.

Summarising, the suggestion of a general strategy for the integration of remote sensing data with additional spatial and non-spatial information is complicated by differences in their existence, availability and quality. Especially spatially differentiated information on climate, bedrock, soils etc. would be desirable. Given the current situation, flexible use must be made considering the respective local conditions. Two important points can be noted. Firstly, many processes of relevance in Mediterranean rangelands are influenced by topography (e.g. del Barrio et al., 1997). Given the wide availability of DEMs as a result of the Shuttle Radar Topography Mission, these data should be considered in any interpretation strategy. Secondly, trends in grazed areas can only be assessed in relation to information on grazing animals. If no other census data are available, statistics provided by the statistical service of the European Union (EUROSTATS) related to different administrational levels offer a feasible alternative.

Concluding, a scientifically sound monitoring and assessment framework for Mediterranean rangelands should comprise the following elements.

- A data set at the scale required and covering maximum observation time. The data selection strategy depends on the underlying rationale. One image per year was rated a good compromise to meet many analysis objectives, but this may require modification depending on data availability and processing capacities
- A precise standardisation of data, ensuring exact geometric co-location as well as radiometric consistence devoid of influences of sensor calibration, atmospheric conditions and illumination effects due to topography.
- Appropriate indicators that are tangible using the chosen data types and that adequately represent target processes directly or indirectly. Furthermore, the utilisation of methodologies to derive these with adequate precision is of great importance.

While these steps form a general baseline, diverse processes, such as fire or grazing, need to be addressed in a differentiated manner and in dependence of available auxiliary information.

- A fire analysis needs to satisfy mapping requirements for burnt area identification and labelling, which can be based on sequential diachronic data sets. A subsequent spatial and temporal stratification allows to draw conclusions on post-fire dynamics through trend analysis. In a further step, this information can be interpreted in relation to topography or other additional information to identify driving factors.
- With respect to grazing, long-term data sets allow to infer trends and statistical parameters. Based on these, the formulation of a degradation index was shown to highlight spatial patterns, which can be integrated with information on animal numbers and topography as major driving factors. Provided the availability of suitable base data sets, modelling of livestock animal distribution in rangelands may serve as a valuable element to complement the understanding of complex rangeland dynamics.

A schematic representation of the different steps involved in this research can be found in the site-related chapters in section 9.6 and 10.3.

12 Perspectives

The interpretation framework presented in this work is based on the present status of operational data availability and focuses on two major drivers of rangelands processes. As indicated in section 2, there are other factors that might entail a loss in ecological diversity or biological productivity. Hence, future perspectives include both conceptual extensions of the framework as well as technical improvements of different steps involved.

Conceptual extensions

A combination of short-term and long-term processes was addressed in this research, which were represented by fire and grazing. However, further threats to rangelands have to be noted, the most severe of which is the general loss of rangeland areas. This is owed to the mosaic of landscapes in the Mediterranean basin, resulting in manifold interfaces between rangelands as extensive resources, with more intensified land uses such as agriculture or (urban) settlements. Growing economic demands lead to corresponding land use conversions in some places, as for instance observed in southern Spain. This is an important aspect given the ecological value of rangelands. Such processes follow a completely different pattern than those investigated here. If they are at the focus of research, multi-temporal classification and change analysis approaches as described in section 3.4 represent an appropriate additional element of a monitoring framework. The analysis of land use at different time steps using change vectors or matrices and linked to socio-economic data is an efficient means to assess such transformations, while often being less costly in terms of data requirements and processing efforts (e.g. Johnson & Kasischke, 1998; Petit et al., 2001). Where agricultural areas are at the focus of analyses, texture- and object-oriented approaches offer further potential to precisely identifying parcel boundaries (Blaschke & Hay, 2001).

Data processing and analysis

Radiometric processing of satellite data involves considerable efforts to characterise sensor calibration and parameterise radiative transfer models. While the first is an engineering task, the lack of information on atmospheric conditions is a major limiting factor in the accuracy of radiometric correction. New sensor systems offer the potential to parameterise atmospheric conditions for base images with information on aerosols or atmospheric water vapours derived from dedicated sensor systems (e.g. MISR, MOPPITT on Terra) that are acquired at only short temporal lags in tandem or formation orbits (e.g. Terra and Landsat-7, or the currently commissioned ‘A-Train’ sensor suite). Alternatively, a regularly spaced network of meteorological stations recording major input parameters to radiative transfer models would certainly advance radiometric processing provided easy and timely access to data. As it is desirable to keep data processing efforts low, it is presently investigated to which degree the accuracy of radiometric correction and subsequent SMA is reduced if standard parameter sets are employed instead of individualised models.

As indicated, validation of remote sensing data on local scales is complicated by the heterogeneity of Mediterranean rangelands. Concerning the validation of radiometric correction, the lack of suitable reference targets is often a drawback. The establishment of a cadastre of vali-

dation sites with regularly documented spectral properties is a desirable perspective, albeit not very probable. Concerning the validation of derived indicators, such as green vegetation cover, validation is equally critical. Frequently, data used are not specifically mapped, but relate to phyto-sociological analyses in their own right, hence focussing on fine rather than on aggregated scales. It is suggested to conduct specific validations of vegetation cover to support remote sensing based indicator derivation by mapping cover on pre-selected, homogeneous areas that can be precisely located in satellite imagery. Different sampling schemes may be adopted, such as using frames along transects and independently estimating ground cover by a number of researchers for averaging.

Ecozoning

As indicated in different sections throughout this research, the accuracy of interpretation approaches benefits from detailed knowledge of the respective environments. For instance, information on soils, bedrock and typical plant communities improves the definition of appropriate endmember models for SMA. Usually, this is based on specific, site-related data and hence confined to these. A general stratification of large areas, i.e. on national to global level, into zones of similar climatological, lithological, pedological, socio-economic etc. properties would be desirable to optimise these tasks. It could be based on available data sets such as the European Soil Database, CORINE land cover surveys or widely available Natura 2000 habitat maps. This would require considerable conceptual efforts to integrate these and other information layers, as the mapping scales are often different, transition rules between national classification systems are sometimes not well defined and in the case of remote sensing derived land cover information an independence of data is not maintained. Nonetheless, if monitoring approaches as the one presented in this research are to be transferred to other regions, the availability of such ‘ecozones’ would be of substantial benefit.

Metadata

As with most aspects raised here, data availability is a crucial issue. Especially the integration of multiple data sources and information layers addressed before necessitates that data are shared and exchanged. An important aspect in this sense is the adequate documentation of data, which is a prerequisite for ensuring their usability in different contexts. Given this, especially data acquired by EC, EEA or FAO should be consistently documented by generally accepted metadata standards such as the FGDC- (FGDC, 1998) or the CEN/TC287 standard promoted by the European Committee for Standardization. On a European level, the ‘INfrastructure for SPatial InfoRmation in Europe’ (INSPIRE, http://inspire.jrc.it) aims at providing harmonised and documented geographic information for various purposes.

Multi-scale integration

The most important perspective on the regular and standardised assessment of Mediterranean rangelands, however, lies in the promotion of multiple-scale data interpretation. In this sense, the framework presented here should be conceptually embedded in a larger scheme where different observation levels exist depending on the target process and area. Recent advances in sensor design offer a unique potential (compare Fig. 1.1), with the NOAA-AVHRR series being complemented by a range of coarse resolution sensors with different spectral capabili-

ties and temporal resolutions, such as MODIS, MERIS, SPOT-Vegetation or METEOSAT-SG. Similarly, a range of operational and experimental sensors for local scale monitoring have been deployed, such as ASTER and ALI or the hyperspectral sensor Hyperion. These complement the Landsat sensor family with increased spectral resolutions that might support an enhanced spectral discrimination of surface materials. At even finer scales, the IKONOS, QuickBird and SPOT-V sensors offer unprecedented spatial detail at multiplspectral resolution. Finally, airborne systems offer hyperspectral data although being limited to specific campaigns. (Kramer, 2002)

Due to its continuous heritage, there is great interest in a continuation of the Landsat mission (e.g. Woodcock et al., 2001). Complemented by the range of new sensor system there is an outstanding potential of earth observation to support a regular monitoring framework. This notwithstanding, the technical innovations bear numerous challenges that equal their potential. Beside data costs, these include technical issues such as sensor cross-calibration, calibration of hyperspectral sensors, the derivation of information products from coarse resolution sensors or the geometric rectification of very high spatial resolution imagery. Most importantly, putting the technical potential into practice requires corresponding conceptual improvements.

Although a variety of approaches and methods exist that address the monitoring and assessment of ecosystems at a particular scale, a coherent concept should integrate multiple scales and support up- and down-scaling in different contexts. The interpretation of coarse-scale, hypertemporal imagery allows characterising linear and non-linear trend components. In the context of fire mapping and post-fire analysis, such information might be used to identify ‘hot spots’ for subsequent analysis at finer scales. Alternatively, the analysis of grazing effects draws great benefit from the integration of VHR imagery and further approaches involving textural or object based analysis may emerge. The application of canopy reflectance models using a combination of local scale and VHR sensors could potentially characterise rangelands using alternative variables, such as leaf water content, LAI, chlorophyll content etc. Although there are numerous studies integrating data from different scales and sources (e.g. Lambin, 1996; Cain et al., 1997; Sester, 1999; Petit & Lambin, 2001; Wang et al., 2004), a comprehensive conceptual approach is not yet available.

In the context of ecosystem monitoring and assessment, the implementation of interpretation approaches that are fully integrated across various spatial and temporal scales and incorporate socio-economic information from national to household levels is an enormous challenge. Among decision-makers at all levels there is a growing interest in relevant geospatial information that complies with their specific demands. Different approaches exist to integrate spatial with non-spatial sources, which incorporate the economic dimension (Mertens et al., 2000), and ‘translate’ scientific information into information products usable on different administrational levels (e.g. White & Engelen, 1997; Engelen, 2002).

Such an interpretation framework for Mediterranean rangelands may only be realised upon thorough conceptual knowledge of driving factors and relevant processes. This research work proposes a framework to assessing and monitoring rangelands based on a quantitative indicator. Addressing fire and grazing as major driving factors, it provides a concept to assess

spatio-temporal patterns using remote sensing data and techniques, following which options for integration with auxiliary information and analyses according to local prerequisites are demonstrated. The formalisation of a data processing strategy is based on explicit consideration of relevant processes and scales, ensuring the scientific credibility of the results. Different elements of this framework show a particular value as information products for land managers. These include the detailed mapping and labelling of fire perimeters, or the characterisation of temporal trends to evaluate past management interventions and identify priority areas both with respect to fire mitigation and grazing impact. In particular, the cost surface approach may be extended to serve as a prediction tool for rangeland managers, as their decisions affecting economic boundary conditions from local to global levels often have immediate ecological consequences.

Besides direct implications at the landscape level, this framework provides an important link for up- and down-scaling between different resolution and aggregation levels from coarse, national scales to plot scales. Complementary approaches are being developed or already exist on these levels. Hence, future research needs to concentrate on establishing clearly defined links and transitions, as these are crucial in proceeding from single scales to a true multi-scale approach.

References

Adams, J.B., Smith, M.O., & Johnson, P.E. (1986). Spectral mixture modelling: a new analysis of rock and soil types at Viking Lander. *Journal of Geophysical Research, 91*, 8113-8125

Adams, J.B., Smith, M.O., & Gillespie, A.R. (1989). *Simple models for complex natural surfaces: A strategy for the hyperspectral era of remote sensing* (pp. 16-21). Proceedings IEEE International Geoscience and Remote Sensing Symposium New York, 1

Adams, J.B., Smith, M.O., & Gillespie, A.R. (1993). Imaging spectroscopy: Interpretation based on spectral mixture analysis. In C.M. Pieters, & P. Englert (Eds.), *Remote Geochemical Analysis: Elemental and Mineralogical Composition* (pp. 145-166). Cambridge: Cambridge University Press

Adams, J.B., Sabol, D.E., Kapos, V., Almeida, R., Filho, R., Roberts, D.A., Sith, M.O., & Gillespie, A.R. (1995). Classification of multispectral images based on fractions of endmembers: application to land-cover change in the Brazilian Amazon. *Remote Sensing of Environment, 52*, 137-154

Adriaensen, F., Chardon, J.P., De Blust, G., Swinnen, E., Villalba, S., Gulinck, H., & Matthysen, E. (2003). The application of 'least-cost' modelling as a functional landscape model. *Landscape and Urban Planning, 64 (4)*, 233-247

Agee, J.K. (1995). Fire and pine ecosystems. In D.M. Richardson (Ed.), *Ecology and biogeography of Pinus* (pp. 193-218). Cambridge, New York, Melbourne: Cambridge University Press

Aguado, I., Chuvieco, E., Martín, P., & Salas, J. (2003). Assessment of forest fire dange conditions in southern Spain from NOAA images and meteorological indices. *International Journal of Remote Sensing, 24(8)*, 1653-1668

Ahern, F.J., Goodenough, D.G., Jain, S.C., Rao, V.R., & Rochon, G. (1977). *Use of clear lakes as standard reflectors for atmospheric measurements* (pp. 731-755). Proceedings of the 11th International Symposium on Remote Sensing of the Environment. Ann Arbor, Michigan

Alados, C.L., El Aich, A., Papanastasis, V.P., Ozbek, H., Navarro, T., Freitas. H., Vrahnakis, M., Larossi, D., & Cabezudo, B. (2004). Change in plant spatial patterns and diversity along the successional gradient of Mediterranean grazing ecosystems. *Ecological Modeling, 180(2004)*, 523-535

Alvarez, R., Bonifaz, R., Lunetta, R.S., Garcia, C., Gomez, G., Castro, R., Bernal, A., & Cabrera, A.L. (2003). Multitemporal land-cover classification of Mexico using Landsat MSS imagery. *International Journal of Remote Sensing, 24(12),* 2501-2514

Anderson, H.E. (1982). *Aids to determining fuel models for estimating fire behaviour.* USDA Forest Service, Gen. Techn. Rep. INT-122. Intermountain Forest and Range Experiment Station. Ogden UT

Andres, L., Salas, W. A., & Skole, D. (1994), Fourier analysis of multi-temporal AVHRR data applied to land cover classification. *International Journal of Remote Sensing, 15*, 115-1121

Andrew, M.H., & Lange, R.T. (1986). Development of a new biosphere in arid chenopod shrubland grazed by sheep - 2. Changes to the vegetation. *Australian Journal of Ecology, 11*, 411-424

Ångstrom, A. (1964). The parameters of atmospheric turbidity. *Tellus,* 16, 64

Anyamba, A., & Eastman, J.R. (1996). Interannual variability of NDVI over Africa and its relation to El Nino/Southern oscillation. *International Journal of Remote Sensing, 17*, 2533-2548

Aranuvachapun, S. (1983). Variation of atmospheric optical depth for remote sensing radiance calculation. *Remote Sensing of Environment, 13*, 131-147

Aranuvachapun, S. (1985). Satellite remote sensing of atmospherical optical depth spectrum. In E.M. Rollin, M.D. Steven, & P.M. Mather (Eds.), *Atmospheric Corrections for Remote Sensing.* Proceedings of a Remote Sensing Workshop on Atmospheric Corrections, 22nd May 1985. University of Nottingham

Arnold, G.W. (1987). Grazing behaviour. In R.W. Snaydon (Ed.), *Ecosystems of the world*, Vol. 17B: Managed grasslands – analytical studies (pp. 129-134). New York: Elsevier

Asner, G.P., & Heidebrecht, K.B. (2002). Spectral unmixing of vegetation, soil and dry carbon cover in arid regions: comparing multispectral and hyperspectral observations. *International Journal of Remote Sensing*, *23 (19),* 3939-3958

Aubreville, A. (1949). *Climats, Forêts et Désertification de l'Afrique tropicale*. Société des Editions Géographiques Maritimes et Coloniales, Paris

Bähr, H.-P. (1985). Geometrische Modelle. In H.-P. Bähr (Ed.), *Digitale Bildverarbeitung – Anwendung in Photogrammetrie und Fernerkundung* (pp. 349-391). Karlsruhe

Bahrenberg, G., Giese, E., Nipper, J. (1990). *Statistische Methoden in der Geographie. Band 1 Univariate und bivariate Statistik*. Stuttgart: Teubner

Barbosa, P.M.; Grégoire, J.-M., & Pereira, J.M.C. (1999). An algorithm for extracting burned areas from time series of AVHRR GAC data applied at continental scale. *Remote Sensing of Environment, 69*, 253-263

Barbosa, P. M., San Miguel-Ayanz, J., Martinez, B., & Schmuck, G. (2002). Burnt area mapping in southern Europe using IRS-WiFS. In D.X. Viegas (Ed.), Forest Fire Research & Wildland Fire Safety. Rotterdam: Millpress (CD-ROM publication)

Baret, F., & Guyot, G. (1991). Potentials and limits of vegetation indices for LAI and APAR assessment. *Remote Sensing of Environment, 35*, 161-173

Baret, F., Jacquemoud, S., & Hanocq, J.F. (1993). The soil line concept in remote sensing. *Remote Sensing Reviews, 7*, 65-82

Bateson, A., Curtis, B. (1996). A method for manual endmember selection and spectral unmixing. *Remote Sensing of Environment, 55*, 229-243

Benedetti, R., Rossini, P., & Taddei, R. (1994). Vegetation classification in the Middle Mediterranean area by satellite data. *International Journal of Remote Sensing, 15*, 583-596

Berk, A., Anderson, G.P., Acharya, P.K., Chetwynd, J.H., Bernstein, L.S., Shettle, E.P., Matthew, M.W., & Adler-Golden, S.M. (1999). *MODTRAN4 user's manual.* Hanscom AFB, MA 01731-3010: Air Force Research Laboratory, Space Vehicles Directorate, Air Force Material Command

Bertram, J.E.A. (2005). Constrained optimisation in human walking: cost minimization and gait plasticity. *Journal of Experimental Biology, 208(6)*, 979-991

Biggar, S.F., Slater, P.N., & Gellmann, D.I. (1994). Uncertainties in the in-flight calibration of sensors with reference to measured ground sites in the 0.4 to 1.1 μm range. *Remote Sensing of Environment, 48(2),* 242-252

Black, S.E., Helder, D.L., & Schiller, S.J. (2003). Irradiance-based cross-calibration of Landsat-5 and Landsat-7 Thematic Mapper sensors. *International Journal of Remote Sensing, 24(2),* 287-304

Blaschke, T., & Hay, G.J. (2001). Object-oriented Image Analysis and Scale-space: Theory and Methods for Modelling and Evaluating Multiscale Landscape Structures. *International Archives of Photogrammetry and Remote Sensing, 34 (Part 4/W5)*, 22-29

Blondel, J., & Aronson, J. (1995). Biodiversity and ecosystem function in the Mediterranean basin: human and non-human determinants. In G.W. Davis, & D.M. Richardson (Eds.), *Mediterranean-type ecosystems.* (*Ecological Studies 109*) (pp. 43-104). New York, Berlin, Heidelberg: Springer

Boardman, J.W., Kruse, F.A., & Green, R.O. (1995). *Mapping target signatures via partial unmixing of AVIRIS data* (pp. 23-26). Proceedings of the 5th annual JPL Airborne Earth Science Workshop, JPL Publication 95-1, 1

Boer, M. (1999). *Assessment of dryland degradation: linking theory and practice through site water balance modelling*. Nederlandse Geografische Studies, 251, Utrecht

Boer, M., Del Barrio, G., & Puigdefabregas, J. (1996). Mapping soil depth classes in dry Mediterranean areas using terrain attributes derived from a digital elevation model. *Geoderma, 72*, 99-118

Bonham-Carter, G. (1998). *Geographic information systems for geoscientists. Modelling with GIS. Computer methods in the geosciences (vol. 13).* Oxford, New York, Tokyo: Pergamon/Elsevier Science

Borel, C.C., & Gerstl, S.A.W. (1994). Nonlinear spectral mixing models for vegetation and soil surfaces. *Remote Sensing of Environment, 47,* 403-416

Boyazoglou, J., & Flamant, J.C. (1990). Mediterranean systems of animal production. In J.G. Galaty, & D.L. Johnson (Eds.), *The world of pastoralism* (pp. 353-393). New York: Guilford Press

Braun-Blanquet, J. (1952): *Les groupements vegetaux de la France Méditerranéenne*. Macabet Frères, Vaison la Romaine

Briske, D.D., & Noy-Meir, I. (1998). Plant responses to grazing: a comparative evaluation of annual and perennial grasses. In V.P. Papanastasis, & D. Peter (Eds.), *Ecological basis of livestock grazing in Mediterranean ecosystems* (pp. 13-26). Proceedings of the International Workshop held in Thessaloniki (Greece), October 23-25, 1997. Luxembourg: Office for Official Publications of the European Communities

Brockmann, K. (1992). Zur Nutzung des Thematic Mapper für die Ozeanographie. *Phd dissertation,* University of Hamburg

Brogaard, S., & Ólafsdóttier, R. (1997). Ground-truths or ground-lies? *Lund electronic reports in Physical Geography, 1*, 1-14

Brown, A.G. (1990). Soil erosion and fire in areas of Mediterranean type vegetation: results from chaparral in Southern California, USA, and matorral in Andalucia, Spain. In J.B. Thornes (Ed.), *Vegetation and erosion: Processes and environments* (pp. 269-288). Chichester, New York, Brisbane: Wiley & Sons

Brunsell, N.A., & Gillies, R.R. (2003). Determination of scaling characteristics of AVHRR data with wavelets: Application to SGP97. *International Journal of Remote Sensing, 24 (14)*, 2945-2957

Burrough, P., & Mc Donnell, R. (1998). *Principles of geographic information systems.* Oxford

Caetano, M.S., Mertes, L.A.K., & Pereira, J.M.C. (1994). *Using spectral mixture analysis for fire severity mapping* (pp. 667-677)*.* Proceedings of the 2nd international Conference on forest fire research, Coimbra Portugal, November 21-24, 1994, Coimbra

Cain, D.H., Riitters, K., & Orvis, K. (1997). A multi-scale analysis of landscape metrics. *Landscape Ecology, 12 (4)*, 1999-212

Calvao, T., & Palmeirim, J.M. (2004). Mapping Mediterranean scrub with satellite imagery: biomass estimation and spectral behaviour. *International Journal of Remote Sensing, 20 (25/16),* 3113-3126

Camacho-De Coca, F., García-Haro, F.J., Gilabert, M.A., & Meliá, J. (2004). Vegetation cover seasonal changes assessment from TM imagery in a semi-arid landscape. *International Journal of Remote Sensing, 25(17)*, 3451-3476

Chander, G. & Markham, B. (2003). Revised Landsat-5 TM radiometric calibration procedures and postcalibration dynamic ranges. *IEEE Transactions on Geoscience and Remote Sensing, 41(11)*, 2674-2677

Chavez, P.S., Jr. (1989). Radiometric calibration of Landsat Thematic Mapper multispectral images. *Photogrammetric Engineering & Remote Sensing, 55,* 1285-1294

Cheng, P., Toutin, Th., & Zhang, Y. (2003a*). QuickBird - geometric correction, data fusion, and automatic DEM extraction.* Proceedings of the 24th Asian Conference on Remote Sensing & International Symposium on Remote Sensing, Busan, Korea, 3-7 November, 2003

Cheng, P., Toutin, Th., Zhang, Y., & Wood, M. (2003b). QuickBird-geometric correction, path and block processing and data fusion. *EOM, 12(3)*, 24-30

Chiarucci, A., Wilson J.B., Anderson, B.J., & De Dominicis, V. (1999). Cover versus biomass as an estimate of species abundance: does it make a difference to the conclusions? *Journal of Vegetation Science, 10,* 35-42

Chouvardas, D., & Papanastasis, V.P. (2004). *Stocking rate evolution in Lagadas County.* Unpublished Presentation at the GeoRange Science Meeting, March 11th-12th,2004, Ispra, Italy

Christensen, N.L. (1985). Shrubland fire regimes. In S.T.A. Pickett, & P.S. White (Eds.), *The ecology of natural disturbance and patch dynamics* (pp. 3-16). Amsterdam, Oxford, New York: Elsevier

Christensen, N.L. (1994). Fire and soil in Mediterranean shrublands. In J.M. Moreno, & W.C. Oechel (Eds.), *The role of fire in Mediterranean-type ecosystems* (pp. 79-95). New York, Berlin, Heidelberg: Springer

Chuvieco, E. (Ed., 1999). *Remote sensing of large wildfires in the European Mediterranean Basin.* Berlin, Heidelberg, New York: Springer

Chuvieco, E., & Congalton, R.G. (1988). Mapping and inventory of forest fires from digital processing of TM data. *Geocarta International, 4,* 41-53

Chuvieco, E., Riano, D., Aguado, I., & Cocero, D. (2002a). Estimation of fuel moisture content from multitemporal analysis of Landsat thematic mapper reflectance data: Applications in fire danger assessment. *International Journal of Remote Sensing*, *23(11),* 2145-2162

Chuvieco, E., Martin, M.P., & Palacios, A. (2002b). Assessment of different spectral indices in the red-near-infrared spectral domain for burned land discrimination. *International Journal of Remote Sensing, 23,* 5103-5110

Chuvieco, E., Aguado, I., Cocero, D., & Riano, D. (2003). Design of an empirical index to estimate fuel moisture content from NOAA-AVHRR images in forest fire danger studies. *International Journal of Remote Sensing, 24(8),* 1621-1637

Cihlar, J. (2000). Land cover mapping of large areas from satellites: status and research priorities. *International Journal of Remote Sensing, 21 (6&7)*, 1093-1114

Civco, D.L. (1989). Topographic normalization of Landsat Thematic Mapper Digital Imagery. *Photogrammetric Engineering & Remote Sensing, 55 (9)*, 1303-1309

Cochrane, M.A., & Souza Jr., C.M.(1998). Linear mixture model classification of burned forests in the eastern Amazon. *International Journal of Remote Sensing, 19*, 3433-3440.

Colby, J.D. (1991). Topographic normalization in rugged terrain. *Photogrammetric Engineering & Remote Sensing, 57 (5)*, 531-537

Conese, C., Maracci, G., Miglietta, F., Maselli, F., & Sacco, V.M. (1988). Forest classification by principal components analyses of TM data. *International Journal of Remote Sensing*, *9 (10/11),* 1597-1612

Conese, C., Gilabert, M.A., Maselli, F., & Bottai, L. (1993). Topographic normalization of TM scenes through the use of an atmospheric correction method and digital terrain models. *Photogrammetric Engineering & Remote Sensing, 59 (12)*, 1745-1753

Congalton, R.G., & Green, K. (1999). *Assessing the accuracy of remotely sensed data. Principles and practices.* Boca Raton: CRC Press

Coppin, P., Jonckheere, I., Nackaerts, K., & Mys, B. (2004). Digital change detection methods in ecosystem monitoring: a review. *International Journal of Remote Sensing*, *25(9),* 1565-1596

Coppock, D.L., Detling, J.K., Ellis, J.E., & Dyer, M.I. (1983). Plant-herbivore interactions in a North American mixed-grass prairie - I. Effects of black-tailed prairie dogs on intraseasonal above-ground plant biomass and nutrient dynamics and plant species diversity. *Oecologia, 56*, 1-9

Corona, P., & Zeide, B. (1999). Contested issues in forest ecosystem management. In A. Farina (Ed.), *Perspectives in Ecology* (pp. 315-322). Leiden: Backhuys Publishers

Cosnefroy, H., Leroy, M., & Briottet, X. (1996). Selection and characterization of Saharan and Arabian desert sites for the calibration of optical satellite sensors. *Remote Sensing of Environment, 58(1),* 101-114

Cosnefroy, H., Briotett, X., Leroy, M., Lecomte, P., & Santer, R. (1997). A field experiment in Saharan Algeria for the calibration of optical satellite sensors. *International Journal of Remote Sensing, 18(16),* 3337-3359

Costa, M. (1987). La region Valenciana. In M. Peinado, & S. Rivas-Martínez (Eds.), *La vegetación de España* (pp. 283-307). Madríd: Universidad de Alcalán de Henares

Cowen, D.J., Jensen, J.R., Hendrix, C., Hodgson, M.E., & Schill, S.R. (2000). A GIS-assisted rail construction economic model that incorporates LIDAR data. *Photogrammetric Engineering and Remote Sensing, 66(11),* 1323-1328

Cracknell, A.P. (1998). Synergy in remote sensing - What's in a pixel? *International Journal of Remote Sensing, 19(11)*, 2025-2047

Dafis, S. (1975). Vegetationsgliederung Griechenlands. In S. Dafis, & E. Landolt (1975). *Zur Vegetation und Flora von Griechenland. Ergebnisse der 15. Internationalen Pflanzen-geographischen Exkursion (IPE) durch Griechenland 1971. Band 1 Einführung; allgemeine Vegetationskunde; Kreta und Ägäische Inseln* (pp. 23-26). Veröffentlichungen des Geobotanischen Instituts der ETH, Stiftung Rübel, Zürich, 55. Heft. Zürich

Dafis, S., E. Papstergiadou, E., & E. Lazaridou (1999). *Technical manual of recognition, description and mapping of habitat types of Greece*. Thessaloniki:Greek Biotopes & Wetlands

DeFries, R.S., Hansen, M. & Townshend, J.R.G. (1995). Global dsicrimination of land cover types from metrics derived from AVHRR pathfinder data, *Remote Sensing of Environment, 54*, 209-222

Dekker, A.G., & Peters, S.W.M. (1993). The use of the thematic mapper for the analysis of eutrophic lakes: A case study in the Netherlands. *International Journal of Remote Sensing, 14,* 799-821

Dekker, A., & Donze., M. (1994). Imaging spectrometry as a research tool for inland water resources analysis. In J. Hill, & J. Mégier (Eds.), *Imaging spectrometry – a tool for environmental observations* (pp. 295-318). Dordrecht, Boston, London: Kluwer Academic Publishers

Dekker, A.G., Malthus, T.J., Wijnen, M.M., & Seyhan, E. (1992). The effect of spectral band width and positioning on the spectral signature analysis of inland waters. *Remote Sensing of Environment, 41 (2/3)*, 211-226

Del Barrio, G., Boer, M., & Puigdefábregas, J. (1996). Selecting representative drainage basins in a large research area using numerical taxonomy on topographic and climatic raster overlays. In M. Rumor, M.C. Millan, & H.F.L. Ottens (Eds.), *Geographical information, from research to application through cooperation, 1* (pp. 398-407). Amsterdam: IOS Press

Del Barrio, G., Alvera, B., Puigdefábregas, J., & Diez, C. (1997). Response of high mountain landscape to topographic variables: Central Pyrenees. *Landscape Ecology, 12(2)*, 95-115

Del Barrio, G., Puigdefabregas, J., Boer, M., Sanjuan, M., & Hilt, K. (2001). Indicators of rangeland condition based on the spatial structure of ecosystems. GeoRange – Geomatics in the assessment and sustainable management of Mediterranean rangelands. *1st annual report. unpublished project report.* Brussels

Del Barrio & G., Puigdefabregas (2004). Assessment of the rangeland condition based on the spatial structure of the landscape within the test sites and generalisation of spatial indicators. GeoRange – Geomatics in the assessment and sustainable management of Mediterranean rangelands. *3rd annual report. unpublished project report.* Brussels

Detchmendy, D.M., & Pace, W.H. (1972). *A model for spatial signature variability for mixtures* (pp. 596-620). Proceedings Earth Resources Observations and Information Analysis Conference, Tullahoma, Tennessee

Di Castri, F. (1981). Mediterranean type shrublands of the world. In F. Di Castri, D.W. Goodall, & R.L. Specht (Eds.), *Mediterranean-type shrublands, ecosystems of the world, 11* (pp. 1-42). Amsterdam, Oxford, New York: Elsevier

Di Castri, F. (1991). The biogeography of Mediterranean animal invasions. In F. Di Castri, & R.H. Groves (Eds.), *Biogeography of Mediterranean invasion* (pp. 439-452). Cambridge: Cambridge University Press

Di Pasquale, G., Di Martino, P., & Mazzoleni, S. (2004). Forest history in the Mediterranean region. In S. Mazzoleni, G. Di Pasquale, M. Mulligan, P. Di Martino, & F. Rego (Eds.), *Recent dynamics of Mediterranean vegetation and landscape* (pp. 13-20). New York: Wiley & Sons

Díaz-Delgado, R., Lloret, F., & Pons, X. (2003). Influence of fire severity on plant regeneration through remote sensing imagery. *International Journal of Remote Sensing, 24(8)*, 1751-1763

Diner, D.J., & Martonchik, J.V. (1984a). Atmospheric transfer of radiation above an inhomogeneous non-lambertian reflective ground. I. Theory. *Journal of Quantitative Spectroscopy and Radiative Transfer, 13 (2)*, 97-125

Diner, D.J., & Martonchik, J.V. (1984b). Atmospheric transfer of radiation above an inhomogeneous non-lambertian reflective ground. II. Computational considerations and results. *Journal of Quantitative Spectroscopy and Radiative Transfer, 13 (2)*, 279-304

Dinguirard, M., & Slater, P. (1999). Calibration of space-multispectral imaging sensors: a review. *Remote Sensing of Environment, 68,* 194-205

Douglas, D.H. (1994). Least cost path in GIS using an accumulated cost surface and slope lines. *Cartographica, 31(3),* 37-51

Drake, N.A., & Settle, J.J. (1989). *Linear mixture modelling of thematic mapper data of the Peruvian Andes* (pp. 490-495). Proceedings of the 9th EARSeL Symposium, Helsinki, Finland, 27th June - 1st July 1989

Du., Y., Teillet, P.M., & Cihlar, J. (2002). Radiometric normalization of multitemporal high-resolution satellite images with quality control for land cover change detection. *Remote Sensing of Environment, 82,* 123-134

Dubost, M. (1998). European policies and livestock grazing in Mediterranean ecosystems. In V.P. Papanastasis, & D. Peter (Eds.), *Ecological basis of livestock grazing in Mediterranean ecosystems* (pp. 298-311). Proceedings of the International Workshop held in Thessaloniki (Greece) on October 23-25, 1997. Luxembourg: Office for Official Publications of the European Communities

Duguy, B, Alloza, J.A., Vallejo, R., Röder, A., & Hill, J. (2005). Use of the FARSITE fire growth model to design strategies for fire prevention and landscape diversity and resilience promotion in a fire-prone area (Ayora, Eastern Spain). *5th International EARSeL Workshop on Remote Sensing and GIS applications to forest fire management: fire effects assessment. June 16th-18th*, Zaragoza, Spain (accepted)

DWD (2003): Klimadaten, URL: http://www.dwd.de/de/WundK/Klimadaten

Eastman, J.R. (1989). Pushbroom algorithms for calculating distances in raster grids. *Autocarto, 9*, 288-297

Eastman, J.R., & Fulk, M. (1993). Long sequence time series evaluation using standardized principal components. *Photogrammetric Engineering & Remote Sensing, 59*, 991-996

EC (Ed., 2001). *Forest fires in Europe. Report No.1 - 2000 fire campaign*. Official Publication of the European Commission, S.P.I01.85.EN

EC (Ed., 2002). *Forest fires in Europe. Report No.2 - 2001 fire campaign*. Official Publication of the European Commission, S.P.I02.72.EN

EC (Ed., 2003). *Forest fires in Europe. Report No.2 - 2002 fire campaign*. Official Publication of the European Commission, S.P.I03.83.EN

EC (Ed., 2004). *Forest fires in Europe. Report No.2 - 2003 fire campaign*. Official Publication of the European Commission, S.P.I04.124.EN

Ehrlich D., & Lambin E.F. (1996). Broad scale land cover classification and interannual climatic change. *International Journal of Remote Sensing, 17*, 845-862

Elachi, C. (1987). *Introduction to the physics and techniques of remote sensing*. New York: Wiley & Sons

Elmore A.J., Mustard, J.F., Manning, S.J., & Lobell, D.B. (2000). Quantifying vegetation change in semiarid environments: Precision and accuracy of spectral mixture analysis and the normalized difference Vegetation index. *Remote Sensing of Environment, 73*, 87-102

Engelen G. (2003). Development of a decision support system for the integrated assessment of policies related to desertification and land degradation in the Mediterranean. In C.G. Giupponi, & M. Shecter (Eds.), *Climate change and the Mediterranean: Socioeconomic perspectives of impacts, vulnerability and adaptation* (pp. 159-195). Cheltenham: Edward Elgar

Etienne, M., Aronson, J., & Le Floc'h (1998). Abandoned lands and land use conflicts in Southern France. In Rundel, P.W., Montenegro, G., & Jaksic, F.M. (Eds.), *Landscape disturbance and biodiversity in Mediterranean-type ecosystems* (pp. 127-140). Berlin, Heidelberg, New York: Springer

European Union Publication Office (2004). *European Soil Database Version 1.0.* CD-ROM Publication (ISBN: 92-894-1947-4). Brussels

Fang, H., Lian, S., McClaran, M.P., van Leeuwen, W.J.D., Drake, S., Marsh, S.E., Thomson, A.M., Izaurralde, R.C., & Rosenberg, N. (2005). Biophysical characterization and management effects on semiarid rangeland observed from Landsat ETM+ data. *IEEE Transaction on Geoscience and Remote Sensing, 43 (1)*, 125-134

Feldman, S.C., Pelletier, R.W., Walser, E., Smoot, J.C., & Ahl, D. (1995). A prototype for pipeline routing using remotely sensed data and geographic information system analysis. *Remote Sensing of Environment, 53(2)*, 123-131

Fensham, R.J., Holman, J.E., & Cox, M.J. (1999). Plant species responses along a grazing disturbance gradient in Australian grassland. *Journal of Vegetation Science, 10*, 77-86

Fernández, A., Illera, P., & Casanova, P. (1997), Automatic mapping of surfaces affected by forest fires in Spain using AVHRR NDVI composite data. *Remote Sensing of Environment, 60*, 153-162

Fernandez-Gimenez, M., & Allen-Diaz, B. (2001). Vegetation change along gradients from water sources in three grazed Mongolian ecosystems. *Plant ecology, 157*, 101-118

FGDC – The Federal Geospatial Data Committee (1998). *Content standard for digital geospatial data.* Report FGDC-STD-001-1998, The Metadata Ad-Hoc Working Group, Reston, Virginia

Finney, M.A. (1994). *Modelling the spread and behaviour of prescribed natural fires* (p. 138-143). Proceedings of the 12th Conference of Fire and Forest Meteorology. Society of American Foresters, Jekyll Island, Georgia

Finney, M.A., & Ryan, K.C. (1995). *Use of the FARSITE fire growth model for fire prediction in US national parks* (pp. 183-189). Proceedings of the International Emergency Management and Engineering Conference, May 1995, Sofia Antipolis

Fisher, P. (1997). The Pixel: A snare and a delusion. *International Journal of Remote Sensing, 18(3)*, 679-685

Fisher, W.B., & Bowen-Jones, H. (1969). *Spain. A geographical background*. London

Foody, G.M., & Cox, D.P. (1994). Sub-pixel land cover composition estimation using a linear mixture model and fuzzy membership functions. *International Journal of Remote Sensing, 15*, 619-631

Foody, G.M., Lucas, R.M., Curran, P.J., & Honzak, M. (1997). Non-linear mixture modeling without end-members using an artificial neural network. *International Journal of Remote Sensing, 18(4)*, 937-953

Foran, B.D. (1987). Detection of yearly cover change with Landsat MSS on pastoral landscapes in Central Australia. *Remote Sensing of Environment, 23(2),* 333-350

Forman, R.T., & Godron, M. (1981). Patches and structural components for landscape ecology. *Bioscience, 31*, 733-740

Forman, R.T.T. (1995). *Land mosaics: The ecology of landscapes and regions.* Cambridge: Cambridge University Press

Forman, R.T.T., & Collinge, S.K. (1996). The "spatial solution" to conserving biodiversity in landscapes and regions. In R.M. DeGraaf, & R.I. Miller (Eds.), *Conservation of Faunal Diversity in Forested Landscapes* (pp. 537-568). London: Chapman and Hall

Fox, B.J., & Fox, M.D. (1986). Resilience of animal and plant communities to human disturbance. In B. Dell, A.J.M. Hopkins, & B.B. Lamont (Eds.), *Resilience in Mediterranean-type ecosystems* (pp. 39-64). Dordrecht, Boston, Lancaster: Kluwer Academic Publishers

Fox, J., Rindfuss, R.R., Walsh, S.J., & Mishra, V. (2002). *People and the environment: approaches for linking household and community surveys to remote sensing and GIS.* Dordrecht, Boston, Lancaster: Kluwer Academic Publishers

Francis, C.F., & Thornes, J.B. (1990). Runoff hydrographs from three Mediterranean vegetation cover sites. In J.B. Thornes (Ed.), *Vegetation and geomorphology* (pp. 363-385). London: Wiley & Sons

Friedl, M.A., & Brodley, C.E. (1997). Decision tree classification of land cover from remotely sensed data. *Remote Sensing of Environment, 61*, 399-409

Frohn, R.C. (1997). *Remote sensing for landscape ecology: new metric indicators for monitoring, modeling, and assessment of ecosystems.* Lewis Publishers

Furlan, D. (1977). The climate of Southeast Europe. In C.C. Wallén (Ed.), *World survey of climatology. Volume 6 – Climates of Central and Southern Europe* (pp. 185-236). Amsterdam, Oxford, New York: Elsevier Scientific Publishing

Ganskopp, D., Cruz, R., & Johnson, D.E. (2000). Least-effort pathways?: a GIS analysis of livestock trails in rugged terrain. *Applied animal behaviour science*, *68(3),* 179-190

Garcìa-Haro, F.J., Gilabert, M.A., & Melìa, J. (1996). Linear spectral mixture modelling to estimate vegetation amount from optical spectral data. *International Journal of Remote Sensing*, *17,* 3373-3400

Garcìa-Haro, F.J., Gilabert, M.A., & Melìa, J. (1999). Extraction of endmembers from spectral mixtures. *Remote Sensing of Environment*, *68*, 237-253

Garcìa-Haro, F.J., Gilabert, M.A., & Melìa, J. (2001). Monitoring fire-affected areas using Thematic Mapper data. *International Journal of Remote Sensing, 22(4)*, 533-549

Garcìa-Haro, F.J., Sommer, S., & Kemper, T. (2005). A new tool for variable multiple endmember spectral mixture analysis (VMESMA). *International Journal of Remote Sensing, 26(10),* 2135-2162

Geerken, R. & Ilaiwi, M. (2004). Assessment of rangeland degradation and development of a strategy for rehabilitation. *Remote Sensing of Environment, 90*, 490-504

Geeson, N.A., Brandt, C.J., & Thornes, J. (2002). *Mediterranean desertification: A mosaic of processes and responses.* London, New York: Wiley & Sons

Ghossub, R. (2003). Impact of piospheric points on Mediterranean rangelands. *Unpublished master thesis, Mediterranean Agronomic Institute of Chania (MAICh),* Chania, Greece

Gilabert, M.A., Gonzàles-Piqueras, J., Garcìa-Haro, F.J., & Melìa, J. (2002). A generalized soil-adjusted vegetation index. *Remote Sensing of Environment, 82,* 303-310

Gillespie, A.R., Smith M.O., Adams, J.B., Willis, S.C., Fischer A.F., & Sabol, D.E. (1990). *Interpretation of Residual Images: Spectral Mixture Analysis of AVIRIS Images, Owens Valley, California* (pp. 243-270). Proceedings of the 2nd AVIRIS Workshop, Pasadena, California

Goel, N.S. (1989). Inversion of canopy reflectance models for estimation of biophysical parameters from reflectance data. In G. Asrar (Ed.), *Theory and applications of optical remote sensing* (pp. 205-251). New York: Wiley & Sons

Goldsworthy, M., Jackson, J., & Haines, J. (2002). The continuity of active fault systems in Greece. *Geophysical Journal International, 148,* 596-618

Gomez-Sal, A. (1998). Relationships between ecological and socio-economic evaluations of grazing in Mediterranean ecosystems. In V.P. Papanastasis, & D. Peter (Eds.), *Ecological basis of livestock grazing in Mediterranean ecosystems* (pp. 275-286). Proceedings of the International Workshop held in Thessaloniki (Greece) on October 23-25, 1997,. Luxembourg: Office for Official Publications of the European Communities

Goward, S.N., & Williams, D.L. (1997). Landsat and earth systems science: development of terrestrial monitoring. *Photogrammetric Engineering & Remote Sensing, 63(7),* 887-900

Goward, S.N., Masek, J.G., Williams, D.L., Iron s, J.R., & Thompson, R.J. (2001). The Landsat 7 mission. Terrestrial research and applications for the 21st century. *Remote Sensing of Environment, 78,* 3-12

Graetz, R.D. (1996). Empirical and Practical Approaches to Land Surface Characterisation and Change Detection. In J. Hill, & D. Peter (Eds.), *The Use of Remote Sensing for Land Degradation and Desertification Monitoring in the Mediterranean Basin - State of the Art and*

Future Research. Proc. of a Workshop, jointly organized by JRC/IRSA and DGXII/D-2/D-4, Valencia, 13-15 June 1994, Valencia, EUR 16732 EN (pp. 9-23). Luxembourg: Office for Official Publications of the European Communities

Green, A.A., Berman, M., Switzer, P, & Craig, M.D. (1988). A transformation for ordering multispectral data in terms of image quality with implications for noise removal. *IEEE Transactions on Geoscience and Remote Sensing, 26 (1)*, 65-74

Grignetti, A., Salvatori, R., Casacchia, R., & Manes, F. (1997). Mediterranean vegetation analysis by multi-temporal satellite sensor data. *International Journal of Remote Sensing, 18*, 1307-1318

Groves, R.H. (1991). The biogeography of Mediterranean plant invasions. In F. Di Castri, & R.H. Groves (Eds.), *Biogeography of Mediterranean invasion* (pp. 427-438). Cambridge: Cambridge University Press

Groves, R.H. (1998). Ecological indicators of landscape degradation. In P.W Rundel, G. Montenegro, & F.M. Jaksic (Eds.), *Landscape disturbance and biodiversity in Mediterranean-type ecosystems* (pp. 55.64). Berlin, Heidelberg: Springer

Gu, D., & Gillespie, A.R. (1998). Topographic normalization of TM images of forests based on sun-canopy-sensor geometry. *Remote Sensing of Environment, 64*, 166-175

Gu, X.F. (1992). Étalonnage et intercomparison des données satellitaire en utilisant le test site de La Crau. *PhD-dissertation, Université Paris VII,* Paris

Gutiérrez Elorza, M. (1994). Introduccion a la geomorfologia española. In M. Gutiérrez Elorza (Ed.), *Geomorfologia de España* (pp. 251-286)

Gutiérrez Elorza, M., & Peña Monné, J.L. (1994). Cordillera Ibérica. In M. Gutiérrez Elorza (Ed.), *Geomorfologia de España* (pp. 1-24)

Guyot, G. (1990). Optical Properties of Vegetation Canopies. In M.D. Steven, & J.A. Clark (Eds.), *Applications of Remote Sensing in Agriculture* (pp. 19-43). London: Butterworths

Haboudane, D., Bonn, F., Sommer, S., Mehl, W., & Royer, A. (2000). Land degradation and erosion risk mapping by fusion of spectrally-based information and digital geomorphometric attributes. *International Journal of Remote Sensing, 23(18)*, 3795-3820

Haddjigeorgiou, I., Vallerand, F., Tsimpoukas, K., & Zervas, G. (1998). *The socio-economics of sheep and goat farming in Greece, and the implications for rural development.* Proceedings of the LSIRD Conference, Bray, Dublin, Dec. 3rd to 5th, 1998

Hadjimitsis, D.G., Clayton, C.R.I., & Hope, V.S. (2004). An assessment of the effectiveness of atmospheric correction algorithms through the remote sensing of some reservoirs. *International Journal of Remote Sensing, 25 (18)*, 3651-3674

Hake, G. (1982). *Kartographie, Bd. 1.* 6th edition. Berlin, New York

Hall, F.G., Strebel, D.E., Nickeson, J.E., & Goetz, S.J. (1991). Radiometric rectification – toward a common radiometric response among multidate, multisensor images. *Remote Sensing of Environment, 35(1)*, 11-27

Harris, A.T., & Asner, G.P. (2003). Grazing gradient detection with airborne imaging spectroscopy on a semi-arid rangeland. *Journal of Arid Environment, 55(2003),* 391-404

Hay, J.E., & McKay, D.C. (1985). Estimating solar irradiance on inclined surfaces: A review and assessment of methodologies. *International Journal of Solar Energy*, *3*, 203-240

Hay, J.E., Perez, R. & McKay, D.C. (1986). Addendum and errata to the paper estimating solar irradiance on inclined surfaces: A review and assessment of methodologies. *International Journal of Solar Energy, 4*, 321-324

Heady, H.F., & Child, D.R. (1994). *Rangeland Ecology and Management*. Boulder: Westview Press

Helldén, U. (1991). Desertification – time for an assessment?. *Ambio, 20 (8)*, 372-383

Henry, M.C., & Hope, A.S. (1998). Monitoring post-burn recovery of chapparal vegetation in southern California using Multitemporal satellite data. *International Journal of Remote Sensing, 19 (16)*, 3097-3107

Henyey, L.G., & Greenstein, J.L. (1941). Diffuse radiation in the galaxy. *Astrophysical Journal, 93*, 70-83

Herold, M., Müschen, B., Müller, A., Klenke, M., & Steinnocher, K. (2000). Zur radiometrischen Reliefkorrektur von Fernerkundungsdaten. *Photogrammetrie – Fernerkundung – Geoinformation, 5,* 347-354

Heshmatti, G.A., Facelli, J.M., & Conran, J.G. (2002). The piosphere revisited: plant species patterns close to waterpoints in small, fenced paddocks in chenopod shrublands of South Australia. *Journal of Arid Environments, 51,* 547-560

Hill, J. (1990). *Radiometric comparison and calibration of remotely sensed data from polar-orbiting earth observation satellites* (pp. 42-53). Proceedings of the 5th Australasian Remote Sensing Conference, 8-12 October, Perth/Australia

Hill, J. (1993). High precision land cover mapping and inventory with multi-temporal earth observation satellite data. The Ardèche experiment. *Dissertation University of Trier, EUR 15271 EN.* Luxembourg: Office for Official Publications of the European Community

Hill, J., & Sturm, B. (1991). Radiometric correction of multi-temporal Thematic Mapper data for the use in agricultural land-cover classification and vegetation monitoring. *International Journal of Remote Sensing, 12 (7)*, 1471-1491

Hill, J., & Schütt, B. (2000). Mapping complex patterns of erosion and stability in dry Mediterranean ecosystems. *Remote Sensing of Environment, 74*, 557-569

Hill, J., & Mehl, W. (2003). Geo- und radiometrische Aufbereitung multi- und hyperspektraler Daten zur Erzeugung langjähriger kalibrierter Zeitreihen. *Photogrammetrie, Fernerkundung, Geoinformation, 1/2003,* 7-14

Hill, J., Mégier, J., & Mehl, W. (1995a). Land degradation, soil erosion and desertification monitoring in Mediterranean ecosystems. *Remote Sensing Reviews, 12,* 107-130

Hill, J., Mehl, W., & Radeloff, V. (1995b). Improved forest mapping by combining corrections of atmospheric and topographic effects. In J. Askne (Ed.), *Sensors and environmental applications of remote sensing* (pp. 143-151). Proceedings of the 14th EARSeL Symposium, Göteborg, Sweden, 6-8 June 1994. Rotterdam, Brookfield: A.A. Balkeman

Hill, J., Sommer, S., Mehl, W., & Mégier, J. (1995c). Use of earth observation satellite data for land degradation mapping and monitoring in Mediterranean ecosystems: Towards a satellite observatory. In J. Hill, & D. Peter (Eds.), *Environmental Monitoring and Assessment*, *37* (pp. 1-16). Dordrecht: Kluwer Academic Publishers

Hill, J., Sommer, S., Mehl, W., & Mégier, J. (1996). A conceptual framework for mapping and monitoring the degradation of Mediterranean ecosystems with remote sensing. In J. Hill, & D. Peter (Eds.), *The use of remote sensing for land degradation and desertification monitoring in the Mediterranean basin - state of the art and future research* (pp. 23-45). Proceedings of a workshop, jointly organized by JRC/IRSA and DGXII/D-2/D-4, Valencia, 13-15 June 1994, Valencia, EUR 16732 EN. Luxembourg: Office for Official Publications of the European Communities

Hill, J., Hostert, P., Tsiourlis, G., Kasapidis, P., Udelhoven, T., & Diemer, C. (1998). Monitoring 20 Years of increased grazing impact on the Greek island of Crete with earth observation satellites. *Journal of Arid Environments, 39*, 165-178

Hill, J., Röder, A., Tsiourlis, G.M., Sommer, S., Mehl, W., Papanastasis, V., Vallejo, R., del Barrio, G., Puigdefabregas, J., & Brundu, G. (2001). Geomatics in the assessment and sustainable management of Mediterranean rangelands. The GeoRange approach. In K. Radoglou (Ed.), *Proceedings of the International Conference on Forest Research: A challenge for an integrated European approach, vol. 1* (pp. 147-152). August 2001, Thessaloniki

Hill, J., Hostert, P., & A. Röder (2003). Observation and long-term monitoring of Mediterranean ecosystems with satellite remote sensing and GIS. *Management of Environmental Quality, 14 (1)*, 51-68

Hill, J., Hostert, P., & Röder, A. (2004). Long-term observation of mediterranean ecosystems with Satellite Remote Sensing. In S. Mazzoleni, G. Di Pasquale, M. Mulligan, P. Di Martino, & F. Rego (Eds.), *Recent dynamics of Mediterranean vegetation and landscape* (pp. 29-39). New York: Wiley & Sons

Hobbs, R.J., Richardson, D.M., & Davis, G.W. (1995), Mediterranean-type ecosystems: opportunities and constraints for studying the function of biodiversity. In G.W. Davis, & D.M. Richardson (Eds.), *Mediterranean-type ecosystems. The function of biodiversity* (pp. 1-42). Berlin, Heidelberg, New York: Springer

Holben, B.N., & Justice, C.O. (1981). An examination of spectral Band ratioing to reduce the topographic effect of remotely sensed data. *International Journal of Remote Sensing, 2*, 115-123

Holechek, J.L., Pieper, R.D., & Herbel, C.H (1989). *Range management. Principles and practices.* 3rd edition. New Jersey

Holm, R.G. (1987). The absolute radiometric calibration of space based sensors. *PhD-dissertation University of Arizona.* Tucson, AZ

Horwitz, H.M., Nalepka, R.F., Hyde, P.D., & Morganstern, J.P. (1971). *Estimating the Proportions of Objects within a Single Resolution Element of a Multispectral Scanner.* University of Michigan, Ann Arbor: NASA Contract NASA-9-9784

Horwitz, H.M., Lewis, J.T., & Pentlend, A.P. (1975). *Estimating the Proportions of Objects from Multi-Spectral Scanner Data*. University of Michigan, Ann Arbor: NASA Contract NASA-14123

Hostert, P. (2001). Monitoring von Degradationserscheinungen im europäisch-mediterranen Raum mit Methoden der Fernerkundung und GIS Untersuchungen am Beispiel der Weidegebiete Zentralkretas. *PhD Thesis University of Trier.* Trier

Hostert, P., & Preissler, H. (1997). *Spectral data catalogue of the field in campaign in Crete, Greece (27.4.-11.5.1997).* Project report, EU-Contract ENV4-CT95-0166, University of Trier, Remote Sensing Department, unpublished

Hostert, P., & Hill, J. (2004). Combining trend parameters from EOS data time series. An analysis of plant composition at landscape level. In P. Smits, & L. Bruzzone (Eds.), *Analysis of multi-temporal remote sensing images* (pp. 216-232). Proceedings of the Second International Workshop, Joint Research Centre Ispra, Italy, 16-18 July, 2003. Series in Remote Sensing Vol. 3. New Jersey, London, Singapore: World Scientific

Hostert, P., Röder, A., & Hill, J. (2003a). Coupling spectral unmixing and trend analysis for monitoring of long-term vegetation dynamics in Mediterranean rangelands. *Remote Sensing of Environment, 87,* 183-197

Hostert, P., Röder, A., Hill, J., Udelhoven, T., & Tsiourlis, G. (2003b). Retrospective studies of grazing-induced land degradation: a case study in central Crete, Greece. *International Journal of Remote Sensing, 24(20),* 4019-4034

Huete, A.R. (1988). A Soil-Adjusted Vegetation Index (SAVI). *Remote Sensing of Environment, 25,* 295-309

Huete, A.R., Jackson, R.D., & Post, D.F. (1985). Spectral response of a plant canopy with different soil backgrounds. *Remote Sensing of Environment, 17*, 37-53

Huttary, J. (1950). Die Verteilung der Niederschläge auf die Jahreszeiten im Mittelmeergebiet. *Meteorologische Rundschau, 3,* 111-119

Instituto Geologico y Minero de España (IGME) (1987). *Mapa geologico de España 1:20000. Sintesis de la Cartografia existente.* Hoja 63: Albacete Onteniente (segunda edicion). Madrid

Iqbal, M. (1983). *An introduction to solar radiation*. New York: Academic Press

Irvine, W.M. (1965). Multiple scattering by large particles. *Astrophysical Journal, 142 (2),* 1563-1575

Itten, K., Meyer, P., Kellenberger, T., Leu, R., Sandmeier, S., Bitter, P., & Seidel, K. (1992). *Correction of the impact of topography and atmosphere on Landsat-TM Forest Mapping of alpine regions.* Remote Sensing Series, 18. Universität Zürich

Jacobshagen, V. (1985). Einführung. In V. Jacobshagen (Ed), *Geologie von Griechenland. Beiträge zur regionalen Geologie der Erde Band 19* (pp. 1-10). Berlin, Stuttgart: Borntraeger

Jacquemoud, S. (1995). Extraction of vegetation biophysical parameters by inversion of the PROSPECT+SAIL models on sugar beet canopy reflectance data. Application to TM and AVIRIS sensors. *Remote Sensing of Environment, 52*, 163-172

Jacquemoud, S., & Baret, F. (1992). Modeling spectral and directional soil reflectance. *Remote Sensing of Environment, 34*, 75-91

James, C.D., Landsberg, J., & Morton, S.R. (1999). Provision of watering points in the Australian arid zone: A review of effects on biota, *Journal of Arid Environments, 41*, 481-484

Janvier, P., & Mayaux, P. (2005). Exploring the synergy between environmental geo-referenced field data and remote sensing spatial information in Central Africa. How to combine the Cyber-Tracker with TREES information system. *www.cybertracker.org/Trees_Ecofac.html*

Jeftic, L., Milliman, J.D., & Sestini, G. (Eds., 1994). *Climatic change and the Mediterranean: 1*. Chichester: Wiley & Sons

Jeftic, L., Keckes, S., & Pernetta, J.C. (Eds., 1996). *Climatic Change and the Mediterranean: Environmental and societal impacts of climatic change and sea level rise in the Mediterranean region: 2.* Chichester: Wiley & Sons.

Johnson, R.D., & Kasischke, E.S. (1998). Change vector analysis: a technique for the multispectral monitoring of land cover and condition. *International Journal of Remote Sensing, 19(3)*, 411-426

Justice, C.O., Wharton, S.W., & Holben, B.N. (1981). Application of digital terrain data to quantify and reduce the topographic effect on Landsat data. *International Journal of Remote Sensing, 2(3)*, 213-230

Justice, C.O., Townshend, J.R.G., Holben, B.N., & Tucker, C.J. (1985). Analysis of the phenology of global vegetation using meteorological satellite data. *International Journal of Remote Sensing, 6*, 1271-1318

Karavokyris, G., & partners (1998). *Environmental Rehabilitation of Lake Koronia, Greece. A Master Plan. Final Report (with annexes).* European Commission, Directorate General XVI, Regional Policy and Cohesion

Kaufman, Y.C., & Sendra, C. (1988). Algorithm for automatic atmospheric correction to visible and near-IR satellite imagery. *International Journal of Remote Sensing, 9(8),* 1357-1381

Kauth, R.J., & Thomas, G.S. (1976). *The tasseled cap – a graphic description of the spectral-temporal development of agricultural crops as seen by Landsat* (pp. 41-57). Proceedings of Remotely Sensed Data. West Lafayett: Purdue University Press.

Kayser, B., & Thompson, K. (1964). *Social and economic atlas of Greece*. Athens

Keeley, J.E. (1986). Resilience of Mediterranean shrub communities to fire. In B. Dell, A.J.M. Hopkins, & B.B. Lamont (Eds.), *Resilience in Mediterranean-type ecosystems* (pp. 95-112). Dordrecht, Boston, Lancaster: Kluwer Academic Publishers

Kieffer, H.H., & Wildey, R.L.(1996). Establishing the moon as a spectral radiance standard. *Journal of Atmospheric Ocean. Techn., 13,* 360-375

King, R., Proudfoot, L., & Smith, B. (1997). *The Mediterranean – Environment and society*. London, New York: Arnold Publication

Kirkby, M.J. (1980). The stream head as a significant geomorphic threshold. In D.R Coates & J.D. Vitek (Eds.). *Thresholds in Geomorphology* (pp. 53-74). London: George Allen and Unwin

Kirkby, M.J., Atkinson, K., & Lockwood. J. (1990). Aspect, vegetation cover and erosion on semi-arid hillslopes. In J.B. Thornes (Ed.), *Vegetation and erosion: Processes and environments* (pp. 25-40). Chichester, New York, Brisbane: Wiley & Sons

Klug, H., Langanke, T., & Lang, S. (2003). IDEFIX – Integration einer Indikatorendatenbank für landscape metrics in ArcGIS 8.x. In S. Strobl, T. Blaschke, & G. Griesebner (Eds.), *Angewandte Geographische Informationsverarbeitung XV* (pp. 224-233). Salzburg

Kneizys, F.X., Shettle, E.P., Gallery, W.O., Chetwynd, J.H., Abreu, L.W., Selby, J.E.A., Fenn, R.W., & McClatchey, R.A. (1980). *Atmospheric Transmittance/ Radiance – Computer Code LOWTRAN 5.* Environmental Research Papers 697. Hanscom AFB, Massachusetts: Air Force Geophysics Laboratory, Optical Physics Division, AFGL-TR-89-0067

Kneizys, F.X., Shettle, E.P., Abreu, L.W., Chetwynd, J.H., Anderson, G.P., Gallery, W.O., Selby, J.E.A., & Clough, S.A. (1988). *User's Guide to LOWTRAN-7*. Hanscom AFB, Massachusetts: Air Force Geophysics Laboratory, AFGL-TR-88-0177

Konstantinidis, P., & Tsiourlis, G. (2003). *Description – analysis and mapping of vegetation units (habitats) of Lagadas County (Thessaloniki, Greece).* NAGREF – Forest Research Institute, GeoRange project

Kosmas, C. Kirkby, M.J., & Geeson, N. (1999). *Manual on key indicators of desertification and mapping environmentally sensitive areas to desertification.* European Commission publication EUR 18882

Kötz, B., Schaepman, M., Morsdorf, F., Bowyer, P., Itten, K., & Allgöwer, B. (2004). Radiative transfer modelling within a heterogeneous canopy for estimation of forest fire fuel properties. *Remote Sensing of Environment, 92*, 332-344

Koutsias, N., & Karteris, M. (1998). Logistic regression modelling of Multitemporal Thematic Mapper data for burned area mapping. *International Journal of Remote Sensing*, *19(18)*, 3499-3514.

Koutsias, N., & Karteris, M. (2000). Burned area mapping using logistic regression modelling of a single post-fire Landsat-5 Thematic Mapper image. *International Journal of Remote Sensing*, *214(4)*, 673-687

Kramer, H.J. (2002). *Observation of the Earth and its environment. Survey of missions and sensors.* Berlin, Heidelberg, New York, Barcelona, Hong Kong, London, Milano, Paris, Tokyo: Springer

Kraus, K. (1996). *Photogrammetrie, Band 2, Verfeinerte Methoden und Anwendungen.* 3rd edition. Bonn: Dümmler

Kraus, K. (1997). *Photogrammetrie, Band 1, Grundlagen und Standardverfahren.* 6th edition. Bonn: Dümmler

Kuhnhotz-Lordat, G. (1958). L'écran vert. *Mémorial du Musé National de la Histoire Naturelle*, *9,* 1-276

Kuemmerle, T. (2003). Investigating the impact of livestock grazing by means of remote sensing and GIS. A case study in Northern Greece using multi-date spectral mixture analyis and cost surface modelling. *Diploma thesis University of Trier.* Trier, unpublished

Kuemmerle, T., Röder, A., & Hill, J. (2006). Separating grassland and shrub vegetation by multidate pixel-adaptive spectral mixture analysis. *International Journal of Remote Sensing* (in print).

Kushla, J.D., & Ripple, W.J. (1998). Assessing wildfire effects with Landsat Thematic Mapper data. *International Journal of Remote Sensing, 19(13),* 2493-2507

Lacaze, B. (1996). Spectral characterisation of vegetation communities and practical approaches to vegetation cover changes monitoring. In J. Hill, & D. Peter (Eds.), *The use of remote sensing for land degradation and desertification monitoring in the Mediterranean basin - state of the art and future research* (pp. 149-166). Proceedings of a workshop, jointly organized by JRC/IRSA and DGXII/D-2/D-4, Valencia, 13-15 June 1994, Valencia, EUR 16732 EN. Luxembourg: Office for Official Publications of the European Communities

Lacaze, B. (2005). Remotely-sensed optical and thermal indicators of land degradation. In M. Oluic (Ed.), *New strategies for European Remote Sensing* (pp. 211-217). Proceedings of the 24th Symposium of the European Association of Remote Sensing Laboratories, Dubrovnik, Croatia, 25-27 May 2004

Lacaze, B., Caselles, V., C. Coll, Hill, J., Hoff, C., de Jong, S., Mehl, W., Negendank, J.F.W., Riezebos, H., Rubio, F., Sommer, S., Teixeira Filho, J., & Valor, E. (1996). *Integrated approaches to desertification mapping and monitoring in the Mediterranean basin. Final report of the DeMon-1 project*, edited by J. Hill, EUR 16448 EN. Luxembourg: Office for Official Publications of the European Communities

Lambin, E.F. (1996). Change detection at multiple temporal scales: seasonal and annual variation in landscape variables. *Photogrammtric Engineering and Remote Sensing, 62*, 931-938

Lambin, E.F., & Strahler, A.H. (1994a). Change-vector analysis in multitemporal space: a tool to detect and categorize land-cover change processes using high temporal resolution satellite data. *Remote Sensing of Environment, 48*, 231-244

Lambin, E.F., & Strahler, A.H. (1994b). Indicators of land-cover change for change-vector analysis in multitemporal space at coarse spatial scales. *International Journal of Remote Sensing, 15,* 2099-2199

Lambin, E.F., & Ehrlich, D. (1997). Land-cover changes in sub-Saharan Africa (1982-1991): application of a change index based on remotely sensed surface temperature and vegetation indices at a continental scale. *Remote Sensing of Environment, 61,* 181-200

Lange, R.T. (1969). The Piosphere: Sheep track and dung patterns. *Journal of Range Management, 22(6)*, 396-400

Lange, R.T., & Graham, C.J. (1983). Rabbits and the failure of regeneration in Australia's arid zone Acacia. *Australian Journal of Ecology, 8,* 377-81

Le Houérou, N.H. (1981). Impact of man and his animals on Mediterranean vegetation. In F. Di Castri, W. Godall, & R.I. Specht (Eds.), *Ecosystems of the world*, *11: Mediterranean-type shrublands* (pp. 479-521). New York: Elsevier

Le Houérou, N.H. (1998). Environmental constraints to livestock husbandry in arid lands. In V.P. Papanastasis, & D. Peter (Eds.), *Ecological basis of livestock grazing in Mediterranean ecosystems* (pp. 210-226). Proceedings of the International Workshop held in Thessaloniki (Greece) October 23-25, 1997. Luxembourg: Office for Official Publications of the European Communities

Legakis, A. (Ed.) (1998). *Ministry of Environment, Physical Planning and Public Works: First national report on the Convention on Biological Diversity.* Athens

Legg, C., Papanastasis, V.P., Heathfield, D., Arianoutsou, M., Kelly, A., Muetzelfeldt, R., & Mazzoleni, S. (1998). Modelling the impact of grazing on vegetation in the Mediterranean: the approach of the ModMED project. In V.P. Papanastasis, & D. Peter (Eds.), *Ecological basis of livestock grazing in Mediterranean ecosystems* (pp. 189-199). Proceedings of the International Workshop held in Thessaloniki (Greece) on October 23-25, 1997. Luxembourg: Office for Official Publications of the European Communities

Leica Geosystems (2003a). *Erdas Field Guide™*. 7th edition. Atlanta, Georgia: GIS & Mapping, LLC

Leica Geosystems (2003b). *Leica photogrammetry suite. Orthobase / orthobase Pro user's guide.* Atlanta, Georgia: GIS & Mapping, LLC

Lewis, M., Jooste, V., & De Gasparis, A (2000). *Hyperspectral discrimination of arid vegetation* (pp. 148-151). Proceedings 28th International Symposium on Remote Sensing of Environment, 27-31 March 2000, Cape Town

Lienau, C. (1989). *Griechenland: Geographie eines Staates der europäischen Südperipherie.* Wissenschaftliche Länderkunden Band 32. Darmstadt: Wissenschaftliche Buchgesellschaft Darmstadt

Lillesand, T.M., & Kiefer, R.W. (2000). *Remote sensing and image interpretation*. New York: Wiley & Sons

Linés Escardó, A. (1970). The climate of the Iberian peninsula. In C.C. Wallén (Ed.), *Climates of Northern and Western Europe.* World survey of climatology, vol. 5. (pp. 195-227). Amsterdam, London, New York: Elsevier

Lobo, A, Legrendre, P., Rebollar, J.L.G., Carreras, J., & Ninot , J.-M. (2004). Land cover classification at a regional scale in Iberia: separability in a multi-temporal and multi-spectral data set of satellite images. *International Journal of Remote Sensing, 25,* 205-213

Lock, G., & Stancic, Z. (1995). *Archaeology and geographical information systems.* London: Taylor & Francis

Lu, D., Batistella, M., Moran, E., & Mausel, P. (2004a). Application of spectral mixture analysis to Amazonian land-use and land-cover classification. *International Journal of Remote Sensing, 25 (23)*, 5345-5358

Lu, D., Mausel, P., Brondízio, E., & Moran, E. (2004b). Change detection techniques. *International Journal of Remote Sensing, 25(12),* 2365-2407

Lu, H., Raupach, M., & McVicar, T.R. (2001). *Decomposition of vegetation cover into woody and herbaceous components using AVHHR NDVI time series.* CSIRO Land and Water Canberra, Technical Report 35/01, Australia

Mainguet, M. (1994): Desertification – Natural Background and Human Mismanagement. Berlin, Heidelberg: Springer-Verlag

Malling, D.H. (1992). *Coordinate Systems and Map Projections*. New York: Pergamon Press

Marchetti, M., Ricotta, C. & Volpe, F. (1995). A qualitative approach to the mapping of post-fire regrowth in Mediterranean vegetation with Landsat-TM. *International Journal of Remote Sensing*, *16,* 2487-2494

Margaris, N.S. (1981). Adaptive strategies in plants dominating Mediterranean-type shrublands. In F. Di Castri, W. Godall, & R.I. Specht (Eds.), *Ecosystems of the world, vol. 11: Mediterranean-type shrublands* (pp. 309-316). New York: Elsevier

Markham, B.L., & Barker, J.L. (1986). Landsat MSS and TM post-calibration dynamic ranges, exo-atmospheric reflectances and at-satellite temperatures. In EOSAT (Eds.), *Landsat Technical Notes – New Look-Up Tables.* Lanham, MD

Markham, B.L., & Barker, J.L. (1987). Radiometric properties of U.S. processed Landsat-MSS data. *Remote Sensing of Environment, 22(1),* 39-71

Markham, B.L., Barker, J.L., Boncyk, W.C., Kaita, E., & Helder, D.L. (1996). Landsat-7 Enhanced Thematic Mapper Plus in-flight radiometric calibration. *International Geoscience and Remote Sensing Symposium, 2,* 1270-1272

Markham, B.L., Barker, J.L. Kaita, E., Seiferth, E., & Morfitt, R. (2003). On-orbit performance of the Landsat-7 ETM+ radiometric calibrators. *International Journal of Remote Sensing, 24(2),* 265-285

Masek, J.G., Honzak, M., Goward, S.N., Liu, P., & Pak, E. (2001). Landsat-7 ETM+ as an observatory for land cover initial radiometric and geometric comparisons with Landsat-5 Thematic Mapper. *Remote Sensing of Environment, 78,* 118-130

May, A.M.B., Pinder, J.E., & Kroh, G.C. (1997). A comparison of Landsat Thematic Mapper and SPOT multi-spectral imagery for the classification of shrub and meadow vegetation in northern California. *International Journal of Remote Sensing*, *18,* 3719-3728

Mazzoleni, S., Di Pasquale, G., & Mulligan, M. (2004). Conclusion: reversing the consensus on Mediterranean Desertification. In S. Mazzoleni, G. Di Pasquale, M. Mulligan, P. Di Martino, & F. Rego (Eds.), *Recent dynamics of Mediterranean vegetation and landscape* (pp. 281-286). New York: Wiley & Sons

McGarigal, K. (2002). Landscape pattern metrics. In A.H. El-Shaarawi, & W.W. Piegorsch (Eds.), *Encyclopedia of environmentrics, vol. 2* (pp. 1135-1142). Sussex: Wiley & Sons

McGwire, K., Minor, T., Fenstermaker, L. (2000). Hyperspectral mixture modelling for quantifying sparse vegetation cover in arid environments. *Remote Sensing of Environment*, *72,* 360-374

Mertens, B., Sunderlin, W., Ndoye, O., & Lambin, E.F. (2000). Impact of macro-economic changes on deforestation in south Cameroon: Integration of household survey and remotely sensed data. *World Development, 28(6)*, 983-999

Meyer, F., & Kockel, F. (1985). Das nordostgriechische Kristallin. In V. Jacobshagen (Ed), *Geologie von Griechenland.* Beiträge zur regionalen Geologie der Erde, Band 19 (pp. 188-201). Berlin, Stuttgart: Borntraeger

Mika, A.M. (1997). Three decades of Landsat instruments. *Photogrammetric Engineering & Remote Sensing, 63(7),* 839-852

Milchunas, D.G., Sala, O.E., & Lauenroth, W.K. (1988). A generalised model of the effects of grazing by large herbivores on grassland community structures. *American Naturalist, 130*, 168-198

Millán, M.M., Estrela, M.J., & Badenas, C. (1998). Synoptic analysis of processes relevant to forest fire dynamics on the Spanish Mediterranean coast. In J.M. Moreno (Ed.), *Large forest fires* (pp. 1-30). Leiden: Blackhuys Publishers

MODMED (1998). *ModMED - Modelling vegetation dynamics and degradation in Mediterranean ecosystems*, Final Report, [EU-DGXXII, ENV4-CT95-0139], Brussels

Moody, A., & Johnson, D.M. (2001). Land-surface phenologies from AVHRR using the discrete Fourier transform. *Remote Sensing of Environment, 75*, 305-323

Mooney, H.A., & Hobbs, R.J. (1986). Resilience at the individual plant level. In B. Dell, A.J.M. Hopkins, & B.B. Lamont (Eds.), *Resilience in Mediterranean-type ecosystems* (pp. 65-82). Dordrecht, Boston, Lancaster: Kluwer Academic Publishers

Moran, M.S., Bryant, R., Thome, K., Ni, W., Nouvellon, Y., Gonzalez-Dugo, M.P., Qi, J., & Clarke, T.R. (2001). A refined empirical line approach for reflectance factor retrieval from Landsat-5 TM and Landsat-7 ETM+. *Remote Sensing of Environment, 78,* 71-82

Moreno, J.M. (1999). Forest Fires: Trends and implications in desertification prone areas of southern Europe. In P. Balabanis, D. Peter, A. Ghazi, & M. Tsogas (Eds.), *Mediterranean desertification. Research results and policy implications* (pp. 115-150). Proceedings of the International Conference, 29th October to 1st November, 1996, Crete, Greece

Moreno, J.M., & Oechl, W.C. (1994). *Global change and Mediterranean-type ecosystems.* Berlin: Springer

Moreno, J.M., Vázquez, A., & Vélez, R. (1998). Recent history of forest fires in Spain. In J.M. Moreno (Ed.), *Large forest fires* (pp. 159-185). Leiden: Blackhuys Publishers

Müller, M. (1996). *Handbuch ausgewählter Klimastationen der Erde*. 5th edition. Trier.

Mulligan, M., Burke, S.M., & Ramos, C. (2004). Climate change, land-use change and the "desertification" of Mediterranean Europe. In S. Mazzoleni, G. Di Pasquale, M. Mulligan, P. Di Martone, & F. Rego (Eds.), *Recent dynamics of the Mediterranean vegetation and landscape* (pp. 259-280). Chichester: Wiley & Sons

Mulligan, M., & Wainwright, J. (2004). Modelling and model building. In J. Wainwright, & M. Mulligan (Eds.), *Environmental modelling: finding simplicity in complexity* (pp. 7-73). Chichester: Wiley & Sons

Narjisse, H. (1998). Ecological health of Mediterranean rangelands: is grazing livestock the prominent driving force? In V.P. Papanastasis, & D. Peter (Eds.), *Ecological basis of livestock grazing in Mediterranean ecosystems* (pp. 287-298). Proceedings of the International Workshop held in Thessaloniki (Greece) on October 23-25, 1997. Luxembourg: Office for Official Publications of the European Communities

Nastis, A.S. (1998). Plant-animal interactions. In V.P. Papanastasis, & D. Peter (Eds.), *Ecological basis of livestock grazing in Mediterranean ecosystems* (pp. 200-209). Proceedings of the International Workshop held in Thessaloniki (Greece) on October 23-25, 1997. Luxembourg: Office for Official Publications of the European Communities

National Statistical Service of Greece (2002). *Catalogue of statistical publications*. General Secretary of the National Statistical Service of Greece. Athens

Naveh, Z. (1988). Multifactorial reconstruction of semiarid Mediterranean landscapes for multi-purpose land uses. In E.B. Allen (Ed.), *The reconstruction of disturbed arid lands – an ecological approach* (pp. 234-256). Boulder: Westview Press

Naveh, Z. (1994). The role of fire and its management in the conservation of Mediterranean ecoystems and landscapes. In J.M. Moreno, & W.C. Oechel (Eds.), *The role of fire in Mediterranean-type ecosystems* (pp. 163-186). New York, Berlin, Heidelberg: Springer

Nouvellon, Y., Moran, M. S., Seen, D. L., Bryant, R., Rambal, S., Ni, W., Bégué, A., Chehbouni, A., Emmerich, W. E., Heilman, P., & Qi, J. (2001). Coupling a grassland ecosystem model with Landsat imagery for a 10-year simulation of carbon and water budgets. *Remote Sensing of Environment, 78,* 131-149

Noy-Meir, I. (1998). Effects of grazing on Mediterranean grasslands: the community level. In V.P. Papanastasis, D. & Peter (Eds.), *Ecological basis of livestock grazing in Mediterranean ecosystems* (pp. 27-39). Proceedings of the International Workshop held in Thessaloniki (Greece) on October 23-25, 1997. Luxembourg: Office for Official Publications of the European Communities

Oba, G., Post, E., Stenseth, N.C., & Lusigi, W.J. (2000). The role of small ruminants in arid zone environments: a review of research perspectives. *Annals of arid zone, 39(3)*, 305-332

Okin, G.S., Okin, W.J., Roberts., D.A., & Murray, B. (1998). Multiple endmember spectral mixture analysis: application to an arid/semi-arid landscape. In R.O. Green (Ed.), *Proceedings 10th Airborne Visible/Infrared Imaging Spectrometer (AVIRIS) Workshop, Pasadena, 1998*

Okin, G.S., Roberts, D.A., Murray, B., & Okin, W.J. (2001). Practical limits on hyperspectral vegetation discrimination in arid and semiarid environments. *Remote Sensing of Environment, 77*, 212-225

Organsiation for Economic Cooperation and Development (OECD) (Ed., 2001). *OECD Environmental indicators. Towards sustainable development.* Paris http://www.oecd.org/dataoecd/7/47/24993546.pdf)

Osborn, F.V., & Parker, G.E. (2003). Linking two elephant refuges with a corridor in the communal lands of Zimbabwe. *African Journal of Ecology*, *41(1)*, 68-74

Pala, V., & Pons, X. (1995). Incorporation of relief in polynom-based geometric correction. *Photogrammetric Engineering & Remote Sensing, 61(7)*, 935-944

Papachristou, T.G., & Platis, P.D. (1998). Small ruminant grazing in Mediterranean kermes oak shrublands. In V.P. Papanastasis, & D. Peter (Eds.), *Ecological basis of livestock grazing in Mediterranean ecosystems* (pp. 254-258). Proceedings of the International Workshop held in Thessaloniki (Greece) on October 23-25, 1997. Luxembourg: Office for Official Publications of the European Communities

Papanastasis, V.P. (1998). Livestock grazing in Mediterranean ecosystems: an historical and policy perspective. In V.P. Papanastasis, & D. Peter (Eds.), *Ecological basis of livestock grazing in Mediterranean ecosystems* (pp. 5-10). Proceedings of the International Workshop held in Thessaloniki (Greece) on October 23-25, 1997. Luxembourg: Office for Official Publications of the European Communities

Papanastasis, V.P. (2003a). *Alternative management strategies in the Lagadas test site.* The GeoRange Project, Final Report, University of Trier, Trier, GeoRange Project [DGXII, EESD, EVK2-CT2000-00091

Papanastasis, V.P. (2003b). *Analysis of range management histories.* The GeoRange Project, Final Report, University of Trier, Trier, GeoRange Project [DGXII, EESD, EVK2-CT2000-00091

Papanastasis, V.P. & Kazaklis, A. (1998). Land use changes and conflicts in the Mediterranean-type ecosystems of Western Crete. In Rundel, P.W., Montenegro, G., & Jaksic, F.M. (Eds.), *Landscape disturbance and biodiversity in Mediterranean-type ecosystems* (pp. 141-153). Berlin, Heidelberg, New York: Springer

Papoulia, S., Kazantzidis, S., & Tsiourlis, G. (2003). *Distribution of the bird fauna in shrub lands and forests of Lagadas area (Thessaloniki, Greece).* NAGREF – Forest Research Institute, GeoRange project

Patterson, M.W., & Yool, S.R. (1998). Mapping fire-induced vegetation mortality using Landsat 5 Thematic Mapper data: a comparison of linear transformation techniques. *Remote Sensing of Environment, 65*, 122-132

Pausas, J.G., & Vallejo, V.R. (1999). The role of fire in European Mediterranean ecosystems. In E. Chuvieco (Ed.), *Remote sensing of large wildfires* (pp. 3-16). Berlin: Springer

Pax-Lenney, M., & Woodcock, C.E. (1997). Monitoring Agricultural Lands in Egypt with Multitemporal Landsat TM Imagery: How Many Images Are Needed? *Remote Sensing of Environment, 59*, 522-529

Pech, R.P., Davies, A.W., Lamacraft, R.R., & Graetz, R.D. (1986). Calibration of Landsat data for sparsely vegetated semi-arid rangelands. *International Journal of Remote Sensing*, *7,* 1729-1750

Pereira, J.M.C (1999). A comparative evaluation of NOAA/AVHRR vegetation indexes for burned surface detection and mapping. *IEEE Transactions on Geoscience and Remote Sensing, 37(1)*, 217-226

Pereira, J.M.C., Chuvieco, E., Beaudoin, A., & Desbois, N. (1997). Remote sensing of burned areas: a review. In E. Chuvieco (Ed.). *A review of remote sensing methods for the study of large wildland fires* (pp. 127-184). Megafires project ENV-CT96-0256. Alcalá de Henares

Perez-Trejo, F. (1994). *Desertification and Land Degradation in the European Mediterranean*. EUR 14850 EN. Luxembourg: Office of Official Publications of the European Communties

Petit, C.C., & Lambin, E.F. (2001). Integration of multi-source remote sensing data for land cover change detection. *International Journal of Geographical Information Science, 15*, 785-803

Petit, C.C., Scudder, T., & Lambin, E.F. (2001). Quantifying processes of land-cover change by remote sensing: resettlement and rapid land cover change in south-eastern Zambia. *International Journal of Remote Sensing, 22,* 3435-3456

Pickup, G. (1996). Estimating the effects of land degradation and rainfall variation on productivity in rangelands: An approach using Remote Sensing and models of grazing and herbage dynamics. *Journal of Applied Ecology, 33,* 819-832

Pickup, G., & Chewings, V.H. (1988). Estimating the distribution of grazing and patterns of cattle movement in a large arid zone Paddock: an approach using animal distribution models and Landsat imagery. *International Journal of Remote Sensing, 9(9)*, 1469-1490

Pickup, G., & Chewings, V.H. (1994). A grazing gradient approach to land degradation assessment in arid areas from remotely-sensed data. *International Journal of Remote Sensing, 15(2)*, 597-617

Pickup, G., Bastin, G.N., & Chewings, V.H. (1998). Identifying trends in land degradation in non-equilibrium rangelands. *Journal of Applied Ecology, 35(3)*, 365-377

Pinty, B., & Verstraete, M. (1991). GEMI: A non-linear index to monitor global vegetation from satellites. *Vegetatio, 101,* 15-20

Pinty, B., & Verstraete, M. (1992). On the design and validation of bidirectional reflectance and albedo models. *Remote Sensing of Environment, 41,* 155-167

Pippan, Th. (1976). Überblick über die Geologie Festlandgriechenlands und des Peloponnes. In H. Riedl (Ed.), *Beiträge zur Landeskunde von Griechenland* (pp. 59-90). Arbeiten aus dem Geographischen Institut der Universität Salzburg Band 6. Salzburg

Preissler, H. (1996). *Spectral Data Catalogue of the Field Campaign in Crete, Greece (2.10.-9.10. 1996).* Project report EU-contract ENV4-CT95-0166, JRC, Italy

Preissler, H., Bohbot, H., Mehl, W., & Sommer, S. (1998). MESPEC – a Spectral Database as a Tool to Support the Use of Imaging Spectroscopy Data for Environmental Monitoring. In M. Schaepman, D. Schlaepfer, & K. Itten. (Eds.), *1st EARSeL Workshop on Imaging Spectroscopy* (pp. 455-462). Zürich, 6-8 October 1998

Price, J.C. (1987a). Radiometric calibration of satellite sensors in the visible and near infrared – history and outlook. *Remote Sensing of Environment, 22(1),* 3-9

Price, J.C. (1987b). Calibration comparison for the Landsat-4 and 5 multispectral scanners and thematic mappers. *Applied Optics, 28(3),* 265-471

Psilovikos, A.A. (1993). The main physicogeographical problems of northern Greece (Thrace and Macedonia). In H. Riedl (Ed.), *Beiträge zur Landeskunde von Griechenland IV* (pp. 9-34). Salzburger Geographische Arbeiten Band 22. Salzburg

Psilovikos, A.A., & Sotiriadis, L.D. (1983). The neotectonic graben complex of the Serbo-Macedonian Massif at the area of Promygdonia Basin in Northern Greece. In L.D. Sotiriadis, A.A. Psilovikos, E. Vavliakis, & G. Syrides (Eds.), *Some tertiary and quarternary basins of Macedonia/Greece. Formation and Evolution* (pp. 21-54). Clausthaler Geologische Abhandlungen 44. Clausthal-Zellerfeld

Quézel, P. (1981). Floristics and phytosociology of Mediterranean matorral. In F. Di Castri, D.W. Goodall, & R.L. Specht (Eds.), *Mediterranean-type shrublands, Ecosystems of the world, 11* (pp. 107-121). Amsterdam, Oxford, New York: Elsevier

Quézel, P. (2004). Large-scale post-glacial distribution of vegetation structures in the Mediterranean region. In S. Mazzoleni, G. Di Pasquale, M. Mulligan, P. Di Martino, & F. Rego (Eds.), *Recent dynamics of Mediterranean vegetation and landscape* (pp. 3-12). New York: Wiley & Sons

Quinn, R.D. (1986). Mammalian herbivory and resilience in mediterranean-climate ecosystems. In B. Dell, A.J.M. Hopkins, & B.B. Lamont (Eds.), *Resilence in mediterranean-type ecosystems* (pp. 113-128). Dordrecht, Boston, Lancaster: Kluwer Academic Publishers

Quinn, R.D. (1994). Animals, fire, and vertebrate herbivory in Californian chaparral and other Mediterranean-type ecosystems. In J.M. Moreno, & W.C. Oechel (Eds.), *The role of fire in Mediterranean-type ecosystems* (pp. 46-78)**.** New York, Berlin, Heidelberg: Springer

Rackham, O., & Moody, J. (1996). *The making of the Cretan landscape.* Manchester, New York: University Press

Rambal, S., & Hoff, C. (1998). Mediterranean ecosystems and fire: the threats of global change. In J.M. Moreno (Ed.), *Large forest fires* (pp. 187-213). Leiden: Blackhuys Publishers

Rashed, T., Weeks, J. R., Stow, D., & Fugate, D. (2005). Measuring temporal composition of urban morphology through spectral mixture analysis: toward a soft approach to change analysis in crowded cities. *International Journal of Remote Sensing, 26 (4)*, 699-718

Raven, P.H. (1973). The evolution of the Mediterranean flora. In F. Castri., & H.A. Mooney (Eds.), *Mediterranean type ecosystems – Origin and structure* (pp. 213-224). Berlin: Springer

Ray, N., Lehmann, A., & Joly, P. (2002). Modeling spatial distribution of amphibian populations: a GIS approach based on habitat matrix permeability. *Biodiversity and Conservation, 11(12)*, 2143-2165

Ray, T.W., & Murray, B.C. (1996). Nonlinear Spectral Mixing in Desert Vegetation. *Remote Sensing of Environment, 55*, 59-64

Rees, W.G. (2004). Least-cost paths in mountainous terrain. *Computers & Geosciences, 30(3)*, 203-209

Retzlaff, R., Stöver, O., Hill, J., & Stelzer, K. (1998). *Spectral Catalogue of the Field Campaign in the Serranja Baja de la Cuenca, Spain.* University of Trier, Remote Sensing Department, unpublished

Rhoades, E.D., Locke, L.F., Taylor, H.M., & Mcilvain, E.H. (1964). Water intake on a sandy range as effected by 20 Years of differential cattle stocking rates. *Journal of Range Management, 17*, 185-196

Riaño, D., Chuvieco, E., Ustin, S., Zomer, R., Dennison, P., Roberts, D.A., & Salas, J. (2002). Assessment of vegetation regeneration after fire through multitemporal analysis of AVIRIS images in the Santa Monica Mountains. *Remote Sensing of Environment*, *79*, 60-71

Riaño, D., Chuvieco, R., Salas, J., & Aguado, I. (2003). Assessment of different topographic corrections in Landsat-TM data for mapping vegetation types. *IEEE Transactions on Geoscience and Remote Sensing, 41 (5),* 1056-1061

Richards, J.A., & Jia, X. (1999). *Remote Sensing Digital Image Analysis. An Introduction.* 4th edition. Berlin, Heidelberg, New York: Springer Verlag

Ricotta, C., Avena, G.C., Olsen, E.R., Ramsey, R.D., & Winn, D.S. (1998). Monitoring the landscape stability of the Mediterranean vegetation in relation to fire with a fractal algorithm. *International Journal of Remote Sensing*, *19(5),* 871-881

Riggan, P.J., Franklin, S.E., Brass, J.A., & Brooks, F.E. (1994). Perspectives on fire management in Mediterranean ecosystems of southern California. In J.M. Moreno, & W.C. Oechel (Eds.), *The role of fire in Mediterranean-type ecosystems* (pp. 140-162). New York, Berlin, Heidelberg: Springer

Rindfuss, R.R., Walsh, S.J., Turner II, B.L. Fox, J., & Mishra, V. (2004). Developing a science of land change: Challenges and methodological issues. *PNAS, 39(101),* 13976-13981

Rivas-Martinez, S. (Ed.) (1987). *Mapa de Series de Vegetacion de España 1:400000 y Memoria.* Ministerio de Agricultura, Pesca y Alimentación, Serie Técnica, Madrid

Roberts, D.A., Yamaguchi, Y., & Lyon, R.J.P. (1986). *Comparison of various techniques for calibration of AIS data.* Proceedings 2nd AIS workshop, JPL Publications 86-35 (pp. 21-30). Pasadena, CA: Jet Propulsion Laboratory

Roberts, D.A., Smith, M.O., Adams, J.B., & Gillespie, A.R. (1991). Leaf spectral types, residuals and canopy shade in an AVIRIS image. In R.O. Green (Ed.), *Proceedings 3rd Airborne Visible/Infrared Imaging Spectrometer (AVIRIS) Workshop*, Pasadena, 1991

Roberts, D.A, Smith, M.O & Adams, J.B. (1993). Green vegetation, non-photosynthetic vegetation and soils in AVIRIS Data. *Remote Sensing of Environment*, *44*, 255-269

Roberts, D.A., Gardner, M., Church, R., Ustin, S., Scheer, G., & Green, R.O. (1998). Mapping chaparral in the Santa Monica Mountains using multiple endmember spectral mixture models. *Remote Sensing of Environment, 65*, 267-279

Röder, A. (2002). *Spectral data catalogue of the field campaign in Lagadas, Greece (May 2002).* Project report, EU contract EVK2-CT-2000-00091, University of Trier, Remote Sensing Department, unpublished

Röder, A., & Hostert, P. (1998). *Spectral data catalogue of the field campaign in Crete, Greece (September 1998).* Project report, EU contract ENV4-CT95-0166, University of Trier, Remote Sensing Department, unpublished

Röder, A., Hill, J., & Hostert, P. (2001). Radiometric intercalibration of Landsat-TM and -MSS data for quantitative long-term environmental monitoring, In M.F. Buchroithner (Ed.), *A Decade of Trans-European Remote Sensing Cooperation* (pp. 213-218). Proceedings of the 20th EARSeL Symposium, held 14-16 June, 2000, Dresden, Germany

Röder, A., Hill, J., Sommer, S., Mehl, W., Kemper, T., Brundu, G., Vallejo, R., del Barrio, G., Puigdefabregas, J., Papanastasis, V., & Tsiourlis, G. (2002) Geomatics in the assessment and sustainable management of Mediterranean rangelands – The GeoRange project. *Second Workshop of the EARSeL Special Interest Group on Remote Sensing for Developing Countries, 18-20 September 2002, Bonn, Germany*. CD-ROM publication

Röder, A., Hostert, P. Tsiourlis,G., Kasapidis, P., & Hill, J. (2003). Resource Assessment to Support the Sustainable Management of Mediterranean Ecosystems - An Approach Integrating Remote Sensing and Ecology. In A. Belward, E. Binaghi, P.A. Brivio, G.A. Lazarone, & G. Tosi (Eds.), *Proceedings of the International Workshop on Geo-Spatial Knowledge Processing for Natural Resource Management* (pp. 303-309), 28th-29th June 2001, Varese, Italy

Röder, A., Kümmerle, T., & Hill, J. (2004). Extending time-series of satellite images by radiometric intercalibration. In P. Smits, & L. Bruzzone (Eds.), *Analysis of Multi-Temporal Remote Sensing Images* (pp. 21-29). Proceedings of the Second International Workshop on the Analysis of Multitemporal Remote Sensing Images, 16-18 July 2003, EC-JRC, Ispra (VA), Italy. Series in Remote Sensing, 3. New Jersey, London, Singapore: World Scientific

Röder, A., Kümmerle, T., & Hill, J. (2005). Extension of retrospective datasets using multiple sensors. An approach to radiometric intercalibration of Landsat-TM and -MSS data. *Remote Sensing of Environment, 95*, 195-210

Rogan, J., & Yool, S.R. (2001). Mapping fire-induced vegetation depletion in the Peloncillo Mountains, Arizona and New Mexico. *International Journal of Remote Sensing, 22(16)*, 3101-3121

Rogan, J., Franklin, J., & Roberts, D.A. (2002). A comparison of methods for monitoring Multitemporal vegetation change using Thematic Mapper imagery. *Remote Sensing of Environment, 80*, 143-156

Román-Cuesta, R.M., Retana, J., Gracia, M., & Rodriguez, R. (2005). A quantitative comparison of methods for classifying burned areas with LISS-III imagery. *International Journal of Remote Sensing, 26 (9)*, 1979-2003

Rondeaux, G. (1995). Vegetation monitoring by remote sensing: a review of biophysical indices. *Photo-Interprétation*, *95-3,* 197-213

Rondeaux, G., Steven, M.D., Clark, J.A., & Mackay, G. (1998). La Crau: a European test site for remote sensing validation. *International Journal of Remote Sensing, 19(14),* 2775-2788

Rother, K. (1984). *Die mediterranen Subtropen: Mittelmeerraum, Kalifornien, Mittelchile, Kaplan, Südwest- u. Südaustralien.* Braunschweig

Rothermel, R.C. (1972). *A mathematical model for predicting fire spread in wild land fuels*. USDA Forest Service, Research Paper INT-115

Rowntree, K., Duma, M., Kakembo, V., & Thornes, J.B. (2004). Debunking the myth of overgrazing and soil erosion. *Land degradation & development, 15,* 203-214

Royer, A., Charbonneau, L., Brochu, R., Murphy, J., & Teillet, P. (1987). Radiometric comparison of the Landsat-5 TM and MSS sensors. *International Journal of Remote Sensing, 8(4),* 579-591

Royer, A., Charbonneau, L., & Teillet, P.M. (1988). Interannual Landsat-MSS reflectance variation in an urbanized temperate zone. *Remote Sensing of Environment, 24(3),* 423-446

Rubio, J.L. (1995). Desertification - evolution of a concept. In R. Fantechi, D. Peter, P. Balabanis, & J.L. Rubio (Eds.), *Desertification in a European context: physical and socio-economic aspects*. EUR 15415 EN, European Commission, DG XIII, Luxembourg

Ruiz de la Torre, J. (1971). *Arboles y arbustos de la España peninsular.* Madrid: Inst. For. Invest. Exper.

Sabol, D.E., Adams, J.B., & Smith, M.O. (1992). Quantitative subpixel detection of targets in multispectral images. *Journal of Geophysical Research, 97/E2,* 2672-2699

Sabol, D.E., Gillespie, A.R., Adams, J.B., Smith, M.O., & Tucker, C.J. (2002). Structural stage in Pacific Northwest forests estimated using simple mixing models of multispectral images. *Remote Sensing of Environment, 80,* 1-16

Sala, M., & Calvo, A. (1990). Response of four different Mediterranean vegetation types to runoff and erosion. In J.B. Thornes (Ed.), *Vegetation and erosion: Processes and environments* (pp. 347-362). Chichester, New York, Brisbane: Wiley & Sons

Salvador, R., Valeriano, J., Pons, X., & Diaz-Delgado, R. (2000). A semi-automatic methodology to detect fire scars in shrubs and evergreen forests with Landsat MSS time series. *International Journal of Remote Sensing, 21(4),* 655-671

San Miguel-Ayanz, J., & Biging, G.S. (1996). An iterative classification approach for mapping natural resources from satellite imagery. *International Journal of Remote Sensing, 17*, 957-981

Santer, R., Gu, X., Guyot, G., Deuzé, J.L., Devaux, C., Vermote, E., & Verbrugghe, M. (1992). Spot calibration at the La Crau test site (France). *Remote Sensing of Environment, 41(2-3),* 227-237

Sathendryanath, S., Prieur, L., & Morel, A. (1989). A three-component model of ocean colour and its application to remote sensing of phytoplankton pigments in coastal waters. *International Journal of Remote Sensing, 10 (8)*, 1373-1394

Savvaidis, A.S., Pedersen, L.B., Tsokas, G.N., & Dawes, G.J. (2000). Structure of the Mygdonia basin (N. Greece) inferred from MT and gravity data. *Tectonophysics, 317*, 171-186

Schachtschabel, P., Blume, H.-P., Brümmer, G., Hartge, K.-H., & Schwertmann, U. (1989). *Lehrbuch der Bodenkunde.* 12th rev. edition. Stuttgart: Enke

Schlittgen, R., & Streitberg, B.H.J. (1999). *Zeitreihenanalyse*. München, Wien: Oldenburg Verlag

Schmidt, K.S., Skidmore, A.K., Kloosterman, E.H., van Oosten, H., Kumar, L., & Janssen, J.A.M. (2004). Mapping coastal vegetation using an expert system and hyperspectral imagery. *Photogrammetric Engineering & Remote Sensing, 6*, 703-715

Schott, J.R. (1997). *Remote Sensing. The image chain approach*. Oxford, New York: Oxford University Press

Schott, J.R., Salvaggio, C., & Volchok, W.J. (1988). Radiometric scene normalization using pseudo invariant features. *Remote Sensing of Environment, 26(1)*, 1-16

Schüle, W. (1990). Landscapes and climate in prehistory. Interaction of wildlife, man and fire. In J.C. Goldammer (Ed.), *Fire in the tropical biota. Ecosystem processes and global challenges* (pp. 273-318). Ecological Studies 84. Berlin, Heidelberg: Springer

Schultz, J. (2000). *Handbuch der Ökozonen*. Stuttgart: Ulmer

Seligman, N.G., & Perevolotsky, A. (1992). Has the intensive herbivory by domestic ungulates degraded the dominant terrestrial Mediterranean ecosystems of the old world? In C. Thanos (Ed.), *Plant-animal interaction in Mediterranean-type ecosystems* (pp. 47-53). Proceedings of MEDECOS VI, Athens

Seligman, N.G., & Perevolotsky, A. (1994). Has intensive grazing by domestic livestock degraded Mediterranean Basin rangelands? In M. Arianoutsou, & R.H. Groves (Eds.), *Plant-animal interactions in Mediterranean-type ecosystems* (pp. 93-104). Berlin, Dordrecht: Kluwer

Sester, M. (1999). Acquiring transition rules between multiple representations in a GIS: an experiment with area aggregation. *Computers, Environment and Urban Systems*, *23 (1),* 5-17

Settle, J.J., & Drake, N.A. (1993). Linear mixing and the estimation of ground cover proportions. *International Journal of Remote Sensing, 14(6)*, 1159-1177

Shandley, J., Franklin, J., & White, T. (1996). Testing the Woodcock-Harward image segmentation algorithm in an area of southern Californian chaparral and woodland vegetation. *International Journal of Remote Sensing, 17*, 983-1004

Shimabukuro, Y.E., Carvalho, V.C., & Rudorff, B.F.T. (1997). NOAA-AVHRR data processing fort he mapping of vegetation cover. *International Journal of Remote Sensing, 18 (3)*, 671-677

Shimabukuro, Y.E., Batista, G.T., & Mello, E.M.K. (1998). Using shade fraction image segmentation to evaluate deforestation in Landsat Thematic mapper images of the Amazon region. *International Journal of Remote Sensing, 19 (3)*, 535-541

Shoshany, M. (2000). Satellite remote sensing of natural Mediterranean vegetation: a review within an ecological context. *Progress in Physical Geography*, *24(2),* 153-178

Shoshany, M. & Svoray, T. (2002). Multidate adavptive unmixing and its application to analysis of ecosystem transition along a climatic gradient. *Remote Sensing of Environment, 82*, 5-20

Siljeström, P., & Moreno, A. (1995). Monitoring burnt areas by principal components analysis of multitemporal TM data. *International Journal of Remote Sensing, 16(9),* 1577-1587

Slater, P.N., Biggar, S.F., Holm, S.F., Jackson, R.D., Mao, Y., Moran, S., Palmer, M., & Yuan, B. (1986). Absolute radiometric calibration of the Thematic Mapper. *SPIE-Proceedings, 660,* 2-8

Slater, P.N., Biggar, S.F., Holm, R.G., Jackson, R.D., Mao, Y., Moran, M.S., Palmer, J.M., & Yuan, B. (1987). Reflectance- and radiance based methods for in-flight absolute calibration of multispectral sensors. *Remote Sensing of Environment, 22(1),* 11-37

Small, C. (2003). High spatial resolution spectral mixture analysis of urban reflectance. *Remote Sensing of Environment, 88 (1-2)*, 170-186

Small, C. (2004). The Landsat ETM+ spectral mixing space. *Remote Sensing of Environment, 93 (2004)*, 1-17

Small, C. (2005). A global analysis of urban reflectance. *International Journal of Remote Sensing, 26 (4)*, 661-681

Smith, M.O., Johnson, P.E., & Adams, J.B. (1985). Quantitative determination of mineral types and abundances from reflectance spectra using principal component analysis. *Journal of Geo-physical Research, 90,* 792-804

Smith, M.O., Ustin, S.L., Adams, J.B., & Gillespie, A.R. (1990a). Vegetation in deserts: I. A regional measure of abundance from multispectral images. *Remote Sensing of Environment, 31*, 1-26

Smith, M.O., Adams, J.B., & Gillespie, A.R. (1990b). *References endmembers for spectral mixture analysis* (pp. 1-26). Proceedings of the 5th Australasian Remote Sensing Conference, Perth, 1

Smith, M.O., Adams, J.B., & Sabol, D.E. (1994). Spectral mixture analysis – New strategies for the analysis of multispectral data. In J. Hill, & J. Mégier (Eds.), *Imaging spectrometry – A tool for environmental observations* (pp. 221-236). Dordrecht, Boston, London: Kluwer Academic Publishers

Sneath, P.H., & Sokal, R.R. (1973). *Numerical taxonomy.* San Francisco: Freeman

Society for Range Management (1995). New concepts for assessment of rangeland condition. *Journal of Range Management, 48,* 271-283

Sole Sabaris, L. (1978a). El relieve de la Peninsula Ibérica. In M. De Terran & L. Sole Sabaris (Eds.), *Geografia general de España* (pp. 17-25). Barcelona: Editorial Ariel

Sole Sabaris, L. (1978b). Los rebordes oriental y meridional de la Meseta: Cordillera Ibérica y Sierra Morena. In M. De Terran, & L. Sole Sabaris (Eds.), *Geografia general de España* (pp. 74-85). Barcelona: Editorial Ariel

Sole Sabaris, L. (1978c). Las Aguas : Ríos y Lagos. In M. De Terran, & L. Sole Sabaris (Eds.), *Geografia general de España* (pp. 182-208). Barcelona: Editorial Ariel

Song, C., Woodcock, C.E., Seto, K.C., Pax-Lenney, M., & Macomber, S.A. (2001). Classification and change detection using Landsat TM data: When and how to correct atomspheric effects? *Remote Sensing of Environment, 75,* 230-244

Spanos, K., Trakolis, D., Spanos, I., & Malamidis, G. (1998). Classification of forest vegetation in Greece. In T.-B. Larsson (Ed., 2001), *Biodiversity evaluation tools for European forests*. Ecological Bulletin 50, Oxford

Specht, R.L. (1981). Primary production in mediterranean-climate ecosystems regenerating after fire. In F. Di Castri, D.W. Goodall, & R.L. Specht (1981), *Mediterranean-type shrublands. Ecosystems of the world, 11* (p. 643). Amsterdam: Elsevier

Stafford-Smith, D. M., &Reynolds, J.F. (2002). The Dahlem desertification paradigm: a new approach to an old problem. In J.F. Reynolds, & M.D. Stafford-Smith (Eds.), *Global desertification. Do humans cause deserts?* (pp. 403-424). Dahlem workshop report 88. Berlin: Dahlem University Press

Sutcliffe, O.L., Bakkestuen, V., Fry, G., & Stabbetorp, O.E. (2003). Modelling the benefits of farm-land restoration: methodology and application to butterfly movement. *Landscape and Urban Planning, 63(1)*, 15-31

Tabarant, F. (2000). Apport de la télédection et de la modélisation à l'étude de la dynamique de production d'un écosystème méditerranéen de chênes verts (*Quercus ilex*) dans le sud de la France. *PhD Thesis,* Université de Paris

Tanré, D., Herman, M., Deschamps, P.Y., & De Leffe, A. (1979). Atmospheric modelling of the background contribution upon space measurements of ground reflectance including bidirectional properties. *Applied Optics, 18*, 3587-3594

Tanré, D., Herman, M., & Deschamps, P.Y. (1981). Influence of the background contribution upon space measurements of ground reflectance. *Applied Optics, 20*, 3676-3684

Tanré, D., Deroo, C., Duhaut, P., Herman, M., Morcrette, J.J., Perbos, J., & Deschamps, P.Y. (1985). *Effets atmosphériques en télédétection, logiciel de simulation du signal satéllitaire dans le spectre solaire* (pp. 315-319). Proceedings of the 3rd International Colloquium on Spectral Signatures of Objects in Remote Sensing, 16th-20th Dec., Les Arcs, France

Tanré, D., Deschamps, P.Y., Duhaut, P., & Herman, M. (1987). Adjacency effect produced by the atmospheric scattering in Thematic Mapper data. *Journal of Geophysical Research, 92, D10*, 12000-12006

Tanré, D., Deroo, C., Duhaut, P., Herman, J.J., Perbos, J., & Deschamps, P.Y. (1990). Description of a computer code to simulate the signal in the solar spectrum – the 5S code. *International Journal of Remote Sensing, 11(4),* 659-668

Teillet, P.M. (1986). Image correction for radiometric effects in remote sensing. *International Journal of Remote Sensing, 7(12),* 1637-1651

Teillet, P.M. (1997). A status overview of Earth observation calibration/validation for terrestrial applications. *Canadian Journal of Remote Sensing, 23(4),* 291-298

Teilet, P.M., & Fedosojevs, G. (1995). On the dark target approach to atmospheric correction of re-motely sensed data. *Canadian Journal of Remote Sensing, 21*, 374-387

Teillet, P.M., Barker, J.L., Markham, B.L., Irish, R.R., Fedosejevs, G., & Storey, J.C. (2001a). Radiometric cross-calibration of the Landsat-7 ETM+ and Landsat-5 TM sensors based on tandem data sets. *Remote Sensing of Environment, 78,* 39-54

Teillet, P.M., Fedosojevs, G., Gauthier, R.P., O'Neill, N.T., Thome, K.J., Biggar, S.F., Ripley, H., & Meygret, A. (2001b). A generalized approach to vicarious calibration of multiple Earth observation sensors using hyperspectral data. *Remote Sensing of Environment, 77,* 304-327

Thirgood, J.V. (1981). Man and the Mediterranean forest. A history of resource depletion. London: Academic Press

Thomas, D.S.G., & Middleton, N.J. (1994). *Desertification - Exploding the Myth*. London: Wiley & Sons

Thome, K.J. (2001). Absolute radiometric calibration of Landsat 7 ETM+ using the reflectance-based method. *Remote Sensing of Environment, 78,* 27-38

Thome, K.J., Markham, B., Barker, J., Slater, P., & Biggar, S. (1997a). Radiometric calibration of Landsat. *Photogrammetric Engineering & Remote Sensing, 63(7),* 853-858

Thome, K.J., Crowther, B.G., & Biggar, S.F. (1997b). Reflectance- and irradiance-based calibration of Landsat-5 Thematic Mapper. *Canadian Journal of Remote Sensing, 23(4),* 309-317

Thornes, J.B. (1985). The ecology of erosion. *Geography, 70(3),* 222-236

Thornes, J.B. (1990). The interaction of erosional and vegetational dynamics in land degradation: spatial outcomes. In J.B. Thornes (Ed.), *Vegetation and erosion: Processes and environments* (pp. 41-54). Chichester, New York, Brisbane, Toronto, Singapore: Wiley & Sons

Thrash, I. (1997). Infiltration rate around drinking troughs in the Kruger National Park. *Journal of Arid Environment, 35*, 617-625

Thrash, I., & Derry, J.F. (1999). The nature and modeling of biospheres: A review. *Koedoe, 42(2)*, 73-94

Tomaselli, R. (1981). Main physiognomic types and geographic distribution of shrub systems related to Mediterranean climates. In F. Di Castri, D.W. Goodall, & R.L. Specht (Eds.), *Mediterranean-type shrublands, Ecosystems of the world, 11* (pp. 95-106). Amsterdam, Oxford, New York: Elsevier

Tomlin, C.D. (1990). *Geographic information systems and cartographic modelling.* New Jersey: Prentice Hall

Tompkins, S., Mustard, J.F., Pieters, C.M., & Forsyth, D.W. (1997). Optimization of endmembers for spectral mixture analysis. *Remote Sensing of Environment, 56*, 472-489

Toutin, Th. (2002). Error tracking in IKONOS geometric processing using a 3D parametric model. *Photogrammetric Engineering & Remote Sensing, 68 (11)*, 9-30

Toutin, Th. (2004). Geometric processing of remote sensing images: models, algorithms and methods. *International Journal of Remote Sensing, 25 (10)*, 1893-1924

Toutin, Th., Chénier, R., & Carbonneau, Y. (2002). 3D models for high resolution images: examples with Quickbird, Ikonos and Eros. In *International Archives of ISPRS Symposium, vol. 43, Part 4* (p. 547-551). Ottawa, Ontario, Canada, July 8-12, 2002

Townshend, J.R.G., Justice, C.O., & Kalb, V.T. (1987). Characterization and classification of South American land cover types using satellite data. *International Journal of Remote Sensing, 8,* 1189-1207

Trabaud, L. (1981). Impact of man and fire. In F. Di Castri, D.W. Goodall, & R.L. Specht (Eds.), *Mediterranean-type shrublands, Ecosystems of the world, 11* (pp. 523-534). Amsterdam, Oxford, New York: Elsevier

Trabaud, L. (1994). Postfire plant community dynamics in the Mediterranean basin. In J.M. Moreno, & W.C. Oechel (Eds.), *The role of fire in Mediterranean-type ecosystems* (pp. 1-15). New York, Berlin, Heidelberg: Springer

Trimble, S.W. (1990). Geomorphic effects of vegetation cover and management: some time and space considerations in prediction of erosion and sediment yield. In J.B. Thornes (Ed.), *Vegetation and Erosion: Processes and environments* (pp. 55-67). Chichester, New York, Brisbane, Toronto, Singapore: Wiley& Sons

Tsiourlis, G.M. (1997). Evolution of biomass and productivity of grazed and ungrazed kermer oak shrubs in an insular phryganic ecosystem of Naxos, Greece. In V.P. Papanastasis, & D. Peter (Eds.), *Ecological basis of livestock grazing in Mediterranean ecosystems* (pp. 86-89). Proceedings of the International Workshop held in Thessaloniki (Greece) on October 23-25, 1997. Luxembourg: Office for Official Publications of the European Communities

Tsiourlis, G.M. (2003). Personal communications

Tsiouvaras, C.N., Koukoura, Z., Platis, P., & Ainalis, A. (1998). Yearly changes in vegetation of a semi-arid grassland under various stocking rates and grazing systems. In V.P. Papanastasis, & D. Peter (Eds.), *Ecological basis of livestock grazing in Mediterranean ecosystems* (pp. 58-61). Proceedings of the International Workshop held in Thessaloniki (Greece) on October 23-25, 1997. Luxembourg: Office for Official Publications of the European Communities

Tucker, C.J., Vanpraet, C., Sharman, M.I., & van Ittersum, G. (1985). Satellite remote sensing of total herbaceous biomass production in Senegalese Sahel. *Remote Sensing of Environment, 14*, 233-149

Tueller, P. (1991). Remote sensing applications for monitoring rangeland vegetation. *Journal of the Grassland Society of South Africa, 8(4)*, 160-167

Tueller, P. (1995). Remote sensing in the management of rangelands. *Annals of Arid Zone, 34(3)*, 191-207

Tueller, P. (2001). Remote sensing of range utilization and production. *Journal of Range Management, 54*, 77-89

Turcotte, K.M., Lulla, K., & Venugopal, G. (1993). Mapping small scale vegetation changes of Mexico. *Geocarta International, 4*, 73-85

Turner, D.P.; Cohen, W.B.; Kennedy, R.E.; Fassnacht, K.S., & Briggs, J.M. (1999). Relationships between leaf area index and Landsat TM spectral vegetation indices across three temperate zone sites. *Remote Sensing of Environment, 70,* 52-68

Turner, M.G., Hargrove, W.W., Gardner, R.H., & Romme, W.H. (1994). Effects of fire on landscape heterogeneity in Yellowstone National Park, Wyoming. *Journal of Vegetation Science, 5*, 731-742

Turner, M.G., Gardner, R.H., & O'Neill, R.V. (2001). *Landscape ecology in theory and practice. Pattern and processes*. New York, Berlin, Heidelberg: Springer

Twele, A. (2004). *Post-fire vegetation regeneration. The case study of the Masif de l'Étoile fire.* European Commission, Directorate General Joint Research Centre (EUR 21010)

Ungar, E.U., Henkin, Z., Gutamn, M., Dolev, A., Genizi, A., & Ganskopp, D. (2005). Inference of animal activity from GPS collar data on free-ranging cattle. *Rangeland ecology & management, 58(3)*, 256-266

United Nations Convention to Combat Desertification - UNCCD (Ed., 1994). *United Nations Convention to Combat Desertification in Countries Experiencing Serious Drought and/or Desertification, Particularly in Africa.* Bonn

United Nations Environmental Programme (UNEP) (2003). Convention on Biological Diversity, Expert Meeting on Indicators of Biological Diversity including Indicators for Rapid Assessment of Inland Water Ecosystems, Montreal, Canada, 10-12 February 2003. UNEP/CDB/EM-Indicators/1/2 (http://www.biodiv.org/doc/meetings/ind/emind-01/official/emind-01-02.en.pdf)

United States Geological Service (USGS) (1979). *Landsat data user handbook*. Arlington

United States Geological Service (USGS) (1984). *Landsat data user handbook.* Alexandria

Ustin, S.L., Smith, M.O., & Adams, J.B. (1993). Remote sensing of ecological processes: A strategy for developing and testing ecological models using spectral mixture analysis. In J. Ehlringer, & C. Field (Eds.), *Scaling physiological processes: Leaf to globe* (pp. 339-357). New York: Academic Press

Ustin, S.L., Hart, Q.J., Duan, L., & Scheer, G. (1996). Vegetation mapping on Hardwood rangelands in California. *International Journal of Remote Sensing, 17(15)*, 3015-3036

Vallejo, R., & Alloza, J.A. (1998). The restoration of burned lands: The case of eastern Spain. In J.M. Moreno (Ed.), *Large Forest Fires* (pp. 91-108). Leiden: Blackhuys Publishers

Vallejo, R., Duguy, B., Alloza, J.A., Valdecantos, A., & Beaza, J. (2001). *GeoRange – Geomatics in the assessment and sustainable management of Mediterranean rangelands.* 1st report of the GeoRange project (EVK2-2000-22089). Unpublished project report, Brussels

Vallejo, R., Duguy, B., Alloza, J.A., Valdecantos, A., & Beaza, J. (2002). *GeoRange – Geomatics in the assessment and sustainable management of Mediterranean rangelands.* 2nd report of the GeoRange project (EVK2-2000-22089). Unpublished project report, Brussels

Vallejo, R., Duguy, B., Alloza, J.A., Valdecantos, A., & Beaza, J. (2003). *GeoRange – Geomatics in the assessment and sustainable management of Mediterranean rangelands.* 3rd report of the GeoRange project (EVK2-2000-22089). Unpublished project report, Brussels

Vallejo, R., Bautista, S., & Cortina, J. (1999). Restoration for soil protection after disturbances. In L. Trabaud (Ed.), *Life and environment in the Mediterranean* (pp. 301-344). Southampton: WIT press

Van der Leeuw, S.E. (Ed. 1998). *Understanding the natural and anthropogenic causes of land degradation and desertification in the Mediterranean basin – the Archeomedes project. Research Results.* EU-Report 18181 EN. Luxembourg

Van der Leeuw, S.E. (1999). Degradation and desertification: Some lessons from the longterm perspective. In P. Balabanis, D. Peter, A. Ghazi, & M. Tsogas (Eds.), *Mediterranean desertification – Research results and policy implications, vol. 1* (pp. 17-31). Proceedings of the International Conference, Oct 29th-Nov 1st, Crete, Greece

Van der Leeuw, S.E. (2000). Some potential problems with the implementation of Annex IV of the convention to combat desertification. In G. Enne, Ch. Zanolla, & D. Peter (Eds.), *Desertification in Europe: mitigation strategies, land-use planning.* Proceedings of the advanced study course held in Alghero, Sardinia, Italy, from 31 May to 10 June 1999. EUR 19390. Luxembourg: Office for Official Publications of the European Communities

Van Wagtendonk, J.W. (1996). *Use of a Deterministic Fire Growth Model to Test Fuel Treatments.* Sierra Nevada Ecosystem Project, Final Report to Congress. Vol. II: 1471-1492. UC Davis. Davis, CA

Vázquez, A., & Moreno, J.M. (1993). Sensitivity of fire occurrence to meteorological variables in Mediterranean and Atlantic areas of Spain. *Landscape and Urban Planning, 24,* 129-142

Vermote, E., Tanré, E., Deuzé, J.L., Herman, M., & Morcrette, J.J. (1997). Second simulation of the satellite signal in the solar spectrum. An overview. *IEEE Transactions on Geoscience and Remote Sensing, 35,* 675-686

Verstraete, M. (1994a). Retrieving canopy properties from remote sensing measurements. In J. Hill, & J. Mégier (Eds.), *Imaging spectrometry – A tool for environmental observations* (pp. 109-125). Dordrecht, Boston, London: Kluwer Academic Publishers

Verstraete, M. (1994b). The contribution of remote sensing to monitor vegetation and to evaluate its dynamic aspects. In F. Veroustraete, & R. Ceulemans (Eds.), *Vegetation, modeling and climatic change effects* (pp. 207-212). The Hague: SPB Academic Publishing

Viedma, O., Melia, J., Segarra, D., & García-Haro (1997). Modeling rates of ecosystem recovery after fires by using Landsat TM data. *Remote Sensing of Environment, 61,* 383-398

Viegas, D.X. (1998). Weather, fuel status and fire occurrence: predicting large fires. In J.M. Moreno (Ed.), *Large forest fires* (pp. 31-48). Leiden: Blackhuys Publishers

Vinas, O., & Baulies, X. (1995). 1:250,000 land-use map of Catalonia (32,000 km^2) using multi-temporal Landsat-TM data. *International Journal of Remote Sensing 16*, 129-146

Vogelmann, J.E., Helder, D., Morfitt, R., Choate, M.J., Merchant, J.W., & Bulley, H. (2001). Effects of Landsat 5 Thematic Mapper and Landsat 7 Enhanced Thematic Mapper Plus radiometric and geometric calibrations and corrections on landscape characterization. *Remote Sensing of Environment, 78,* 55-70

Wagner, H.G. (2001). *Mittelmeerraum*. Darmstadt

Walker, B. (1993). Rangeland ecology: understanding and managing change. *Ambio, 22 (2-3),* 80-87

Walther, H. (1955). Die Klima-Diagramme als Mittel zur Beurteilung der Klimaverhältnisse für ökologische, vegetationskundliche und landwirtschaftliche Zwecke. *Berichte der Deutschen Botanischen Gesellschaft, 68*, 321-344

Wang, G., Gertner, G., & Anderson, A. B. (2004). Up-scaling methods based on variability-weighting and simulation for inferring spatial information across scales. *International Journal of Remote Sensing*, *25(22),* 4961-4979

Waske, B. (2003). Bewertung des Landschaftszustandes in mediterranen Trockenräumen auf der Basis einer Fernerkundungs- und GIS-gestützten Wasserhaushaltsmodellierung. *Unpublished diploma thesis, University of Trier.* Trier

Welch, R., Jordan, T.R., & Ehlers, M. (1985). Comparative evaluations of the geodetic accuracy and cartographic potential of Landsat-4 and Landsat-5 Thematic Mapper Image Data. *Photogrammetric Engineering & Remote Sensing, 51 (9)*, 1249-1262

Westman, W.E. (1978). Measuring the inertia and resilience of ecosystems. *Bioscience, 28,* 705-710

Westoby, M., Walker, B., & Noy-Meir, I. (1989). Opportunistic management for rangelands not at equilibrium. *Journal of Range Management, 42(4)*, 266-274

Whelan, R.J. (1995). *The ecology of fire*. Cambridge, New York, Melbourne: Cambridge University Press

White R., & Engelen G. (1997). Cellular automata as the basis of integrated dynamic regional modelling. *Environment and Planning, B, 24*, 235-246

White, D.H. (1987). Stocking Rate. In R.W. Snaydon (Ed.), *Ecosystems of the world, vol. 17B: Managed grasslands – Analytical studies* (pp. 227-235). New York: Elsevier

White, P.S., & Pickett, S.T.A. (1985). Natural disturbance and patch dynamics: an introduction. In S.T.A. Pickett, & P.S. White (Eds.), *The ecology of natural disturbance and patch dynamics* (pp. 3-16). Orlando: Academic Press

Wiens, J.A. (1995). Landscape mosaics and ecological theory. In L. Hansson, L. Fahrig, & G. Merriam (Eds.), *Mosaic landscapes and ecological processes* (pp. 1-26). London: Chapman & Hall

Wilkinson, G.G. (1996). A review of current issues in the integration of GIS and remote sensing. *International Journal of Geographical Information Systems, 10 (1)*, 85-101

Williams, R.E., Allred, B.E., DeNio, R.M., & Paulsen, H.E. (1968). Conservation, development and use of world's rangelands. *Journal of Range Management, 21,* 355-360

Woodcock, C.E., Macomber, S.A., Pax-Lenney, M., & Cohen, W.B. (2001). Monitoring large areas for forest change using Landsat: Generalization across space, time and Landsat sensors. *Remote Sensing of Environment, 78,* 194-203

Woodham, R.J., & Gray, M.H. (1987). An analytic method for radiometric correction of satellite multispectral scanner data. *IEEE Transactions on Geosciences and Remote Sensing, GE-25 (3)*, 258-271

Wu, C. (2004). Normalized spectral mixture analysis for monitoring urban composition using ETM+ imager. *Remote Sensing of Environment, 93*, 480-492

Yiakoulaki, M.D., & Papanastasis, V.P. (2003). Die selection of sheep and goats grazing on cereal stubble in Northern Greece. *Unpublished project report* (GeoRange science meeting)

Yiakoulaki, M.D., Zarovali, M.P., Ispikoudis, I., & Papanastasis, V.P. (2002). *Evaluation of small ruminant production systems in the area of Lagadas County.* Proceedings of 3rd National Rangeland Congress. Karpenisi, Greece, 4-6 September 2002, (in press)

Yiakoulaki, M.D., Pantazopoulos, Ch.I., & Papanastasis, V.P. (2003). *Sheep and goat behaviour grazing on stubble in northern Greece.* Proceedings of the International Symposium "Animal Production and Natural Resources Utilization in the Mediterranean Mountain Areas", Ioannina, Eprius, Greece (in press)

Yu, C.Q., Lee, J., & Munro-Stasiuk, M.J. (2003). Extensions to least-cost path algorithms for roadway planning. *International Journal of Geographical Information Science, 17(4)*, 361-376

Zervas, G. (1998). Quantifying and optimizing grazing regimes in Greek mountain systems. *Journal of Applied Ecology, 35*, 983-986

Appendix A: Base data sets and information

A.1 Ayora

A.1.1 Satellite images

Description: Depending on data availability and cloud cover, images were acquired to correspond to the date of maximum photosynthetic activity of vegetation.

Platform	Sensor	Path/Row	Acquisition date	Processing level	Resampling	Provider
Landsat-7	ETM+	199/33	21. 06. 2000	System corr.	NN	Eurimage
Landsat-5	TM	199/33	27. 06. 1999	System corr.	NN	Eurimage
Landsat-5	TM	199/33	07. 05. 1998	System corr.	NN	Eurimage
Landsat-5	TM	199/33	21. 06. 1997	System corr.	NN	Eurimage
Landsat-5	TM	199/33	02. 04. 1997	System corr.	NN	Eurimage
Landsat-5	TM	199/33	04. 07. 1996	System corr.	NN	Eurimage
Landsat-5	TM	199/33	31. 05. 1995	System corr.	NN	Eurimage
Landsat-5	TM	199/33	28. 05. 1994	System corr.	NN	Eurimage
Landsat-5	TM	199/33	07. 04. 1993	System corr.	NN	Eurimage
Landsat-5	TM	199/33	02. 04. 1991	System corr.	NN	Eurimage
Landsat-5	TM	199/33	17. 07. 1989	System corr.	NN	Eurimage
Landsat-5	TM	199/33	23. 06. 1986	System corr.	NN	Eurimage
Landsat-5	TM	199/33	22. 07. 1985	System corr.	NN	Eurimage
Landsat-5	TM	199/33	01. 06. 1984	System corr.	NN	Eurimage
Landsat-5	MSS	199/33	22. 07. 1985	System corr.	NN	Eurimage
Landsat-5	MSS	199/33	01. 06. 1984	System corr.	NN	Eurimage
Landsat-3	MSS	199/33	10. 06. 1982	System corr.	NN	Eurimage
Landsat-2	MSS	214/33	06. 06. 1981	System corr.	NN	Eurimage
Landsat-2	MSS	214/33	02. 06. 1980	System corr.	NN	Eurimage
Landsat-2	MSS	214/33	12. 05. 1979	System corr.	NN	Eurimage
Landsat-2	MSS	214/33	10. 07. 1978	System corr.	NN	Eurimage
Landsat-1	MSS	214/33	18. 06. 1976	System corr.	NN	Eurimage

A.1.2 Digital Elevation Model

Description: DEM interpolated from 10 m contour lines in topographic maps 1:10,000

Source: Instituto Nacional de Información Geográfica (CNIG)

Resolution: 25 m, estimated vertical accuracy 3 m

Reference projection: UTM zone 30, International 1909 ellipsoid, European 1950 (Portugal, Spain) datum

A.1.3 Topographic reference maps

Description	Topographic maps; available map frames: 745, 746, 768, 769, 793, 794, for each frame sheets 11, 12, 13, 14, 21, 22, 23, 24, 31, 32, 33, 34, 41, 42, 43, 44 (all in digital format)
Source	Instituto Valenciano de Cartografia
Scale	1:10,000
Reference projection	UTM zone 30, International 1909 ellipsoid, European 1950 (Portugal, Spain) datum

A.1.4 Land use

Description	Vector data set describing major land cover / land use types
Source	Forest Inventory, Ministerio de Medio Ambiente (published 1994)
Scale	1:50,000
Reference projection	UTM zone 30, International 1909 ellipsoid, European 1950 (Portugal, Spain) datum

A.1.5 Vegetation

Description	Vector data set describing major vegetation types, crown cover classes and density classes; fire areas are included
Source	Forest Service: Plan de Selvicultura Preventiva. Conselleria de Territori i Habitage – Valencia Region Autonomous Government (published 1993), based on 1989 information
Scale	1:50,000
Reference projection	UTM zone 30, International 1909 ellipsoid, European 1950 (Portugal, Spain) datum

A.1.6 Lithology map

Description	Vector data set indicating main associations of bedrock types and lithology classes
Source	Conselleria d'Obres Publiques, Urbanisme i Transports- Valencia Region Autonomous Government, Lithology, industrial rocks use and slide risk in the Valencia region, CD-ROM (published 1998)
Scale	1:50,000
Reference projection	UTM zone 30, International 1909 ellipsoid, European 1950 (Portugal, Spain) datum

A.1.7 Villages

Description	Vector data set characterising urban areas within and near the Ayora site, including information about their main characteristics (type of urban area, density of urbanisation)
Source	Conselleria d'Obres Publiques, Urbanisme i Transports- Valencia Region Autonomous Government, Colección Cartografía Temática, CD-ROM (published 1998)
Scale	1:50,000
Reference projection	UTM zone 30, International 1909 ellipsoid, European 1950 (Portugal, Spain) datum

A.1.8 Road network

Description	Vector data set describing the road network
Source	Conselleria d'Obres Publiques, Urbanisme i Transports- Valencia Region Autonomous Government, Colección Cartografía Temática, CD-ROM (published 1998)
Scale	1:50,000
Reference projection	UTM zone 30, International 1909 ellipsoid, European 1950 (Portugal, Spain) datum

A.1.9 Fire perimeter maps

Description	Vector data set containing fire perimeters from 1978 to 1996, digitised from perimeters drawn on topographic maps
Source	Forest Services - Conselleria de Agricultura i Medi Ambient- Valencia Region Autonomous Government
Scale	1:50,000
Reference projection	UTM zone 30, International 1909 ellipsoid, European 1950 (Portugal, Spain) datum

A.1.10 Meteorological data

Description	Long-term climate records (different observation periods) from meteorological stations around the Ayora test area
Source	Spanish meteorological service, made available through Fundacion CEAM.

A.1.11 Spectral database

Description	Hyperspectral reflectance measurements acquired in the context of different campaigns in Mediterranean countries; DeMon-II (Preissler, 1996; Hostert & Preissler, 1997; Röder & Hostert, 1998), Lucifer (Retzlaff et al., 1998), GeoRange (Röder & Hostert, 1998); field-based and laboratory measurements
Source	ASD II Fieldspec Spectroradiometer, Spectralon Panel
Reference projection	all measurements are located using non-differential GPS

A.1.12 Vegetation sampling

Description	Botanical field surveys (summer months 2002, 2003); 113 plots, x-shaped 40 m transects, point-intersect method with 40 cm sampling interval
Source	Researchers from Fundacion CEAM
Reference projection	UTM zone 30, International 1909 ellipsoid, European 1950 (Portugal, Spain) datum; centre of transect located using non-differential GPS

A.1.13 Field observations

Description	Protocols from various field visits, Photographs
Source	Visual observations by researchers from Fundacion CEAM and RSD, University of Trier
Reference projection	UTM zone 30, International 1909 ellipsoid, European 1950 (Portugal, Spain) datum; located using non-differential GPS

A.1.14 European Soil database

Description	Soil units of Europe at a scale of 1:1,000,000 based on information from archives of national soils information
Source	European Soil Bureau, http://eusoils.jrc.it; http://dataservice.eea.eu.int/
Scale	1:1,000,000
Reference projection	Lambert Azimuthal, user-defined Sphere

A.1.15 Miscellaneous

Description	Different types of reference information including socio-economic characterisation
Source	Project reports to the GeoRange project supplied by Fundacion CEAM (Beatriz Duguy, José Antonio Alloza, Jaime Beaza, Alejandro Valdecantos, Ramon Vallejo)

A.2 Lagadas

A.2.1 Satellite Images

A.2.1.1 Landsat

Description: Depending on data availability and cloud cover, images were acquired to correspond to the date of maximum photosynthetic activity of vegetation. In addition, a late summer image was acquired from August, 2000, characterise evergreen vegetation.

Platform	Sensor	Path/Row	Acquisition date	Proc. level	Resampling	Provider
Landsat-5	TM	183/32	16. 08. 2000	System corr.	NN	Eurimage
Landsat-7	ETM+	183/32	05. 06. 2000	System corr.	NN	Eurimage
Landsat-5	TM	183/32	11. 06. 1999	System corr.	NN	Eurimage
Landsat-5	TM	183/32	10. 07. 1998	System corr.	NN	Eurimage
Landsat-5	TM	183/32	21. 06. 1997	System corr.	NN	Eurimage
Landsat-5	TM	183/32	04. 07. 1996	System corr.	NN	Eurimage
Landsat-5	TM	183/32	02. 07. 1995	System corr.	NN	Eurimage
Landsat-5	TM	183/32	28. 05. 1994	System corr.	NN	Eurimage
Landsat-5	TM	183/32	12. 07. 1993	System corr.	NN	Eurimage
Landsat-5	TM	183/32	23. 06. 1992	System corr.	NN	Eurimage
Landsat-5	TM	183/32	04. 07. 1990	System corr.	NN	Eurimage
Landsat-5	TM	183/32	14. 07. 1988	System corr.	NN	Eurimage
Landsat-5	TM	183/32	10. 06. 1987	System corr.	NN	Eurimage
Landsat-5	TM	183/32	23. 06. 1986	System corr.	NN	Eurimage
Landsat-5	TM	183/32	19. 05. 1985	System corr.	NN	Eurimage
Landsat-5	TM	183/32	03. 07. 1984	System corr.	NN	Eurimage

A.2.1.2 Quickbird

Description: A Quickbird VHR image was acquired in 2003 to characterise late summer rangeland conditions. It was custom-ordered to match the core test area (Kryoneri, Ossa, Eksalofos, Kolhiko and Analipsi) and recorded in off-nadir mode at two different dates (two tiles each) due to Digitalglobe's image acquisition policy.

Platform	Sensor	Path/Row	Acquisition date	Processing level	Resampling	Provider
Quickbird	Mulit, Pan	Custom	03. 07. 2003	Standard imgagery.	CC	Digitalglobe
Quickbird	Mulit, Pan	Custom	03. 07. 2003	Standard imgagery.	CC	Digitalglobe
Quickbird	Mulit, Pan	Custom	03. 08. 2003	Standard imgagery.	CC	Digitalglobe
Quickbird	Mulit, Pan	Custom	03. 08. 2003	Standard imgagery.	CC	Digitalglobe

A.2.1.3 Digital Elevation Model

Description	DEM derived from photogrammetric analysis of aerial orthophotographs (Scale 1:40,000)
Source	Geoapikonisis Ltd., Athens, Greece
Resolution	30 m; estimated vertical accuracy better than 3 m
Reference projection	Transverse Mercator; GRS 1980 spheroid, EGSA87 ellipsoid

A.2.2 Topographic reference maps

Description	Topographic maps; available map sheets: Kilkis, Lakhanas, Sokhos, Sitokhorion, Stavros, Zangliverion, Thermi (all in digital format)
Source	Hellenic Military Geographic Service, publication date 1969
Scale	1:50,000
Reference projection	Transverse Mercator; GRS 1980 spheroid, EGSA87 ellipsoid

A.2.3 Habitats / land use

Description	Vector data set describing major land cover / land use types and habitats according to the Natura 2000 key and EU directive 92/43 (Konstantinidis & Tsiourlis, 2003)
Source	Aerial orthophotos (acquired 1984) complemented by field surveys and plant-physiological studies; mapping and field survey by NAGREF – Forest Research Institute
Scale	1:20,000
Reference projection	Transverse Mercator; GRS 1980 spheroid, EGSA87 ellipsoid

A.2.4 Geology

Description	Simplified vector data set describing major geological formations digitised from paper maps; available map sheets: Kilkis, Lakhanas, Sokhos, Sitokhorion, Stavros, Zangliverion, Thermi
Source	Greek Institute of Geology and Mineral Exploration (publication date 1978), digitised by staff from Laboratory of Range Ecology, Aristotle University of Thessaloniki and NAGREF – Forest Research Institute
Scale	1:50,000
Reference projection	Transverse Mercator; GRS 1980 spheroid, EGSA87 ellipsoid

A.2.5 Administrative borders

Description	Vector data set indicating county and community borders
Source	Lagadas County Administration
Scale	1:50,000
Reference projection	Transverse Mercator; GRS 1980 spheroid, EGSA87 ellipsoid

A.2.6 Villages

Description	Vector data set indicating major villages
Source	Hellenic Military Geographic Service, digitised by staff from the Laboratory of Range Ecology, Aristotle University of Thessaloniki
Scale	1:50,000
Reference projection	Transverse Mercator; GRS 1980 spheroid, EGSA87 ellipsoid

A.2.7 Animal census

Description	Animal census differentiated according to goats, sheep, and cattle; identified by communities; available for 1961, 1971, 1981, 2002
Source	National Statistical Survey of Greece

A.2.8 Meteorological data

Description	Long-term climate records (different observation periods) from meteorological stations within and around the Lagadas test area
Source	National Agricultural Research Foundation, Forest Research Institute, Forest Meteorological Station Network

A.2.9 Spectral database

Description	Hyperspectral reflectance measurements acquired in the context of different campaigns in Mediterranean countries; DeMon-II (Preissler, 1996; Hostert & Preissler, 1997; Röder & Hostert, 1998), Lucifer (Retzlaff et al., 1998), GeoRange (Röder & Hostert, 1998); field-based and laboratory measurements
Source	ASD II Fieldspec Spectroradiometer, Spectralon panel
Reference projection	all measurements are located using non-differential GPS

A.2.10 Vegetation sampling

Description	12 field plots were established to represent different typical grass-land/*Quercus coccifera* shrubland patches. On these patches, surveys characterising the structure of vegetation communities, projected ground cover of major woody species and woody biomass estimations were carried out. In addition, selected indicators of rangeland health (Papanastasis, 2003) were mapped using x-shaped 40 m transects with 16 circle plots of 1 m diameter and at 5 m distance.
Source	Mapping by researchers from NAGREF – Forest Research Institute and Laboratory of Range Ecology, Aristotle University Thessaloniki
Reference projection	Transverse Mercator; GRS 1980 spheroid, EGSA87 ellipsoid; centre of plot/transect located using non-differential GPS

A.2.11 Field observations

Description	Protocols from various field visits, Photographs
Source	Visual observations by researchers from NAGREF – Forest Research Institute; Laboratory of Range Ecology, Aristotle University Thessaloniki; and RSD, University of Trier
Reference projection	Transverse Mercator; GRS 1980 spheroid, EGSA87 ellipsoid; located using non-differential GPS

A.2.12 European Soil database

Description	Soil units of Europe at a scale of 1:1,000,000 based on information from archives of national soils information
Source	European Soil Bureau, http://eusoils.jrc.it; http://dataservice.eea.eu.int/
Scale	1:1,000,000
Reference projection	Lambert Azimuthal, user-defined Sphere

A.2.13 Miscellaneous

Description	Different types of reference information including socio-economic characterisation, animal behaviour, management recommendations etc.
Source	Project reports to the GeoRange project supplied by NAGREF – Forest Research Institute (Georgios Tsourlis) and Laboratory of Range Ecology, Aristotle University Thessaloniki (Vasilios Papanastasis)

Table A.1: Animal numbers in Lagadas County (Source, National Statistical Service Greece) - B: Bovide; S: Sheep; G: Goats

VILLAGE	B_61	B_71	B_91	B_02	S_61	S_71	S_91	S_02	G_61	G_71	G_91	G_02
ADAM	175	125	20	200	1420	1231	797	640	678	688	425	190
AGIOS VASILIOS	207	223	188	45	1624	1569	947	0	703	722	550	662
ANALIPSI	696	354	582	500	5017	2990	2585	3100	3446	1383	2788	2840
APOLLONIA	383	441	155	435	2938	2008	1579	2300	921	873	564	300
ARDAMERI	128	12	33	0	1041	679	601	1600	2461	1704	2603	1280
ARETHOYSA	589	452	311	240	1201	2318	2180	3213	3667	3129	3841	6055
ASKOS	996	650	880	800	3198	1927	3092	2000	3701	3129	3653	4530
ASSIROS	1044	781	757	286	5170	2216	2472	0	866	788	1449	415
EKSALOFOS	560	311	151	11	2887	2231	1325	1200	2103	1383	938	1150
EVAGELISMOS	0	205	31	137	0	1161	1786	2350	0	1453	2420	3000
FILADELFIO	1161	620	1072	1102	1895	1828	349	1615	3166	1898	2794	2825
GERAKAROY	694	425	263	150	1058	589	433	1500	307	92	1012	1040
HRISAVGI	335	273	39	510	1468	1115	1053	1200	147	102	883	860
KALAMOTO	482	148	39	64	3043	2830	3536	4300	1477	1181	4113	2800
KARTERES	815	459	297	545	4161	4840	3107	2300	329	497	953	1800
KAVALLARI	496	1112	3297	2600	3382	2586	2389	1750	632	33	121	1000
KOLHIKO	1066	1064	166	685	7175	5001	3526	0	2849	2500	3765	4025
KRYONERI	871	480	742	670	2986	3211	3734	4200	4161	1497	5365	6400
KSILOPOLI	568	322	93	12	3678	3497	4279	2700	185	173	882	820
LAGKADAS	1546	2365	1443	590	3695	1365	1332	800	96	24	188	120
LAGKADIKI	302	186	161	200	823	453	1196	1900	1081	65	137	1112
LAHANAS	780	294	106	16	1830	2442	1073	2900	149	54	67	1500
LEYKOHORI	310	212	117	136	1354	2030	1974	1400	342	308	344	600
LIVADI	206	93	3	0	1879	1320	1993	1400	5326	3521	4630	6100
LOFISKOS	768	492	578	240	4400	2978	2771	2000	4997	4405	2223	3000
MAYROYDA	0	402	455	175	0	1109	565	220	0	1325	943	1520
MELISSOYRGOS	227	95	49	45	521	576	130	900	2757	1619	1509	4700
NEA APOLLONIA	581	772	2125	2224	5940	3157	4345	7500	2203	1825	3900	5000
NEA MADYTOS	176	129	18	170	644	1454	1088	836	2339	1956	1208	1745
NIKOMIDINO	139	126	96	0	1154	562	649	850	714	296	553	150
NIKOPOLI	424	118	34	0	654	695	749	240	131	87	49	80
NYMFOPETRA	488	320	352	1325	4413	3189	2066	3800	3898	3599	850	1780
OSSA	846	354	113	0	3895	2214	2069	2500	3300	1835	2660	2000
PERISTERA	245	178	165	160	1558	1283	866	1200	2295	3336	9737	9820
PERISTERONAS	468	179	195	0	3026	1335	679	2000	3470	2537	624	2600
PERIVOLAKI	618	1051	1169	1150	721	286	230	0	3	31	160	300
PROFITIS	880	421	367	8	3068	2301	1740	2210	1606	502	1975	1150
SARAKINA	119	59	0	0	852	297	421	440	1009	737	702	560
SHOLARI	464	492	351	19	2284	841	2154	2040	15	30	624	440

continued on next page

Table A.1: Animal numbers in Lagadas County (Source, National Statistical Service Greece) - B: Bovide; S: Sheep; G: Goats

VILLAGE	B_61	B_71	B_91	B_02	S_61	S_71	S_91	S_02	G_61	G_71	G_91	G_02
SKEPASTO	1328	579	238	815	3474	1588	1057	1500	3563	505	1761	3780
SOHOS	1109	634	2494	3870	6389	4612	3409	3300	4393	5480	8105	9300
STEFANINA	253	249	483	421	918	1158	739	850	2390	2093	1565	3060
STIVOS	257	172	138	330	1674	911	965	3000	726	1044	168	800
VASILOYDI	315	163	21	3	651	200	29	538	255	104	284	720
VERTISKOS	311	124	152	320	2487	2510	320	0	303	318	334	0
VOLVI	459	395	126	820	3649	3724	1597	4200	15576	17592	14770	13250
ZAGKLIVERI	251	222	252	290	4119	1647	2437	3400	2764	2931	2498	3600

Appendix B: Data processing

Table B.1: Number of GCPs and error estimates for the Ayora satellite images

	GCPs	RMS x	RMS y	Total RMS (pixel)
am19750629	66	0.1725	0.1653	0.2384
am19760518	67	0.2407	0.1773	0.2989
am19780710	64	0.2938	0.1291	0.3209
am19790512	67	0.2633	0.1764	0.3169
am19800602	70	0.2531	0.2026	0.3242
am19810606	71	0.2587	0.1406	0.2944
am19820610	65	0.2493	0.2003	0.3198
am19840601	61	0.2542	0.1669	0.3041
am19850722	61	0.2496	0.1611	0.2971
at19840601	21	0.4265	0.400	0.5851
at19850722	21	0.3968	0.3688	0.5417
at19860623	20	0.3043	0.354	0.4668
at19890717	19	0.5148	0.5174	0.7299
at19910402	20	0.4701	0.3558	0.5896
at19930407	21	0.3979	0.3886	0.5562
at19940528	18	0.5526	0.4033	0.6841
at19950531	18	0.2885	0.4109	0.5021
at19960704	21	0.3711	0.3694	0.5237
at19970402	19	0.5092	0.3686	0.6286
at19970621	20	0.5195	0.4501	0.6874
at19980507	21	0.4812	0.4276	0.6437
at19990627	19	0.5814	0.4250	0.7202
at20000621	17	0.5378	0.4279	0.6873

Table B.2: Number of GCPs and error estimates for the Lagadas satellite images

	GCPs	RMS x	RMS y	Total RMS (pixel)
lt19840703	142	0.1573	0.1394	0.2102
lt19850519	104	0.1956	0.1683	0.2581
lt19860623	121	0.1592	0.1400	0.1220
lt19870610	141	0.1839	0.1394	0.2307
lt19880714	116	0.1553	0.1497	0.2157
lt19900704	111	0.1901	0.1495	0.2418
lt19920623	118	0.1641	0.1343	0.2121
lt19930712	91	0.1738	0.1370	0.2213
lt19940528	108	0.1633	0.1328	0.2105
lt19950702	104	0.1612	0.1604	0.2274
lt19960704	86	0.1584	0.1121	0.1940
lt19970621	79	0.118	0.1383	0.1818
lt19980710	89	0.1408	0.1327	0.1935
lt19990611	85	0.1384	0.1224	0.1850
Lt20000605	48	0.3591	0.4091	0.5444
lt20000816	66	0.1736	0.1410	0.2236

Table B.3: Landsat-5 TM calibration gains (offsets set to 0)

DATE	TM1	TM2	TM3	TM4	TM5	TM7
Empirical function	2E-06x + 0.0183	4E-06x + 0.0279	1E-06x + 0.0607	9E-07x + 0.0624	4E-08x + 0.0125	5E-08x + 0.005
01/01/1984	0.079664	0.150628	0.091382	0.0900138	0.01372728	0.0065341
01/07/1984	0.080028	0.151356	0.091564	0.0901776	0.01373456	0.0065432
01/01/1985	0.080396	0.152092	0.091748	0.0903432	0.01374192	0.0065524
01/07/1985	0.080758	0.152816	0.091929	0.0905061	0.01374916	0.00656145
01/01/1986	0.081126	0.153552	0.092113	0.0906717	0.01375652	0.00657065
01/07/1986	0.081488	0.154276	0.092294	0.0908346	0.01376376	0.0065797
01/01/1987	0.081856	0.155012	0.092478	0.0910002	0.01377112	0.0065889
01/07/1987	0.082218	0.155736	0.092659	0.0911631	0.01377836	0.00659795
01/01/1988	0.082586	0.156472	0.092843	0.0913287	0.01378572	0.00660715
01/07/1988	0.08295	0.1572	0.093025	0.0914925	0.013793	0.00661625
01/01/1989	0.083318	0.157936	0.093209	0.0916581	0.01380036	0.00662545
01/07/1989	0.08368	0.15866	0.09339	0.091821	0.0138076	0.0066345
01/01/1990	0.084048	0.159396	0.093574	0.0919866	0.01381496	0.0066437
01/07/1990	0.08441	0.16012	0.093755	0.0921495	0.0138222	0.00665275
01/01/1991	0.084778	0.160856	0.093939	0.0923151	0.01382956	0.00666195
01/07/1991	0.08514	0.16158	0.09412	0.092478	0.0138368	0.006671
01/01/1992	0.085508	0.162316	0.094304	0.0926436	0.01384416	0.0066802
01/07/1992	0.085872	0.163044	0.094486	0.0928074	0.01385144	0.0066893
01/01/1993	0.08624	0.16378	0.09467	0.092973	0.0138588	0.0066985
01/07/1993	0.086602	0.164504	0.094851	0.0931359	0.01386604	0.00670755
01/01/1994	0.08697	0.16524	0.095035	0.0933015	0.0138734	0.00671675
01/07/1994	0.087332	0.165964	0.095216	0.0934644	0.01388064	0.0067258
01/01/1995	0.0877	0.1667	0.0954	0.09363	0.013888	0.006735
01/07/1995	0.088062	0.167424	0.095581	0.0937929	0.01389524	0.00674405
01/01/1996	0.08843	0.16816	0.095765	0.0939585	0.0139026	0.00675325
01/07/1996	0.088794	0.168888	0.095947	0.0941223	0.01390988	0.00676235
01/01/1997	0.089162	0.169624	0.096131	0.0942879	0.01391724	0.00677155
01/07/1997	0.089524	0.170348	0.096312	0.0944508	0.01392448	0.0067806
01/01/1998	0.089892	0.171084	0.096496	0.0946164	0.01393184	0.0067898
01/07/1998	0.090254	0.171808	0.096677	0.0947793	0.01393908	0.00679885
01/01/1999	0.090622	0.172544	0.096861	0.0949449	0.01394644	0.00680805
01/01/1999	0.090622	0.172544	0.096861	0.0949449	0.01394644	0.00680805
01/07/2000	0.090984	0.173268	0.097042	0.0951078	0.01395368	0.0068171
01/07/2000	0.090984	0.173268	0.097042	0.0951078	0.01395368	0.0068171

Table B.4: Landsat-7 ETM+ calibration constants

	ETM+ 1	ETM+ 2	ETM+ 3	ETM+ 4	ETM+ 5	ETM+ 7
at20000621 - offset	-0.6869	-0.7174	-0.5206	-0.5409	-0.1075	-0.0373
at20000621 - gain	0.0782	0.0796	0.0616	0.0968	0.0127	0.0044
lt20000605 - offset	-0.68685	-0.71744	-0.52060	-0.54090	-0.1075	-0.03733
lt20000605 - gain	0.07815	0.07957	0.06159	0.09677	0.0127	0.00377

Table B.5: Parameterisation of the radiative transfer model and the topography correction - Ayora

Scene ID	Calib. targets	Ångstrom-relation: β; α	Aerosol phase f.: g^1; g^2; α	Atmospheric water vapour [gm/cm^2]	Max. angle Lambertian correction [°]	Sun azimuth angle [°]	Sun zenith angle [°]
at19840601	13	0.150; 1.5	0.8270; 0.5130; 0.9520	0.000710	50	117.75	29.08
at19850722	13	0.150; 2.5	0.8270; 0.5130; 0.9520	0.146116	50	117.42	31.13
at19860623	13	0.100; 1.0	0.8360; 0.5370; 0.9680	0.146116	50	112.47	29.66
at19890717	13	0.150; 2.5	0.8270; 0.5130; 0.9520	0.292232	50	115.45	30.95
at19910402	15	0.080; 1.5	0.8360; 0.5370; 0.9680	2.337857	50	133.11	44.40
at19930407		0.080; 1.5	0.8360; 0.5370; 0.9680	4.383482	50	132.1	42.61
at19940528	14	0.080; 1.5	0.8360; 0.5370; 0.9680	2.337857	50	115.89	30.94
at19950531	13	0.080; 1.5	0.8360; 0.5370; 0.9680	0.292232	50	111.63	32.89
at19960704	13	0.080; 1.5	0.8360; 0.5370; 0.9680	1.168929	50	110.11	31.93
at19970402	13	0.100; 2.5	0.8360; 0.5370; 0.9680	2.922321	50	134.74	43.72
at19970621	13	0.100; 2.5	0.8360; 0.5370; 0.9680	2.337857	50	116.80	27.20
at19980507	13	0.080; 1.5	0.8360; 0.5370; 0.9680	2.337857	50	128.59	31.2
at19990627	13	0.080; 1.5	0.8360; 0.5370; 0.9680	0.584464	50	116.85	27.22
at20000621	13 (24)	0.150; 2.0	0.8360; 0.5370; 0.9680	0.000710	50	122.08	24.65

Table B.6: Number of targets included in the normalisation steps of the MSS data - Ayora

Scene ID	Targ.	MSS band 1	MSS band 2	MSS band 3	MSS band 4
am19750629	41	y=1.7066x-55.656 (r^2=0.9748)	y=1.2364x-32.937 (r^2=0.9739)	y=1.3019x-43.639 (r^2=0.9694)	y=1.7232x-48.381 (r^2=0.9566)
am19760518			Not used due to strong haze		
am19780710	47	y=1.6678x-23.581 (r^2=0.982)	y=1.2684x-15.233 (r^2=0.9783)	y=1.2546x-18.864 (r^2=0.9813)	y=1.2174x-9.736 (r^2=.9792)
am19790512	65	y=1.359x-2.9771 (r^2=0.9858)	y=1.0844x-2.2973 (r^2=0.9818)	y=1.0545x-0.4058 (r^2=0.982)	y=1.0016x+8.418 (r^2=0.9767)
am19800602	62	y=1.3864x-16.142 (r^2=0.9859)	y=1.1738x-3.5572 (r^2=0.9776)	y=1.1805x-4.1953 (r^2=0.982)	y=0.9297x+4.029 (r^2=0.9757)
am19810606	64	y=1.3251x-14.715 (r^2=0.9801)	y=1.027x-9.0377 (r^2=0.983)	y=1.0365x-13.608 (r^2=0.9821)	y=1.0103x-5.5697 (r^2=0.9757)
am19820610	57	y=1.3666x-23.927 (r^2=0.9892)	y=1.1526x-10.545 (r^2=0.9862)	y=1.1809x-11.481 (r^2=0.9803)	y=0.9797x-4.5496 (r^2=0.9729)
			Second normalization step		
am19750629	41	y=0.9527x-1.1735 (r^2=0.9583)	y=0.9453x+0.648 (r^2=0.9584)	y=0.9478x+2.263 (r^2=0.9522)	y=0.9526x+3.991 (r^2=0.9402)
am19760518			Not used due to strong haze		
am19780710	47	y=1.6384x-9.455 (r^2=0.9797)	y=1.2639x-11.199 (r^2=0.9734)	y=1.2439x-14.108 (r^2=0.9699)	y=1.2247x-9.994 (r^2=0.9696)
am19790512	65	y=0.9921x-4.0556 (r^2=0.9742)	y=0.9886x-2.4904 (r^2=0.9674)	y=0.9827x-1.2793 (r^2=0.9609)	y=0.9864x-0.4847 (r^2=0.9534)
am19800602	62	y=1.0097x-4.8069 (r^2=0.9738)	y=1.0127x-3.8304 (r^2=0.9601)	y=0.9959x-2.6892 (r^2=0.9705)	y=1.0023x-2.1782 (r^2=0.9652)
am19810606	64	y=1.0055x-4.4172 (r^2=0.9693)	y=1.0048x-3.1939 (r^2=0.9744)	y=1.0041x-2.7651 (r^2=0.9748)	y=1.0024x-1.5405 (r^2=0.9668)
am19820610	57	y=0.9855x-3.8609 (r^2=0.9765)	y=0.9747x-1.9389 (r^2=0.9704)	y=0.9783x-1.1427 (r^2=0.9644)	y=0.9894x-0.6216 (r^2=0.9568)

Table B.7: Parameterisation of the radiative transfer model and the topography correction - Lagadas

Scene ID	Calib. targets	Ångstrom-relation: β; α	Aerosol phase f.: g^1; g^2; α	Atmospheric water vapour [gm/cm^2]	Max. angle f. Lambertian correction [°]	Sun azimuth angle [°]	Sun zenith angle [°]
lt19840703	26	0.150; 2	0.8270; 0.5130; 0.9520	3.945134	40	116.78	29.64
lt19850519	26	0.150; 2	0.8360; 0.5370; 0.9680	3.799018	40	124.67	30.67
lt19860623	26	0.150; 2	0.8360; 0.5370; 0.9680	4.091250	40	115.17	29.99
lt19870610	26	0.080; 1.5	0.8360; 0.5370; 0.9680	4.383482	40	117.32	29.64
lt19880714	26	0.080; 1.5	0.8360; 0.5370; 0.9680	3.799018	40	118.57	30.39
lt19900704	26	0.080; 1.5	0.8360; 0.5370; 0.9680	4.091250	40	114.24	31.19
lt19920623	26	0.080; 1.5	0.8360; 0.5370; 0.9680	4.091250	40	115.11	30.69
lt19930712	26	0.120; 1.8	0.8360; 0.5370; 0.9680	2.337857	40	115.77	31.54
lt19940528	26	0.080; 1.5	0.8360; 0.5370; 0.9680	2.337857	40	118.41	31.36
lt19950702	26	0.080; 1.5	0.8360; 0.5370; 0.9680	3.068437	40	110.06	33.66
lt19960704	26	0.080; 1.5	0.8360; 0.5370; 0.9680	2.337857	40	112.61	32.20
lt19970621	26	0.080; 1.5	0.8360; 0.5370; 0.9680	2.337857	40	117.48	28.74
lt19980710	26	0.080; 1.5	0.8360; 0.5370; 0.9680	2.337857	40	120.52	28.67
lt19990611	26	0.080; 1.5	0.8360; 0.5370; 0.9680	2.922321	40	121.62	27.39
lt20000605	26	0.080; 1.5	0.8360; 0.5370; 0.9680	2.630089	40	128.16	25.50
lt20000816	26	0.150; 1.8	0.8360; 0.5370; 0.9680	1.168929	40	133.99	33.45

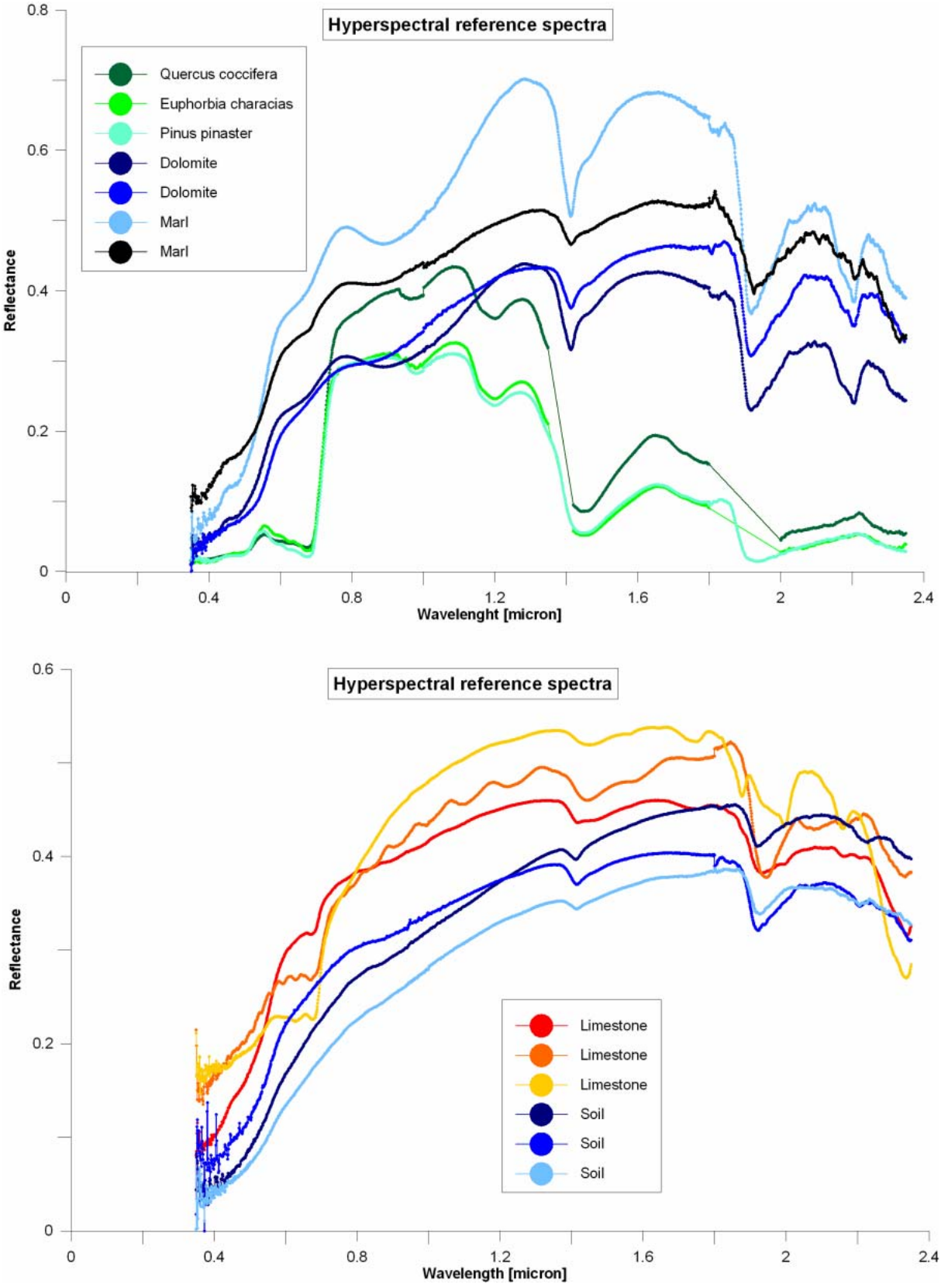

Fig. B.1: Hyperspectral reflectance measurements used for radiometric correction validation of the master image - Ayora

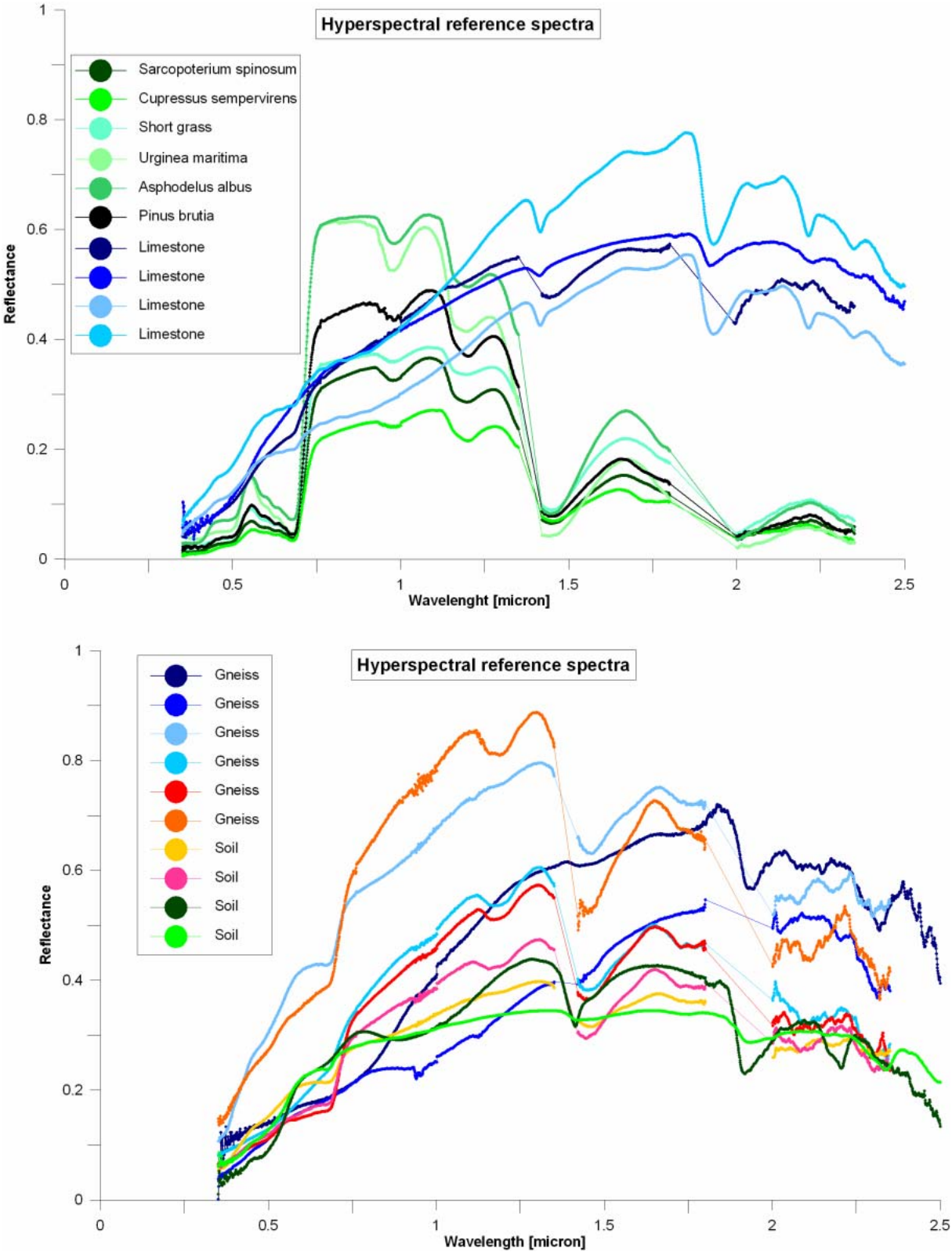

Fig. B.2: Hyperspectral reflectance measurements used for radiometric correction validation of the master image - Lagadas

Appendix C: The Lagadas case study

Table C.1: Trend for the full observation period averaged by elevation classes – full area

Elevation (m)	Area (ha)	Min	Max	Mean
0 - 250	17540	-0.777765	0.918121	0.01926
> 250 - 500	50615	-0.735954	0.73961	0.0135643
> 500 - 750	29484	-0.694892	0.690302	0.0105958
> 750 - 1000	3833	-0.432235	0.594817	0.0331616
> 1000	171	-0.387608	0.313056	0.041944

Table C.2: Area (ha) assigned to degradation index classes by elevation classes– full area

Degradation index	0 – 250 m	> 250 – 500 m	> 500 – 750 m	> 750 – 1000 m	> 1000 m
strong neg./low	276.93	286.2	47.61	2.61	0
strong neg./med.	913.14	2640.6	1732.95	91.89	0.81
strong neg./high	22.68	97.02	325.17	57.15	0.18
neg./low	707.04	669.87	87.21	3.15	0.09
neg./med.	2546.46	8874.27	5133.6	295.74	3.87
neg./high	64.71	560.7	775.35	214.65	3.42
neutral/low	1177.02	947.43	111.69	4.05	0.27
neutral/med.	6342.12	18514.98	10135.98	779.94	19.08
neutral/high	452.25	3833.37	4043.61	1018.98	82.98
incr./low	503.1	408.96	68.4	1.62	0
incr./med.	4502.97	9975.24	5174.19	573.3	17.1
incr./high	877.14	4084.2	3648.15	909.81	56.79
strong incr./low	109.08	82.26	27	0.45	0
strong incr./med.	1068.84	2683.62	1125.18	77.04	1.62
strong incr./high	241.92	862.56	677.61	194.22	2.43

Table C.3: Trend for the full observation period averaged by elevation classes – focus area 1

Elevation (m)	Area (ha)	Min	Max	Mean
0-250	11665800	-0.550726	0.5853	-0.001970
> 250-500	51819300	-0.735954	0.739617	0.037126
> 500-750	49654800	-0.657032	0.690302	0.005114
> 750-1000	23212800	-0.422104	0.450380	0.042257
> 1000	1713600	-0.387608	0.313056	0.041944

Table C.4: Trend for the full observation period averaged by elevation classes – focus area 2

Elevation (m)	Area (ha)	Min	Max	Mean
0-250	26710200	-0.6186	0.633441	0.0190588
> 250-500	63713700	-0.623528	0.384428	0.0409694
> 500-750	26415000	-0.435623	0.362903	0.0766797

Table C.5: Trend for the full observation period averaged by elevation classes – focus area 3

Elevation (m)	Area (ha)	Min	Max	Mean
0-250	1846	-0.430593	0.373314	0.0233251
> 250-500	5583	-0.434114	0.484045	0.00755576

Table C.6: Area (ha) assigned to degradation index classes by elevation – focus area 1

Class	0 – 250 m	> 250 – 500 m	> 500 – 750 m	> 750 – 1000 m	> 1000 m
	area (ha)	area (ha)	area (ha)	area (ha)	area (ha)
strong neg./low	31.77	22.86	5.31	2.16	0
strong neg./med.	42.21	253.08	294.03	22.41	0.81
strong neg./high	0.09	8.46	24.21	2.34	0.18
neg./low	58.14	40.86	8.01	2.88	0.09
neg./med.	304.65	836.37	578.16	106.2	3.87
neg./high	0.45	17.91	112.41	22.68	3.51
neutral/low	74.16	42.12	9.45	2.7	0.27
neutral/med.	462.51	1042.2	966.69	328.95	18.36
neutral/high	3.06	78.57	534.24	316.26	83.7
incr./low	49.95	17.28	5.04	0.9	0
incr./med.	208.26	641.25	544.95	232.29	16.74
incr./high	5.04	149.94	353.52	415.62	56.43
strong incr./low	19.53	18.45	0.45	0	0
strong incr./med.	65.7	794.61	248.76	24.3	1.35
strong incr./high	0.81	32.67	31.32	116.55	2.88

Table C.7: Area (ha) assigned to degradation index classes by elevation – focus area 2

Degradation index	0 – 250 m	> 250 – 500 m	> 500 – 750 m
strong neg./low	29.88	8.82	0.18
strong neg./med.	80.46	166.86	18.27
strong neg./high	2.16	1.89	0.99
neg./low	118.17	26.46	0.63
neg./med.	361.35	713.43	86.76
neg./high	2.34	20.61	15.39
neutral/low	218.34	40.14	1.26
neutral/med.	1114.65	2243.43	479.88
neutral/high	7.47	356.76	274.32
incr./low	110.7	23.85	0.36
incr./med.	655.92	1689.12	497.88
incr./high	9.72	973.26	1091.25
strong incr./low	36.45	4.23	0.09
strong incr./med.	185.94	334.35	99.36
strong incr./high	7.2	222.84	255.6

Table C.8: Area (ha) assigned to degradation index classes by elevation – focus area 3

Degradation index	0 – 250 m	> 250 – 500 m
strong neg./low	7.02	33.84
strong neg./med.	10.26	99.36
strong neg./high	0	0
neg./low	91.44	179.46
neg./med.	189.09	1303.02
neg./high	0	0.9
neutral/low	303.12	442.17
neutral/med.	775.35	3601.89
neutral/high	0	20.97
incr./low	125.01	194.94
incr./med.	503.91	1573.47
incr./high	1.62	42.21
strong incr./low	12.78	23.67
strong incr./med.	48.96	262.08
strong incr./high	0.63	20.7

Table C.9: Trend for the full observation period averaged by terrain classes – full area

Terrain class	Area (ha)	Min	Max	Mean
Low elevation divides	13616100	-0.7472	0.614722	-0.0233506
Gentle areas	5353200	-0.701038	0.684279	-0.0146494
Convex upperslopes	123379000	-0.6961	0.602888	0.00177792
Hill tops	816300	-0.358749	0.406673	0.013259
High elevation ridges and divides	113434000	-0.606352	0.661973	0.0290645
Steep mid and low slopes	254965000	-0.61206	0.572649	0.0297243
Channels	47608200	-0.597268	0.440897	0.0388857

Table C.10: Area (ha) assigned to degradation index classes by terrain classes – full area

Degradation index	Low elevation divides	Gentle areas	Convex upper slopes	Hilltops	High elevation ridges & divides	Steep mid- & low slopes	Channels
strong neg./low	138.96	57.24	312.48	0.99	55.62	145.17	36.36
strong neg./med.	232.2	100.35	962.28	7.2	420.12	721.89	215.01
strong neg./high	3.42	5.94	18.54	0.45	22.41	32.22	13.59
neg./low	227.7	89.37	688.5	2.79	206.28	437.22	106.11
neg./med.	743.94	213.84	4073.13	51.57	2291.94	4354.02	1161.81
neg./high	17.01	9.36	122.04	2.79	148.59	240.75	82.71
neutral/low	241.74	106.65	916.2	4.32	367.74	898.38	233.55
neutral/med.	1263.51	366.84	8910.27	127.08	6352.92	13123.62	3938.94
neutral/high	79.74	35.37	720.09	17.46	1116.45	1966.59	662.22
incr./low	87.57	57.69	310.32	1.98	146.79	368.28	128.07
incr./med.	604.53	232.74	4773.51	59.4	3660.39	8409.96	3129.48
incr./high	104.58	51.48	1108.08	27.81	1883.25	3084.66	1167.84
strong incr./low	16.2	16.29	43.92	0.27	21.24	48.69	24.03
strong incr./med.	123.21	67.77	880.65	7.56	757.08	1648.17	651.24
strong incr./high	25.56	12.51	270.09	3.06	406.26	730.35	255.33

Table C.11: Trend for the full observation period averaged by terrain classes – focus area 2

Terrain class	Area (ha)	Min	Max	Mean
Low elevation divides	1665000	-0.374629	0.390621	0.00637404
Gentle areas	1098000	-0.591167	0.431508	-0.0258625
Convex upperslopes	16913700	-0.623528	0.427575	0.031812
High elevation ridges and divides	26404200	-0.435623	0.362903	0.0534299
Steep mid and low slopes	47725200	-0.516463	0.371138	0.0542905
Channels	8935200	-0.438239	0.302756	0.0609532
Hill tops	170100	-0.358749	0.267048	0.058921

Table C.12: Trend for the full observation period averaged by terrain classes – focus area 3

Terrain class	Area (ha)	Min	Max	Mean
Low elevation divides	1312200	-0.357749	0.353218	-0.0129711
Gentle areas	244800	-0.21567	0.255665	0.00199515
Convex upperslopes	12769200	-0.46152	0.468262	-0.000817109
High elevation ridges and divides	9474300	-0.328828	0.437174	0.00224471
Steep mid and low slopes	40769100	-0.434114	0.484045	0.0193184
Channels	5499900	-0.368282	0.440897	0.0276518
Hill tops	53100	-0.144742	0.267833	-0.0112946

Table C.13: Area (ha) assigned to degradation index classes by terrain classes – focus area 2

Degradation index	Low elevation divides	Gentle areas	Convex upper slopes	Hilltops	High elevation ridges & divides	Steep mid- & low slopes	Channels
strong neg./low	2.61	5.4	11.97	0	0.99	6.12	1.71
strong neg./med.	18.45	24.39	73.71	1.44	32.76	51.93	18.99
strong neg./high	0.09	0.36	0.9	0	1.17	0.99	0.72
neg./low	13.59	13.32	39.33	0	10.53	40.5	7.83
neg./med.	88.11	44.19	395.64	3.15	258.93	452.34	127.8
neg./high	1.26	0.54	12.6	0.18	15.03	12.15	5.58
neutral/low	20.97	22.32	64.26	0.54	25.92	91.26	17.37
neutral/med.	162.9	57.06	1033.74	16.83	1181.16	2069.73	560.07
neutral/high	14.22	2.61	165.51	5.13	246.96	290.52	97.65
incr./low	9.99	13.5	27	0.27	9.81	44.55	11.61
incr./med.	91.26	35.91	740.16	16.11	869.22	1649.07	606.87
incr./high	26.01	5.76	452.7	17.46	879.75	1125.45	417.33
strong incr./low	3.69	7.2	5.22	0.09	0.99	7.65	2.61
strong incr./med.	19.08	10.26	122.94	2.34	132.3	336.15	132.93
strong incr./high	8.1	0.81	111.06	1.98	167.85	303.57	107.19

Table C.14: Area (ha) assigned to degradation index classes by terrain classes – focus area 3

Degradation index	Low elevation divides	Gentle areas	Convex upper slopes	Hilltops	High elevation ridges & divides	Steep mid- & low slopes	Channels
strong neg./low	2.97	0.72	14.67	0.18	4.68	12.42	2.43
strong neg./med.	8.55	1.17	44.73	0.36	13.95	37.35	9.45
strong neg./high	0	0	0	0	0	0	0
neg./low	14.31	2.25	82.62	0.18	38.34	100.08	17.46
neg./med.	97.65	12.69	531.9	6.39	306	842.58	158.04
neg./high	0	0	0.27	0	0	0.9	0
neutral/low	29.88	6.21	181.44	0.18	86.49	293.58	67.59
neutral/med.	191.52	43.38	1256.94	10.8	811.62	2634.93	642.42
neutral/high	0.18	0	6.93	0.09	1.89	18.09	3.06
incr./low	10.98	3.24	67.77	0	37.8	142.02	41.04
incr./med.	60.66	15.48	449.01	1.98	284.04	1246.86	347.4
incr./high	0.81	0.18	9.09	0	3.24	37.8	9.27
strong incr./low	0.54	0.27	7.02	0	6.57	17.37	5.76
strong incr./med.	7.02	1.26	86.76	0.99	29.25	206.28	47.25
strong incr./high	0.72	0	6.84	0	0.72	18.72	2.07

Table C.15: Friction assignment for cost factor ‘attractiveness’ based on Natura 2000 habitat codes

N. 2000 code	Habitat type	Habitat cover class	Friction surface
934A	Kermes oak shrublands (*Quercus coccifera*)	10-40	5
6290	Mediterranean subnitrophyllous meadows (Poa bulbosa, Dactylis glomerata, Thymus spp., Bromus spp., Quercus coccifera)		10
	Abandoned field		25
934A	Kermes oak shrublands (see above)	40-70	30
92A4	Balkanic thermophilous oak forests (*Quercus pubescens, Quercus frainetto*)	10-40	50
9280	Deciduous mixed woods (Fagus sylvatica, Quercus frainetto)	10-40	50
5350	Pseudomaquis (Quercus coccifera, Juniperus oxycedrus, Carpinus orientalis, Ostrya carpinifolia)	40-70	75
9130	Neutrophilous beech forests (*Fagus sylvatica*)	40-70	75
92A4	Balkanic thermophilous oak forests (see above)	40-70	75
9280	Deciduous mixed woods (see above)	40-70	75
1030	Reforestation (Pinus halepensis, P. brutia, P. nigra, P. maritima)		75
5350	Pseudomaquis (see above)	70-100	100
72A0	Reed beds (Phragmites australis, Arundo donax, Typha angustifolia)		100
9110	Acidophilous beech forests (*Fagus sylvatica)*		100
9130	Neutrophilous beech forests (see above)	70-100	100
92A4	Balkanic thermophilous oak forests (see above)	70-100	100
9280	Deciduous mixed woods (see above)	70-100	100
92C0	Oriental plane woods (*Platanus orientalis*)	70-100	100
	Agricultural		100
	Barren field		100
	Village		100

Table C.16: Friction assignment for cost factor 'attractiveness' based on Natura 2000 habitat codes and Landsat-7 ETM+

N. 2000 code	Habitat type	Habitat cover class	Biomass (green vegetation cover June 2000)	Friction surface
934A	Kermes oak shrublands (*Quercus coccifera*)	0-40	3	1
934A	Kermes oak shrublands (see above)	0-40	2	5
6290	Mediterranean subnitrophyllous meadows (Poa bulbosa, Dactylis glomerata, Thymus spp., Bromus spp., Quercus coccifera)		3	5
934A	Kermes oak shrublands (see above)	0-40	1	10
6290	Mediterranean subnitrophyllous meadows		2	10
	Abandoned field		2	15
6290	Mediterranean subnitrophyllous meadows (see above)		1	15
	Abandoned field		1	20
	Abandoned field		3	20
934A	Kermes oak shrublands (see above)	40-70	3	25
934A	Kermes oak shrublands (see above)	40-70	2	30
934A	Kermes oak shrublands (see above)	40-70	1	35
92A4	Balkanic thermophilous oak forests (*Quercus pubescens, Quercus frainetto*)	0-40	3	40
9280	Deciduous mixed woods (Fagus sylvatica, Quercus frainetto)	0-40	3	40
934A	Kermes oak shrublands (see above)	70-100	3	40
92A4	Balkanic thermophilous oak forests (see above)	0-40	2	45
9280	Deciduous mixed woods (see above)	0-40	2	45
934A	Kermes oak shrublands (see above)	70-100	2	45
92A4	Balkanic thermophilous oak forests (see above)	0-40	1	50
9280	Deciduous mixed woods (see above)	0-40	1	50
934A	Kermes oak shrublands (see above)	70-100	1	50
92A4	Balkanic thermophilous oak forests (see above)	40-70	3	55
9280	Deciduous mixed woods (see above)	40-70	3	55
92A4	Balkanic thermophilous oak forests (see above)	40-70	2	60
9280	Deciduous mixed woods (see above)	40-70	2	60
92A4	Balkanic thermophilous oak forests (see above)	40-70	1	65
9280	Deciduous mixed woods (see above)	40-70	1	65
5350	Pseudomaquis (Quercus coccifera, Juniperus oxycedrus, Carpinus orientalis, Ostrya carpinifolia)	40-70	3	70
92A4	Balkanic thermophilous oak forests (see above)	70-100	3	70
9280	Deciduous mixed woods (see above)	70-100	3	70
5350	Pseudomaquis (see above)	40-70	2	75
92A4	Balkanic thermophilous oak forests (see above)	70-100	2	75

continued on next page

Table C.16: Friction assignment for cost factor ‘attractiveness’ based on Natura 2000 habitat codes and Landsat-7 ETM+

N. 2000 code	Habitat type	Habitat cover class	Biomass (green vegetation cover June 2000)	Friction surface
9280	Deciduous mixed woods (see above)	70-100	2	75
5350	Pseudomaquis (see above)	40-70	1	80
92A4	Balkanic thermophilous oak forests (see above)	70-100	1	80
9280	Deciduous mixed woods (see above)	70-100	1	80
5350	Pseudomaquis (see above)	70-100	1	100
5350	Pseudomaquis (see above)	70-100	2	100
5350	Pseudomaquis (see above)	70-100	3	100
72A0	Reed beds (Phragmites australis, Arundo donax, Typha angustifolia)		1-3	100
9110	Acidophilous beech forests (*Fagus sylvatica)*		1-3	100
9130	Neutrophilous beech forests (*Fagus sylvatica*)	70-100	1-3	100
9130	Neutrophilous beech forests (*Fagus sylvatica*)	40-70	1-3	100
92C0	Oriental plane woods (*Platanus orientalis*)	70-100	1-3	100
1030	Reforestation (Pinus halepensis, P. brutia, P. nigra, P. maritima)		1-3	100
	Agricultural			100
	Barren field			100
	Village			100

Table C.17: Friction assignment for cost factor ‘accessibility’ based on Natura 2000 habitat codes

N. 2000 code	Description	Cover class	Friction value
	Barren field		5
6290	Mediterranean subnitrophyllous meadows (Poa bulbosa, Dactylis glomerata, Thymus spp., Bromus spp., Quercus coccifera)	0-10	5
92A4	Balkanic thermophilous oak forests (*Quercus pubescens, Quercus frainetto*)	10-40	25
9280	Deciduous mixed woods (Fagus sylvatica, Quercus frainetto)	10-40	25
934A	Kermes oak shrublands (*Quercus coccifera*)	10-40	25
	Abandoned field		25
5350	Pseudomaquis (Quercus coccifera, Juniperus oxycedrus, Carpinus orientalis, Ostrya carpinifolia)	40-70	55
9130	Neutrophilous beech forests (*Fagus sylvatica*)	40-70	55
92A4	See above	40-70	55
9280	See above	40-70	55
934A	Kermes oak shrublands (*Quercus coccifera*)	40-70	55
5350	See above	70-100	85
9110	Acidophilous beech forests (*Fagus sylvatica)*		85
9130	See above	70-100	85
92A4	See above	70-100	85
9280	See above	70-100	85
92C0	Oriental plane woods (*Platanus orientalis*)	70-100	85
934A	See above	70-100	85
1030	Reforestation (Pinus halepensis, P. brutia, P. nigra, P. maritima)		85
72A0	Reed beds (Phragmites australis, Arundo donax, Typha angustifolia)		100
	Agriculture		100
	Village		100

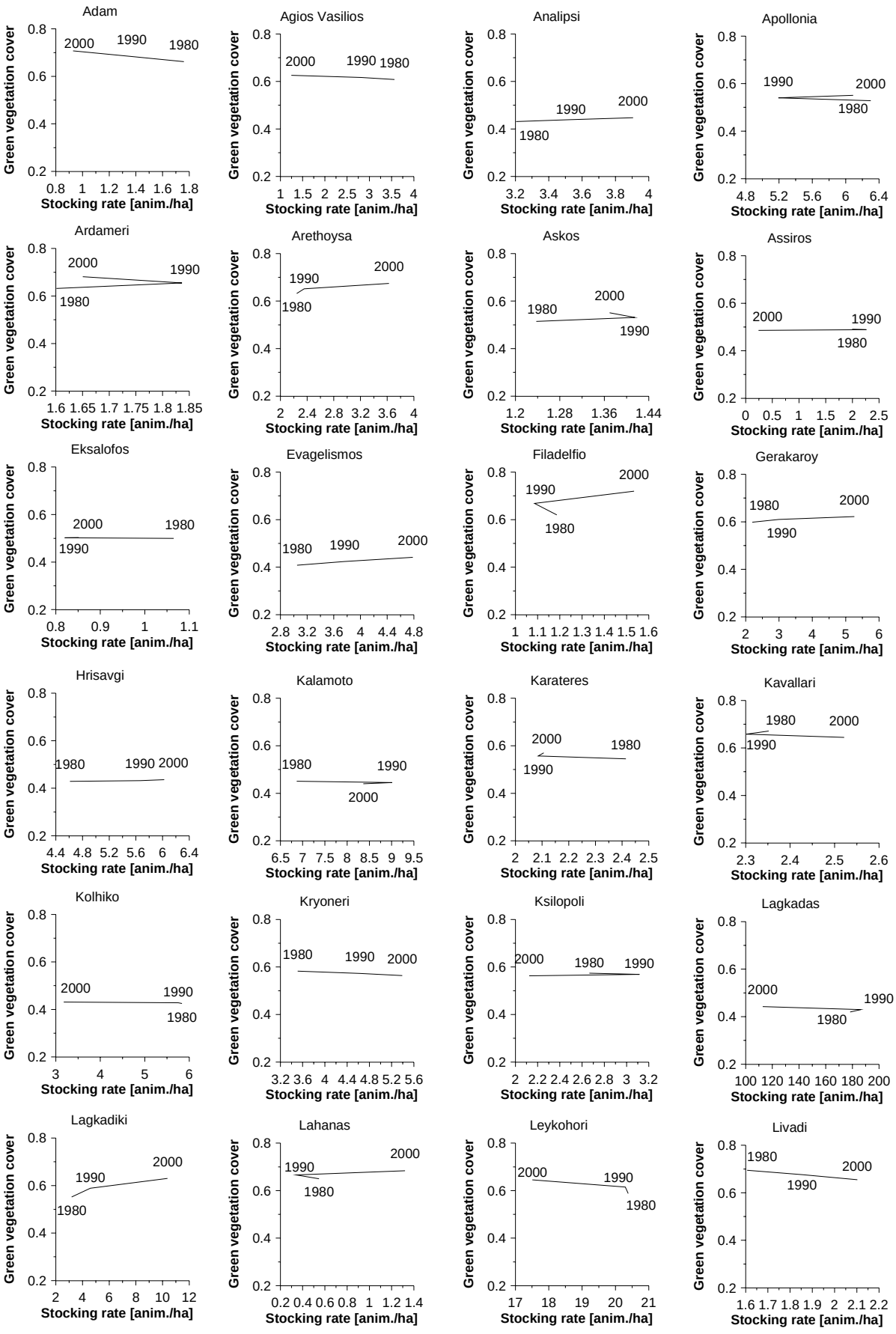

Fig. C.1: Temporal trajectories of development of vegetation cover in relation to animal stocking rates in Lagadas County

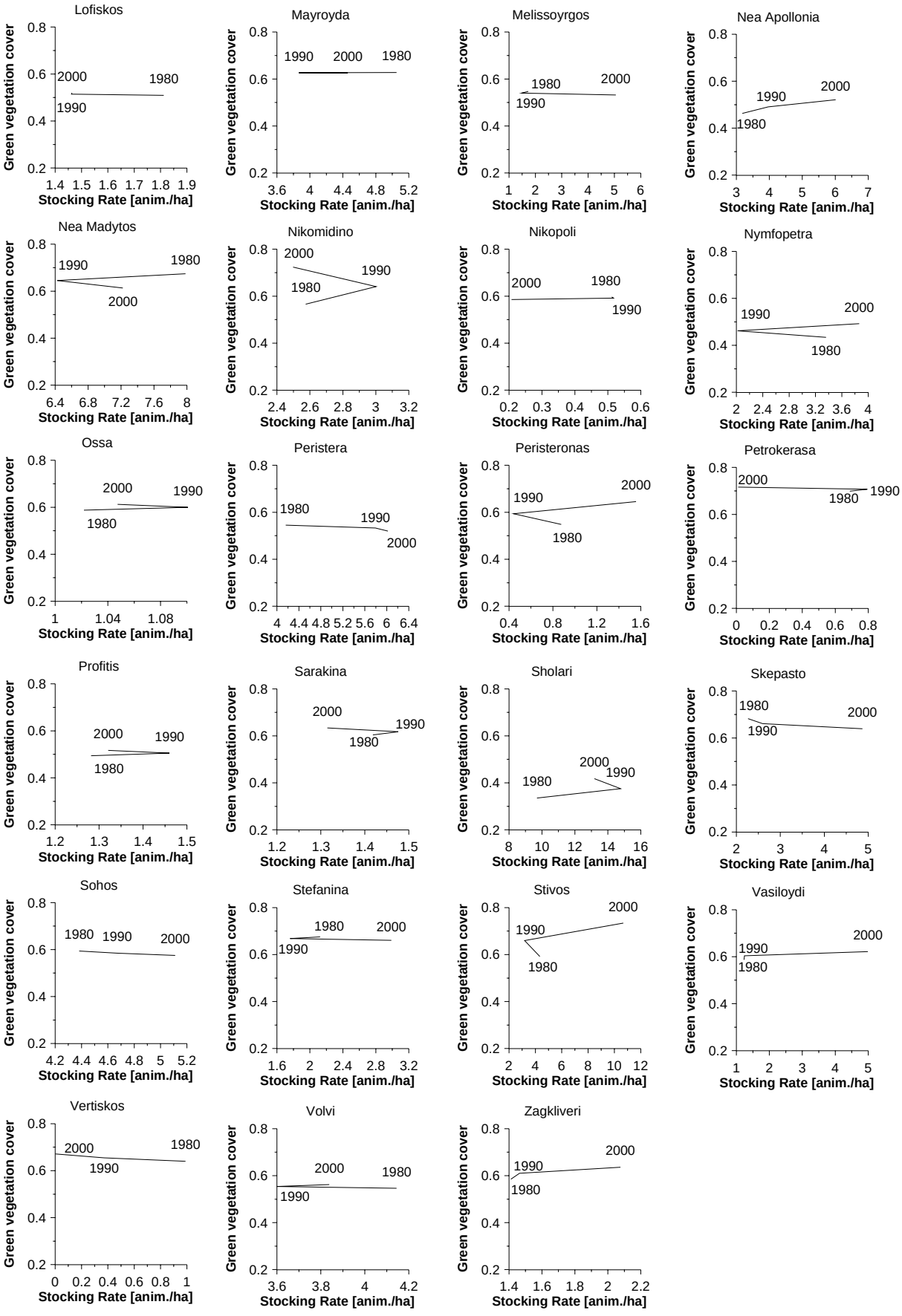

Fig. C.2: Temporal trajectories of development of vegetation cover in relation to animal stocking rates in Lagadas County (continued)

Appendix D: Maps Ayora

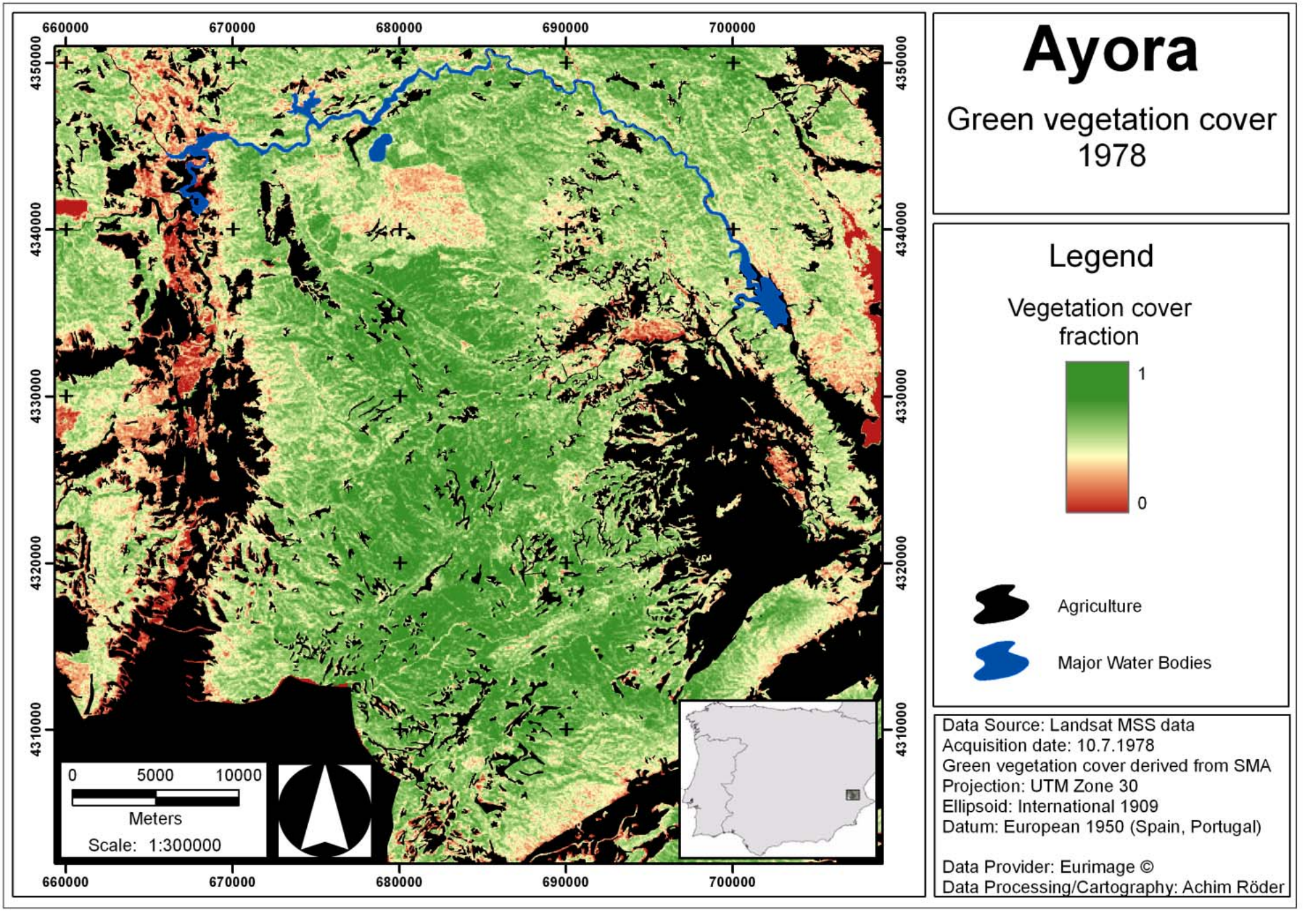

Map D.1: Proportional vegetation cover - Ayora (1978)

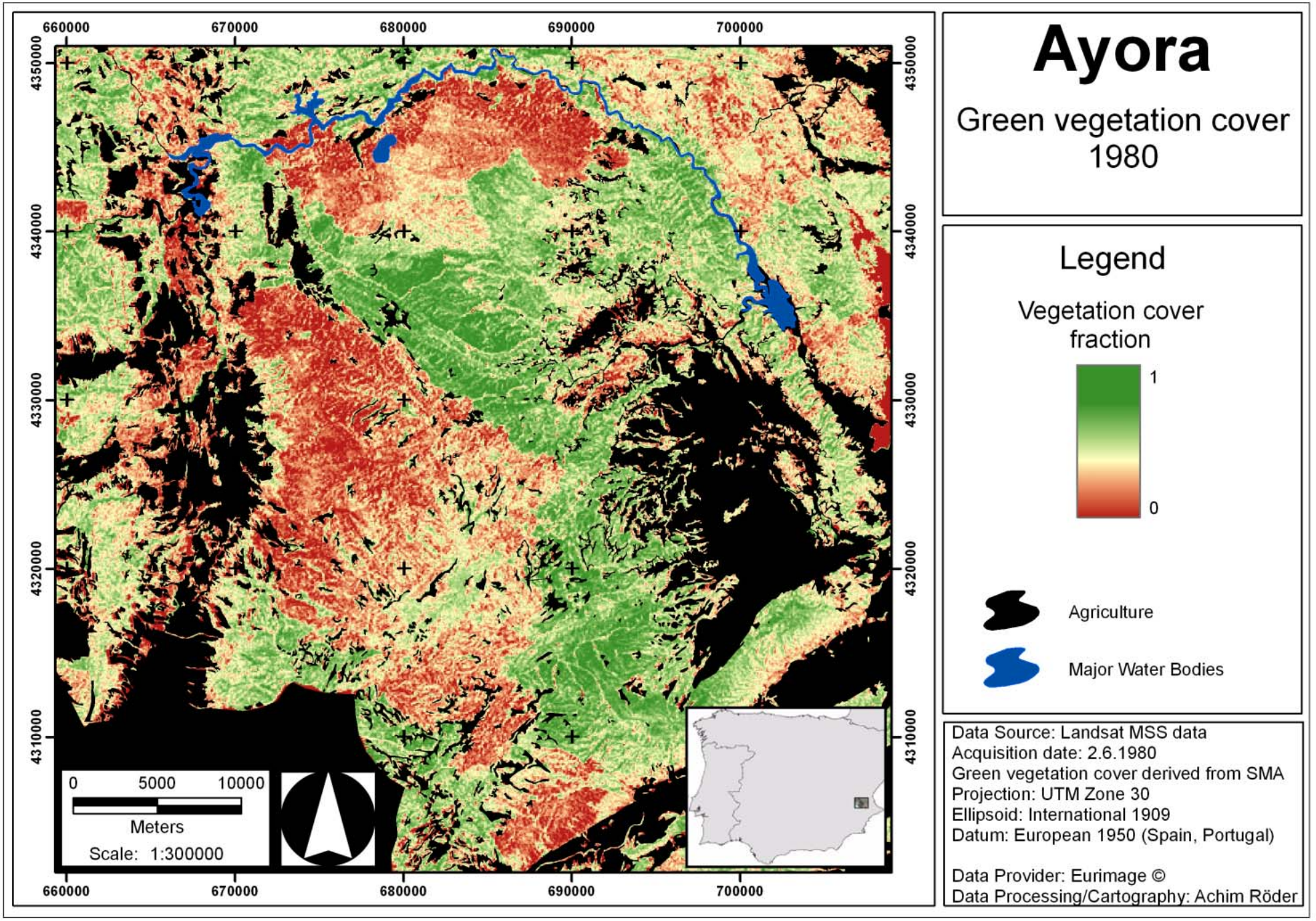

Map D.2: Proportional vegetation cover - Ayora (1978)

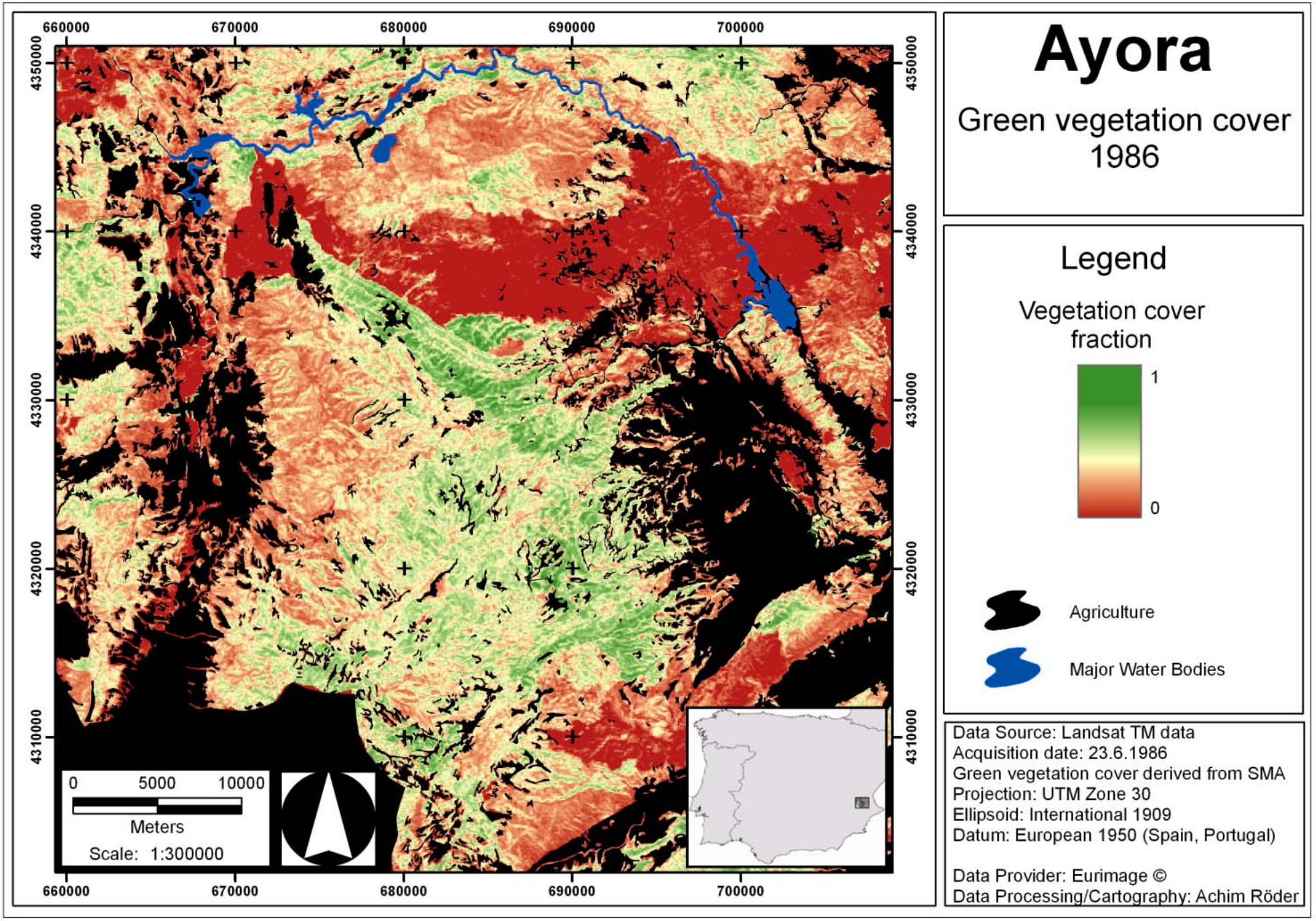

Map D.3: Proportional vegetation cover - Ayora (1986)

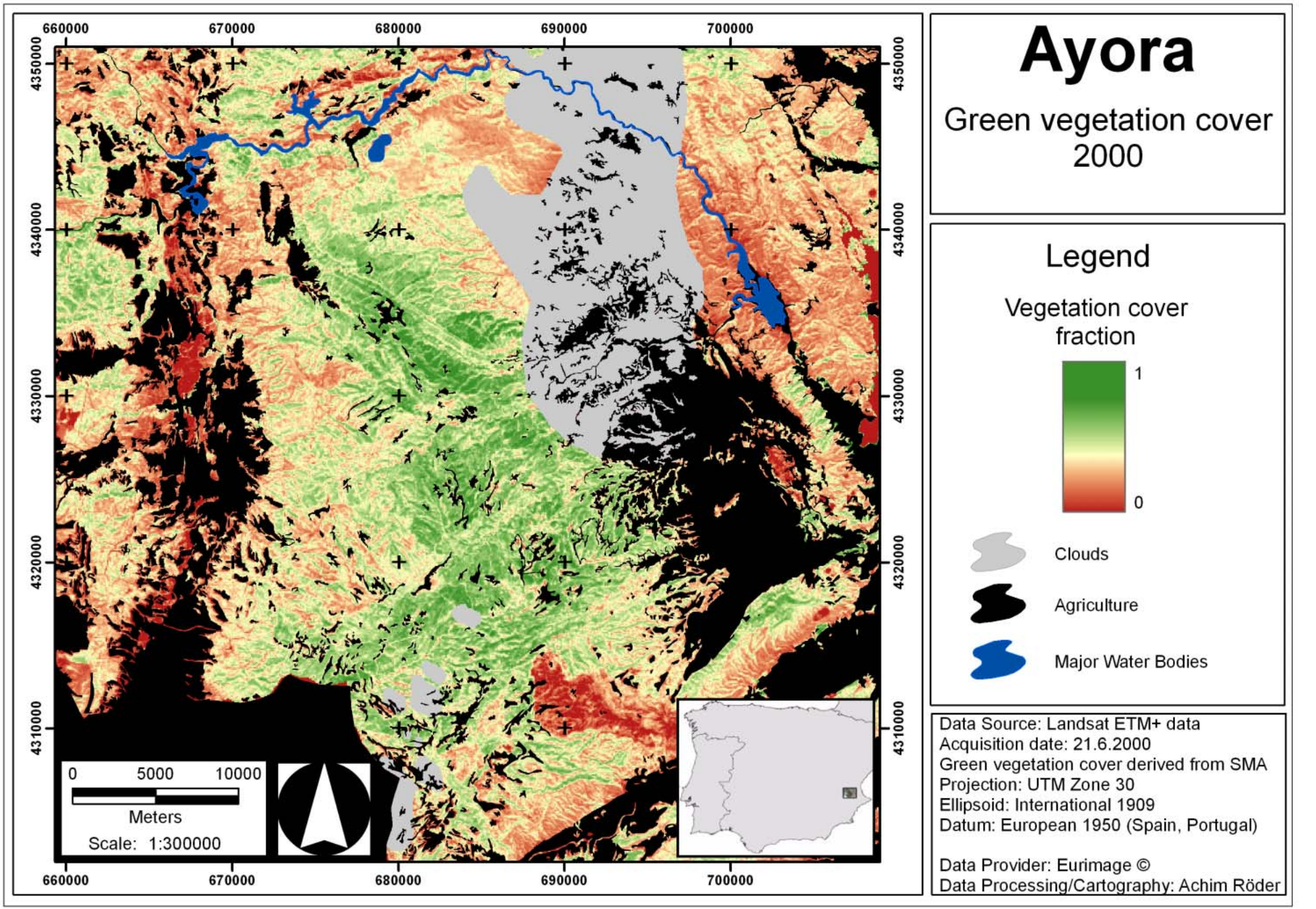

Map D.4: Proportional vegetation cover - Ayora (2000)

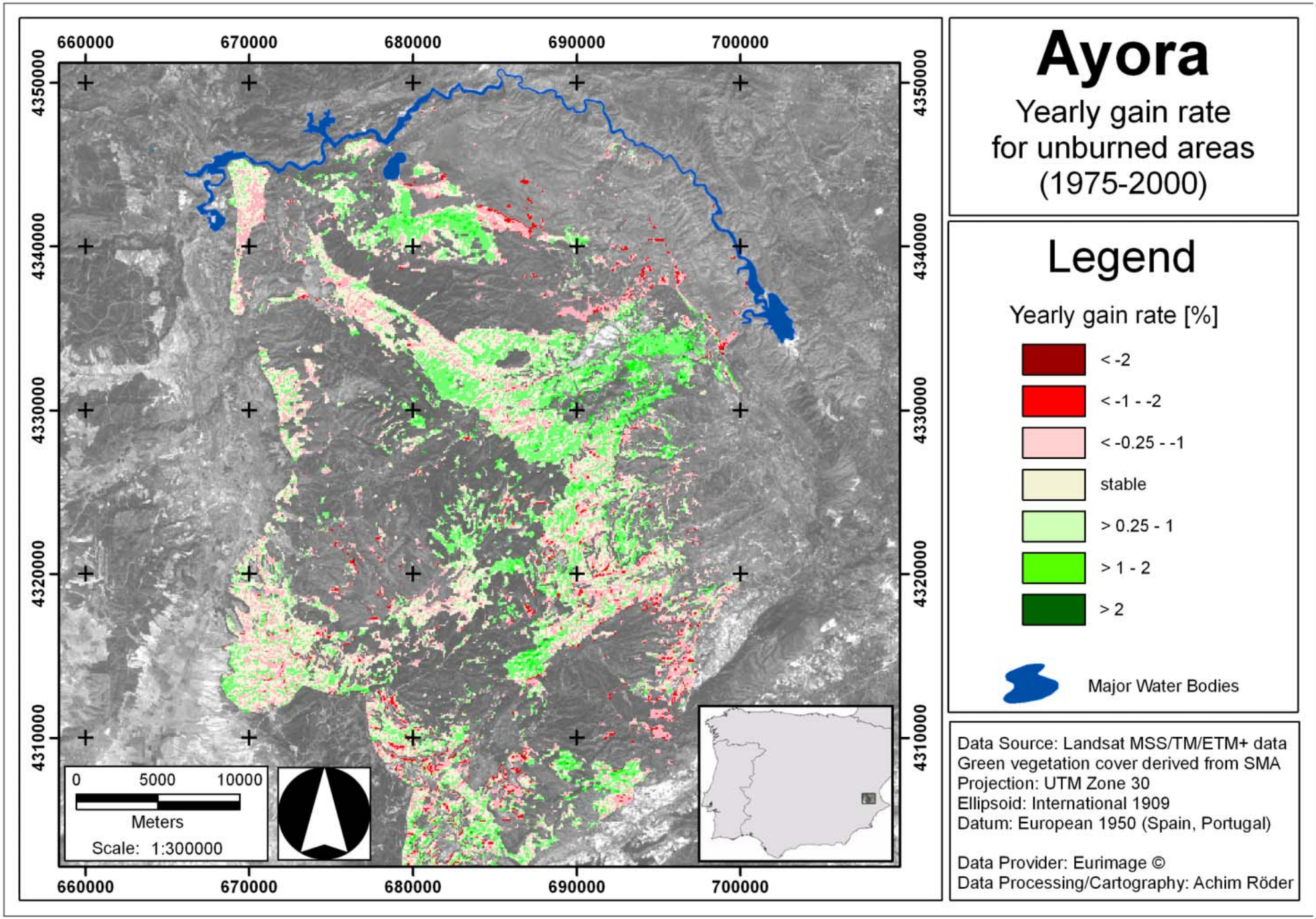

Map D.5: Yearly gain rate for unburned areas - Ayora (1975-2000)

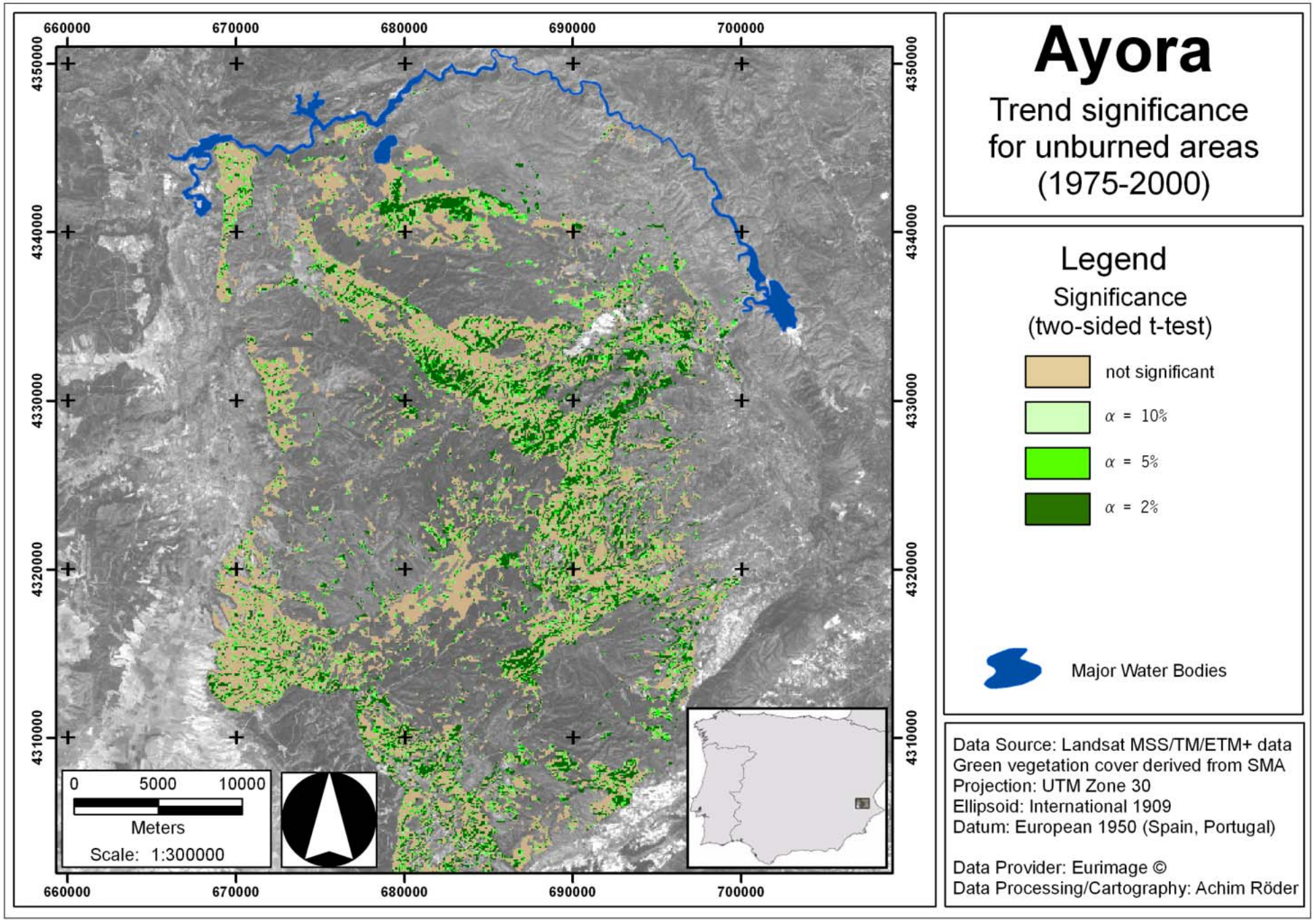

Map D.6: Trend significance for unburned areas - Ayora (1975-2000)

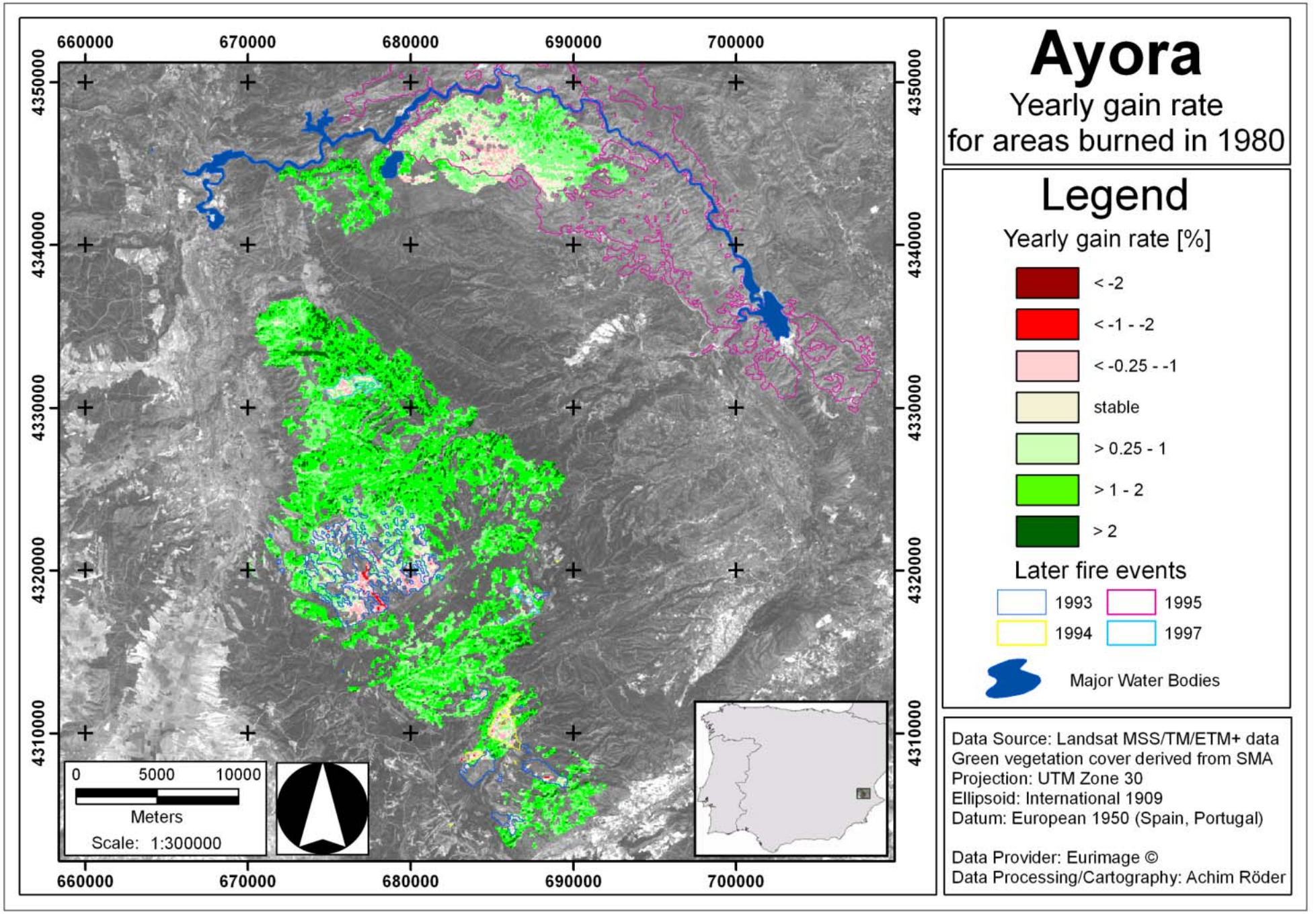

Map D.7: Yearly gain rate for the area affected by the fire in 1980 - Ayora

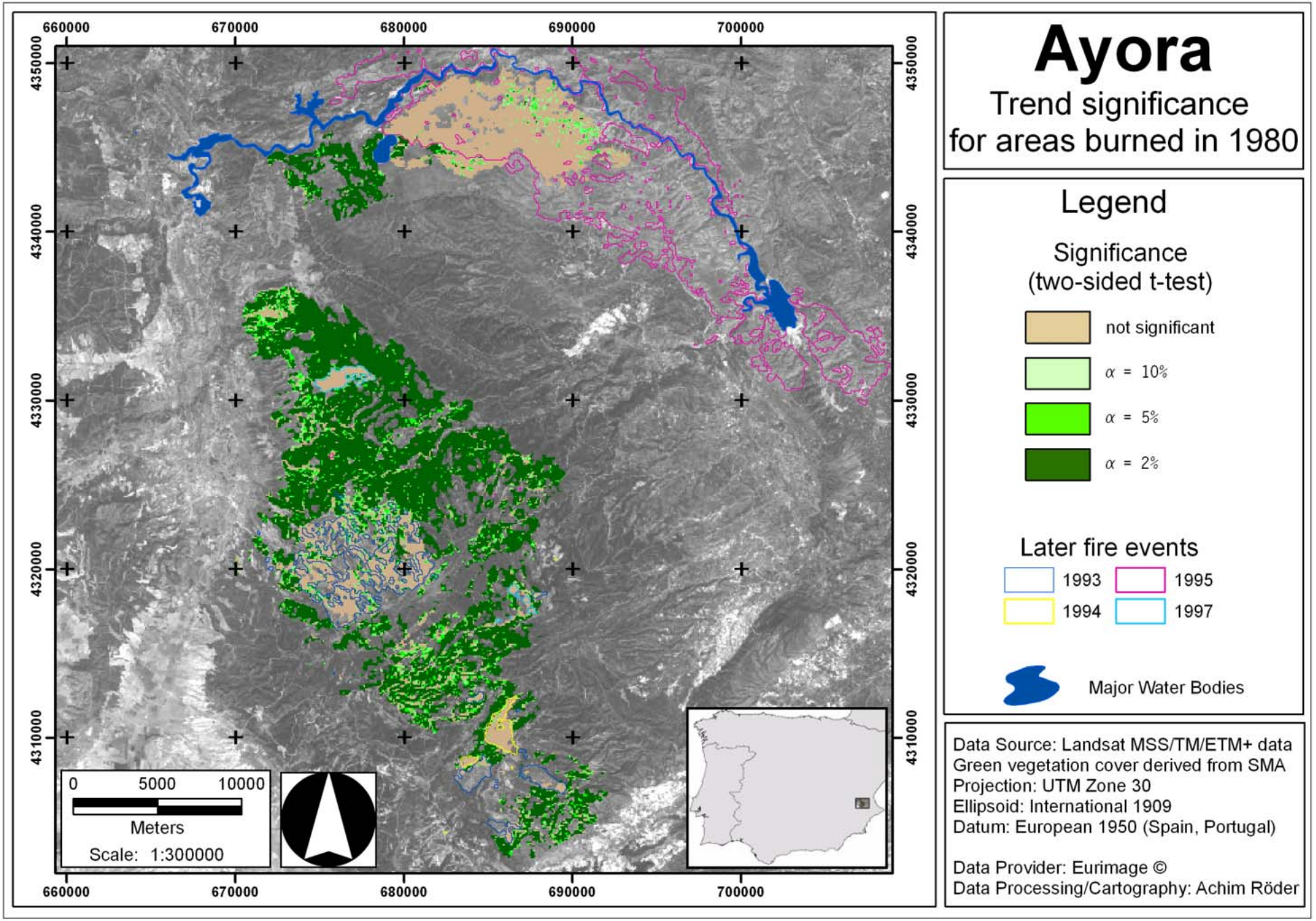

Map D.8: Trend significance for the area affected by the fire in 1980 - Ayora

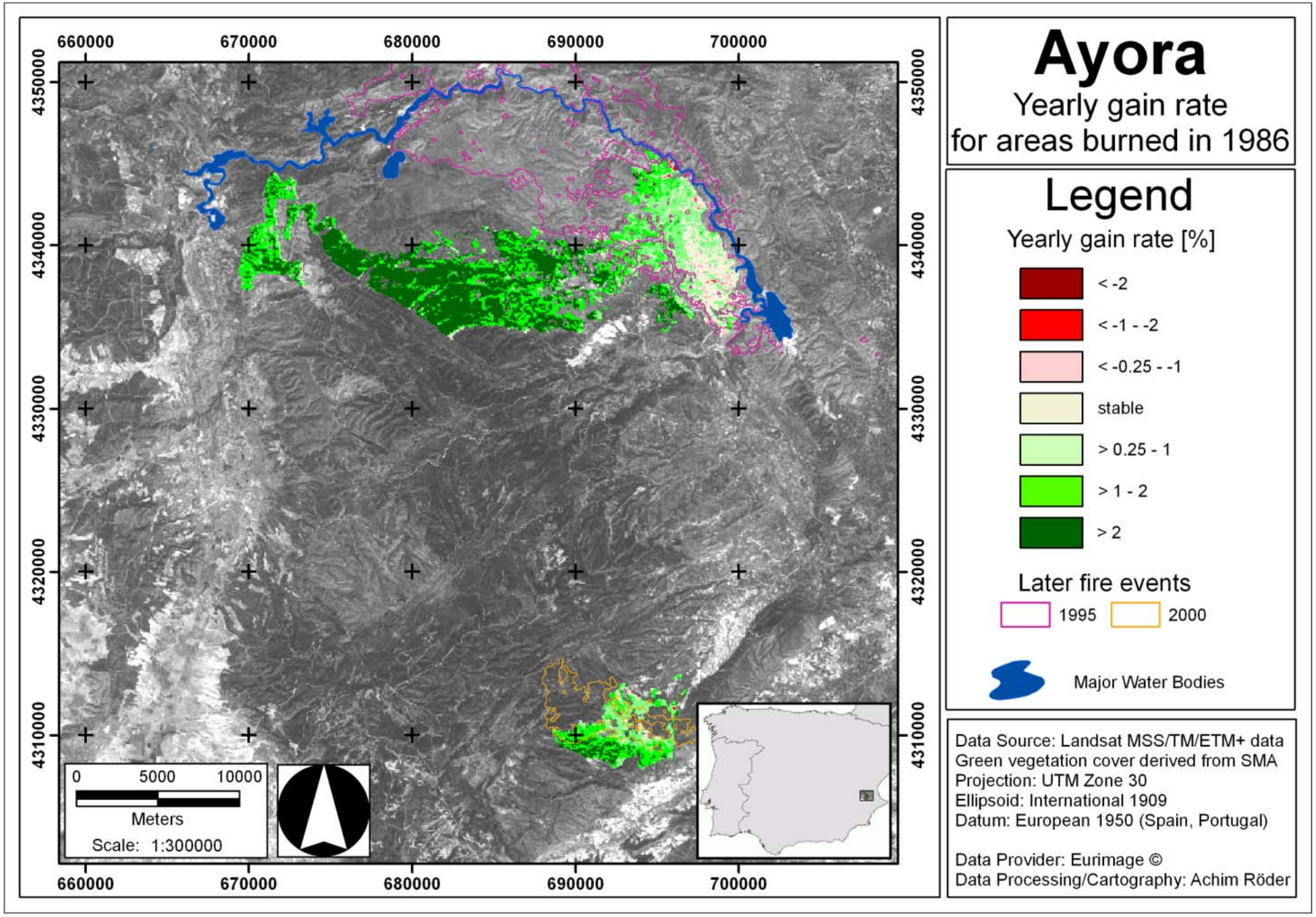

Map D.9: Yearly gain rate for the area affected by the fire in 1986 - Ayora

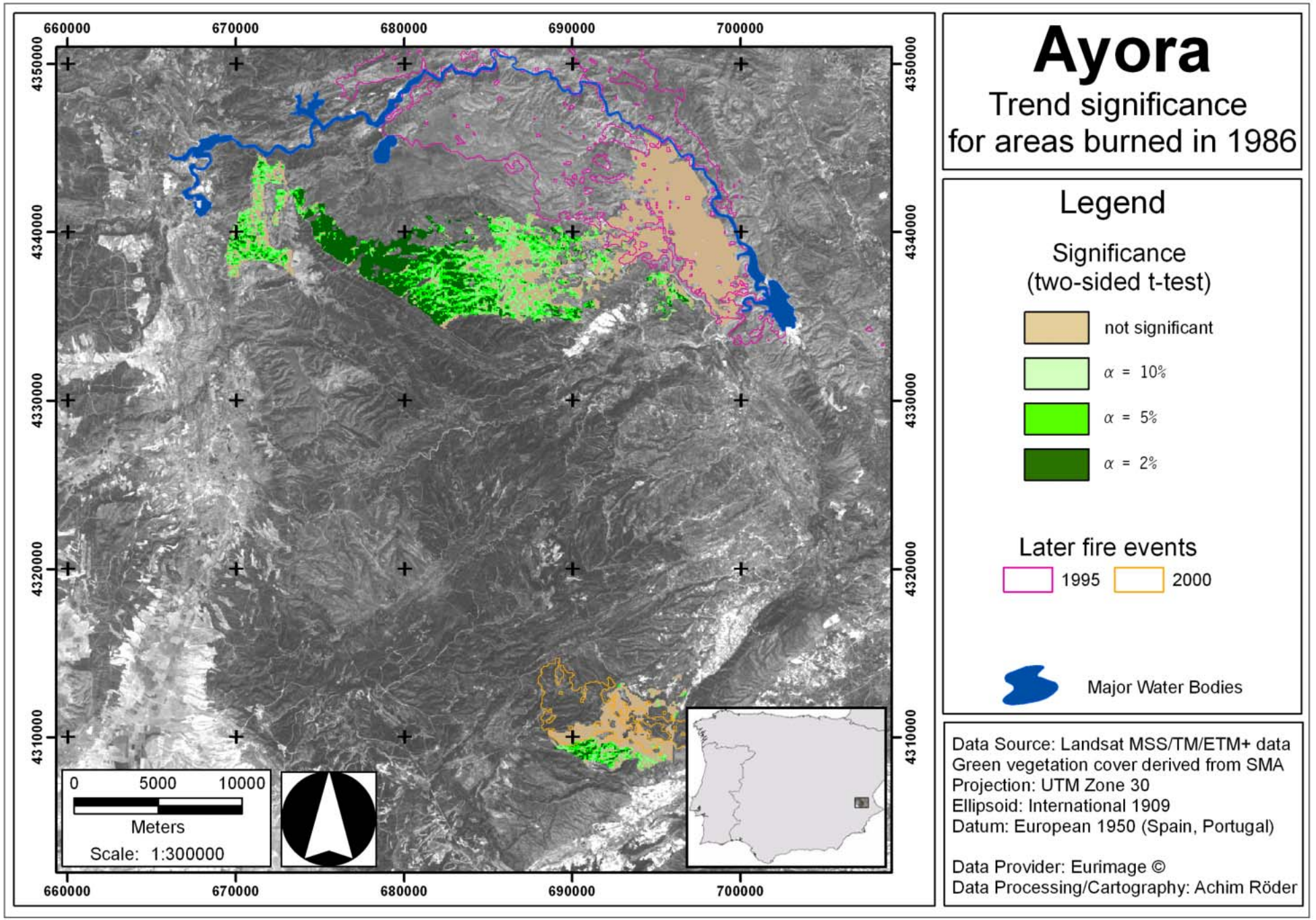

Map D.10: Trend significance for the area affected by the fire in 1986 - Ayora

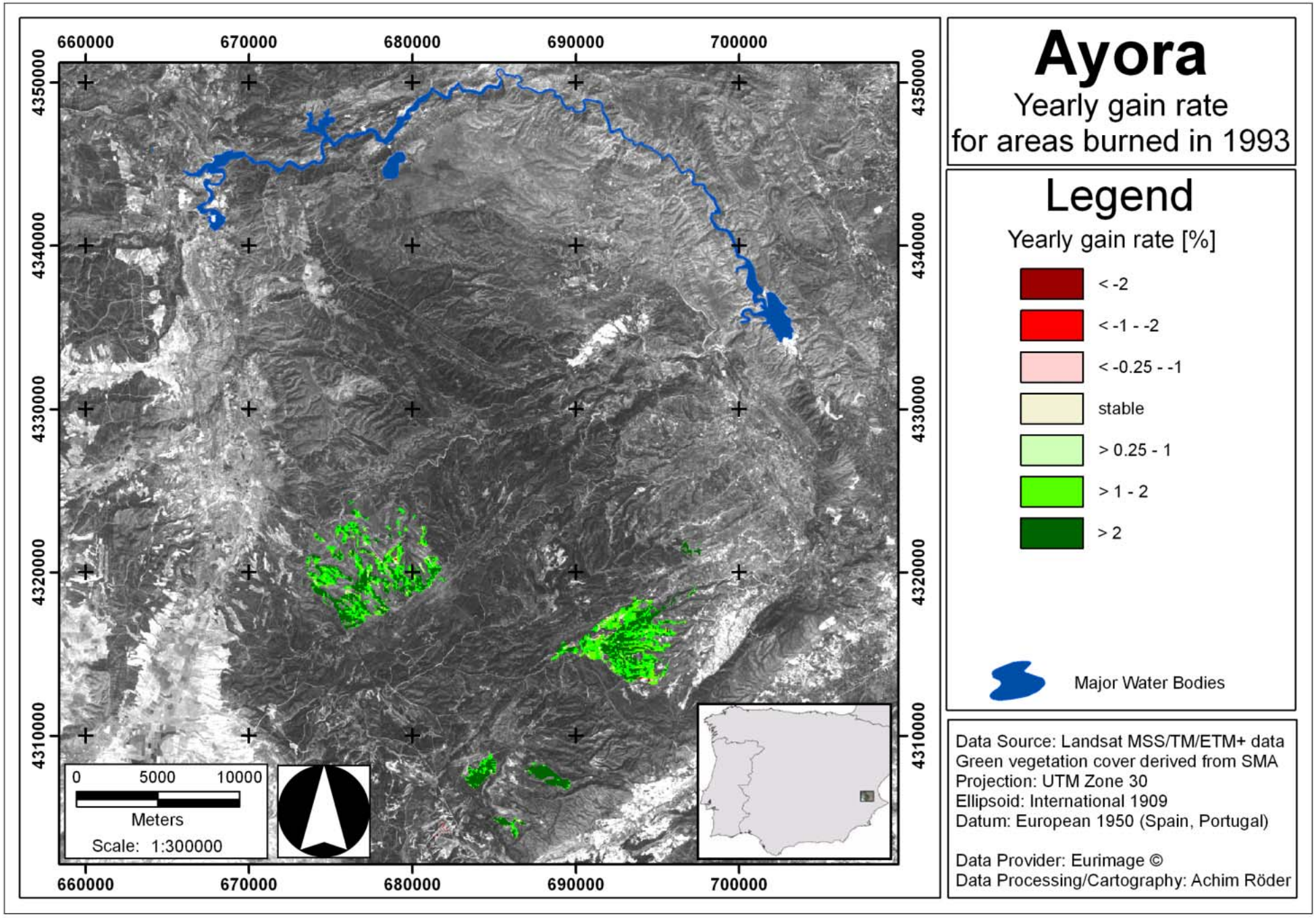

Map D.11: Yearly gain rate for the area affected by the fire in 1993 - Ayora

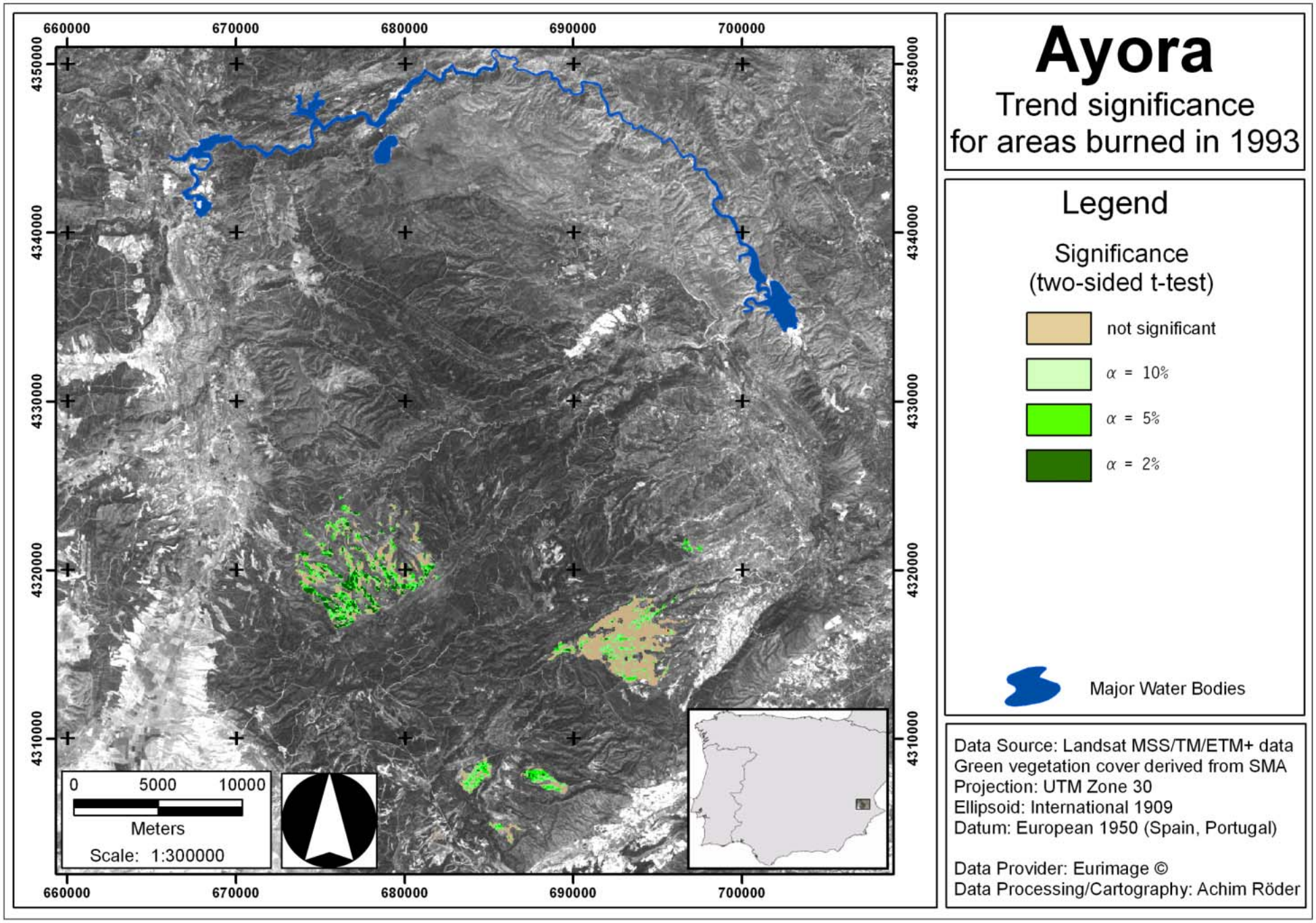

Map D.12: Trend significance for the area affected by the fire in 1993 - Ayora

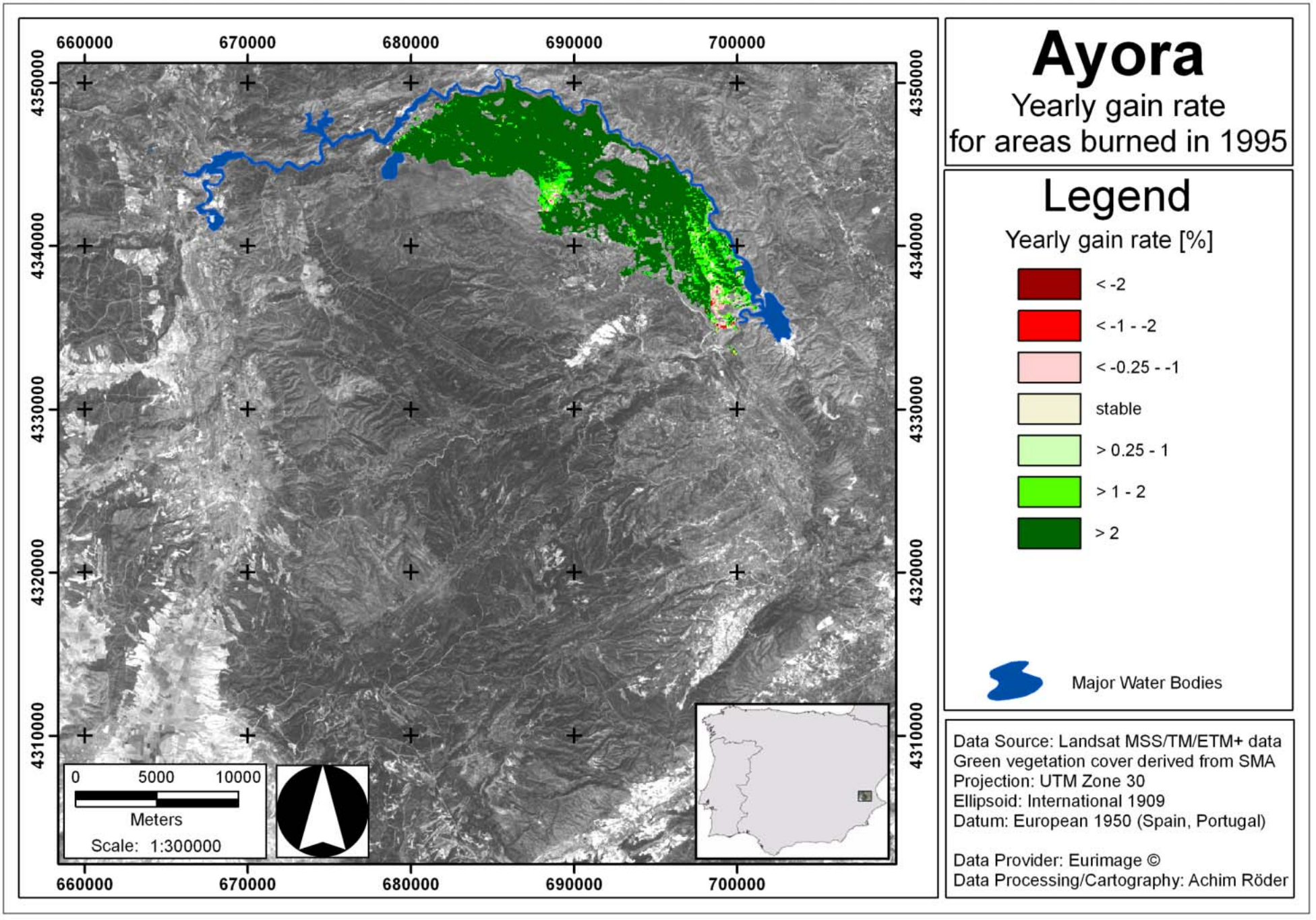

Map D.13: Yearly gain rate for the area affected by the fire in 1995 - Ayora

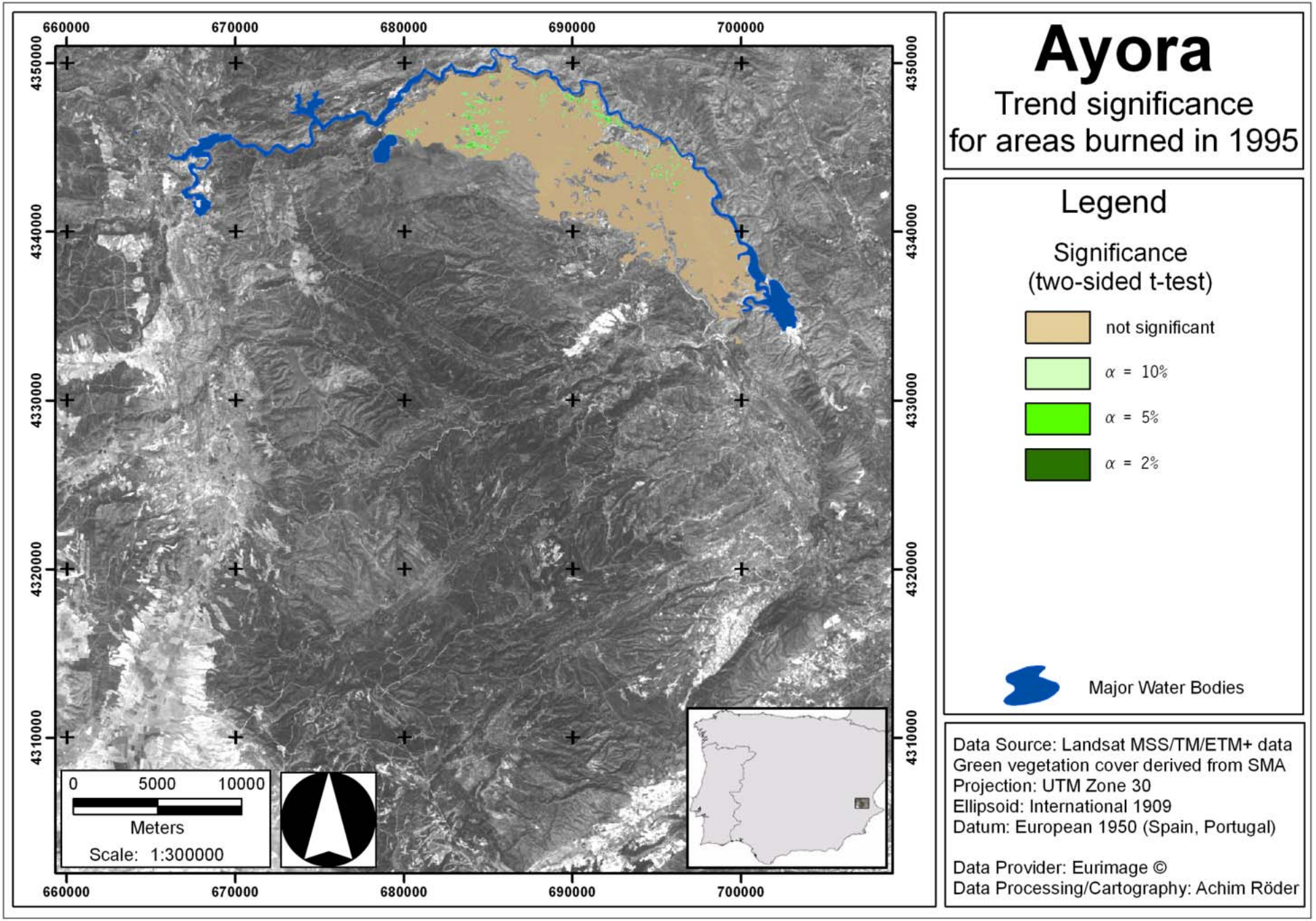

Map D.14: Trend significance for the area affected by the fire in 1995 - Ayora

Appendix E: Maps Lagadas

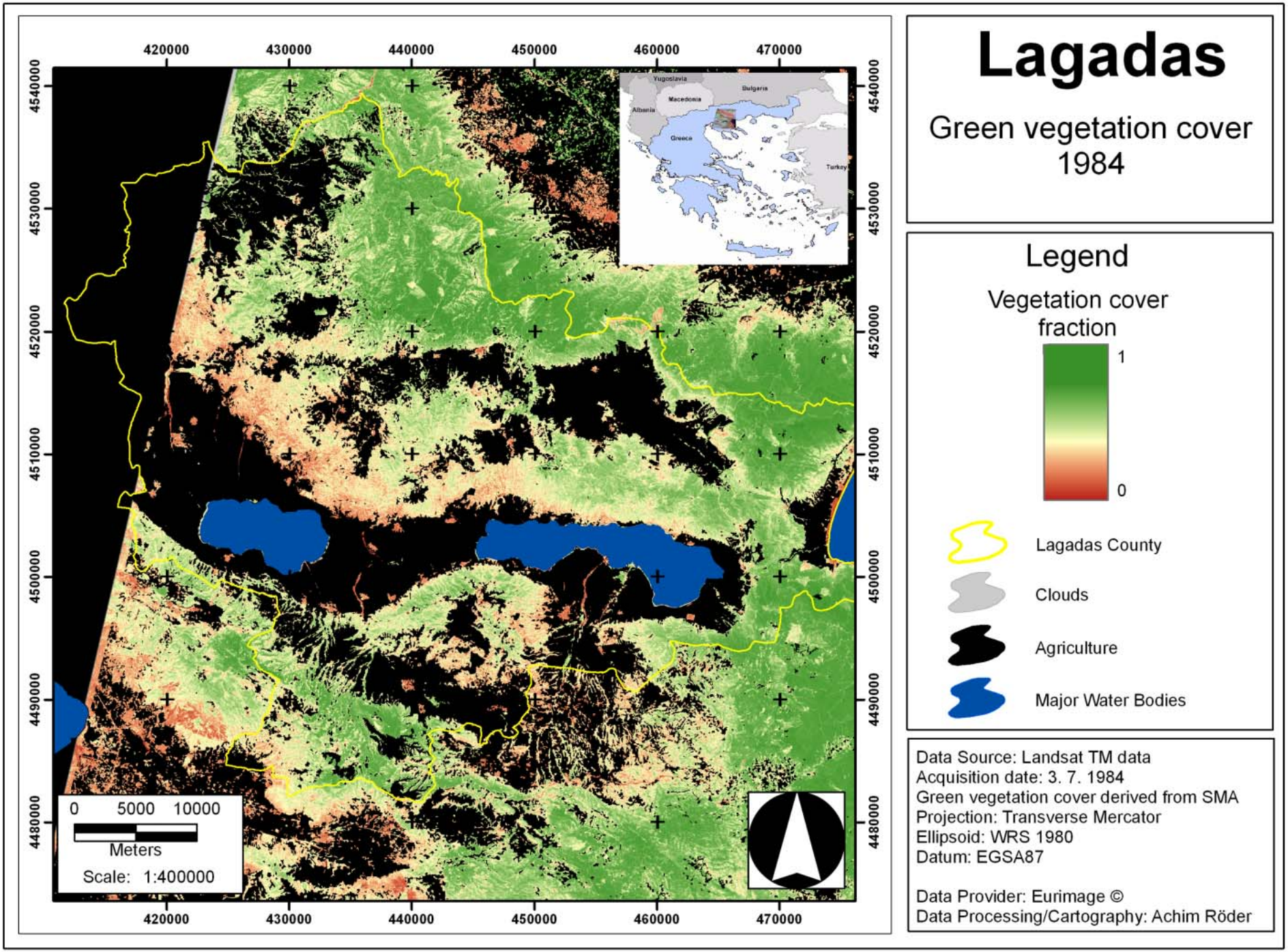

Map E.1: Proportional green vegetation cover - Lagadas (1984)

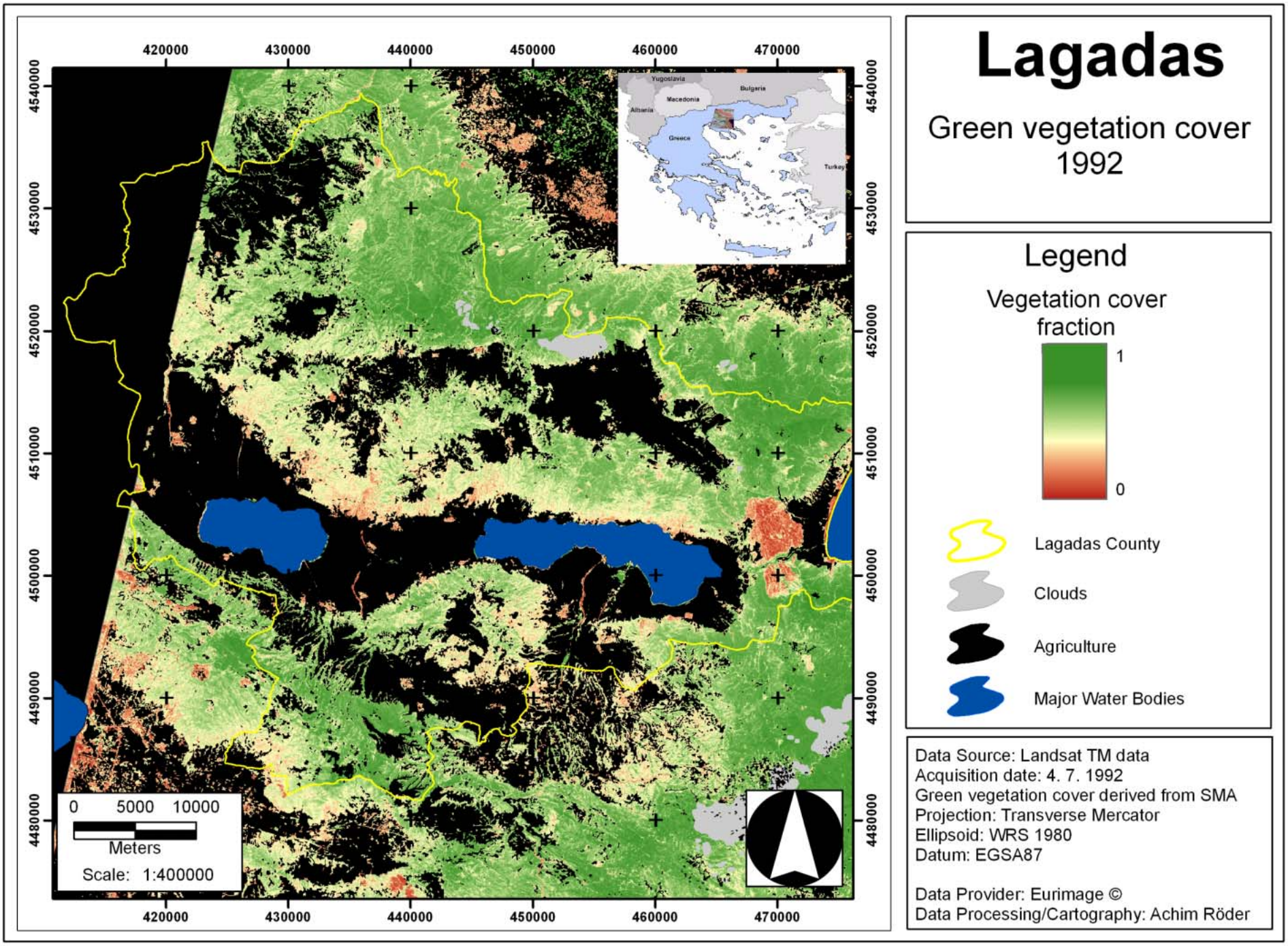

Map E.2: Proportional vegetation cover - Lagadas (1992)

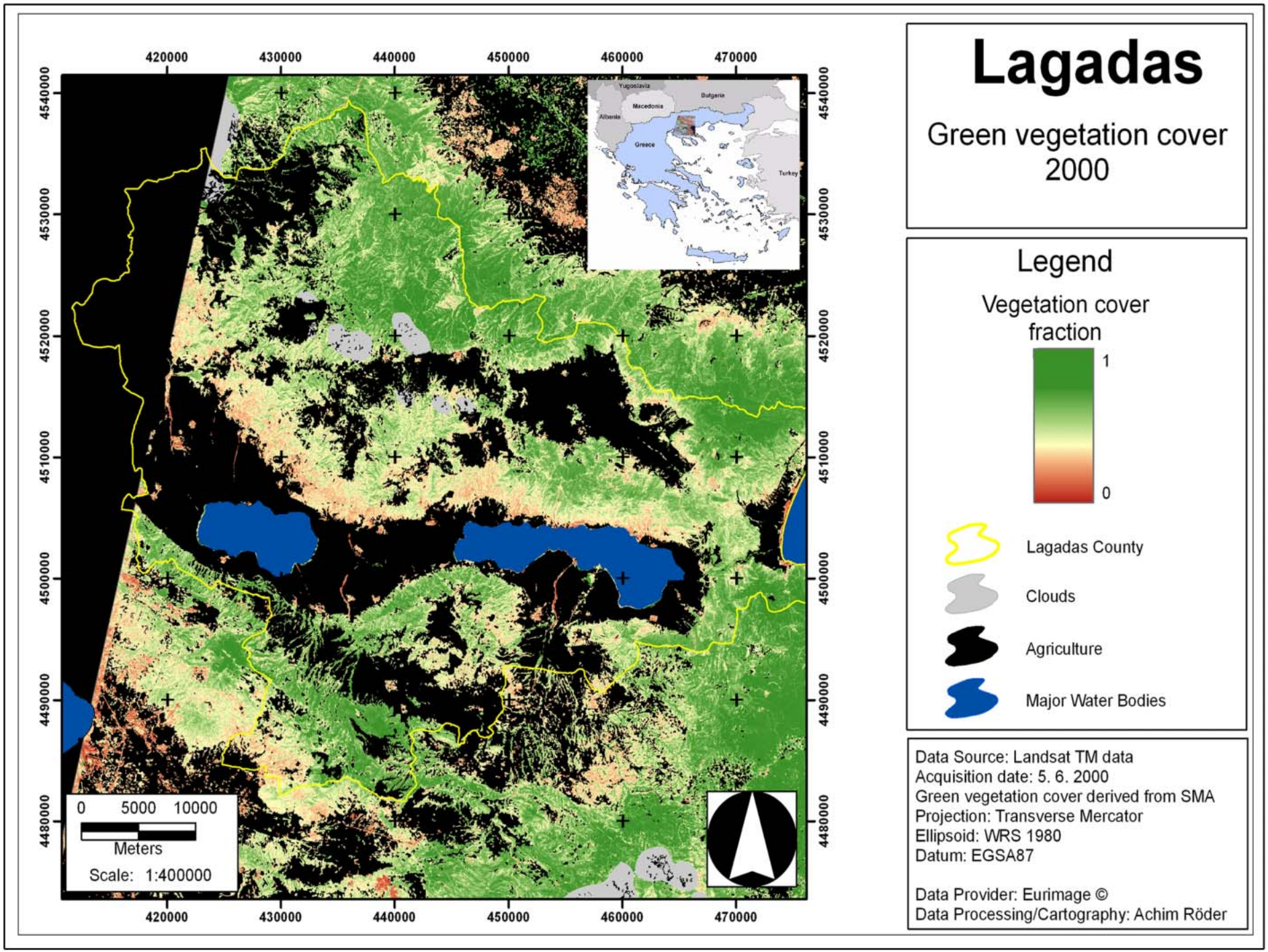

Map E.3: Proportional vegetation cover - Lagadas (2000)

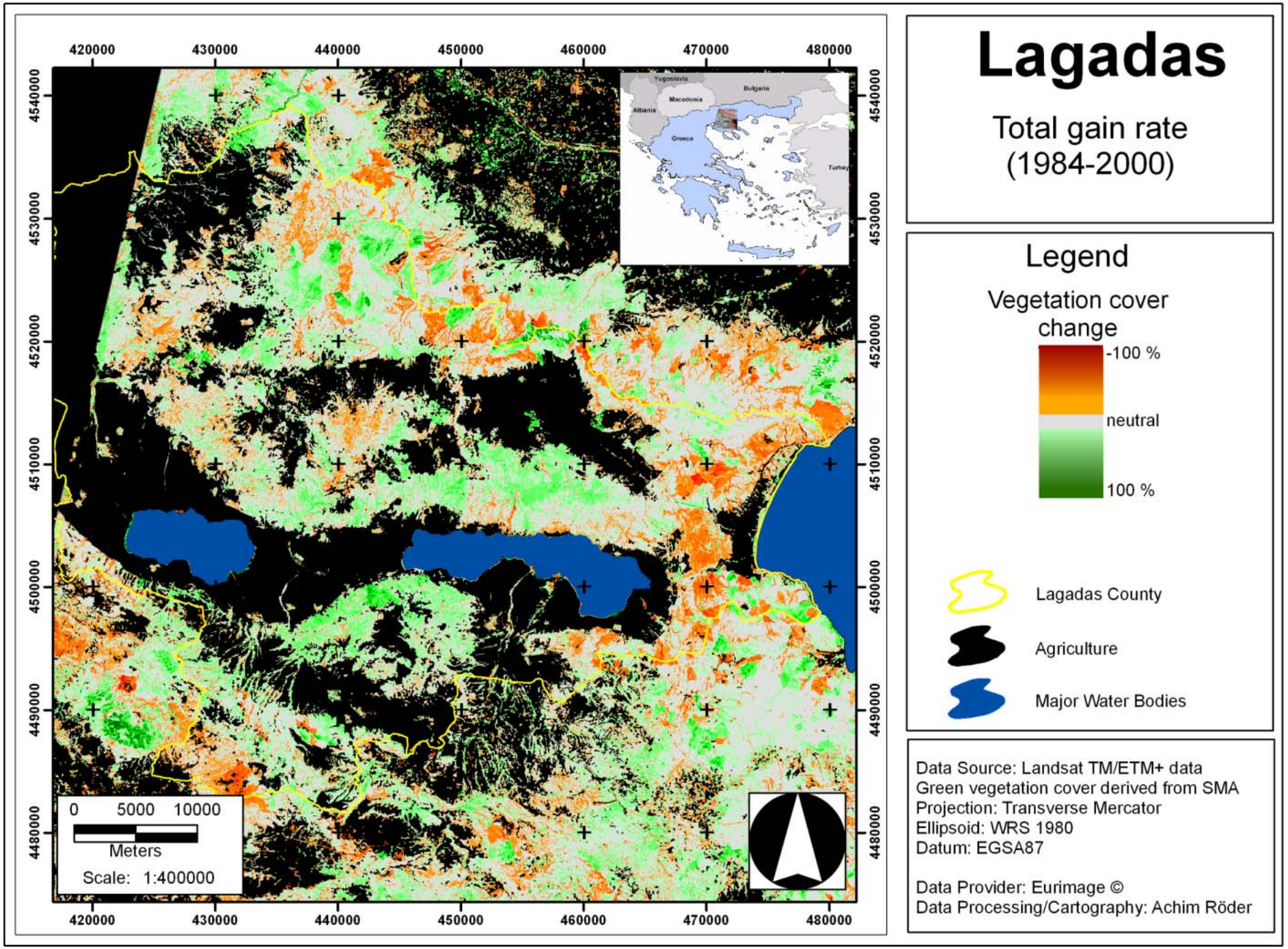

Map E.4: Total gain rate - Lagadas (1984-2000)

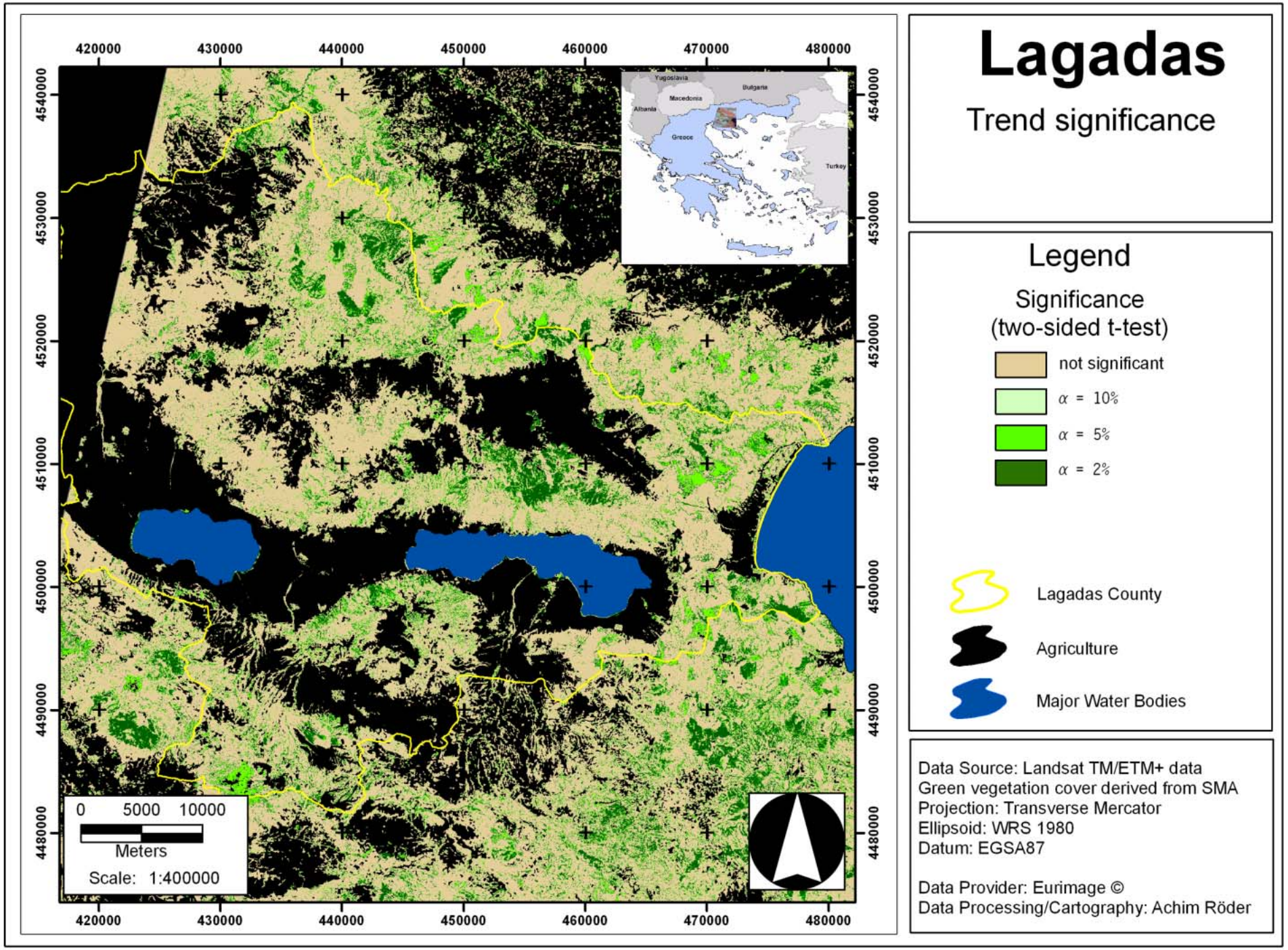

Map E.5: Trend significance - Lagadas

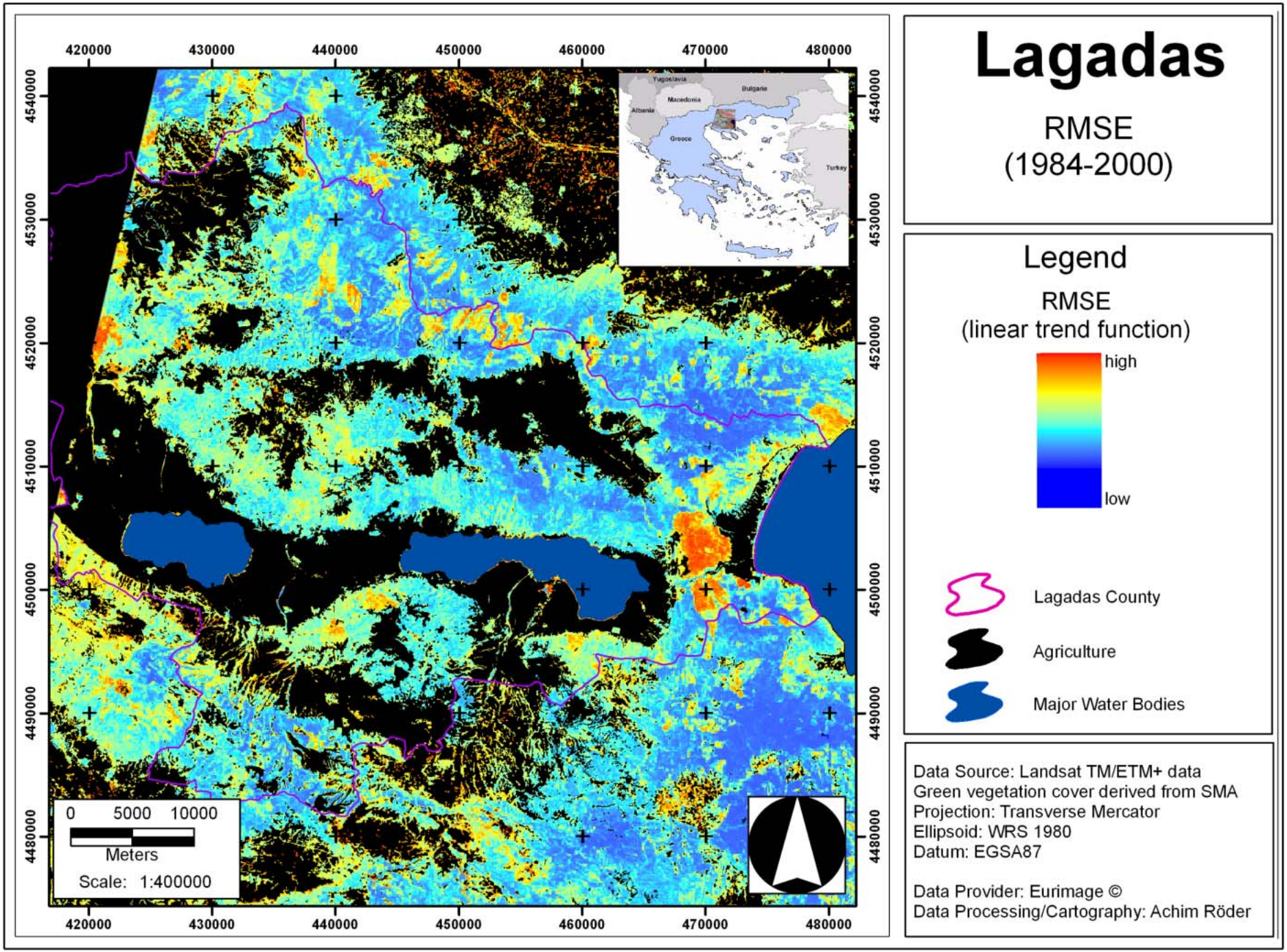

Map E.6: RMSE - Lagadas

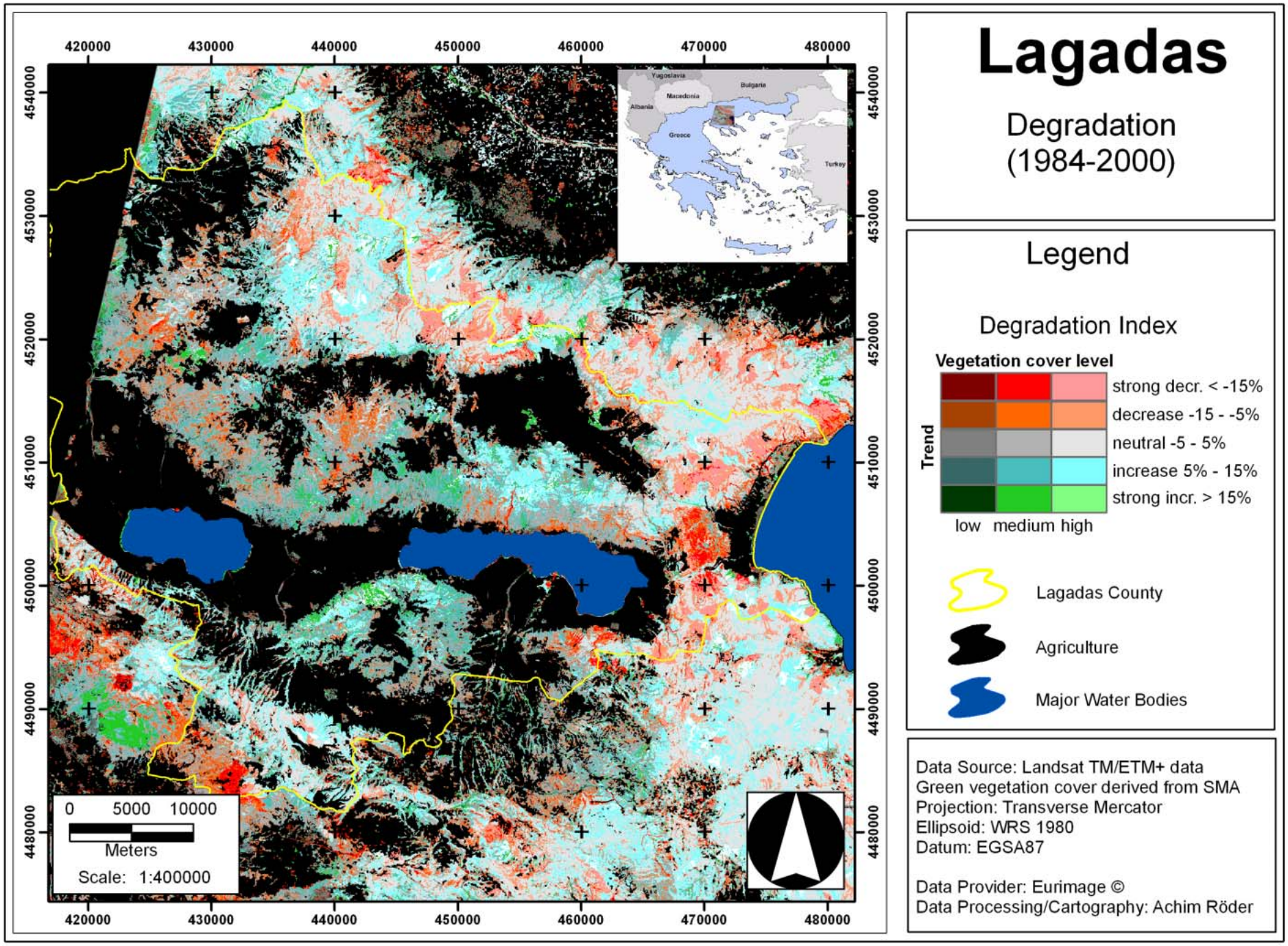

Map E.7: Degradation index - Lagadas

A Remote Sensing Based Framework for Monitoring and Assessing Mediterranean Rangelands. Case Studies from Two Test Sites in Spain and Greece

Zusammenfassung

Aufgrund seiner naturräumlichen Grundlagen gilt der europäische Mittelmeerraum als ein von Desertifikation bzw. Landdegradation gefährdeter Raum und wird in Annex IV der Konvention zur Bekämpfung von Wüstenbildung (UNCCD) geführt. Diese betont den Einfluss des wirtschaftenden Menschen, durch den häufig - vor dem Hintergrund ungünstiger Naturfaktoren – der Prozess der Desertifikation erst initiiert wird. Der in dieser Arbeit verwendete Begriff der ‚Landdegradation' bezieht sich dabei auf Prozesse, die das natürliche Potenzial von Ökosystemen nachhaltig stören. Dies schließt weit reichende Aspekte mit ein, wie z.B. biologische Produktivität, Landschaftsstruktur, ökosystemare Kreisläufe, oder ökonomische, soziale und kulturelle Strukturen. Als Zielraum dienen in dieser Arbeit so genannte ‚Rangelands'. Es handelt sich dabei um marginale Räume, die keiner primären Nutzung unterliegen, aber von großer Bedeutung als Weideland, für die Holzgewinnung, für lokale Wasserkreisläufe oder als Rückzugsgebiete für Flora und Fauna sind. Durch ökonomische und gesellschaftliche Veränderungen, insbesondere in den europäischen Mittelmeerländern, wird das über lange Zeiträume entwickelte Gleichgewicht in diesen Räumen zunehmend bedroht. Diese Prozesse führen zu einem Nebeneinander von Extensivierung durch Auflassung und Intensivierung zur Steigerung landwirtschaftlicher Produktion.

Fernerkundliche Ansätze ermöglichen die kontinuierliche Überwachung von Ökosystemen auf der Basis objektiver Daten. Insbesondere die Verfügbarkeit der Landsat-Sensoren seit 1972 erlaubt ein retrospektives Monitoring von Umweltveränderungen und somit die Bewertung zurückliegender externer Einflüsse. Letzteres ist von großer Bedeutung im Kontext von politischer Entscheidungsfindung auf unterschiedlichen administrativen Ebenen. Um dies über einzelne Fallstudien hinaus zu unterstützen, ist ein konzeptioneller, übertragbarer Interpretationsrahmens notwendig. Die vorliegende Arbeit zielt darauf ab, Kernpunkte eines solchen Rahmens zu identifizieren und Vorschläge zu deren Umsetzung zu machen.

Stellvertretend für zwei der wichtigsten Prozessregime mediterraner Rangelands wurden zwei Gebiete ausgewählt. In der Provinz von Lagadas (Griechenland), östlich von Thessaloniki, ist die Beweidung mit Schafen und Ziegen ein wichtiger Faktor der ländlichen Volkswirtschaft und wird durch landwirtschaftliche Nutzung geeigneter Gebiete ergänzt. Die Region um Ayora (Spanien), westlich von Valencia gelegen, gilt als eine der am stärksten von Feuer betroffenen Regionen Spaniens. Die Faktoren ‚Beweidung' und ‚Feuer' stehen stellvertretend für wichtige Prozess-Skalen: längerfristige im ersten Fall, deren Einfluss nur im Laufe der Zeit sichtbar wird; eine Kombination aus kurz- und längerfristigen im zweiten Fall, da die direkten Konsequenzen großer Feuer kurzfristig auftreten, während Auswirkungen auf Pflanzengesellschaften, Bodenerosion etc. erst in längeren Zeiträumen erfasst werden können.

Zunächst wurden für beide Gebiete Zeitreihen auf Basis der Landsat-Sensoren aufgebaut, die den Zeitraum von 1976 (Ayora) bzw. 1984 (Lagadas) bis 2000 mit einer Szene pro Jahr umfassen. Alle Daten wurden, unter Berücksichtigung des Reliefs, mit Hilfe digitaler Höhenmodelle geometrisch und radiometrisch korrigiert. Dabei lag das Augenmerk auf der exakten Sensorkalibrierung, der Interkalibrierung von TM- und MSS-Daten sowie einer optimierten Prozessierung dieser langen Datenreihen. Der Bedeckungsrad photosynthetisch aktiver Vegetation wurde als geeigneter Indikator für die Bewertung des Landschaftszustandes identifiziert und mit Hilfe der Spektralen Mischungsanalyse (SMA) als quantitativer Parameter für jede verfügbare Szene abgeleitet.

Die somit verfügbare Datenbasis erlaubte für Ayora zunächst eine exakte Kartierung von Auftrittsjahr und Perimeter von Feuern sowie die räumlich differenzierte Kartierung ihrer Häufigkeit. Die gestiegene Feuerhäufigkeit wird dabei unter anderem auf verstärkte Abwanderung aus der Region und die damit verbundene Auflassung und Verbuschung zurückgeführt. Auf der Basis der ersten Analyseergebnisse konnte mittels räumlich und zeitlich stratifizierter linearer Trendanalyse die Dynamik der Wiederbesiedlung durch Pflanzen erfasst und quantifiziert werden. Infolge der langen Beeinflussung durch Feuer kommt es in solchen Gebieten häufig zu einer Autosukzession, die nach einer anfänglichen Dominanz von Gräsern und Krautigen letztendlich zu ähnlichen Pflanzengesellschaften führt, wie sie vor dem Feuer vorhanden waren. Die hierfür typischen exponentiellen Kurvenverläufe wurden in dieser Arbeit ebenfalls festgestellt. Außerdem zeigte sich deutlich der Einfluss von Exposition und Hangneigung auf die Regeneration von Pflanzen; dabei erwiesen sich Gebiete mit besserer Wasserversorgung infolge niedrigerer solarer Einstrahlung als günstiger. Darüber hinaus wurden nach den Feuern nur selten die davor beobachteten Bedeckungsrade wieder erreicht. Dies unterstreicht die Theorie einer Verarmung und verringerten Produktivität feuerbeinflusster Ökosysteme wenn die Feuerhäufigkeit einen kritischen Wert überschreitet.

In der Region von Lagadas konnte mittels linearer Trendanalyse und eines abgeleiteten Degradationsindex ein eng verzahntes Muster von Vegetationszuwachs und –abnahme aufgezeigt werden. Dessen räumliche Verteilung zeigte einen deutlichen Einfluss von Geländeform und –höhe. Diese wurden als Indizien für den Einfluss lokaler Erreichbarkeit bewertet, denn insbesondere steile, enge Täler zeigten positive Trends, während negative Trends vor allen Dingen auf wenig geneigten, niedrig gelegenen Gebieten auftraten. Vieh-Bestandszahlen auf Gemeindeebene ermöglichten die Untersuchung eines Zusammenhangs zwischen Vegetationsbedeckungsraden und Bestockungsdichte. Durch die Berechnung zeitlicher Trajektorien wurde deutlich, dass lediglich ein Teil der beobachteten Gemeinden den erwarteten negativen Zusammenhang aufweist. Davon abweichend zeigt sich häufig ein positiver Zusammenhang oder ein wechselndes Verhalten über den Beobachtungszeitraum. Eine stellenweise beobachtete Zunahme der Vegetationsbedeckung bei gleichzeitig steigenden Besatzdichten weist beispielsweise deutlich auf jüngere Trends im Weideverhalten hin, in Folge derer es zu einem deutlichen Rückgang traditioneller Wanderungen von Schäfern und Herden kommt. Im Gegensatz dazu finden signifikante Konzentrationsprozesse durch verlängerte Aufenthaltszeiten in Ställen und die verstärkte Beweidung nahe gelegener Gebiete statt. Um potenzielle Auswirkungen dieses Verhaltens auf räumliche Trends beurteilen zu können, wurde schließlich anhand verfügbarer Geodaten der Aufwand zur Erreichung verschiedener Gebiete als Kostenoberfläche modelliert. Die Ableitung von Bedeckungsgraden für solche Kostenzonen in Relation zur Lage von Stallungen, die aus geometrisch höchstauflösenden QuickBird-Daten kartiert wurden, verdeutlichte diesen Zusammenhang in Form eines klar gegliederten Gradienten.

Auf der Basis dieser beiden Pilotstudien konnten schließlich die zu Beginn definierten Elemente eines Interpretationskonzeptes bewertet und formal dargestellt werden. Von besonderer Wichtigkeit ist dabei die Trennung klar vorgegebener Prozessierungsketten der Fernerkundungsdaten im Vergleich zur weiteren Datenintegration und Interpretation. Diese benötigt eine flexible Handhabung, da gerade in den Ländern des europäischen Mittelmeerraums die Datenlage äußerst heterogen ist. Während vielerorts der Bereitstellung von Geodaten großes Gewicht beigemessen wird, sind solche Informationen in anderen Regionen häufig von nicht ausreichender Qualität oder in ihrer Verfügbarkeit eingeschränkt. Ein übertragbares Monitoring-Konzept für Prozesse mediterraner Rangelands kann deshalb nur als zweigeteilter Ansatz erfolgreich sein, der der klar definierten fernerkundlichen Analyse eine flexible weitere Interpretation auf der Basis tatsächlich verfügbarer Daten gegenüberstellt.

Summary

The European Mediterranean is characterised by a unique combination of natural factors, which contribute to its vulnerability to desertification and land degradation. Consequently, the region is listed in Annex IX for the 'UN Convention to Combat Desertificiation (UNCCD)'. The Convention particularly emphasises the anthropogenic influence, which – augmented by unfavourable natural conditions – is often responsible for desertification processes. In the present research, the term 'land degradation' is used to characterise processes which negatively affect the natural potential of ecosystems. This relates to biological productivity, landscape structure, nutrient cycles, or economic, social and cultural structures etc. 'Rangelands' – generally defined as areas which by reason of physical limitations are unsuited to cultivation – make up for most of the land surface of the Mediterranean basin. They relate to marginal, non-arable lands and provide forage for free-roaming native and domestic animals, as well as a source of wood products, water and important retreat areas for flora and fauna. In combination with the typical Mediterranean climate regime, strong relief gradients and less developed soils frequently cause a high erosive potential of these areas.

There is a long history of human settlement and intervention in Mediterranean rangelands, which have led to an equilibrium state in many areas and resulted in the typical landscapes found today. Substantial economic and societal changes of the recent past have caused land use transitions that increasingly threaten these ecosystems. Depending on local conditions there is a mosaic of land uses, ranging from extensification due to land abandonment to intensification to increase rural production.

Remote sensing supports the monitoring of ecosystems, as it provides objective and consistent data on a regular basis. In particular, the range of Landsat sensors allows to retrospectively characterise land use and land cover change back until 1972, which enables to assess the effects of external interventions. This is especially important in the context of land management and decision making. This research work intends to contribute to this process by identifying elements of a transferable monitoring concept and demonstrating their potential implementation in the frame of two case studies.

Two areas were selected to represent major process regimes of Mediterranean rangelands. In the County of Lagads (Greece), situated east of the city of Thessaloniki, livestock grazing with sheep and goats is a major factor of the rural economy. In suitable areas, it is complemented by agricultural use. The region of Ayora (Spain) is located west of the city of Valencia. It is one of regions most affected by fires in Spain. The factors 'grazing' and 'fire' are representative of important process scales: gradual processes the results of which manifest on a longer term in the first case; and a combination of singular and gradual processes in the second, as fire effectuates often catastrophic short-term effects, while their eventual impact on plant composition, soil erosion etc. becomes visible only after longer periods.

First of all, long time series of satellite data were compiled for both regions on the basis of Landsat sensors, which cover the time until 1976 (Ayora) and 1984 (Lagadas) with one image per year. The data were geometrically and radiometrically corrected and a digital elevation model was used to account for non-systematic geometric distortions and topography-induced illumination variations. Specific attention was given to an exact sensor calibration, the radiometric intercalibration of Landsat-TM and –MSS and the optimisation of processing such volumes of data. Proportional cover of photosynthetically active vegetation was identified as a suitable quantitative indicator for assessing the state of rangelands. Using Spectral Mixture Analysis (SMA) it was inferred for all data sets.

The extensive data base procured this way enabled to map fire events in the Ayora area based on sequential diachronic sets and provide fire dates, perimeter as well as fire recurrence for

each pixel. The increasing fire frequency in the past decades is in large parts attributed to the accelerated abandonment of the area that leads to an encroachment of shrublands and the accumulation of combustible biomass. On the basis of the fire mapping results, a spatial and temporal stratification of the data set allowed to asses plant recovery dynamics on the landscape level through linear trend analysis. The long history of fire events in the Mediterranean frequently leads to processes of auto-succession. Following an initial dominance of herbaceous vegetation this commonly leads to similar plant communities as the ones present before the fire. On a temporal axis, this results in typical exponential post-fire trajectories which could also be shown in this study. The analysis of driving factors for post-fire dynamics confirmed the importance of aspect and slope. Locations with lower amounts of solar irradiation and favourable water supply yielded faster recovery rates and higher post-fire vegetation cover levels. In most cases, the vegetation cover levels observed before the fire were not reached within the post-fire observation period. This supports the hypothesis of a general loss in biological productivity of ecosystems affected by fires, if fire recurrence cycles exceed a tolerance threshold and deny plant species to reach sexual maturity.

In the area of Lagadas, linear trend analysis and additional statistical parameters were used to infer a degradation index. This could be used to illustrate a complex pattern of stability, regeneration and degradation of vegetation cover. These different processes and states are found in close proximity and are clearly determined by topography and elevation. Following a sequence of analyses, it was found that in particular steep, narrow valleys show positive trends, while negative trends are more abundant on plain or gently undulating areas. Considering the local grazing regime, this spatial differentiation was related to the accessibility of specific locations. Subsequently, animal numbers on community level were used to calculate efficient stocking rates and assess the temporal development of their relation with vegetation cover. This calculation of temporal trajectories illustrated that only some communities show the expected negative relation. To the contrary, a positive relation or even changing relation patterns are observed. For instance, some communities exhibit increasing vegetation cover with increasing stocking rates. This signifies recent concentration and intensification processes in the grazing scheme, as a result of which animals are kept in sheds where additional feedstuffs are provided. In these cases, free roaming of livestock animals is often confined to some hours every day, which explains the spatial preference of easily accessible areas by the shepherds. Beyond these temporal trends it was analysed whether the grazing pattern is equally reflected in a spatial trend. Making use of available geospatial information layers, the efforts required to reach each location (i.e. pixel) was expressed as a cost. Then, cost zones could be defined and woody vegetation cover as a grazing indicator could be inferred for the different zones. Animal sheds were employed as starting features for this piospheric analysis, which could be mapped from very high spatial resolution Quickbird image data. The result was a clearly structured gradient showing increasing woody vegetation cover with increasing cost distance.

On the basis of these two pilot studies, the elements of a monitoring and interpretation framework identified at the beginning of the work were evaluated and a formal interpretation scheme was presented. It is based on two separated components: a clearly defined and structured component for standardised processing of remote sensing data; and a second component aiming at the integration with other data sources and interpretation. The latter can not be completely formalised as the availability of such data is highly variable in different regions affected by land degradation processes. In the frame of the two case studies presented in this work, it was demonstrated how specific data may be used in this context to illustrate potential data integration and interpretation pathways.

Lebenslauf

Adresse:	Achim Röder
	Kurfürstenstraße 31
	D-54295 Trier
Staatsangehörigkeit:	deutsch
Geburtsdatum:	7. 03. 1969
Geburtsort:	Calw / Württemberg

Schulbildung:

8/1975 - 7/1979:	Gundschule Feldrennach
8/1979 - 7/1988:	Mathematisch-naturwissenschaftliches Gymnasium Neuenbürg (Württemberg)

Studium:

10/1990 - 7/1997:	Angewandte Physische Geographie / Geowissenschaften (Abschluss Dipl.-Geograph) an der Universität Trier Thema der Abschlussarbeit: Möglichkeiten der Interkalibrierung von Landsat TM und MSS zur Ableitung vergleichbarer Vegetations- und Bodenparameter - dargestellt am Beispiel Kreta.
10/2003-heute:	Promotionsstudium Geographie / Geowissenschaften an der Universität Trier

Berufliche Tätigkeiten

1/1998 - heute:	Mitarbeiter in verschiedenen Forschungsprojekten im FB VI Geographie / Geowissenschaften der Universität Trier, Abteilung Fernerkundung